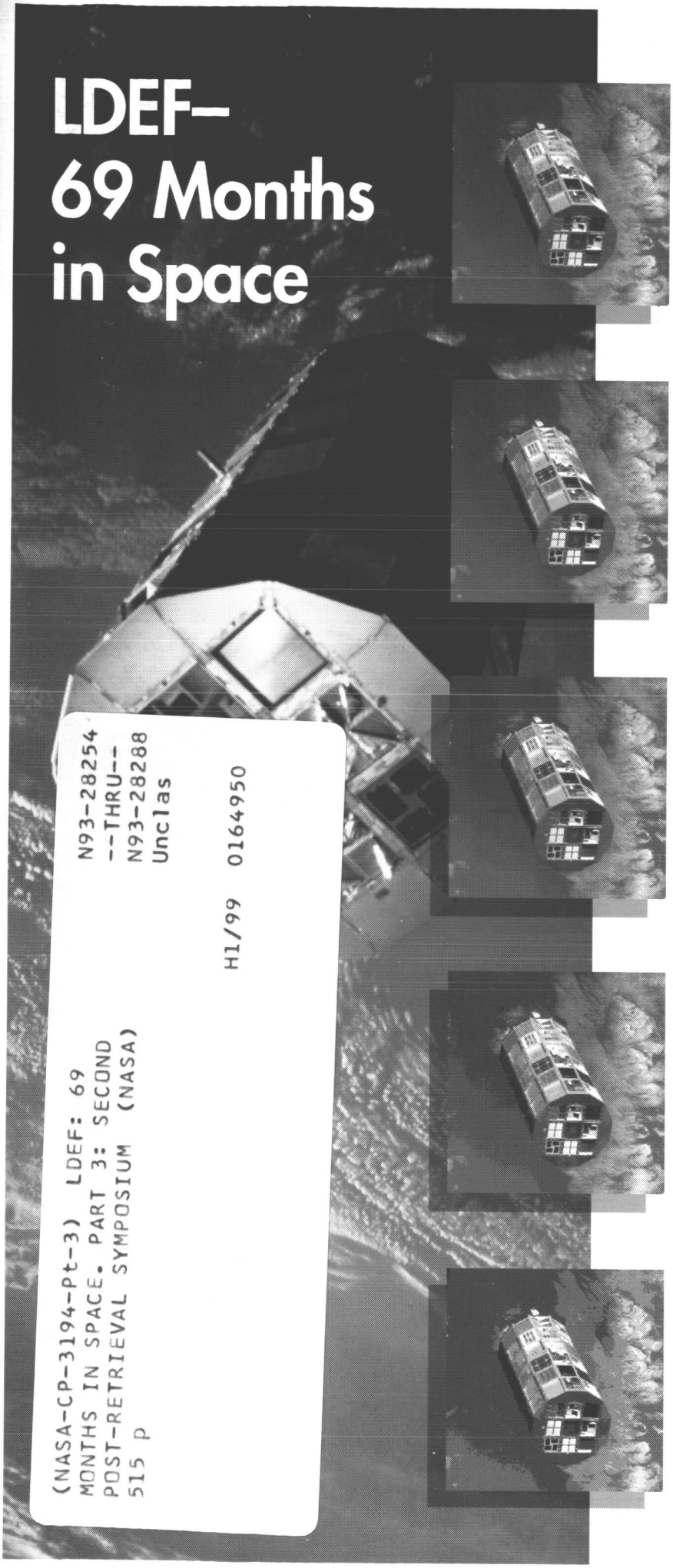

LDEF–69 Months in Space

Second Post - Retrieval Symposium

June 1-5, 1992
San Diego, California

Sponsors:

LDEF Science Office
NASA Langley Research Center

American Institute of
Aeronautics and Astronautics

NASA Conference Publication 3194
Part 3

National Aeronautics and
Space Administration

American Institute of
Aeronautics and Astronautics

(NASA-CP-3194-Pt-3) LDEF: 69 MONTHS IN SPACE. PART 3: SECOND POST-RETRIEVAL SYMPOSIUM (NASA) 515 p
N93-28254 --THRU-- N93-28288 Unclas
H1/99 0164950

LDEF–
69 Months
in Space

NASA Conference Publication 3194
Part 3

Second Post - Retrieval Symposium

Edited by
Arlene S. Levine
NASA Langley Research Center
Hampton, Virginia

Proceedings of a symposium sponsored by the National Aeronautics and Space Administration, Washington, D.C., and the American Institute of Aeronautics and Astronautics, Washington, D.C., and held in San Diego, California
June 1-5, 1992

National Aeronautics and
Space Administration

Office of Management

Scientific and Technical
Information Program

1993

FOREWORD

Nineteen hundred ninety-two, designated The International Space Year (ISY), coincided with the 35th anniversary of the International Geophysical Year (IGY). The International Space Year honored space exploration and the planet Earth and also marked the 500th Anniversary of Christopher Columbus's discovery of the New World. Langley Research Center, the home of the Long Duration Exposure Facility (LDEF), celebrated its 75th anniversary. In addition, 1992 marked the second anniversary of the LDEF retrieval. Since publication of the First LDEF Post-Retrieval Symposium Conference Publication in January 1992, the LDEF principal investigators, co-investigators, and collaborating investigators have had an additional 12 months to analyze and interpret the data from LDEF's 57 onboard experiments and to reach a better understanding of the space environment (ionizing radiation, meteoroids, space debris, and atomic oxygen in the upper atmosphere) and the effects that prolonged exposure in this environment will have on future spacecraft such as large low-Earth orbit (LEO) platforms, Earth-orbiting spacecraft, and on future manned and unmanned spacecraft to the Moon and to other planets.

Results of the second year LDEF studies were presented at the Second LDEF Post-Retrieval Symposium, held at the Town and Country Hotel, San Diego, California, June 1 to 5, 1992. This symposium was co-sponsored by NASA Langley Research Center and the American Institute of Aeronautics and Astronautics. This document contains the full-length papers presented at the second symposium. The collection includes invited review papers on ionizing radiation, meteoroids and debris, environmental effects on materials, environmental effects on systems, and archiving of the LDEF data. Contributed papers on ionizing radiation, meteoroids and debris, space effects on materials and systems, the LDEF mission and induced environments, microgravity, and life science are also included. The document organization is very similar to that of the symposium.

LDEF Mission and Induced Environments
Space Environments - Ionizing Radiation
Space Environments - Meteoroid and Debris
Space Environments - Microgravity
Space Environmental Effects - Materials
Space Environmental Effects - Systems
Space Environmental Effects - Biology
The Future

During the symposium William H. Kinard chaired the first half of the general session containing the invited review papers, and Bland A. Stein chaired the second half of the general session containing the invited review papers, plus the Mission and Induced Environments papers, and a Microgravity paper. Thomas Parnell chaired the Ionizing Radiation sessions; J.A.M. McDonnell, Jean-Claude Mandeville, Dale R. Atkinson, Michael Zolensky, and Donald Humes chaired Meteoroid and Debris sessions; Joan Funk and John Davis chaired the Data basing session; Ann Whitaker and Bruce Banks chaired the Coating session; Philip Young chaired the Polymer session, and R.C. Tennyson chaired the Polymer Matrix Composites session. Roger Linton chaired the Metals and Metal Matrix Composites session. Gale Harvey and Bland Stein chaired the Contamination session. James Mason, Joel Edelman, and Harry Dursch chaired the Systems sessions. William H. Kinard chaired the closing general session containing papers on biology and future activities.

PRECEDING PAGE BLANK NOT FILMED

I wish to thank the contributing authors whose research greatly enhanced the knowledge of space environments and their effects on materials, systems, and biology. The papers contained in this volume underwent a technical review by peer reviewers and an editorial review. I also wish to thank the technical reviewers for their time and effort in making this collection as current and accurate as it is. I would like to thank Maureen Sgambelluri, who assisted with the symposium logistics, and who cheerfully reformatted some of the papers contained in this publication. I would like to gratefully acknowledge Susan Hurd, Mary Edwards, Lisa Levine, Alisa Hollins, and Jeanne Gordon, for their support in editing this document.

This conference publication is the second in a series of three LDEF Post-Retrieval documents. In June 1991, over 400 LDEF investigators and data users convened in Kissimmee, Florida for the First LDEF Post-Retrieval Symposium. The results of the symposium (130 papers) are printed in a three-part NASA Conference Publication, ***LDEF-69 Months in Space: First LDEF Post-Retrieval Symposium,*** January 1992, (NASA CP-3134.) The LDEF Science Office plans to hold a third symposium in November 1993, in Williamsburg, Virginia. Published abstracts for the third symposium will be available at the meeting. Additional information on these symposia may be obtained by contacting:

Arlene S. Levine
LDEF Science Office M/S 404
NASA Langley Research Center
Hampton, Virginia 23681-0001
Telephone: 804 864-3318
Fax: 804 864-8094

The use of trade names or manufacturers in this publication does not constitute an official endorsement of such products or manufacturers, either expressed or implied, by the National Aeronautics and Space Administration.

CONTENTS

FOREWORD.....iii

Part 1*

Mission and Induced Environments

Refinements on the Pinhole Camera Measurements of the LDEF Attitude.....3
Palmer N. Peters, Paul L. Whitehouse and John C. Gregory

LDEF Microenvironments, Observed and Predicted.....13
R.J. Bourassa, H.G. Pippin, and J.R. Gillis

A Generalized Approach to the Thermal Analysis of the Long Duration Exposure Facility's Flight Experiments.....27
Thomas R. Sampair*

ENVIRONET: On-Line Information for LDEF.....51
Michael Lauriente

Space Environments - Ionizing Radiation

Status of LDEF Ionizing Radiation Measurements and Analysis.....69
Thomas A. Parnell

Sensitivity of LDEF Foil Analyses Using Ultra-Low Background Germanium Vs. Large NaI(Tl) Multidimensional Spectrometers.....79
James H. Reeves, Richard J. Arthur, and Ronald L. Brodzinski

Radioactivities Induced in Some LDEF Samples.....87
Robert C. Reedy, Calvin E. Moss, S. George Bobias, and Jozef Masarik

A Photon Phreak Digs the LDEF Happening.....97
Alan R. Smith and Donna L. Hurley

Charged Particle Activation Studies on the Surface of LDEF Spacecraft.....107
Ilhan Olmez, Forest Burns, and Paul Sagalyn

Collection, Analysis, and Archival of LDEF Activation Data.....111
C.E. Laird, B.A. Harmon, G.J. Fishman, and T.A. Parnell

---

* Part 1 is presented under separate cover.

Induced Activation Study of LDEF 125
B.A. Harmon, G.J. Fishman, T.A. Parnell, and C.E. Laird

Revised Prediction of LDEF Exposure to Trapped Protons 137
John W. Watts, T. W. Armstrong, and B. L. Colborn

A Measurement of the Radiation Dose to LDEF by Passive Dosimetry 147
J. B. Blake and S. S. Imamoto

LDEF: Dosimetric Measurement Results (AO 138-7 Experiment) 157
J. Bourrieau*

Absorbed Dose Measurements and Predictions on LDEF 163
A.L. Frank, E.V. Benton, T.W. Armstrong, and B.L. Colborn

LET Spectra Measurements of Charged Particles in P0006 Experiment of LDEF 171
E.V. Benton, I. Csige, K. Oda, R.P. Henke, A.L. Frank, E.R. Benton, L.A. Frigo, T.A. Parnell, J.W. Watts, Jr., and J.H. Derrickson

Light-Heavy Ion Measurements in CR-39 Located on the Earth Side of LDEF 181
I. Csige, E.V. Benton, S. Soundararajan, and E.R. Benton

Three-Dimensional Shielding Effects on Charged Particle Fluences Measured in the P0006 Experiment of LDEF 187
I. Csige, E.V. Benton, L. Frigo, T.A. Parnell, J.W. Watts, Jr., T.W. Armstrong, and B.L. Colborn

Development and Application of a 3-D Geometry/Mass Model for LDEF Satellite Ionizing Radiation Assessments 195
B.L. Colborn and T.W. Armstrong

Radiation Model Predictions and Validation Using LDEF Satellite Data 207
T.W. Armstrong and B.L. Colborn

Future Directions for LDEF Ionizing Radiation Modeling and Assessments 221
T.W. Armstrong and B.L. Colborn

Cosmogenic Radionuclides on LDEF: An Unexpected ^{10}Be Result 231
J.C. Gregory, A. Albrecht, G. Herzog, J. Klein, R. Middleton, B. Dezfouly-Arjomandy, and B.A. Harmon

Heavy Ion Measurement on LDEF 239
D. Jonathal, R. Beaujean, and W. Enge

Progress Report on the Heavy Ions in Space (HIIS) Experiment 247
James H. Adams, Jr., Lorraine P. Beahm, Paul R. Boberg, and Allan J. Tylka

Progress Report on the Ultra Heavy Cosmic Ray Experiment (AO 178) 261
A. Thompson, D. O'Sullivan, J. Bosch, R. Keegan, K.-P. Wenzel, F. Jansen, and C. Domingo

Author Index 269

Part 2*

Space Environments - Meteoroid and Debris

Interim Report of the Meteoroid and Debris Special Investigation Group 277
Michael E. Zolensky, Herbert A. Zook, Fred Hörz, Dale R. Atkinson, Cassandra R. Coombs, Alan J. Watts, Claire Dardano, Thomas H. See, Charles Simon, and William H. Kinard

Micrometeoroids and Debris on LDEF 303
Jean-Claude Mandeville

Continued Investigation of LDEF's Frame and Thermal Blankets by the Meteoroid and Debris Special Investigation Group 313
Thomas H. See, Kimberly S. Mack, Jack L. Warren, Michael E. Zolensky, and Herbert A. Zook

Predicted and Observed Directional Dependence of Meteoroid/Debris Impacts on LDEF Thermal Blankets 325
Gerhard Drolshagen

3-D Crater Analysis of LDEF Impact Features from Stereo Imagery 339
Clyde A. Sapp, Thomas H. See, and Michael E. Zolensky

Further Analysis of LDEF FRECOPA Micrometeoroid Remnants 347
Janet Borg, Ted E. Bunch, Filippo Radicati di Brozolo, and Jean-Claude Mandeville

Long Duration Exposure Facility (LDEF) Experiment M0003 Meteoroid and Debris Survey 357
M.J. Meshishnek, S.R. Gyetvay, K.W. Paschen, and J.M. Coggi

Derivation of Particulate Directional Information from Analysis of Elliptical Impact Craters on LDEF 417
P.J. Newman, N. Mackay, S.P. Deshpande, S.F. Green, and J.A.M. McDonnell

---

* Part 2 is presented under separate cover.

Characteristics of Hypervelocity Impact Craters on LDEF Experiment S1003 and Implications of Small Particle Impacts on Reflective Surfaces 431
Michael J. Mirtich, Sharon K. Rutledge, Bruce A. Banks, Christopher De Vries, and James E. Merrow

Hypervelocity Impact Survivability Experiments for Carbonaceous Impactors 453
T.E. Bunch, Luann Becker, Jeffrey Bada, John Macklin, Filipo Radicati di Brozolo, R.H. Fleming, and Jozef Erlichman

Hypervelocity Impact Facility for Simulating Materials Exposure to Impact by Space Debris 479
M.F. Rose, S. Best, T. Chaloupka , B. Stephens, and G. Crawford

Analysis of LDEF Micrometeoroid/Debris Data and Damage to Composite Materials 493
R. C. Tennyson and G. Manuelpillai

SIMS Chemical Analysis of Extended Impacts on the Leading and Trailing Edges of LDEF Experiment AO187-2 513
S. Amari, J. Foote, P. Swan, R.M. Walker, E. Zinner, and G. Lange

Cratering in Glasses Impacted by Debris or Micrometeorites 529
David E. Wiedlocher and Donald L. Kinser

Scanning Electron Microscope/Energy Dispersive X-Ray Analysis of Impact Residues in LDEF Tray Clamps 541
Ronald P. Bernhard, Christian Durin, and Michael E. Zolensky

Projectile Compositions and Modal Frequencies on the "Chemistry of Micrometeoroids" LDEF Experiment 551
Ronald P. Bernhard, Thomas H. See and Friedrich Hörz

Asteroidal Versus Cometary Meteoroid Impacts on the Long Duration Exposure Facility (LDEF) 575
Herbert A. Zook

Interplanetary Meteoroid Debris in LDEF Metal Craters 577
D.E. Brownlee, D. Joswiak, J. Bradley, and F. Hörz

Origin of Orbital Debris Impacts on LDEF's Trailing Surfaces 585
Donald J. Kessler

Damage Areas on Selected LDEF Aluminium Surfaces 595
Cassandra R. Coombs, Dale R. Atkinson, Martha K. Allbrooks, Alan J. Watts, Corey J. Hennessy, and John D. Wagner

LDEF Data: Comparisons with Existing Models 619
Cassandra Coombs, Alan Watts, John Wagner, and Dale Atkinson

New Meteoroid Model Predictions for Directional Impacts on LDEF 665
Neil Divine and Rene Agüero

Long Duration Exposure Facility (LDEF) Attitude Measurements of the Interplanetary Dust Experiment 667
Philip C. Kassel, Jr., William R. Motley III, S. Fred Singer, J. Derral Mulholland, John P. Oliver, Jerry L. Weinberg, William J. Cooke, and Jim J. Wortman

Elemental Analyses of Hypervelocity Microparticle Impact Sites on Interplanetary Dust Experiment Sensor Surfaces 677
C.G. Simon, J.L. Hunter, D.P. Griffis, V. Misra, D.A. Ricks, J.J. Wortman, and D.E. Brownlee

Long-Term Microparticle Flux Variability Indicated by Comparison of Interplanetary Dust Experiment (IDE) Timed Impacts for LDEF's First Year in Orbit with Impact Data for the Entire 5.77-Year Orbital Lifetime 693
C.G. Simon, J.D. Mulholland, J.P. Oliver, W.J. Cooke, and P.C. Kassel

The Interstellar Gas Experiment: Analysis in Progress 705
F. Bühler, D.L. Lind, J. Geiss, and O. Eugster

Space Environments - Microgravity

Follow Up on the Crystal Growth Experiments of the LDEF 725
K.F. Nielsen and M.D. Lind

Author Index 733

Part 3

Space Environmental Effects - Materials

LDEF Materials Overview 741
Bland A. Stein

Oxygen Isotopes Implanted in the LDEF Spacecraft 791
J.M. Saxton, I.C. Lyon, E. Chatzitheodoridis, P. Van Lierde, J.D. Gilmour, and G. Turner

Silizane to Silica 797
Gale A. Harvey

Stability and Reactivity of Dimethylethoxysilane 811
Richard E. Johnson and Douglas I. Ford

LDEF Polymeric Materials: 10 Months Vs. 5.8 Years of Exposure 827
Philip R. Young, Wayne S. Slemp, and Alice C. Chang

Viscoelastic Characterization of Thin-Film Polymers Exposed to Low-Earth Orbit 849
Alan Letton, Allan Farrow, and Thomas Strganac

A Study of the UV and VUV Degradation of FEP 867
Graeme A. George, David J.T. Hill, James H. O'Donnell, Peter J. Pomery, and Firas A. Rasoul*

Outgassing and Dimensional Changes of Polymer Matrix Composites in Space 877
R.C. Tennyson and R. Matthews

High-Toughness Graphite/Epoxy Composite Material Experiment 889
David K. Felbeck*

LDEF Fiber-Composite Materials Characterization 905
C.J. Miglionico, C. Stein, R.E. Roybal, and L.E. Murr

Space Environmental Effects on LDEF Composites: A Leading Edge Coated Graphite Epoxy Panel 923
Pete E. George, Harry W. Dursch, and Sylvester G. Hill

The Effects of Long-Duration Space Exposure on the Mechanical Properties of Some Carbon-Reinforced Resin Matrix Composites 941
Richard F. Vyhnal

An XPS Study of Space-Exposed Polyimide Film 957
Myung Lee, William Rooney, and James Whiteside

Surface Analyses of Composites Exposed to the Space Environment on LDEF 963
Joseph J. Mallon, Joseph C. Uht, and Carol S. Hemminger

Thermal Expansion Behavior of LDEF Metal Matrix Composites 977
Tuyen D. Le and Gary L. Steckel

Spectral Infrared Hemispherical Reflectance Measurements for LDEF Tray Clamps 1001
B.K. Cromwell, Capt. S.D. Shepherd, C.W. Pender, and B.E. Wood

Surface Characterization of Selected LDEF Tray Clamps 1015
T.F. Cromer, H.L. Grammer, J.P. Wightman, P.R. Young, and W.S. Slemp

Contamination on LDEF: Sources, Distribution, and History 1023
Gary Pippin and Russ Crutcher

Contamination Measurements on Experiment M0003 1033
Eugene N. Borson and F. Barry Sinsheimer

Optical Characterization of LDEF Contaminant Film 1035
Brian K. Blakkolb, Lorraine E. Ryan, Howard S. Bowen, and Thomas J. Kosic

Evaluation of Seals, Lubricants, and Adhesives Used on LDEF 1041
Harry Dursch, Bruce Keough, and Gary Pippin

The Continuing Materials Analysis of the Thermal Control Surfaces Experiment (S0069) 1061
Donald R. Wilkes, Edgar R. Miller, James M. Zwiener, and Richard J. Mell

Thermal Control Paints on LDEF: Results of M0003 Sub-Experiment 18 1075
C.H. Jaggers, M.J. Meshishnek, and J.M. Coggi

LDEF Thermal Control Coatings Post-Flight Analysis 1093
Wayne S. Slemp and Philip R. Young

Selected Results for LDEF Thermal Control Coatings 1099
Johnny L. Golden

Fluorescence Measurements of the Thermal Control Experiments Coatings on LDEF S0069 and AO114 1111
J.M. Zwiener, R.J. Mell, P.N. Peters, J.C. Gregory, D.R. Wilkes, and E.R. Miller

Atomic Oxygen Effects on LDEF Experiment AO171 1125
Ann F. Whitaker, Rachel R. Kamenetzy, Miria M. Finckenor, and Joseph K. Norwood

Monte Carlo Modeling of Atomic Oxygen Attack of Polymers with Protective Coatings on LDEF 1137
Bruce A. Banks, Kim K. de Groh, Bruce M. Auer, Linda Gebauer, and Jonathan L. Edwards

Second LDEF Post-Retrieval Symposium Interim Results of Experiment AO034 1151
Roger C. Linton and Rachel R. Kamenetzky

The Interaction of Atomic Oxygen with Copper: An XPS, AES, XRD, Optical Transmission and Stylus Profilometer Study 1169
Ganesh N. Raikar, John C. Gregory, Ligia C. Christl, and Palmer N. Peters

LDEF Materials Data Analysis: Representative Examples 1187
Gary Pippin and Russ Crutcher

Materials and Processes Technical Information System (MAPTIS) - LDEF Materials Data Base 1201
Joan G. Funk, John W. Strickland, and John M. Davis

Data Bases for LDEF Results 1223
Gail Bohnhoff-Hlavacek

Long Duration Exposure Facility Experiment M0003 Deintegration Observation Data Base 1235
S.R. Gyetvay, J.M. Coggi, and M.J. Meshishnek

Color Photographs 1247

Author Index 1249

Part 4*

Space Environmental Effects - Systems

Overview of the Systems Special Investigation Group Investigation 1257
James B. Mason, Harry Dursch, and Joel Edelman

Post-Flight Analyses of the Crystals from the M0003-14 Quartz Crystal Microbalance Experiment 1269
W.K. Stuckey, G. Radhakrishnan, and D. Wallace

Radiation Sensitivity of Quartz Crystal Oscillators Experiment for the Long Duration Exposure Facility (LDEF)--Part II 1285
J.S. Ahearn and J.D. Venables

The Effect of the Low Earth Orbit Environment on Space Solar Cells: Results of the Advanced Photovoltaic Experiment (S0014) 1291
David J. Brinker, John R. Hickey, and David A. Scheiman

LEO Effects on Candidate Solar Cell Cover Materials 1303
Paul M. Stella

New Results from FRECOPA Analysis 1315
Christian Durin

Degradation of Electro-Optic Components Aboard LDEF 1333
M.D. Blue

* Part 4 is presented under separate cover.

LDEF Space Plasma-High Voltage Drainage Experiment Post-Flight Results 1343
J.Y. Yaung, B.K. Blakkolb, W.C. Wong, L.E. Ryan, H.J. Schurig, and W.W.L. Taylor

In Orbit Degradation of EUV Optical Components in the Wavelength Range 10-140 nm AO 138-3 1355
J.P. Delaboudinière, Ch. Carabétian, and J.F. Hochedez

Degradation of Optical Components in a Space Environment 1361
Linda L. DeHainaut, John R. Kenemuth, Cynthia E. Tidler, and David W. Seegmiller

Studies of Effects on Optical Components and Sensors: LDEF Experiments AO-147 (ERB Components) and S-0014 (APEX) 1375
John R. Hickey, David J. Brinker, and Philip Jenkins

Effects Of Long Term Space Environment Exposure on Optical Substrates and Coatings (S0050-2) 1389
Keith Havey, Arthur Mustico, and John Vallimont

LDEF Space Optics Handbook 1399
Robert J. Champetier, Dale R. Atkinson, and William T. Kemp

Ruled and Holographic Experiment (AO 138-5) 1401
Francis Bonnemason

Holographic Data Storage Crystals for the LDEF 1403
W. Russell Callen and Thomas K. Gaylord

Characterization of a Space Orbited Incoherent Fiber Optic Bundle 1413
Stephen A. DeWalt and Edward W. Taylor

Analyses of Space Environment Effects on Active Fiber Optic Links Orbited Aboard the LDEF 1425
E.W. Taylor, T.W. Monarski, J.N. Berry, A.D. Sanchez, R.J. Padden, and S.P. Chapman

Radiation and Temperature Effects on LDEF Fiber Optic Samples 1439
A.R. Johnston, R. Hartmayer, and L.A. Bergman

Long Duration Exposure Facility (LDEF) Low-Temperature Heat Pipe Experiment Package (HEPP) Flight Results 1455
Roy McIntosh, Craig McCreight, and Patrick J. Brennan

Space Environmental Effects - Biology

Final Results of Space Exposed Experiment Developed for Students 1479
Doris K. Grigsby

Continued Results of the Seeds in Space Experiment 1493
Jim A. Alston*

The Future

LDEF Archival System Plan 1499
Brenda K. Wilson

Retrievable Payload Carrier -- Next Generation Long Duration Exposure Facility: Update '92 1511
A.T. Perry, J.A. Cagle, and S.C. Newman †

Next Generation Optical Instruments and Space Experiment Based on the LDEF Thermal Control Surfaces Experiment (S0069) 1521
Donald R. Wilkes

An LDEF II Dust Instrument for Discrimination Between Orbital Debris and Natural Dust Particles in Near-Earth Space 1535
A.J. Tuzzolino, J.A. Simpson, R.B. McKibben, H.D. Voss, and H. Gursky

Future Radiation Measurements in Low Earth Orbit 1551
James H. Adams, Jr.

Color Photographs 1563

Author Index 1565

*Poster Presentation
† Oral and Poster Presentation

PART 3

SPACE ENVIRONMENTAL EFFECTS

MATERIALS

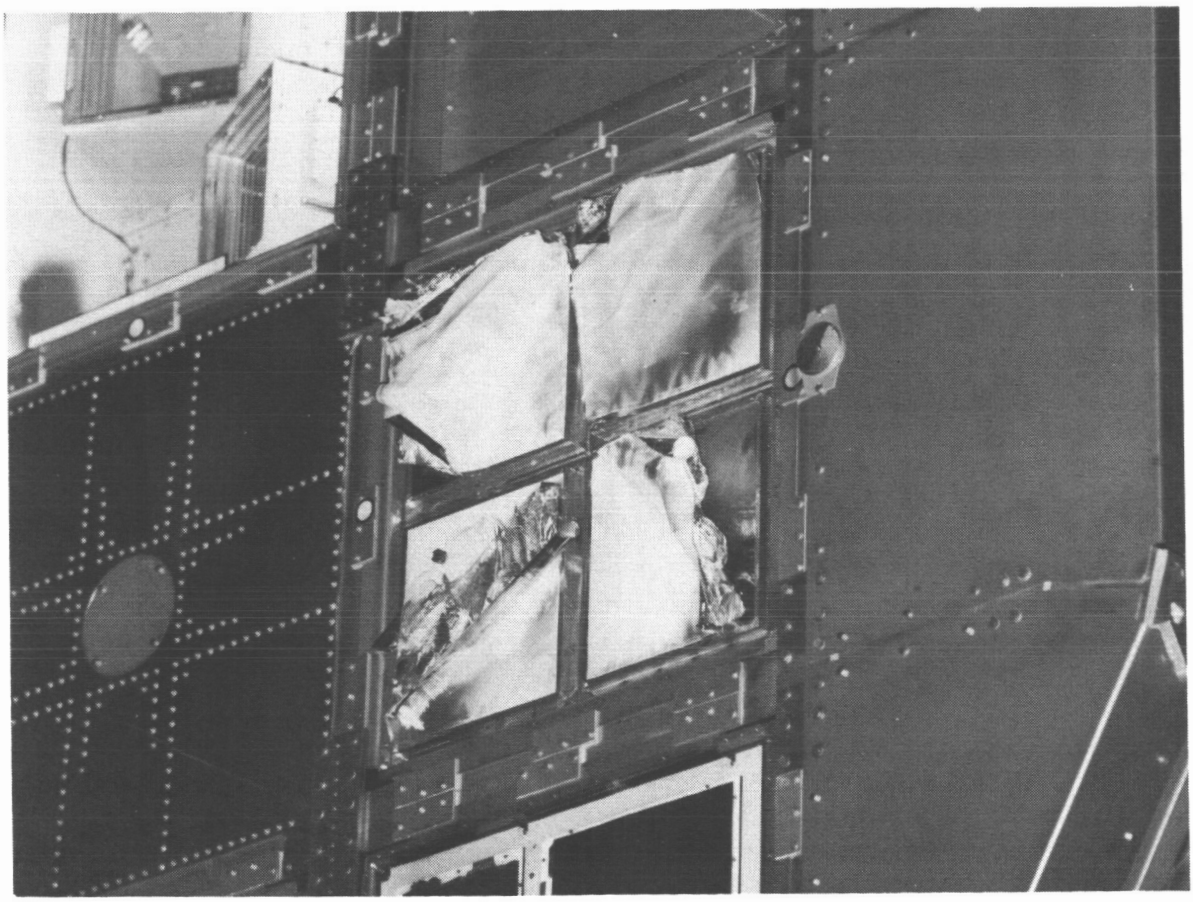

L-90-1275

PRECEDING PAGE BLANK NOT FILMED

N93-28255

LDEF MATERIALS OVERVIEW

Bland A. Stein
NASA - Langley Research Center
Hampton, VA 23665-5225
Phone: 804/864-3492, Fax: 804/864-7729

SUMMARY

The flight and retrieval of the National Aeronautics and Space Administration's Long Duration Exposure Facility (LDEF) provided an opportunity for the study of the low-Earth orbit (LEO) environment and long-duration space environmental effects (SEE) on materials that is unparalleled in the history of the U. S. Space Program. The 5-year, 9-month flight of LDEF greatly enhanced the potential value of all materials on LDEF to the international SEE community, compared to that of the original 1-year flight plan. The remarkable flight attitude stability of LDEF enables specific analyses of individual and combined effects of LEO environmental parameters on identical materials on the same space vehicle. NASA recognized this potential by forming the LDEF Space Environmental Effects on Materials Special Investigation Group (MSIG) to address the greatly expanded materials and LEO space environment analysis opportunities available in the LDEF structure, experiment trays, and corollary measurements so that the combined value of all LDEF materials data to current and future space missions will be addressed and documented.

This presentation provides an overview of the interim LDEF materials findings of the principal investigators and the Materials Special Investigation Group. These revelations are based on observations of LEO environmental effects on materials made in space during LDEF retrieval and during LDEF tray deintegration at the Kennedy Space Center, and on findings of approximately 1.5 years of laboratory analyses of LDEF materials by the LDEF materials scientists. These findings were extensively reviewed and discussed at the MSIG-sponsored LDEF Materials Workshop '91. The results are presented in a format that categorizes the revelations as "clear findings" or "obscure preliminary findings" (and progress toward their resolution), plus resultant needs for new space materials developments and ground simulation testing/analytical modeling, in seven categories: Materials/Environmental Parameters and Data Bases; LDEF Contamination; Thermal Control Coatings and Protective Treatments; Polymers and Films; Polymer-Matrix Composites; Metals, Ceramics, and Optical Materials; and Systems-Related Materials. The utilization of LDEF materials data for future low-Earth orbit missions is also discussed, concentrating on Space Station Freedom.

In general, the LDEF data is remarkably consistent; LDEF will provide a "benchmark" for materials design data bases for satellites in low-Earth orbit. Some materials were identified to be encouragingly resistant to LEO SEE for 5.8-years; other "space qualified" materials displayed significant environmental degradation. General contamination levels on LDEF were low, but molecular contamination was widespread; LDEF offers an unprecedented opportunity to provide a unified perspective of unmanned LEO spacecraft contamination mechanisms. New material development requirements for long-term LEO missions have been identified and current ground simulation testing methods/data for new, durable materials concepts can be validated with LDEF results. LDEF findings are already being integrated into the design of Space Station Freedom.

PRECEDING PAGE BLANK NOT FILMED

INTRODUCTION

The National Aeronautics and Space Administration / Strategic Defense Initiative Organization Space Environmental Effects on Materials Workshop, June 1988, identified and prioritized candidate materials spaceflight experiments needed to validate long-term performance of materials on future spacecraft (reference 1). The highest priority identified by all participants of that workshop was virtually unanimous: The return of the NASA Long Duration Exposure Facility (LDEF) safely to earth, followed by a detailed analysis of its materials to compare with data obtained in previous relatively short in-space exposures and to validate, or identify deficiencies in, ground testing and simulation facilities and materials durability analytical models. As the First LDEF Post-Retrieval Symposium proved (ref. 2), the expectations of the NASA/SDIO Workshop were well founded. The initial in-space and experiment deintegration observations of LDEF at the end of its remarkable flight provided to the LDEF investigators an unparalleled opportunity to define space environment parameters and their long-term individual and combined effects on critical properties of materials for spacecraft applications.

The National Aeronautics and Space Administration Long Duration Exposure Facility (ref. 3) was launched into low-Earth orbit (LEO) from the payload bay of the Space Shuttle Orbiter Challenger in April 1984 (figure 1). It was retrieved from orbit by the Columbia in January 1990 (fig. 2). The 57 LDEF experiments (Table 1) covered the fields of materials, coatings, and thermal systems; space science; power and propulsion; and electronics and optics. LDEF was designed to provide a large number of economical opportunities for science and technology experiments that require modest electrical power and data processing while in space and which benefit from post-flight laboratory investigations of the retrieved experiment hardware on Earth. It was also designed to maintain these experiments in a stable orbital attitude to enable determination of directional effects of the space environment parameters. Most of the materials experiments were completely passive; their data must be obtained in post-flight laboratory tests and analyses.

The 5.8-year flight of LDEF greatly enhanced the potential value of most LDEF materials, compared to that of the original 1-year flight plan. NASA recognized this potential by forming the LDEF Space Environmental Effects on Materials Special Investigation Group (MSIG) to address the expanded opportunities available in studies of the LDEF structure and experiment tray material, which were not originally considered to be materials experiments, so that the value of all LDEF materials data to current and future space missions would be assessed and documented. Similar Special Investigation Groups were formed for the disciplines of Systems, Ionizing Radiation, and Meteoroids/Debris.

This paper provides an overview of the interim LDEF materials findings of the Principal Investigators and the Materials Special Investigation Group. These revelations are based on observations of LEO environmental effects on materials made in-space during LDEF retrieval and during LDEF tray deintegration at the Kennedy Space Center, and on findings of approximately 1.5 years of laboratory analyses of LDEF materials by the LDEF materials scientists. These findings were extensively reviewed and discussed at the MSIG-sponsored LDEF Materials Workshop '91 (ref. 4). The results are presented in a format which categorizes the revelations as "clear findings" or "obscure preliminary findings" (and progress toward their resolution) in seven categories: Environmental Parameters and Data Bases; LDEF Contamination; Thermal Control Coatings and Protective Treatments; Polymers and Films; Polymer-Matrix Composites; Metals, Ceramics, and Systems-Related Materials. Resultant needs for new space materials developments and ground simulation testing/analytical modeling are enumerated. The utilization of LDEF materials data for future low-Earth orbit missions is also discussed, concentrating on Space Station Freedom. Some directions for continuing studies of LDEF materials are outlined.

THE LDEF MISSION, SCIENCE TEAM, AND MSIG

LDEF was a free-flying, 12-sided cylindrical structure, approximately 30-feet long and 14 -feet in diameter (ref. 3). It had the capability to accommodate 86 experiment trays, most of which were 50-inches long and 34-inches wide. LDEF had no central power or data systems and no capability to transmit data to Earth while in orbit. Thus, experiments which took data during the flight had power systems (batteries) and data recorders on the inside of their trays, designed for 1-year of operation. Despite the obvious constraints of such arrangements and the much longer flight than planned, these data systems worked exceedingly well in almost all cases. The in-flight data recovered from the data tapes was of high quality. The skeletal structure of LDEF weighed approximately 8000 lb; the combined structure and experiment weight launched into orbit was approximately 21,400 lb. The initial orbit was nearly circular, at 257 nautical miles, with a 32° inclination. General information concerning the flight period, experiments, and participants is shown in Table 1 and further detailed in refs. 2 and 3.

The orientation of the spacecraft with respect to the Earth during the mission is shown in figure 3. Values of key parameters of the low-Earth orbit environment which LDEF encountered are listed in Table 2. This orientation was sustained throughout the flight, from release by the Shuttle Challenger Payload Bay Remote Manipulator System to retrieval by the Columbia Remote Manipulator. Precision placement (release) into its orbit, plus a design which included gravity gradient stabilization, careful consideration of mass distribution, and a passive viscous magnetic damper system were the key factors in orienation maintenance. The remarkable flight attitude stability of LDEF (within less than 1° of movement in yaw, pitch, or roll) enables specific analyses of various individual and combined effects of LEO environmental parameters on identical materials and systems on the same space vehicle. NASA recognized this potential by forming four LDEF Special Investigation Groups (SIGs) (Table 1) to address the greatly expanded materials and LEO space environment parameter analysis opportunities available in the LDEF structure, experiment trays, and corollary measurements.

The LDEF Science Team management structure is shown in figure 4. The LDEF Science Office is located in the Materials Division of the NASA Langley Research Center; it is responsible for coordination of all LDEF experiment data, supporting data, and data generated by the SIGs.

The LDEF Environmental Effects on Materials Special Investigation Group (MSIG) was chartered to investigate the effects of the long-term LEO exposure on structure and experiment materials, which were not originally planned to be test specimens, and to integrate the results of these investigations with data generated by the Principal Investigators of the LDEF experiments into the LDEF Materials Data Base. The LDEF Materials Data Analysis Workshop (ref. 6) addressed the plans resulting from that charter. MSIG membership includes approximately 25 technical experts in the fields of atomic oxygen, radiation, contamination and other space environment effects on materials. Researchers with experimental and analytical experience in chemical, mechanical and physical properties of spacecraft materials and data basing are included. Several members provide liaison with the other LDEF Special Investigation Groups. The members represent technical laboratories and organizations throughout the United States, and laboratories in Canada and Europe. A number of MSIG members are also Principal Investigators of LDEF experiments.

Initial considerations of MSIG related to significant issues concerning space environmental effects on materials and the data potentially available from LDEF analyses to address these issues, is outlined in fig. 5. The general plan for MSIG operations is as follows:

- Systematically examine identical materials in multiple locations around LDEF to establish directionality of atomic oxygen erosion, ultraviolet radiation degradation, contamination, etc.

- Analyze selected samples from LDEF "non-materials" experiments and samples contributed from LDEF materials experiments.

- Establish central materials analysis capability:
  - Standardized, non-contaminating procedures for sampling / shipping / archiving
  - Uniform test / analysis procedures and ground simulation tests
  - Basis for assessment of laboratory-to-laboratory variations in materials data

- Focal point for coordination of all LDEF materials analyses:
  - Sponsor LDEF materials workshops / symposia
  - Generate unified LDEF Materials Data Base, including data from principal investigators, supporting data groups, and special investigation groups

The Boeing Defense and Space Group Laboratories in Seattle and Kent, Washington were selected as the MSIG Central Analysis Laboratory by the MSIG, shortly after its formation in 1989.

The LDEF Materials Workshop '91 (ref. 4) was scheduled to elucidate, compare, and assess the results of the initial 1.5 years of observations and laboratory analyses of LDEF materials by the LDEF materials scientists. Figure 6 outlines the Workshop objectives and the materials disciplines addressed. The results in each discipline were extensively discussed and reviewed by technical teams consisting of technologists from the International Space Materials Community, with various degrees of familiarity with LDEF. Their findings are detailed in ref. 4. The next section of this paper (LDEF Materials Findings) includes information generated in recent space environmental effects on materials modeling studies and data-basing activities, information presented to and generated during the workshop, plus information based on previous observations of LEO environmental effects on materials made in-space during LDEF retrieval and during LDEF tray deintegration at the Kennedy Space Center in 1990 (See, for example, ref. 2).

LDEF MATERIALS FINDINGS

In this section, 9 categories of LDEF materials results are presented in a format which classifies them as "clear findings" or "obscure preliminary findings". Many of the clear findings were made during the initial months after LDEF retrieval, as the LDEF trays were de-integrated from the structure for shipment to the laboratories of the principal investigators, but others periodically appear as the PIs and the MSIG investigators report on their continuing studies . Currently, the LDEF investigators are quantifying and modeling the clear findings and defining the phenomena involved in the obscure findings. In a previous, complementary report (ref. 5), this author has summarized these findings with examples of observations from a number of experiments and from the materials on the LDEF structure. In the present report, examples of

specific findings are illustrated with interim results of laboratory material analyses which have been in progress since June of 1990. The status of the resolution of the obscure findings is also addressed. The October 1992 Huntsville Alabama Conference on "LDEF Materials Results for Spacecraft Applications" (ref. 7) was the most recent update on LDEF Materials; ref. 8 is a general exposition of the applicability of LDEF results.

Environments and Data Bases

Table 3 is such a listing for the environments encountered by the materials on LDEF and the considerations for LDEF materials data basing. Most of the clear findings were illustrated and discussed in refs. 2, 4, and 5 and will not be repeated, or only briefly summarized here.

However, new information has emerged in some cases. Perhaps the most significant regards the general classification of the degree of LDEF contamination. LDEF had been regarded by many observers as a "dirty" spacecraft, because of the visible molecular and particulate contaminants on its external surfaces during retrieval and deintegration. That perjorative designation may have been due to the unfamiliarity of these observers with the appearance of other spacecraft after extended exposures in orbit, since very few spacecraft have been returned to earth undamaged. At the October 1992 at Huntsville Conference on "LDEF Materials Results for Spacecraft Applications", two respected authorities in spacecraft contamination expressed an opposing view. Based on their recent findings, Dr. Wayne Stuckey of the Aerospace Corporation and Dr. Alain Paillous of CERT - CNES asserted that LDEF may be one of the cleaner spacecraft flown in recent years. Dr. Stuckey illustrated that comment with fig. 7, which shows the increase in solar absorptance for fused silica mirrors as a function of time in orbit (ref. 9). Fused silica is not degraded by LEO environmental parameters; changes in absorptance are considered to be due to contamination. LDEF mirror absorptance increases were equivalent to those observed on SCATHA, which had stringent cleanliness requirements and has generally been regarded as having very low levels of contamination during its flight.

Since the publication of ref. 5, atomic oxygen fluence calculations have been further refined. Fig 8 shows the revised AO fluences for each LDEF tray on the 12 side rows, the earth-facing end, and the space-facing end. The highest AO fluence was 9.0×10^{21} atoms/cm^2 , on the LDEF leading edge, about 8.1° off row 9 (towards row 10). Experiment trays on the side rows experienced different AO fluences because of the 8° ram vector angle. The Earth and Space end AO fluences were more than one order of magnitude lower than the ram fluence. The lowest AO fluence on LDEF was 2.7×10^3 atoms/cm^2, between rows 3 and 4. During the LDEF flight, the total fluence for rows 2 through 4 was in the same order of magnitude as the lowest fluence listed in fig. 8. However, during the retrieval mission, after LDEF was safely clamped in the shuttle payload bay, an "anomaly" occurred when LDEF rows 1 through 3 (which faced out of the bay) were inadvertently subjected to atomic oxygen at the retrieval altitude for approximately 15 minutes. That inadvertent exposure raised AO fluence from values on the order of the 10^3 to 10^{17} atoms/cm^2 for the experiment trays on those rows.

It has become clear that geometric details of the exposed surfaces in conjunction with their flight attitude are keys to understanding some of the space environmental effects that occurred differently on different parts of experiment trays. Such effects as atomic oxygen atoms which do not "stick" to a surface but deflect onto another surface and react with it, and partial shadowing of atomic oxygen and solar ultraviolet radiation on exposed surfaces will affect fluences of these environmental factors. MSIG is developing analysis schemes to account for these "microenvironments". The methodology is outlined in refs. 10 and 11; initial results were

presented in those references; further results were presented by Dr. Roger Bourassa at the October 1992 at Huntsville Conference. The objective and general scope of the microenvironments modeling task for atomic oxygen is shown in fig. 9. The outline of the AO exposure models is given in fig. 10 and Fig. 11 shows the orientation of surfaces on LDEF that were studied. The following discussion (and figures 12 and 13) focus on case number 2, tray B7 FEP Teflon thermal blanket edge shown in fig. 11. Predicted FEP surface recession from the model is seen in the plot of silvered Teflon blanket thickness as a function of the distance from the blanket edge, fig. 12. Fig. 13 shows a cross-section sketch of the geometry involved and the comparison of the predicted Teflon blanket thickness changes due to AO erosion with those experimentally measured on two specimens. The microenvironments model shows very good correlation with the experimental data and holds promise as a very useful tool for quantitative predictions of environmental effects on spacecraft surfaces in LEO.

As indicated in the "LDEF Mission, Science Team, And MSIG" section of this paper, development of LDEF materials data bases is an important MSIG responsibility. The LDEF Materials Workshop '91 participants clearly indicated their expectations of two kinds of materials data bases: one for the spacecraft design community and another for the space environmental effects on materials research community (ref. 4). Potential users of these data bases have requested early release of the interim data. In order to satisfy these needs, MSIG is concentrating on two electronic data basing activities. Early data releases are being accomplished by means of the "mini-databases" described in ref. 12. Fig. 14 indicates the mini-data bases which are currently available through Dr. Gary Pippin of Boeing Defense and Space Group, P. O. Box 3999, M. S. 82-32, Seattle WA 98124. The second MSIG electronic data basing activity is underway at the NASA Marshall Spaceflight Center as the LDEF Materials Database on MAPTIS - the NASA Materials and Processes Technical Information System, as described in ref. 13. Quoting from that reference, this database is intended to encompass the "wide variety and vast quantities of materials data being generated by the MSIG members and other LDEF investigators". A preliminary version of the LDEF Materials Data Base Menu is shown in fig. 15. Completion of this database will not be accomplished for several years, but a preliminary version was released to the LDEF community in June of 1992. Continuous updating is in progress. A third LDEF materials data base has been developed for the comprehensive materials and system components on experiment M0003, located on four LDEF trays. This data base, The M0003 Deintegration Observation Record Database, is described in ref. 14, which also contains information for obtaining a copy.

In the lower part of Table 3, the obscure preliminary findings in this category are noted. Some of these findings have been resolved or at least qualitatively explained, while others remain enigmatic. Work in progress should resolve some of the remaining unexplained findings.

LDEF Contamination

Contamination control was not a priority for the LDEF mission. Preflight cleaning procedures were those utilized for any shuttle payload to maintain the cleanliness of the payload bay. As described in the previous section, observers not familiar with contamination levels on other LEO spacecraft initially believed that LDEF had high contamination levels, a belief that was recently disproved. LDEF was actually a "relatively clean" satellite in LEO, compared to other LEO spacecraft (fig. 7).

As low as contamination levels on LDEF were, the contamination was both widely dispersed for some contaminants and quite localized in others, which sometimes exhibited heavy concentrations. Detailed study of residual contaminants is straightforward via visual and spectroscopic surface examination of experiment samples, trays, and structural elements in LDEF archival storage. LDEF provides a unique opportunity to provide a unified perspective of unmanned spacecraft contamination mechanisms in low-Earth orbit. LDEF was the ultimate

witness plate for the shuttle orbiter payload bay. It was a molecular film deposition experiment. LDEF provided data for many potential studies of orbital effects on surface contaminants, both molecular and particulate. LDEF research provides data for validation of current and future contamination monitoring systems for spacecraft. However, current funding limitations severely limit the future progress of LDEF contamination research.

Table 4 is a listing of the clear findings, the obscure preliminary findings and their resolutions, new materials development requirements, and ground simulation testing requirements based on 1.5-years of LDEF contamination studies. Most of the clear findings were illustrated and discussed in ref. 5. The following will concentrate on developing an interim perspective based on these studies.

Although all materials used on the spacecraft structure and experiments were nominally "space qualified", LDEF carried a significant amount of both particulate and molecular contaminants when it was placed in orbit. Fig. 16 is a general overview of the contamination history of LDEF. Figs. 17 through 21 summarize information from a number of sources, including refs. 2 and 4 and 15 through 27. These figures were prepared by E. R. Crutcher and H. G. Pippin for the October 1992 Huntsville Conference (ref. 7). Fig. 17 defines the three categories of LDEF contamination exposures: Pre Flight, On-Orbit, and Post Flight. Fig. 18 categorizes the contamination sources into three classes: those which produce carbon based contamination films, those which produce silicon or silica based films, and those which produce particulate contamination. The widespread "nicotine stain" molecular contamination formation and degradation processes observed on many LDEF surfaces are summarized in fig. 19. On-orbit effects on the LDEF contamination are described in fig. 20. Fig. 21 summarizes these interim LDEF contamination findings.

In the center of Table 4 are listed the initial LDEF contamination findings that were not explained during the initial observations of the retrieved LDEF in 1990. As indicated in the figures and references discussed in the preceding paragraph, the sources of silicon-containing films and the mechanisms of film deposition have been identified and defined in many cases. They can be complex. The contribution of products of atomic oxygen degradation of LDEF materials to the contamination and the quantitative effects of LDEF contamination on analyses for other space environmental effects has not yet been significantly addressed in published LDEF research.

At the bottom of Table 4 are comments on new materials development requirements to avoid, in future spacecraft, the most significant contamination sources found on or in proximity to LDEF. Foremost among these include the development of non-contaminating alternates to the silicones used in spacecraft for adhesives, coatings, and flexible films. Non-contaminating lubricants and polymers are also important spacecraft materials development needs. Ground simulation testing requirements which have resulted from the initial LDEF contamination studies include the re-evaluation of current outgassing criteria and testing methods for selection and screening of materials for long-term (>10-year) missions in LEO.

Thermal Control Coatings and Protective Treatments

Table 5 outlines the interim findings of the LDEF materials studies on thermal control coatings and protective treatments. Most of the clear findings were illustrated and discussed in ref. 5, based on information presented in refs. 2 and 4 and 28 through 41. Additional studies, presented in refs. 42 through 46, have not significantly changed the "clear findings" listed in Table 5, but have quantified some of the effects, correlated LDEF data with ground tests and analyses, and put individual experiment findings into context with each other. An example of such a study is shown in figs. 22 and 23, from ref. 45. Fig. 22 shows a laser profilometer scan along the surface of a polyurethane-based thermal control coating, A276, on LDEF tray D9, where unprotected areas

were exposed to the highest atomic oxygen fluences. Such areas eroded to a depth of approximately 10μm (0.4 mils). Fig 23 shows that the solar absorptance of such LDEF leading edge specimens was unaffected, because the surface of the polyurethane binder of the A276 which was being degraded (darkened) by ultraviolet radiation was being eroded away. Fig. 23 also shows the correlation of solar absorptance with solar UV fluence for LDEF trailing edge exposures (low AO fluence) for specimens from various LDEF experiments and MSIG evaluations. The degradation in solar absorptance due to UV darkening of polyurethane is consistent. Also shown in fig. 23 is a ground test correlation line, based on an assumed equivalency of LEO solar fluence with ground test exposures using 40 kev electrons and protons and a scaling factor. This correlation is one of a number of possible ways to utilize combinations of LDEF and ground test data.

These additional studies have also concentrated on analysis of the LDEF data to define trends in coating thermal control properties which will enable prediction of stability of coatings and protective treatments for LEO exposures longer than the LDEF coatings received (such as for those to be used on Space Station Freedom). Fig. 24, from ref. 46, shows a regression analysis using a power law to predict absorptance changes in Z93 white thermal control coatings for 30-year exposures in LEO. This coating promises excellent thermal control property stability, based on the LDEF data.

The obscure findings in Table 5 include a fluorescence shift in surfaces of several LDEF coating specimens. Whereas the unexposed coatings fluoresced in the ultraviolet portion of the spectrum when subjected to UV radiation, the exposed coatings fluoresced in the visible portion of the spectrum (refs. 30 and 42). This phenomenon has been noted previously (see, for instance, ref. 41). The details of the surface chemistry changes for the LDEF specimens have not yet been defined, but studies such as those reported in ref. 42 are making good progress.

Two important coatings, S-13GLO (ref. 33) and black chromium (ref. 45) showed variabilities in their thermal control properties which have not yet been explained; studies continue. The microenvironment analysis methodology, discussed earlier in this paper, may provide avenues to the resolution of such enigmas. The synergistic roles of UV, electron and proton radiation in the atomic oxygen erosion of certain polymeric materials such as FEP Teflon have not yet been quantitatively defined.

New materials development requirements in thermal control coatings and protective treatments for long-term LEO missions are listed in Table 5. Included are thin, transparent silicate overcoats resistant to crazing and alternate sources of pure silicates for coating binders. New processes for application of adhesive-backed Ag/FEP to substrate panels are being developed which show promise of avoiding microcracking. The final item in the new materials category regards the need for a flexible white thermal control coating with demonstrated long-term LEO durability. The PCBT coating developed by the MAP Company in France has shown promise in a 9-month exposure (in a FRECOPA canister) during the LDEF missions and in another short LEO flight (ref. 34). Self explanatory ground simulation testing requirements in the coatings category are also listed in Table 5.

Polymers and Films

Table 6 outlines the interim findings of the LDEF materials studies on polymers and polymer films. Most of the clear findings were illustrated and discussed in ref. 5, based on information presented in refs. 2 and 4 and 47 through 58. Additional studies, presented in refs. 59 through 64, have not significantly changed the "clear findings" listed in table 6, but have modeled some of the effects and explained previous inconsistencies. An example of such a modeling study

is reported in ref. 61, a study of polymer "undercutting" at defects in a protective coating. The atomic oxygen erosion yield at such sites is approximately twice that of an uncoated polymer surface, because of multiple impacts of AO atoms in the undercut cavity. The Monte Carlo model assumptions and parameters were adjusted to reasonably correlate with LDEF results. However, it is interesting to note that assumptions in the model, which accurately predicted ground laboratory "asher" facility simulation test results, did not accurately predict LDEF results.

Detailed chemistry studies of the FEP surfaces of LDEF silvered Teflon blankets (ref. 64) show that atomic oxygen dominated the environmental interactions on LDEF leading edge surfaces, leaving virgin FEP on the surfaces. Beginning at row 6, the interactions transitioned to solar UV dominated interactions on LDEF trailing edge surfaces.

Ref. 59 provides an excellent explanation of a phenomenon which was previously considered to be an inconsistency in LDEF results: Molecular-level effects present in polymer specimens exposed for 10 months in canisters (which were closed during the flight) were no longer present after 5.8 years of exposure. The relative flux ratios of solar UV to atomic oxygen were quite different early in the LDEF mission than they were at the end of the mission. AO erosion at the 10-month point did not "scrub away" the surface material which was affected by UV. Near the conclusion of the mission, AO flux was so high that all UV-affected material was eroded away.

The obscure preliminary findings for polymers and polymer films (Table 6) include higher erosion for some polymeric materials on LDEF than predicted on the basis of previous short-term flight exposure data, the sources of thermal effects, and the degree of confounding of polymer surface analyses due to the molecular contamination. The high erosion rates of some polymers appear to be an example of AO/UV synergism wherein a threshold of UV exposure is reached, after an extended time in orbit, which affects the polymer surface and makes it more susceptible to reactions with atomic oxygen (ref. 5). After that time, the erosion is accelerated, as postulated in ref. 50.

The localized thermal effects noted in some LDEF external regions during the initial inspections of the retrieved spacecraft in 1990 have not yet been fully explained; the microenvironment analysis methodology, discussed earlier in this paper, will probably explain many of these effects. The effects of molecular film contamination on LDEF polymers has not yet been defined in many cases and contributes to the difficulty of analyzing for the effects of the LEO environment on a non-contaminated surface.

Near the bottom of Table 6 is a list of new polymeric material development requirements for durability in long term LEO environments and ground simulation testing requirements based on LDEF polymers and polymer film analyses thus far. No current polymeric material appears to be completely resistant to atomic oxygen and/or UV attack. If such polymers can be developed, they must have the additional attribute of non-contamination of other materials on a spacecraft due to outgassing, reaction products from AO or other LEO environmental parameter interactions, etc. Some suggested avenues for polymer synthesis are noted in the Polymers and Films section of the Panel Discussion Summary in ref. 4. Ground simulation testing requirements, listed at the bottom of Table 6, were also extensively discussed at the workshop. These discussions are also summarized in ref. 4.

Polymer-Matrix Composites

Table 7 outlines the interim findings of the LDEF materials studies on polymer-matrix composites. Most of the clear findings were illustrated and discussed in ref. 5, based on information presented in refs. 2 and 4 and 65 through 71. Additional studies, presented in refs. 72 through 78, have not significantly changed the "clear findings" listed in Table 7, but have quantified and modeled some of the effects and explained previous inconsistencies.

Atomic oxygen impinging on a bare Gr/Ep composite on the leading edge of LDEF eroded 0.0034-inch (on average) of material from the specimen surface, ref. 73. Figures 25 and 26, from ref. 74, indicate the quality of the data. The AO reactivity calculated from these erosion measurements was calculated to be $0.99 \times 10^{-24} cm^3$/atom, which correlates with other LDEF data (e.g. refs. 67 and 78) and data from other space experiments (e.g. ref. 79). Correlations such as those made for specimens of polymers, polymer-matrix composites, paints, and metals in ref. 78, and other correlations on areas of LDEF which had widely varying AO fluences, give high credibility to LDEF data and indicate that contamination is not confounding analyses of AO interactions with composites.

Outgassing of LDEF composite specimens, which had been previously shown to be the key factor in dimensional stability of graphite/epoxy composites in space (ref. 67), was modeled; these modeling studies are reported in ref. 77. The model assumptions followed the data trends well, but diffusion constants measured on earth do not result in an accurate prediction of flight data outgassing; further studies are required.

An excellent study of microcracking in LDEF graphite/epoxy composites was reported in ref. 74. A T300/934 panel was divided into areas, one of which was bare and others which had black and white coatings. The thermal histories of these areas are shown in fig. 27; the dashed curve shows that the subsurface thermal cycling temperature range was much smaller than those of the panel areas. Microcrack densities are shown in fig. 28. White coatings, which significantly reduced the thermal cycling temperature range, thus prevented significant microcracking. The bare and black coated portions of the panel had significant microcracks in the 3 outer plies on both outer (exposed to LEO environment) and inner surfaces. AO exposure eroded microcracked areas, even under coatings. Other LDEF experimenters reported composite microcracking (e.g. ref. 75) or showed data indicating that it may have been present (e.g. ref. 76).

The effects of meteoroid and debris impacts on composites were reported in refs. 73 and 74. Many impacts were studied, with the general conclusion that composite material structural integrity was not affected by any LDEF impact. Ref. 73 reported that quartz/phenolic composites exhibited less degradation due to impact and subsequent AO erosion than do Gr/Ep composites. The latter, "...because of their melt/vapor features and fiber weave can serve as an efficient absorber of impacting particle residue..." (ref. 73), compared to impacts on metals, which vaporize the particles, or on fiberglass composites, where fiber fragmentation confounds the studies. This leads to an interesting conjecture that further cross-section studies of LDEF graphite fiber reinforced polymer matrix composites could provide elemental space particles to elucidate the chemical compositions of objects both within and outside the solar system.

The obscure preliminary findings for polymer-matrix composites (Table 7) include effects of contamination on AO erosion rates, explanations for detailed differences in eroded surfaces, and mechanical property degradation differences. The effects of contamination on degradation mechanisms for certain materials and in confounding the analyses of the degradation mechanisms was discussed previously in this report. Although the qualitative understanding is slowly

appearing, quantitative information and modeling have not progressed. This is a fruitful area for further LDEF studies.

Recent studies of surprising differences in AO erosion morphologies and "ash" residues in graphite fiber reinforced composite surfaces were reported in refs. 59 and 74. "Stripes" on the composite surfaces were first illustrated (but the phenomenon was not defined) in ref. 64. Figure 29 (from ref. 74) shows that these stripes or bands are areas of differing surface heights while the schematic in fig. 30 shows that the widths of the bands definitely correspond to graphite fiber tow widths. Detailed chemical analyses reveal sodium and sulfur differences in the different bands, indicating that chemical differences in the fiber/matrix interface (and, thus, possibly, in the matrix and/or fiber tow sizing) provide the explanation for these stripes. Recent studies of the "ash" residue on AO-eroded composites are reported in refs. 59, 73, and 74. The definitive chemical analysis, reported in ref. 59, identifies the ash to be the remnant of sulfates from the DDS curing agents used in epoxy- and polysulfone-matrix composites. Differences in the appearance and quantity of the ash are related to the concentration of the DDS in the specific regions of the AO-eroded LDEF composites being studied.

The obscure preliminary finding of a lack of mechanical property degradation in uncoated LDEF composites, excepting on the leading edge specimens is probably a result of the considerably lower AO fluences on all LDEF surfaces, compared to the leading edge fluence. AO erosion on non-leading edge specimens probably affected the outer polymer layer, but did not reach into the first ply of the composite and did not disbond that ply from the matrix. Given this scenario, mechanical properties would not be affected.

Near the bottom of Table 7 are new materials development requirements for polymer-matrix composites resulting from the LDEF materials studies reported to date. The excellent protection afforded to small polymer specimens by very thin inorganic coatings (see, for example, ref. 5) requires scale-up and verification in tests of full-size parts. Flexible coatings for specialized uses such as springs which must operate in the LEO environment should be developed and verified. Given such development, there is good reason to believe that surface-protected polymer-matrix composites will perform well in structural applications for extended missions in LEO.

Ground simulation testing requirements (bottom of Table 7) for polymer-matrix composites are similar to those noted for other materials categories, including increases in size of specimen areas subjected to atomic oxygen exposures, simultaneous simulation of space environment parameters for synergistic effects, and analytical modeling of such effects. The size limitations for specimens in current facilities may be inadequate for the parts mentioned in the previous paragraph.

Metals, Ceramics, and Optical Materials

Table 8 outlines the interim findings of the LDEF materials studies on metals, ceramics, and optical materials. Most of the clear findings were illustrated and discussed in ref. 5, based on information presented in refs. 2 and 4 and 80 through 94. Additional studies, presented in refs. 62 and 96 through 99, have not significantly changed the "clear findings" listed in Table 8, but have made good contributions in quantification and modeling of some of the effects. Additional studies of LDEF clamps (refs. 96 and 97) continue to document the inherent stability of chromic acid anodized aluminum alloy in the LEO environment, noted in ref. 5. Although the effect is small, it appeared that solar UV incident flux contributed more to a slight (<1%) decrease in emittance than did atomic oxygen (ref. 96). Ref. 97 documented the stable surface chemistry of the clamps and the change in molecular contamination chemistry from organo-silicon (silicone) to inorganic silicon (silicate), due to AO interactions with the contamination film.

Details of the interactions of copper with atomic oxygen were reported in ref. 98. On a thin film sample, 55 nm of Cu was converted stoichiometrically to Cu_2O. The outer surface of that oxide on a solid copper specimen appears to have been hydrated to $Cu(OH)_2$ after the samples were returned and stored on earth. Copper grounding straps from LDEF indicated the same phenomenon. This is another indication of post-exposure effects in earth storage, which was previously noted for polymeric materials in refs. 53 and 56. The thermal control properties (absorptance and emittance) of LDEF copper grounding straps were reported in ref. 64. For LDEF leading edge exposures, large increases in absorptance correlate with atomic oxygen fluence (fig. 31). On the LDEF trailing edge, where AO fluences were low, absorptance increases were still noted and correlated with solar exposure during the early part of the LDEF LEO exposure (fig. 32). The trailing edge copper specimen increases were of lower magnitude than those in the leading edge specimens. Emittance values were not significantly affected by these environmental parameters.

A detailed study of graphite fiber reinforced metal-matrix composites, Gr/Al and Gr/Mg, flown on LDEF is reported in ref. 99. As noted previously (ref. 5) for oxidation behavior, Gr/Al was shown in ref. 99 to be more stable in thermal expansion behavior than Gr/Mg. Gr/Al showed linear, near zero hysteresis, thermal expansion behavior which stabilized with prolonged thermal cycling. Even after extensive thermal cycling, Gr/Mg showed non-linear expansion with hysteresis. Thermal bending of Gr/Mg samples was noted, due to low thermal conductivity (as compared to that of Gr/Al, where no bending was noted).

The only obscure preliminary findings for metals, ceramics, and optical materials (Table 8) related to the sources of molecular contamination. As noted previously herein, those sources have been identified to be organics and silicones, both internal and external to LDEF.

Near the bottom of Table 8 are new materials development requirements for metals, ceramics, and optical materials resulting from the LDEF materials studies reported to date. Clear, craze-resistant coatings and flexible coatings, which are stable in LEO and do not contaminate other surfaces, are of prime interest. Ground simulation testing requirements (bottom of Table 8) for metals, ceramics, and optical materials are similar to those noted previously for other materials categories.

Systems-Related Materials

This materials category covers lubricants, adhesives, seals, mechanical fasteners, solar cells, and batteries. The studies on materials aspects of systems on LDEF were conducted jointly by the LDEF Systems and LDEF Materials Special Investigation Groups; a detailed exposition of findings is presented in ref. 100. In general, LDEF systems functioned well; the system materials met their requirements.

Table 9 outlines the interim findings of studies on LDEF systems-related materials. Most of the clear findings were briefly discussed in ref. 5, based on information presented in refs. 2 and 4 and 100 through 106. A recent summary paper, ref. 107, is an excellent compilation of comments on the systems materials performance. Figs. 33 and 34 are examples of data from that reference. Fig. 33 lists the findings on lubricants flown on LDEF. The overall conclusions on lubricants are that they should be protected or shielded from direct contact with the LEO environment and that fasteners must be carefully lubricated to prevent galling during installation, if post-flight disassembly is required. Aside from galling problems which complicated fastener removal during experiment tray disassembly, fastening systems on LDEF performed satisfactorily (ref. 104). No "cold welding" was observed on LDEF systems.

Seals on LDEF (ref. 107) were predominantly in the form of O-rings, with a few cases of sheet rubber seals. The seal materials included butyl, ethylene propylene, ethylene propylene diene monomer, acrylonitrile butadiene, silicone, and Viton. All rubber seals were protected from the LEO environment and all performed well, excepting for an ethylene propylene O-ring on a LiCF battery. That O-ring failed due to a "compression set" from contact with the dimethyl sulfite electrolyte, a failure not attributed to the space exposure.

Fig. 34, from ref. 107, lists findings on LDEF epoxy adhesives. Where no information is listed for an adhesive in the comments column of fig. 34, evaluations were not performed due to a lack of resources. Most LDEF adhesives performed satisfactorily. A failure of a strain gage adhesive is noted in ref. 107. Some acrylic and RTV adhesives (ref. 108) degraded in one experiment, but silicone adhesives performed well in another (ref. 101).

Solar cells on LDEF (ref. 105), showed major performance degradation resulting only from meteoroid and debris impacts. Minor degradation was caused by contamination, UV effects on cover glass adhesives, and atomic oxygen/UV effects on antireflection coatings.

The first of the obscure preliminary findings for LDEF systems-related materials (Table 9) regards "dynamic" effects; the microenvironment analysis methodology, discussed earlier in this paper, will probably explain many of these effects. The degradation in solar cell output, was found to be a result of contamination, UV, and AO effects, as described earlier in this section.

Near the bottom of Table 9 are new materials development requirements for systems-related materials resulting from the LDEF materials studies reported to date. Non-contaminating, low outgassing lubricants and seals, which are stable when directly exposed to the LEO environment, are of prime interest. Ground simulation testing requirements (bottom of Table 9) for systems-related materials are similar to those noted previously for other materials categories.

LDEF MATERIALS CONTRIBUTIONS TO SPACE TECHNOLOGY

The promise that LDEF offered (ref. 1) for providing unparalleled data on long-term space environmental effects on materials in low-Earth orbit is being fulfilled. Ref. 5 places the LDEF materials data in context with that from previous LEO environmental effects on materials studies conducted in flight tests and ground simulation tests. The needs of Space Station Freedom designers and the applicability of the LDEF data to those needs were addressed. Ref. 5 also indicated some of the early LDEF materials findings that are already being utilized for SSF. The third of the LDEF materials forums, the October 1992 conference at Huntsville, Alabama on "LDEF Materials Results for Spacecraft Applications" was planned to provide a review and critical assessment of the relevance, significance, and impact on spacecraft design practice of the interim results of LDEF materials research. The proceedings of that conference will undoubtedly be an important addition to the libraries of spacecraft designers and materials analysts.

Ref. 5 also reviewed the general directions for continuing LDEF materials studies under MSIG. The focus of these studies gradually is changing from preliminary observations and physical analyses of LDEF materials specimens to phenomenological understanding, documentation, archiving, and data basing. LDEF specimens and hardware will be archived and will be available to researchers worldwide, into the foreseeable future, through the LDEF Science Office and NASA.

CONCLUSIONS

This paper, as a supplement to ref. 5, has presented a broad overview of interim findings of observations and analyses from ongoing studies of materials from the National Aeronautics and Space Administration Long Duration Exposure Facility, and concentrates on explaining those initial findings which were obscure in the preliminary evaluations. These interim findings on LDEF materials are summarized in Table 10. The column at the upper left lists materials which demonstrated high resistance to degradation for the entire 5.8-year flight. The column at the upper right lists materials which may be perfectly adequate for flights up to several years in LEO but which, if unprotected, will exhibit various degrees of degradation during flights as long or longer than the LDEF mission (5.8 years). As a result of these findings, new materials development requirements and general ground simulation testing requirements have been identified, as listed in the lower parts of Table 10.

In general, LDEF met or surpassed all of its goals regarding the generation of long-term low-Earth obit space environmental effects on spacecraft materials. The ongoing studies outlined herein indicate LDEF to be the definitive source of long-term exposure verification of low-Earth orbit effects on materials. The quantitative data / micro-environment / mechanistic understanding being developed will strongly contribute to future spacecraft design and new materials development guidelines. LDEF furnishes an unprecedented opportunity to provide a unified perspective of unmanned low-Earth orbit spacecraft contamination mechanisms and interactions. The LDEF materials data bases under development should become the basis of a new family of design guidelines for space environmental effects on materials.

ACKNOWLEDGMENTS

The author is pleased to express his appreciation for the efforts of the outstanding LDEF planners and scientific investigators, and particularly the members of the LDEF Materials Special Investigation Group, whose remarkably competent efforts made this review paper possible.

REFERENCES

1. Teichman, Louis A. and Stein, Bland A. (Compilers): NASA/SDIO Space Environmental Effects on Materials Workshop. NASA Conference Publication 3035, 1989.

2. Levine, Arlene S. (Editor): LDEF - 69 Months in Space: First Post-Retrieval Symposium. NASA Conference Publication 3134, 1992.

3. Clark, Lenwood G.; Kinard, William H.; Carter, David J. Jr.; and Jones, James L. Jr. (Editors): The Long Duration Exposure Facility (LDEF). NASA SP-473, 1984.

4. Stein, Bland A. and Young, Philip R. (Compilers): LDEF Materials Workshop '91. NASA Conference Publication 3162, 1992.

5. Stein, Bland A.: LDEF Materials: An Overview of the Interim Findings. In LDEF Materials Workshop '91 (Bland A. Stein and Philip R. Young, compilers). NASA Conference Publication 3162, part 1, 1992, p. 1.

6. Stein, Bland A. and Young, Philip R. (Compilers): LDEF Materials Data Analysis Workshop. NASA Conference Publication 10046, 1990.

7. LDEF Materials Results for Spacecraft Applications Conference, Huntsville, AL, October 1992.

8. Whitaker, Ann F.; Stuckey, Wayne K.; and Stein, Bland A.: What LDEF Means for Development and Testing of Materials. Presented at LDEF Materials Results for Spacecraft Applications Conference, Huntsville, AL, October 1992.

9. Stuckey, Wayne K.: An Overview of the On-Orbit Contamination of LDEF. LDEF Materials Results for Spacecraft Applications Conference, Huntsville, AL, October 1992. Quoted in LDEF Spaceflight Environmental Effects Newsletter, Vol. III, No. 6, November 15, 1992.

10. Bourassa, Roger J. and Gillis, J. R.: LDEF Atomic Oxygen Fluence Update. In LDEF Materials Workshop '91 (Bland A. Stein and Philip R. Young, compilers). NASA Conference Publication 3162, part 1, 1992, p. 59.

11. Bourassa, R. J.; Pippin, H. G.; and Gillis, J. R.: LDEF Microenvironments, Observed and Predicted. **Presented at the Second LDEF Post-Retrieval Symposium, San Diego, CA, June 1992.** NASA CP-3194, 1993.

12. Bohnhoff-Hlavacek, Gail: Databases for LDEF Results. **Presented at the Second LDEF Post-Retrieval Symposium, San Diego, CA, June 1992.** NASA CP-3194, 1993.

13. Funk, Joan G.; Strickland, John W.; and Davis, John M.: Materials and Processes Technical Information System (MAPTIS) LDEF Materials Data Base. **Presented at the Second LDEF Post-Retrieval Symposium, San Diego, CA, June 1992.** NASA CP-3194, 1993.

14. Gyetvay, S. R.; Coggi, J. M.; and Meshishnek, M. J.: Long Duration Exposure Facility Experiment M0003 Deintegration Observation Database. **Presented at the Second LDEF Post-Retrieval Symposium, San Diego, CA, June 1992.** NASA CP-3194, 1993.

15. Crutcher, E. R.; Nishimura, L. S.; Warner, K. J.; and Wascher, W. W.: Migration and Generation of Contaminants from Launch through Recovery: LDEF Case History. In LDEF-69 Months in Space, NASA Conference Publication 3134 (Arlene S. Levine, editor), Part 1, 1991, p. 121.

16. Crutcher, E. R.; Nishimura, L. S.; Warner, K. J.; and Wascher, W. W.: Quantification of Contaminants Associated with LDEF. In LDEF-69 Months in Space, NASA Conference Publication 3134 (Arlene S. Levine, editor), Part 1, 1991, p. 141.

17. Crutcher, E. R. and Warner, K. J.: Molecular Films Associated with LDEF. In LDEF-69 Months in Space, NASA Conference Publication 3134 (Arlene S. Levine, editor), Part 1, 1991, p. 155.

18. Harvey, G. A.: Organic Contamination of LDEF. In LDEF-69 Months in Space, NASA Conference Publication 3134 (Arlene S. Levine, editor), Part 1, 1991, p. 179.

19. Maag, C. R. and Linder, W. K.: Measured Space Environmental Effects to LDEF During Retrieval. In LDEF-69 Months in Space, NASA Conference Publication 3134 (Arlene S. Levine, editor), Part 1, 1991, p. 85.

20. Crutcher, Russ: Materials SIG Quantification and Characterization of Surface Contaminants. In LDEF Materials Workshop '91 (Bland A. Stein and Philip R. Young, Compilers), NASA Conference Publication 3162, Part 1, 1992, p. 95.

21. Golden, Johnny L.: Z306 Molecular Contamination Ad Hoc Committee Results. In LDEF Materials Workshop '91 (Bland A. Stein and Philip R. Young, Compilers), NASA Conference Publication 3162, Part 1, 1992, p. 115.

22. Gordon, Tim and Rantanen, Ray: Long Duration Exposure Facility (LDEF) Contamination Modeling. In LDEF Materials Workshop '91 (Bland A. Stein and Philip R. Young, Compilers), NASA Conference Publication 3162, Part 1, 1992, p. 141.

23. Hemminger, Carol S.: Surface Contamination on LDEF Exposed Materials. In LDEF Materials Workshop '91 (Bland A. Stein and Philip R. Young, Compilers), NASA Conference Publication 3162, Part 1, 1992, p. 159.

24. Harvey, Gale A.: Sources and Transport on Silicone NVR. In LDEF Materials Workshop '91 (Bland A. Stein and Philip R. Young, Compilers), NASA Conference Publication 3162, Part 1, 1992, p. 175.

25. Harvey, Gale A.: Silizane to Silica. **Presented at the Second LDEF Post-Retrieval Symposium, San Diego, CA, June 1992.** NASA CP-3194, 1993.

26. Pippin, Gary and Crutcher, Russ: Contamination on LDEF: Sources, Distribution, and History. **Presented at the Second LDEF Post-Retrieval Symposium, San Diego, CA, June 1992.** NASA CP-3194, 1993.

27. Blakkolb, Brian K. and Ryan, Lorraine E.: Optical Characterization of LDEF Contaminant Film. **Presented at the Second LDEF Post-Retrieval Symposium, San Diego, CA, June 1992.** NASA CP-3194, 1993.

28. Plagemann, W. L.: Space Environmental Effects on the Integrity of Chromic Acid Anodized Coatings. In LDEF-69 Months in Space, NASA Conference Publication 3134 (Arlene S. Levine, editor), Part 2, 1991, p. 1023.

29. Wilkes, D. R.; Brown, M. J.; Hummer, L. L.; and Zwiener, J. M.: Initial Materials Evaluation of the Thermal Control Surfaces Experiment (S0069). In LDEF-69 Months in Space, NASA Conference Publication 3134 (Arlene S. Levine, editor), Part 2, 1991, p. 899.

30. Zwiener, J. M.; Herren, K. J.; Wilkes, D. R.; Hummer, L. L.; and Miller, E. R.: Unusual Materials Effects Observed on the Thermal Control Surfaces Experiment (S0069). In LDEF-69 Months in Space, NASA Conference Publication 3134 (Arlene S. Levine, editor), Part 2, 1991, p. 919.

31. deGroh, K. K. and Banks, B. A.: Atomic Oxygen Undercutting of LDEF Aluminized-Kapton Multilayer Insulations. In LDEF-69 Months in Space, NASA Conference Publication 3134 (Arlene S.Levine, editor), Part 2, 1991, p. 781.

32. Wilkes, Donald R.; Whitaker, Ann; Zwiener, James M.; Linton, Roger C.; Shular, David; Peters, Palmer; and Gregory, John: Thermal Control Surfaces on the MSFC LDEF Experiments. In LDEF Materials Workshop '91 (Bland A. Stein and Philip R. Young, compilers). NASA Conference Publication 3162, part 1, 1992, p. 187.

33. Hurley, C. J.: Long Duration Exposure Facility Experiment M0003-5: Thermal Control Materials. In LDEF-69 Months in Space, NASA Conference Publication 3134 (A. Levine, editor), Part 2, 1991, p. 961.

34. Guillaumon, J-C.: Thermal Control Paints for Satellites. Presented at the Canadian Space Agency Space Station Program Forum: Protection of Materials and Surface Finishes from the Low Earth Orbit Space Environment, Toronto, Canada, Feb. 1992.

35. Golden, Johnny L.: Anodized Aluminum on LDEF: A Current Status of Measurements. In LDEF Materials Workshop '91 (Bland A. Stein and Philip R. Young, compilers). NASA Conference Publication 3162, part 1, 1992, p. 211.

36. Kamenetzky, Rachel R. and Whitaker, Ann F: Performance of Thermal Control Tape in the Protection of Composite Materials. In LDEF Materials Workshop '91 (Bland A. Stein and Philip R. Young, compilers). NASA Conference Publication 3162, part 1, 1992, p. 223.

37. Zwiener, James M.; Mell, Richard J.; Peters, Palmer N.; Wilkes, Donald R.; Miller, Edgar R.; and Gregory, John C.: Fluorescence of Thermal Control Coatings on S0069 and A0114. In LDEF Materials Workshop '91 (Bland A. Stein and Philip R. Young, compilers). NASA Conference Publication 3162, part 1, 1992, p. 233.

38. Hurley, Charles J. and Lehn, William L.: Long Duration Exposure Facility M0003-5 Thermal Control Coatings on DoD Flight Experiment. In LDEF Materials Workshop '91 (Bland A. Stein and Philip R. Young, compilers). NASA Conference Publication 3162, part 1, 1992, p. 245.

39. Hashimoto, Yoshihiro; Ito, Masaaki; and Ishii, Masahiro: Element Material Exposure Experiment by EFFU. In LDEF Materials Workshop '91 (Bland A. Stein and Philip R. Young, compilers). NASA Conference Publication 3162, part 1, 1992, p. 283.

40. Lehn, William L. and Hurley, Charles J.: Skylab D024 Thermal Control Coatings and Polymeric Films Experiment. In LDEF Materials Workshop '91 (Bland A. Stein and Philip R. Young, compilers). NASA Conference Publication 3162, part 1, 1992, p. 293.

41. Dyer, J. R.: Applications of Absorption Spectroscopy of Organic Compounds. Prentice-Hall, Englewood Cliffs, NJ, 1965

42. Zwiener, J. M.; Mell, R. J.; Peters, P. N.; Gregory, J. C.; Wilkes, D. R.; and Miller, E. R. : Fluorescence Measurements of the Thermal Control Coatings on LDEF Experiments S0069 and A0014. **Presented at the Second LDEF Post-Retrieval Symposium, San Diego, CA, June 1992.** NASA CP-3194, 1993.

43. Linton, Roger C.: Second LDEF Post-Retrieval Symposium Interim Results of Experiment A0034. **Presented at the Second LDEF Post-Retrieval Symposium, San Diego, CA, June 1992.** NASA CP-3194, 1993.

44. Slemp, Wayne S. and Young, Philip R.: LDEF Thermal Control Coatings Post-Flight Analysis. **Presented at the Second LDEF Post-Retrieval Symposium, San Diego, CA, June 1992.** NASA CP-3194, 1993.

45. Golden, Johnny L.: Selected Results for LDEF Thermal Control Coatings. **Presented at the Second LDEF Post-Retrieval Symposium, San Diego, CA, June 1992.** NASA CP-3194, 1993.

46. Wilkes, Donald R.; Miller, Edgar R.; Zwiener, James M.; and Mell, Richard J.: The Continuing Materials Analysis of the Thermal Control Surfaces Experiment (S0069).

Presented at the Second LDEF Post-Retrieval Symposium, San Diego, CA, June 1992. NASA CP-3194, 1993.

47. Banks, B. A.; Dever, J. A.; Gebauer, L.; and Hill, C. M.: Atomic Oxygen Interactions with FEP Teflon and Silicones on LDEF. In LDEF-69 Months in Space, NASA Conference Publication 3134 (Arlene S. Levine, editor), Part 2, 1991, p. 801.

48. Young, P. R.. and Slemp, W. S.: An Analysis of LDEF-Exposed Silvered FEP Teflon Thermal Blanket Material. NASA TM 104096, 1991.

49. Visentine, J. T.; Leger, L. J.; Kuminecz, J. F.; and Spiker, I. K.: STS-8 Atomic Oxygen Effects Experiment. AIAA Paper 85-0415, 1985.

50. Koontz, S; Leger, L.; and Albyn, K.: Vacuum Ultraviolet Radiation/Atomic Oxygen Synergism in Materials Reactivity. Journal of Spacecraft and Rockets, May-June 1990

51. Rousslang, K.: Crutcher, R.; and Pippin, G.: Results of Examination of Silvered Teflon from the Long Duration Exposure Facility. In LDEF-69 Months in Space, NASA Conference Publication 3134 (Arlene S. Levine, editor), Part 2, 1991, p. 847.

52. Brinza, David E.; Stiegman, A. E.; Staszak, Paul R.; Laue, Eric G.; and Liang, Ranty H.: Vacuum Ultraviolet (VUV) Radiation-Induced Degradation of Fluorinated Ethylene Propylene (FEP) Teflon Aboard the Long Duration Exposure Facility (LDEF). In LDEF-69 Months in Space, NASA Conference Publication 3134 (Arlene S. Levine, editor), Part 2, 1991, p. 817.

53. Young, P. R. and Slemp, W. S.: Chemical Characterization of Selected LDEF Polymeric Materials. In LDEF-69 Months in Space, NASA Conference Publication 3134 (Arlene S. Levine, editor), Part 2, 1991, p. 687.

54. Levadou, Francois and Pippin, Gary: Effects of the LDEF Environment on the Ag/FEP Thermal Blankets. In LDEF Materials Workshop '91 (Bland A. Stein and Philip R. Young, compilers). NASA Conference Publication 3162, part 1, 1992, p. 311.

55. Pippin, H. Gary: Recession of FEP Specimens from Trays D11 and B7. In LDEF Materials Workshop '91 (Bland A. Stein and Philip R. Young, compilers). NASA Conference Publication 3162, part 1, 1992, p. 345.

56. Young, P. R.. and Slemp, W. S.: Characterization of Selected LDEF-Exposed Polymer Films and Resins. In LDEF Materials Workshop '91.(Bland A. Stein and Philip R. Young, compilers). NASA Conference Publication 3162, Part 1, 1992, p.357.

57. Brower, William E., Jr.; Holla, Harish; and Bauer, Robert A.: Effect of Orbital Exposure on Halar During the LDEF Mission. In LDEF Materials Workshop '91.(Bland A. Stein and Philip R. Young, compilers). NASA Conference Publication 3162, Part 1, 1992, p.391.

58. Hurley, Charles L. and Jones, Michele: Long Duration Exposure Facility M0003-5 Results on Polymeric Films. In LDEF Materials Workshop '91.(Bland A. Stein and Philip R. Young, compilers). NASA Conference Publication 3162, Part 1, 1992, p.417.

59. Young, P. R.; Slemp, Wayne S; and Chang, Alice C.: LDEF Polymeric Materials: 10 Months vs. 5.8 Years of Exposure. **Presented at the Second LDEF Post-Retrieval Symposium, San Diego, CA, June 1992.** NASA CP-3194, 1993.

60. Lee, Myung; Rooney, William; and Whiteside, James: An XPS Study of Space-Exposed Polyimide Film. **Presented at the Second LDEF Post-Retrieval Symposium, San Diego, CA, June 1992.** NASA CP-3194, 1993.

61. Banks, Bruce A.; deGroh, Kim K.; Auer, Bruce M.; Gebauer, Linda; and Edwards, Jonathan L.: Monte Carlo Modeling of Atomic Oxygen Attack of Polymers with Protective Coatings on LDEF. **Presented at the Second LDEF Post-Retrieval Symposium, San Diego, CA, June 1992.** NASA CP-3194, 1993.

62. George, Graeme A.; Hill, David J. T.; O'Donnell, James H.; Pomery, Peter J.; and Rasoul, Firas A.: A Study of the UV and VUV Degradation of LDEF. **Presented at the Second LDEF Post-Retrieval Symposium, San Diego, CA, June 1992.** NASA CP-3194, 1993.

63. Letton, Alan; Farrow, Allan; and Stragnac, Thomas: Viscoelastic Characterization of Thin-Film Polymers Exposed to Low Earth Orbit. **Presented at the Second LDEF Post-Retrieval Symposium, San Diego, CA, June 1992.** NASA CP-3194, 1993.

64. Pippin, Gary and Crutcher, Russ: LDEF Materials Data Analysis: Representative Examples. **Presented at the Second LDEF Post-Retrieval Symposium, San Diego, CA, June 1992.** NASA CP-3194, 1993.

65. Slemp, W. S.; Young, P. R.; Witte, W. G., Jr., and Shen, J. Y.: Effects of LDEF Flight Exposure on Selected LDEF Polymer Matrix Resin Composite Materials. In LDEF-69 Months in Space, NASA Conference Publication 3134 (Arlene S. Levine, editor), Part 2, 1991, p. 1149.

66. Young, P. R.; Slemp, W. S.; Witte, W. G., Jr., and Shen, J. Y.: Characterization of Selected LDEF Polymer Matrix Resin Composite Materials. SAMPE International Symposium, 36 (1), 1991, p. 403.

67. Tennyson, R. C., Mabson, G. E., Morison, W. D., and Kleiman, J: Preliminary Results form The LDEF/UTIAS Composite Materials Experiment. In LDEF-69 Months in Space, NASA Conference Publication 3134 (Arlene S. Levine, editor), Part 2, 1991, p. 1057.

68. Steckel, Gary L.; Cookson, Thomas; and Blair, Christopher: Polymer Matrix Composites on LDEF Experiments M0003-9 and 10. In LDEF Materials Workshop '91 (Bland A. Stein and Philip R. Young, compilers). NASA Conference Publication 3162, part 2, 1992, p. 515.

69. George, Pete: Space Environmental Effects on LDEF Low Earth Orbit Exposed Graphite Reinforced Polymer Matrix Composites. In LDEF Materials Workshop '91 (Bland A. Stein and Philip R. Young, compilers). NASA Conference Publication 3162, part 2, 1992, p. 543.

70. Tennyson, R. C.: Additional Results on Space Environmental Effects on Polymer Matrix Composites - Experiment A0180. In LDEF Materials Workshop '91 (Bland A. Stein and Philip R. Young, compilers). NASA Conference Publication 3162, part 2, 1992, p. 571.

71. Tennyson, R. C.; George, P.; Steckel, G., and Zimcik, D. G.: Proposed Test Program and Data Base for LDEF Polymer Matrix Composites. In LDEF Materials Workshop '91 (Bland A. Stein and Philip R. Young, compilers). NASA Conference Publication 3162, part 2, 1992, p. 593.

72. Felbeck, David K.: High Toughness Graphite/Epoxy Composite Material Experiment. **Presented at the Second LDEF Post-Retrieval Symposium, San Diego, CA, June 1992.** NASA CP-3194, 1993.

73. Miglionico, C. J.; Stein, C.; Roybal, R. E.; and Murr, L. E.: LDEF Fiber-Composite Materials Characterization. **Presented at the Second LDEF Post-Retrieval Symposium, San Diego, CA, June 1992.** NASA CP-3194, 1993.

74. George, Pete; Dursch, Harry; and Hill, Sylvester: Space Environmental Effects on LDEF Composites. **Presented at the Second LDEF Post-Retrieval Symposium, San Diego, CA, June 1992.** NASA CP-3194, 1993.

75. Vynhal, Richard F.; Welch, Douglas W.; and Powell, Howard J.: Evaluation of Long-Duration Exposure to the Natural Space Environment on Graphite-Polyimide and Graphite-Epoxy Mechanical Properties. **Presented at the Second LDEF Post-Retrieval Symposium, San Diego, CA, June 1992.** NASA CP-3194, 1993.

76. Mallon, Joseph J.; Uht, Joseph C.; and Hemminger, Carol S.: Surface Analysis of Composites Exposed to the Space Environment on LDEF. **Presented at the Second LDEF Post-Retrieval Symposium, San Diego, CA, June 1992.** NASA CP-3194, 1993.

77. Tennyson, R. C.: Outgassing and Dimensional Changes of Polymer Matrix Composites in Space. **Presented at the Second LDEF Post-Retrieval Symposium, San Diego, CA, June 1992.** NASA CP-3194, 1993.

78. Whitaker, Ann F.; Kamenetzky, Rachel R.; Fickenor, Maria M.; and Norwood, Joseph K.: Atomic Oxygen Effects on LDEF Experiment A0171. **Presented at the Second LDEF Post-Retrieval Symposium, San Diego, CA, June 1992.** NASA CP-3194, 1993.

79. Banks, Bruce A.; Atomic Oxygen Interaction with Materials on LDEF. LDEF Materials Data Analysis Workshop (Bland A. Stein and Philip R. Young, compilers). NASA Conference Publication 10046, 1990, p. 191.

80. Stein, B. A. and Pippin, H. G.: Preliminary Findings of the LDEF Materials Special Investigation Group. In LDEF-69 Months in Space, NASA Conference Publication 3134 (Arlene S. Levine, editor), Part 2, 1991, p. 617.

81. Meshishnek, M. J.; Gyetvay, S. R.; and Jaggers, C. H.: Long Duration Exposure Facility Experiment M0003 Deintegration/Findings and Impacts. In LDEF-69 Months in Space, NASA Conference Publication 3134 (Arlene S. Levine, editor), Part 2, 1991, p. 1073.

82. Spear, W. S. and Dursch, H. W.: LDEF Mechanical Systems. In LDEF-69 Months in Space, NASA Conference Publication 3134 (Arlene S. Levine, editor), Part 3, 1991, p. 1549.

83. Miglionico, C.; Stein, C.; Roybal, R.; Robertson, R.; Murr, L. E.; Quinones, S.; Rivas, J.;Marques, B.;Advani, A. H.; Fisher, W. W., and Arrowood, R.: Effects of Space Environment on Structural Materials. In LDEF-69 Months in Space, NASA Conference Publication 3134 (A. Levine, editor), Part 2, 1991, p. 663.

84. Plagemann, W. L.: Space Environmental Effects on the Integrity of Chromic Acid Anodized Coatings. In LDEF-69 Months in Space, NASA Conference Publication 3134 (Arlene S. Levine, editor), Part 2, 1991, p. 1023.

85. Mason, J. B.; Dursch, H.; and Edelman, J: Systems Special Investigation Group Overview. In LDEF-69 Months in Space, NASA Conference Publication 3134 (Arlene S. Levine, editor), Part 3, 1991, p. 1217.

86. Assié, J-P. and Condé, E.: Microwelding (or Cold-Welding) of Various Metallic Materials Under the Ultra-Vacuum LDEF Experiment A0138-10. In LDEF-69 Months in Space, NASA Conference Publication 3134 (Arlene S. Levine, editor), Part 3, 1991, p. 1613.

87. Gregory, J. C.; Christl, L.; Raikar, G. N.; Weimer, J. J.; Wiser, R.; and Peters, P. N.: Interactions of Atomic Oxygen With Material Surfaces in Low Earth Orbit: Preliminary Results from Experiment A0114. In LDEF-69 Months in Space, NASA Conference Publication 3134 (Arlene S. Levine, editor), Part 2, 1991, p. 753.

88. Linton, R. C.; Kamenetzky, R. R.; Reynolds, J. M.; and Burris, C. L.: LDEF Experiment A0034: Atomic Oxygen Stimulated Outgassing. In LDEF-69 Months in Space, NASA Conference Publication 3134 (Arlene S. Levine, editor), Part 2, 1991, p. 763.

89. Peters, Palmer N.; Gregory, J. C.; Christi, L. C.; and Raikar, G. N.: Effects on LDEF Exposed Copper Film and Bulk. In LDEF-69 Months in Space, NASA Conference Publication 3134 (Arlene S. Levine, editor), Part 2, 1991, p. 755.

90. Tredway, W. K. and Prewo, K. M. Analysis of the Effect of Space Environmental Exposure on Carbon Fiber Reinforced Glass. United Technologies Research Center Report R91-112542-4, 1991.

91. Whitaker, Ann F.: Selected Results for Metals from LDEF Experiment A0171. In LDEF Materials Workshop '91 (Bland A. Stein and Philip R. Young, compilers). NASA Conference Publication 3162, part 2, 1992, p. 467.

92. de Rooij, A.: Some Results of the Oxidation Investigation of Copper and Silver Samples Flown on LDEF. In LDEF Materials Workshop '91 (Bland A. Stein and Philip R. Young, compilers). NASA Conference Publication 3162, part 2, 1992, p. 479.

93. Golden, Johnny L.: Changes in Oxidation State of Chromium During LDEF Exposure. In LDEF Materials Workshop '91 (Bland A. Stein and Philip R. Young, compilers). NASA Conference Publication 3162, part 2, 1992, p. 491.

94. Robertson, James B. Effect of Space Exposure on Pyroelectric Infrared Detectors. In LDEF Materials Workshop '91 (Bland A. Stein and Philip R. Young, compilers). NASA Conference Publication 3162, part 2, 1992, p. 501.

95. Bohnhoff-Hlavacek, Gail: Long Duration Exposure Facility (LDEF) Optical Systems SIG Summary and Database. In LDEF Materials Workshop '91 (Bland A. Stein and Philip R. Young, compilers). NASA Conference Publication 3162, part 2, 1992, p. 507.

96. Cromwell, B. K.; Shepherd, S. D.; Pender, C. W.; and Wood, B. E.: Spectral Infrared Hemispherical Reflectance Measurements for LDEF Tray Clamps. **Presented at the Second LDEF Post-Retrieval Symposium, San Diego, CA, June 1992.** NASA CP-3194, 1993.

97. Cromer, T. F.; Grammer, H. L.; and Wightman, J. P.: Surface Characterization of Selected LDEF Tray Clamps. **Presented at the Second LDEF Post-Retrieval Symposium, San Diego, CA, June 1992.** NASA CP-3194, 1993.

98. Raikar, Ganesh N.; Gregory, John C.; Christl, Ligia C.; and Peters, Palmer N.: The Interaction of Atomic Oxygen with Copper: An XPS, AES, XRD, Optical Transmission, and Stylus Profilometry Study. **Presented at the Second LDEF Post-Retrieval Symposium, San Diego, CA, June 1992.** NASA CP-3194, 1993.

99. Le, T. D.; and Steckel, G. L.: Thermal Expansion Behavior of LDEF Metal Matrix Composites. **Presented at the Second LDEF Post-Retrieval Symposium, San Diego, CA, June 1992.** NASA CP-3194, 1993.

100. Dursch, H. W., et. al.: Analysis of Systems Hardware Flown on LDEF - Results of the Systems Special Investigation Group. NASA CR 189628, April, 1992.

101. Whitaker, A. F. and Young, L. E.: An Overview of the First Results on the Solar Array Materials Passive LDEF Experiment (AO171). In LDEF-69 Months in Space, NASA Conference Publication 3134 (Arlene S. Levine, editor), Part 3, 1991, p. 1241.

102. Keough, Bruce: Identification and Evaluation of Lubricants, Adhesives, and Seals Used on LDEF. In LDEF Materials Workshop '91 (Bland A. Stein and Philip R. Young, compilers). NASA Conference Publication 3162, part 2, 1992, p. 603.

103. Spear, Steve; Dursch, Harry; and Johnson, Chris: Results from Testing and Analysis of LDEF Batteries. In LDEF Materials Workshop '91 (Bland A. Stein and Philip R. Young, compilers). NASA Conference Publication 3162, part 2, 1992, p. 619.

104. Spear, Steve and Dursch, Harry: Effects of Long-Term Exposure on LDEF Fastener Assemblies. In LDEF Materials Workshop '91 (Bland A. Stein and Philip R. Young, compilers). NASA Conference Publication 3162, part 2, 1992, p. 633.

105. Dursch, Harry: Results from Testing and Analysis of Solar Cells Flown on LDEF. In LDEF Materials Workshop '91 (Bland A. Stein and Philip R. Young, compilers). NASA Conference Publication 3162, part 2, 1992, p. 649.

106. Durin, Christian: Systems Related Testing and Analysis of FRECOPA. In LDEF Materials Workshop '91 (Bland A. Stein and Philip R. Young, compilers). NASA Conference Publication 3162, part 2, 1992, p. 661.

107. Dursch, Harry; Keough, Bruce; and Pippin, Gary: Evaluation of Seals, Lubricants, and adhesives used on LDEF. **Presented at the Second LDEF Post-Retrieval Symposium, San Diego, CA, June 1992.** NASA CP-3194, 1993.

108. Meshishnek, M. J.; Gyetvay, S. R.; and Jaggers, C. H.: Long Duration Exposure Facility Experiment M0003 Deintegration/Findings and Impacts. In LDEF-69 Months in Space, NASA Conference Publication 3134 (Arlene S. Levine, editor), Part 2, 1991, p. 1073.

TABLE 1

LONG DURATION EXPOSURE FACILITY

LAUNCH:

- April, 1984
  (into 255 nautical mile orbit)

RETRIEVAL:

- January, 1990
  (from 178 nautical mile orbit)

EXPERIMENTS:

- 57 Technology, Science, and Applications Experiments
- Potential for >25000 test specimens from experiment trays and structure

PARTICIPANTS:

- >200 Principal Investigators from 9 Countries
  - 33 Industry
  - 7 NASA Centers
  - 21 University
  - 4 DoD Laboratories
- 4 Special Investigation Groups, >75 Participants
  - Materials
  - Meteoroid and Debris
  - Systems
  - Ionizing Radiation

TABLE 2

LDEF EXPOSURE CONDITIONS

HIGH VACUUM:
- 10^{-6} to 10^{-7} torr

UV RADIATION:
- 100 - 400 nm; 4,500 to 15,500 equivalent sun hours

ELECTRON AND PROTON RADIATION:
- ~2.5 x 10^5 Rads surface fluence

ATOMIC OXYGEN:
- ~10^3 to 9 x 10^{21} atoms/cm^2 (wake- to ram-facing)

METEOROID AND DEBRIS IMPACTS:
- >36000 particles from ~0.1 mm to ~2 mm
- High fluence on ram-facing surfaces

COSMIC RADIATION:
- ~6 Rads
- ~20 tracks Thorium and Uranium

THERMAL CYCLING:
- ~34,000 cycles
- [±20°F] to [~ -30°F to ~+190°F]

TABLE 3

ENVIRONMENTAL PARAMETERS AND DATA BASES

Clear Findings

- All polymers on LDEF were attacked by atomic oxygen (AO).
- Metals and oxides protect against AO.
- Although widespread contamination occurred, continuing studies indicate LDEF to have low levels of general contamination, compared to other spacecraft.
- LDEF mission environments were defined:
  - Atomic oxygen
  - Total solar exposures
  - Contamination history
- "Microenvironment" analysis methodology is in development for detailed understanding of space environmental effects.
- AO fluence models must be revised to account for thermal velocity distribution.
- Impacts occur in temporal bursts.
- Data bases are required for both design and research technical communities.

Obscure Preliminary Findings	Resolution
• Sources of general "nicotine stain" contamination	• Silicones and organic materials, both internal and external to LDEF
• Contamination mechanisms	• Not yet defined in many cases
• AO degradation mechanisms	• Defined in most cases
• AO/UV synergism	• Work in progress for a number of cases

TABLE 4

LDEF CONTAMINATION

Clear Findings

- LDEF was not a "dirty spacecraft"
- Molecular contamination was widespread:
  - Multiple sources, external and internal
  - Surface temperature dependent
  - Cross-contamination from Shuttle sources
  - Environmental interactions with AO & UV
  - Leading edge deposits more transparent
- Particulate contamination was deposited pre-flight, in-flight, post-flight; can be differentiated
- LDEF provides an opportunity for a unified perspective of unmanned LEO spacecraft contamination mechanisms

Obscure Preliminary Findings	Resolution
• Sources of silicones/silicates	• Silicones internal and external to LDEF
• Deposition mechanisms	• Defined in many cases
• Contribution of AO degradation products	• Undefined in most cases
• Effects on analyses for other space environmental effects	• Undefined in most cases

New Materials Development Requirements:
- Alternate, non-silicone materials
- Non-contaminating lubricants, polymers

Ground Simulation Testing Requirements:
- Re-evaluation of current outgassing criteria/tests for long-term missions
- Combined exposure testing and analytical modeling
- System level testing and analytical modeling

TABLE 5

THERMAL CONTROL COATINGS AND PROTECTIVE TREATMENTS

Clear Findings

- Chromic Acid Anodized Aluminum is stable for long LEO exposures.
- Z-93, YB-71, PCB-Z white TC paints and D-111 black TC paint are stable.
- A276 is affected by AO and UV.
- Potassium silicate binders are stable; organic binders are not stable.
- UV accelerates AO erosion of Teflon; FEP erodes more rapidly than predicted.
- Microcracking was found in adhesively bonded Ag/FEP.
- Surface crazing was found in clear silicone coatings.
- Atomic-oxygen undercutting of polymer substrates under protective coatings was evident.

Obscure Preliminary Findings	Resolution
• Fluorescence shift from UV to VIS	• General phenomena explained; LDEF chemistry details undefined
• Variable results for black chromium	• "Microenvironment" effect ?
• Variable results for S-13GLO	• VUV plus "Microenvironment" ?
• Roles of UV, e-, p+ in AO erosion of FEP	• Not defined in most cases

New Materials Development Requirements:

- Thin silicate overcoats for AO protection
- New silicate source for Z-93
- Application process for Ag/FEP
- Durable flexible coating to replace S-13GLO

Ground Simulation Testing Requirements:

- Temperature effects on AO, UV degradation
- Single/combined effects data for analytical modeling
- In-situ measurement capabilities for AO and UV testing
- Addition of e^- and p^+ to simulation facilities
- Verified accelerated testing and analytical modeling

TABLE 6

POLYMERS AND FILMS

Clear Findings

- Ag/FEP blankets remained functional, but were eroded by atomic oxygen (AO).
- No significant changes were found in α/ε of Ag/FEP; diffuse reflectance was increased.
- Sizable delaminations of Ag from FEP were found at meteoroid/debris impacts; thermal "lag" resulted from these delaminations.
- Mechanical properties of polymers such as FEP and polyethylene were affected by UV.
- Siloxane-modified materials resist AO.
- Non-silicone polymers are attacked by AO.
- Contamination is an important effect.
- AO erosion of Kapton is linearly predictable; Kapton will be a good "witness" specimen.
- Greater erosion was found than that predicted for FEP, polystyrene, and PMMA.
- Minimal chemical change detected in bulk polymers from AO exposures.
- Extensive heating was apparent for some films on LDEF.
- Atomic oxygen attack on carbon films was observed.

Obscure Preliminary Findings	Resolution
• More erosion was found on some materials than predicted.	• UV/AO synergism effects are most likely responsible.
• Localized thermal effects were evident.	• "Microenvironment" effect ?
• Effects of contamination	• Not yet defined in many cases

New Materials Development Requirements:

- Non-contaminating materials resistant to AO attack
- Non-contaminating materials resistant to UV degradation

Ground Simulation Testing Requirements:

- High fluence AO testing (directed beam)
- High fluence UV/VUV testing
- Simultaneous AO/UV exposure testing and analytical modeling
- Verified accelerated testing and analytical modeling
- Large area exposures for mechanical testing
- Thermal cycling
- Temperature effects
- Quantitative definition of thermal "lag" at delaminations in silvered Teflon second-surface-mirror thermal blankets

TABLE 7

POLYMER-MATRIX COMPOSITES

Clear Findings

- AO causes surface degradation of uncoated composites, but no bulk polymer property changes.
- Thin inorganic coatings prevent AO erosion
- Outgassing dictates dimensional stability of Gr/Ep; other CTE changes minor
- Optical properties: No change for Gr PMC except on LDEF LE; fiberglass darkened
- Sequential effects of impact/AO erosion
- Thermal cycling causes microcracking
- No catastrophic failure from impacts

Obscure Preliminary Findings	Resolution
• Effects of contamination on AO erosion rates.	• Not yet defined in most cases.
• Differences in AO erosion morphologies; stripes on T300/934 with 5-mil tape.	• Tow material variability, particularly sodium and sulfur concentrations.
• Differences in appearance and quantity of "ash" on AO-eroded specimens.	• Sulfates from DDS curing agent.
• No AO degradation of mechanical properties except on LDEF leading edge.	• AO erosion did not reach deep into outer ply of composite.

New Materials Development Requirements:
- Scale up of coating process to full size parts
- Flexible coatings (for composite springs, etc.)

Ground Simulation Testing Requirements:
- Current capabilities adequate for individual effects
- Capacity and size for AO inadequate
- Synergistic effects (AO, UV, thermal cycling, vacuum, contamination)
- AO simulation on UV degraded LDEF specimens
- Analytical modeling of individual parameter and synergistic effects

TABLE 8

METALS, CERAMICS, AND OPTICAL MATERIALS

Clear Findings

- Structural Al and Ti alloys are unaffected.
- Many surfaces are contaminated.
- 1000Å Al coating on stainless steel is a very stable mirror/reflector.
- Thin anodized coatings on Al show small but measurable α/ε increases.
- Heavy oxidation of Ag and Cu.
- All metallic films except Sn and Pt show some oxidation.
- Al-matrix composites are not degraded; Mg-matrix composites oxidize at edges.
- Gr/glass composites are stable.
- Ceramics and glasses are generally stable unless damaged by impacts.
- Optical properties of glasses are affected in UV spectral regions only.
- Black coatings become more absorbing

Obscure Preliminary Findings	Resolution
• Sources of contamination	• Multiple sources internal and external to LDEF. Predominantly organics and silicones.

New Materials Development Requirements:

- Non-contaminating, craze-resistant clear coatings
- Non-contaminating flexible coatings

Ground Simulation Testing Requirements:

- Synergistic effects (AO, UV, thermal cycling, vacuum, contamination)
- Analytical modeling of synergistic effects

TABLE 9

SYSTEMS-RELATED MATERIALS

Clear Findings

- Lubricants--OK only when protected
- Fasteners--no cold welding failures were observed; galling was evident
- Seals--no failures (all protected)
- Adhesives--a few indications of failure
- Solar cells--degradation due to impacts
- Batteries--no space-related failures

Obscure Preliminary Findings	Resolution
• Dynamic effects	• "Microenvironment" effect ?
• Solar cells--minor degradation in output	• Possibly due to contamination plus UV and AO

New Materials Development Requirements:

- Non-contaminating dry film lubricants for exposed applications
- Non-contaminating seals for exposed applications

Ground Simulation Testing Requirements:

- Combined thermal vacuum / UV / AO / dynamic testing

TABLE 10

SUMMARY OF LDEF MATERIALS INTERIM FINDINGS

Resistant Materials	Degraded Materials
• Chromic acid anodized Al alloys	• Various thermal control coatings
• Many metals and Al-matrix composites	• Silicone conformal coatings
• Ceramics, glasses, and Gr/glass composites	• Polymers
• YB-71, Z-93, PCB-Z, D-111 paints	• Polymeric-matrix composites
• Inorganic coatings	• Silver & copper
• Some siloxane-based polymers	• Ag/FEP second surface mirrors
• Al-coated stainless steel reflectors	• Exposed lubricants

New Materials Development Requirements:

- Non-contaminating, atomic-oxygen-resistant polymers and polymer-matrix composites
- AO-durable flexible polymer for electrical insulation
- Replacement for Ag/FEP with low α_s/ε
- Flexible white paint replacement for S-13GLO
- Non-contaminating lubricants and seals for exposed applications
- Durable transparent polymer coatings
- Efficient concepts for hypervelocity impact resistance

Ground Simulation Testing Requirements:

- Synergistic effects testing and analytical modeling
- Validated accelerated tests for combined UV, AO, thermal cycling

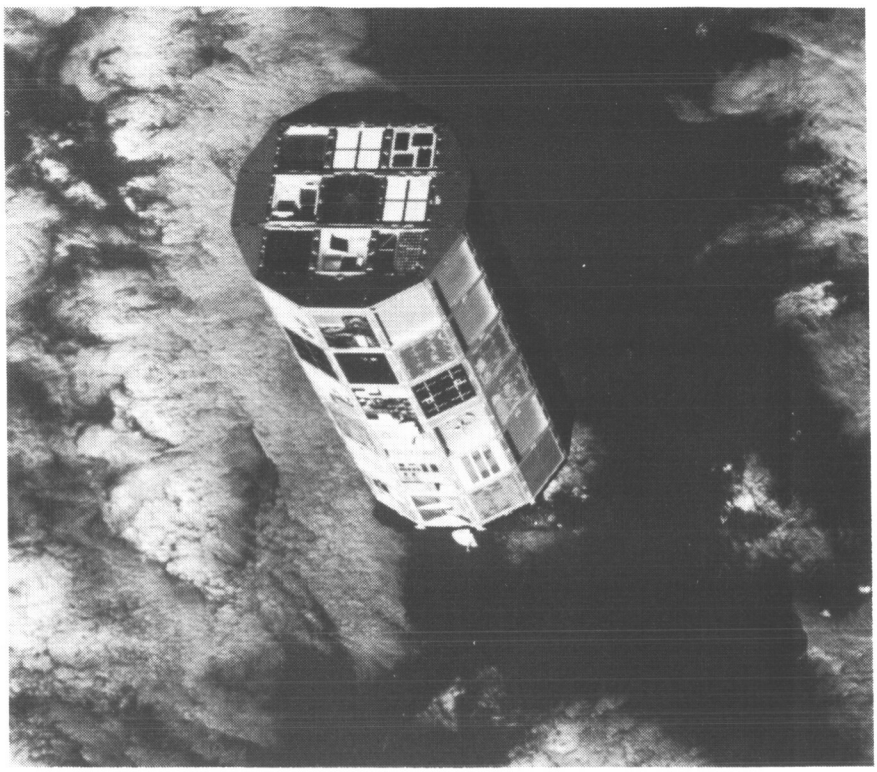

1. LDEF in orbit, April 1984.

2. LDEF retrieval after 5.8 years in low-Earth orbit, January 1990.

LDEF ORIENTATION

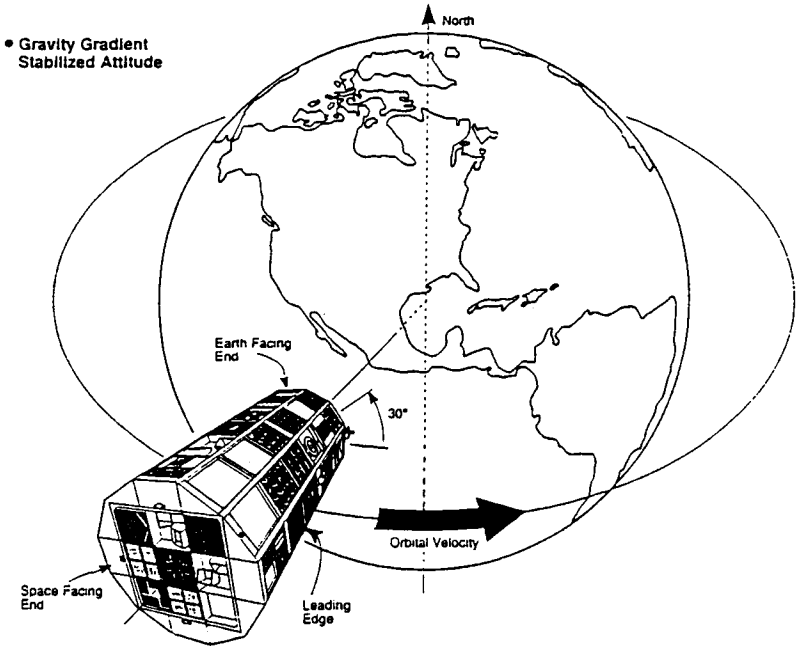

3. LDEF orientation.

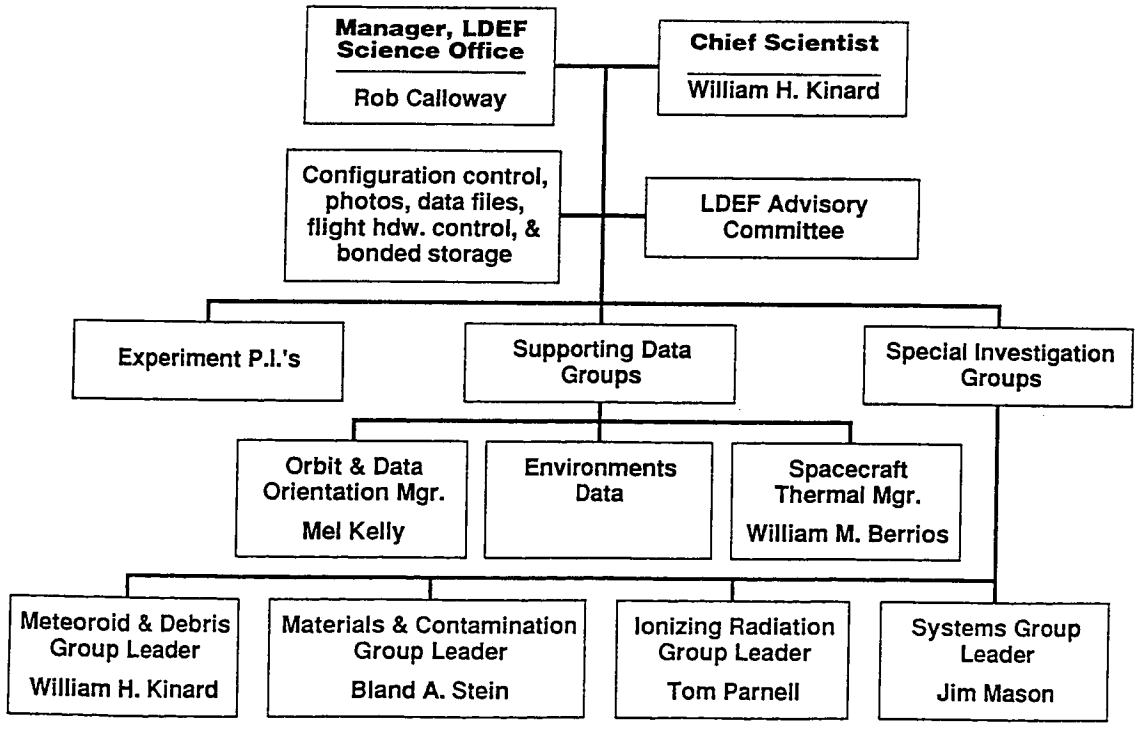

4. LDEF Science Team.

Materials Issue	Data Available from LDEF
• Stability of Material Properties - Optical - Mechanical - Thermal - Physical - Chemical	• Polymers, Metals, Composites, Ceramics, Glasses, Coatings, Films
• Combined Space Environment Effects Models	• AO, Electrons, Protons, UV, ΔT, M & D, Vacuum • Control Specimens on LDEF and in Ground Storage
• Atomic Oxygen Effects	• Erosion Rates and Mechanisms • Modifications to Fluence Models
• Meteoroid/Debris Impact Effects	• Delamination of Blankets, Composites • Crater/Impact Particle Chemistry
• Contamination	• Molecular & Particulate Levels/Chemistry

5. LDEF data available to address current issues in space environmental effects on materials.

SPONSOR: Long Duration Exposure Facility - Materials Special Investigation Group

OBJECTIVES:
- In-depth exposition of LDEF Materials Findings from Principal Investigators and MSIG
- Workshop discussions and theme reports on LDEF materials disciplines, data-basing requirements, ground simulation testing and analytical modeling needs, and future flight experiments

TUTORIAL AND WORKSHOP DISCUSSION DISCIPLINES:
- LDEF Materials, Environmental Parameters, and Data Bases
- LDEF Contamination
- Metals, Ceramics, and Optical Materials
- Lubricants, Fasteners, Adhesives, Seals, Solar Cells, and Batteries
- Thermal Control Coatings, Protective Coatings, and Surface Treatments
- Polymers and Films
- Polymer-Matrix Composites

ATTENDANCE:
- ~200 technologists from the International Space Materials Community

REPORT:
- NASA Conference Publication 3162 (1992)

6. LDEF Materials Workshop '91.

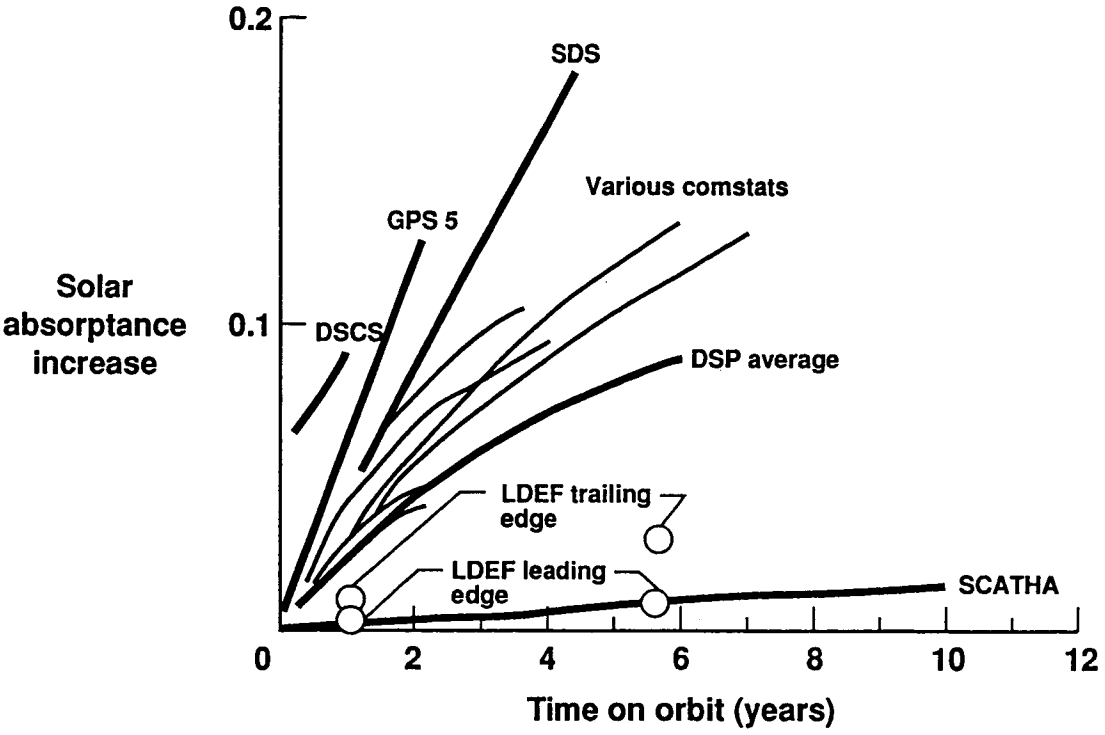

7. Fused silica mirror radiator degradation. (From ref. 9.)

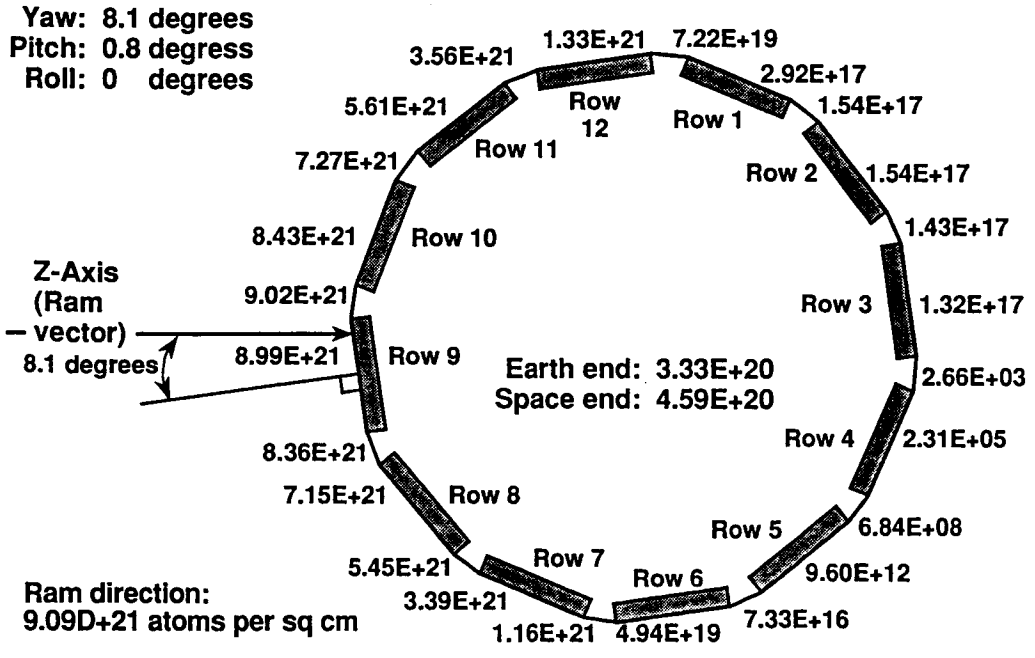

Atomic oxygen fluences at end of mission for all row, longeron, and end bay locations including the fluence received during the retrieval attitude excursion.

8. Atomic oxygen fluence for each LDEF tray location.

Objective

Over the surface of an object of arbitrary shape and placement on a spacecraft, determine atomic oxygen flux while accounting for direct exposure, shadowing, specular reflectance, and diffuse reflectance of oxygen atoms.

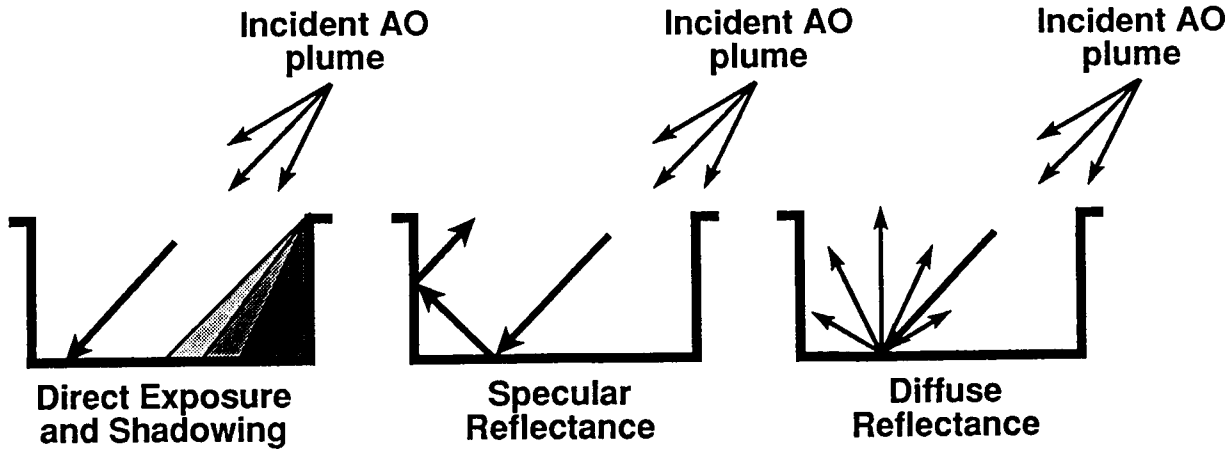

9. Atomic oxygen microenvironments model (from ref. 11).

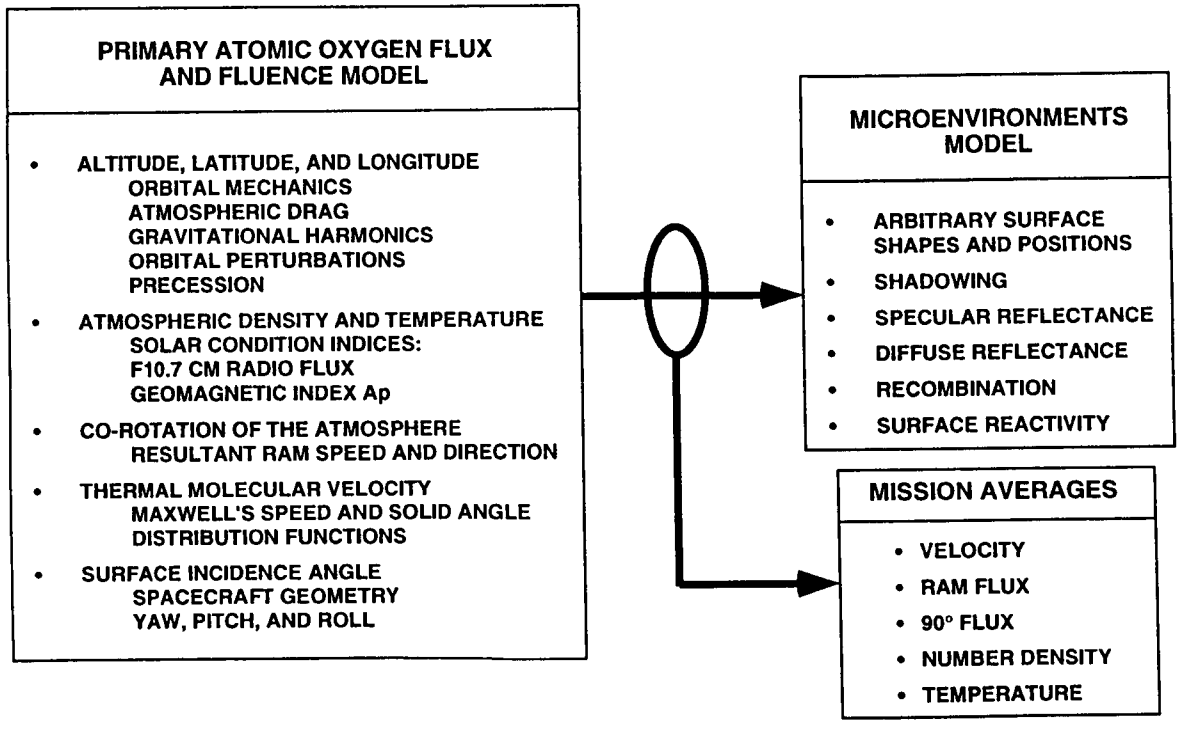

10. Atomic oxygen exposure models (from ref. 11).

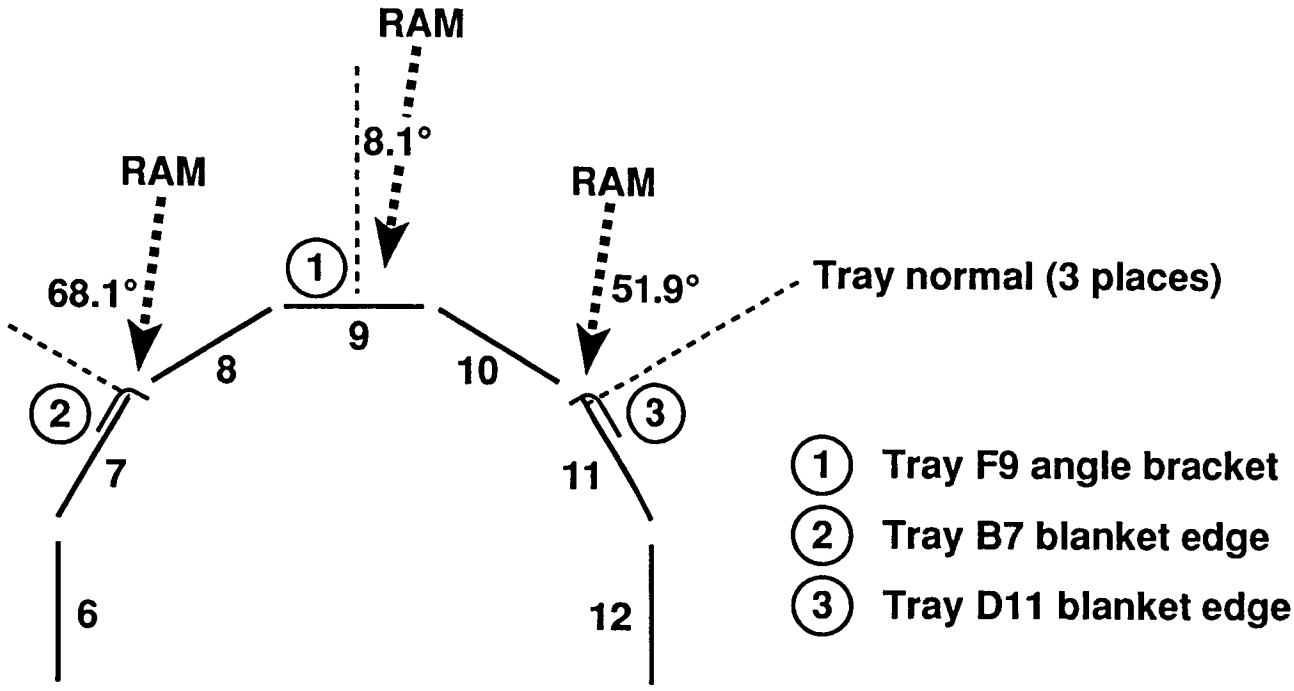

11. Orientation of specimens (from ref. 11).

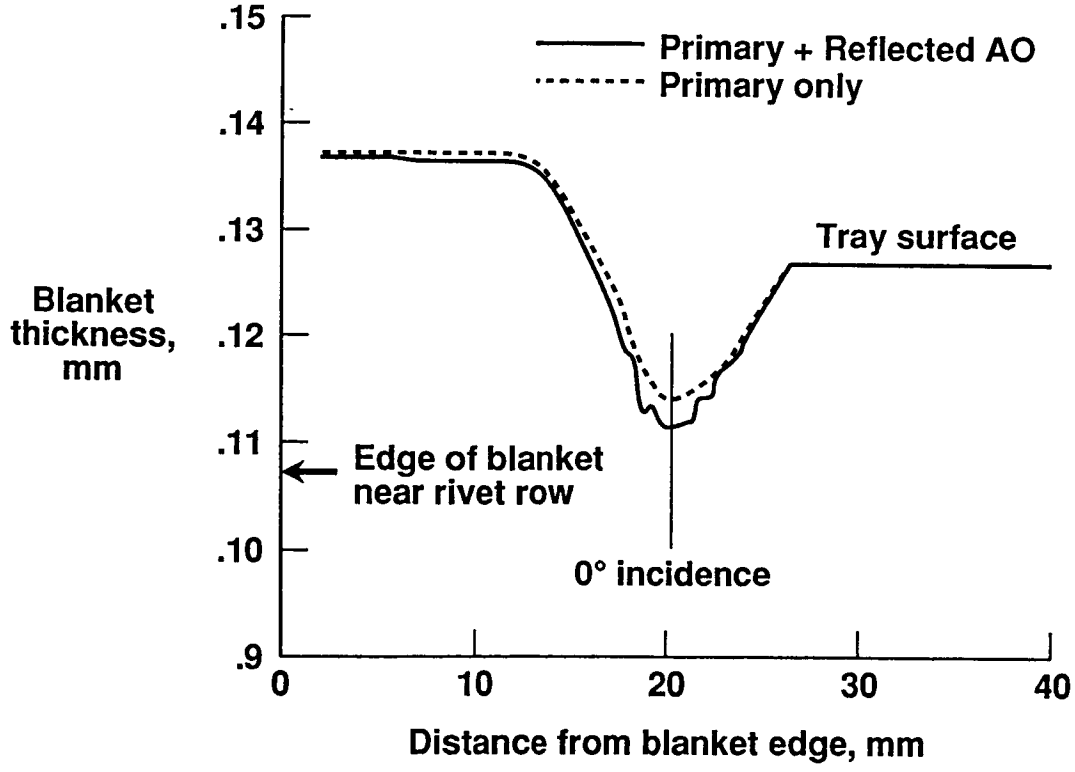

12. FEP blanket, B7 tray, 68.1° between tray normal and ram vector (from ref. 11).

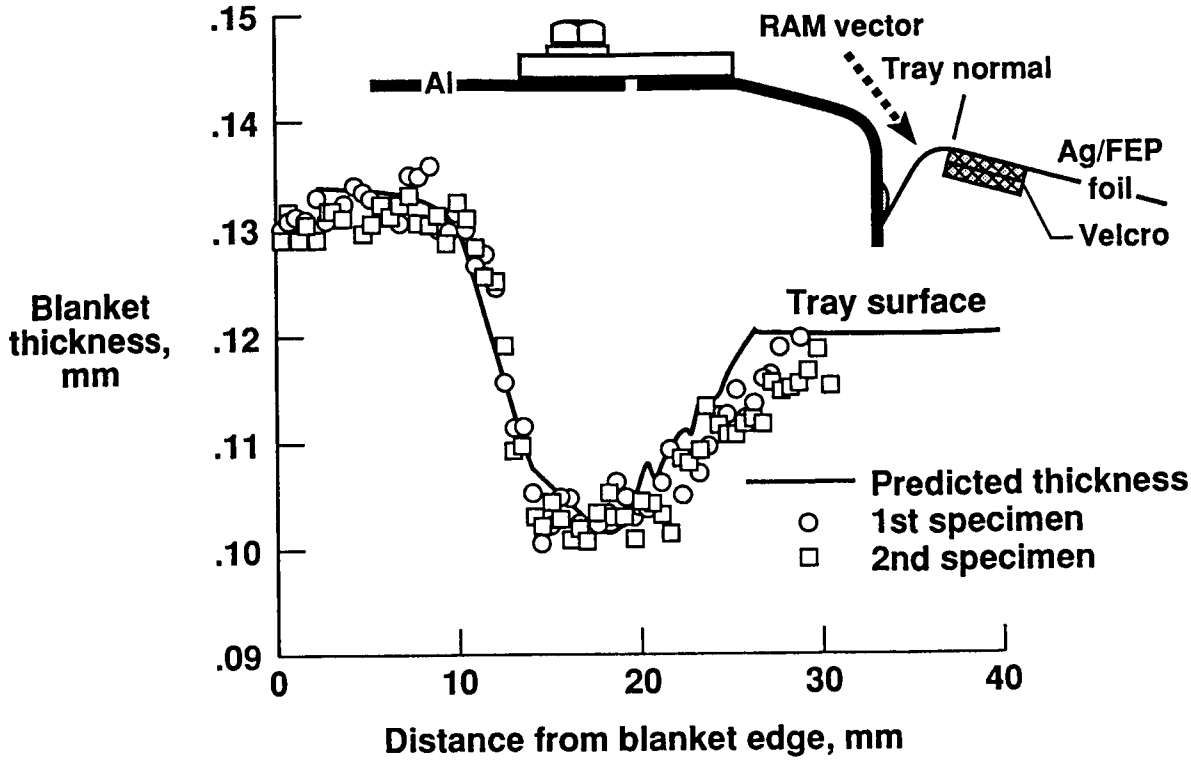

13. LDEF silvered Teflon blanket AO erosion predicted by new atomic oxygen model (from ref. 11).

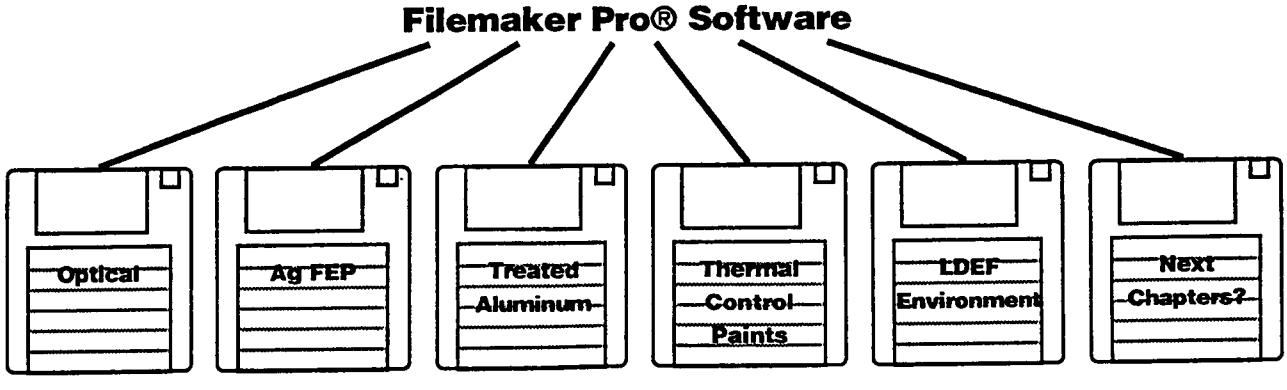

- Independent self-contained units of information
- Application specific
- Optical experiments database supported by the Systems SIG (1991); all other databases supported by the Materials SIG (1992)
- Next chapters? Composites, metals, contamination

14. Status of LDEF "Mini-data bases" (from ref. 12).

1. Basic Data

2. All Data

3. General Properties
   A. All General Properties
   B. Change in Mass
   C. Change in Thickness
   D. Optical Density
   E. Surface Roughness

4. Mechanical Properties
   A. All Mechanical Properties
   B. Elastic Properties
   C. Tensile Strength
   D. Hardness
   E. Maximum Load

5. Electrical Properties
   A. Surface Resistance

6. Optical/Thermal Properties
   A. All Optical/Thermal Properties
   B. Absorptivity
   C. Emissivity
   D. Absorptivity/Emissivity
   E. Reflectance
   F. Transmittance

7. Data Sources
   A. Primary Facility
   B Author or Secondary Facility
   C. Document Title

15. MAPTIS - LDEF materials database (from ref. 13).

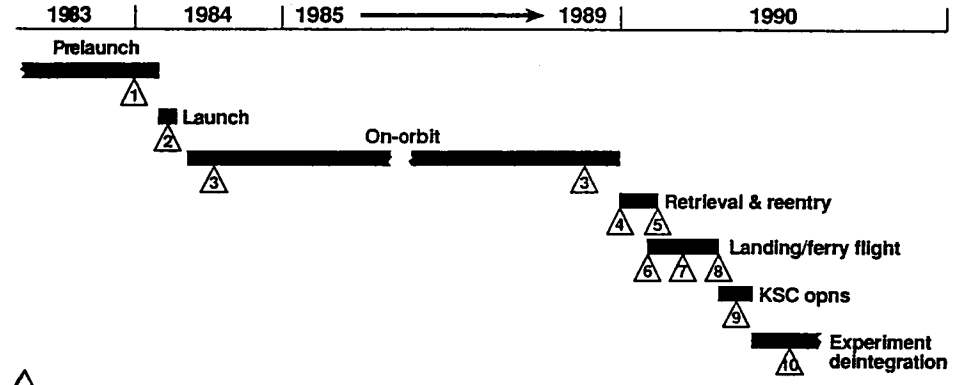

1. **Pre-launch;** Condition of LDEF prior to launch: > MIL STD 1246 level 1000 C for some trays.
2. **Launch;** During launch particulate contaminants are redistributed and Shuttle Bay Debris is added.
3. **On-orbit;** Contaminants are modified and new contaminants are generated in the orbital environment.
4. **Retrieval;** Grappling jars particles and films free, some may have relocated.
5. **Re-entry;** During reentry particles and molecular contaminants relocate or are created.
6. **Landing;** The Shuttle is exposed the Edwards Environment, accumulation of natural dusts.
7. **Ferry flight;** High humidity conditions, high velocity flow, thermal and pressure stresses occur.
8. **Ferry flight;** HEPA filter fibers appear on tape lifts after exposure to new filter.
9. **KSC Ground operations;** Ground operations prior to SAEF 2 include many manipulations of LDEF in complex environment.
10. **De-integration;** SAEF 2 exposure

16. Contamination exposure history of LDEF.

- **Pre Flight:** Ground based processing created particles and contamination films which were carried into orbit

- **On-Orbit:** Exposures and subsequent degradation. Venting and outgassing produced new particles and molecular contamination films

These events must be evaluated as to how they influence spacecraft performance

- **Post Flight:** Particulate deposition, moisture absorption

These processes must be viewed as artifacts to be factored out of materials performance analyses

17. LDEF contamination exposure categories.

Carbon based film contamination

- Paint solvents
- Polymeric thin films
- Composite materials

Silicon/silica based film contamination

- Adhesives
- Coatings on specimens
- Coatings on support hardware
- Solar cells
- Paints

Particulate contamination

- Fibers, pollen, dust
- Degraded materials

18. LDEF contamination sources.

- **Complex process - Several contributing factors. Outgassed hydrocarbons and silicones deposit on surface**
- **Degraded by solar UV; polymerized crosslinked, fixed to surface**
- **Co-deposited silicones are oxidized to silica/silicates and trap hydrocarbons, which are then darkened by UV exposure**
- **Heat from thermal cycling may accelerate degradation for part of each orbit**

19. Brown ("nicotine stain") contamination observed on external aluminum surface of LDEF.

Creation of contaminants

- Particulate contamination created as materials deteriorated or failed on leading edges
- Thin films created on many surfaces as materials out gassed

Removal of contaminants

- Thermal cycling
- Oxidation

Fix contaminants in place and change their identity

- Breaks bonds, crosslinks polymers
- Oxidizes
  - Volatile products
  - Cross-linked structure

End products indentified after flight

- Relatively few species - thermodynamically stable
  - Non volatile
  - Physically trapped

20. On-orbit effects on LDEF contamination.

- Minimal influence on thermal status of satellite
- Films interfered with LDEF surface analysis and recession rate determination
- On-orbit generation of particles may be an issue for sensitive optics
- Oxygen atoms will clean some surfaces
- Contamination extensive, but site specific
  - Heavy molecular contamination deposition is line-of-sight
- Uncertainties for outgassing of materials
  - Is rate linear or does it decay with time
  - Total amount of material outgassed
  - Details of interaction of outgassed material with environment

21. Interim LDEF contamination summary.

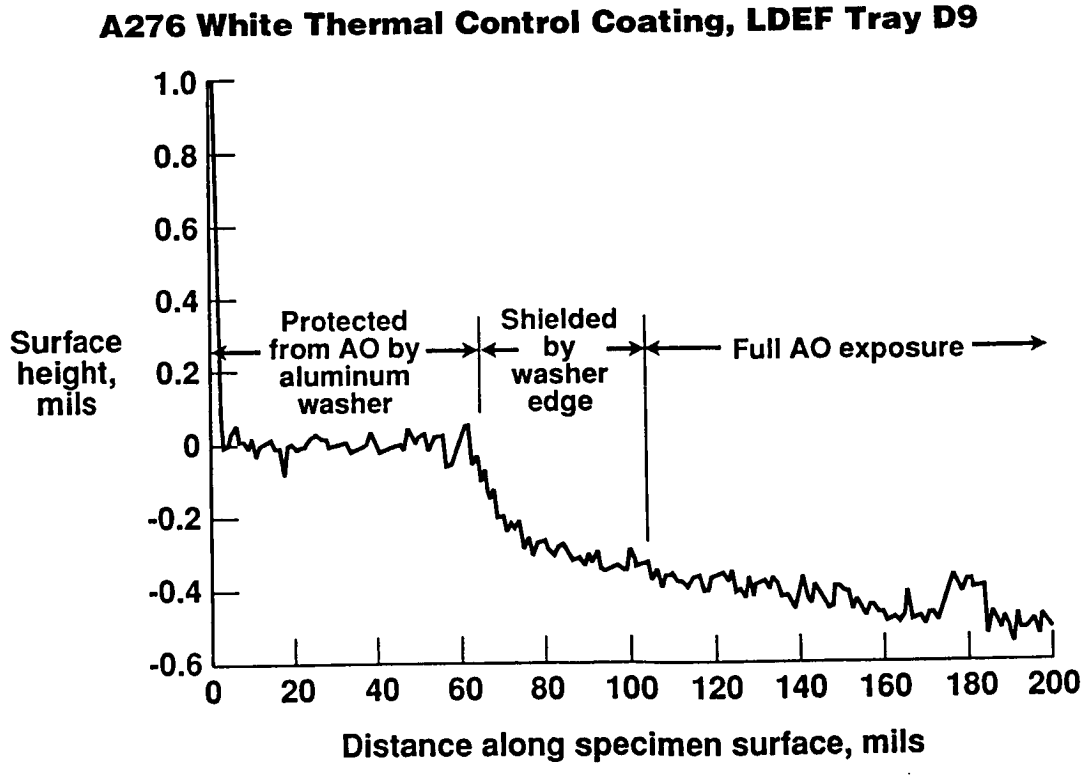

22. Laser profilometry scan for atomic oxygen erosion (from ref. 45).

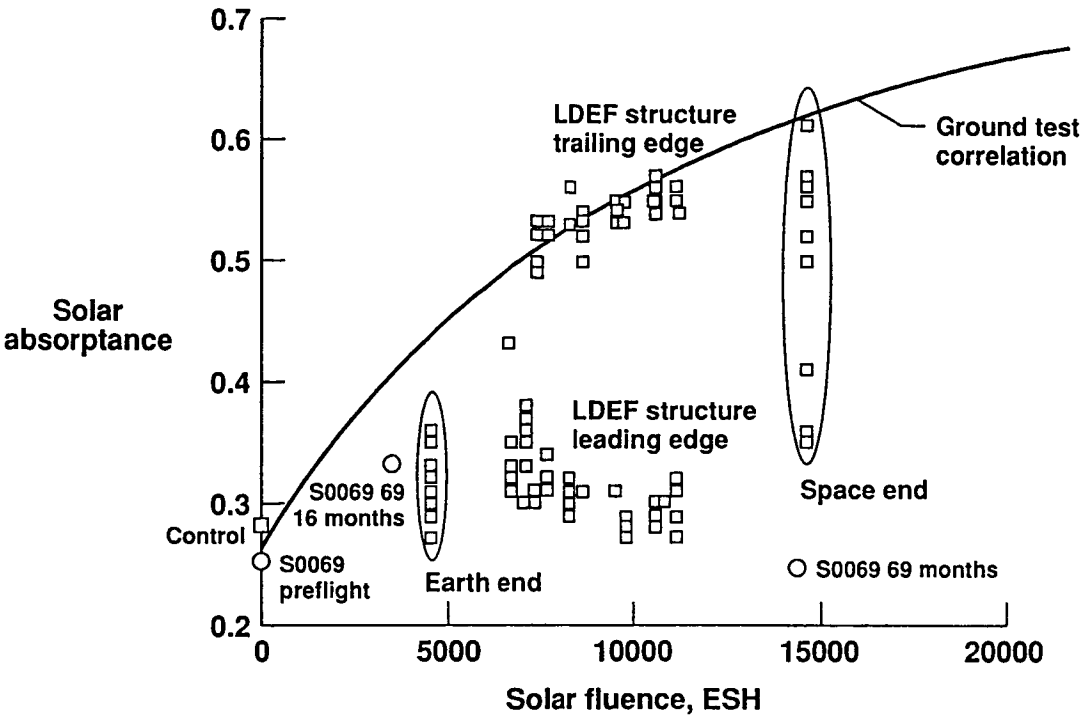

23. Solar fluence effects on solar absorptance (from ref. 45).

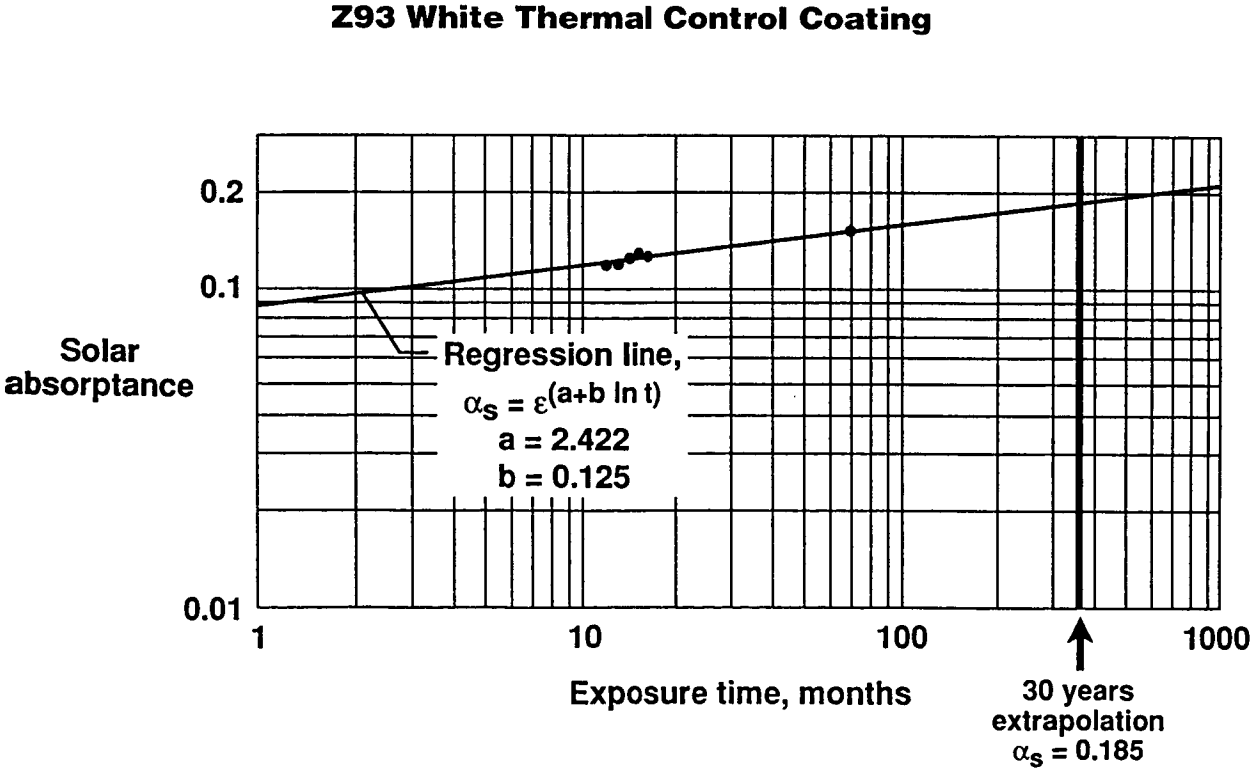

24. Solar absorptance degradation analysis (from ref. 46).

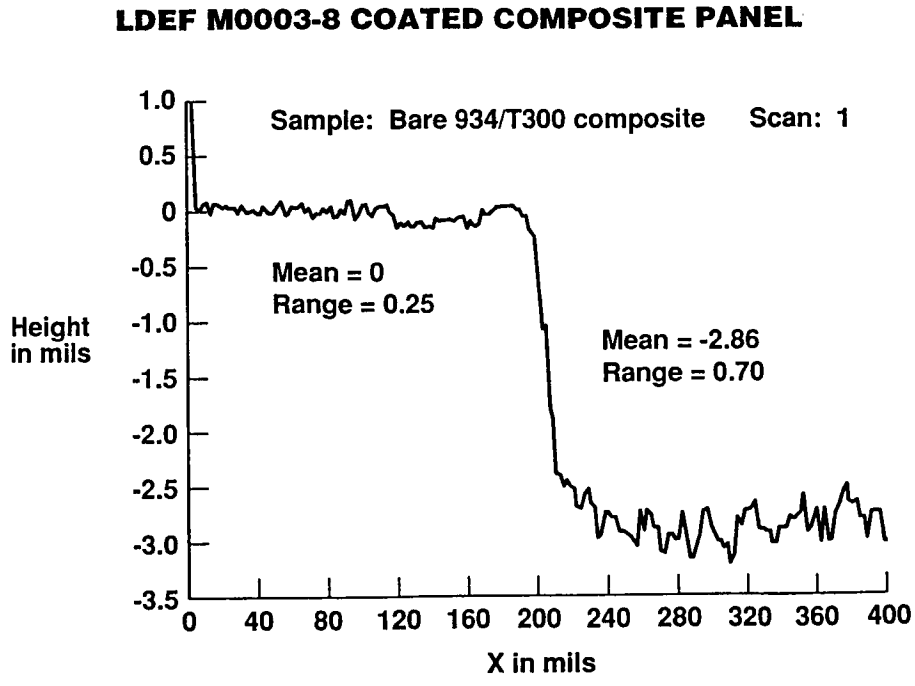

25. Laser profilometry scan of LDEF atomic oxygen erosion (from ref. 74).

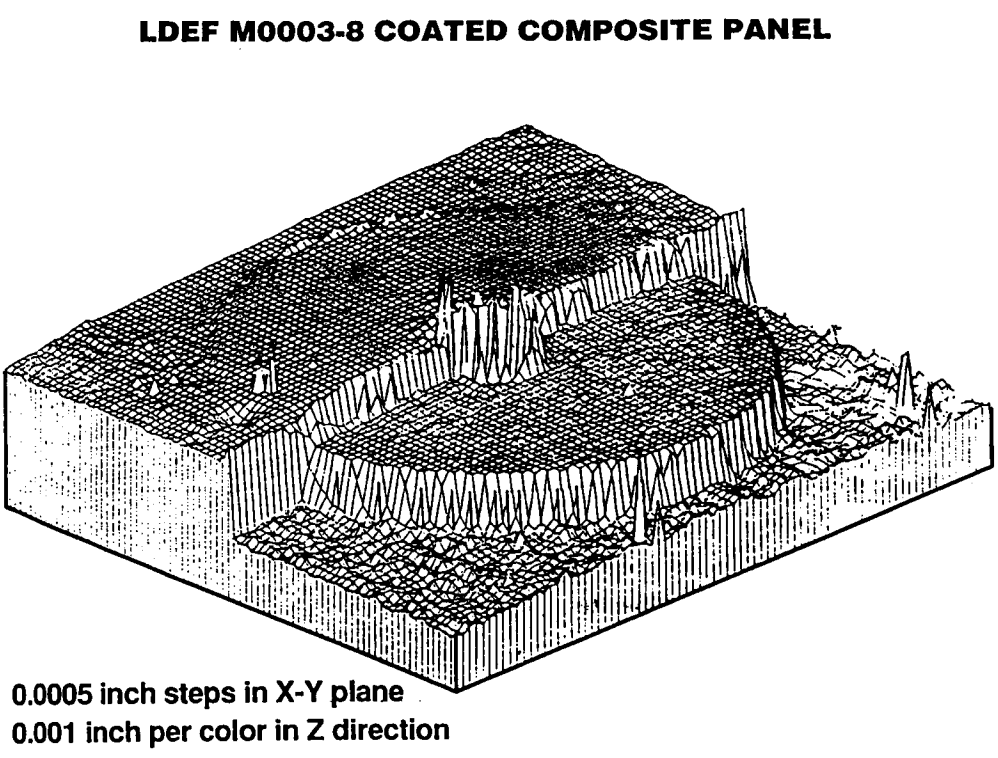

26. Laser profilometry raster scan of washer region (from ref. 74).

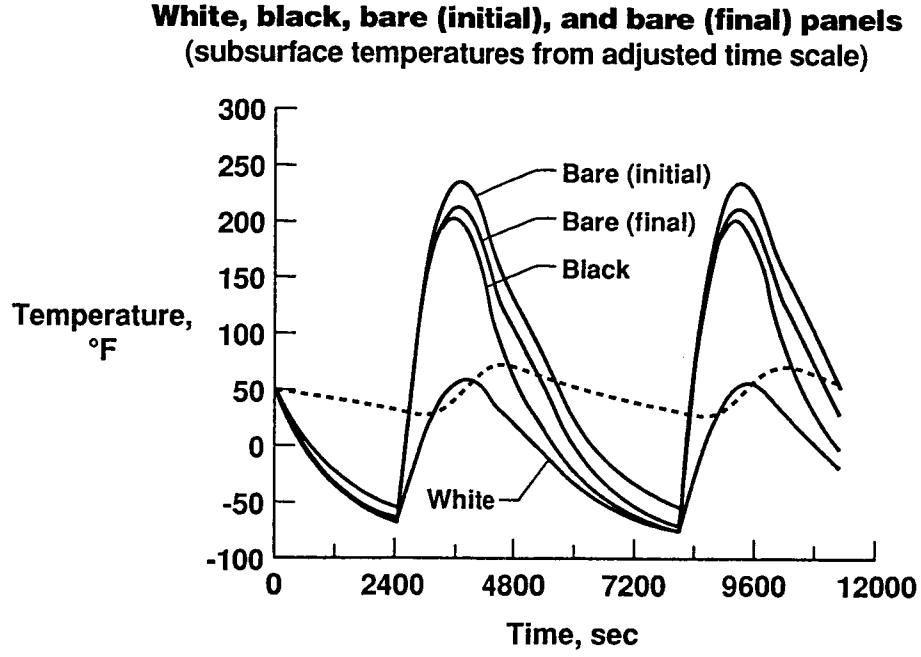

27. LDEF panel and subsurface temperatures (from ref. 74).

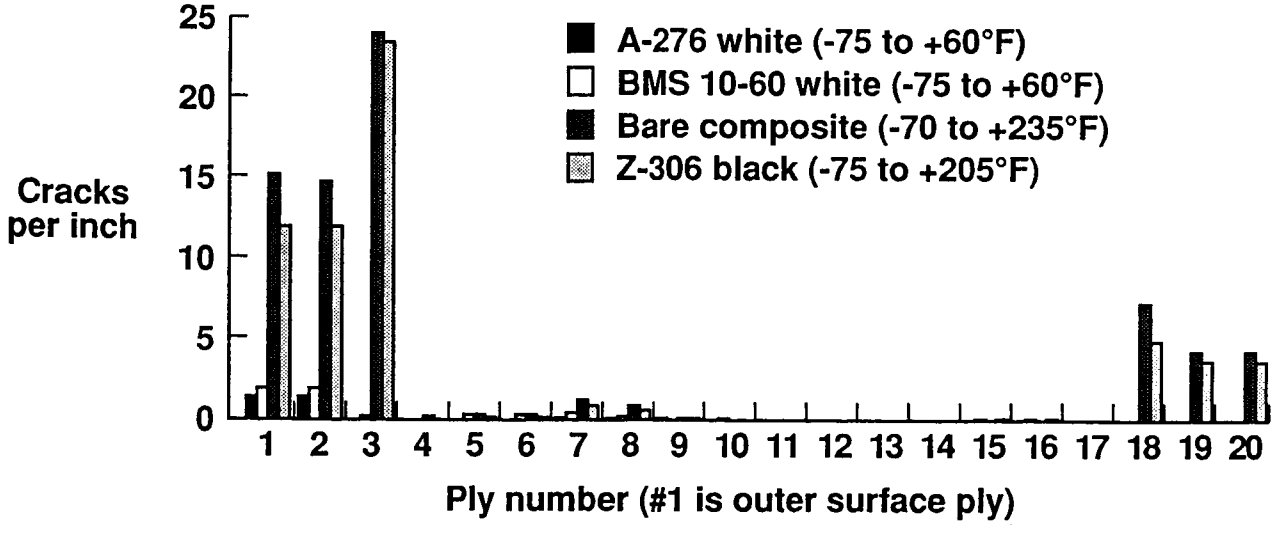

28. Microcrack density vs. location for coated and uncoated composite (from ref. 74).

LDEF M0003-8 COATED COMPOSITE PANEL

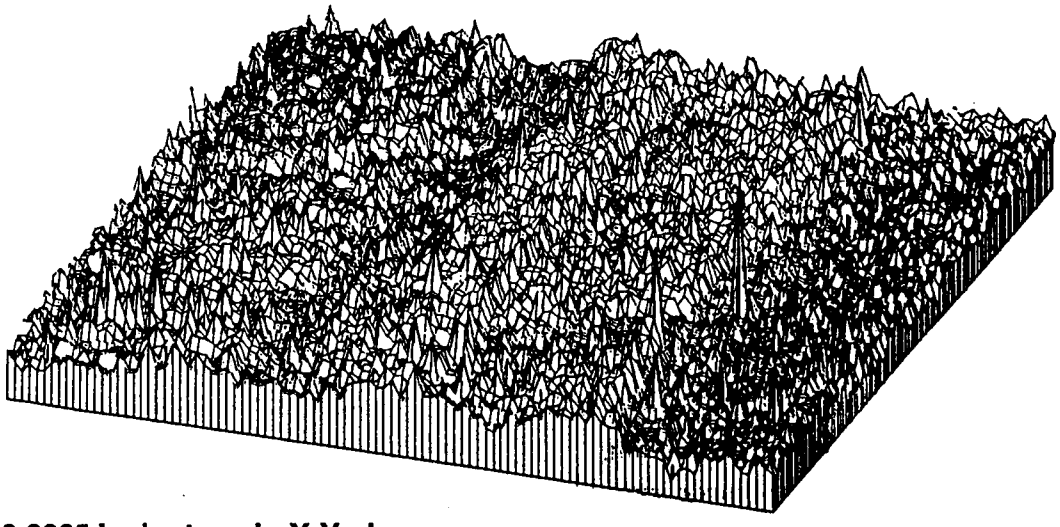

0.0005 inch steps in X-Y plane
0.00025 inch per color in Z direction

29. Laser profilometry raster scan of band pattern (from ref. 74).

LDEF M0003-8 COATED COMPOSITE PANEL

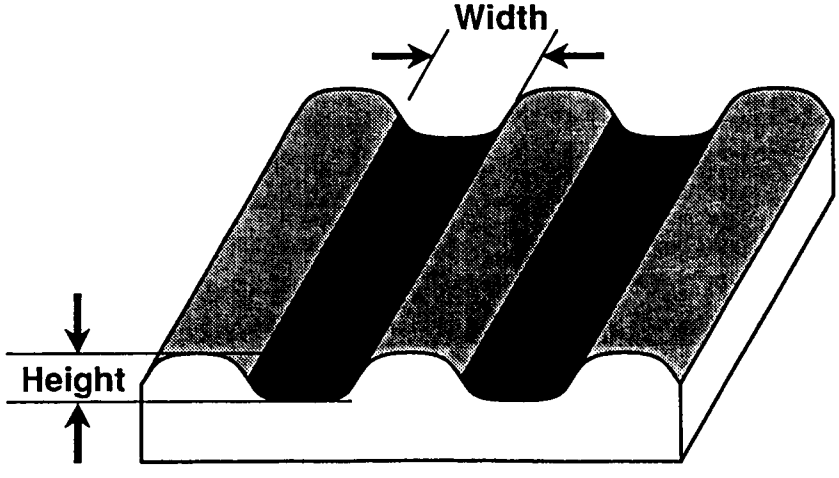

Width (10 measurements): 0.059" ± 0.003"
Compare to 0.056" tow width as prepregged

Height (from raster scan): approx. 0.0005" or 15% of erosion depth

30. Band pattern dimensions (from ref. 74).

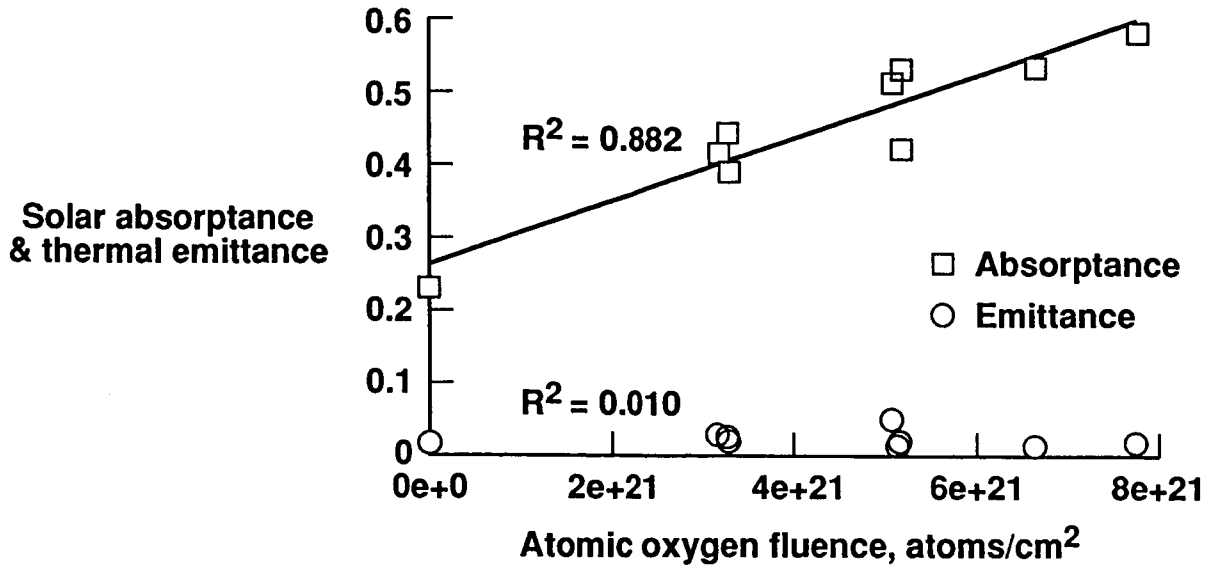

31. Thermal control properties of LDEF copper grounding straps on leading edge surfaces (from ref. 64).

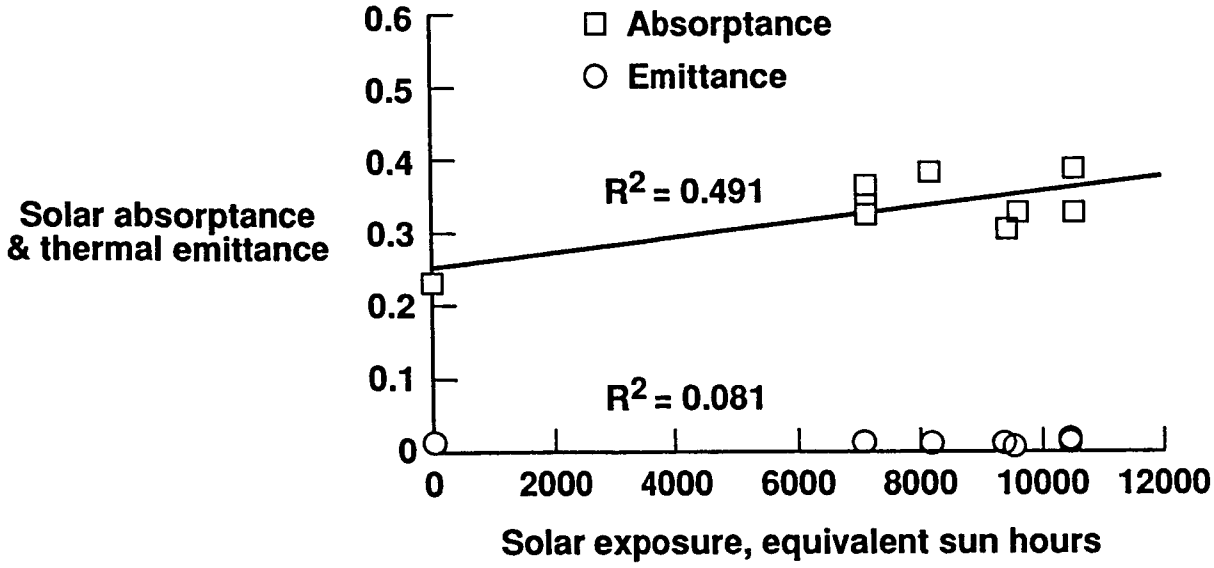

32. Thermal control properties of LDEF copper grounding straps on trailing edge surfaces (from ref. 64).

Material - Description	Location	Findings (5/92)
Cetyl alcohol	A1 & A7	Failed
MoS_2	A1 & A7	Used on nut plates, appears to be nominal
MoS_2 - air cured dry film lubricant (MIL-L-23398)	EECCs (shielded & exposed)	Nominal, further testing required
MoS_2 - chemically deposited	B3	Degraded
Molykote Z - MoS_2	B3 (shielded)	Not tested
WS_2 (tungsten disulfide)	Grapples	Bulk properties nominal, no difference between leading and trailing edge
Apiezon H - petroleum based thermal grease	F9 (shielded)	Outgassing tests nominal
Apiezon L- petroleum based lubricant	D12	Not tested
Apiezon T - petroleum based lubricant	H3 & H12 (space end)	Slight separation of oil from filler, some migration
Ball Aerospace VacKote 18.07 - MoS_2 with polyimide binder	A9 (shielded)	Not tested
Ball Brothers 44177 - hydrocarbon oil with lead naphthanate and clay thickener	EECCs (shielded)	Not tested, extensive offgassing

33a. Lubricants on LDEF (from ref. 107).

Material - Description	Location	Findings (5/92)
Castrol Braycote 601 - PTFE filled perfluoronated polyether lubricant	A3	Extensive testing, to date results show no change
Dow Corning 340 - Silicone heat sink compound	Shielded	IR spectra unchanged
Dow Corning 1102 - Mineral oil based heat sink compound	Shielded	Visual examination nominal
Dow Corning Molykote Z - MoS_2	Shielded	Not tested
DuPont Vespel 21 - Graphite filled polyimide	D3	Optical, EDX, and friction tests nominal
DuPont Vespel bushings - polyimide	Various	Nominal
E/M Lubricants Everlube 620C - MoS_2 with modified phenolic binder	D3	Complete binder failure
Exxon Andok C - petroleum grease	Shielded	System test results nominal, lubricant not evaluated
Mobil Grease 28 - Silicone grease	MTMs (shielded)	System test results nominal, lubricant not evaluated
Rod end bearings with PTFE coated Nomex liner	D3	Extensive test results nominal

33b. Lubricants on LDEF (concluded) (from ref. 107).

Vendor	Product	Experiment	Comments
Ciba-Geigy	Araldite AV 100/HV 100	A0056 A0139	
	Araldite AV 138/HV 998	A0023 A0056 A0138-1 S1002	
	Araldite AV 138/HW 2951	A0138-1	
	Araldite AW 136/HY 994	M0002	
	Araldite AW 2101/HW 2951	A0138-1	
	Araldite MY 750/HY 956	A0056	
Crest	3135/7111	A0180	1, 2, 3

Key to comments
1: Performed as expected
2: Discolored where exposed to U.V.
3: Further testing is planned./Results to be published later

34a. Epoxy adhesives on LDEF (from ref. 107).

Vendor	Product	Experiment	Comments
Emerson & Cuming	Eccobond 55	A0056 A0139 A0147 S0014	 1 1, 2
	Eccobond 55 + 10% Ecosil	S1002	
	Eccobond 56C	A0076 A0171 S0069	1 1, 3 1
	Eccobond 56C + silver powder	S1002	
Epoxy Technology	Epo-Tec 301	A0147 S0014	1 1
	Epo-Tec 331	M0004	1
Furane	Epi-Bond 104	S0014	1
Hysol	EA 934	A0180 M0024 S1001	1, 2, 3 1 1
	EA 956	A0054	1
	EA 9210/109519	M0004	1
	EA 9628	M0003	1, 3

Key to comments
1: Performed as expected
2: Discolored where exposed to U.V.
3: Further testing is planned./Results to be published later

34b. Epoxy adhesives on LDEF (continued) (from ref. 107).

Vendor	Product	Experiment	Comments
Rome & Haas	K-14	A0171	1, 3
	N-580	A0171	1, 3
Shell	Epon 828	A0056 A0180 P0003 S1001	 1, 2, 3 1 1
3M	AF-143	M0003	1
	EC 2216	A0076 A0138-1 A0178 M0003 S1005 Viscous damper	 1 1 1
Varian	Torrseal	M0006	

Key to comments
1: Performed as expected
2: Discolored where exposed to U.V.
3: Further testing is planned./Results to be published later

34c. Epoxy adhesives on LDEF (concluded) (from ref. 107).

N93-28256

OXYGEN ISOTOPES IMPLANTED IN THE LDEF SPACECRAFT

J M Saxton, I C Lyon, E Chatzitheodoridis, P Van Lierde*, J D Gilmour and G Turner

Department of Geology, University of Manchester, MANCHESTER, M13 9PL, UK
Phone 44-(0)61-275-3842 Fax 44-(0)61 -275-3947

*also VG Isotech, Aston Way, Middlewich, Cheshire, UK

SUMMARY

We have used secondary ion mass spectrometry to study oxygen implanted in the surface of copper from LDEF. Oxidation that occurred in orbit shows a characteristic oxygen isotope composition, depleted in ^{18}O. The measured depletion is comparable to the predicted depletion (45%) based on a model of the gravitational separation of the oxygen isotopes. The anomalous oxygen was contained within 10nm of the surface. Tray E10 was calculated to have received 5.14×10^{21} atoms of oxygen cm^{-2} during the LDEF mission[1] and so there is sufficient anomalous implanted oxygen present in the surface to obtain a reliable isotopic profile.

INTRODUCTION

The atomic oxygen to which LDEF was exposed in orbit is expected to be depleted in ^{18}O in comparison with ground level atomic oxygen due to gravitational separation of the oxygen isotopes above the turbopause (about 110km). Below this altitude the isotopes are well mixed but above it the scale heights for ^{18}O and ^{16}O differ by a factor of 18/16. Oxidation that occurred in orbit should therefore show a characteristic oxygen isotopic composition. We have used an ion microprobe to study the oxide layer on a sample of copper grounding strap from tray E10 on LDEF in order to determine the oxygen isotopic composition of the atmosphere at LDEF orbital altitudes.

EXPERIMENTAL TECHNIQUE

The sample was studied by SIMS (secondary ion mass spectrometry) using a VG Isolab 54 ion probe. A Cs^+ beam (of total energy 18keV on the target) was used to sputter oxygen from the sample surface; secondary O^- ions were then analysed in a double focussing mass spectrometer. We measured ^{16}O and ^{18}O simultaneously using different detectors: a Faraday cup for the ^{16}O beam and a microchannel plate detector for ^{18}O. This multicollection facility was a vital feature of the experiment, since the anomalous oxide layer on the LDEF samples was very thin and the signal short lived (typically of the order of a few minutes). A primary ion beam of 2 nA focussed to a spot size of approximately 100 μm reduced the sputtering rate sufficiently that consistent and reproducible isotopic depth profiles were obtained, even in very near surface layers where the oxygen abundance and isotopic ratio were highly variable. The beam was held static on the surface as we did not have the facility for rastered depth profiling. Undoubtedly this reduced the depth resolution and contributed significant edge effects when the ion beam had sputtered through the anomalous layer, but the near surface profile is thought to be quite accurate. We are in the process of improving our depth resolution by using Köhler illumination to give uniform ion beam density across the primary beam and we will re-examine the samples to improve the isotopic depth profiles.

The ease with which the surface layer was sputtered meant that no ion beam imaging, peak centring or beam optimisation could be performed on any part of the surface which was to be analysed. The experimental procedure adopted therefore was to first obtain high precision and consistent $^{18}O/^{16}O$ ratios from ordinary copper sheet or an area of the LDEF copper sheet which had already been analysed, peak centre and optimise the ion beams, and just at the point at which software starts to measure isotopic ratios, move the sample under the primary ion beam to an area which had not been analysed. The LDEF copper always showed large depletions of ^{18}O near the surface, rising up to

PRECEDING PAGE BLANK NOT FILMED

'normal' terrestrial ratios as the beam sputtered away near surface layers. When the Cs^+ beam was defocussed to greater than 100μm spot size to reduce the sputtering rate, consistent values of the most extreme surface depletions were recorded. We also used identical experimental procedures on ordinary (non-LDEF) copper sheet and unexposed LDEF stainless steel surfaces, but no experimental artifacts were ever observed which could have produced the observed isotopic profiles.

RESULTS AND DISCUSSION

We have studied copper grounding strap from position E10 (near the forward edge). The exposed side of the copper (ie facing along the velocity vector) was visibly darkened whilst the unexposed side appeared bright and shiny. Figure 1 shows the ^{16}O signal as a function of time for the darkened (exposed) side of the E10 copper in which the depth scale was determined by using a Talystep 1 (manufactured by Rank Taylor and Hobson with a depth resolution of 50Å). Oxygen is clearly concentrated within 10nm of the surface. Unfortunately the depth measurement proved very difficult to perform accurately due to the surface roughness of the copper. (Figure 2 shows a back scattered SEM image of the surface illustrating the micron sized irregularity of the surface.) The surface roughness also makes simple models of implantation of oxygen in the surface questionable and the depth profiles difficult to interpret. The depth calibration is assumed to be linear with time since we have no way at present of obtaining a more accurate depth calibration. Indeed we were only able to obtain a depth calibration by sputtering a crater for an hour and measuring the final crater depth (1μm). The Talystep profile of this crater is shown in figure 3 along with surface irregularities.

Figures 1 and 4 show the variation of $\delta^{18}O$ with time (and hence depth) for the exposed and unexposed sides, respectively, of the E10 copper. The ratio is expressed as permil variation from 'normal' oxygen (i.e., the isotopic composition at sea level calibrated by obtaining an isotopic ratio from the bulk copper when the depth profile reached a constant isotopic value - which agreed with the value obtained from copper gently oxidised by a heat gun in the laboratory).

The variation of $\delta^{18}O$ with depth is different for the two sides but several spots on both sides yielded consistent profiles for each side. The exposed side appears to have a layer of isotopically more normal material at the surface. Viewing the sample optically whilst the darkened surface was sputtered showed that the minimum isotopic value for this side occurred when the primary beam just sputtered through this dark layer to reveal bright copper underneath. Although the exposed side profile appears to have a shallower gradient than the unexposed side, this is probably an artifact produced by a lower primary beam density. One of our objectives in the near future is to improve the precision of depth profiles for both sides of the copper.

The oxygen in the LDEF surface is clearly depleted in ^{18}O with respect to normal oxygen. The exact value of the depletion is difficult to determine precisely due to a variable admixture of normal oxygen from the bulk copper. Extrapolation of a graph of $^{18}O/^{16}O$ vs $1/^{16}O$ (Lyon et al.[2]) suggests a value for $\delta^{18}O$ of -450 ± 50 $^{o}/_{oo}$ (though a single value as low as -550 $^{o}/_{oo}$ has been recorded, see fig. 4). The ^{18}O and total oxygen signal decrease with time as we begin to sample the residual (impurity) oxygen in the bulk copper. We have calculated the expected depletion in $\delta^{18}O$ over the whole of the 6 year mission to account for solar cycle variations in the atmosphere using data from the MSIS86 model[3]. The oxygen density and calculated $\delta^{18}O$ value at a particular height and time were integrated over the spacecraft's orbit for the six year mission and a total integrated $\delta^{18}O$ value for the implanted oxygen determined. LDEF received most of its atomic oxygen exposure between days 2000-2106 of the mission during a rapid descent from 400km to 300km, so we took the isotopic and density parameters every 6 months for the first 5 years and every 1 month for the final year. The average $\delta^{18}O$ value integrated over the whole mission was $-450^{o}/_{oo}$ but this value is probably uncertain by $\pm50^{o}/_{oo}$. This uncertainty arises mainly from having to assume hydrostatic equilibrium in calculating the $\delta^{18}O$ values (an assumption we know to be not strictly true) and partly from uncertainty in the height of the turbopause. The calculation of $\delta^{18}O$ as a function of height is a subject we intend to study in more detail.

An obvious implication of the difference in isotopic depth profile between the outward and inward facing surfaces is that the contamination layer was deposited on surfaces very late in the LDEF mission, a conclusion which runs contrary to expectations from other experiments. Such a novel

conclusion must therefore be treated with caution. Other studies have shown that atomic oxygen reacts with surfaces in a complex fashion[4], some surface contaminants proving much more resistant to erosion than normal surface materials and considerable sub-surface erosion occurring as atomic oxygen penetrates through microscopic pin pricks in resistant surfaces. The surface roughness of the copper also makes simple models questionable.

The observation of anomalous profiles on both sides of the copper requires scattering of oxygen atoms behind the copper. We are now studying how profiles vary with distance from edges of the copper and it is clear that extensive further work is required to understand the measured profiles and predict the effects of space exposure on materials.

FUTURE WORK

We are in the process of extending our measurements to ^{17}O, to see if the ^{17}O depletion is also that expected by simple theory. In order to provide an accurate calibration at these extreme depletions, we have also prepared samples of copper, oxidised on the surface with a known amount of ^{16}O enriched oxygen. In addition to calibrating isotope ratios these should allow us to quantify the dose of atomic oxygen received by the samples of copper from LDEF. We will also study copper strap from other trays; we have samples from D07 (close to the RAM atomic oxygen vector) and E02 (from the trailing side of LDEF which should have received a very small flux of anomalous oxygen). We also intend to study the effect of LDEF surface contamination on our measurements.

ACKNOWLEDGEMENTS

We gratefully acknowledge the support of Dr P K Wenzel and Dr F Levadou of the European Space Agency division ESTEC, NASA and Professor J A M McDonnell and Dr T Stevenson of the Space Sciences Group at the University of Kent, UK, for the provision of information and materials. We also thank Mr M McGowan and Mr S Barnes at the Department of Electrical Engineering at the University of Manchester Institute of Science and Technology who instructed us and gave us freedom to use their Talystep 1. We also thank Drs C G Simon and D Griffis for a constructive review of this paper.

REFERENCES

1.'LDEF Atomic Oxygen Flux and Fluence Calculations'. R J Bourassa and J R Gillis, NASA Contract Report, NAS1-18224, Task 12 (1991)
2.'Oxygen isotopes implanted in the LDEF spacecraft' I C Lyon, J D Gilmour, J M Saxton and G Turner. Meteoritics, **26**, 368-369 (1991)
3. MSIS86 (Mass Spectrometer - Incoherent Scatter) computer model of the upper atmosphere, run at the World Data Centre, SERC Rutherford Appleton Laboratory, Chilton, Didcot, Oxon. UK. Full details given in A E Hedin. J. Geophys. Res. **88**, p10170-10188, (1983)
4. LDEF Spaceflight Environmental Effects Newsletter. Vol 1, No2 12th April 1990

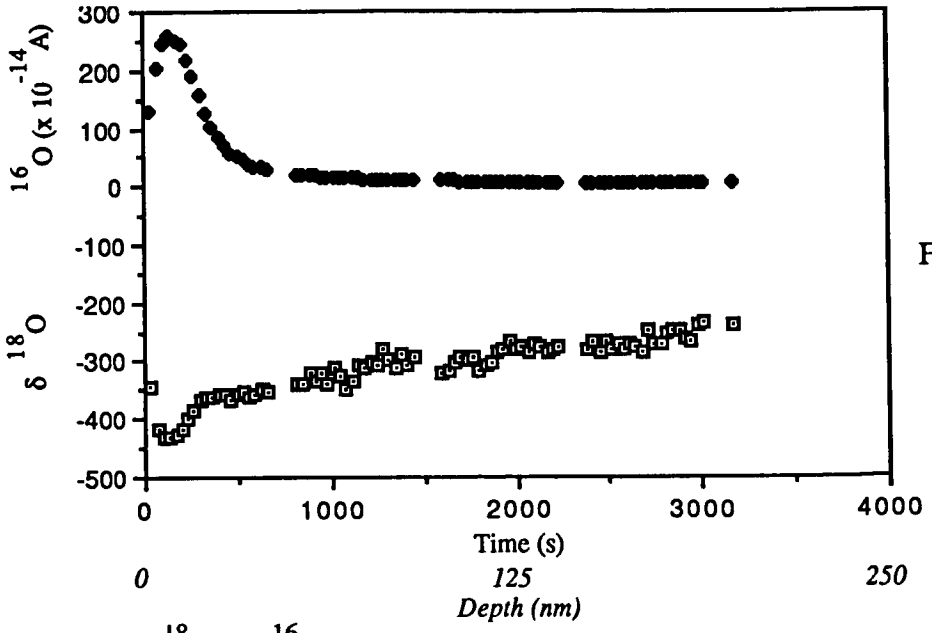

Figure 1

$\delta^{18}O$ and ^{16}O as a function of time for the exposed side of E10 copper (depth equivalent estimated from final crater depth measured by a Talystep)

Figure 2.
A back scattered scanning electron photograph of the surface of the E10 copper showing micron scale roughness and an ion beam burn mark.

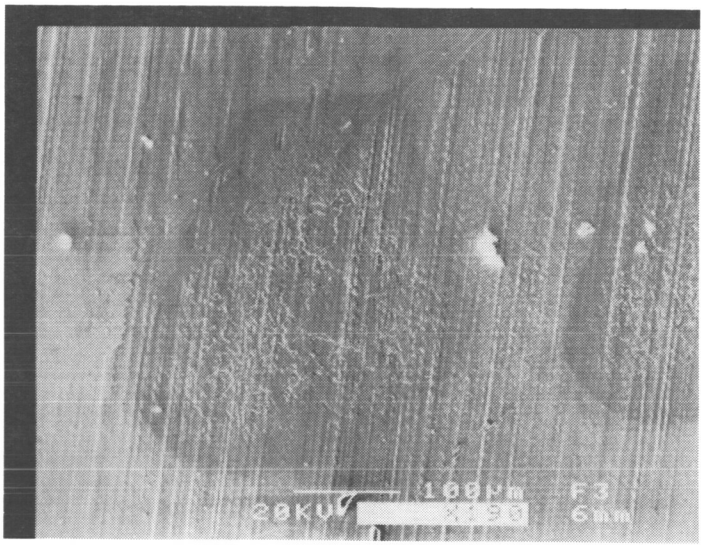

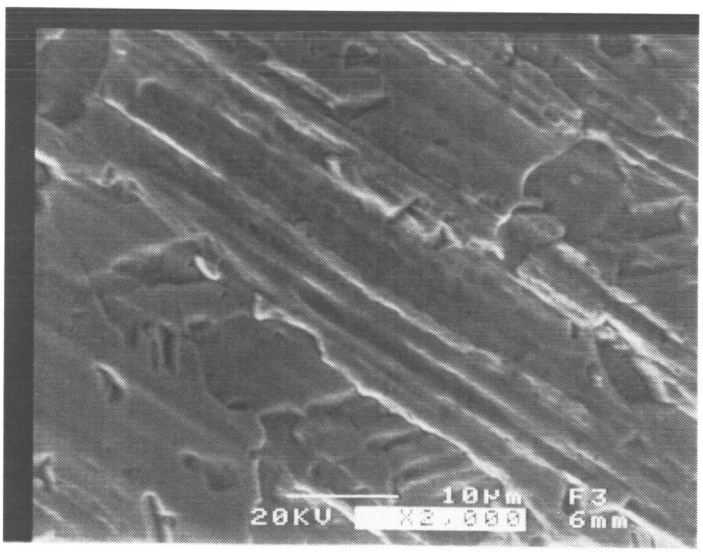

Figure 3

Talystep Profile of the Ion Beam Burn Mark

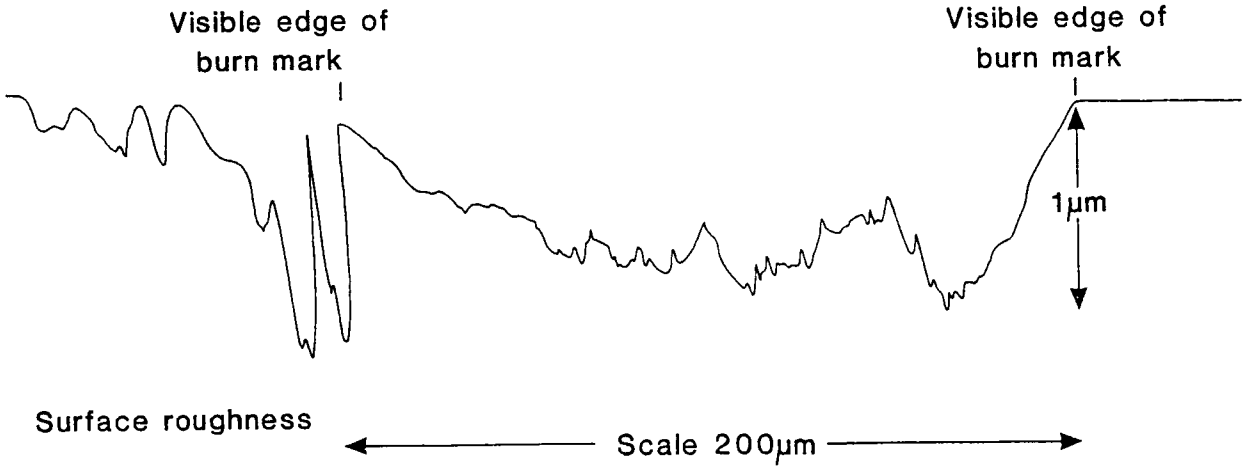

Figure 4

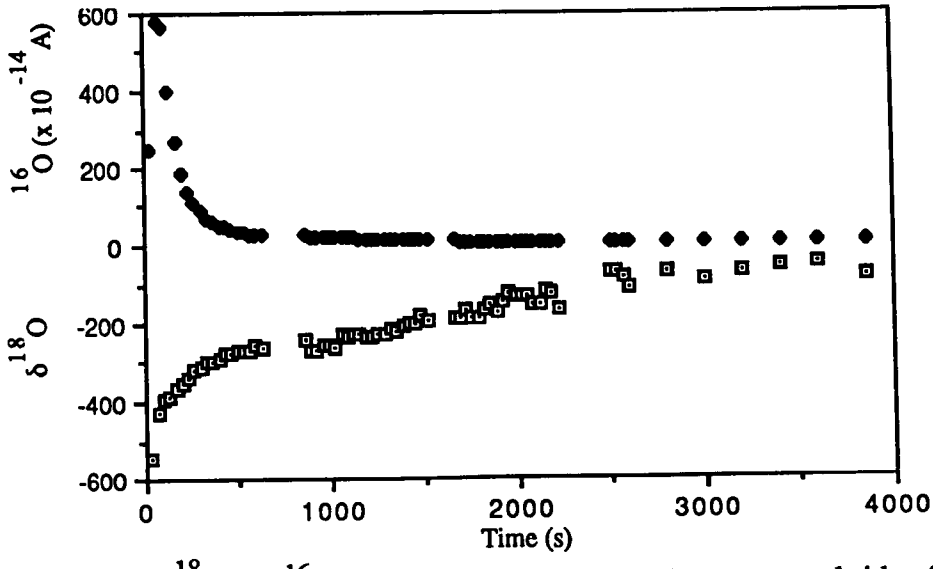

$\delta^{18}O$ and ^{16}O as a function of time for the unexposed side of E10 copper (no depth calibration for this side)

N93-28257

SILAZANE TO SILICA

Gale A. Harvey
NASA Langley Research Center
Hampton, VA 23665-5225
Phone: 804-864-6742, FAX: 804-864-7790

ABSTRACT

Thin film silica and/or methyl silicone have been detected on most external surfaces of the retrieved LDEF. Both solar ultraviolet radiation and atomic oxygen can convert silicones to silica. Known sources of silicone in or on the LDEF appear inadequate to explain the ubiquitous presence of the silica and silicone films. Hexamethyldisilazane (HMDS) was used as the Challenger tile waterproofing compound for the Challenger/LDEF deployment mission. HMDS is both volatile and chemically reactive at STP. In addition, HMDS releases NH_3 which depolymerizes silicone RTV's. Polyurethanes are also depolymerized. Experiments are reported that indicate much of the silicone and silica contamination of LDEF resulted directly or indirectly from HMDS.

INTRODUCTION

A brown stain of varying thickness was present on much of the external surfaces of LDEF (ref. 1). This visible contamination resulted primarily from outgassing of the thermal-control paints and will not be discussed in this paper. However, mixed in with the visible contamination and on visually clean surfaces are films of methyl silicones and silica (refs: 2-4). Organic film cleanliness measurements of facility wash plates during processing of the Upper Atmosphere Research Satellite (UARS) suggested silicone contamination of payloads from orbiter rewaterproofing compounds (ref. 2).

The orbiters are protected from heating during reentry by the thermal protection system (TPS) of reusable surface insulation tiles and fibrous insulation blankets. The tiles and blankets are waterproofed prior to installation on the orbiters by treatment in an oven that contains methyltrimethoxysilane (MTMS) vapor (ref. 5). This initial waterproofing is burned off by high-temperatures during reentry. Scotchguard was used early in the shuttle flight program to rewaterproof the orbiters at KSC, but was ineffective (ref. 5). Hexamethyldisilazane (HMDS) was used for rewaterproofing of the orbiters starting with the Challenger in 1983. This continued, including LDEF/Challenger (April 1984), until the sixth flight of the Challenger (October 1984) when a tile was lost during reentry. Widespread degradation (depolymerization) of the silicone adhesives used to attach the tiles, RTV-560 and 577, was traced to reaction products from HMDS, particularly ammonia (ref. 5). Subsequently, the chemistry of HMDS and silicones was studied extensively by Rockwell International (ref. 6). Additional information regarding silane surface chemistry is in reference 7. Since 1988 (STS-26) dimethylethyoxysilane (DMES) has been used to rewaterproof the tiles and external blankets. The chemistry of DMES and other silanes for waterproofing of silica surfaces has been studied by Johnson et. al. (refs. 8 and 9). Table 1 lists the schedule for the shuttle flights and the associated rewaterproofing agents. Two cc/6"x 6" tile of waterproofing compound are injected into each of approximately 25,000 tiles. About 200 pounds of waterproofing compound, DMES, was applied to the orbiter for mission STS-48.

TABLE 1
SHUTTLE SCHEDULE

Flight		Date	Waterproofing	Comments
STS-1	Columbia	4/12/81	MTMS	
STS-2	Columbia	11/12/81	SG (Scotchguard)	
STS-3	Columbia	3/22/82	SG	
STS-4	Columbia	6/27/82	SG	
STS-5	Columbia	11/11/82	SG	
STS-6	Challenger	4/4/83	MTMS	
STS-7	Challenger	6/18/83	HMDS	
STS-8	Challenger	8/30/83	HMDS	
STS-9	Columbia	11/28/83	HMDS	
STS-41B	Challenger	2/3/84	HMDS	
STS-41C	Challenger	4/6/84	HMDS	LDEF Deployed
STS-41D	Discovery	8/30/84	MTMS	
STS-41G	Challenger	10/5/84	HMDS	Tiles Off
STS-51A	Discovery	11/8/84	HMDS	Brown Stain
STS-51C	Discovery	1/24/85	SG	
STS-51D	Discovery	4/12/85	SG	
STS-51B	Challenger	4/29/85	SG	Challenger Return to Flight
STS-51G	Discovery	6/17/85	SG	
STS-51F	Challenger	7/29/85	SG	
STS-51I	Discovery	8/27/85	SG	
STS-51J	Atlantis	10/3/85	MTMS	
STS-61A	Challenger	10/30/85	SG	
STS-61B	Atlantis	11/26/85	SG	
STS-61C	Columbia	1/12/86	SG	
STS-51L	Challenger	1/28/86	SG	In-Flight Explosion
STS-26	Discovery	9/29/88	DMES	Return to Flight
STS-27	Atlantis	12/2/88	DMES	
STS-29	Discovery	3/13/89	DMES	
STS-30	Atlantis	5/4/89	DMES	
STS-28	Columbia	8/8/89	DMES	
STS-34	Atlantis	10/18/89	DMES	
STS-33	Discovery	11/22/89	DMES	
STS-32	Columbia	1/9/90	DMES	LDEF Retrieval
STS-36	Atlantis	2/28/90	DMES	
STS-31	Discovery	4/24/90	DMES	HST
STS-41	Discovery	10/6/90	DMES	
STS-38	Atlantis	11/15/90	DMES	
STS-35	Columbia	12/2/90	DMES	
STS-39	Discovery	3/ /91	DMES	
STS-37	Atlantis	4 / /91	DMES	
STS-40	Columbia	5/ /91	DMES	
STS-43	Discovery	7/ /91	DMES	
STS-44	Atlantis	8/ /91	DMES	
STS-48	Discovery	9/13/91	DMES	UARS
STS-42	Atlantis	1/ /92	DMES	Brown Stain
STS-46	Discovery	2/ /92	DMES	
STS-45	Atlantis	4/ /92	DMES	

MEASUREMENT TECHNIQUE

Fourier transform infrared spectroscopy (FTIR) was used for the identification of silicones and silica. The spectra are 4 cm^{-1} resolution and the spectrometer was optimized for the 900-1800 cm^{-1} spectral region. The sample spectra are generally ratioed to equivalent background spectra to give transmission spectra. Sample residues and films are placed on IR transmitting windows (i.e., CaF_2, MgF_2, NaCL) and centered in the IR beam at the beam focus in the sample compartment. Additional information regarding FTIR spectroscopy for contamination measurement and analysis is in reference 10.

Absorption bands resulting from chemical bonds in molecules are useful in identifying classes of chemical compounds. For example, the sharp absorption at 1260 cm^{-1} results from the silicon-methyl bond and indicates $SiCH_3$ in the compound. The absorption bands of major interest in this paper are: 940 cm^{-1} (SiN), 1000-1100 cm^{-1} (O-Si-O), 1050-1200 cm^{-1} (O-C-O), 1185 cm^{-1} (SiNH), 1260 cm^{-1} ($SiCH_3$) and 1730 cm^{-1} (O=C-O). A broad single peak near 1050 cm^{-1} is indicative of silica (SiO_2). Most contamination films are mixtures of compounds, and discretion should be used in the interpretation of IR spectra of residues.

HMDS CHEMICAL PATHWAYS

Hexamethyldisilazane $[(CH_3)_3SiNHSi(CH_3)_3]$ is a clear liquid at STP with a molecular weight of 161.4 Daltons and a vapor pressure of 1.04 mm at 20°C (ref. 11). The chemical structure is shown in figure 1. An IR spectrum of HMDS is presented as figure 2. The $SiCH_3$ absorption at 1260 cm^{-1} is very strong, but the SiO at 1000-1100 cm^{-1} (strong in silicones and silica) and the SiH absorption at 2200 cm^{-1} (strong in DMES) are absent. The strong, sharp absorption at 1180 cm^{-1} (NH) serves as a convenient identifier for HMDS.

There are several chemical pathways by which HMDS can produce a silicone residue, or a thin film of SiO_2 on a surface. A silicone residue is left in a vessel after evaporation of HMDS. Commercial HMDS is generally specified as 98% pure. The residue may be impurities in delivered HMDS. An IR spectrum of current production (HULS America CH7300, January 1992) HMDS residue is presented as figure 3. The residue has the visual appearance of clear oil. A few small, translucent particles ≈10 microns diameter are imbedded in the residue. An IR spectrum of residue from aged HMDS (Pfaltz and Bauer, Inc. ≈1983) is presented as figure 4. More, and larger gel-like particles are imbedded in the residue (figure 5).

A pathway by which HMDS can be converted directly to thin film silica is by exposure to ultraviolet radiation. A few drops of HMDS were transferred to CaF_2 and NaCL windows placed on a deuterium lamp and exposed for 5 minutes to the ultraviolet radiation. The IR spectra of the residue films are shown in figures 6 and 7. A silica film is present on the CaF_2 window. No silica film is present on the NaCl window. This indicates that HMDS surface chemistry is substrate dependent.

A third chemical pathway in which HMDS can produce silicone residue is by the depolymerization of silicone sealants and potting compounds (ref. 6, 7). A film of RTV-142 (which had been previously cleaned by soaking for 30 minutes in IPA, ref. 2) was placed in a sealed glass vessel with HMDS vapor for 7 days. The film of RTV was then soaked again in IPA for 30 minutes and the IPA allowed to evaporate. The IR spectra of residue from the RTV is presented in figure 8. The molecular weight distribution of the residue is presented as figure 9. The residue mass from the HMDS-vapor-exposed RTV was 6 percent. The residue mass from a film of RTV-560 exposed to HMDS vapor for 7 days was 0.1 percent. A silicone adhesive, DC6-1104, was used to attach velcro strips to the LDEF experiment

trays (≈17) with silvered teflon blankets. The LDEF materials handbook lists 7.5 grams of DC6-1104 for each tray. That is, only a small amount of silicone material is listed on the LDEF manifest. The total mass loss (ASTM E-595) for DC6-1104 is about 0.2% (ref. 12).

A previously cleaned film of Chemglaze Z306 (ref. 2), the polyurethane based thermal control paint used on LDEF, was also placed in a sealed glass vessel with HMDS vapor for 8 days. The film of Z306 was soaked in IPA for 30 minutes and the IPA allowed to evaporate. The spectra of residue from the Z306 is presented in figure 10. The residue mass from the HMDS-vapor-exposed Z306 was 1%. Thus, HMDS vapor depolymerizes Z306 as well as RTV's.

A fourth chemical pathway for HMDS to produce silicone films is the polymerization of products of reaction of HMDS with moisture. HMDS reacts with water to form ammonia (NH_3) and trimethylsilanol ($(CH_3)_3SiOH$) (ref. 5). But trimethylsilanol is very reactive and quickly polymerizes to hexamethyldisiloxane ($(CH_3)_6\ Si_2O$) and water. Hexamethyldisiloxane is relatively stable, but has a high vapor pressure (201 mbar/122°F) and hence will be transported by convection at standard temperature and pressure. The silicone compounds trimethylsilanol, hexamethylcyclotrisiloxane, and octamethylcyclotetrasiloxane were detected in the Challenger crew compartments during the LDEF deployment mission (Table 2, ref. 13). Trimethylsilanol is an immediate reaction product of HMDS and H_2O. It is not clear if the crew compartment siloxanes are related to HMDS.

TABLE 2
STS-13 (41-C) INFLIGHT ATMOSPHERIC ANALYSIS

	SAMPLE			
Compound	S/N-1016	S/N-1013	S/N-1014	S/N-1015
Carbon Monoxide	<0.500(<0.572)	<0.500(<0.572)	<0.500(<0.572)	<0.500(<0.572)
Methane	3.360(2.198)	19.240(12.588)	57.219(37.435)	80.904(52.931)
Bromotrifluoromethane	1.054(6.422)	1.073(6/537)	1.323(8.060)	0.707(4.307)
1.1.2-Trichloro-1,2,2-Trifluoroethane	0.001(6.422)	0.011(0.084)	0.008(0.061)	0.008(0.061)
Ethanal 0.002(0.004)	0.008(0.015)	0.011(0.019)	0.022(0.040)	
2-Propanone	0.002(0.004)	0.049(0.115)	0.054(0.129)	0.037(0.088)
Dichloromethane	nd	0.006(0.022)	0.010(0.034)	0.015(0.051)
2-Propanol	nd	0.019(0.040)	0.015(0.036)	0.018(0.044)
Ethanol nd	1.335(2.510)	0.586(1.102)	1.551(2.917)	
Hexamethylcyclotri-siloxane	nd	0.004(0.037)	0.002(0.020)	0.010(0.092)
Trimethylsilanol	nd	0.003(0.011)	0.003(0.012)	0.009(0.032)
Toluene	nd	0.002(0.006)	0.001(0.003)	0.001(0.005)
Octamethylcyclotetra-siloxane	nd	0.004(0.040)	0.003(0.033)	0.013(0.158)
Silicone, M.W. = 452	nd	0.032(0.595)	0.021(0.393)	0.067(1.232)

[a]Concentrations not in parenthesis are ppm; in parenthesis are mg/m3.

ORBITER FACILITIES DATA

Silicone residues were obtained from the Payload Changeout Room (PCR Pad A) during processing of STS-48 (Upper Atmosphere Research Satellite, 8/92) (ref. 2). Additional NVR measurements of orbiter processing facilities have subsequently been made in order to confirm and better understand these residues.

Four NVR wash plates were exposed in the PCR (3/12 to 4/5/84) during processing of STS-41C. Two NVR wash plates were exposed (12/18/91 to 1/21/92) in the PCR during processing of STS-42. Two other NVR wash plates were exposed (1/15 to 1/29/92) in the Orbiter Processing Facility (OPF) where the rewaterproofing agent DMES was applied. The residue masses from these wash plates are listed in Table 3. A different gravemetric procedure is used for the OPF wash plates than is used for the PCR wash plates. The residue transfer is with dimethyl chloride for the PCR plates and with carbon tetrachloride for the OPF plates. Significant residue masses were measured from PCR wash plates.

An IR spectrum of hexane-transferred residue from the STS-48 processing in the PCR is presented as figure 11. The strongest absorption is from the silicone band (1000 cm^{-1} to 1100 cm^{-1}). Alkaline water reacts with both the hydrogen and ethoxy groups to give DMES bifunctionality and results in the formation of silicone polymers (ref.8).

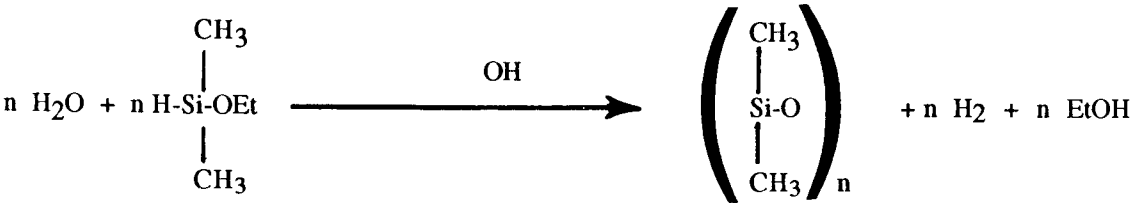

(DMES) (silicones)

Thus, figure 11 is compatible with expected reaction product of DMES. The 1730 cm^{-1} carbonyl absorption indicates other compounds are also present in the PCR residue.

An IR spectrum, of methylene chloride-transferred residue from the STS-42 processing in the PCR, is presented as figure 12. The strongest absorptions are carboxyl (1100 cm^{-1}) and carbonyl (1730 cm^{-1}) and obscure any silicone absorption. Some type of chromatography (i.e. hexane transfer for silicones followed by methylene chloride transfer for phathalates) is needed to clearly identify silicones in residues.

TABLE 3 - ORBITER FACILITY RESIDUE MASSES

Wash Plate	Facility	Date	NVR Mass (mg)
2 Side 2	PCR	3/12-4/5/84	.94
3 Side 4	PCR	"	.64
4 Side 2	PCR	"	.42
5 Side 4	PCR	"	.30
6	PCR	7/23-8/13/91	.27
7	PCR	8/13-9/9/91	.35
8	PCR	12/18-1/21/92	.40
9	PCR	"	.22
7W-X	OPF	1/15-1/29/92	.027
7E-V	OPF	"	.031

CONCLUSIONS

HMDS is capable of producing silicone and silica films by both direct and indirect pathways. Direct pathways include the absorption of HMDS vapor on surfaces with subsequent reactions and polymerization, and absorption of reaction products, such as hexamethyldisiloxane, and subsequent polyermization. Outgassing of polymerized residues in HMDS is also likely. Indirect pathways are: depolymerization of silicone materials such as RTV's which subsequently outgas and produce silicone films on surfaces. Subsequent exposure to solar UV and or atomic oxygen could convert the silicones to silica. Depolymerization of other plastics such as urethanes can increase the total organic film on some surfaces. The surface chemistry of HMDS is dependent on surface material. Much of the silicone and silica contamination on LDEF resulted from several chemical processes in which HMDS, its reaction products, or depolymerized organic materials are deposited on surfaces during payload processing and in orbit.

CONCLUDING REMARKS

During the 1970's the space shuttle program was in its development stage; LaRC was conceiving a proposed first shuttle payload that was to become LDEF, and the Viking Project was the largest program at LaRC. The Viking Project expended much effort to insure that the Viking Mars Landers were biologically sterile and would not biologically contaminate Mars with viable organisms from Earth. A general concern at LaRC was that payloads from manned launch vehicles would not be as clean as those from unmanned launch vehicles. Fifteen years later, this early concern has largely been forgotten.

The NASA space-flight centers, LaRC and GSFC, generally go to great efforts to insure flight instrument cleanliness. Assembly, testing, and integration of flight hardware are typically performed in class 100 clean rooms and organic films are restricted to budgets of 1 milligram per 0.1 square meter of surface area. Rigorous material selection criteria are imposed. Beta cloth, which sometimes has a phenymethyl silicone oil with a vapor pressure about 1×10^{-7} Torr at room temperature, is a borderline material for space flight qualification. The silanes used to rewaterproof the shuttle tiles and blankets have vapor pressure almost a billion times higher, and hence are subject to transport on the ground as well as in space.

The STS-48 launch of HALOE/UARS was possibly the first mission in which a payload program requested IR analyses of wash plate residues from orbiter processing facilities. Evidently, payload programs have relied on early cleanliness assessments from STS-2, 3, and 4 which did not indicate contamination (at 1970's cleanliness levels) during launch and short term on-orbit operations. Needless to say, the flight instrument centers have been remiss in not following through on their cleanliness programs to include the orbiter processing, and launch and deployment phases of launch operations.

In addition to silicone residues, orbiter tile and beta cloth fibers (ref. 14), and shuttle waste dump residues (ref. 3) are present on the LDEF and indicate cross-contamination from shuttle operations. Even though both HMDS and Chemglaze Z306 are no longer widely used in the space program, a sustained, broadly based measurement and analysis program for residues from all flight-hardware-flow facilities is still needed.

REFERENCES

1. Harvey, G. A., "Organic Contamination of LDEF," Proc. of First LDEF Post-Retrieval Symposium, June 1991, NASA CP 3134, pp. 179-197, January 1992.

2. Harvey, G. A., "Sources and Transport of Silicone NVR," Proc. of LDEF Materials Workshop, November 1991, NASA CP 3162, pp. 175-184, 1992.

3. Crutcher, E. R., and K. T. Warner, "Molecular Films Associated with LDEF," Proc. of First LDEF Post-Retrieval Symposium, June 1991, NASA CP 3134, pp. 155-177, January 1992.

4. Henninger, C. S., and W. K. Stuckey, and J. C. Uht, "Space Environmental Effects on Silvered Teflon Thermal Control Surfaces," Proc. of First LDEF Post-Retrieval Symposium, June 1991, NASA CP 3134, pp. 831-845, January 1992.

5. Hill, W. L., and S. M. Mitchell, "Certification of Rewaterproofing Agent for Shuttle Thermal Protection Systems," 199th Am. Chem. Soc. Conf., Boston, Massachusetts, April 1990.

6. Hill, W. L., "Certification for New Shuttle Orbiter TPS Waterproofing Agent, February 1988 through September 1988," Rockwell International Laboratory Test Report LTR 4917-4285, January 1989.

7. Leyden, D. E., "Silanes, Surfaces, and Interfaces," Chemically Modified Surfaces Series; Gordon and Breach Science Publishers: New York, 1986.

8. Johnson, R. E., D. Ford, F. Fangio, and J. Lawton, "Final Report - The Study of Silanes and HRSI Tiles Using Infrared Spectroscopy," Research and Advanced Development Institute, LeTourneau University, Longview, Texas, June 1988.

9. Johnson, R. E., and D. Ford, "Final Report - Studies of Silane Stability to Humidity and Temperature," Research and Advanced Development Institute, LeTourneau University, Longview, Texas, April 1990.

10. Harvey, G. A., and J. L. Raper, "Halogen Occultation Experiment (HALOE) Optical Witness-Plate Program," NASA TM 4081, February 1989.

11. Material Safety Data Sheet - Hexamethyldisilazane, HULS America Inc., P. O. Box 365, Piscataway, New Jersey 08855-0365.

12. Campbell, W. A., and J. J. Scialdone, "Outgassing Data for Selecting Spacecraft Materials," NASA RP 1124, November 1990.

13. Bafus, Donald A., "STS-13 (41-C) Flight Atmospheric Sample Analysis," Krug Life Sciences, 1290 Hercules Drive, Suite 120, Houston, Texas 77058.

14. Crutcher, E. R., "Particle Types and Sources Associated with LDEF," Proc. of First LDEF Post-Retrieval Symposium, June 1991, NASA CP 3134, pp. 101-119, January 1992.

ACKNOWLEDGEMENTS

Randy Ponticiello (HULS America, Inc.) and Bill Sobieski (Miles, Inc.) supplied samples of new HMDS for testing. Bill Hill, Shirley Mitchell, and Howard Massey (Rockwell International) provided copies of their reports and detailed discussions. Richard Johnson (LeTourneau University) provided vintage DC 6079 HMDS, reports, and discussions. Hector Garcia (Krug Life Sciences) provided the STS-41C air sample analysis report. Fred Gross (Goddard Space Flight Center) critically reviewed the paper, "Sources and Transport of Silicone NVR". Mark Scarbrough (Lockheed) provided useful discussions. Lubert Leger (Johnson Space Center) provided information on the tile rewaterproofing problems and certification. Jaime Palou (Kennedy Space Center) provided invaluable orbiter processing data, NVR samples, and information regarding key processes and individuals involved in orbiter rewaterproofing. His open, professional attitude toward dissemination of information is especially appreciated.

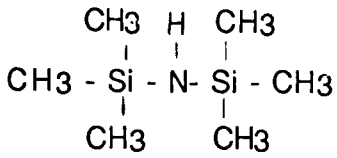

Figure 1. Molecular structure of hexamethyldisilazane (HMDS).

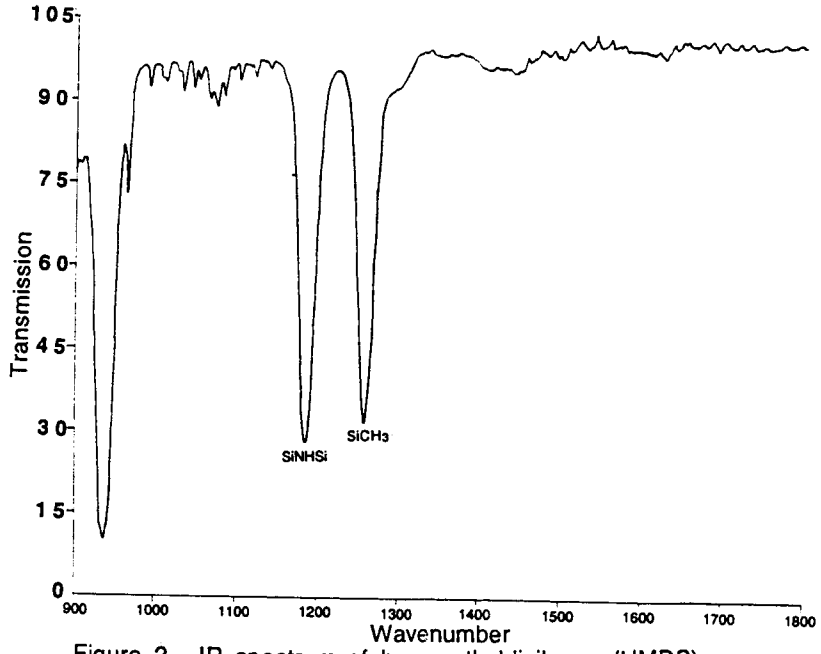

Figure 2. IR spectrum of hexamethyldisilzane (HMDS).

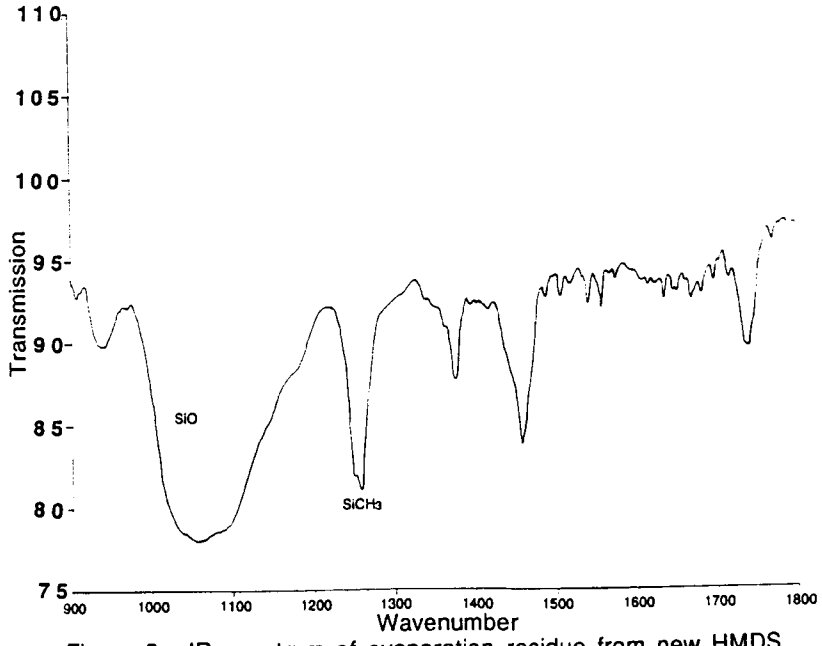

Figure 3. IR spectrum of evaporation residue from new HMDS.

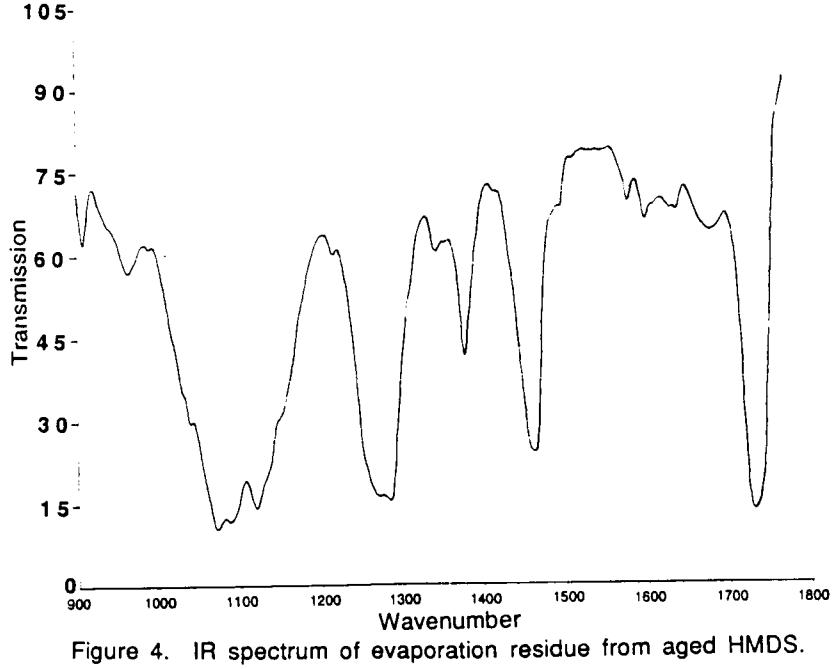

Figure 4. IR spectrum of evaporation residue from aged HMDS.

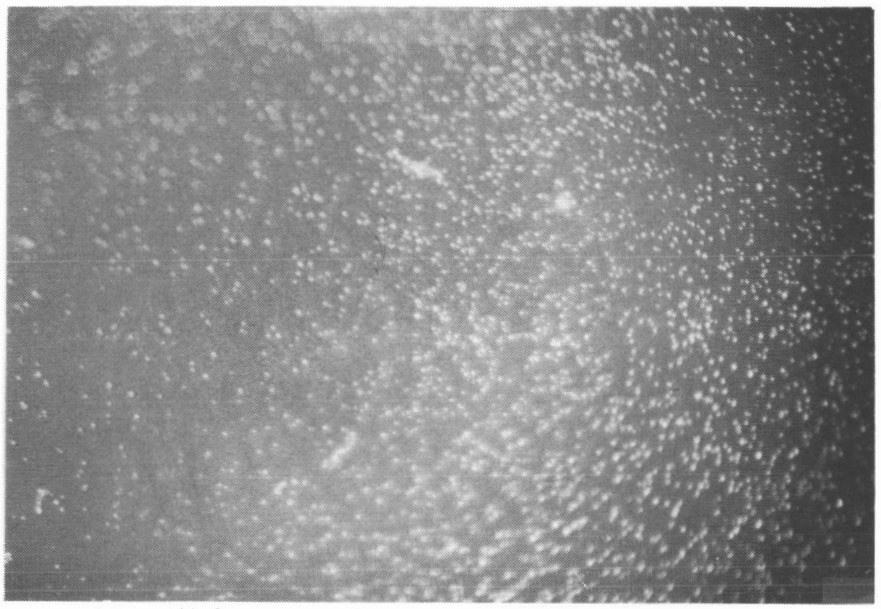

Figure 5. Photograph of evaporation residue from aged HMDS.

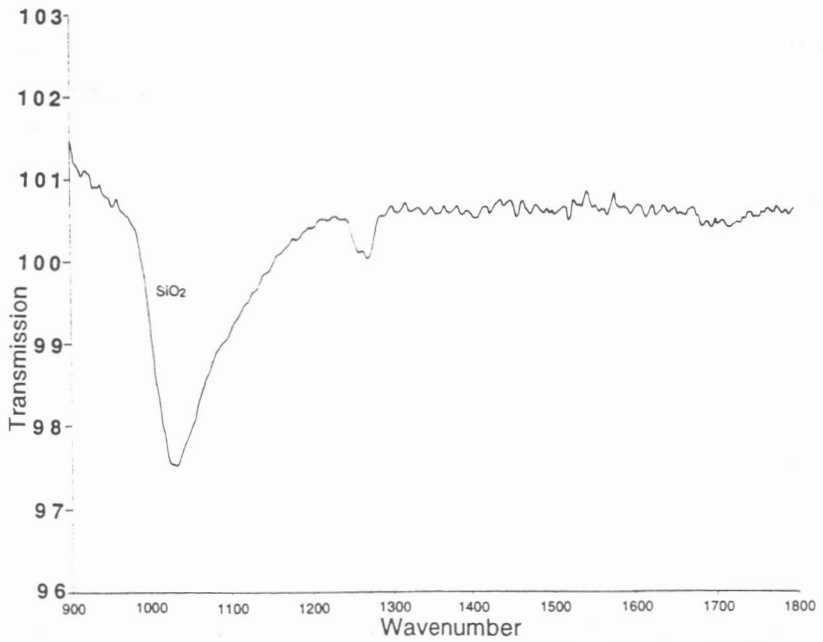

Figure 6. IR spectrum of UV exposed HMDS residue on CaF2.

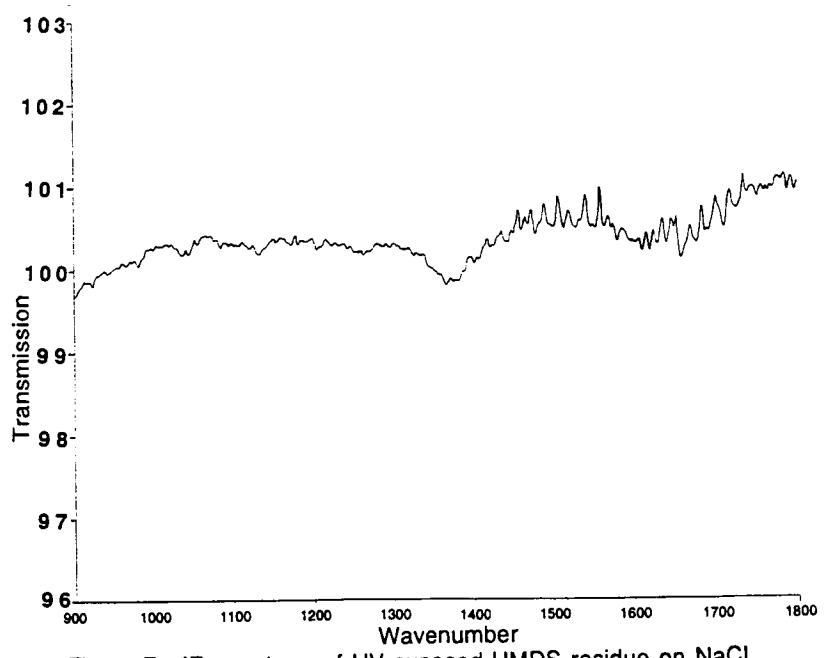

Figure 7. IR spectrum of UV exposed HMDS residue on NaCL.

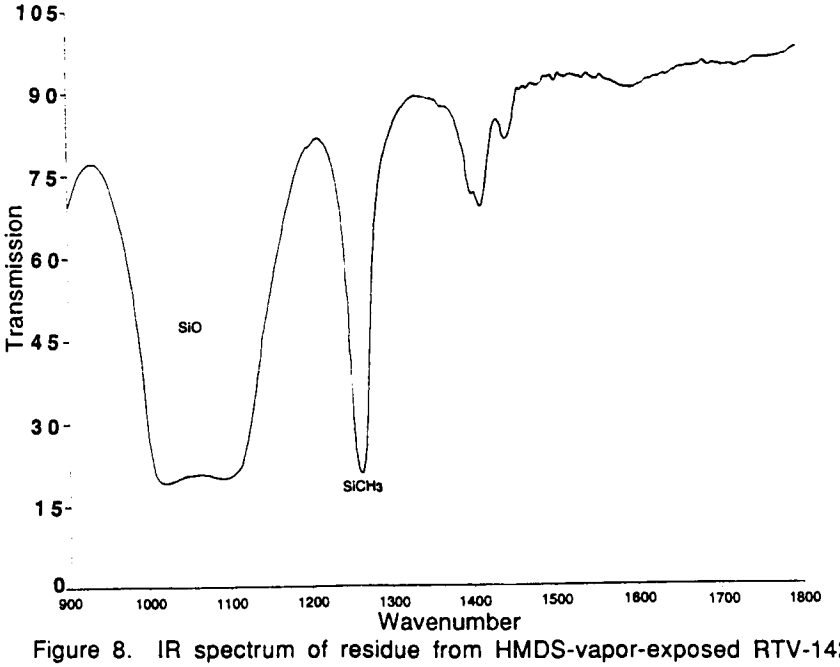

Figure 8. IR spectrum of residue from HMDS-vapor-exposed RTV-142.

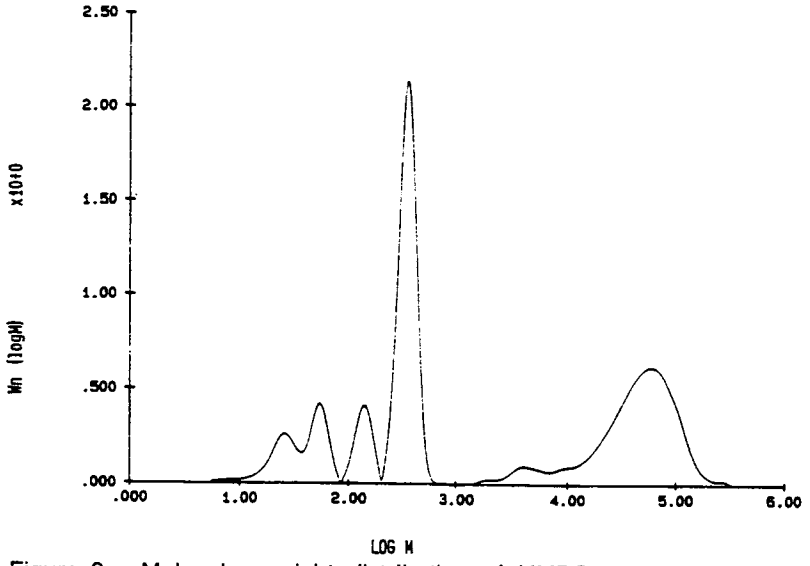

Figure 9. Molecular weight distribution of HMDS-vapor-exposed RTV residue.

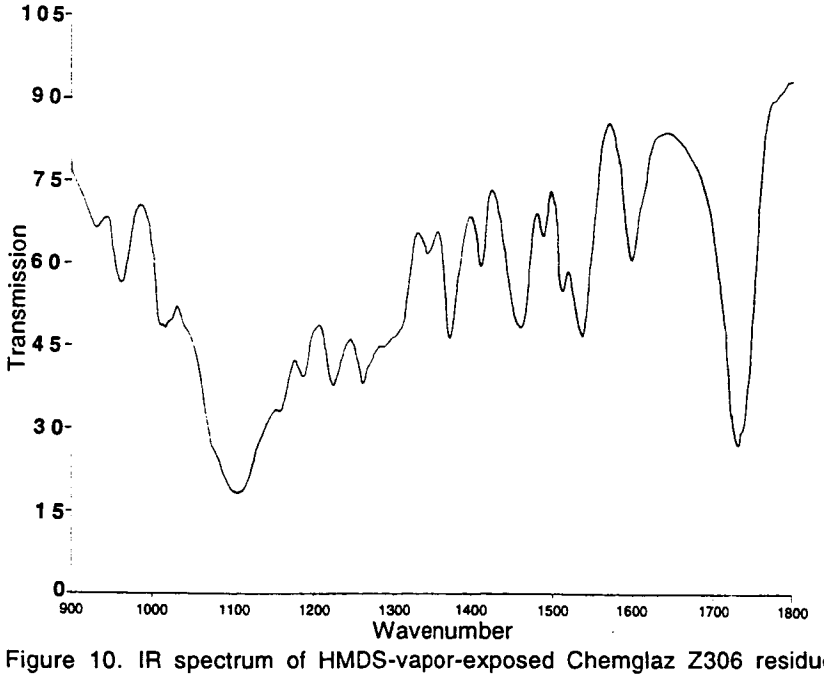

Figure 10. IR spectrum of HMDS-vapor-exposed Chemglaz Z306 residue.

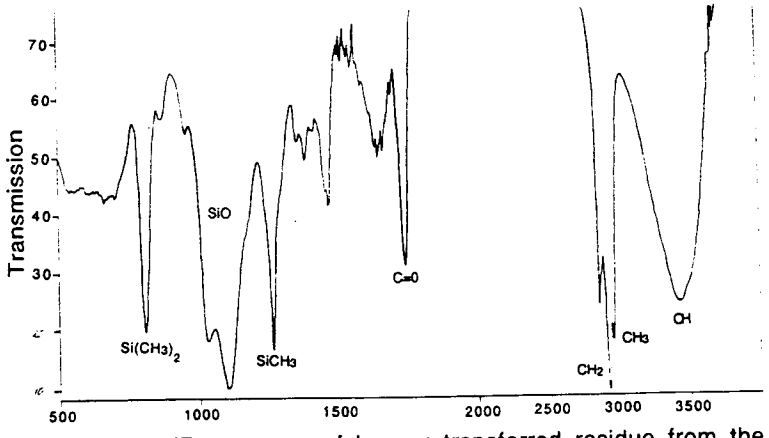

Figure 11. IR spectrum of hexane-transferred residue from the PCR (STS-48).

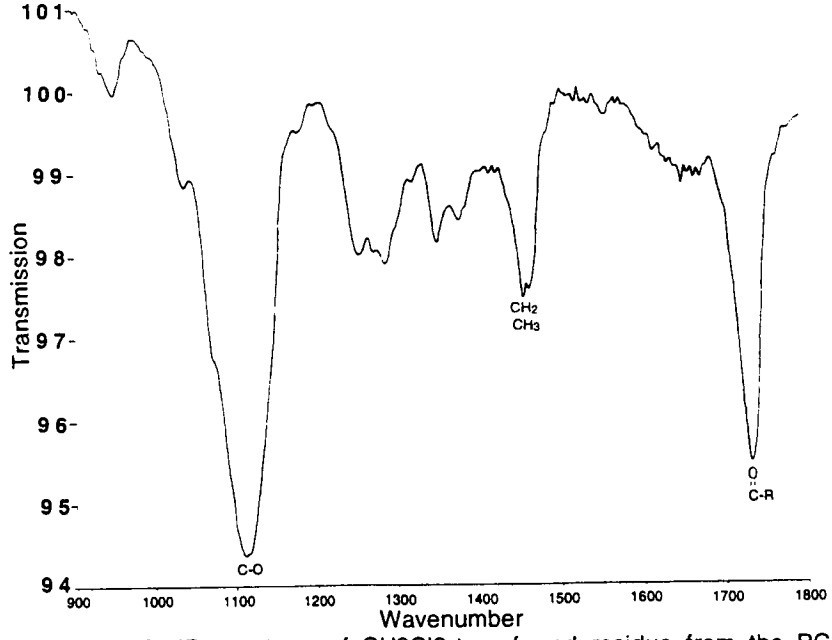

Figure 12. IR spectrum of CH2Cl2-transferred residue from the PCR (STS-42).

N93-28258

STABILITY AND REACTIVITY OF DIMETHYLETHOXYSILANE

Richard E. Johnson
LeTourneau University
Longview, TX 75607-7001
Phone: 903/753-0231, ext. 222; Fax: 903/237-2732

Douglas I. Ford
LeTourneau University
Longview, TX 75607-7001
Phone: 903/753-0231, ext. 378; Fax: 903/237-2732

INTRODUCTION

In this paper, the chemistry of the compound dimethylethoxysilane (DMES) is discussed especially as it relates to waterproofing silica surfaces. Some of the desirable properties of this compound are that it readily reacts with silica in the vapor phase, it is a low boiling point liquid (54°C) and the by-product of its reaction with silica is the rather inert substance, ethanol. It is currently used by NASA to re-waterproof the HRSI shuttle tiles before relaunching the vehicle.

Very little information is available on this particular compound in the literature or even on related silane compounds that have both a hydride group and an alkoxy group. Since the close proximity of two groups often drastically affects the chemical behavior of each group, chemical reactions were carried out in the laboratory with DMES to verify the expected behavior of these two functional groups located on DMES. Some of the reactions tested would be potentially useful for quantitative or qualitative measurements on DMES. To study the reactions of DMES with silica surfaces, cabosil was used as a silica substrate because of its high surface area and the ease of detection by infrared spectroscopy as well as other techniques. (This paper cites references 1-11 and figures 1-10.)

CHEMICAL REACTIONS OF DIMETHYLETHOXYSILANE (DMES)

DMES has the following structure and physical properties.

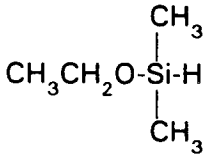

Density 0.751 g/ml at 25°C

Boiling point 54°C

Refractive index 1.365

The methyl-silicon bonds are chemically inert toward ordinary chemical reagents (acids, bases, water, oxidizing and reducing agents). Most of the chemistry of this compound is due to the ethoxy and hydride groups. In contrast to carbon-ethoxy linkages, the silicon-ethoxy bond is readily hydrolyzed by water. The hydrogen of the Si-H linkage is a fairly strong reducing agent, whereas

the C-H linkage is quite inactive as a reducing agent. This is probably due to the smaller electronegativity of the silicon atom compared to carbon. DMES, then, has two fairly aggressive functional groups. These two groups account for most of its chemical reactions at ordinary temperatures and ordinary chemical environments.

In the following section, reactions of DMES which were investigated are discussed. Various applications of each reaction are also given. Figures 1 and 2 summarize these reactions.

Water Hydrolysis

When water is added to DMES, separation in two layers occurs due to immiscibility. Agitation of the liquids for a few minutes produces a homogeneous solution. The obvious hydrolysis reaction would be

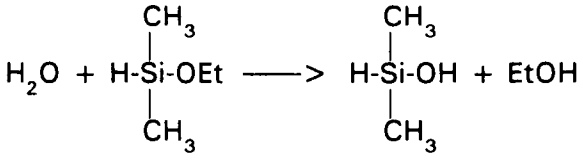

(1)

However, the resulting silanol has not been isolated (ref. 1). Indeed, the combination H-Si-OH does not occur in any known stable compound and is at best a very reactive intermediate. It is in this respect that DMES is unique compared to other common silylating agents. GCMS confirmed that the reaction of DMES and water produced ethanol and 1,1,2,2 tetramethylsiloxane. The net reaction is therefore

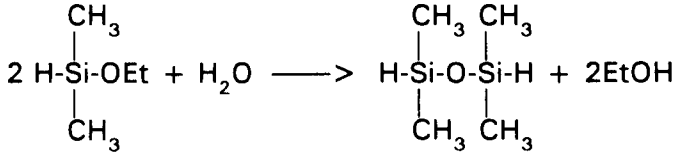

(2)

When DMES is applied to wet silica, this reaction will compete with the reaction of the DMES with silanol groups. However, infrared studies indicate that this is not a major factor for silica surfaces with physically adsorbed water, but could certainly be a major reaction if liquid water is present.

Reaction With Silica-OH Groups

Silylating agents typically hydrolyze to silanols which then react with the fixed silanols of the silica surface to produce the Si-O-Si (siloxane) linkage. However, since DMES does not produce a stable silanol, it is likely that it reacts directly with the surface hydroxyls:

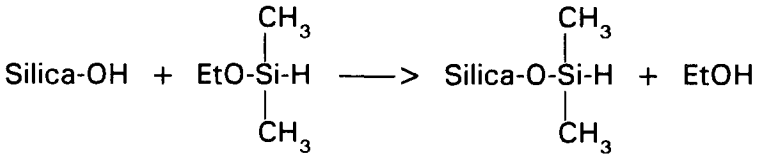

(3)

The reaction occurs reasonably fast even at room temperature, although it does not appear to replace all of the hydroxyl groups. The retention of the Si-H group during this reaction is confirmed by infrared spectra of cabosil treated with DMES (figures 3, 4).

Disproportionation

A major impurity in "old" DMES samples is found by GCMS to be diethoxydimethylsilane. For example, a bottle of DMES which was about two or three years old contained about 5% of the diethoxy compound. It has been noted in the literature that compounds containing H-Si-OEt disproportionate especially in the presence of a strong base which acts as a catalyst (ref. 2). Indeed, when dry NaOH is added to DMES, a vigorous reaction occurs accompanied by a small amount of heat released (which is characteristic of disproportionation) and also with the evolution of a gas. The disproportionation reaction is as follows.

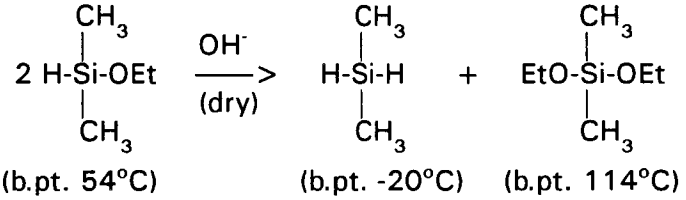

(4)

Both of the products have been confirmed by GCMS.

The above reaction might account for the slow pressure build up observed in containers of DMES and the presence of the diethoxy impurity. Reactions 5 and 6 (discussed in the next section) could also contribute H_2 gas as well. Figure 5 shows this pressure increase over a period of several days. The non-congruency of the lines of figure 5 is likely due to the absence of light during the night hours of the experiment, indicating a sensitivity of the reaction to light. Decomposition did continue to occur in an amber polypropylene bottle as well, indicating that some reaction occurs without catalytic effects of the glass surface or exposure to light.

The Si-H Group as a Reducing Agent

Hydrides of silicon are known to be good reducing agents. The -1 oxidation state of the hydrogen can be increased to 0 to produce H_2 gas or to +1 to produce water or hydrogen ions. Reactions which were examined involving the oxidation of DMES are given below.

1. Base catalyzed oxidation with alcohols.

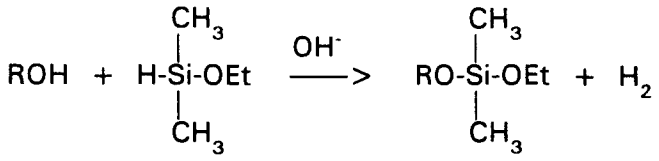

(5)

This reaction was utilized to synthesize diethoxydimethylsilane in order to verify its peak as a decomposition product in the GC of DMES. Ethanol was used as the alcohol and the reaction was vigorous even at room temperature.

2. Base catalyzed oxidation with water.

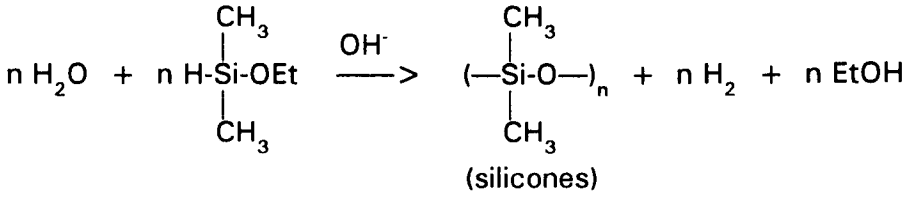

(6)

Alkaline water reacts with both the hydride and ethoxy groups to give a bifunctional monomer which can then form silicone polymers.

3. Oxidation with $Hg^{+2}(aq)$.

An aqueous solution of mercuric chloride is rapidly reduced by DMES to produce mercurous chloride and silicones. The combination of an oxidizing agent and water with DMES can always be expected to produce silicones. This reaction can be used to detect the Si-H group in silanes by the observation of the white precipitate, Hg_2Cl_2.

4. Oxidation with aqueous I_2 or Br_2.

Both I_2 and Br_2 oxidize DMES to produce silicones and either HI or HBr. The reaction with I_2, as expected, is slower than with Br_2. Both reactions have been used to perform quantitative oxidation-reduction titrations of DMES. Excess iodine or bromine was allowed to oxidize the DMES and then the excess halogen was determined using standardized sodium thiosulfate. The excess bromine was generated by using potassium bromate and excess potassium iodide.

5. Oxidation with Cu^{+2}.

When a saturated solution of $CuSO_4$ in methanol comes in contact with DMES in liquid or vapor form, it rapidly deposits a brown solid and produces hydrogen gas. The solid is probably metallic copper and Cu^+ salts. It provides a very sensitive test for DMES vapors.

6. Oxidation with Ag^+.

A silver nitrate solution (0.1 M in 50/50 water-methanol) reacts rapidly with DMES to produce H_2 and metallic silver. Initially, a yellow color appears which then disappears or is masked by the gray to black silver precipitate. This was used to examine silica shuttle tiles which had been treated with DMES. When the tile was treated with DMES, spraying it with the silver nitrate solution produced a gray color, presumably due to the reduction of the silver ions by the Si-H.

GAS CHROMATOGRAPHY STUDIES

Gas chromatograms were obtained for DMES in various stages of reaction with water and with sodium hydroxide. Dimethylsilicone stationary phases were employed on both packed and capillary columns in the chromatograph. The packed columns were operated isothermally at 50°C and utilized a flame ionization detector. The capillary columns utilized temperature programming and a mass spectrometer for the detector. All of the major peaks and many of the minor peaks were identified from the mass spectra obtained. Nearly all of the peaks could be accounted for in terms of expected hydrolysis and disproportionation products (reactions 2 and 4), with the disproportionation products then reacting with incidental moisture and the parent DMES molecule.

The following compounds are identified as major peaks coming off before twenty minutes on the capillary column (eight minutes on the packed column): $(CH_3)_2Si(OCH_2CH_3)_2$, $(CH_3)_2HSiOSiH(CH_3)_2$, CH_3CH_2OH, $(CH_3)_2H_2Si$, $(CH_3CH_2O)Si(CH_3)_2O(CH_3)_2SiH$, $(CH_3)_2HSiOSi(CH_3)_2OSiH(CH_3)_2$. Many of the minor components were identified as being polysiloxanes, both linear and cyclic. The above mentioned components were also found in a DMES sample which was two to three years old.

INFRARED STUDIES OF DMES TREATED SILICA

Cabosil is a high surface area silica powder which is chemically similar to crystalline quartz and fibrous silica. Cabosil samples can be prepared for infrared spectroscopy studies by lightly pressing the powder sample between two salt plates of a demountable liquid cell. The apparatus used for room temperature studies of cabosil and DMES is shown in figure 6. After reacting in the apparatus, a portion of the cabosil powder was then pressed between the salt plates to a thickness of about 0.5 mm. Before discussing the results of infrared studies, a brief discussion of silica surfaces is given.

The Nature of Silica Surfaces

Silica is known to have a strong affinity toward water adsorption. This tendency is due to the silica surface hydroxyls of which there are two types, isolated hydroxyls and vicinal hydroxyls (ref. 4). The vicinal hydroxyls can form hydrogen bonds to each other and can retain water on the surface by forming hydrogen bonds to the adsorbed water. Surprisingly, it appears that isolated hydroxyls do not hydrogen bond to water molecules (no infrared shift) and therefore contribute

little to water adsorption (ref. 4). However, Lewis base compounds such as amines are preferentially adsorbed on the isolated hydroxyls. Also, other factors being equal, the isolated hydroxyls are more reactive than the hydrogen bonding hydroxyls (ref. 4, 5, 6).

Figure 8 shows the infrared spectrum of cabosil obtained by pressing the cabosil powder between two salt plates 0.5 mm apart. This sample technique was used previously and the absorption band assignments are as follows (ref. 3).

3750 cm^{-1} is the stretching vibrations of isolated surface hydroxyls (sharp peak due to no interaction of isolated hydroxyls groups)

3660 cm^{-1} is due to vicinal hydroxyl groups which hydrogen bond to each other and thus give a broad absorption band

3450 cm^{-1} is a broad band due to water adsorbed on the silica surface

Typically, silica surfaces have from one to four hydroxyls per 100 square angstroms of surface (ref. 7). Raising the temperature destroys the vicinal hydroxyls by eliminating water. This occurs in the temperature range of 450 - 800°C and is known to be somewhat irreversible. The isolated hydroxyls (usually about one per 100 square angstroms) persist even at these elevated temperatures. Replacement of the surface hydroxyls by non-hydrogen bonding groups drastically reduces the wettability of the material.

A Method for Determining Surface Hydroxyls

Fripiat and Uytterhoeven (ref. 7) determined the OH content of cabosil using the methyl-Mg Grignard reagent to generate methane gas with the surface OH groups. Cabosil was shown to contain one to four hydroxyls per 100 square angstroms of surface area depending upon the temperature. This value should be applicable to the shuttle tile surface as well since it is essentially pure silica except that it would have a much smaller surface area per gram than cabosil. The technique developed here to determine surface hydroxyls on silica is as follows.

1. Substitute Cl for surface OH groups (ref. 8).

$$\text{Silica-OH} + CCl_4 \xrightarrow[N_2]{550^\circ C} \text{Silica-Cl} + COCl_2 + HCl \qquad (7)$$

2. Hydrolyze the chloride (or fluoride) with water.

$$\text{Silica-Cl} + HOH \longrightarrow \text{Silica-OH} + HCl \qquad (8)$$

3. Titrate the liberated HCl (or HF) with standardized NaOH solution.

We were able to replace the hydroxyls of silica using freon 12, CCl_2F_2. The reaction is conjectured to be

$$\text{Silica-OH} + CCl_2F_2 \xrightarrow[550°C]{} \text{Silica-F} + COCl_2 + HF \qquad (9)$$

It was also found that freon 22, $CHClF_2$, worked equally well to produce the fluorinated surface.

Five grams of hydrolyzed cabosil halide neutralized about 35 ml of 0.1 M NaOH. The same amount of shuttle tile treated the same way only neutralized 0.4 ml of the same NaOH solution. From this, it can be calculated that the cabosil contains about 0.7×10^{-3} moles of surface hydroxyls per gram. This is consistent with previous data reported in the literature using a completely different method (ref. 7). The shuttle tile silica by the same calculations then has about two orders of magnitude less hydroxyl groups (due to less surface area) or about 1×10^{-5} moles/gram. From these data, it can be calculated that the stoichiometric amount of DMES needed to completely react with shuttle tiles is about one milligram of DMES per gram of tile. Cabosil is known to have a surface area of about 200 m^2/g and therefore the shuttle tiles silica is estimated to have less than 10 m^2/g silica of surface area. This low hydroxyl content of the shuttle tiles explains why it is difficult to see reacted DMES on treated tiles by infrared spectroscopy but it can be seen on cabosil surfaces.

Figure 7 shows the spectra of cabosil samples before and after treatment with CCl_4 and CCl_2F_2 (freon 12) at 550°C. Both reagents cleanly remove the surface hydroxyls and replace them with chlorine or fluorine atoms. Both chlorinated and fluorinated cabosil surfaces give essentially the same spectra, except for the weakly discernible SiF band at 900 cm^{-1}. The surface treated with CCl_4 was shown to be chlorinated by hydrolysis of the surface and treating the solution with $AgNO_3$ to obtain the white AgCl precipitate. The surface treated with freon 12 is likely to be fluorinated, since a negative test for chloride was obtained for the hydrolyzed product, and a band at 900cm^{-1} is observed in freon-treated samples. Interestingly, both fluorinated and chlorinated cabosils and shuttle tile silica resisted wetting with water until hydrolysis took place, which was after about one hour of contact with water. Similar results for fluorinated porous glass were obtained using an entirely different process (ref. 9).

Infrared Detection of Attached Silyl Groups

Figure 3 shows the effect of reaction of the cabosil with DMES. As water adsorbency decreases, the hydroxyl peaks also diminish as well. Note, however, a new prominent peak at 2150 cm^{-1} which is due to the Si-H group. This peak persists even after heating the cabosil at 130°C under a vacuum. This indicates that the Si-H group does not significantly react with the surface hydroxyls. The small peaks at about 2900 cm^{-1} are due to methyl groups of the silane that have bonded to the surface.

Figure 4 contrasts cabosil surfaces reacted with DMES and hexamethyldisilizane (HMDS). The HMDS provides $(CH_3)_3Si$-O- groups for bonding to the surface by replacing the surface hydroxyls. DMES provides $(CH_3)_2Si(H)$O- groups for bonding. The differences can be seen in the infrared spectra. As expected, both HMDS and DMES treated cabosil give infrared peaks characteristic of C-H groups around 2900 cm^{-1}, but only the DMES spectrum has the Si-H band at 2150^{-1}cm.

Thermal Stability of DMES Treated Cabosil

In order to examine the thermal stability of DMES treated silica, the specially constructed gas cell shown in figure 8 was used. A heating tape was wrapped around the center portion of the cell to control the temperature in the cell. A thin silica wafer was made by pressing cabosil powder between two stainless steel plates in a hydraulic press to a pressure of about 5000 lb/sq in. The resulting wafer was about 1.5 x 2.0 cm and weighed about 40 to 50 mg. The wafer could then be mounted into the holder which was then placed into the cell. Generally, the wafers were dried at room temperature by applying a vacuum and then reacted with DMES vapor at about 100 mm Hg pressure. The excess DMES was removed by vacuum again and the IR spectrum obtained. Subsequently, 50% R.H. air was admitted to the cell and then heated to various temperatures, held at the temperature for twenty minutes, and then the air was expelled and the cell cooled down to room temperature before the IR spectrum was taken. Representative spectra are given in figure 9.

The stability of DMES on silica is inferred by observing the Si-OH, C-H and Si-H peaks. It is evident that the groups C-H and Si-H begin to diminish in the 400 - 500°C range while the Si-OH peaks begin to increase. This range for thermal breakdown is consistent with other work for silylated silica surfaces containing Si-H and Si-CH groups which also report decomposition of these groups in the 400 - 500°C range in air (refs. 10, 11).

After heating to the highest temperature, 640°C, a silica wafer was retreated with DMES under the same conditions as previously described. Figure 10 indicates that there are qualitative differences in the silane bonded to silica upon retreatment as compared to initial treatment. The broad Si-OH peak was smaller in the retreated sample. This can be explained by the known phenomena of irreversible dehydration of silica surfaces at high temperatures (ref. 4). Adjacent Si-OH groups on the surface are converted to Si-O-Si bridges at high temperatures and these bridges persist even when the sample is recooled to room temperature.

More significantly, it is noted that even though the C-H and Si-H peaks reappear on the DMES for the retreated silica, the Si-H peak is diminished in size, suggesting that the thermally degraded surface has oxidized some of the Si-H groups of the reacting DMES. Also it is noted that in figures 9 and 10 the spectra of the samples that have experienced a temperature of 640°C indicate a new kind of surface hydroxyl may be forming. These results are consistent with the following representation of the thermal degradation of the silylated surface.

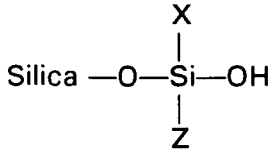

Here X and Z could be additional OH groups or partially oxidized methyl groups which could function as oxidizing agents. Certainly it is evident that repeated retreatment of partially degraded silylated silica surfaces is likely to give new surfaces which are not easily characterized.

CONCLUSIONS

Dimethylethoxysilane has a varied chemistry involving the hydride group which can act as a reducing agent and the ethoxy group which can react with water and silanol groups. These two groups can switch places intermolecularly by disproportionation under basic conditions. In view of this, it is not surprising that DMES readily produces a variety of products in the presence of small amounts of moisture or bases. A major impurity in aged DMES is diethoxydimethylsilane which can hydrolyze to produce silanols which in turn can react with itself and the parent DMES compound. Most of the products identified in an aged sample of DMES by GCMS can be accounted for in terms of this reaction scheme.

Using a high surface area form of silica called cabosil, infrared spectroscopy studies indicate that DMES reacts with the Si-OH groups by way of the ethoxy group. The silylated surface degrades in air beginning at temperatures of about 400°C which coincidentally is the same temperature the vicinal (adjacent) Si-OH groups of silica begin dehydrating to form Si-O-Si bridges. The infrared studies also suggest that the thermally degraded silylated surfaces which are retreated with DMES will produce attached silyl groups which are varied and not easily characterized. After many retreatments with DMES, the structure of the silylated surface could be much different from the initially treated surface.

ACKNOWLEDGMENTS

This work was supported in part by a grant from NASA Johnson Space Center in Houston, Texas. Mr. Keith Albyn and Mr. Randy Peters are acknowledged for their assistance in some of the GCMS work. Also, several undergraduate students from LeTourneau University assisted in the experimental work.

REFERENCES

1. Ebsworth, E. A.: *Volatile Silicon Compounds*. Pergamon Press, 1963, p. 35.

2. Eaborn, C.: *Organosilicon Compounds*. Academic Press, 1960, p. 213.

3. McDonald, R. S.: *J. Am. Chem. Soc.*, 79, 1957, p. 850.

4. Hair, M. L.: *Chemically Modified Surfaces, Vol. 1, Silanes, Surfaces and Interfaces*. Gordon and Breach Science Publishers, 1986, p. 26.

5. Hertl, W.; and Hair, M. L.: *J. Phys. Chem.*, 75, 1971, p. 2181.

6. Basila, M. R.: *J. Chem. Phys.*, 35, 1961, p. 1151.

7. Fripiat, J. J.; and Uytterhoeven, J.: *J. Phys. Chem.*, 66, 1962, p. 800.

8. Peri, J. B.: *J. Phys. Chem.*, 70, 1966, p. 2937.

9. Elmer, T. H.; and Chapman, I. D.; and Nordberg, M. E.: *J. Phys. Chem.*, 67, 1963, p. 2219.

10. Mahias, J.; and Wannamacher, G.: *J. Colloid Interface Sci.*, 1, 1988, p. 125.

11. Pesek, J. J.: *Chemically Modified Oxide Surfaces*, vol. III. Gordon and Breach Science Publishers, 1990, p. 99.

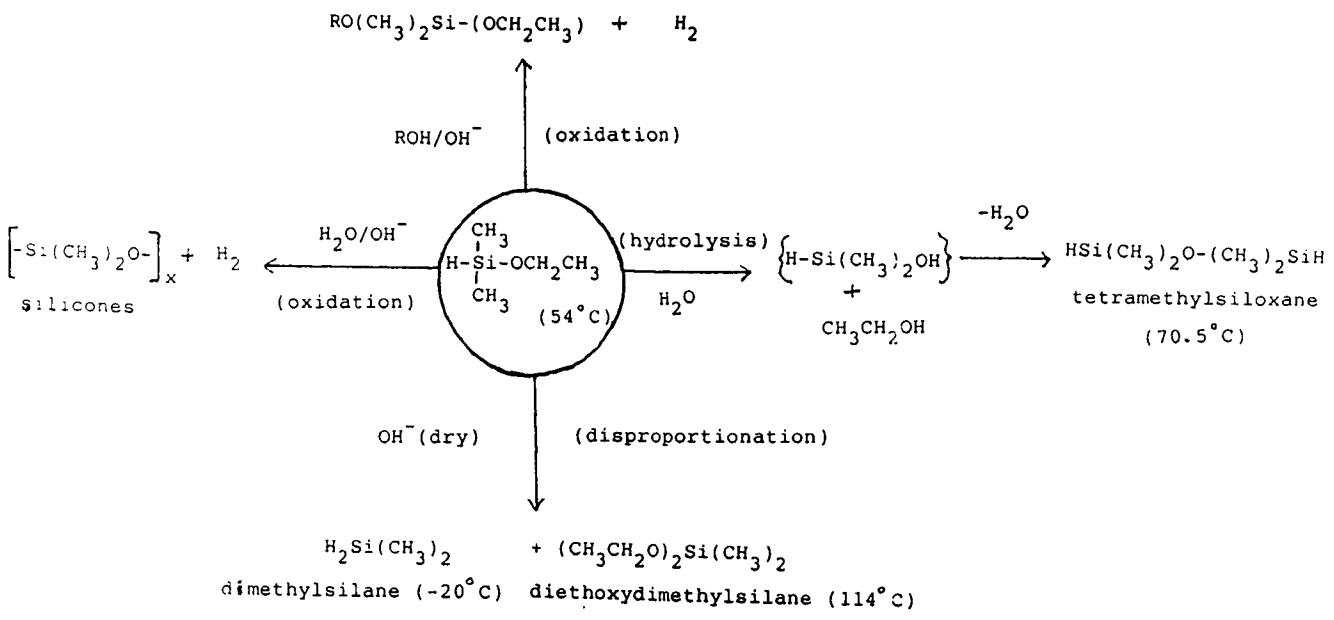

Figure 1. Reactions of dimethylethoxysilane in the presence of water or base.

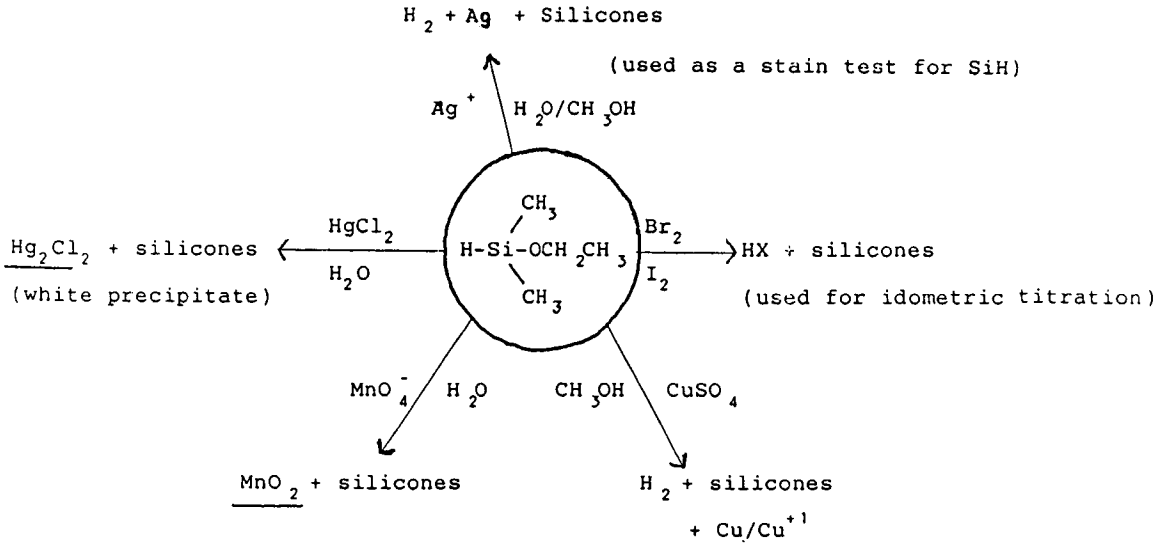

Figure 2. Miscellaneous oxidations of dimethylethoxysilane which can serve for for qualitative and for quantitative determination of the Si-H group.

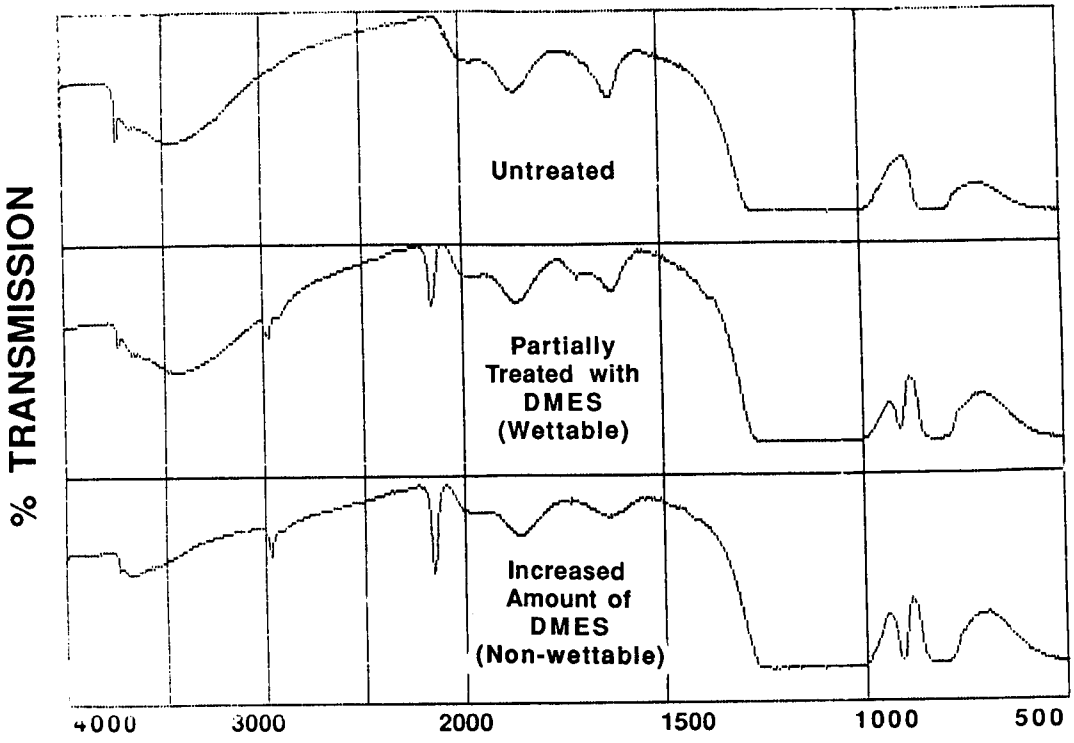

Figure 3. Infrared of cabosil powder in various stages of reaction with dimethylethoxysilane vapors at room temperature.

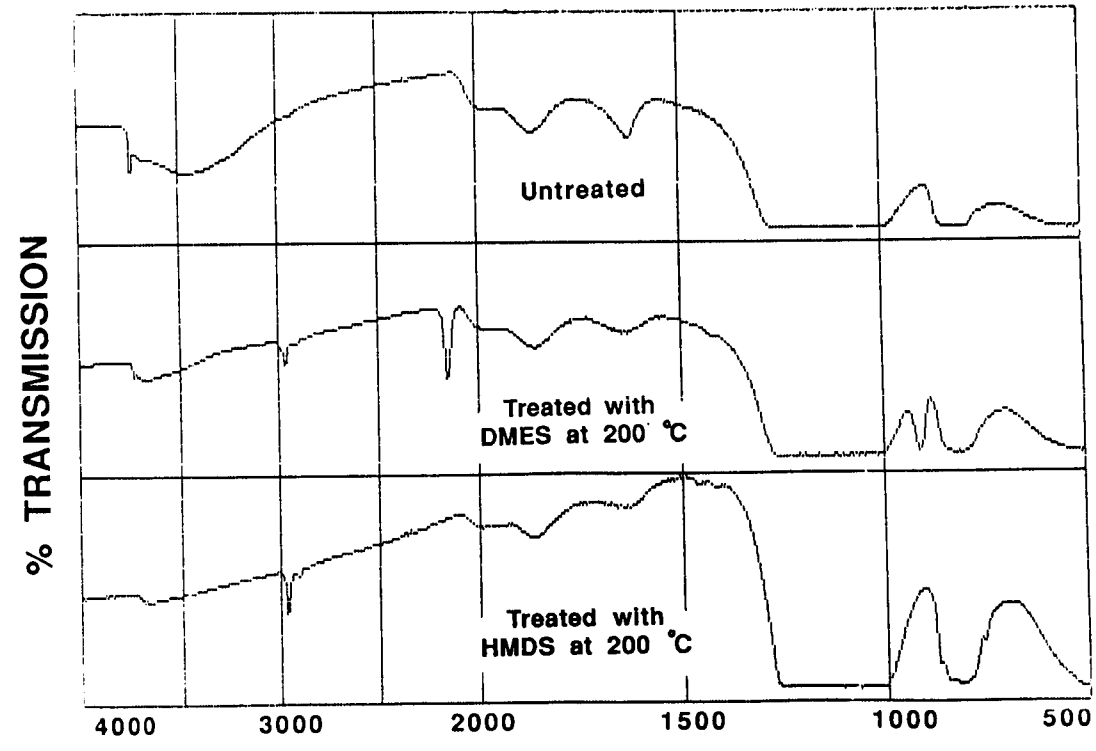

Figure 4. Infrared of cabosil powder before and after treatment with dimethylethoxysilane (DMES) and hexamethyldisilazane (HMDS) vapors.

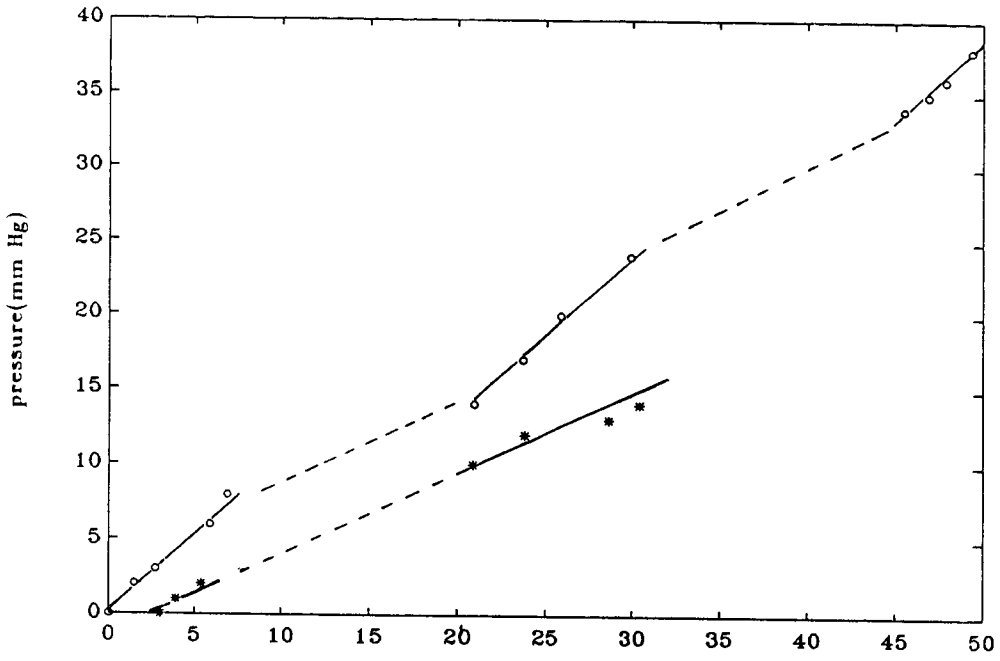

Figure 5. Pressure build-up over DMES in a closed container immersed in a 26°C water bath. Circles denote data collected when using a clear pyrex glass container. Asterisks denote data collected when using an amber polypropylene container. Dashed lines are periods when the lab lights were off.

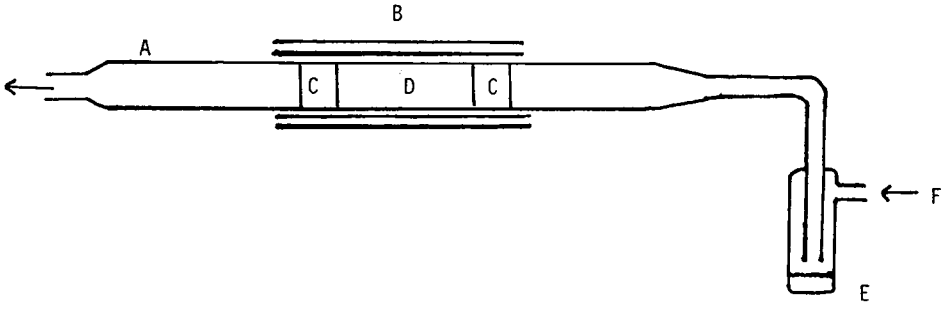

Figure 6. Apparatus for chemical treatment of cabosil powder. Legend:
A - quartz tube, B - furnace, C - porous silica plugs,
D - cabosil sample, E - DMES or other agents,
F - nitrogen gas.

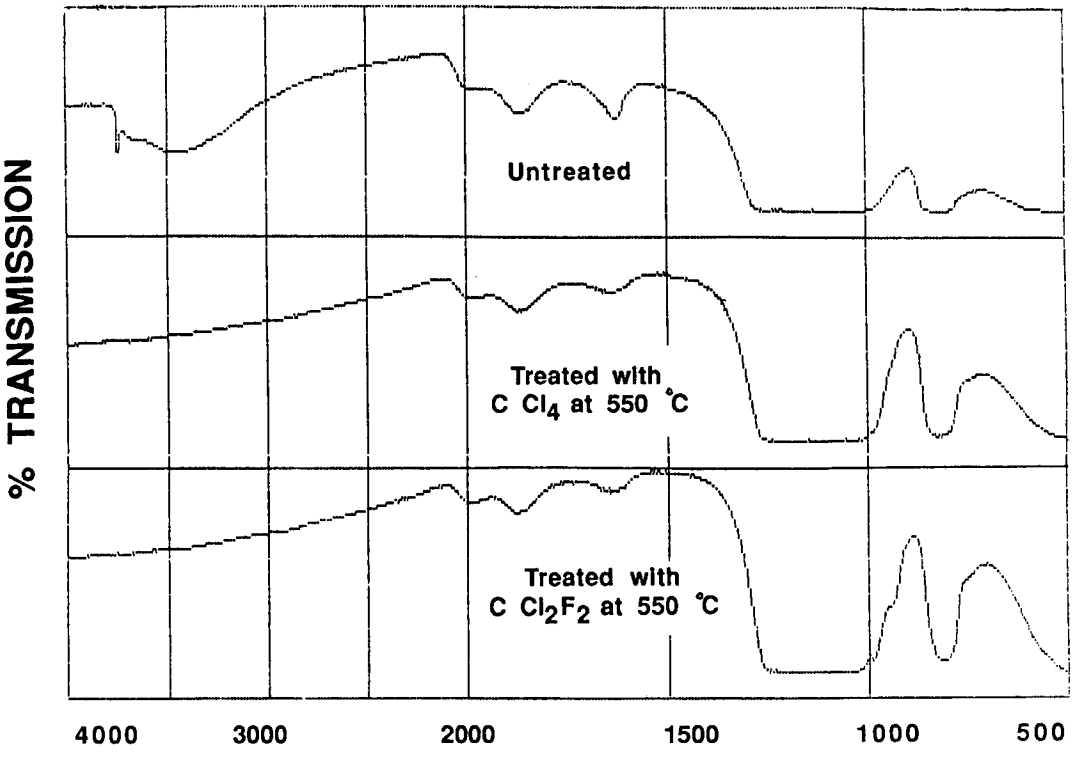

Figure 7. Infrared spectra of cabosil before and after treatment with carbon tetrachloride or freon 12.

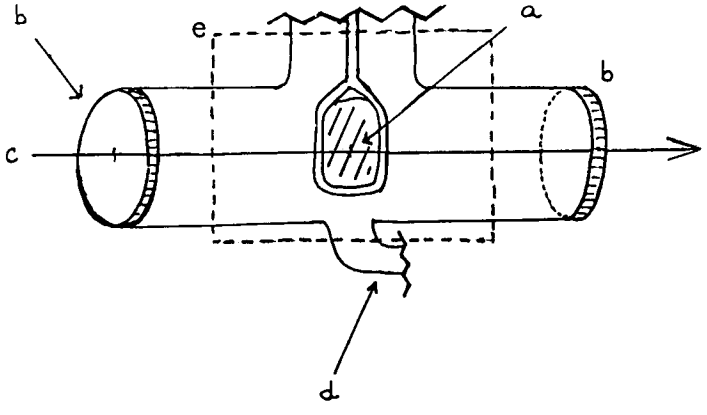

Figure 8. Infrared cell used for thermal studies of DMES-treated cabosil. Legend: a - silica wafer ($\approx$ 3 cm^2 x 0.25 mm, $\approx$ 45 mg, 5000 lb/in^2), b - sodium chloride plates, c - infrared beam, d - access port, e - heated area.

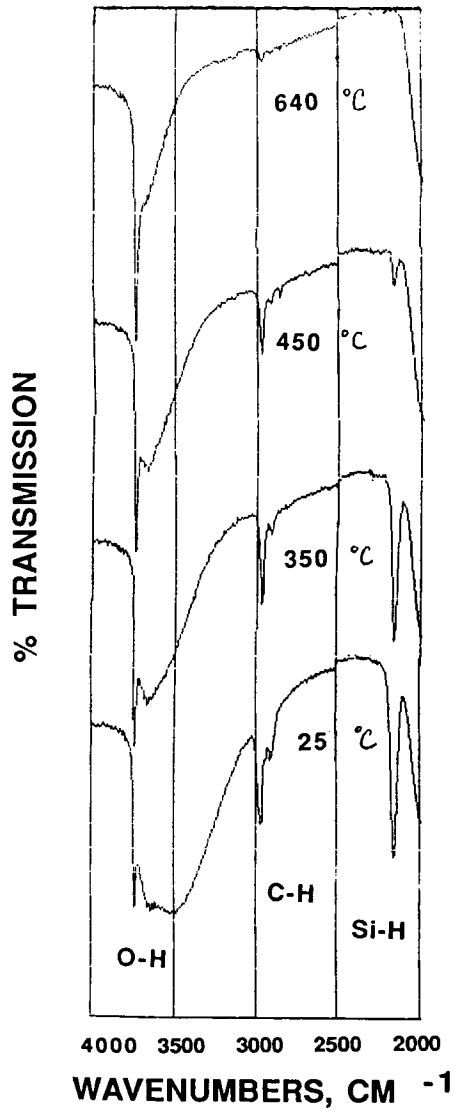

Figure 9. Infrared spectra of DMES-treated cabosil wafers at various temperatures.

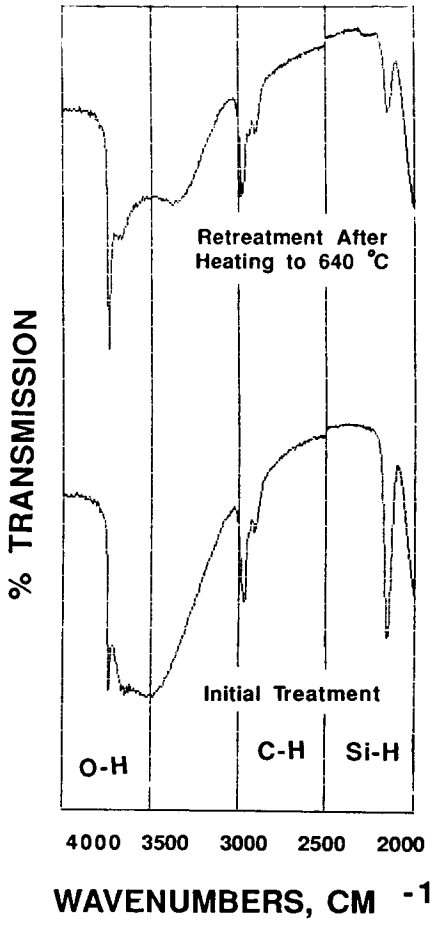

Figure 10. Infrared spectra of DMES-treated cabosil wafer showing the difference in silyation for a new sample as opposed to a sample which had been treated and then thermally degraded before retreatment.

N93-28259

LDEF POLYMERIC MATERIALS: 10 MONTHS VS. 5.8 YEARS OF EXPOSURE

Philip R. Young
NASA Langley Research Center
Hampton, VA 23681-0001
Phone: 804/864-4265, Fax: 804/864-8312

Wayne S. Slemp
NASA Langley Research Center
Hampton, VA 23681-0001
Phone: 804/864-1334, Fax: 804/864-7729

Alice C. Chang
Lockheed Engineering and Science Company
Hampton, VA 23666
Phone: 804/864-4267, Fax: 804/864-8312

SUMMARY

The chemical characterization of several polymeric materials which received 10 months of exposure and 5.8 years of exposure on a Row 9 Long Duration Exposure Facility (LDEF) experiment (A0134) is reported. Specimens include fluorinated ethylene propylene (FEP) teflon film, polysulfone film and graphite fiber reinforced epoxy amd polysulfone matrix composites. The responses of these materials to the two LEO exposures are compared.

The results of infrared, thermal, x-ray photoelectron, and scanning electron microscope analyses are reported. Solution property measurements of various molecular weight parameters are presented for the thermoplastic polysulfone materials. Molecular level effects attributable to exposure that were present in 10-month exposed specimens were not found in 5.8-year exposed specimens. This result suggests that increased atomic oxygen fluence toward the end of the LDEF mission may have eroded away selected environmentally induced changes in surface chemistry for 5.8-year exposure specimens.

INTRODUCTION

The NASA Long Duration Exposure Facility (LDEF) was retrieved from low Earth orbit (LEO) by the Space Shuttle Orbiter Columbia on January 10, 1990. Shortly after that event, the most detailed analysis began of space-exposed materials in the history of the U.S. Space Program. The knowledge being derived from experiments and specimens which spent 5.8 years on LDEF during its 34,000 orbit/three-quarters of a billion mile flight will be the baseline for environmental effects on materials well into the 21st Century. This paper reports the chemical characterization of two sets of polymeric materials which received 10-month and 5.8-year exposures on this remarkable space vehicle.

Previous research in this laboratory dealt with a broad assessment of a variety of polymer films (1-3) and polymer matrix resin composite materials (4,5) on two Langley

PRECEDING PAGE BLANK NOT FILMED

Research Center LDEF experiments. With the completion of that assessment came the opportunity to examine individual polymers and phenomena in greater detail.

Materials in the present study are unique because some specimens were flown inside an Experiment Exposure Control Canister (EECC). This canister was closed when LDEF was launched. The EECC opened as programmed 1 month after deployment and closed 10 months later. Specimens of similar materials were placed outside the canister and, thus, received the full 5.8-year exposure. Table I gives environmental exposure conditions pertinent to these two sets of samples. The analysis of these 10-month materials in the EECC is enabling some interesting comparisons with materials which received full exposure.

Figure 1 gives a preflight photograph of Langley's LDEF materials experiment tray. The tray was integrated onto the LDEF structure on Row 9 and Tray B and flew nominally in the RAM direction on the leading edge (6). Recent LDEF supporting data analyses have determined that the actual RAM direction was 8° of yaw from the perpendicular to Row 9, in the direction of Row 10. This tray contained two materials experiments, one dealing with composites (7), and one dealing with coatings and films (8). Most composite specimens are located on the right side of the panel in the photograph. A matching set of pre-cut flight control specimens flew underneath that panel and, thus, were protected from direct exposure. Additional coatings, films, and smaller composite specimens are shown in the center of the tray. The EECC is shown in the open position on the left side of the experiment tray. Many specimens on the experiment tray were held in place by an aluminum template with machined 0.81-inch and 1.35-inch exposure holes.

The detailed chemical characterization of FEP Teflon film, polysulfone film, and graphite fiber reinforced epoxy and polysulfone matrix composites is examined in this report. This characterization included ultraviolet-visible and infrared spectroscopic analyses, thermal analyses, x-ray photoelectron spectroscopy, scanning electron microscopy, and selected solution property measurements of various molecular weight parameters. The intent of this study is to add to the body of knowledge of space environmental effects on materials being derived from the LDEF mission.

EXPERIMENTAL

A description of film and composite materials is given in Table II. Udel P1700 polysulfone film was fabricated in-house from dried resin pellets by applying pressure to a mold heated to 250-300°C and maintaining that pressure for 1 hour before cooling. Other films were obtained from commercial sources or synthesized at Virginia Tech. (9). The fabrication, quality control, specimen preparation, and baseline testing of the composite materials were covered in previous reports (10,11). In general, composite specimens were cut from larger panels processed at the Langley Research Center using prepreg manufacturers' specifications. Matching sets of specimens remained at Langley in a low humidity environment as controls.

Chemical Characterization. The equipment and techniques used to make solution property measurements have been previously reported (12). Gel Permeation Chromatography (GPC) was performed on a Waters Associates System in chloroform using a $10^6/10^5/10^4/10^3$ Å Microstyragel column bank. The chromatograph was interfaced with a Viscotek (Viscotek Corp., Porter, TX) Model 100 Differential Viscometer (DV). Thermal analyses were conducted using a DuPont 9900 Thermal Analyzer to process data from DuPont's Model 910 Differential Scanning Calorimeter (DSC) or Model 943 Thermomechanical Analyzer (TMA). Infrared spectra were recorded on a Nicolet 60SX Fourier Transform Infrared System (FTIR) either in

the transmission mode or using a diffuse reflectance (DR) technique (13). Ultraviolet-Visible (UV-VIS) spectra were scanned on a Perkin-Elmer Lambda 4A Spectrophotometer.

A Cambridge StereoScan 150 (Cambridge Instruments, Deerfield, IL) was used for Scanning Electron Microscopy (SEM). An EDAX S150 detecting unit (EDAX International Inc., Prairie View, IL) on the SEM was used to perform Energy Dispersive Spectroscopy (EDS) analyses. The visual appearance of selected specimens was documented using various photographic techniques.

X-ray Photoelectron Spectroscopy (XPS) measurements were conducted at the Virginia Tech Surface Analysis Laboratory (14). Measurements were made on a Perkin-Elmer PHI 5300 Spectrometer equipped with a Mg Kα source (1253.6 eV) operating at 15kV/120mA.

DISCUSSION

The chemical and physical response of selected epoxy and polysulfone matrix/graphite fiber reinforced composite materials to 5.8 years of Row 9 exposure has been discussed in previous reports (3-5). The performance of silvered FEP Teflon thermal blanket material after 5.8 years of exposure at various locations has also been the subject of numerous investigations (2,15). The comparison of these materials with identical materials which received only the 10-month, Row 9 exposure provided by the EECC is enabling complementary performance information to be developed.

Polymer Films

FEP Teflon. The only film which survived both the 10-month EECC exposure and the 5.8-year experiment tray exposure was 5 mil thick FEP Teflon. Other thinner, 1 mil thick polymeric films flown outside the canister on this Row 9 experiment failed to survive. Silvered FEP material was flown in both locations; FEP film was only flown inside the EECC. Inspection of FEP and Ag/FEP canister specimens showed no visible effects of exposure. The frosted or diffuse appearance of Ag/FEP after 5.8 years is well documented (2,15).

Figure 2 is the UV-VIS transmission spectrum of the 10-month FEP film. The spectrum was superimposable over that for the control specimen. Figure 3 gives total reflectance curves for Ag/FEP specimens for both exposures. The solar absorptance, α_s, changed only marginally after 5.8 years. Greater detail on the optical and thermal properties of this material may be found elsewhere in this publication (16).

In an earlier study, a small new band near 1730cm^{-1} was found by subtractive FTIR techniques in the 5.8-year Ag/FEP specimen (2,3). In that study, no other significant differences were noted by FTIR or DSC as a result of exposure. This small 1730cm^{-1} band was also found in the 10-month specimen by subtracting the FTIR spectrum of the exposed specimen from that for the control. This band is most likely due to the formation of surface carbonyl groups as the result of exposure to the LEO environment. The carbonyl in the infrared spectrum correlated with a 0.5% atomic concentration of oxygen found in this specimen by XPS. No additional molecular level changes were noted with this 10-month specimen. Thus, except for minor changes in surface chemistry, this material was remarkably stable during 10 months of exposure.

Additional Canister Films. In contrast to FEP Teflon film, which showed no visible effects of exposure, other canister films exhibited effects of 10 months in LEO. Figure 4 gives photographs of P1700, Kapton, Kynar, and PIPSX films. The first three films are polysulfone, polyimide, and fluorinated hydrocarbon materials, respectively. PIPSX is an experimental polyimide-polysiloxane block copolymer (9). The exposed area for all four films are apparent in the photograph, as are template-protected areas around their edges. Figure 5 gives UV-VIS transmission spectra for the four materials. The decrease in transmission with exposure is primarily due to AO and UV. Except for P1700 and PIPSX films, no significant molecular level changes were noted by FTIR or DSC. The siloxane copolymer apparently formed a silica/silicate surface layer attributable to AO exposure (1). The performance of a series of PIPSX copolymers flown inside the EECC will be the subject of a future publication.

934/T300 Epoxy Composites

Figure 6 shows the SEM of T300 carbon fiber reinforced 934 epoxy matrix specimens for the two exposures. The 10-month and 5.8-year samples were placed adjacent to each other to enable simultaneous analyses. The left side low magnification photomicrograph shows both exposed surfaces, and surfaces protected from direct exposure by the aluminum retaining template. The fabric-appearing pattern visible in the micrograph was transferred to the composite surface by a glass cloth peel-ply during processing. The right side photomicrograph shows a higher magnification SEM of exposed regions of two specimens. Individual carbon fibers apparent with the 10-month composite are no longer distinguishable after 5.8 years.

Table III gives XPS data for control, 10-month, and 5.8-year epoxy composites. Surface carbon content increased in the first 10 months of exposure. This probably reflects increased carbon fiber content due to preferential erosion of matrix resin. Oxygen and sulfur did not appear to change significantly. Fluorine on the control likely resulted from release agent used during processing. Fluorine was not detected on exposed composites because this outer surface was eroded away by AO. The increased silicon content with exposure is no doubt due to the well-documented LDEF contamination. Additional chemical characterization including FTIR, TMA, and DSC failed to detect significant differences between the two specimens.

The origin and composition of the "white ash" on selected composite surfaces has become one of the mysteries associated with materials flown on LDEF (17). This ash on the 5.8-year 934/T300 epoxy composite was investigated in some detail. Figure 7 shows high magnification SEM photomicrographs of that specimen. Projections rising from the composite surface were apparently caused by contamination protecting underlying material from attack by atomic oxygen. The right hand photograph, obtained by overlaying three individual micrographs, shows graphite fiber fragments presumedly sheared off by AO. The white ash in question is visible at the base of this finger-like projection.

Figure 8 shows the ash at higher resolution. The residue appears to contain crystals on the order of 0.1μm in diameter. EDS analysis on these crystals, given in Figure 9, revealed sulfur to be a major component. This result was not expected. However, sulfur is present in the diaminodiphenylsulfone (DDS) cured epoxy matrix resin. Similar-appearing residues have been noted on DDS-cured 5208 epoxy and polysulfone composites. The exact chemical composition of this sulfur-containing species has not been established; sodium may be a counter ion. XPS data in Table III shows no unusual sulfur content for the 5.8-year specimen. Apparently, this analysis was not conducted on an ash-rich portion of the exposed composite. Future XPS analyses will focus on this portion (14).

The 934/T300 epoxy composites addressed in this paper were uncoated materials. Thus, they were attacked by the harsh LEO environment. Identical specimens protected with thin coatings, such as 1000Å of nickel followed by 600Å of silicon dioxide, exhibited outstanding resistance to surface erosion. Several inorganic coatings were found to be effective in preventing surface degradation (16).

Polysulfone Film and Composites

Pertinent information on LEO space environmental effects was also obtained by comparing the performance of polysulfone materials after 10 months of exposure with performance after 5.8 years of exposure. Figure 10 shows photographs of 10-month exposed film and 5.8-year exposed composite specimens. Dramatic visual effects in these specimens were primarily due to AO. Protected and exposed surfaces are easily distinguishable in Figure 10.

10-Month Exposed Polysulfone Film. Typical SEM photomicrographs of the polysulfone film are shown in Figure 11. The imprint from scratches on the mold is apparent on the surface of the control film, as are small surface impurities. This contamination, transferred during molding, apparently protected parts of the exposed specimen as evidenced by relief patterns present in that micrograph. AO erosion after 10 months was severe.

UV-VIS spectra of control and exposed film are included in Figure 5. Much of the decrease in transmittance is presumed to be due to UV degradation and AO roughening or "frosting" of the film surface. The glass transition temperature, T_g, of the film apparently was not affected by exposure. Essentially identical glass transition temperatures for control and exposed film were determined by DSC. The T_g of the two specimens determined by TMA and shown in Figure 12 are also identical. No significant change in T_g of any polymer flown on or near the RAM direction of LDEF has been found that could be attributed to LEO exposure.

In contrast to various thermal analyses which detected no difference between control and exposed specimens, FTIR characterization has shown interpretable differences between the two specimens. Figure 13 shows the transmission spectrum of a thin polysulfone film obtained in our laboratory under ideal conditions. Several band assignments have been made in the figure. Since the LDEF specimen was too thick for good quality transmission studies, somewhat poorer quality spectra of control and exposed specimens were obtained by diffuse reflectance (DR). Differences between the two diffuse reflectance spectra were difficult to establish until they were subtracted. The spectrum in Figure 14 is the result of subtracting the DR-FTIR spectrum of the exposed film from that of the control. A downward inflection in the curve is indicative of a larger amount of a particular species in the exposed spectrum.

The band centered around 3400cm^{-1} is most likely due to -OH. Bands at 1485 and 1237cm^{-1} may also be associated with that group. Reports in the literature have noted the 3400cm^{-1} -OH band for polysulfone film exposed to UV (18) and also to 3-MeV protons (19). Additionally, the loss of the 1385cm^{-1} methyl band was noted in at least one study (18). Methyl does not appear to have been lost in the present study. A diminished -CH_3 content would have resulted in an upward inflection in the subtraction spectrum at 1385cm^{-1}; no band is present around 1385cm^{-1} in Figure 14.

The presence of -OH has been explained by cleavage of the ether oxygen in the backbone of the polymer followed by abstraction of a proton (19), or by a photo-Claisen rearrangement of

the ether oxygen to produce an ortho-hydroxy substituted biphenyl linkage (20). This study made no determination of the origin of the -OH group.

Solution property measurements also revealed molecular level effects of the 10-month LEO exposure. Figure 15 shows the molecular weight distributions of three polysulfone specimens as determined by GPC-DV. Curves for control film, a template-protected specimen cut from around the yellowed edge of the sample, and a directly exposed center-cut specimen are given in the figure. Several points should be made. The solubility decreased from 100% to 96% to 87% for the three specimens. Note also the decrease in number average molecular weight (M_n) and the increase in weight- and z-average molecular weights (M_w and M_z) with exposure. This behavior is considered evidence for both chain scission and crosslinking, thus confirming predictions of ground-based simulation of space environment effects on this material (19-24).

10-Month Exposed Polysulfone Composite. The visual effects of 10 months of exposure of the polysulfone composite specimens were evident, but not as dramatic as those observed for similar specimens exposed for 5.8 years. Figure 16 shows the SEM of a 10-month specimen taken at 4250X magnification. While surface erosion is apparent, individual fibers can still be distinguished. TMA measurements of Tg for control and exposed samples, shown in Figure 12, suggest no change as a result of exposure. DSC measurement of Tg on composites in this study were inconclusive. Subtractive FTIR measurements on 10-month composite specimens showed the same behavior observed for 10-month film. The subtraction composite spectrum is included in Figure 17. The spectrum for the 10-month exposed film is repeated in this figure for comparison purposes. The decreased intensity of the 3400cm^{-1} -OH band for the 10-month exposed composite may be due in part to surface resin content dilution by graphite fiber which probably eroded more slowly than the resin. Solution property measurements on 10-month composite specimens show the general behavior observed on film and given in Figure 15 but less dramatically.

5.8-Year Exposed Polysulfone Composites. As illustrated in Figure 10, 5.8 years of exposure led to severe erosion. Almost one ply of the 4-ply composite was lost. Figure 16b shows the SEM of this material. Both resin and fiber degradation are apparent. The "spider-web"-like residue in the micrograph has also been observed with thermoset composites on LDEF and on Kapton film from the space end of the vehicle (3).

TMA determination of T_g of the 5.8-year specimen, shown in Figure 12, did not detect a change attributable to exposure. An earlier more detailed TMA study of the same material also failed to show a change in T_g (4). Figure 12 illustrates the need to use correct controls when analyzing test specimens. While the three materials were processed at the same time, there were apparently sufficient differences in the cure cycles to produce three different glass transition temperatures. The use of the tensile specimen as a control for the 10-month specimen could have led to an erroneous conclusion.

The 5.8-year composite subtraction spectrum given in Figure 17 is essentially a straight line. This result suggests very little difference in infrared spectra of control and 5.8-year exposed composites. A similar y-axis sensitivity was used to obtain the three spectra in the figure.

An earlier study reported molecular weight determinations made on 5.8-year exposed composite specimens (4). Two pertinent pieces of information from that study, the molecular weight distributions of unexposed resin and ground control, flight control, and flight exposed composites, along with a table of molecular weight values, are reproduced for convenience in Figure 18 and Table IV. The molecular weight distributions were separated for clarity when

Figure 18 was drawn. The distributions are virtually superimposable. Expected variations between techniques are noted for absolute molecular weight values in Table IV. However, a careful inspection of data for the same technique suggests no significant differences in various molecular weight parameters.

The XPS analysis of all specimens in this study is given in Table V. The release agent used during fabrication is apparently present on the control composite surface as evidenced by the 4.1% atomic concentration of fluorine for that sample. Calcium and aluminum were also detected. Silicon, the common LDEF contaminant, is also present with most samples, particularly the 5.8-year exposed composite. The oxygen content for that specimen is unusually high due to the likely formation of silica/silicate upon exposure of the contaminant to atomic oxygen (1, 2). These artifacts make a consistent interpretation of data in Table V difficult.

A Perspective. Evidence developed in this study suggests that molecular level effects present in specimens after 10 months of LEO exposure are not present after 5.8 years of exposure. This potentially contradictory observation is best understood by considering the orbit of the spacecraft during its flight. LDEF was deployed in an essentially circular orbit of 257 nautical miles on April 7, 1984 (25). It was retrieved 69 months later at an altitude of 179 nautical miles. Only about 2 months of orbit lifetime remained at retrieval. The atomic oxygen fluence differs greatly at these two altitudes.

Figure 19 is the approximate cumulative percent RAM AO fluence as a function of time. Exact AO exposure for these specimens is given in reference 26. The 10-month specimens were exposed early in the mission when AO fluence was at a minimum. The 5.8-year specimens received significant exposure near the end of the mission. As much as 50% of total AO exposure was received during the last 6 months in orbit. The molecular level effects observed after 10 months, primarily related to changes in surface chemistry, had most likely been eroded away by the time the satellite was retrieved. An earlier retrieval from a higher orbit may have provided different results.

A second point is also offered. The polysulfone film in this study received 10 months of LEO exposure. Subtle differences at the molecular level, most notably, infrared spectra and solution properties, have been documented. Can this information be used as a benchmark to calibrate ground-based simulation of LEO space environmental effects? If effects on materials described in this report can be simulated, then can the same conditions be used to simulate the effects of LEO exposure on other polymeric materials under consideration for space application? If this is possible, synergistic and accelerated effects may also be better understood.

CONCLUDING REMARKS

The LDEF is providing a wealth of information on the effects of exposure of polymeric materials to the LEO environment. The present study examined the response of several specimens to both 10 months and 5.8 years of RAM exposure on the vehicle. AO induced surface erosion was apparent in both film and composite specimens. Changes were detected in the UV-VIS and IR spectra of some materials after 10 months in LEO, as well as shifts in various molecular weight parameters. Those molecular level effects were not as apparent after 5.8 years of exposure. Rapid surface erosion due to increased exposure to AO toward the end of the mission probably erased some of these fundamental effects. The chemical characterization of additional LDEF-exposed polymeric materials is continuing. The ultimate benefits will be increased confidence in models for spacecraft materials performance in LEO and in better ground-based simulation of LEO space environmental effects on materials.

ACKNOWLEDGMENT

This report was not possible without the capable assistance of a number of individuals. The authors thank Carol R. Kalil, Emilie J. Siochi, Judith R. J. Davis, Karen S. Whitley, and Reta R. Barrett.

REFERENCES

1. P. R. Young, W. S. Slemp, and C. R. Kalil; SAMPE Intl. Symp., 37, 159(1992).
2. P. R. Young and W. S. Slemp; NASA TM 104096, December 1991.
3. P. R. Young and W. S. Slemp; NASA CP-3134, Part 2, 687(1991).
4. P. R. Young, W. S. Slemp, W. G. Witte, and J. Y. Shen; SAMPE Intl. Symp., 36(1), 40(1991).
5. W. S. Slemp, P. R. Young, W. G. Witte, and J. Y. Shen; NASA CP-3134, Part 3, 1149(1991).
6. L. G. Clark, W. H. Kinard, D. J. Carter, and J. L. Jones, Eds.; The Long Duration Exposure Facility (LDEF). NASA SP-473, 1984.
7. W. S. Slemp; NASA SP-473, 24(1984).
8. W. S. Slemp; NASA SP-473, 54(1984).
9. NASA Grant NAG-1-343, Virginia Polytechnic Institute and State University, Blacksburg, VA.
10. W. G. Witte, Jr.; NASA TM 87624, 1985.
11. W. G. Witte, Jr.; NASA TM 89069, 1987.
12. P. R. Young, J. R. J. Davis, and A. C. Chang; SAMPE Intl. Symp., 34(2), 1450(1989).
13. P. R. Young, B. A. Stein, and A. C. Chang; SAMPE Intl. Symp., 28, 824(1983).
14. NASA Grant NAG-1-1186, Virginia Polytechnic Institute and State University, Blacksburg, VA.
15. A. S. Levine, Ed.; NASA CP-3134, Parts 1, 2, and 3. LDEF-69 Months in Space, First Post Retrieval Symposium, Kissimmee, FL, June 2-8, 1991.
16. W. S. Slemp and P. R. Young, LDEF Thermal Control Coatings Post Flight Analysis. Presented at the Second LDEF Post-Retrieval Symposium, San Diego, CA, June 1992.
17. B. A. Stein and P. R. Young, Compilers; LDEF Materials Workshop '91, NASA CP-3962, 1992.

18. B. D. Gesner and P. G. Kelleher; J. Appl. Polym. Sci., 12, 1199(1968).

19. D. R. Coulter, M. V. Smith, F. Tsay and A. Gupta; J. Appl. Polym Sci., 30, 1753(1985).

20. S. Kuroda, A. Nagura, K. Horie, and I. Mita; Eur. Polym. J., 25(6), 621(1989).

21. J. R. Brown and J. H. O'Donnell; J. Appl. Polym. Sci., 19, 405(1975).

22. J. R. Brown and J. H. O'Donnell; J. Appl. Polym. Sci., 23, 2763(1979).

23. K. B. Kingsbury, D. S. Hawkins, R. A. Orwoll, R. L. Kiefer, S. A. T. Long, and G. F. Sykes; Macromolecules, 22, 3486(1989).

24. B. Santos and G. F. Sykes; SAMPE Tech. Conf., 13, 256(1981).

25. R. L. O'Neal and E. B Lightner; NASA CP-3134, Part 1, 3 (1991).

26. R. J. Bourassa and J. R. Gillis; Atomic Oxygen Exposure of LDEF Experiment Trays, NASA Contractor Report 189627, Contracts NAS1-18224 and NAS1-19247, May 1992.

TABLE I. ENVIRONMENTAL EXPOSURE PARAMETERS

	10-MONTH SPECIMENS	5.8-YEAR SPECIMENS
• ATOMIC OXYGEN	2.6 x 10^{20} atoms/cm^2	8.7 x 10^{21} atoms/cm^2
• UV RADIATION 100-400 nm	1,600 hours	11,100 hours
• THERMAL CYCLES	~4,900 -20 to 140°F (±20°)	~34,000 -20 to 160°F (±20°)

Integrated Tray Parameters

- PARTICULATE RADIATION
  e^- and p^+: 2.5 x 10^5 rad fluence
  cosmic: <10 rad
- MICROMETEOROID AND DEBRIS
  734 impact craters <0.5 mm
  74 impact craters >0.5 mm
- VACUUM
  10^{-6}-10^{-7} torr
- ALTITUDE/ORBITAL INCLINATION
  255-180 nautical miles/28.5°

TABLE II. MATERIALS

10-MONTH AND 5.8-YEAR SPECIMENS	EXPOSED THICKNESS	EXPOSED DIAMETER
SILVERED FEP TEFLON	5 mil	0.81 and 1.35 in
934/T300 EPOXY COMPOSITE	4 ply[a]	0.81 in
P1700/C6000 POLYSULFONE COMPOSITE	4 ply[a]	0.81 in and tensile specimen (0.024 in x 0.50 in x 8.0 in)
10-MONTH SPECIMENS		
FEP TEFLON FILM	5 mil	0.81 in
P1700 POLYSULFONE FILM	18 mil	0.81 in
KAPTON FILM	1.2 mil	0.81 in
KYNAR FILM	2.4 mil	0.81 in
POLYIMIDE-POLYSILOXANE COPOLYMER FILM	1.0 mil	0.81 in

[a] ~5 mil per ply.

TABLE III. XPS ANALYSIS OF 934/T300 COMPOSITES

Photopeak	Control	10-Month Exposed	5.8-Year Exposed
C 1s B.E.[a] (eV)	285.0 ... 292.3[c]	283.6 ... 289.7	283.9 ... 288.5
A.C.[b] (%)	68.9	73.3	72.1
O 1s B.E. (eV)	531.5/532.7/533.9	531.3 ... 534.0	531.1/532.5/534.8
A.C. (%)	18.1	18.8	19.7
S 2p B.E. (eV)	168.4	168.6	170.0
A.C. (%)	1.1	0.8	0.9
N 1s B.E. (eV)	399.9	399.6	400.6
A.C. (%)	3.4	5.5	0.8
Si 2p B.E. (eV)	103.2	103.7	104.0
A.C. (%)	1.0	0.9	6.4
Na 1s B.E. (eV)	1072.2	——	
A.C. (%)	2.0	NSP[d]	
F 1s B.E. (eV)	689.3	——	——
A.C. (%)	5.5	NSP	NSP

[a] Binding Energy. [b] Atomic Concentration. [c] Multiple Peaks.
[d] No Significant Peak.

TABLE IV. MOLECULAR WEIGHT OF POLYSULFONE MATRIX RESIN

Sample, Technique	[a] M_N	M_W	M_Z	M_W/M_N
Resin control				
GPC	19,000	70,000	117,000	3.8
GPC-DV	18,000	50,000	83,000	2.8
GPC-LALLS	21,000	46,000	74,000	2.2
Static LALLS		45,900		
Langley control				
GPC	18,000	68,000	113,000	3.9
GPC-DV	16,000	50,000	81,000	3.1
GPC-LALLS	18,000	40,000	65,000	2.1
Flight protected				
GPC	19,000	68,000	114,000	3.7
GPC-DV	17,000	53,000	87,000	2.9
GPC-LALLS	21,000	40,000	66,000	1.8
Flight exposed				
GPC	18,000	68,000	114,000	3.7
GPC-DV	17,000	48,000	80,000	2.9
GPC-LALLS	21,000	46,000	71,000	2.2

[a] Molecular weight in g/mole

TABLE V. XPS ANALYSIS OF POLYSULFONE SPECIMENS

Photopeak	Film		P1700/C6000 Composite		
	Control	10-Month Exposed	Control	10-Month Exposed	5.8-Year Exposed
C 1s B.E.[a] (eV)	285.0/286.6/288.9	283.5 ... 288.7[c]	283.6 ... 288.9	283.6 ... 288.9	282.0 ... 293.0
A.C.[b] (%)	82.2	79.2	75.5	66.5	25.0
O 1s B.E. (eV)	532.1/533.2/534.3	528.3 ... 534.9	530.7/532.0/533.2	530.3 ... 534.5	530.2 ... 534.5
A.C. (%)	14.3	18.6	14.6	12.4	52.0
S 2p B.E. (eV)	168.7	168.4	167.9	169.9	169.6
A.C. (%)	1.3	0.4	0.5	2.5	2.9
N 1s B.E. (eV)	400.2	399.9	399.8	399.7	400.6
A.C. (%)	1.2	1.8	1.0	1.1	0.3
Si 2p B.E. (eV)	102.4	—	102.4	103.5	103.7
A.C. (%)	1.1	NSP[d]	1.3	2.3	17.4
F 1s B.E. (eV)			688.9	—	—
A.C. (%)			4.1	NSP	NSP
Ca 2p B.E. (eV)			347.6/351.1		348.5/351.0
A.C. (%)			1.3		1.0
Al 2p B.E. (eV)			74.7	75.3	—
A.C. (%)			1.8	2.0	0.3

[a] Binding Energy. [b] Atomic Concentration. [c] Multiple Peaks. [d] No Significant Peak.

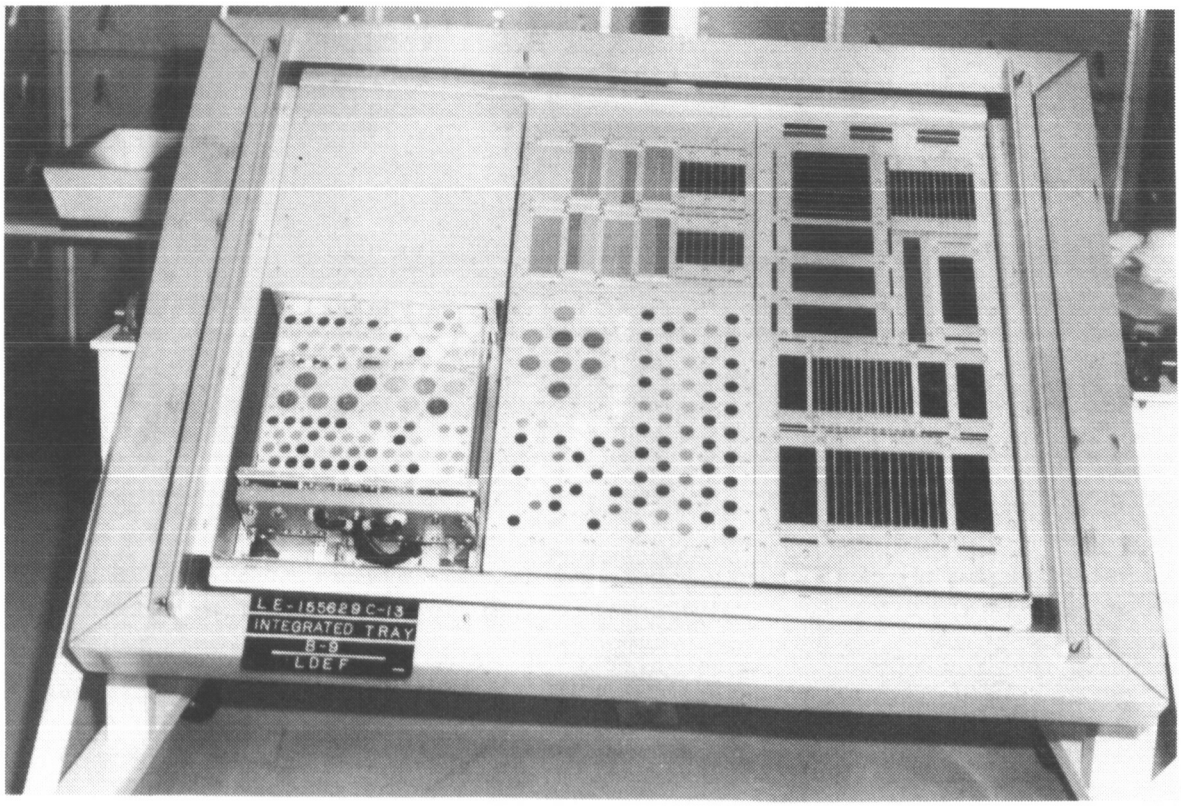

Figure 1. Preflight photograph of LDEF materials experiment tray.

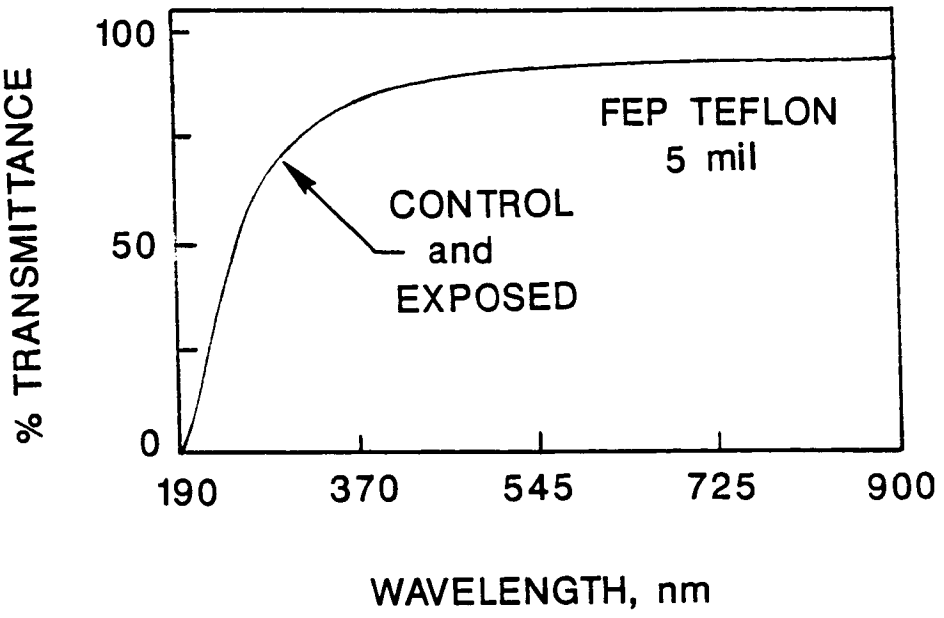

Figure 2. UV-VIS transmission spectrum of 10-month LDEF exposed FEP Teflon film.

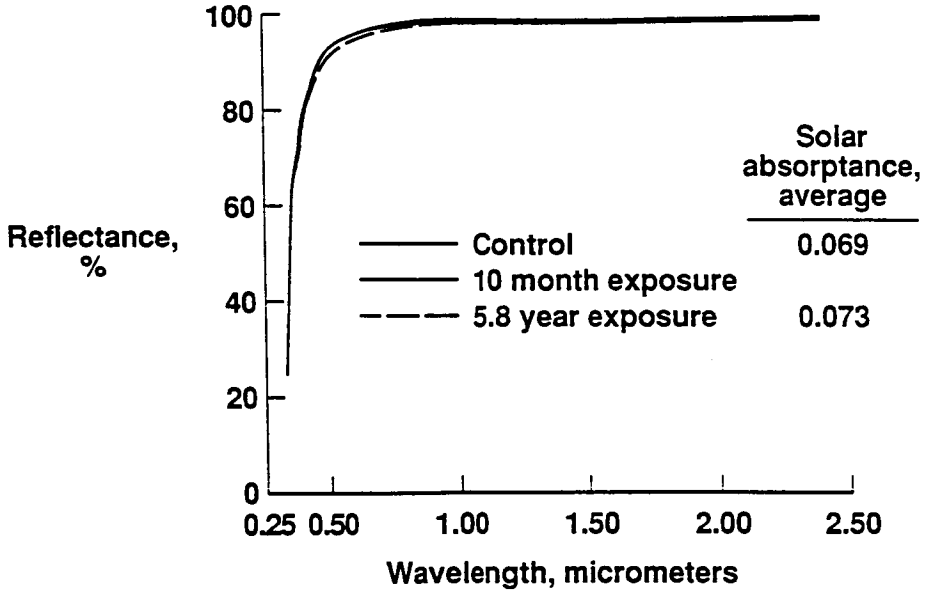

Figure 3. Total reflectance spectra for 10-month and 5.8-year exposed silvered FEP Teflon thermal control coating.

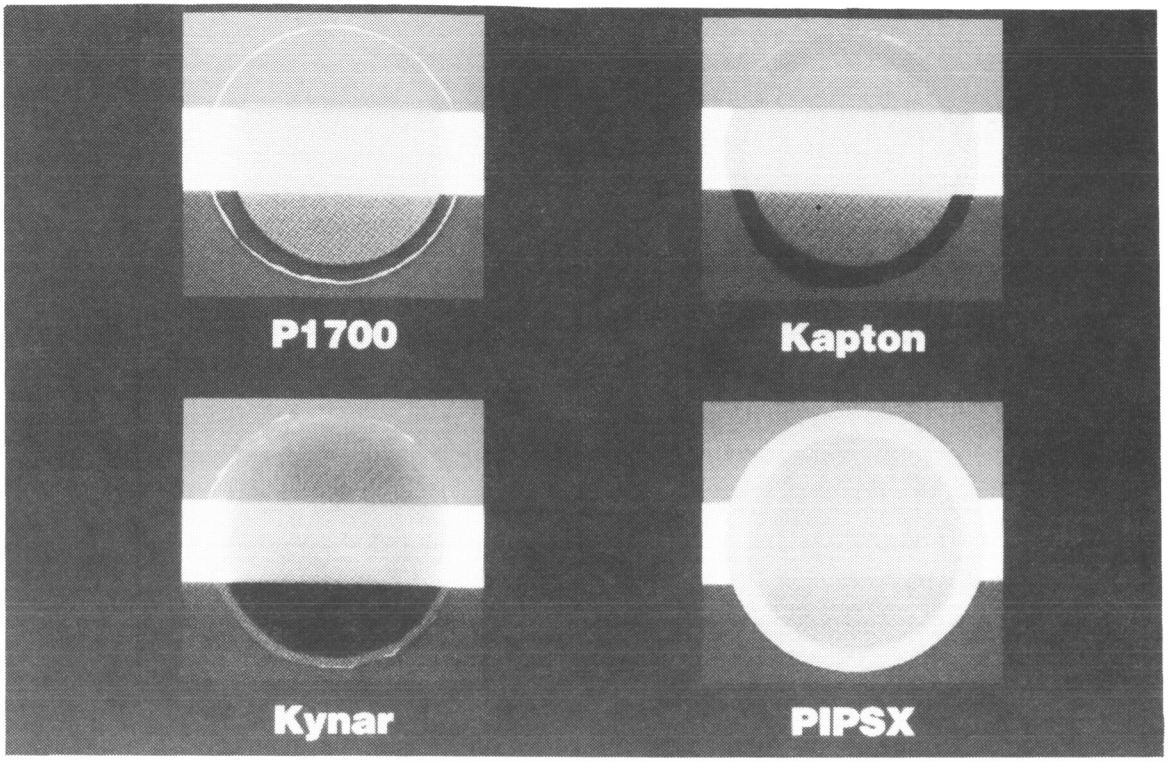

Figure 4. Photographs of 10-month exposed polymer films.

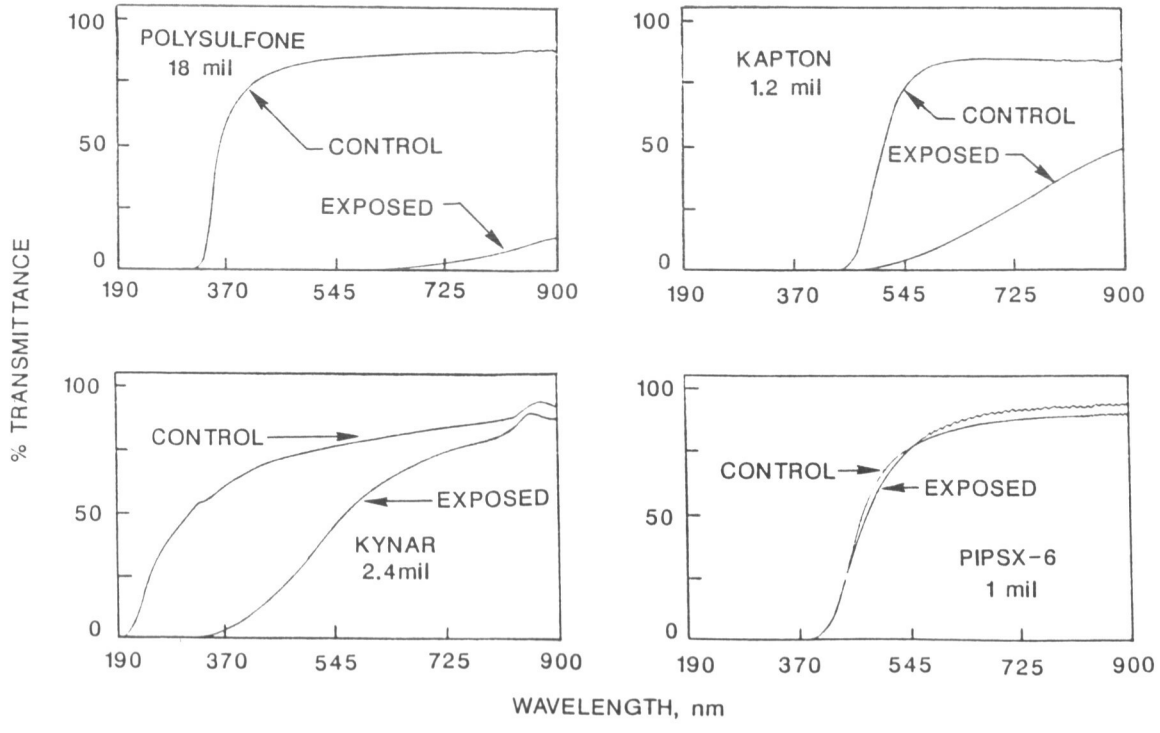

Figure 5. UV-VIS transmission spectra of 10-month exposed polymer films.

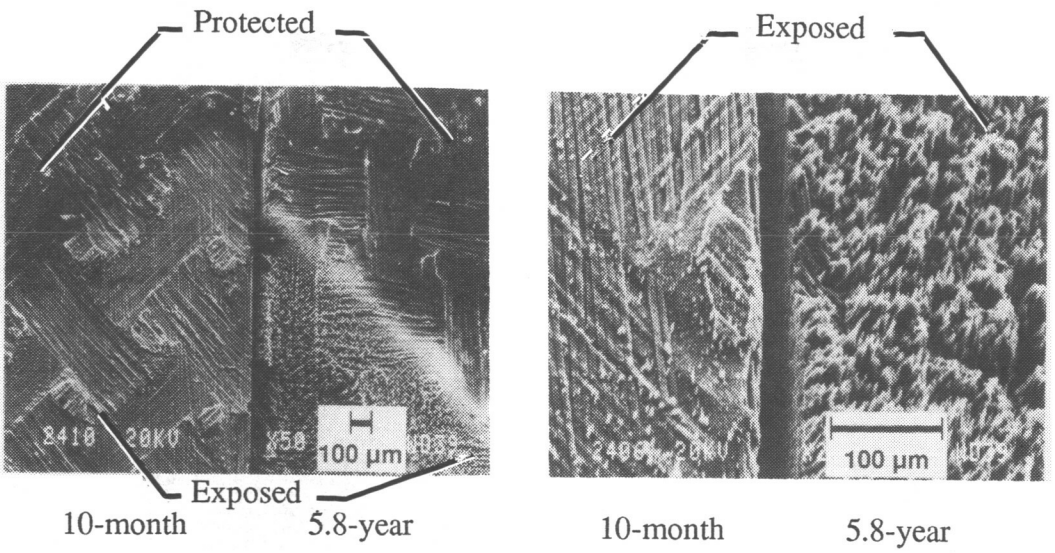

Figure 6. SEM photomicrographs of 934/T300 epoxy composites after 10-month and 5.8-year LDEF exposures.

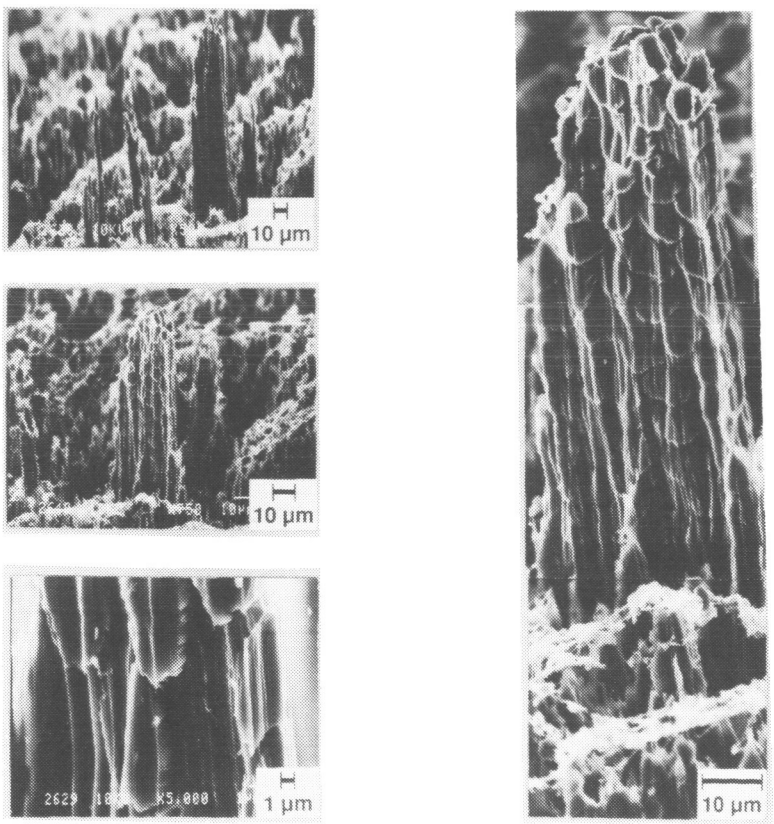

Figure 7. SEM photomicrographs of 5.8-year exposed 934/T300 epoxy composite.

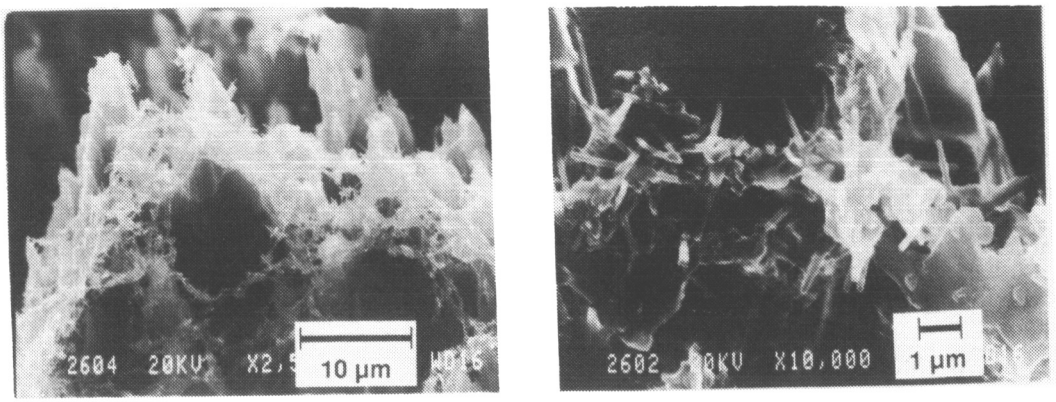

Figure 8. SEM photomicrographs of white ash or residue on exposed epoxy composite.

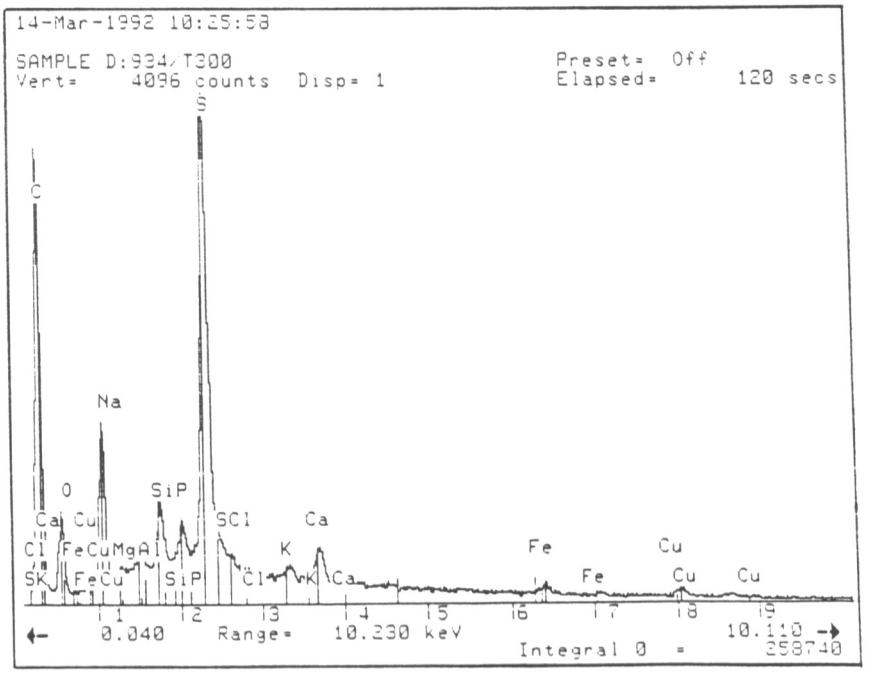

Figure 9. EDS analysis of composite residue.

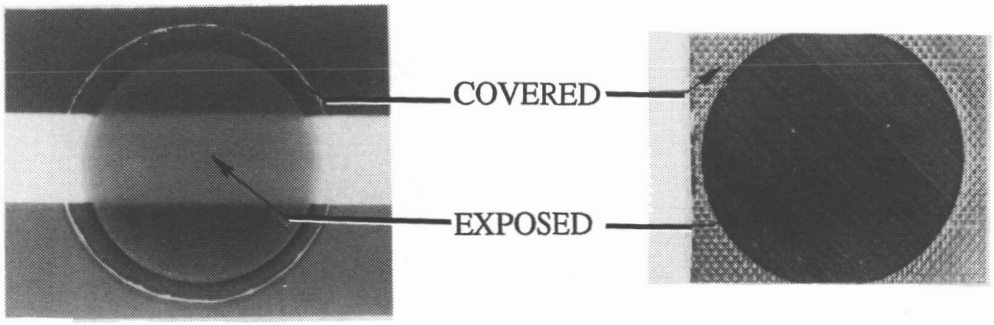

FILM

10-month exposure

COMPOSITE

5.8-year exposure

Figure 10. Photographs of LDEF exposed polysulfone film and composite specimens.

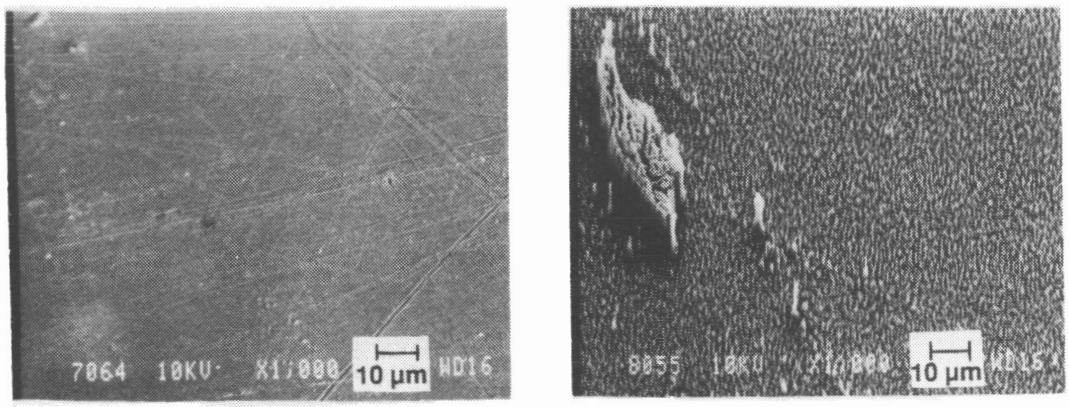

Control

10-month exposure

Figure 11. SEM photomicrographs of polysulfone film.

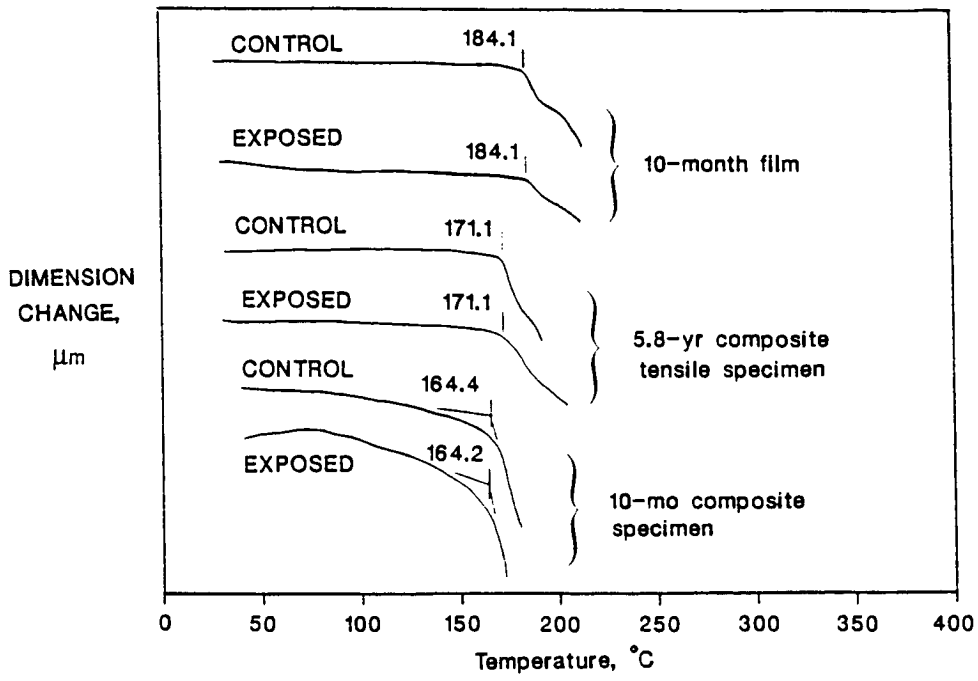

Figure 12. TMA of LDEF exposed polysulfone specimens.

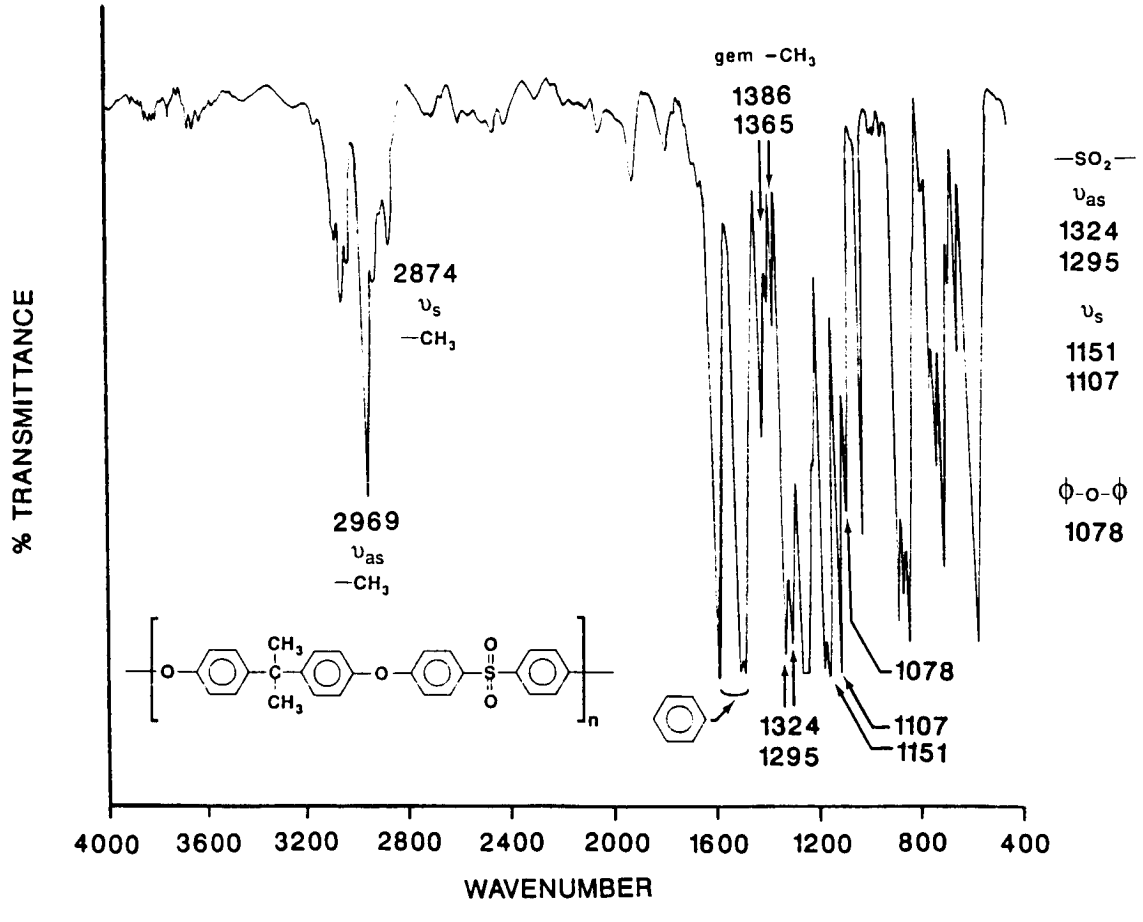

Figure 13. FTIR spectrum of a thin polysulfone film.

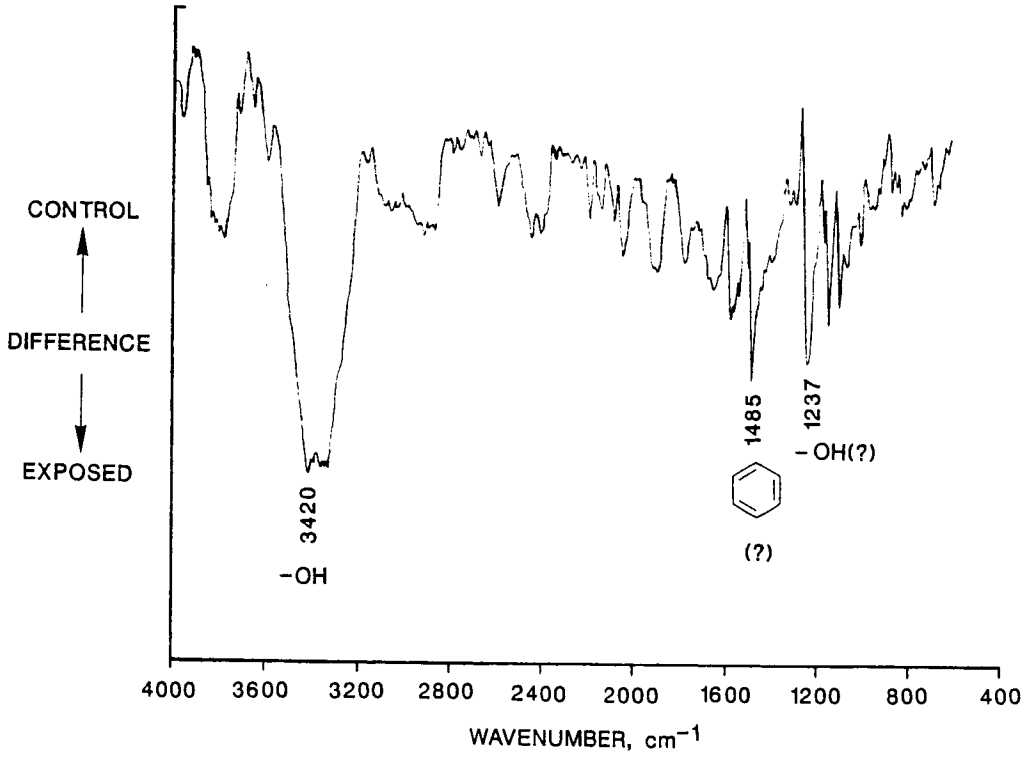

Figure 14. Subtraction DR-FTIR spectra of LDEF exposed polysulfone film specimen.

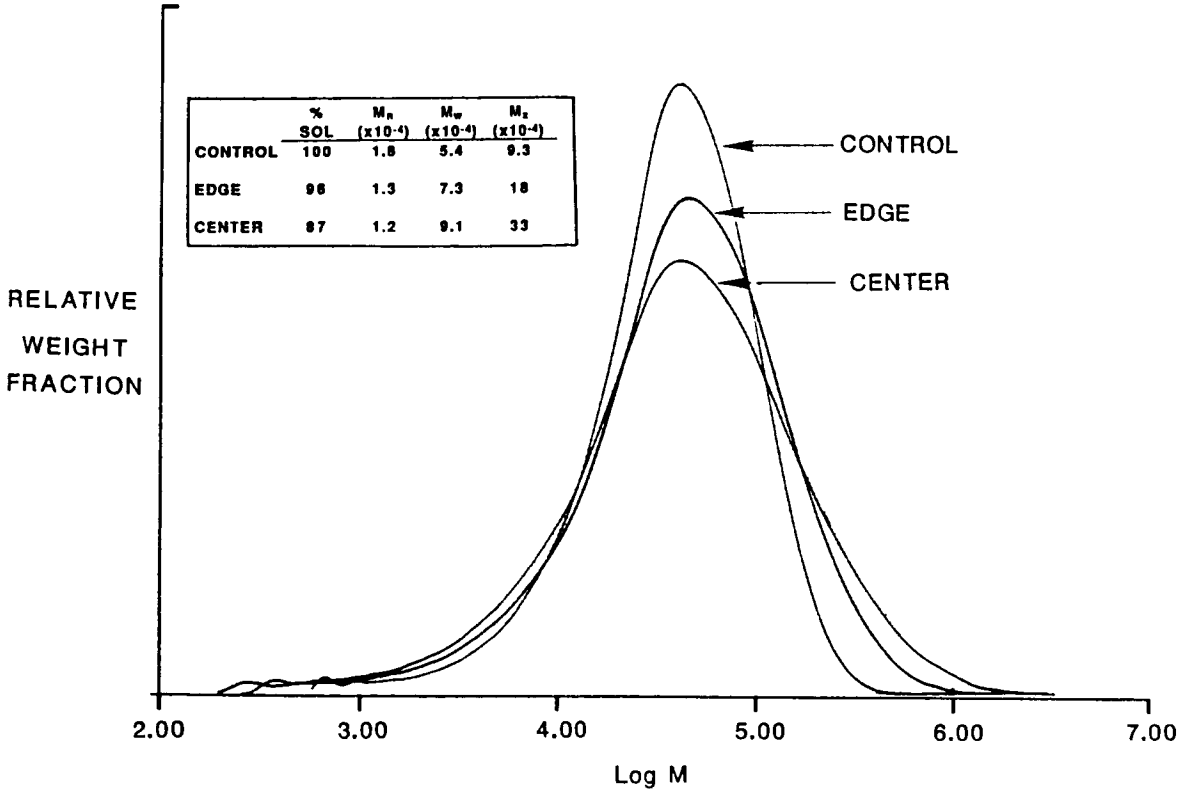

Figure 15. GPC-DV molecular weight distributions of 10-month exposed polysulfone film specimens.

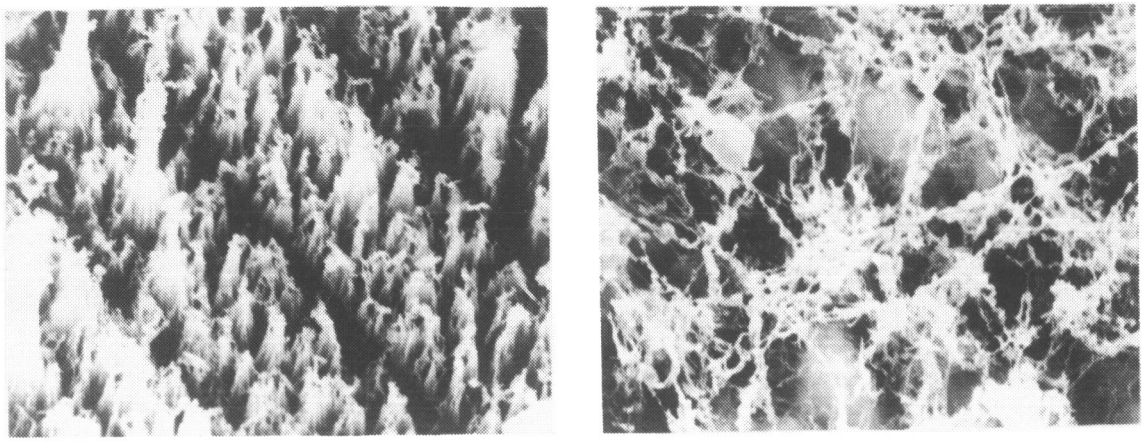

a) 10 months exposure

b) 5.8 years exposure

Figure 16. SEM photomicrographs of 10-month and 5.8-year exposed polysulfone composite specimens.

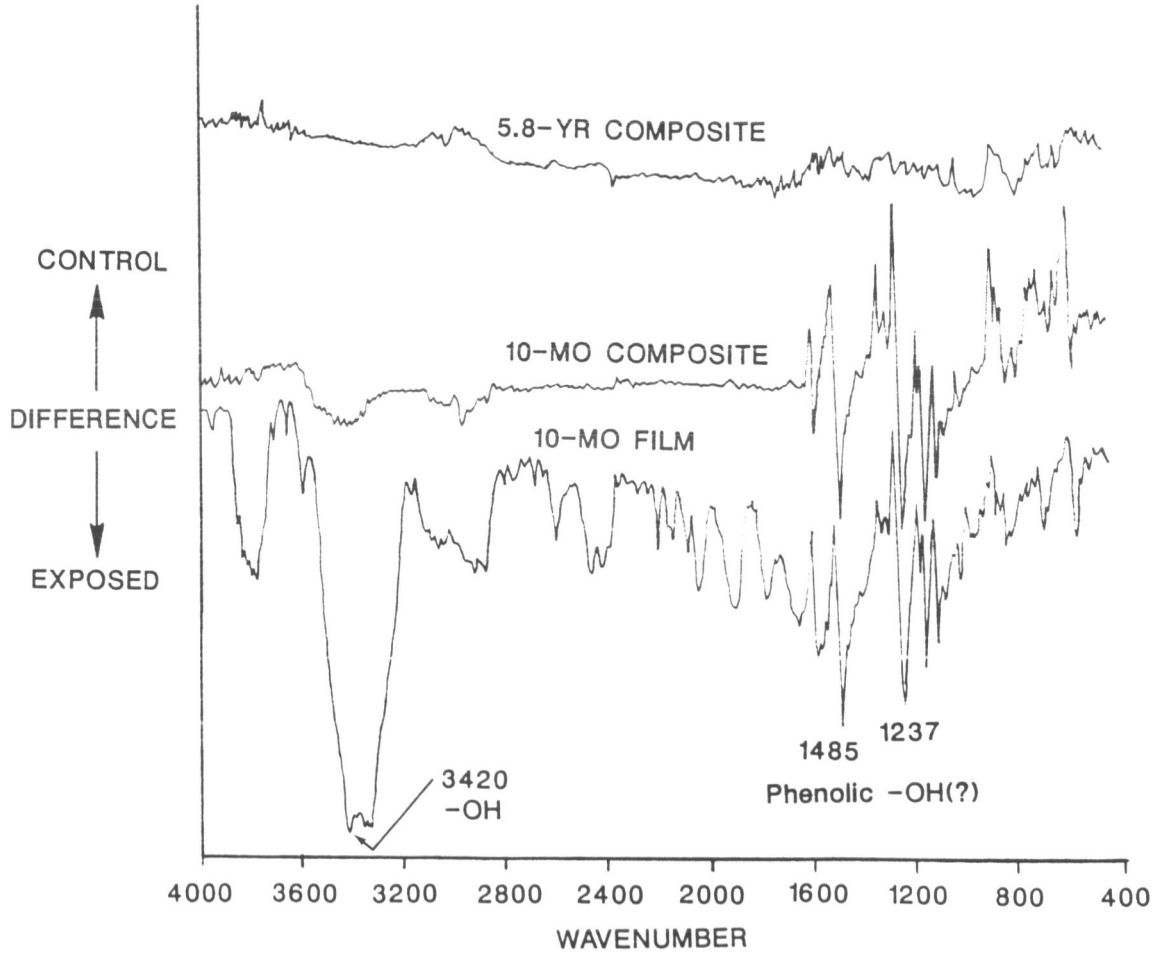

Figure 17. Subtraction DR-FTIR spectra for LDEF exposed polysulfone specimens.

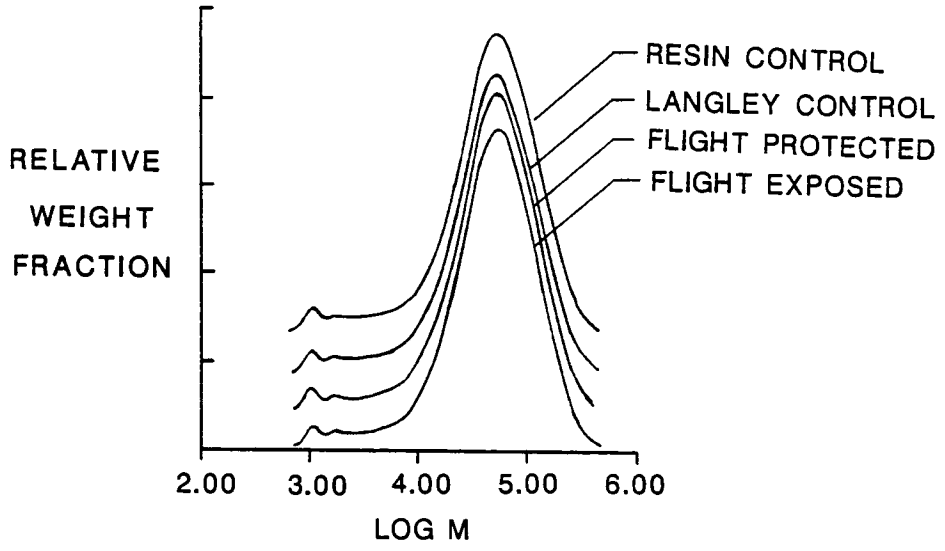

Figure 18. GPC-DV Molecular weight distributions of 5.8-year exposed polysulfone composites.

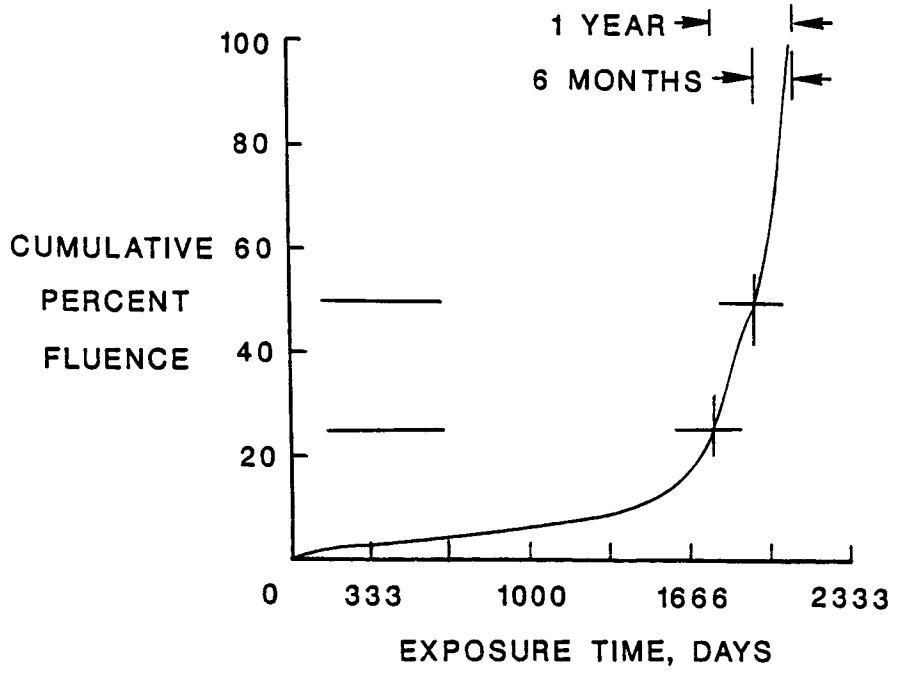

Figure 19. Approximate LDEF cumulative percent atomic oxygen fluence as a function of exposure time.

N93-28260

VISCOELASTIC CHARACTERIZATION OF THIN-FILM POLYMERS EXPOSED TO LOW EARTH ORBIT

Alan Letton
Polymer Technology Center
Mechanical Engineering Department
Texas A & M University
College Station, Texas 77843

Allan Farrow, Thomas Strganac
Aerospace Engineering Department
Texas A & M University
College Station, Texas 77843

ABSTRACT

The materials made available through the LDEF satellite provide a set of specimens that can be well characterized and have a known exposure history with reference to atomic oxygen and ultraviolet radiation exposure. Mechanical characteristics measured from control samples and exposed samples provide a data base for predicting the behavior of polymers in low earth orbit.

Samples of 1.0 mil thick low density polyethylene were exposed to the low earth orbit environment for a period of six years. These materials were not directly exposed to ram atomic oxygen and offer a unique opportunity for measuring the effect of atomic oxygen and UV radiation on mechanical properties with little concern to the effect of erosion. The viscoelastic characteristics of these materials were measured and compared to the viscoelastic characteristics of control samples. To aid in differentiating the effects of changes in crystallinity resulting from thermal cycling, from the effects of changes in chemical structure resulting from atomic oxygen/UV attack to the polymer, a second set of control specimens, annealed to increase crystallinity, were measured as well. The resulting characterization of these materials will offer insight into the impact of atomic oxygen/UV on the mechanical properties of polymeric materials.

The viscoelastic properties measured for the control, annealed, and exposed specimens were the storage and loss modulus as a function of frequency and temperature. From these datum is calculated the viscoelastic master curve derived using the principle of time/temperature superposition.[1] Using this master curve, the relaxation modulus is calculated using the method of Ninomiya and Ferry.[1] The viscoelastic master curve and the stress relaxation modulus provide a direct measure of the changes in the chemical or morphological structure. In addition, the effect of these changes on long-term and short-term mechanical properties is known directly. It should be noted that the dependence on directionality for the polymer films has been considered since these films were manufactured by a blown-film process.[2]

PRECEDING PAGE BLANK NOT FILMED

INTRODUCTION

It is known that thin film polymers unprotected from direct ram impact of atomic oxygen in the low earth orbit (LEO) environment undergo significant degradation. This degradation is synergistically increased in the presence of high levels of ultra-violet (UV) radiation[3]. To date, the large body of knowledge associated with the use of polymers in LEO has probed the chemical mechanisms associated with atomic oxygen attack and UV exposure. The effect of atomic oxygen and UV radiation on engineering properties has been largely ignored. With the increasing importance of polymers' use in orbiting spacecraft it has become necessary to determine how and to what extent the mechanical properties of polymers are affected by the LEO environment.[4]

The polyolefin films studied here offer a unique opportunity since they were not directly exposed to the ram impact of atomic oxygen prevalent in most LEO studies. As a result of the configuration of the test tray aboard the Long Duration Exposure Facility (LDEF), the specimens studied here were exposed to diffuse atomic oxygen only (in the presence of UV radiation). This oxygen does not have the kinetic energy of 5eV typically associated with ram impact atomic oxygen. Materials studied were control, exposed and thermally annealed specimens of 1.0 mil Stratofilm®. Stratofilm® is a low density polyethylene (LDPE) film manufactured for use in scientific balloons.

OVERVIEW OF EXPOSED MATERIALS AND CONDITIONS

It has recently been observed that exposure of polymers to the LEO environment can result in significant weight loss, possibly due to degradation primarily from atomic oxygen attack.[1] Although it is recognized that the presence of atomic oxygen and UV radiation alters the chemical integrity of polymers, it is not known to what extent these chemical alterations affect the mechanical behavior of the material. Fortunately, the extended duration of the LDEF mission significantly enhanced the opportunities to characterize the morphological and mechanical properties of these exposed polymers. The findings of this research contribute to the predictive models of material constitutive characteristics. The balloon materials exposure experiment consists of 38 polymer film specimens and 24 fibrous cord specimens.[3,4]

The mechanics of the orbit were such that one end of LDEF faced the Earth and one specific side was always aligned with the orbital velocity vector (or the "RAM" when referring to the direct exposure of atomic oxygen). The LDEF was inserted into a 476km orbit; when LDEF was retrieved, the orbit had decayed to 333 km.

The balloon materials exposure experiment consisted of 38 thin film polymer samples and 24 fibrous cord samples. The thin-film polymer samples ranged from 0.35 mil to 1.8 mil in thickness and were primarily constructed of polyester and polyethylene. Some of the thin-film specimens were reinforced with nylon, Kevlar, or polyester fibers. These polymeric materials are intended for use in long-duration scientific balloons and, except for the laminates and composite films, are manufactured as a blown film. This manufacturing process is known to introduce a biaxial orientation to the film resulting in anisotropic mechanical properties. Hence, pairs of specimens with mutually perpendicular orientation were included in the experiment package to account for directionality. Each non-reinforced specimen was six inches long and one inch wide. Each reinforced film was six inches long and one and one-half inches wide.

Spacecraft with the orbit of LDEF travel at a rate of 8 km/s. This velocity has the effect of providing the atomic oxygen in LEO with a translational energy of approximately 5 eV as it strikes surfaces perpendicular to the direction of RAM. Under these conditions many polymers are degraded with resulting mass loss. The balloon materials exposure experiment was positioned on row 6; which was oriented 90 degrees from the velocity vector (actually 98 degrees due to a slight misalignment). This yielded a significantly smaller AO fluence (2 orders of magnitude) than RAM facing experiments. Further, the specimens were shielded as the mounting trays were slightly recessed within the supporting LDEF structure.[5]

The fortuitous location of the balloon materials exposure experiment on LDEF minimized direct impact by atomic oxygen. Hence, the effect of the environment on balloon materials has been provided without the worry of atomic oxygen abrasion; as a result a majority of the materials survived the extended LDEF mission. The experiment was exposed to a minimum level of UV radiation by comparison to other locations aboard LDEF.[6] Except for the earth-end experiment locations, the row containing these specimens was exposed to the lowest equivalent sun hours, 6500. By comparison, the space end of LDEF received the maximum exposure, which was 14,500 equivalent sun hours. Further, the slightly recessed position of the specimen trays provided shielding for the specimens.

EXPERIMENTAL PROCEDURE

A Rheometrics Solids Analyzer model II (RSA-II) was used for viscoelastic characterization. The RSA-II applies an oscillating tensile strain to a thin film specimen by clamping the specimen between two grips and driving one of the clamping fixtures at a designated frequency. The RSA-II is capable of testing specimens between the frequencies of 0.1 radians/second and 400 radians/second.

To measure the storage and loss moduli as a function of temperature the RSA II is equipped with an environmental chamber capable of attaining temperatures between -150°C and 450°C. Since the glass transition temperature of all the specimens tested is approximately -40°C, by testing the specimens to -150°C the entire glass transition region can be captured. Similarly, the melting temperature is approximately 100°C for the specimens tested. Therefore, the RSA-II allows the entire temperature range of interest, from the region previous to the glass transition to the melting temperature, to be captured.

Due to the design of the RSA-II there are inherent limitations on the size and compliance of the sample to be tested. The minimum specimen compliance that the RSA-II can measure is 40 μm/kg. Any sample with a compliance less than this will be subject to large measurement errors due to limits in the hardware transducer compliance correction. The maximum allowable compliance of a specimen is based on the sample being capable of generating a force equal to the lower limit of the transducer (1 gram force) with the maximum dynamic oscillation (± 0.5 mm). The combination of these two limiting factors leads to a maximum testable sample compliance of $5x10^5$ μm/kg.

With the modulus of the sample fixed and the thickness of the sample determined by the film that was tested, the sample width was the only parameter available for adjustment in order to test within the RSA-II's recommended operating region. A thickness of approximately 0.02 mm and a estimated modulus of $2x10^{10}$ dynes/cm^2 for the test sample yielded an optimum sample width of between 6.0 mm and 4.5 mm.

In order to insure that the samples would only be tested in their linear range, such that time-temperature superposition is valid, a series of strain sweeps were conducted. This test was conducted at select temperatures and at select frequencies to insure linear measurements over the entire testing range. The nonlinear region of the strain sweep is characterized by a force decrease in the strain versus force curve. There is a simultaneous change in the values of the storage and loss moduli at the same value of strain where the force deviates from its linear behavior. When the storage and loss moduli are no longer independent of the strain, the beginning of the nonlinear region is noted. By performing the strain sweep at a number of temperatures, the linear/nonlinear boundary can be characterized as a function of strain and temperature. When characterizing the storage and loss moduli as functions of frequency and temperature, a strain that is less than the critical strain at which the nonlinear region begins at each temperature and frequency must be used in order to remain in the linear region. Also required is some level of pretension in the

specimen, used to keep the specimen from buckling during dynamic oscillations. The pretension force is chosen so that the dynamic force required to produce the largest strain at the highest frequency to be tested is less than the static pretension force. This will insure that the specimen will never buckle over the range of tested strains and frequencies. The frequency range that was tested was determined by the RSA-II's physical limitations. The maximum frequency of oscillation was 100 radians/second. The smallest frequency of oscillation used for testing was 0.4 radians/second.

Once the linear region of the material has been characterized, the RSA-II was again used to measure the viscoelastic response of the specimens as a function of frequency and temperature. An initial temperature of -150°C was chosen as a starting point for the viscoelastic characterization. The final temperature was determined by the material's melting point, approximately 100°C. The dynamic mechanical characterization of the specimen was continued until the specimen was unable to support the load needed for testing. This occurred at approximately 85°C.

The storage and loss moduli were recorded over a predetermined range of frequencies at discrete temperatures within a specified temperature range. A 5°C step size was chosen for these frequency-temperature sweeps, this step size allowed a significant amount of overlap in the frequency curves when the data was shifted. Although a smaller temperature step size would have allowed more data overlap, it would have also significantly increased the time necessary for the temperature to stabilize and increased the total time necessary to complete a test. To avoid problems associated with long term creep resulting from the static pretension the temperature frequency sweeps were conducted in three sections. The first section of testing covered the temperature range from -150°C to -20°C. The second section of testing covered a temperature region of -50°C to +50°C, and the third region of testing covered a temperature region of 0°C to +90°C. The resulting data were shifted to produce the frequency dependent master curve. The relaxation modulus was then calculated using the method of Ninomiya and Ferry.[1] Typical results are presented in Figures 1 and 2.

RESULTS AND DISCUSSION

Earlier work by the authors suggests that there is extensive crosslinking resulting from atomic oxygen/UV exposure, and a change in crystallinity.[4] To understand the effect of atomic oxygen & UV radiation on the mechanical properties of these thin film materials, the control, exposed and annealed specimens will be compared. Viscoelastic measurements provide the opportunity to relate the mechanical performance of these films to their chemical structure. In particular, we are

interested in understanding the effect of changes due to the presence of atomic oxygen in the presence of UV radiation and differentiate these changes from those related to changes in crystallinity. This analysis is complicated by the fact that the crystallinity of the film was measurably reduced during exposure on the LDEF experiment.[7] The question arises as to the definition of the sequence of events leading to changes in the crystalline structure. Wide angle and small angle x-ray analysis is underway to probe observed changes in the crystallites' structure. Earlier work suggests that the crystalline regions were crosslinked in-situ.[7] This is evidenced by the fact that the crystalline melt temperature and the percent crystallinity for the exposed specimen were unaltered after repeated heating, suggesting a permanent morphology. If the crystalline and amorphous regions were crosslinked in-situ, one would expect the fundamental molecular relaxations to be only slightly altered. Our earlier efforts suggest that only a portion of the chains are crosslinked.[7] At this density of crosslinking there is not enough restriction in molecular mobility to alter the fundamental relaxations in these polymers. Changes in the fundamental relaxations can be quantified by noting changes in the Arrhenius behavior of the viscoelastic shift factors. Typically, there are two quantities of importance used to analyze viscoelastic shift factors; the activation energy associated with a particular relaxation and the temperature range over which the relaxation occurs. Changes in the relaxation process will translate to a change in the activation energy for a particular relaxation (an increase in the activation energy being associated with a decrease in molecular mobility) or a change in the temperature at which the relaxation is observed. For the materials studied here, both changes are monitored.

For a molecular relaxation, the Gibbs' free energy associated with the relaxation process is classically represented by

$$\Delta G = \Delta H - T\Delta S \tag{1}$$

The rate constant associated with this relaxation process can be expressed in terms of the Gibbs free energy.

$$k = e^{-\Delta G/RT} = e^{-\Delta H/RT} e^{\Delta S/R} \tag{2}$$

The entropic term, $e^{\Delta S/R}$ is associated with the frequency at which the relaxation process takes place while the enthalpic term, $e^{-\Delta H/RT}$ is associated with the energy barrier for the process. The rate constant is inversely proportional to time; therefore, the ratio of the inverse of the rate

constant at temperature T, to the inverse of the rate constant at temperature T_o, a reference temperature, can be defined as the viscoelastic shift factor if the rate constant is a measure of the relaxation time scale. This is expressed in the equation below.

$$\frac{1/k}{1/k_0} = Ae^{\frac{\Delta H}{R}\left(\frac{1}{T}-\frac{1}{T_0}\right)} = a_T \qquad (3)$$

where A is a constant. This suggests that a plot of the natural logarithm of the viscoelastic shift factor against the quantity $[1/T - 1/T_o]$ will yield a linear expression with a slope of $\Delta H_a/R$, the apparent activation enthalpy divided by the gas constant. For processes at constant pressure and volume, ΔH_a is equivalent to E_a, the activation energy.

Arrhenius plots derived from the construction of master curves are presented in Figures 3 to 8 for the 6 systems tested (control, annealed and exposed specimens in the machine and transverse directions). In each, the linear regions and the corresponding lease squares fit used to calculate the slope (the apparent activation energy) are presented. The temperatures at which the relaxation processes change are denoted by a change in the apparent activation enthalpy. These temperatures and the corresponding activation enthalpies are summarized in the tables below.

Table 1†

Summary of Transition Temperatures for Control, Exposed and Annealed Specimens

Annealed MD	*Annealed TD*	*Control MD*	*Control TD*	*Exposed MD*	*Exposed TD*	*Relaxation Process*
61°C	*66°C*					α_1
		26°C	*30°C*	*31°C*	*41°C*	α_2
	-34°C		*-34°C*	*-24°C*	*-29°C*	β_1
-63°C		*-54°C*		*-68°C*		β_2

† *In polyethylene, two major relaxations are recognized, the α relaxation located near 50°C and the β relaxation located near -50°C. In this summary there are clearly two "groups" of transition temperatures associated with each relaxation. For clarity in discussions, they have been designated α_1, α_2, β_1 and β_2.*

Table 2
ΔH_a (kcal/mole) for Control, Annealed and Exposed Specimen Machine and Transverse Directions

Temperature Region	*Annealed MD*	*Annealed TD*	*Control MD*	*Control† TD*	*Exposed MD*	*Exposed TD*
Above α relaxation	*108.9*	*135.7*	*74.9*	*76.7*	*80.0*	*88.8*
Between β and α relaxation	*60.3*	*59.6*	*56.5*	*60.6*	*59.2*	*64.4*
Below β relaxation	*21.4*	*29.2*	*17.2*	-	*30.0*	*35.9*

† *Below the β relaxation, a clearly definable linear region is not observed.*

From the information provided in Tables 1 and 2, it is easy to conclude that the changes that took place aboard LDEF are not consistent with changes resulting from crystalline morphology changes. Changes in crystalline structure due to annealing and melting, as would result from thermal cycling, would lead to an increase in the activation enthalpy above the α relaxation but more importantly would result in a higher α relaxation temperature. This is not observed in the exposed specimens. The annealed specimens have an α relaxation near 60°C, a 30°C increase over that recorded for the control specimens. The exposed specimens, while showing a slight increase of 5°C to 10°C, do not demonstrate the dramatic increase associated with the annealed specimen. This would suggest that in the exposed specimens there is a slight increase in the crystalline packing (as occurs in annealed specimens) but not a significant change. This fact is further evidenced by noting the activation energies associated with the α processes. For the annealed specimens, the activation enthalpy is ~110 kcal/mole while for the control specimen the activation energy is ~75 kcal/mole. This increase is due to an increase in packing in the crystalline regions thereby increasing the barrier to molecular motion. The exposed materials show a slight ~10 kcal/mole increase in the apparent activation energy. It is therefore, easy to conclude that any observed changes in the mechanical properties of these materials is not solely due to the observed changes in crystallinity since the fundamental relaxations have not been altered to a great extent.

Earlier analysis of the exposed materials illustrated the presence of crosslinks induced by atomic oxygen/UV radiation.[7] With this information in mind, one can conclude that the crosslinks were introduced into the polymer at an early stage of exposure before a significant amount of melting occurred. The relatively small change in the activation energies and the transition temperatures suggest that the original relaxations have somehow been preserved. In-situ crosslinking would achieve this result. This conclusion is further supported by the fact that repeated heating and cooling of the exposed material always reproduces the same extent of crystallization and the same melting temperature. This can only occur if the local structure preceding crystallization (and melting) is fixed under all conditions. In-situ crosslinking would produce this effect.

The storage and loss modulus master curves resulting from application of time/temperature superposition are presented in Figures 9 to 12. Three relaxations are visible; a relaxation centered at 10^{10} radians/second (α relaxation) with a second relaxation appearing as a shoulder centered at 1 radian/second, and a third relaxation centered at 10^{30} radians/second (β relaxation). In general, the exposed specimen shows a decrease in the E' master curve at all frequencies. There is a corresponding decrease in the E" master curve with an additional shift to lower frequencies for the β relaxation. Although the shift is observed for the annealed specimens, there is not an observed decrease in the E' and E" master curves. A shift to lower frequencies is equivalent to a shift to higher temperatures suggesting an increase in the energy needed to activate the β process. It has been proposed that the β transition is associated with the glass-rubber transition for the constrained amorphous chain components.[8,9] If the proposed in-situ crosslinking mechanism does occur, one would expect to see an increase in the constraint of the amorphous segments of the polymer chain. The shift in the E" master curve β relaxation supports this hypothesis.

Using the master curves, the relaxation modulus for each of the specimens was calculated and is compared in Figures 13 and 14. In general, for the range of times (frequencies) measured, there is an observed decrease in the modulus on exposure to LEO. However, this decrease only applies to the transient response. The long time response for all the systems measured is equivalent, the limiting modulus is the same, which suggests for the times considered, that the equilibrium mechanical behavior of these systems is unaltered by the chemical changes that take place in the polymer. Once the polymer is protected from direct exposure, the chemical changes that take place from diffusing atomic oxygen do not adversely alter the time dependent modulus.

The relaxation modulus, E(t), is one measure of the mechanical or engineering performance of this material. Noting the effects of in-situ crosslinking and smaller effects due to changes in crystallinity, the engineering performance of this material is only slightly altered after exposure to

non-ram impact, atomic oxygen and UV radiation. This result does not however, speak to changes in fracture toughness, fatigue resistance, yield and failure. It only speaks to the primary engineering design property of linear viscoelastic response and modulus.

CONCLUSIONS

For the polyethylene specimen tested, it is clear that erosion typically observed in materials directly exposed to atomic oxygen has been avoided. As a result, an opportunity to study the effects of atomic oxygen with minimum UV exposure is presented. Results of this work and earlier efforts[5] indicate a crosslinking mechanism which occurred simultaneous to thermal cycling. The result is an in-situ crosslinking that makes permanent the crystalline morphology and has little effect on the molecular relaxations associated with the amorphous chains. The exposed specimens demonstrate relaxation behavior that is similar to that of the control specimens with a measurable but small increase in the energy barrier to molecular motion for the amorphous regions. This slight decrease in molecular mobility translates to a decrease in the relaxation modulus. The long term, equilibrium relaxation moduli seem to be equivalent for the control, annealed and exposed specimen although more work is needed to clearly identify the equilibrium behavior. The observed changes in the mechanical properties (linear viscoelastic) are due to the effect of atomic oxygen and the resulting crosslinking and not do to changes in crystalline morphology.

ACKNOWLEDGEMENTS

The authors would like to thank NASA for their support in the form of research funding. In addition we would like to thank Rheometrics Inc. for their continued suppport.

REFERENCES

1. Ferry, J.D., "Viscoelastic Properties of Polymers", John Wiley and Sons, New York, 1980

2. Allen, D.H., in "The Long Duration Exposure Facility (LDEF). Mission 1 Experiments", Eds. Clark, L.G., Kinard, W.H., Carter, D.L., and Jones, J.L.; NASA SP-473, 1984, p.49

3. S.L. Koontz, Proceedings of the NASA/SDIO Space Environmental Effects on Materials Workshop, NASA Conference Publication 3035, Part 1, 241 (1988)

4. Letton, A., Rock, N.I., Williams, K.D., Strganac, T.W., and Farrow, D.A., "Characterization of Polymer Films Retrieved From LDEF" in First LDEF Post-Retrieval Symposium Proceedings, NASA CP-3134, p. 705, 1991

5. Strganac, T.W., Farrow, D.A., Letton, A., Williams, K.D., and Rock, N.I., "Analysis and Simulation of Polymers Exposed to Low Earth (LEO) Environments", in 30th Aerospace Sciences Meeting and Exhibit Proceedings, AIAA 92-0849, 1992

6. LDEF Spaceflight Environmental Effects Newsletter, vol.2, no. 3, June 15,1991

7. Rock, N.; Master's Thesis, Texas A & M University, College Station, Texas, December, 1992

8. Boyd, R.H.; Polymer, Vol. 26, March, pp. 323-347; 1985

9. Boyd, R.H.; Polymer, Vol. 26, August, pp. 1123-1133; 1985

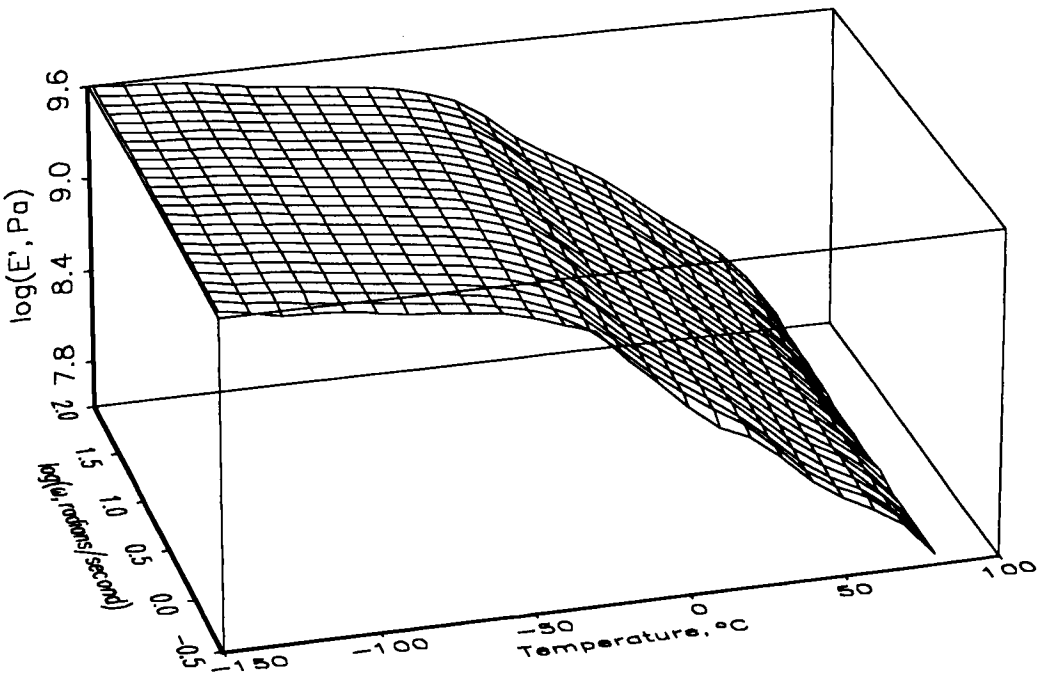

Figure 1, Typical storage modulus data. Presented is the data for the annealed specimen in the machine direction.

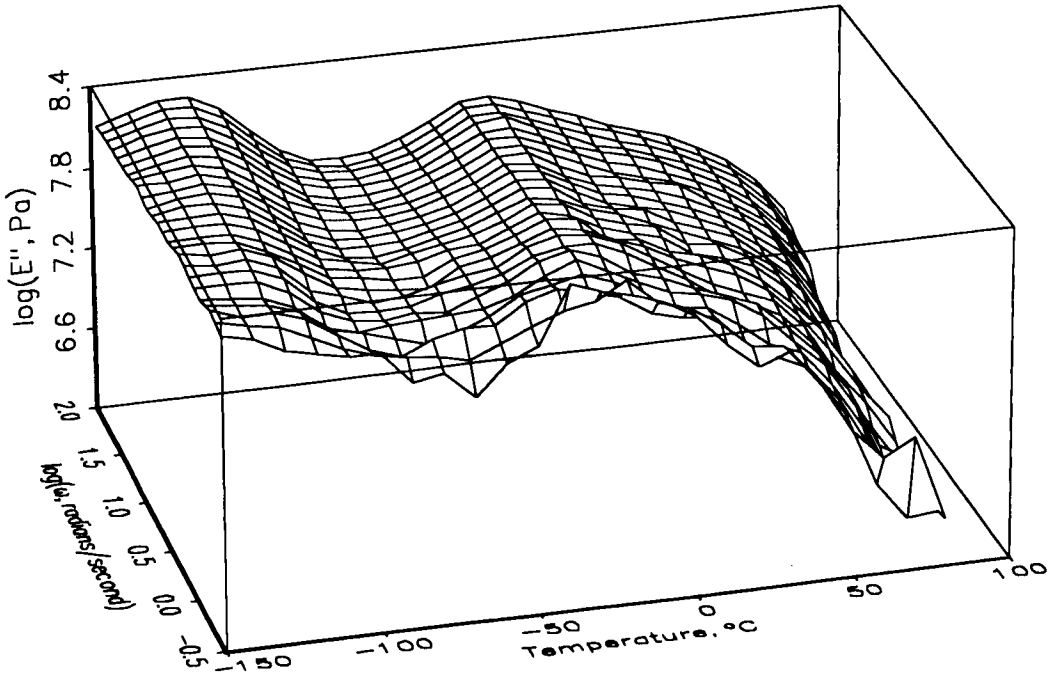

Figure 2, Typical loss modulus data for an annealed, machine direction specimen.

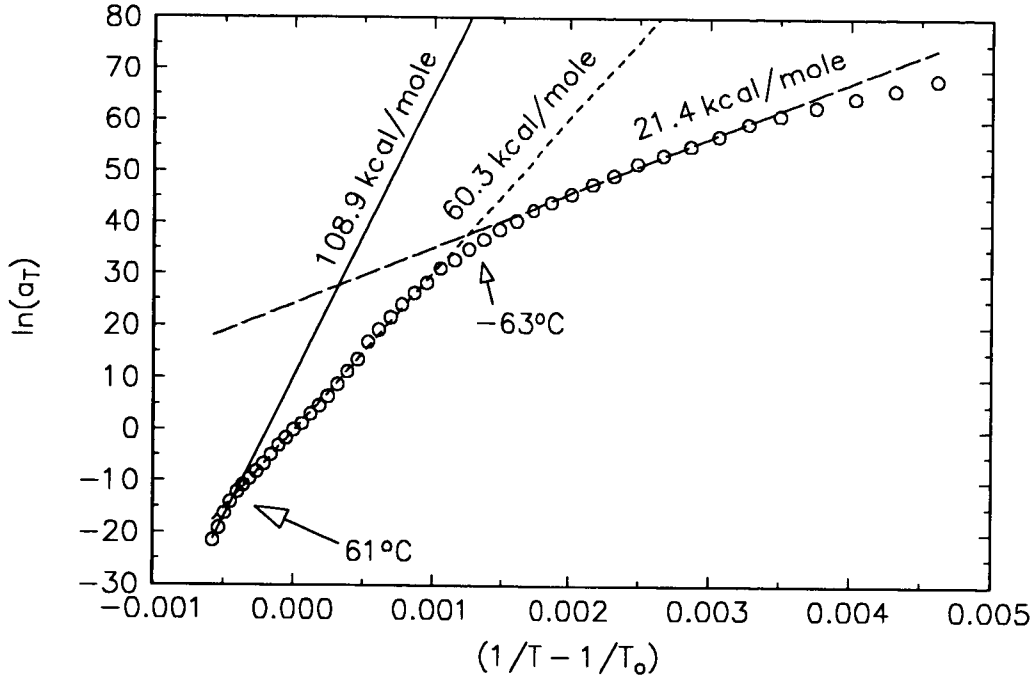

Figure 3, Arrhenius plot of viscoelastic shift factors for annealed specimen in the machine direction. Numbers by each line indicate the calculated activation energy for each relaxation while the line represents the least squares fit used to determine Ea. The arrows indicate the observed transitions and the corresponding temperatures.

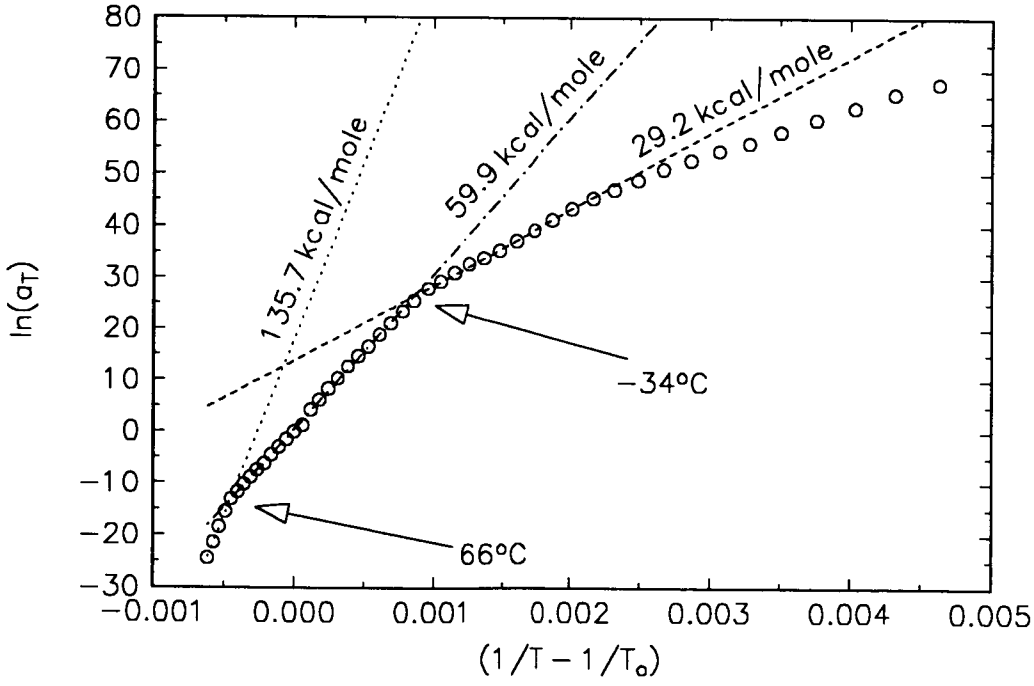

Figure 4, Arrhenius plot of viscoelastic shift factors for annealed specimen in the transverse direction. Numbers by each line indicate the calculated activation energy for each relaxation while the line represents the least squares fit used to determine Ea. The arrows indicate the observed transitions and the corresponding temperatures.

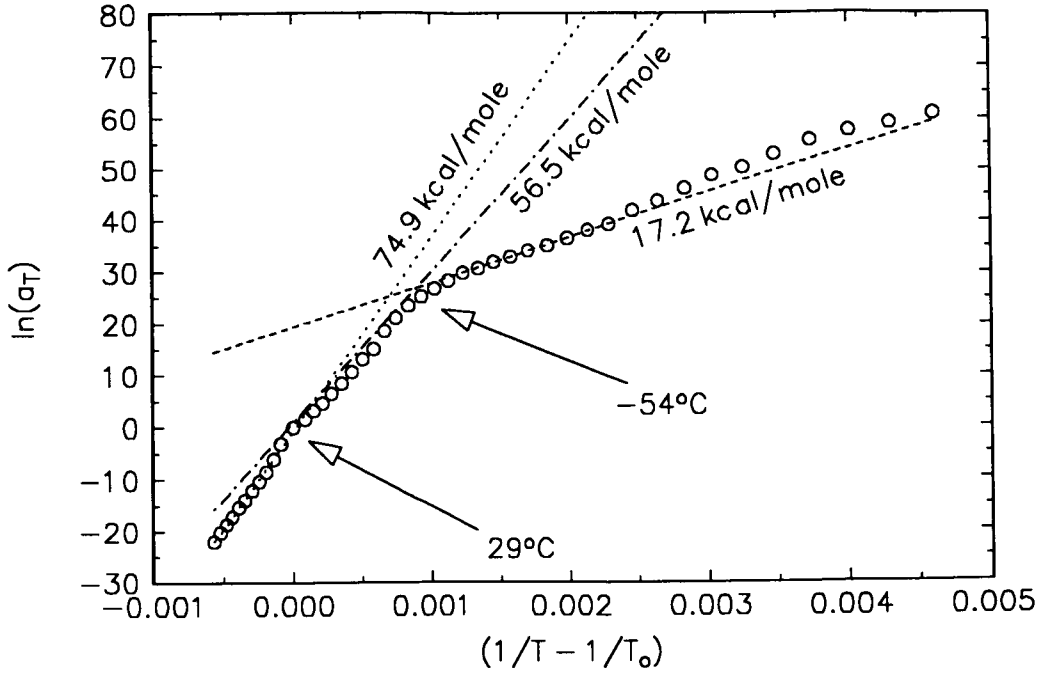

Figure 5, Arrhenius plot of viscoelastic shift factors for the control specimen in the machine direction. Numbers by each line indicate the calculated activation energy for each relaxation while the line represents the least squares fit used to determine Ea. The arrows indicate the observed transitions and the corresponding temperatures.

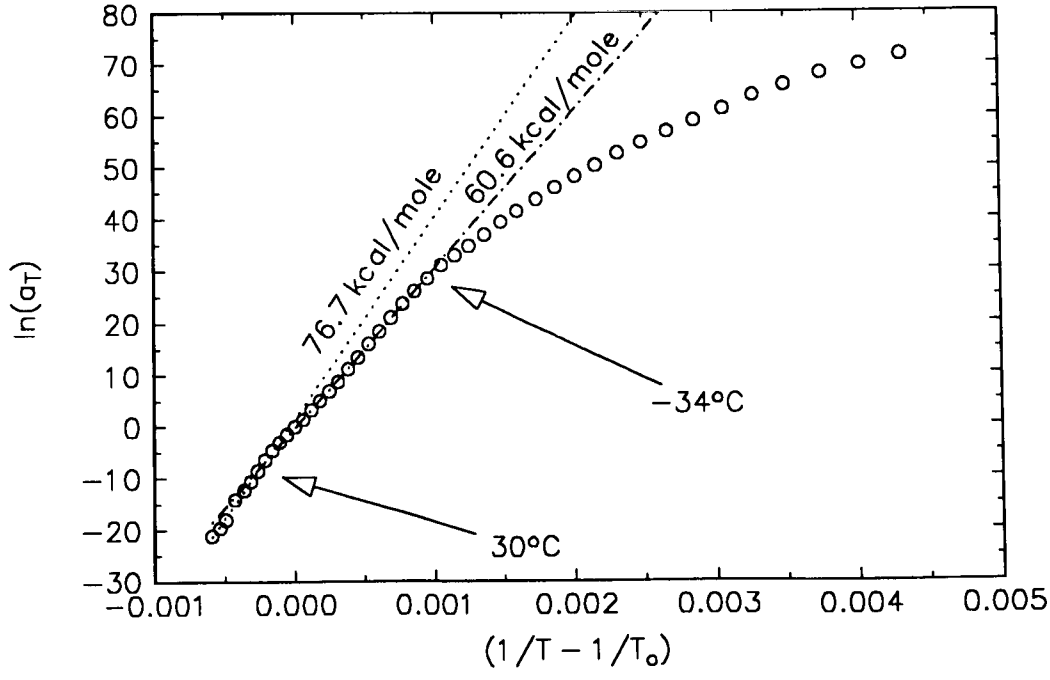

Figure 6, Arrhenius plot of viscoelastic shift factors for the control specimen in the transverse direction. Numbers by each line indicate the calculated activation energy for each relaxation while the line represents the least squares fit used to determine Ea. The arrows indicate the observed transitions and the corresponding temperatures.

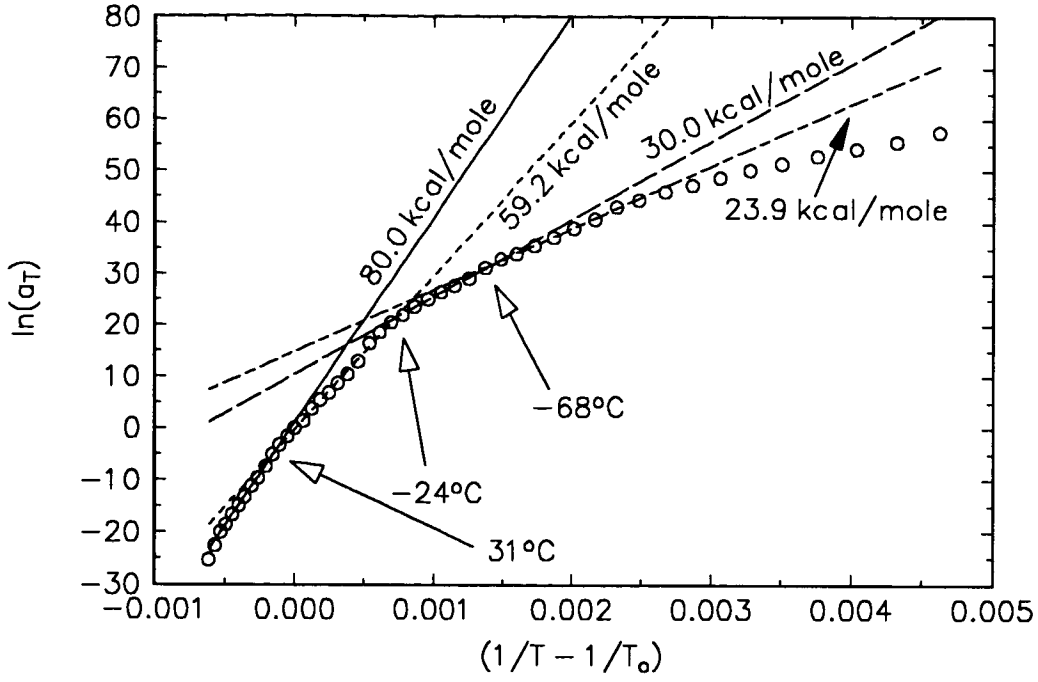

Figure 7, Arrhenius plot of the viscoelastic shift factors for the exposed specimen in the machine direction. Numbers by each line indicate the calculated activation energy for each relaxation while the line represents the least squares fit used to determine Ea. The arrows indicate the observed transitions and the corresponding temperatures.

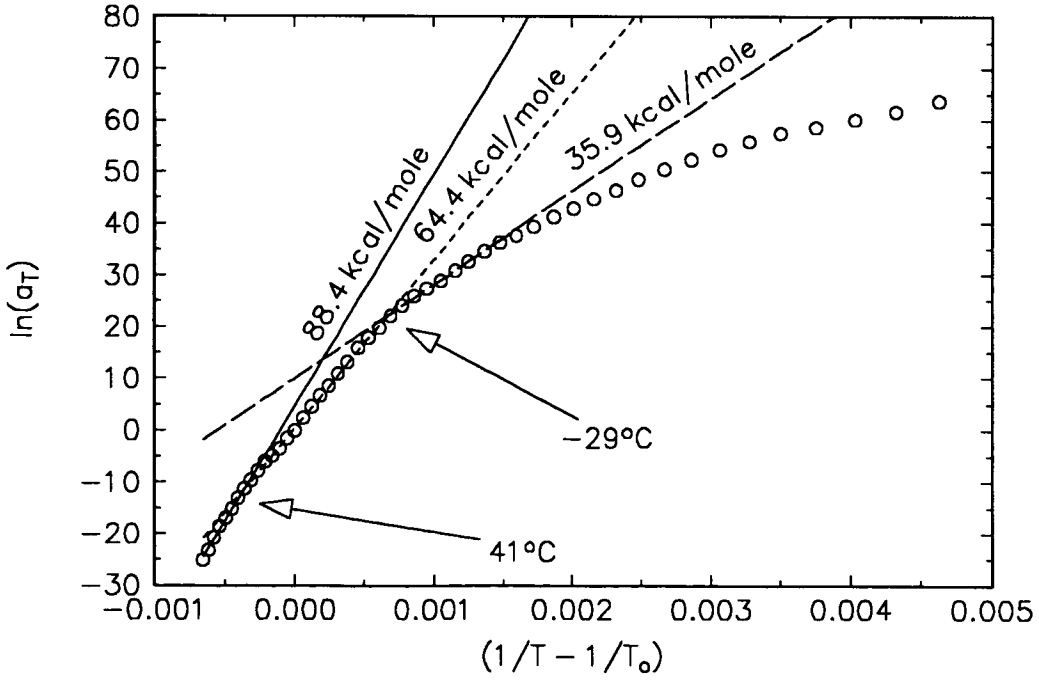

Figure 8, Arrhenius plot of the viscoelastic shift factors for the exposed specimen in the transverse direction. Numbers by each line indicate the calculated activation energy for each relaxation while the line represents the least squares fit used to determine Ea. The arrows indicate the observed transitions and the corresponding temperatures.

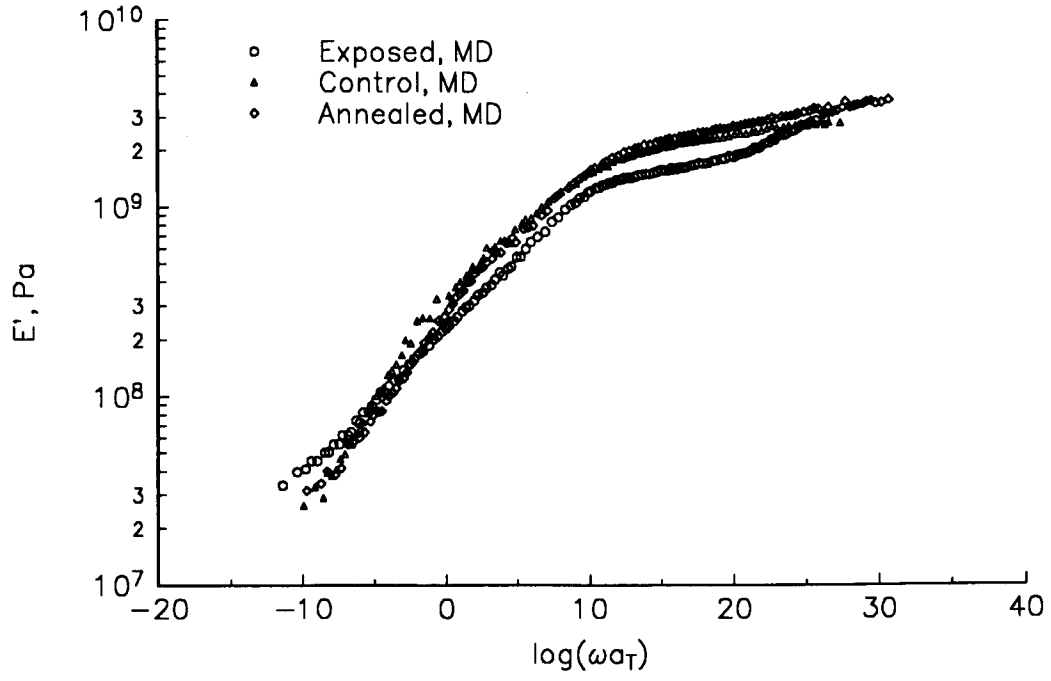

Figure 9, E' master curve for specimen in the machine direction. Every third point is plotted for clarity.

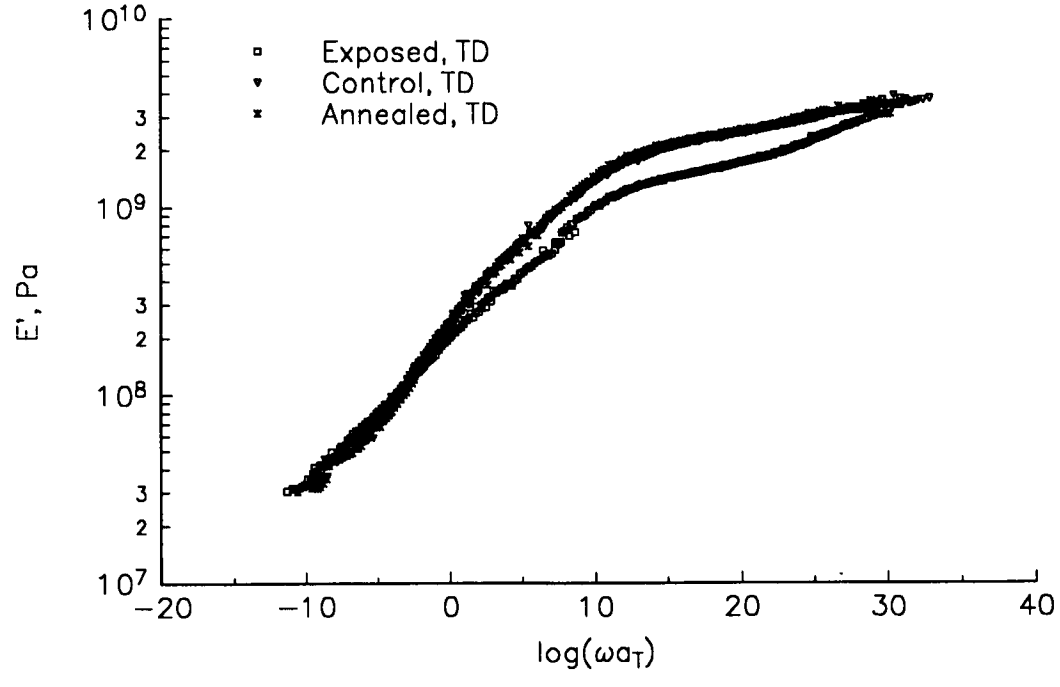

Figure 10, E' master curve for specimen in the transverse direction. Every third point is plotted for clarity.

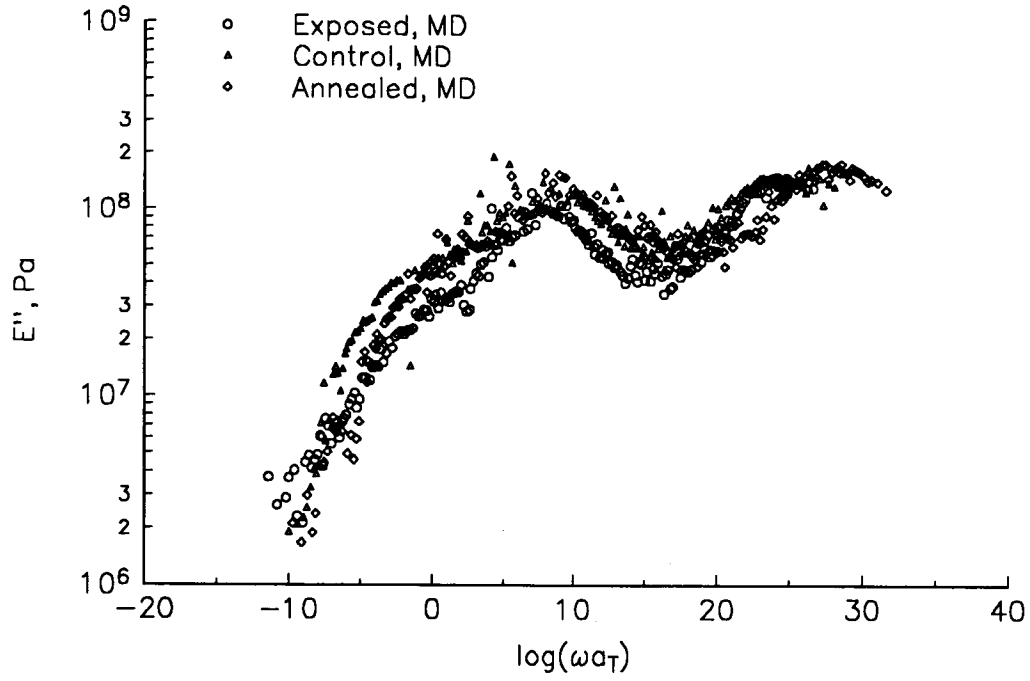

Figure 11, E" master curve for specimen in the machine direction. Every third point is plotted for clarity.

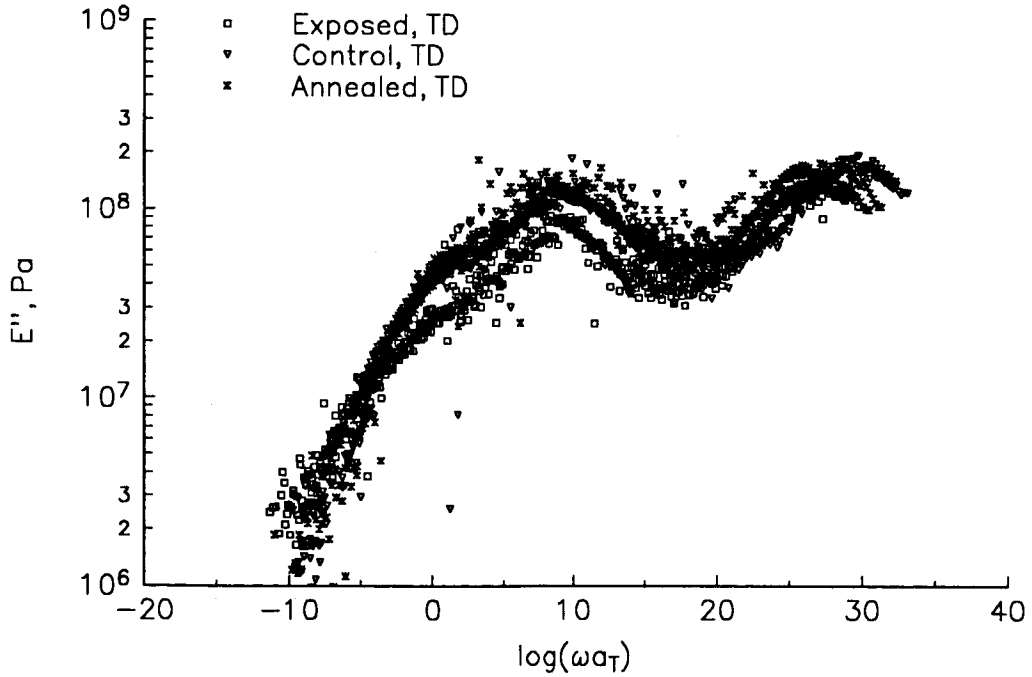

Figure 12, E" master curve for specimen in the transverse direction. All points are included.

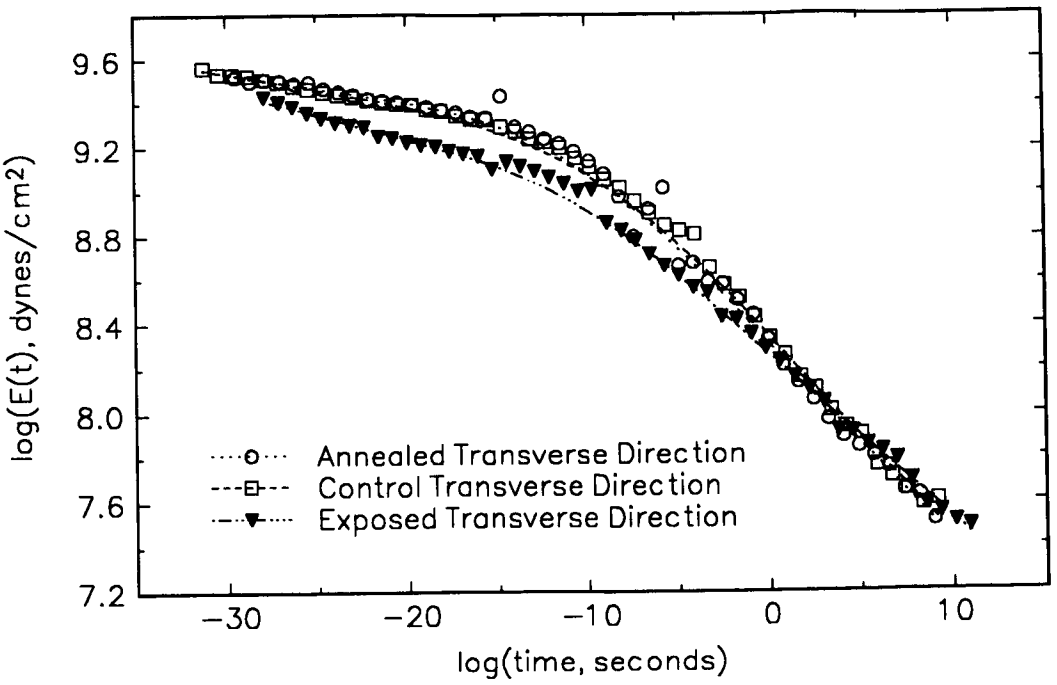

Figure 13, Relaxation modulus calculated for specimens with a transverse orientation.

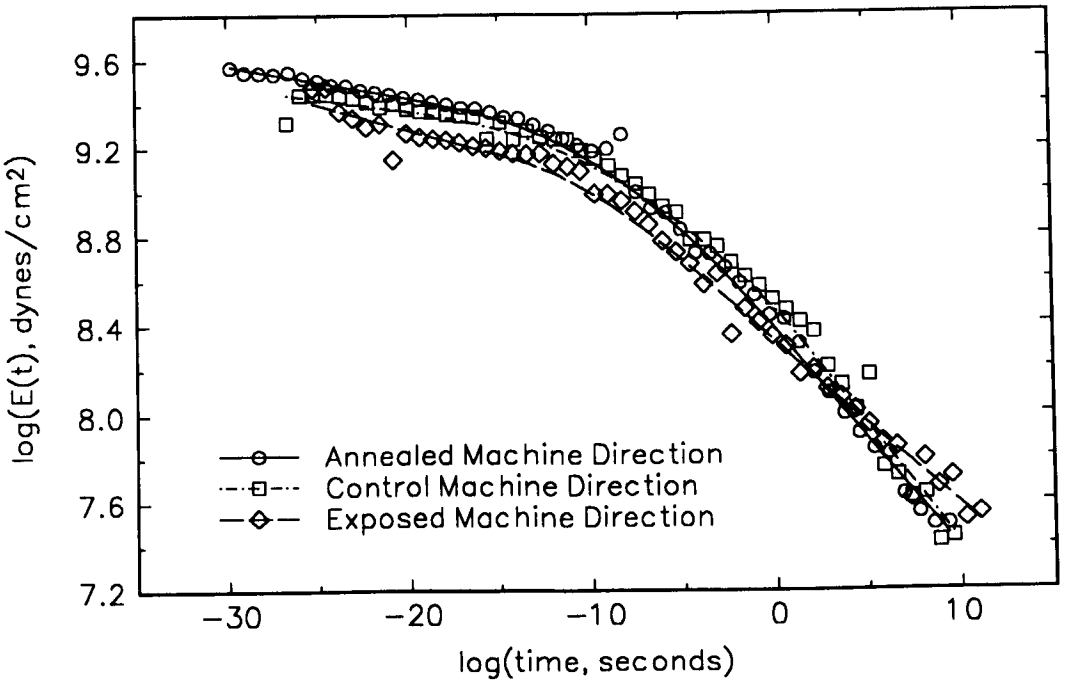

Figure 14, Relaxation modulus calculated for specimens with a machine direction orientation.

N93-28261

A STUDY OF THE UV AND VUV DEGRADATION OF FEP

Graeme A. George, David J.T. Hill,
James H. O'Donnell, Peter J. Pomery and
Firas A. Rasoul*
Polymer Materials and Radiation Group
The University of Queensland
Australia 4072
Phone:07-365 3686, Fax:07- 365 4299

SUMMARY

UV and VUV degradation of fluorinated ethylene propylene (FEP) copolymer was studied using ESR, XPS and SEM. The ESR study revealed the formation of a terminal polymer radical. The stability of this radical has been investigated under different environments. An XPS study of FEP film exposed to VUV and atomic oxygen showed that oxidation takes place on the polymer surface. The study revealed also that the percentage of CF_2 in the polymer surface decreased with exposure time and the percentage of CF, CF_3 and carbon attached to oxygen increased. SEM micrographs of FEP film exposed to VUV and atomic oxygen identified a rough surface with undulations similar to sand dunes.

INTRODUCTION

Spacecraft in low orbit are subjected to significant levels of high energy radiation, including UV and VUV wavelengths. The effects of UV radiation are enhanced over those at the surface of the earth, where the only incident wavelengths are greater than 290 nm (1). In low earth orbit the incident UV wavelengths extend below 290 nm into the VUV region, where the Lyman-α emissions of atomic hydrogen occur at 121 nm (2). In addition to electromagnetic radiation, in low earth orbit polymer materials may also be subjected to atomic oxygen particle radiation, which will result in direct oxidation of the polymer (1).

Thus, polymeric materials for space applications must exhibit a resistance to radiation damage of this type. One class of materials which have this characteristic are the fluorinated ethylene-propylene copolymers (FEP).

FEP is produced commercially by the copolymerisation of tetrafluoroethylene and perfluoropropylene in approximately 6:1 mole ratio. The polymer is an insoluble, semi-crystalline thermoplastic (crystallinity 50-60%) with a glass transition temperature (Tg) of approximately -10° C (1).

The extent of photodegradation of a polymer will be determined by the absorption

characteristics of the material. Optically, FEP is transparent in the visible region of the spectrum, but the absorbance begins to rise slowly below 300 nm. A complete absorption spectrum of FEP is not available in the literature, but the absorption spectrum of polytetrafluoroethylene (PTFE) has been reported,(see Fig.1), and that of FEP would be similar. The spectrum of PTFE is characterised by a strong absorption at 161 nm, which has been assigned to a transition from the HOMO levels for the C-C and C-F bonds to a conduction band (3). This peak has a long tail extending into the UV region. Below 130 nm, the absorbance of FEP again increases, due to the onset of the continuous absorption region of the material.

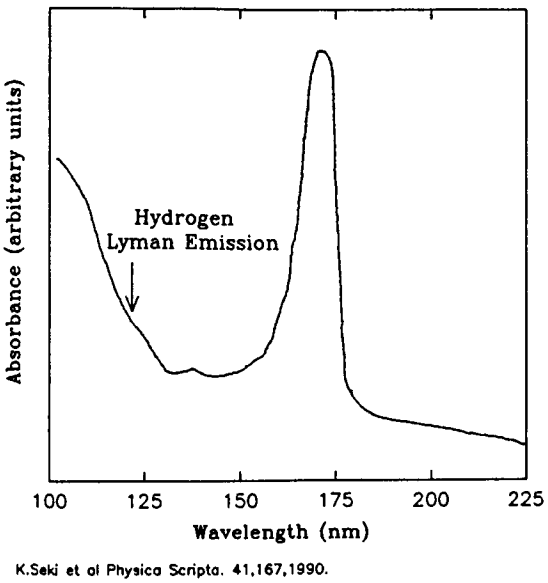

Figure 1: VUV absorption spectrum of PTFE.

Photoinduced degradation can only occur at wavelengths where there is a significant overlap between the solar spectrum and the absorption of the material (4). In the VUV region there is a significant overlap between the absorption spectrum of FEP and Lyman-α line of atomic hydrogen and the continuous solar emission at wavelengths above 150 nm (2).

Two reports published recently by NASA have dealt with studies of the effect of 5 years and 9 months exposure of FEP thermal blankets to the Low-Earth-Orbit environment (LEO) on the Long Duration Exposure Facility (LDEF)(1 and 5). Stiegman et al.(1) investigated the synergistic effect of VUV and atomic oxygen on the FEP surface. They concluded that samples which received only VUV radiation possessed a hard embrittled surface layer, that was absent in the samples which were exposed to VUV and atomic oxygen, and also in the unexposed control samples. Stiegman suggested that this surface layer resulted from a "synergistic" effect between VUV and atomic oxygen. Young and Slemp (5) concluded from the XPS, FTIR and thermal analyses that there was no significant change at the molecular level for FEP thermal blankets exposed to LEO. However, various microscopic analyses revealed a roughening of the surface due to atomic oxygen erosion, which resulted in some materials changing from specular reflectors to diffuse reflectors (5).

As part of a materials evaluation program for space applications, we have studied the effects of UV-VUV induced degradation processes in FEP virgin polymer (FEP100) and unetched commercial films. The studies involve the photo-generation of radical species in the polymer matrices as the initial steps in the degradation process. It is the aim of this paper to obtain molecular level information for the initial stages of photo-degradation processes by using ESR spectroscopy and also to assess the effect of VUV radiation and atomic oxygen on FEP surfaces using Scanning Electron Microscopy (SEM) and X-ray Photoelectron Spectroscopy (XPS).

EXPERIMENTAL

Samples of FEP commercial films and FEP100 virgin polymer beads were irradiated in vacuum in Spectrosil-A grade quartz ESR tubes (i.d. 3.0 mm), at room temperature using a high power xenon lamp (wavelength > 200 nm). The radical concentrations,[$R^{\cdot}$], were determined by ESR spectroscopy (Bruker ER-200D), utilising a strong pitch standard reference (3.0 x 10^{15} spin/cm). Spectra were determined at room temperature using Klystron frequency of 9.25 GHz, microwave power of 27db and magnetic field strength of 0.33 Tesla.

For surface analysis, (XPS and SEM), samples of FEP films were exposed to VUV radiation and atomic oxygen, which are generated using an oxygen plasma source designed specially for this purpose. The plasma tube was equipped with an earthed fine metal grid, which allows the passage of VUV radiation and atomic oxygen only, and prevents the plasma from reaching the polymer. Furthermore, the source was fitted with a removable MgF_2 window so that the polymer films could be separated from the flow of the atomic oxygen stream, to allow exposure to VUV radiation only. A Perkin-Elmer model 560 XPS/SAM/SIMS multi-technique surface analysis system and a JEOL model JSM 6400F Scanning Electron Microscope were used to evaluate the effects of VUV radiation and the synergistic effects of VUV and atomic oxygen on the FEP films.

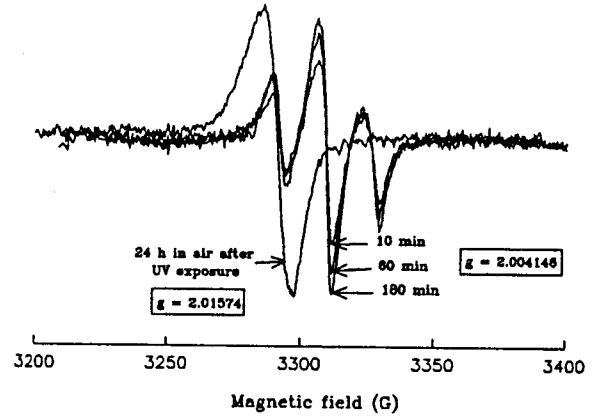

Figure 2: ESR spectra of FEP100 polymer exposed to UV radiation and air.

RESULTS AND DISCUSSION

ESR Studies:

Samples of FEP film and virgin polymer beads were irradiated in vacuum by a high power xenon lamp (Intensity = 9.1 mW/cm²), using quartz tubes at room temperature.

The ESR spectra of the radicals formed on exposure of the virgin FEP polymer beads (FEP100; obtained from DuPont Australia) to UV radiation (10-180 min.) in vacuum at room temperature are shown in Fig.2. The spectra are characterised by a triplet with a splitting of 17-18 G and g = 2.004. This triplet is identical to that observed by Kim and Liang (6), who assigned it to the chain scission radical I.

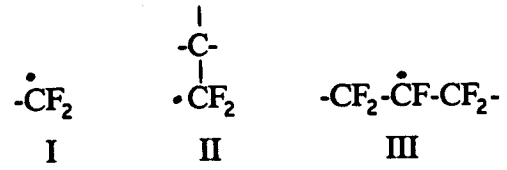

I II III

There was no evidence for the formation of radicals of the type II and III, which is also in agreement with Kim and Liang for irradiation with a xenon lamp.

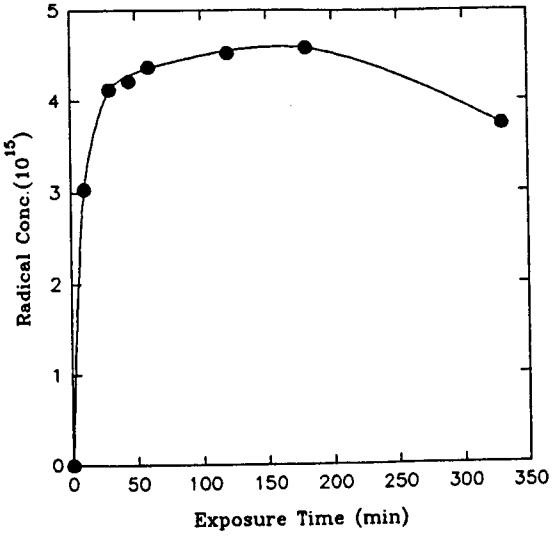

Figure 3: The effect of exposure time on radical concentration for FEP100.

The concentration of the chain scission radical increases with exposure time up to approximately 180 minutes, as shown in Fig.3. For exposure times beyond approximately 200 minutes, the radical concentration started to decline. This decrease in radical concentration could be due to a decrease in the concentration of the species responsible for radical formation.

Samples of irradiated virgin polymer (FEP100) stored in the dark under vacuum show a rapid decrease in the radical concentration due to recombination. After 24 h in the dark at room temperature all the chain scission radicals had decayed.

Samples of virgin polymer exposed to UV radiation under vacuum and then exposed to air have an ESR spectrum with a centre field shifted by 19 G to lower field (g = 2.016). The original triplet spectrum found for irradiation under vacuum is transformed into a broad singlet with a ΔH_{pp} of 9.3 G.

This spectrum can be assigned to the peroxy radical IV (6). A similar peroxy radical is formed on UV exposure of the virgin polymer in air.

IV

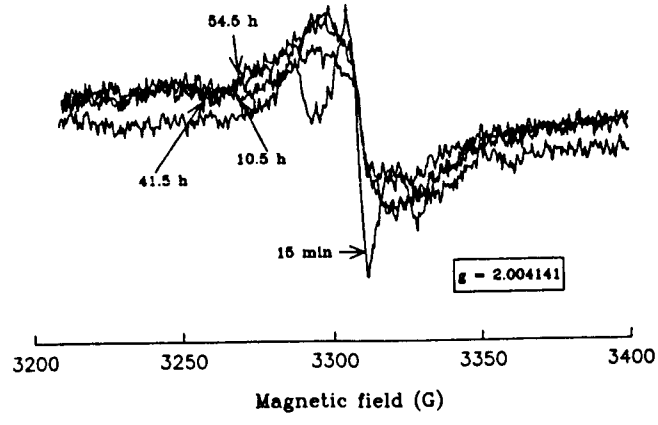

Figure 4: ESR spectra of FEP film exposed to UV radiation.

The ESR spectra of the FEP polymer film shows that samples irradiated for 15 min. produce a radical characterised by a triplet structure with an 18 G splitting (see Fig.4). This triplet is identical to that found for the virgin polymer, and is due to the chain scission radical I. On the other hand, the ESR spectra of the same polymer film irradiated for 1-60 h produces a completely

different spectral shape. The outer peaks of the triplet merge into the central peak. This behaviour could be explained by photodegradation of the FEP to form the chain scission radical, followed by reaction of this radical with an impurity present in the polymer film to form a new and relatively stable carbon centred radical. This impurity in the FEP polymer film could be for example a processing aid used in preparation of the film. The processing aid could be an antioxidant or stabiliser.

Furthermore, it was observed from this experiment that there was a fast build up of radical concentration in the first few minutes (2-15 min) of irradiation and then a sharp drop as the irradiation continued to about 75 min., see Fig.5. This decrease in the radical concentration coincided with the transition from the triplet ESR spectrum to a broad singlet. After approximately 75 minutes, the radical concentration then started to build up to higher values with increasing UV irradiation time (see Fig.5). This behaviour might be related to a time delay between the generation of the first radical species and the activation of the radical scavenger.

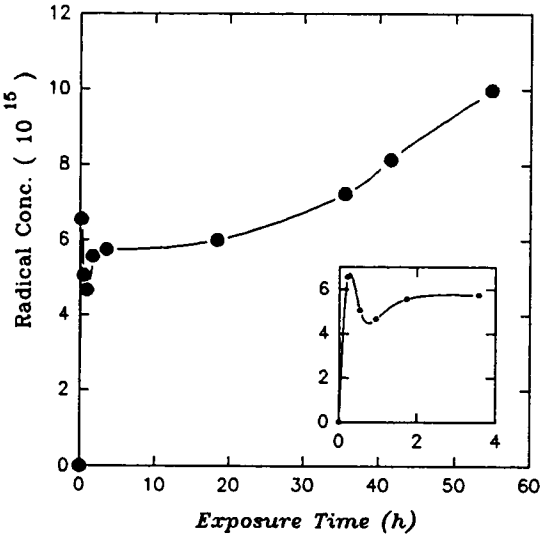

Figure 5: The effect of UV exposure time on radical concentration of FEP film.

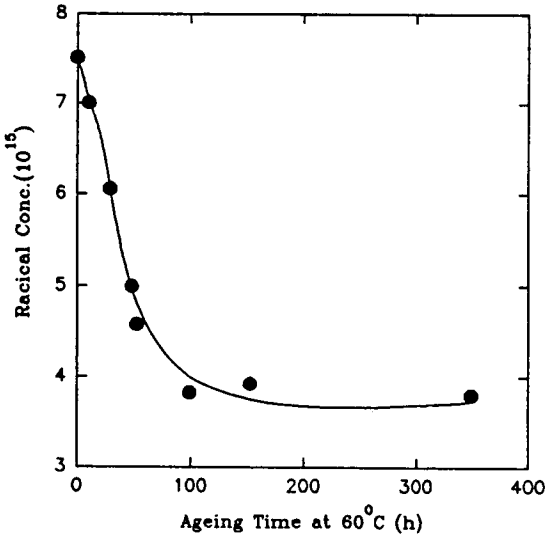

Figure 6: The effect of ageing at 60°C on radical concentration of FEP film exposed to UV radiation.

On ageing, the time dependence of the radical concentration at 60° C exhibited a relatively sharp drop (55%) in the radical concentration up to 100 h (see Fig.6). However, longer ageing to about 400 h produced no significant further change in the radical concentration. A similar trend was observed for the room temperature ageing of the UV irradiated polymer film, however the decay rate in the radical concentration was, as expected, slower than that for 60° c ageing (30% upto 100 h). This behaviour suggests that some of the secondary radicals are restricted from decomposition by their location in the polymer matrix.

The radicals responsible for the broad singlet species (g = 2.004) formed in the FEP polymer film were stable on exposure to air. Thus, their behaviour contrasts with that observed for the radicals formed by irradiation of virgin polymer, which reacted readily with oxygen to form peroxy radicals (g = 2.016).

Surface Analysis:

Surface analyses of FEP films were conducted using XPS spectroscopy and SEM.

The XPS multiplex spectrum at 25 eV pass energy of unirradiated FEP film for the C(1s) and F(1s) regions is shown in Fig.7. Using a set of standard sensitivity factors(7) the ratio of C:F was found to be 1:2, as expected for FEP. Thus, there is no significant contamination of the surface layer of the film, but a close examination of the C(1s) peak reveals a small tail in the lower binding energy region, containing approximately 3.6 percent of the total peak area. The reason for this tail is unclear, but possible contributing sources could include crosslinks, end groups, branches and oxidation of the polymer, although there was no evidence of a significant O(1s) peak. Curve fitting of the carbon peak yielded the analysis shown in Table 1. In this simulation, two minor peaks at 286.6 and 288.3 eV were used to account for the tail, but they are unassigned.

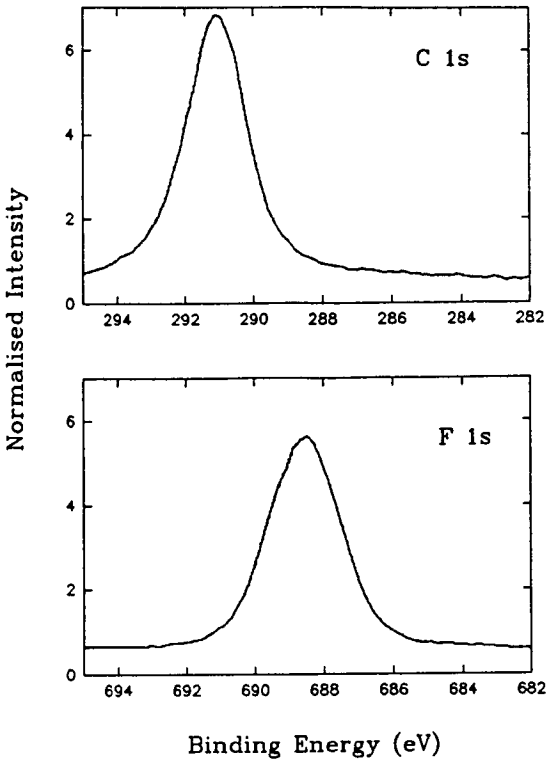

Figure 7: XPS spectrum of unirradiated FEP film.

Table 1: Percent composition of the FEP film from curve fitting of surface analysis data.

Binding Energy(eV)/ Chem.Bond	Unexposed FEP (%)	FEP Exposed to VUV & AO for 15 min. (%)	FEP Exposed to VUV & AO for 75 min. (%)	FEP Exposed to UV rad. then air (%)
285.0/ C-H	-	0.2	0.8	13.8
286.6/ C-C,C-O	1.2	1.2	1.4	5.7
288.3	2.4	2.5	2.7	2.7
289.5/ CF-CF_n	8.5	9.5	9.9	7.1
291.2/ CF_2	79.5	76.0	73.8	64.0
293.3/ CF_3	8.4	9.6	9.8	5.7
287.8/ C=O	-	1.0	1.5	1.0

The curve fitting analysis is consistent with a tetrafluoroethylene : perfluoropropylene ratio in the polymer film of 4.2:1. This ratio in the surface is lower than that generally reported for the composition of FEP copolymers, which is 6:1.

Exposure of FEP film to VUV radiation in the presence of atomic oxygen results in the oxidation of the polymer surface. This is revealed in the XPS spectrum, as demonstrated in Fig.8 by the presence of an oxygen peak. Furthermore, it was observed that the oxygen peak is very broad, which suggests the possible presence of various oxygen species. It is also revealed by an increase in the tail of the carbon peak. The curve fitting analysis of the carbon peak is given in Table 1. This increase in the area of the tail has been accounted for by inclusion of an additional peak at 287.8 eV, which has been assigned tentatively to formation of a carbonyl moeity. (The intensities of the unassigned peaks at 286.6 and 288.3 remain constant within experimental error). The important trends observed in Table 1 with increasing irradiation time are: an increase in the percentage of carbon attached to oxygen, a decrease in the percentage of CF_2 and an increase in the percentage of CF and CF_3. This suggests that oxidation takes place at the fluorinated ethylene units.

The changes in the F(1s):C(1s) and O(1s):C(1s) ratios with increasing irradiation time and atomic oxygen flux are shown in Table 2 and in Figs. 9 and 10, respectively. As the irradiation time increases, the fluorine to carbon ratio decreases and the oxygen to carbon ratio increases. At longer irradiation times, the rate of change in these ratios decreases, and the ratios appear to approach constant values. This observation would be consistent with a

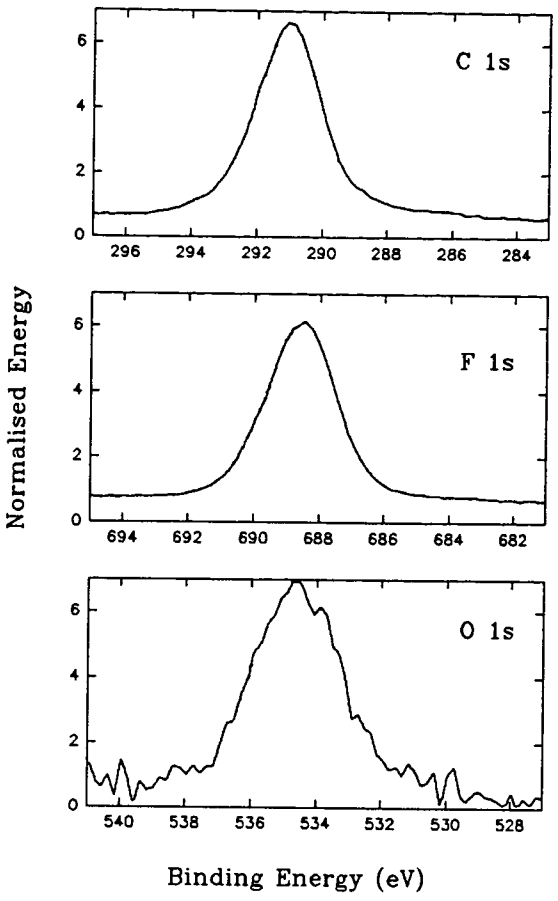

Figure 8: XPS spectrum of FEP film exposed to VUV and atomic oxygen.

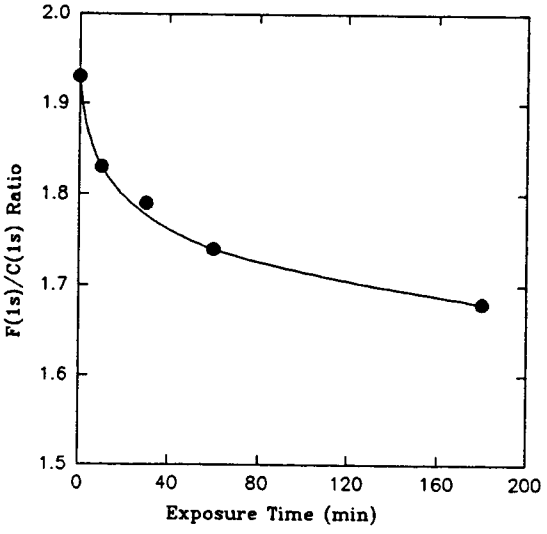

Figure 9: The change of F(1s)/C(1s) ratio in FEP film exposed to VUV and atomic oxygen.

gradual erosion of the polymer surface by the radiation, with a concurrent loss of small molecule products.

The oxygen atom flux was varied by changing the oxygen pressure in the plasma tube and by introduction of a MgF_2 window between the plasma and the polymer film. As shown in Fig. 10, the rate of oxidation of the polymer surface increases with the atomic oxygen flux.

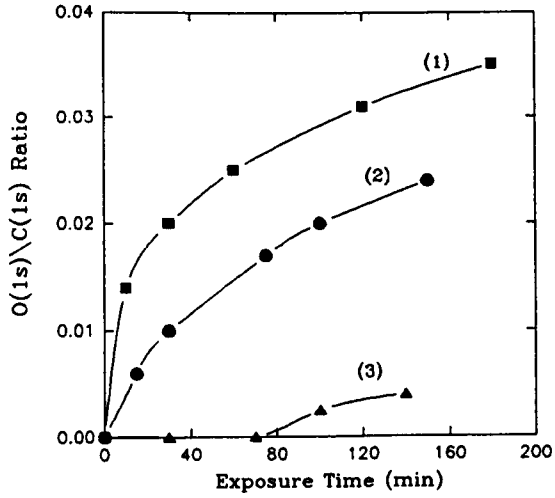

Figure 10: The effect of high(1), medium(2), and zero(3) oxygen atom flux on the surface of FEP film exposed to VUV radiation.

The XPS carbon spectrum (Fig. 11) of FEP polymer film irradiated by UV (xenon lamp) in vacuum and exposed to air immediately after irradiation showed about 1% oxygen atom concentration in the surface. This was attributed to the formation of C=O. Furthermore, additional peaks were observed in the C-C (286.6 eV)(8) and C-H (285.0 eV) binding energy regions of the XPS spectrum, which might be assigned to the formation of crosslinks between polymer chains and to the presence of hydrocarbon contamination, which might have resulted from the increased susceptibility of the oxidised polymer surface to laboratory contamination. A similar small hydrocarbon peak was observed in the FEP films exposed to VUV and atomic oxygen (see Table 1).

Compared with the films irradiated using VUV, the films irradiated with UV then exposed to air have a lower surface F(1s)/C(1s) ratio and a higher concentration of crosslinks. The O(1s) peak also appears narrower, suggesting a different distribution of oxidation products, which arise via peroxide formation in this case.

Table 2: XPS results for FEP polymer films exposed to simulated and actual space environment.

Peaks	FEP Type A	FEP (VUV & AO)	FEP(UV> 200 nm) and air	Control [a]	A10 Opaque [a]	C8 Opaque [a]
C1s(eV) AC (%)	291.1 34	291.1 35.2	291.6 40	290.9 31.6	290.9 28.5	290.9 30.4
F1s(eV) AC (%)	688.6 66	688.6 64.1	688.8 59	689 65.6	688.5 69.8	688.8 66.2
O1s(eV) AC (%)	- 0	534.4 0.7	532 1.0	- -	530.9 1.3	- <0.5

a: Data obtained from NASA technical report no.104096 (5).
AC: Atomic concentration (%).

The surface analysis of the FEP polymer film obtained in the simulated space environment used in the experiments described here are compared in Table 2 with those reported by Young and Slemp (5) for FEP polymer films exposed to the space environment in the LDEF experiments.

SEM micrographs of FEP film before and after exposure to VUV and atomic oxygen showed a dramatic change in the polymer surface (see Figs. 12). These micrographs show the extensive loss of polymer material during the VUV and atomic oxygen irradiation of the film. The texture of the surface becomes rough with regular undulations similar to sand dunes. Thus, as the polymer erodes and "new" surfaces are exposed, the chemical composition of the surface would be expected to approach a constant average value; as found by the XPS analysis.

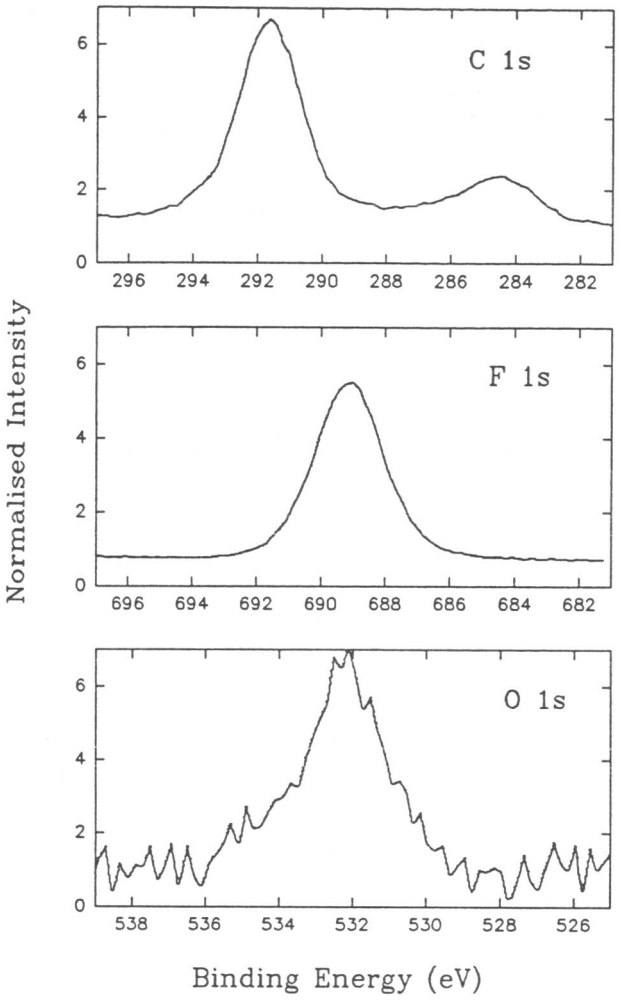

Figure 11: XPS spectrum of FEP film exposed to UV radiation and air.

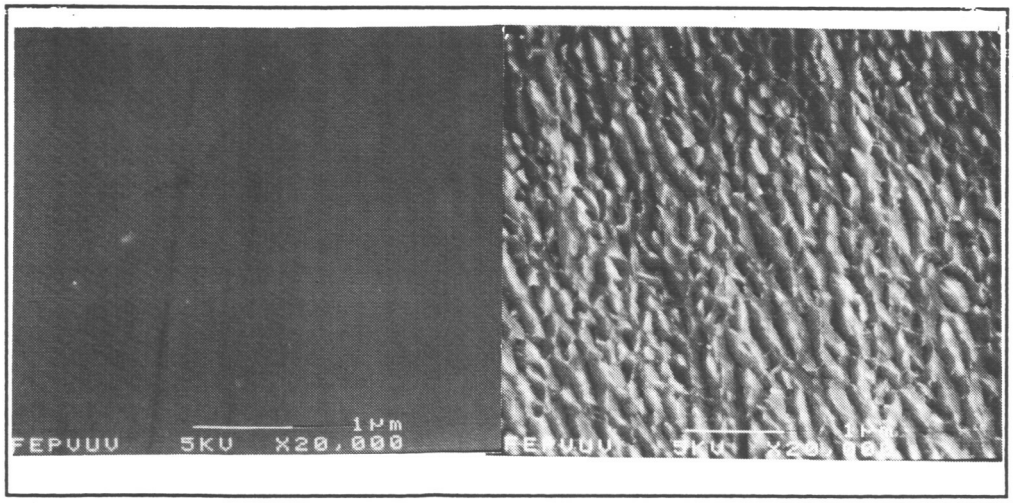

Figure 12: SEM micrograph of FEP film before and after exposure to VUV and atomic oxygen.

REFERENCES

1- A.E. Stiegman, D.E. Brinza, M.S. Anderson, T.K. Minton, and E.G. Liang, Jet Propulsion Laboratory Publication, 91-10, California Institute of Technology; Pasadena, California, USA.

2- D. Heath, and M. Thekaekara, The Solar Output and its Variation, Colorado Associated University Press, Boulder, CO, 1977, p. 193.

3- K. Seki, H. Tanaka, T. Ohta, Y. Aoki, and A. Imamura, Physica Scripta; 1990, 41, 167.

4- N.J. Turro, Modern Molecular Photochemistry, Benjamin/Cummings Publishing, Menlo Park, CA, 1979.

5- P.R. Young and W.S. Slemp, NASA Technical Memorandum 104096, Dec.1991.

6- S.S. Kim and R.H. Liang, Polym. Prepr.(Am.Chem.Soc., Div. Polym. Chem.), 1990, 31, 389.

7- R.J. Ward and B.J. Wood, A comparison of experimental and theoretically derived sensitivity factor for XPS. Surface and Interface Analysis, 1992, 18, 679.

8- D.R. Wheeler and S.V. Pepper, J. Vac. Sci. Technol. 1990, A8(6), 4046.

Acknowledgement

We would like to acknowledge support of this work by the National Aeronautics and Space Administration (NASA), Langley Research Center.

N93-28262

OUTGASSING AND DIMENSIONAL CHANGES OF POLYMER MATRIX COMPOSITES IN SPACE

R. C. Tennyson and R. Matthews
University of Toronto Institute for Aerospace Studies
North York, Ontario, Canada, M3H 5T6
Phone: 416/667-7710, Fax: 416/667-7799

SUMMARY

This report describes a thermal-vacuum outgassing model and test protocol for predicting outgassing times and dimensional changes for polymer matrix composites. Experimental results derived from a "control" sample are used to provide the basis for analytical predictions to compare with the outgassing response of LDEF flight samples.

THERMAL-VACUUM OUTGASSING AND DIMENSIONAL CHANGES OF LDEF POLYMER MATRIX COMPOSITES (AO180)

The UTIAS experiment consisted of a variety of graphite, aramid and boron fiber reinforced epoxy matrix composites located at station D-12 on LDEF (i.e., ~82° relative to velocity vector). Selected samples were instrumented with strain and temperature gauges that were sampled every 16 hours over the first 370 days in orbit. Data were stored on a magnetic tape cassette using a space-qualified data acquisition system designed and constructed at UTIAS. Details on this aspect of our experiment can be obtained from ref. 1. It was found that the strain/thermal gauge measuring system worked flawlessly, as evidenced by the measured response of a stainless steel calibration specimen which remained unchanged throughout the 5.75 years in orbit. Typical time/temperature and strain/temperature data for one material (graphite/epoxy, 5208/T300) are shown in Figs. 1 and 2, respectively. This data can be re-plotted as strain vs. temperature as given in Fig. 3 for the 90° laminate. It can be seen that a "total" dimensional strain change of $\sim 1600 \times 10^{-6}$ occurred after about 80 days in orbit. It should be noted that no microcracks were observed in this laminate and full recovery of the dimensional change occurred once the sample was returned to Earth and exposed to the ambient environment.

From this data, it is possible to estimate the coefficient of thermal expansion (CTE) from the final slope once all outgassing is essentially finished. Using this CTE value, one can correct for the temperature variations on-orbit, giving the strain change of the sample, over time, independent of temperature. The formula used to do this is:

$$\Delta_t = \varepsilon_t - (T_t - T_{Ref}) \cdot \alpha \qquad (1)$$

where

Δ_t = strain change at time t
ε_t = measured strain at time t
T_t = temperature at time t
T_{Ref} = reference temperature = 75°F
α = CTE of material.

Δ_t was then plotted against time and an adjustment factor (Δ adj) was added to every point. This had the effect of shifting the graph so that the final strain was zero, allowing the total strain change to be read easily. Figure 4 shows the adjusted Δ_t versus time curve for graphite/epoxy (5208/T300). From this graph it is

evident that outgassing was completed in about 80~100 days. It is clear that outgassing was very rapid over the first 25 days, then slowed due to the low temperatures encountered (see Fig. 1). Outgassing then increased after 50 days as the sample temperature increased, and eventually no further measured dimensional change occurred after about 80~100 days exposure. Similar behaviour was exhibited by the other composite materials (ref. 1). The outgassing time required to reach an equilibrium state in space depends on such factors as the initial moisture concentration, the volatile content, laminate thickness, ambient temperature and constituent material diffusion properties.

MOISTURE DESORPTION AND DIMENSIONAL CHANGES

As with many other published analyses, the moisture desorption can be estimated using Fick's law, given by (for example, ref. 2):

$$\frac{\partial c}{\partial t} = D \frac{\partial^2 c}{\partial x^2} \tag{2}$$

where
- c = moisture concentration at x
- t = time
- x = thickness coordinate
- h = thickness
- D = diffusion coefficient in the x-direction

and the following boundary conditions apply:

$$c(x, o) = c_o \text{ (initial concentration)}$$

$$c(o, t) = c(h, t) = c_\infty \text{ (ambient concentration)}$$

$$c(x, \infty) = c_\infty$$

Noting that the total mass change over time is given by

$$M = \int_o^h c(x, t)dx \tag{3}$$

a solution was obtained to Eq. (2) in terms of the moisture content variation with time:

$$M(T, t) = M_o(1 - G) \tag{4}$$

where M_o = initial moisture content (wt %), assuming the final moisture content = 0 in space, and

$$G = 1 - \frac{8}{\pi^2} \sum_{k=0}^{\infty} \left(\frac{1}{(2k+1)^2} \exp\left[\frac{-(2k+1)^2 \pi^2 Dt}{h^2} \right] \right)$$

$$\approx 1 - \exp\left[-7.3 \left(\frac{Dt}{h^2} \right)^{0.75} \right] \tag{5}$$

where

$$\begin{aligned} D &= \text{diffusion coefficient} = D_o \exp(-E_d/RT) \text{ (from ref. 3)} \\ R &= \text{gas constant} \\ T &= \text{absolute temperature} \\ E_d &= \text{activation (diffusion) energy} \end{aligned} \tag{6}$$

For constant temperature, Shen and Springer (ref. 4) have shown that the diffusion coefficient (D) can be calculated knowing the moisture content at different times, i.e.,

$$D_{T=const} = \frac{\pi h^2}{16 M_o^2} \left[\frac{M_2 - M_1}{\sqrt{t_2} - \sqrt{t_1}} \right]^2 \tag{7}$$

where

$$\begin{aligned} M_o &= \text{initial moisture content at start of desorption test} \\ M_1, M_2 &= \text{moisture contents at times } t_1 \text{ and } t_2, \text{ respectively} \end{aligned}$$

Rather than measure moisture content during a test, one can employ strain data. Noting that

$$\varepsilon = M\beta \tag{8}$$

where β = coefficient of moisture expansion (CME), then substituting into Eq. (4) yields:

$$\varepsilon(T, t) = \varepsilon_o(1 - G) \tag{9}$$

Substituting Eq. (8) into Eq. (7) also gives

$$D_{T=const} = \frac{\pi h^2}{16 \varepsilon_o^2} \left[\frac{\varepsilon_2 - \varepsilon_1}{\sqrt{t_2} - \sqrt{t_1}} \right]^2 \tag{10}$$

PREDICTING MOISTURE OUTGASSING FOR VARYING TEMPERATURES

To develop a model for predicting outgassing of materials in space, it is necessary to take temperature into account. However, Fick's law as previously described applies to constant temperature, constant

humidity environments. In space, the humidity level (i.e., vacuum) is constant. It is possible to determine the diffusion coefficient by performing outgassing tests at different temperatures (T_1 and T_2). Using the Arrhenius relation given by Eq. (6), one obtains the following two equations:

$$\ln(D_1) = \ln(D_o) - \frac{E^*}{T_1} \tag{11}$$

$$\ln(D_2) = \ln(D_o) - \frac{E^*}{T_2} \tag{12}$$

where $E^* = E_d/R$. Solving for E^* and D_o yields:

$$E^* = \frac{[\ln(D_2) - \ln(D_1)]}{\left[\frac{1}{T_1} - \frac{1}{T_2}\right]} \tag{13}$$

$$D_o = \exp\left[\left(\frac{\ln(D_2) - \ln(D_1)}{1 - \frac{T_1}{T_2}}\right) + \ln(D_1)\right] \tag{14}$$

Substituting back into Eq. (6) gives:

$$D(T) = \exp\left[\frac{\ln(D_2) - \ln(D_1)}{1 - \frac{T_1}{T_2}} + \ln(D_1)\right] \cdot \exp - \left[\frac{(\ln(D_2) - \ln(D_1))}{\left(\frac{1}{T_1} - \frac{1}{T_2}\right) \cdot T}\right] \tag{15}$$

This equation can be used to calculate the diffusion coefficient at any temperature, T, as long as the diffusion coefficients D_1 and D_2 at temperatures T_1 and T_2 are known. All of the above temperatures must be absolute (K).

APPLICATION TO LDEF SAMPLES

Experimental Input

1. Control samples were subjected to vacuum outgassing at elevated temperature to obtain their "dry weight" values.

2. For given temperature (T) and % RH, record moisture uptake (%) for given material from its "dry" state as a function of time (t) to saturation.

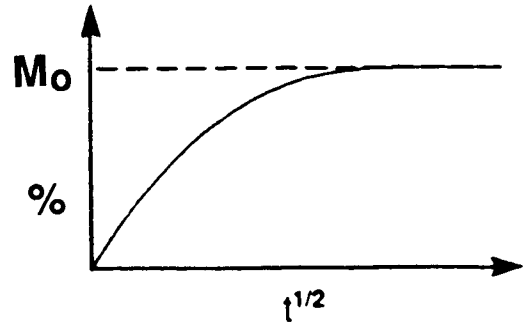

3. Measure sample strain (ε) as a function of time (t) in vacuum for a given temperature (T_1). Repeat experiment at another temperature (T_2). Both experiments employ samples having the same M_o.

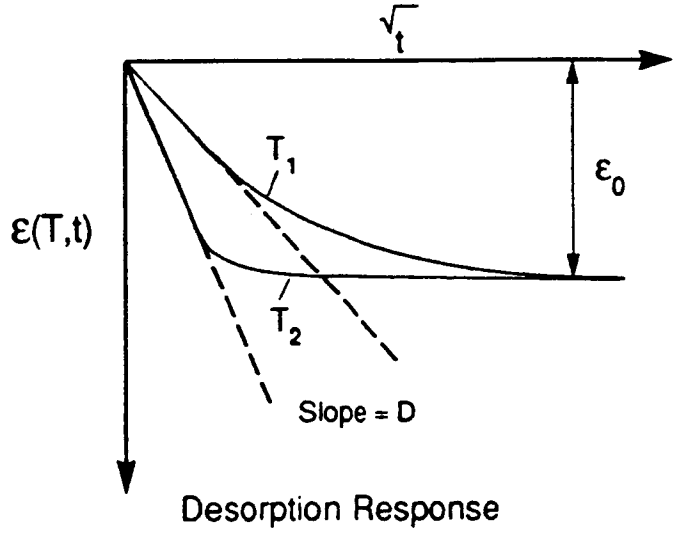

Desorption Response

Analytical Procedure

1. Using the ε(T, t) curves, calculate the initial slope from Eq. (10) to obtain $D_1(T_1)$ and $D_2(T_2)$.
2. Determine D(T) from Eq. (15) based on $D_1(T_1)$, $D_2(T_2)$, T_1 and T_2.
3. Using the LDEF temperature/time profile obtained in-orbit (see Fig. 1), calculate the dynamic strain change ε(t) for given time steps (Δt), using the above D(T) equation evaluated at the appropriate temperature. The ε(t) function is given by

$$\varepsilon_t = \varepsilon_{t-1} - \varepsilon_{t-1}\left(1 - \exp\left[-7.3\left(\frac{D(T_t)\cdot\Delta t}{h^2}\right)^{.75}\right]\right) \qquad (16)$$

where T_t = average temperature over Δt, assuming ε_0 is known at t = 0 from the outgassing test. By using this equation at every time step over the temperature history, it is possible to calculate the strain change of the sample due to outgassing, taking into account temperature effects.

COMPARISON WITH LDEF DATA

Before starting the outgassing tests, the samples were completely dried out under vacuum at elevated temperature. The dry weight and length of each sample were measured and recorded. The samples were then placed in a hygroscopic chamber to absorb moisture. Each sample was left until it absorbed the same amount of moisture as was outgassed from the equivalent LDEF sample. This value was determined by measuring the CME (β) of each material and then dividing the strain change measured on-orbit by β to give the total change in moisture content. Typical moisture absorption curves for three polymer matrix composites flown on LDEF are shown in Fig. 5. At this point in time, results will be presented only for one graphite/epoxy system — T300/5208, having the form of a 4 ply, 90° laminate $[90]_4$. The ground-based simulator tests were conducted on two tubes: a control sample (5T5) that had remained under ambient laboratory conditions since the manufacture of the LDEF flight specimens and a flight sample (2T13). Both 22°C and 50°C outgassing tests were performed on the control and flight samples. From CME calculations, it was determined that the flight data from sample 3T6 (Fig. 3) indicated a total moisture content change of .50%. Therefore, for all the tests on the T300/5208 $[90]_4$ samples, a moisture content as close as possible to this value was used, as summarized in Table I. The initial straight-line portions of the tests are plotted in Figs. 6 to 9 and a comparison of the β and D results presented in Table I. The nonlinearity at the beginning of these curves is due to temperature corrections. For about the first hour the samples had not reached equilibrium. On average, the 22°C and 50°C tests took about 13 days and 6 days to complete, respectively. Note that the diffusion coefficients of the control and flight samples agree quite well, indicating no significant changes occurred after 69 months of space exposure.

Using the temperature history of the flight sample (3T6) shown in Fig. 1, it was possible to predict its outgassing behaviour based on the results in Table I and Eqs. (15) and (16). A comparison with the flight data is given in Fig. 10. It is obvious that the predicted values do not fit the actual results very closely. However, if the predicted diffusion coefficient is reduced to 13.4% of its measured value, the predicted response is extremely close to the actual data as shown in Fig. 11. This indicates that the model itself is correct. The discrepancies may be due to differences between the test conditions and the space environment, such as a higher pressure or the presence of surface contaminants. It is also important to note that there is a large variability in the thickness and uniformity of the samples. Manufacturing variations may have caused the different diffusion coefficients of the samples. Ideally, it would be best to measure D(T) from sample 3T6, and see how well this prediction fits the flight data. Unfortunately, it was not yet possible to perform this test, although this will be done in the near future.

ACKNOWLEDGEMENTS

This research was sponsored by the Canadian Space Agency (CSA) under contract 025SR.9F009-1-1435, and two Ontario Centres of Excellence: the Institute for Space and Terrestrial Science and the Ontario Centre for Materials Research. Special thanks are extended to Dr. D. G. Zimcik of the CSA for his continued support of our work.

REFERENCES

1. Tennyson, R. C.: Composite Materials in Space — Results from the LDEF Satellite. *J. Canadian Aeronautics and Space Institute,* vol. 37, no. 3, Sept. 1991.

2. Crank, J.; and Park, G. S.: *Diffusion in Polymers.* Academic Press, London, 1968.

3. Whitney, J. M.; and Browning, C. E.: Some Anomalies Associated with Moisture Diffusion in Epoxy Matrix Composite Materials. *Advanced Composite Materials - Environmental Effects,* ASTM STP 658, J. R. Vinson, ed.; American Society for Testing and Materials, 1978.

4. Shen, Chi-Hung.; and Springer, George S.: Moisture Absorption and Desorption of Composite Materials. *J. Composite Materials,* vol. 10, Jan. 1976.

Table I. Summary of Simulator Outgassing Test Results for Graphite/Epoxy (T300/5208) Tube Laminates $[90]_4$

Sample No.	Type	Temp [°C]	M_i [%]	$\Delta\varepsilon$ [$\mu\varepsilon$]	CME [$\mu\varepsilon$/%]	D [mm^2/h]
5T5	Control	22	.49	-1200	-2449	.0001
5T5	Control	50	.55	-1939	-3525	.00047
2T13	Flight	22	.505	-1212	-2400	.00013
2T13	Flight	50	.632	-1517	-2400	.00078

Fig. 1 **Thermal History of LDEF Specimen (3T6)**
Graphite/Epoxy [90°]
5208/T300

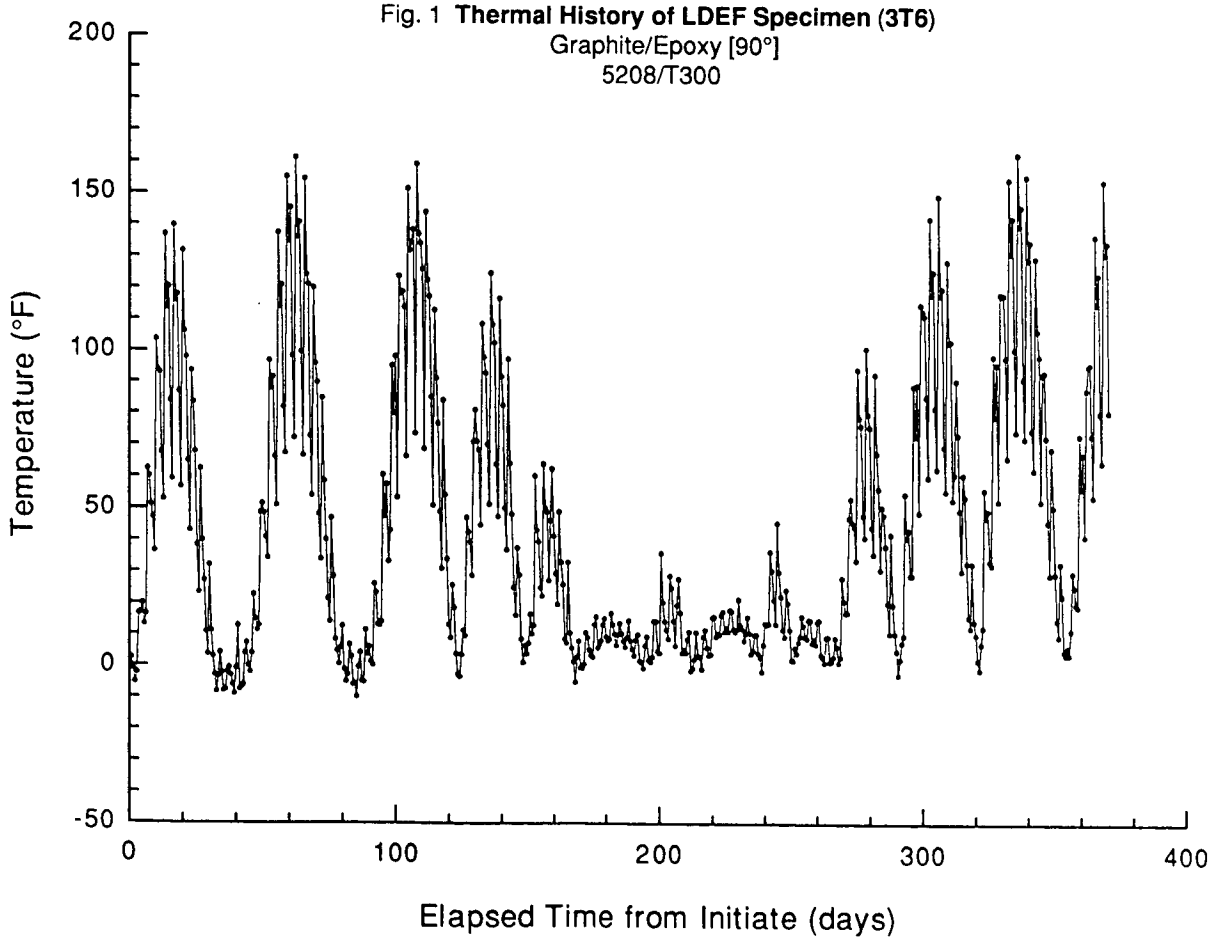

Fig. 2 **Strain-Time History for LDEF Specimen (3T6)**
Graphite/Epoxy [90°]
5208/T300

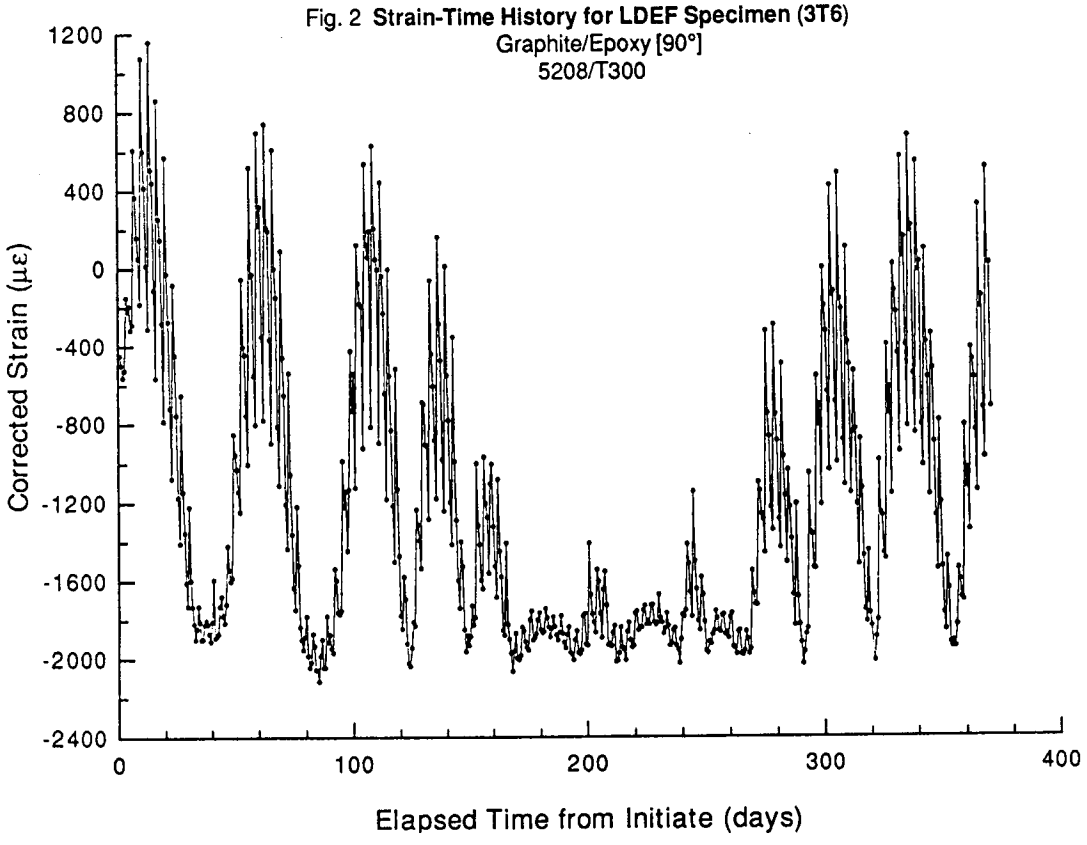

Fig. 3 **Thermal/Strain Response of LDEF Specimen (3T6)**
Graphite/Epoxy [90°]
5208/T300

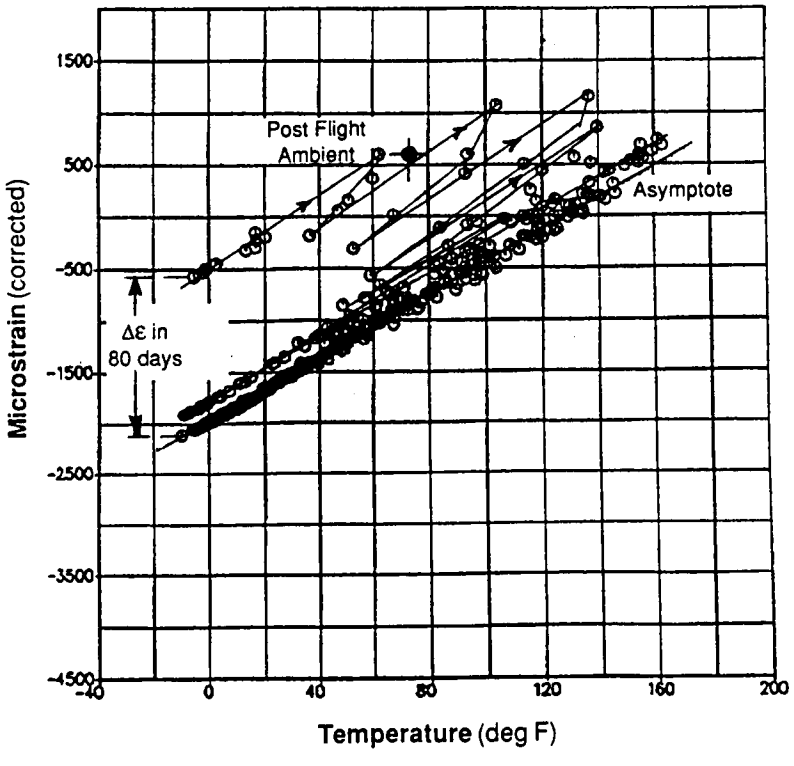

Fig. 4 **Plot of Δ Strain vs Time in Orbit for LDEF Specimen (3T6)**

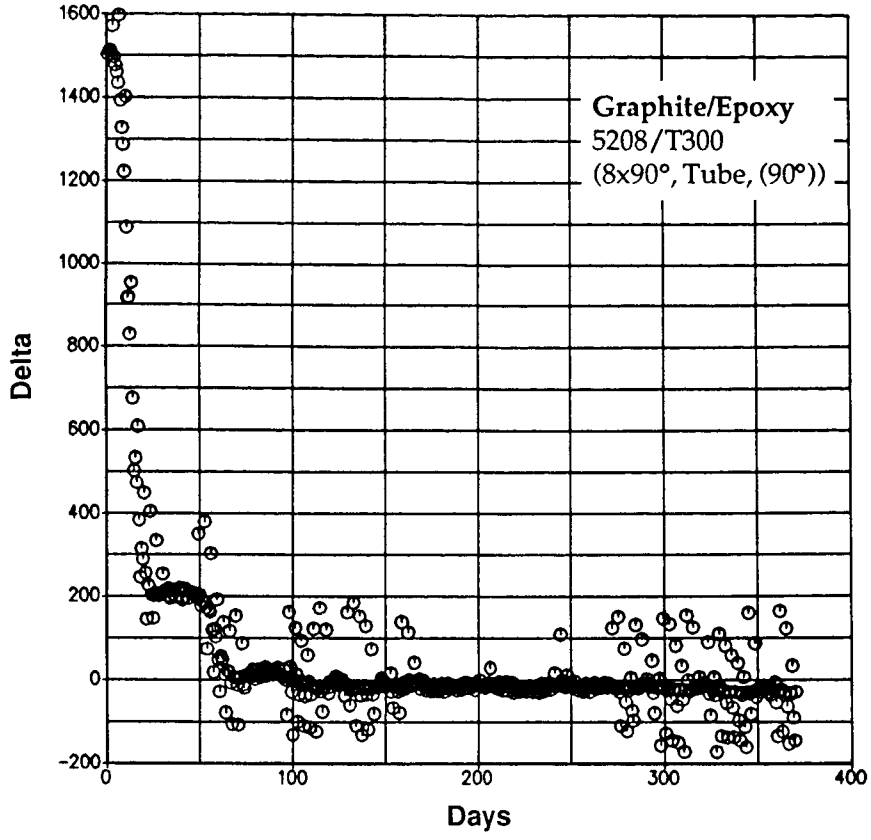

Fig. 5 **LDEF Control Moisture Absorption Test**
4 Ply 90 deg — 50 C — 75% RH

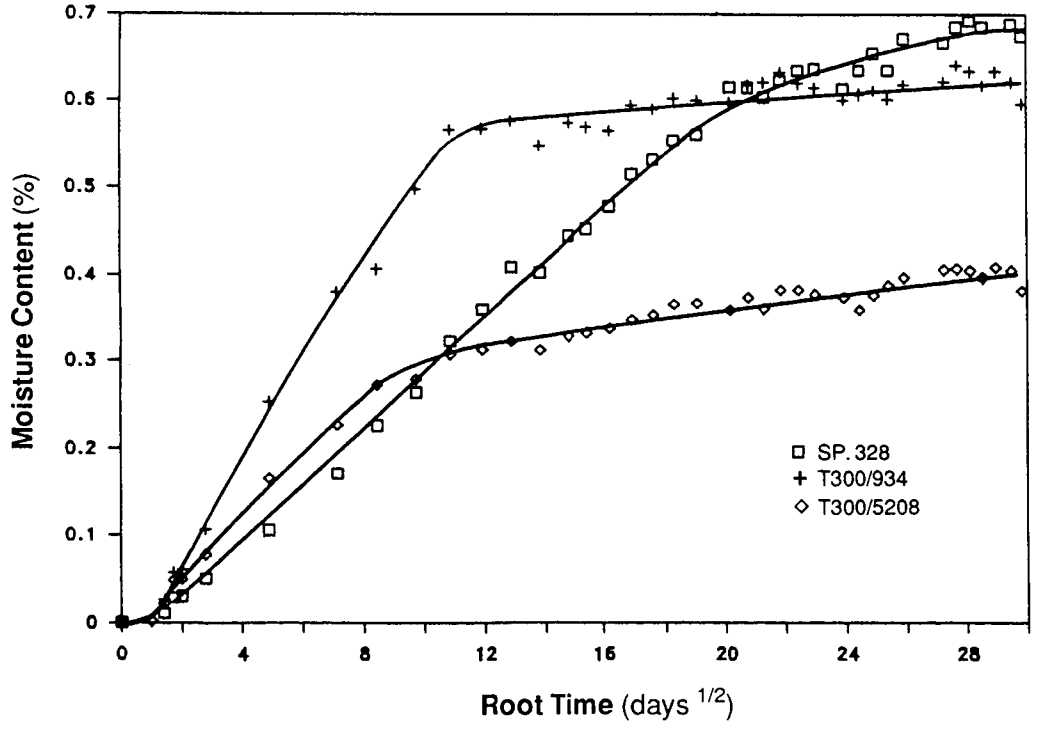

Fig. 6 **Outgassing Test on Control Specimen (5T5) @ 22°C**
Graphite/Epoxy [90°]
5208/T300

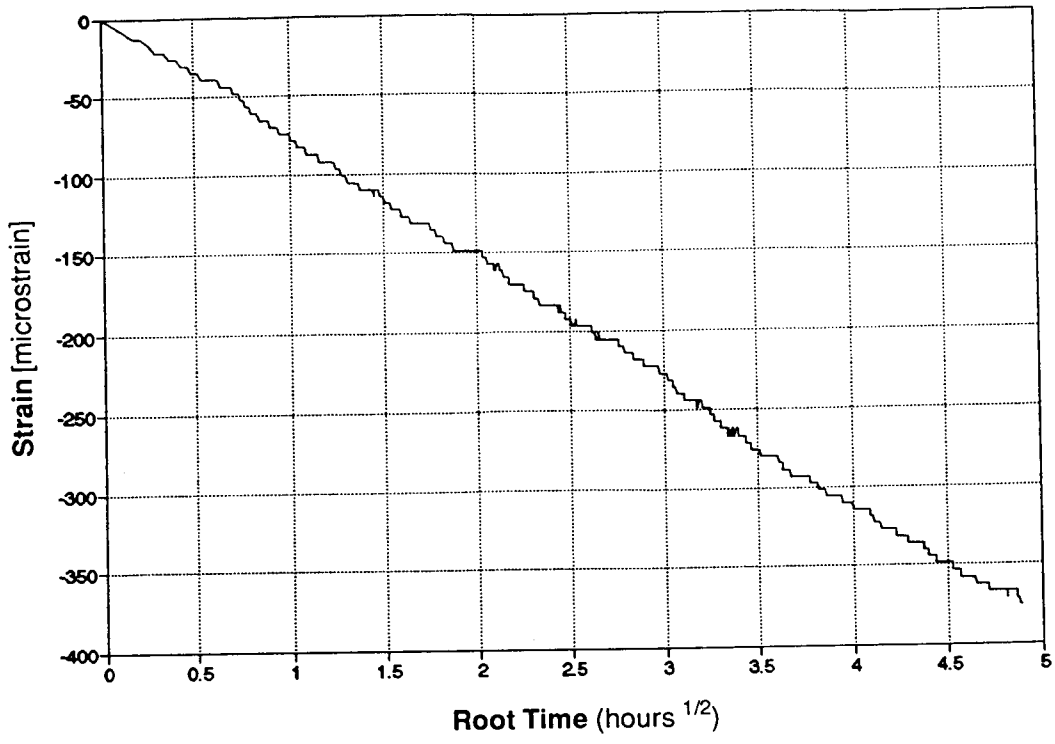

Fig. 7 **Outgassing Test on Control Specimen (5T5) @ 55°C**
Graphite/Epoxy [90°]
5208/T300

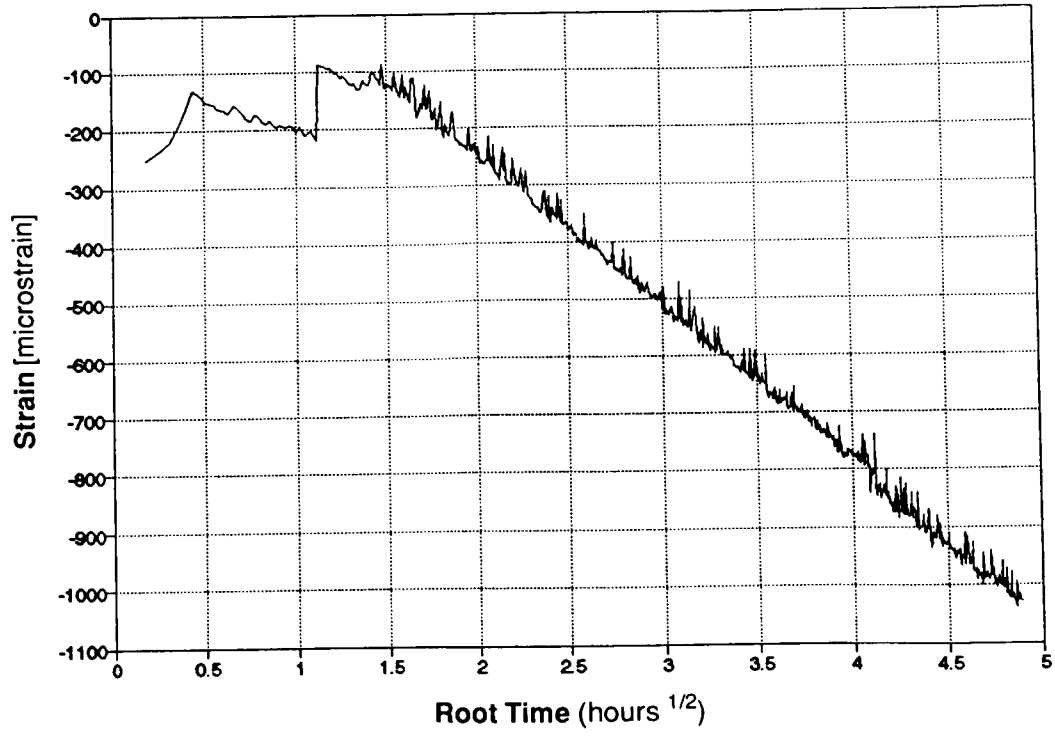

Fig. 8 **Outgassing Test on LDEF Flight Specimen (2T13) @ 22°C**
Graphite/Epoxy [90°]
5208/T300

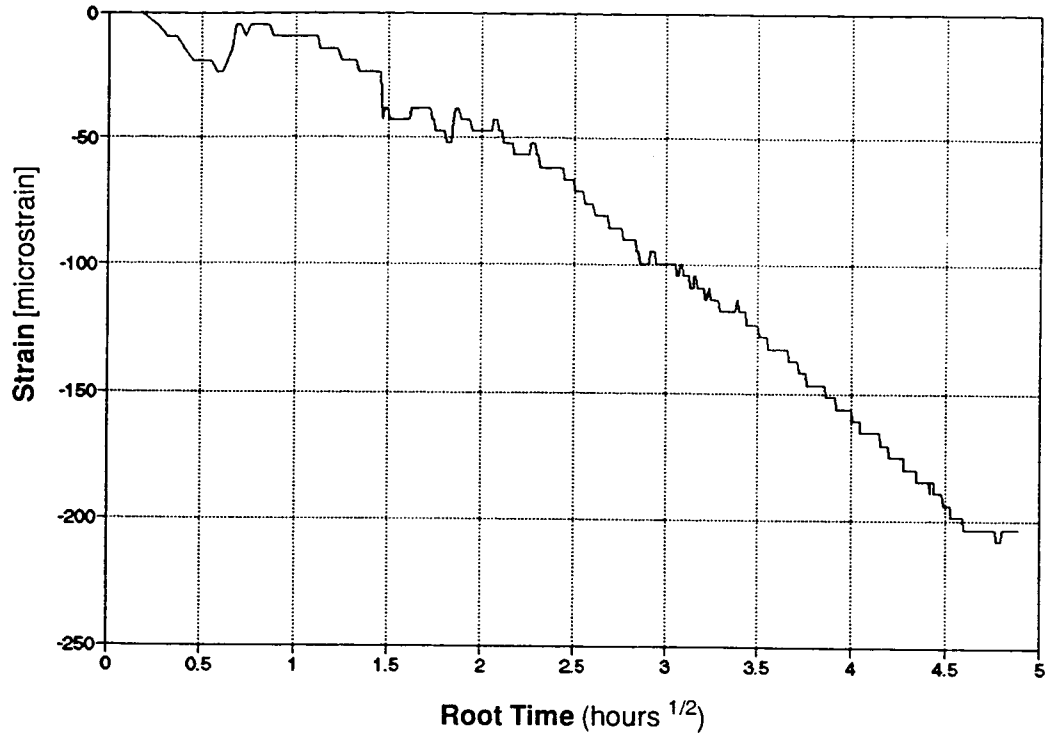

Fig. 9 **Outgassing Test on LDEF Flight Specimen (2T13) @ 50°C**
Graphite/Epoxy [90°]
5208/T300

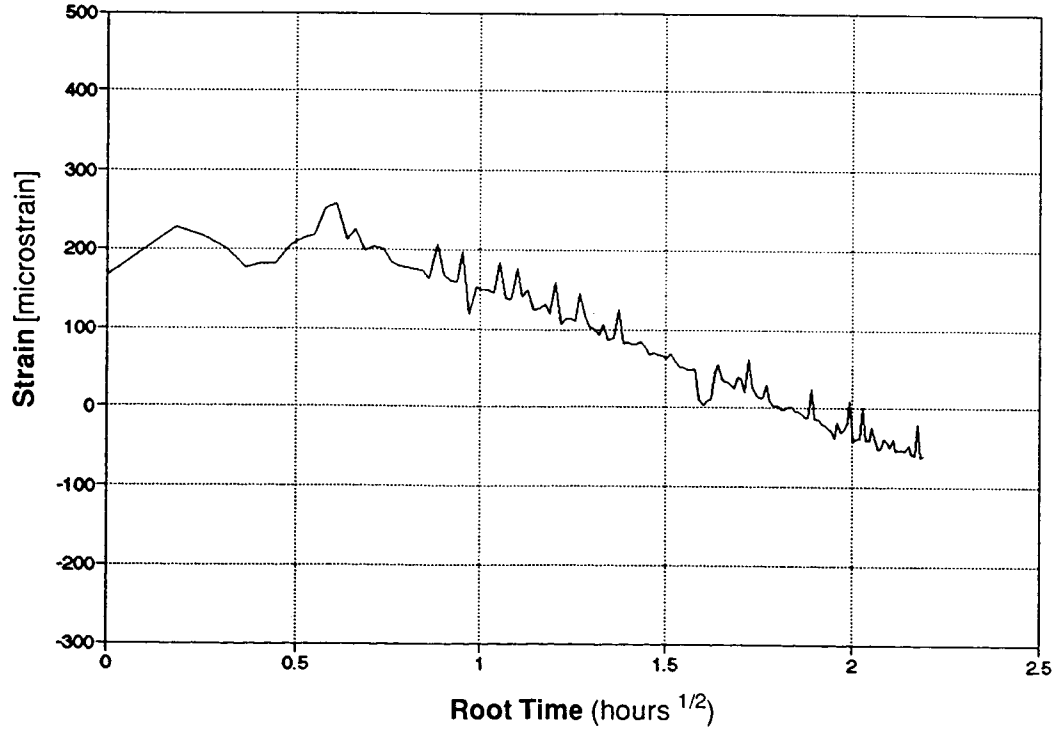

Fig. 10 **Comparison of Predicted Strain/Time Response in Space with LDEF Flight Specimen**
Graphite/Epoxy [90°]
5208/T300

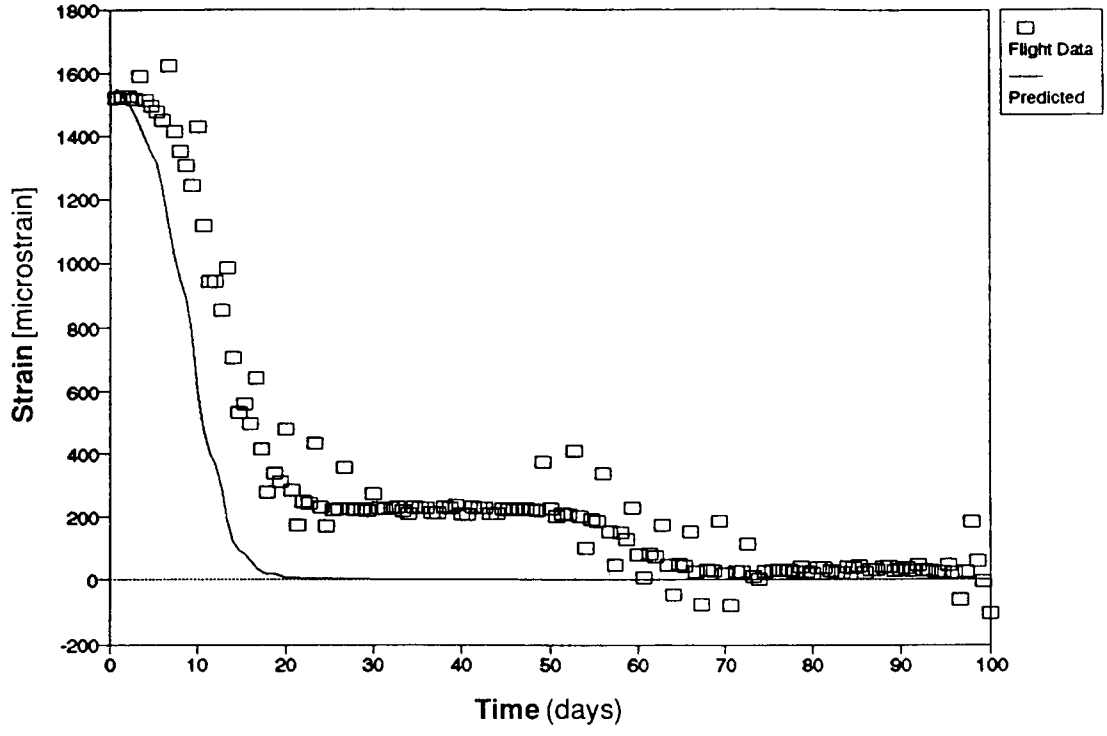

Fig. 11 **Comparison of Corrected Prediction of Strain/Time Response in Space with LDEF Flight Specimen (D* = 0.134D)**
Graphite/Epoxy [90°]
5208/T300

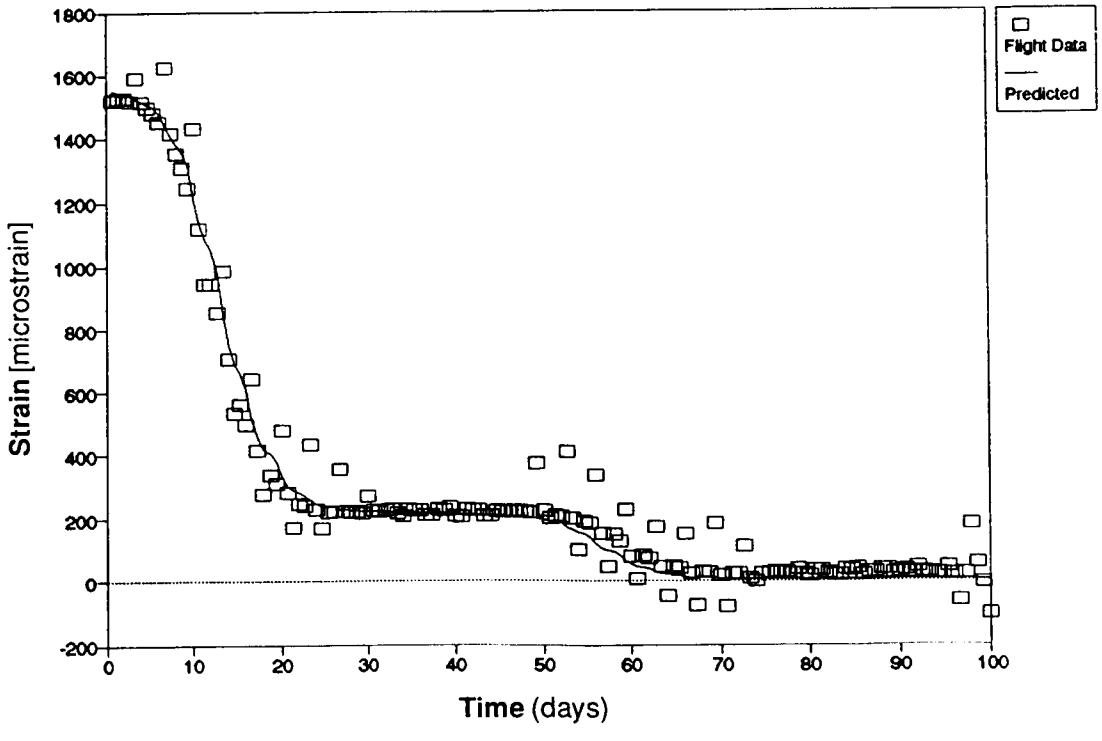

N93-28263

HIGH-TOUGHNESS GRAPHITE/EPOXY COMPOSITE MATERIAL EXPERIMENT*

David K. Felbeck
University of Michigan
2250 G.G. Brown Laboratory
Ann Arbor, MI 48109-2125
Phone: 313-994-6662; Fax: 313-665-9370

SUMMARY

This experiment was designed to measure the effect of near-earth space exposure on three mechanical properties of specially toughened 5208/T300 graphite/epoxy composite materials. The properties measured are elastic modulus, strength, and fracture toughness. Six toughness specimens and nine tensile specimens were mounted on an external frame during the 5.8-year orbit of the Long Duration Exposure Facility (LDEF). Three identical sets of specimens were manufactured at the outset: the flight set, a zero-time non-flight set, and a total-time non-flight set.

INTRODUCTION

The then-recent development of a procedure for improving the toughness of graphite/epoxy composites[1,2] provided an appropriate material for near-earth space exposure testing when the Long Duration Exposure Facility was publicly proposed by NASA/Langley in the late 1970s. This toughening procedure, termed *intermittent interlaminar bonding*, consists of introduction of a thin perforated layer of Mylar film between adjacent plies of a cross-ply composite so as to limit the area of inter-ply bonding. In this way, fracture of the composite is diverted when crossing regions have no bonding between plies, with a consequent substantial increase in total area of fracture and an increase in fracture energy, usually with only minor reduction in strength and elastic modulus.

TEST PROCEDURE

The tensile/modulus dumbbell-shaped specimens are each about 183 mm overall length with test section width about 20 mm, as shown in Fig. 1. All specimens with intermittent interlaminar control consist of eight layers of prepreg unidirectional T300 graphite tape with 5208 epoxy, plus seven layers of 7- μm thick Mylar, and are about 1.1 mm thick. For this study, orientations of the graphite cross-ply were either ±20° or ±45°. The prepreg composite of T300 graphite with 5208 epoxy was Narmco Lot 50548470, batch 20, roll 20, having density of 142.2 g/m² and 32.6% resin. The Mylar used contains evenly spaced holes of 1.1-mm diameter in a matrix spaced appropriately for the per cent contact desired. For specimens with 0% contact, Teflon was sprayed on each of the contacting layers of prepreg

*This work was performed under National Aeronautics and Space Administration Langley Research Center Grant NAS1-17008.

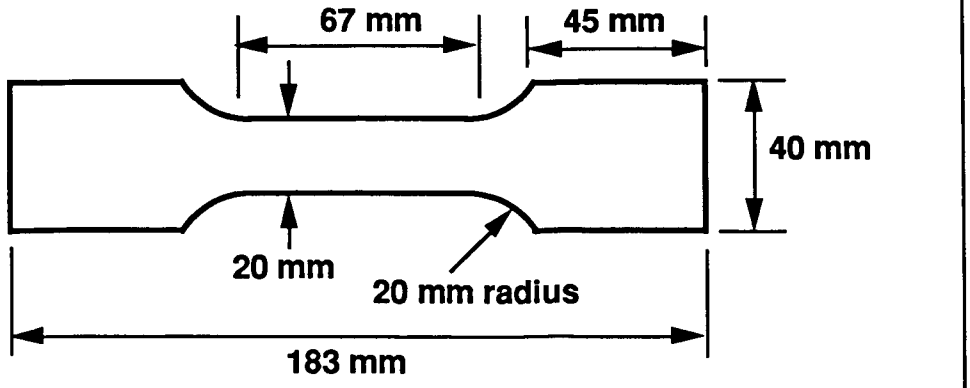

Figure 1. Tensile/modulus specimen.

prior to curing so as to prevent interlaminar bonding. Specimens for 100% contact were cured with nothing between adjacent layers. Curing of all specimens was in accordance with the manufacturer's specifications. Using steel friction grips, each specimen was tested initially for elastic modulus at moderate loads and a crosshead speed of 0.5 mm/min, then later fractured to measure strength as the maximum stress (load/net area) during the test. (Elastic modulus is the ratio of incremental stress to incremental strain at stresses well below the fracture stress; that is, where the stress-strain curve is virtually a straight line.)

The fracture toughness compact-tension specimens are about 190 mm long and about 70 mm wide overall, as shown in Fig. 2. A narrow 27.5-mm transverse slot is machined on the initiation side, and a 22.5-mm 60° notch is cut out on the termination side to control out-of-plane buckling, with a net test section width of approximately 20 mm. Each specimen with intermittent interlaminar control consists of eight layers of prepreg plus seven layers of Mylar in the same manner as for the tensile/modulus specimens. The 100% and zero per cent contact specimens are likewise the same layup (either ±20° or ±45°, as listed in Table 1) as for the tensile/modulus specimens. Each specimen is mounted in a loading frame as shown in Fig. 3. Each half of the frame is made of 8-mm thick structural steel and is loaded as shown by the arrows in Fig. 3. A matrix of compression screws to secure the specimen, not shown here, was found to be necessary to prevent slippage of the specimen.

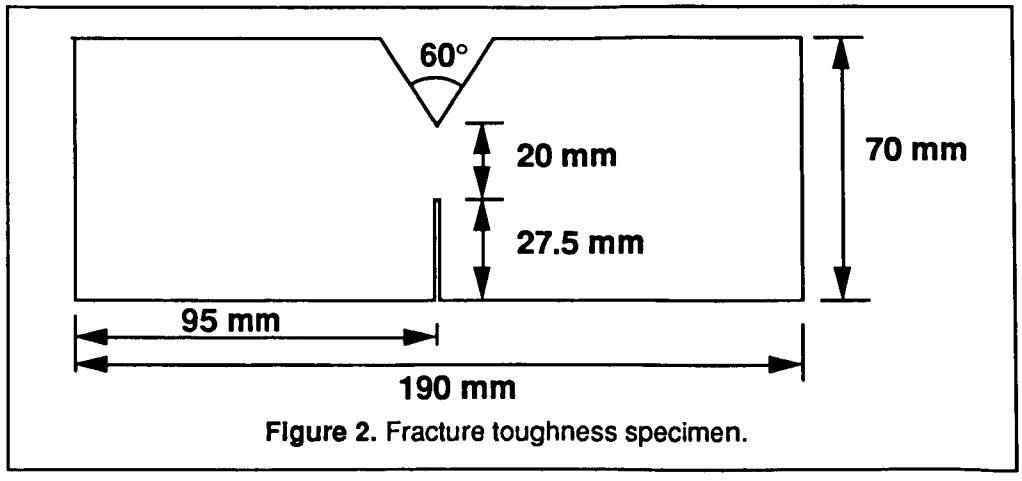

Figure 2. Fracture toughness specimen.

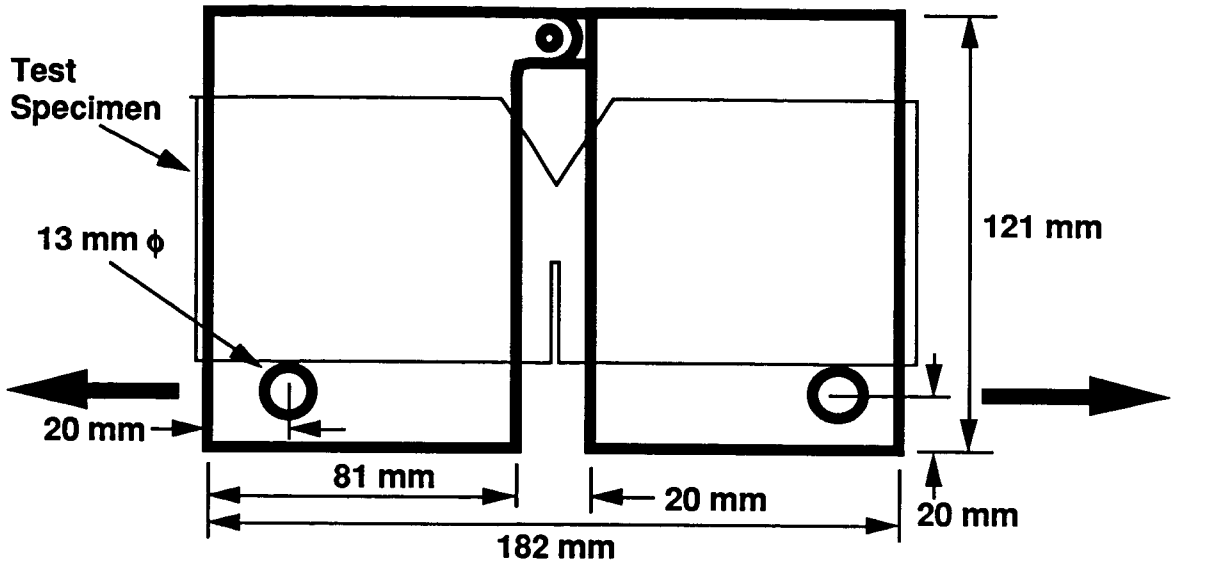

Figure 3. Fracture toughness frame.

Because the compact-tension specimen permits slow stable fracture to occur, the load-displacement curve can be recorded, in accordance with the Gurney method[3], at a crosshead speed of 0.5 mm/min. In this case we made the arbitrary assumption that all work done following an 80% drop from the maximum load is neglected; in fact, each specimen would continue to absorb energy until complete separation is achieved, so this assumption leads to a conservative measure of fracture energy. This additional energy would normally be expected to exceed the elastic energy that would be given up by the specimen if it could return to its initial displacement. The net work done divided by the *apparent* minimum fracture area (specimen thickness times increase in crack length) is thus the fracture toughness R, where stress intensity factor $K_{Ic} = [ER]^{1/2}$; E is the elastic modulus. Note that K_{Ic} is here not plane strain stress intensity factor, but the Mode I critical stress intensity factor. With the relatively large values of toughness measured, the ratio of stress intensity factor divided by yield strength (in this case the fracture stress), upon which the radius of the plastic region depends, would mandate thicknesses one to three orders of magnitude greater than the subject specimens in order to achieve mostly plane strain conditions. Thus the results obtained here for plane stress are meaningful for the range of thickness measured, as well as foreseeable thicknesses that might be used in actual structures.

For each of the two classes of specimens, tensile/modulus and fracture toughness, the cross-ply angle and the fraction (percent) of contact between adjacent plies are varied. The interlaminar contact fraction is controlled by the spacing and thus the fraction of holes in the Mylar sheet.

EXPERIMENT LOCATION

Our experiment was located on LDEF in tray D12, which was oriented so that the vector normal to the plane of the tray was 82° from the velocity vector; this panel received relatively low solar exposure. The layout of the 15 specimens, and their orientation with respect to space and the approximate

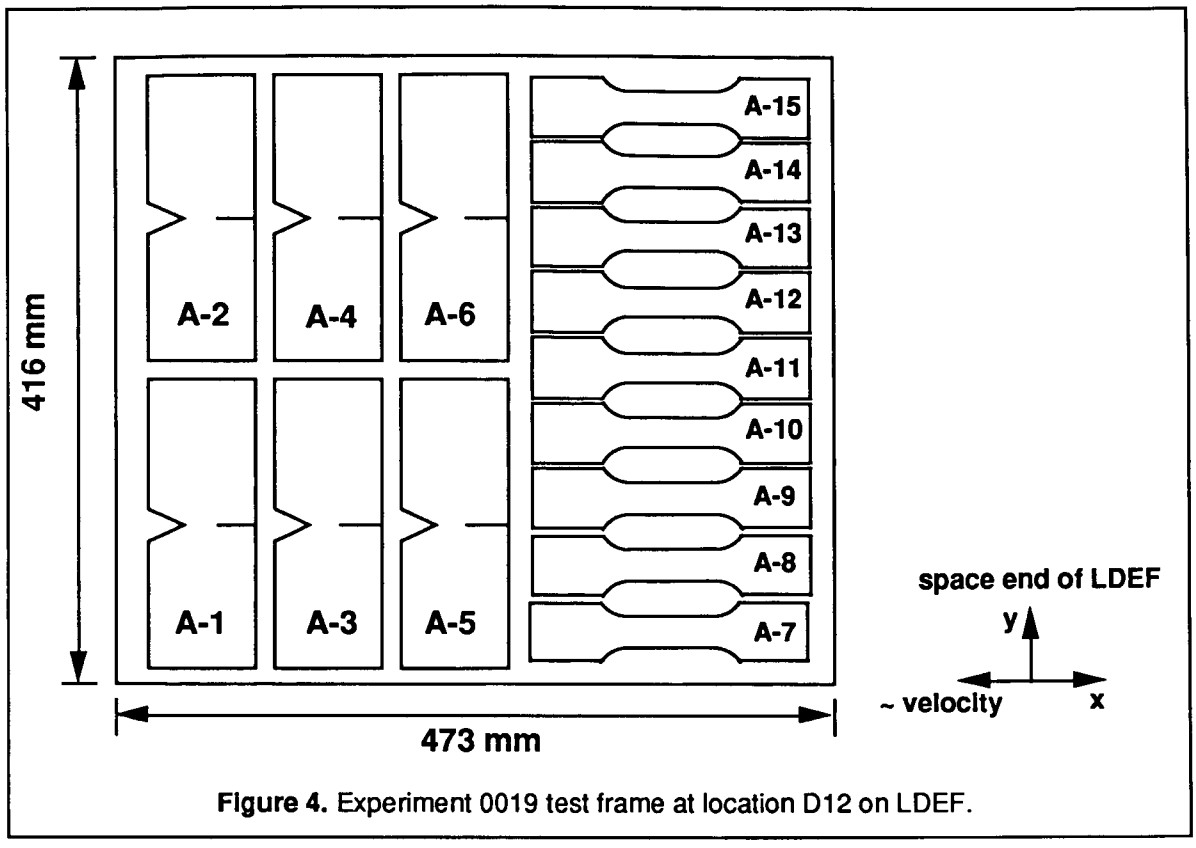

Figure 4. Experiment 0019 test frame at location D12 on LDEF.

velocity vector of LDEF, are shown in Fig. 4. All specimens were held in place with thin aluminum strips bolted to the test frame, not shown in the sketch. Measurement of the extent of atomic oxygen exposure has been made by other LDEF experimenters. Of particular importance here is that atomic oxygen produced erosion only in the surface epoxy but caused no loss of graphite filaments in our experiment.

RESULTS

All specimens were manufactured in December 1982, in preparation for delivery of the flight specimens to Langley the following spring. All specimens for each of the 15 groups were cured at the same time from the same batch. LDEF was launched in April 1984, approximately 16 months after manufacture of our specimens. The three sets of specimens were designated as:

Set A: flight specimens, to be flown on board LDEF
Set B: "zero time" specimens, to be tested at the time of the launch of LDEF
Set C: total time, ground specimens, to be tested after the flight along with Set A

Six fracture toughness specimens (group numbers 1-6) and nine tensile/modulus specimens (group numbers 7-15), of varying layup angle and per cent contact, were manufactured for each of the three sets. Complete descriptions of the characteristics of each group of specimens, date of manufacture, date of testing, and results are compiled in Table 1.

Toughness results are shown in Figs. 5 through 10. Our past experience with composite specimens of the same type had shown some modest scatter in results, but we had never tested specimens that were more than a few months old. In the present program, even the "zero time" specimens, Set B, were approximately 18 months old when tested, and the rest of the specimens were about 100 months old. The scatter in results between the zero-time specimens (Set B) and the total-time ground specimens (Set C) was therefore unanticipated. Because of these substantial changes in properties with time, we have elected to display all test results as a function of time since manufacture. We have no explanation for the observed changes; additional studies of the effects of aging in composite materials of this type are clearly warranted.

Figures 5-10 demonstrate that, in general, fractional per cent contact produces the highest values of toughness, as would be expected from the basic mechanism of partial bonding. Thus the toughness for 18% (Fig. 6) and 36% (Fig. 9) contact are higher than for 0% contact (Figs. 5 and 8), and much higher than for 100% contact (Figs. 7 and 10). In every case, toughness of the flight specimens was less than of the zero-time specimens; this suggests degradation from exposure. But as already noted above, we have no explanation for increases with toughness with time of ground specimens and, in Fig. 5, a marked decrease in toughness with time. (The datum for Set C of Group 3, Fig. 7, was lost.)

Modulus results are shown in Figs. 11 through 19. Elastic modulus of the ground specimens either remained the same or decreased. Both ground specimens having 100% contact (Figs. 14 and 18) show marked decreases in modulus. The scatter in modulus of flight specimens appears to follow no consistent pattern, and the very limited number of tests precludes further conclusions. The testing procedure for measuring modulus is rather critically dependent on control of specimen slippage, with scatter observed in repeated tests; thus we have used average values here. The widely different values of modulus in Groups 8 and 9, which are the same lay-up, demonstrate this problem.

Strength results are shown in Figs. 20 through 28. Measurement of strength of these composites is more precise than measurement of toughness or modulus, as can be noted by the closeness of values for Groups 8 and 9. Scatter of ground specimens is less for the strength specimens, and flight specimens are in every case but one (Fig. 22) lower in strength than total time control specimens. (Datum for Set B in Fig. 23 was lost.) We may conclude that flight exposure led to some degradation in strength in almost all cases.

Toughness of flight specimens is given in Fig. 29, with corresponding lay-ups and per cent interlaminar contact. For each ply angle, the partial per cent contact provides the highest toughness after exposure and the 100% contact the lowest.

Figure 30 shows the elastic modulus of all flight specimens. The ±45° specimens are all of low modulus; all of the ±20° specimens show several times the modulus of the ±45° specimens. That one of the ±20° 18% specimens shows much higher modulus than the corresponding 100% contact specimen suggests that the ±20° 18% datum may be the result of an inaccurate measurement. The strength of the flight specimens, Fig. 31, shows a similar difference between the ±45° specimens and the ±20° specimens. As expected, the 100% contact specimens for both angle layups show the highest strengths.

Fig. 5. Group 1: ±20°, 0% contact

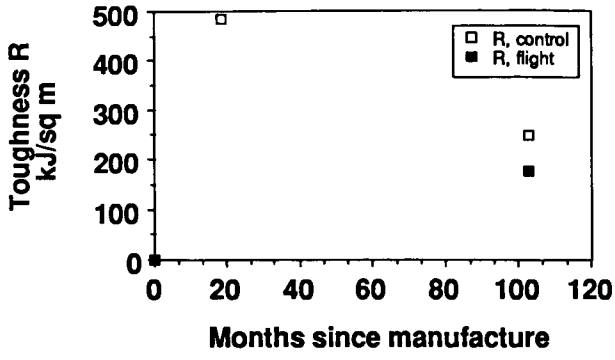

Fig. 6. Group 2: ±20°, 18% contact

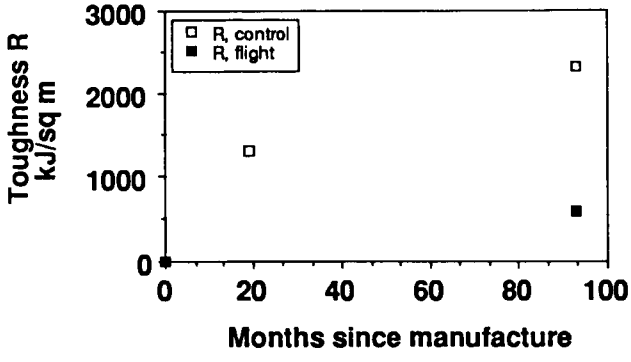

Fig. 7. Group 3: ±20°, 100% contact

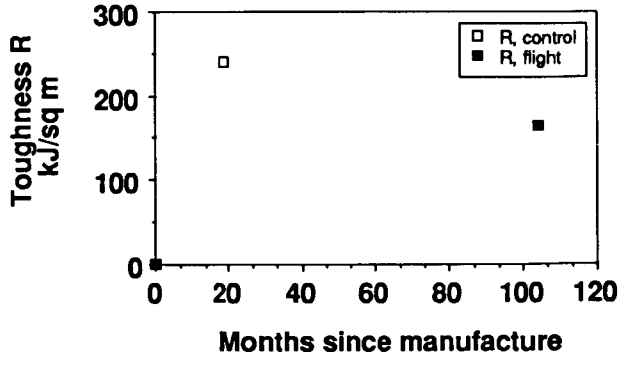

Fig. 8. Group 4: ±45°, 0% contact

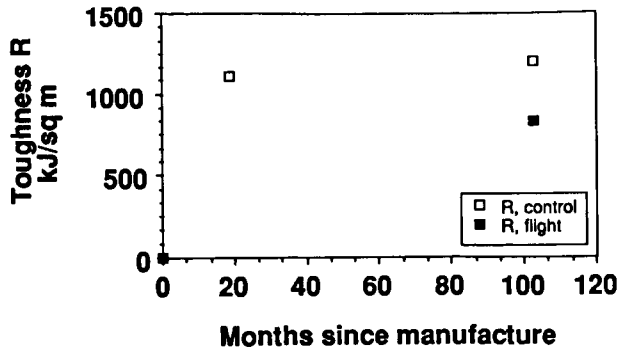

Fig. 9. Group 5: ±45°, 36% contact

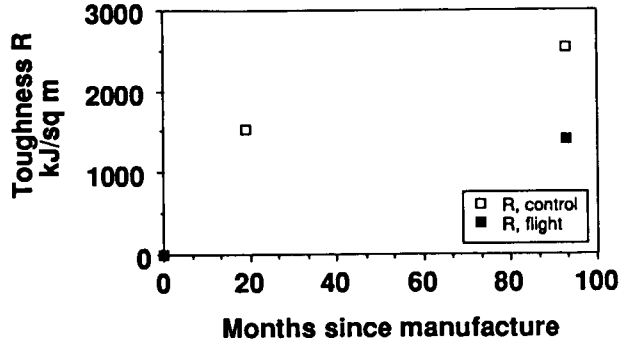

Fig. 10. Group 6: ±45°, 100% contact

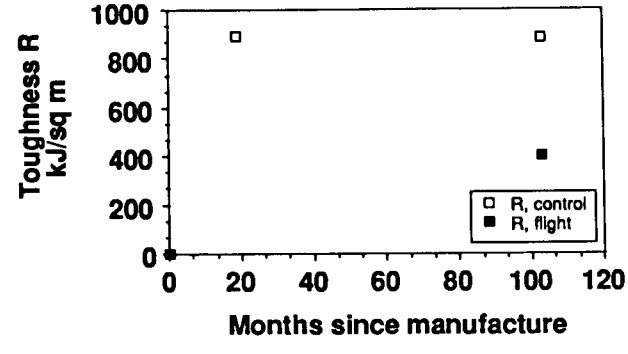

Figures 5-10. Toughness results.

Fig. 11. Group 7: ±20°, 0% contact

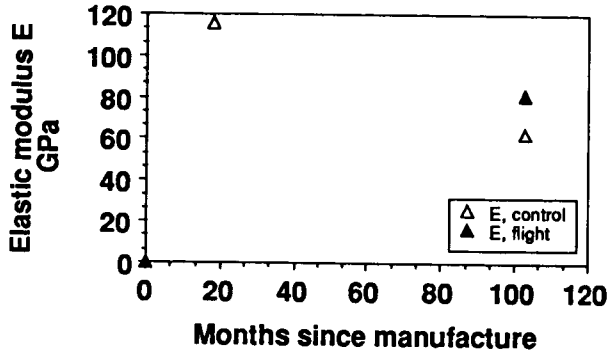

Fig. 12. Group 8: ±20°, 18% contact

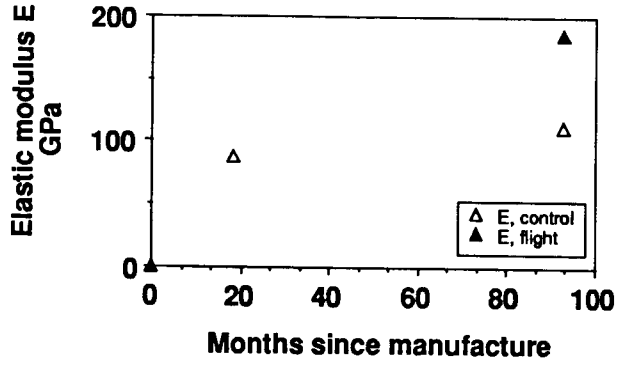

Fig. 13. Group 9: ±20°, 18% contact

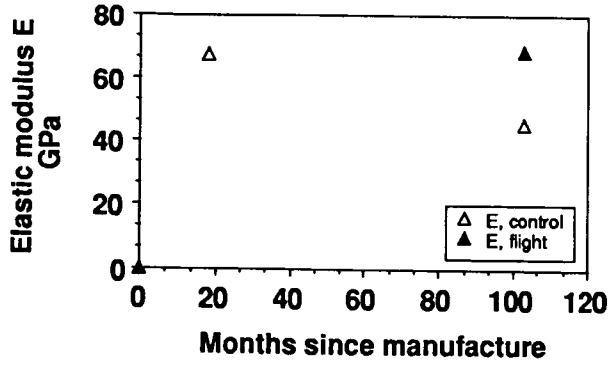

Fig. 14. Group 10: ±20°, 100% contact

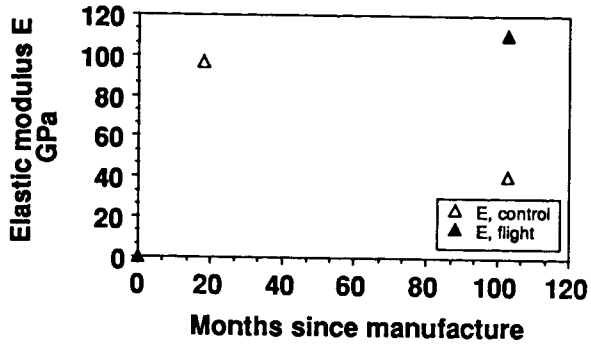

Fig. 15. Group 11: ±45°, 0% contact

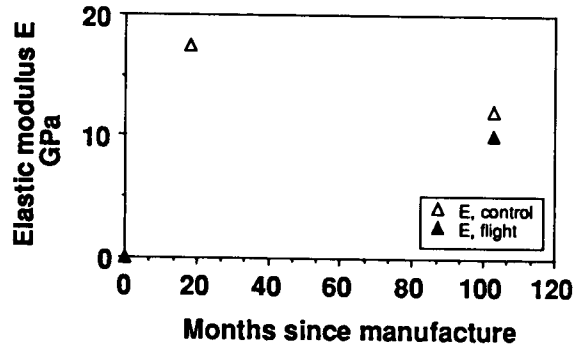

Fig. 16. Group 12: ±45°, 36% contact

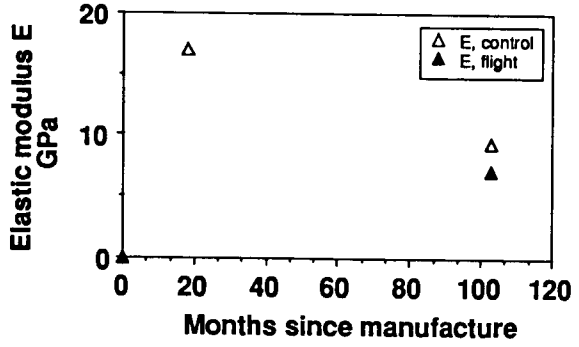

Figures 11-16. Elastic modulus results.

Fig. 17. Group 13: ±45°, 36% contact

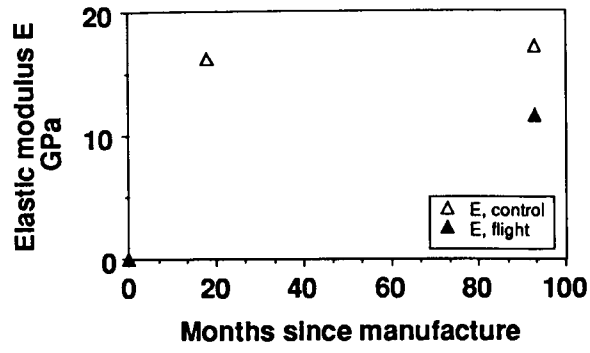

Fig. 18. Group 14: ±45°, 100% contact

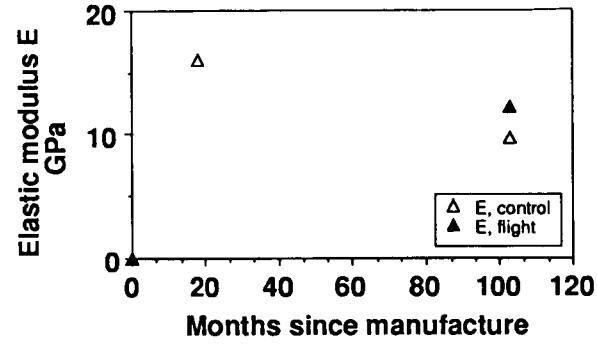

Fig. 19. Group 15: ±20°, 36% contact

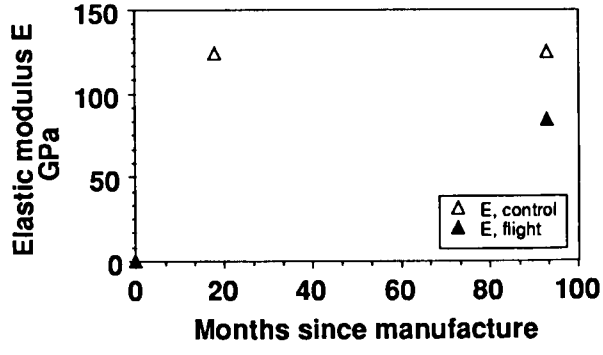

Figures 17-19. Elastic modulus results (cont.).

Fig. 20. Group 7: ±20°, 0% contact

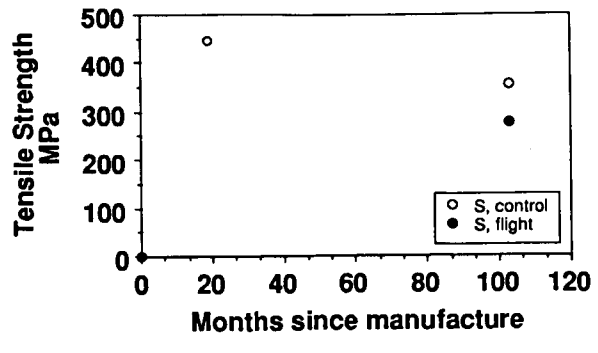

Fig. 21. Group 8: ±20°, 18% contact

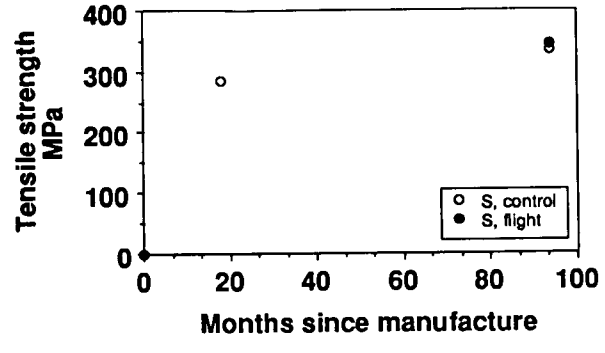

Fig. 22. Group 9: ±20°, 18% contact

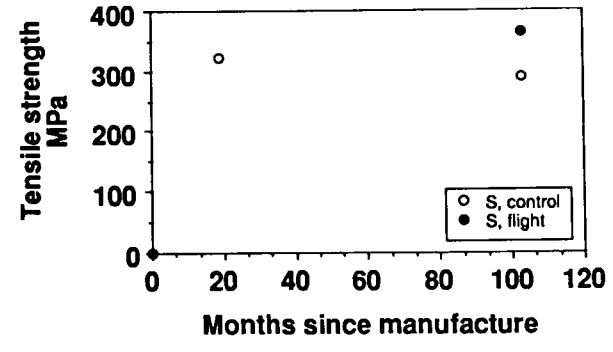

Figures 20-22. Tensile strength results.

Fig. 23. Group 10: ±20°, 100% contact

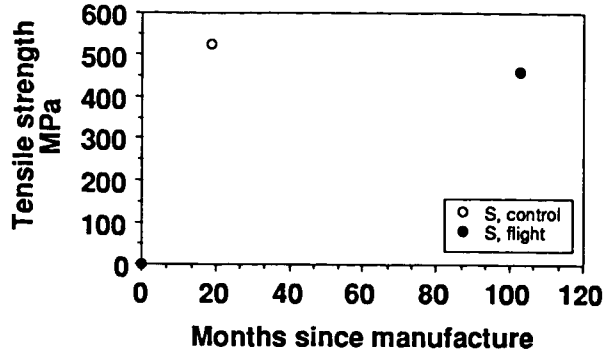

Fig. 24. Group 11: ±45°, 0% contact

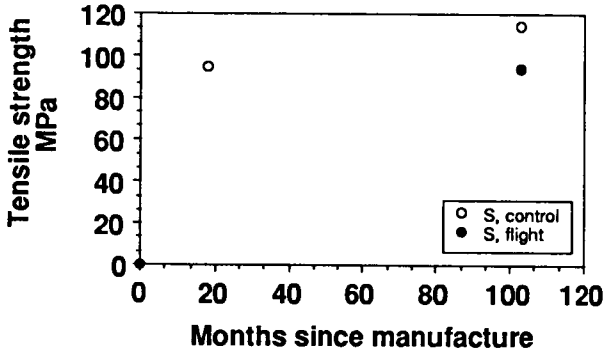

Fig. 25. Group 12: ±45°, 36% contact

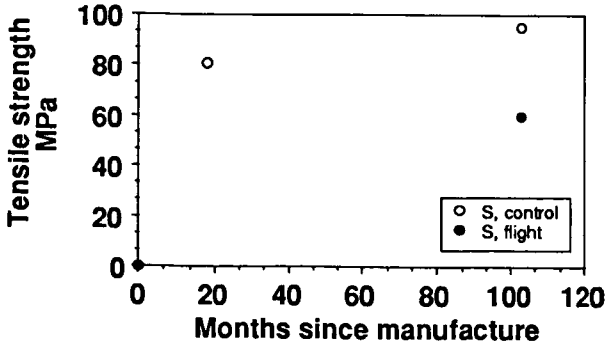

Fig. 26. Group 13: ±45°, 36% contact

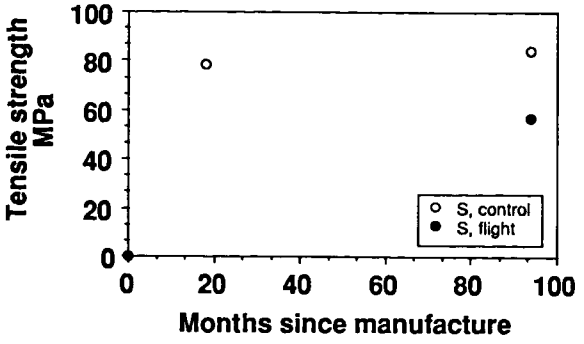

Fig. 27. Group 14: ±45°, 100% contact

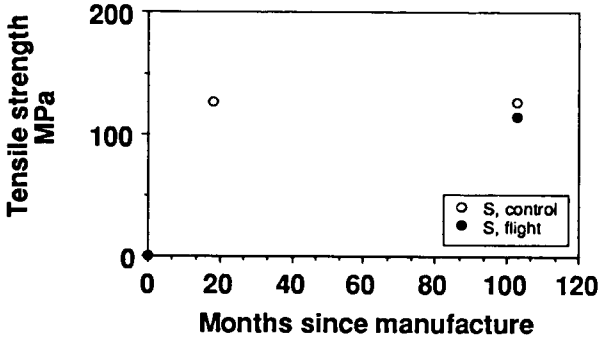

Fig. 28. Group 15: ±20°, 36% contact

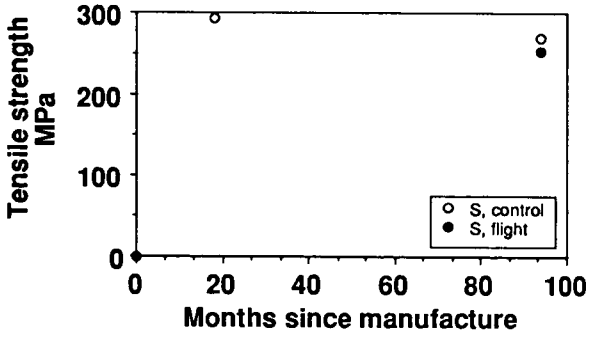

Figures 23-28. Tensile strength results (cont.).

Fig. 29. Toughness of Flight Specimens

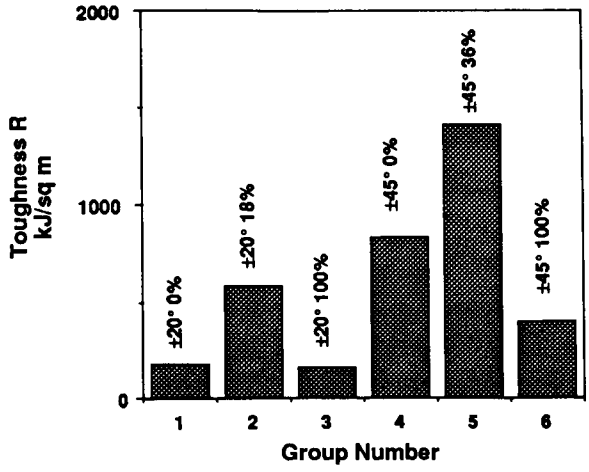

Fig. 30. Modulus of Flight Specimens

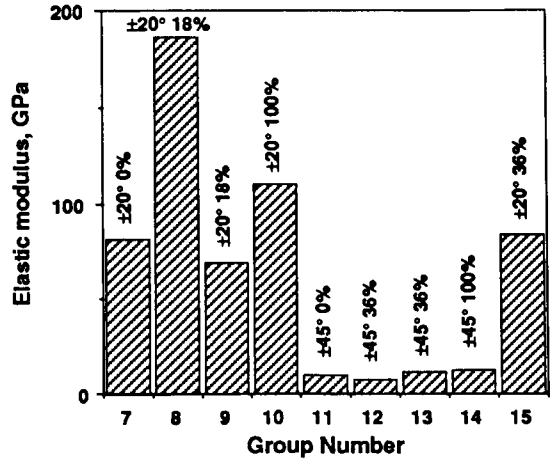

Fig. 31. Strength of Flight Specimens

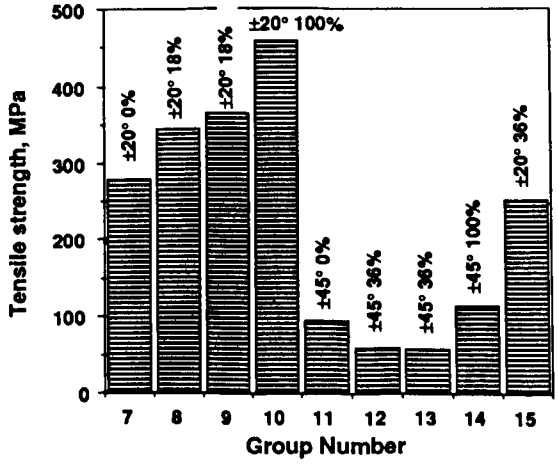

OTHER OBSERVATIONS

We have observed a number of micrometeoroid impact sites on the soft aluminum surface of the frame and on the composite specimens, ranging in size from 0.1 mm down to sub-micron sizes. Since this subject is being given extensive examination by other LDEF experimenters, we have not pursued it systematically and will not report on the subject here.

We also noted some apparently anomalous indentations on our aluminum frame, which we have reported elsewhere.[4,5] We believe now, after further systematic examination of ground control and flight tray clips, that these observations represent artifacts somehow resulting from techniques of fabrication, although we still do not know their origins.

Wahl maximum-temperature sensors were located on the outside (exposed) face of each of the specimens. These sensors indicate maximum temperature reached during ground storage, launch, flight, retrieval, and post-flight storage, in increments of 11°C. The temperatures indicated upon retrieval of the experiment are as follows:

Specimen	Temp., °C	Specimen	Temp., °C	Specimen	Temp., °C
A-1	93	A-6	82	A-11	93
A-2	93	A-7	82	A-12	93
A-3	93	A-8	93	A-13	93
A-4	82	A-9	93	A-14	93
A-5	82	A-10	93	A-15	93

From Fig. 4 it is apparent that Specimens A-4 through A-7 have no special location or orientation with respect to the experiment panel that would explain the lower observed maximum temperature, and no other LDEF experiment in the vicinity is likely to have led to the observed differences. Thus we may conclude that the maximum external temperature reached was close to 93°C, with a small variation below that actuating only the 82°C sensors.

Wahl maximum-temperature sensors were located on the under side (unexposed) surface of the test frame at nine locations. Upon retrieval, all of these sensors read 82°C.

CONCLUSIONS

We observe the following:

- Marked degradation from exposure, of the order of a factor of roughly two from the control specimens, is observed in every one of the six toughness specimens.
- Except for the Group 1 specimen (±20°, 0% contact), the toughness of the other four control specimens (Specimen C-3 datum was lost during the test) increased during the 100 or so months since manufacture. Although an observation that four out of five specimens increased in toughness is significant, the limited amount of this increase probably lies within the range of scatter for the test.

- The elastic modulus of the flight specimens varied rather widely from the control specimens for the same life, both higher and lower. In six of the nine specimens, flight modulus was lower than zero-time modulus; in four of the nine specimens, flight modulus was lower than total time ground specimens. Some of this variation is surely experimental scatter, but we have no way to establish its extent.
- In most cases, the elastic modulus of the control specimens either remained about the same or degraded during the duration of the experiment. In no case did it increase significantly.
- The strength of the flight specimens ranged from moderate increase to moderate decrease, except for Group 7 (±20°, 0% contact) which was about half of the initial strength. In every specimen except ±20° 18% contact, the strength of the flight specimens was less than that of the total time ground specimens.
- The change in strength of the control specimens ranged from moderate increase to moderate decrease. Even with the better precision of the strength results, this modest variation is probably attributable to scatter.
- Substantial differences are observed in the behavior of specimens having different cross-ply angles and fraction of interlaminar contact.
- In general, the 0% and 100% contact layups produced poorer combinations of post-flight properties than partial contact layups with the same cross-ply arrangement.

Fig. 32. ±20°, 18% Contact Specimens: Initial and Final Properties

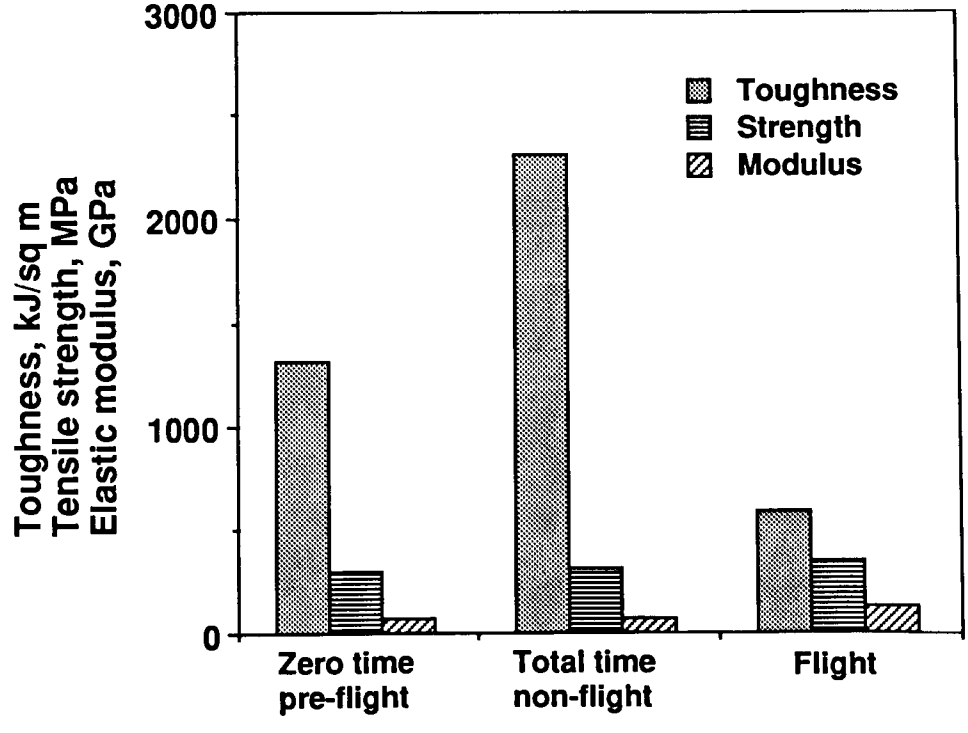

We conclude the following:

- With the proper selection of layup (see discussion below of ±20°, 18% contact) , and also including choices of layups not included in this experiment, graphite/epoxy composites can be used for extended exposure, at least in near-earth orbit, for periods of the order of 5 years without degradation to intolerable levels of toughness, elastic modulus, and strength. This assumes that suitable coating or protection from solar exposure and atomic oxygen is provided, as neither of these problems was severe in our test because of the orientation of the test panel.
- The single best combination of acceptable properties of toughness, elastic modulus, and strength in uniaxial tension after flight exposure is achieved for the Groups 2, 8 and 9 layup: ±20°, 18% contact. These results are shown in Fig. 32. While the toughness dropped to 593 kJ/m^2, this is still an entirely acceptable value, and both the elastic modulus and the tensile strength remained essentially constant as a result of the 5.8-year near-earth space exposure.

REFERENCES

1. Marston, T.U.; Atkins, A.G.; and Felbeck, D.K.: "Interfacial Fracture Energy and the Toughness of Composites," *Jour. of Materials Science*, v. 9 (1974), p. 447.

2. Jea, L.-C.; and Felbeck, D.K.: "Increased Fracture Toughness of Graphite-Epoxy Composites Through Intermittent Interlaminar Bonding," *Jour. of Composite Materials*, v. 14 (July 1980), p. 245.

3. D.K. Felbeck and A.G.Atkins, *Strength and Fracture of Engineering Solids*. (Englewood Cliffs, NJ: Prentice-Hall, Inc., 1984), p. 333-35. More detailed information on the Gurney method can be found in several papers in the *Proceedings of the Royal Society (London)*, e.g., 1974, vol. 340A, p. 213.

4. Felbeck, D.K.; and Durrant, W.H: "Repetitive Orbital Damage,"*Nature*, v. 347, Sept. 27, 1990, p. 341.

5. Felbeck, D.K.: Author's Response to Scientific Correspondence, *Nature*, v. 352, July 25, 1991, p. 289.

Table 1. All Data.

Spec.	Tested	Layup	%contact age,mo.	R, kJ/sq m	E, GPa	Su, MPa	Comment
Group 1		**20 deg**	**0**				**Gp 1 specs mfr 12/9/82**
A-1	7/23/91		103	177			Set A=Flight
B-1	7/11/84		19	484			Set B=Zero time
C-1	7/23/91		103	248			Set C=Ground, total time
Group 2		**20 deg**	**18**				**Gp 2 specs mfr 12/13/82**
A-2	9/20/90		93	593			
B-2	7/11/84		19	1315			
C-2	9/20/90		93	2311			
Group 3		**20 deg**	**100**				**Gp 3 specs mfr 12/7/82**
A-3	7/23/91		104	165			
B-3	7/11/84		19	241			
C-3	7/23/91		104	no result			
Group 4		**45 deg**	**0**				**Gp 4 specs mfr 12/15/82**
A-4	7/23/91		103	839			
B-4	7/11/84		19	1116			
C-4	7/23/91		103	1200			
Group 5		**45 deg**	**36**				**Gp 5 specs mfr 12/17/82**
A-5	9/20/90		93	1410			
B-5	7/11/84		19	1528			
C-5	9/20/90		93	2540			
Group 6		**45 deg**	**100**				**Gp 6 specs mfr 12/16/82**
A-6	7/23/91		103	400			
B-6	7/11/84		19	890			
C-6	7/23/91		103	886			
Group 7		**20 deg**	**0**				**Gp 7 specs mfr 12/3/82**
A-7	7/16l/91		103		80.9		
A-7	7/18/91		103			279	
B-7	6/9/84		18		116		
B-7	6/22/84		19			447	
C-7	7/16/91		103		62.2		
C-7	7/18/91		103			355	
Group 8		**20 deg**	**18**				**Gp 8 specs mfr 12/9/82**
A-8	9/21/90		93		186		
A-8	10/9/90		94			344	
B-8	6/9/84		18		87.9		
B-8	6/22/84		18			285	
C-8	9/21/90		93		111		
C-8	10/9/90		94			336	
Group 9		**20 deg**	**18**				**Gp 9 specs mfr 12/4/82**
A-9	7/16/91		103		68.5		
A-9	7/18/91		103			365	
B-9	6/9/84		18		67.6		
B-9	6/22/84		19			324	
C-9	7/16/91		103		45.6		
C-9	7/18/91		103			290	

Table 1. All Data (cont.).

Spec.	Tested	Layup	%contact age,mo.	R, kJ/sq m	E, GPa	Su, MPa	Comment
Group 10		**20 deg**	**100**				**Gp 10 specs mfr 12/5/82**
A-10	7/16/91		103		111		
A-10	7/18/91		103			460	
B-10	6/9/84		18		97.2		
B-10	6/22/84		19			525	
C-10	7/16/91		103		40.9		
C-10	7/18/91		103			no result	
Group 11		**45 deg**	**0**				**Gp 11 specs mfr 12/16/82**
A-11	7/16/91		103		10.1		
A-11	7/18/91		103			94.1	
B-11	6/9/84		18		17.5		
B-11	6/22/84		18			94.6	
C-11	7/16/91		103		12.1		
C-11	7/18/91		103			114	
Group 12		**45 deg**	**36**				**Gp 12 specs mfr 12/18/82**
A-12	7/16/91		103		7.07		
A-12	7/18/91		103			59.7	
B-12	6/9/84		18		17		
B-12	6/22/84		18			81	
C-12	7/16/91		103		9.3		
C-12	7/18/91		103			95	
Group 13		**45 deg**	**36**				**Gp 13 specs mfr 12/19/82**
A-13	9/21/90		93		11.6		
A-13	10/9/90		94			56.7	
B-13	6/9/84		18		16.2		
B-13	6/22/84		18			78.5	
C-13	9/21/90		93		17.1		
C-13	10/9/90		94			84.7	
Group 14		**45 deg**	**100**				**Gp 14 specs mfr 12/17/82**
A-14	7/16/91		103		12.2		
A-14	7/18/91		103			115	
B-14	6/9/84		18		16.1		
B-14	6/22/84		18			127	
C-14	7/16/91		103		9.68		
C-14	7/18/91		103			127	
Group 15		**20 deg**	**36**				**Gp 15 specs mfr 12/13/82**
A-15	9/21/90		93		84		
A-15	10/9/90		94			253	
B-15	6/9/84		18		124		
B-15	6/22/84		18			292	
C-15	9/21/90		93		125		
C-15	10/9/90		94			269	

All specimens of prepreg unidirectional 5208/T300 epoxy/graphite, 8 plies thick, Narmco Lot 50548470, batch 20, roll 20: 142.2 g/sq m, 32.6% resin. Interleaved with fractionally perforated 7 μm thick Mylar film having evenly spaced 1.14-mm holes. Zero percent contact specimens were made with teflon coating sprayed on all contact surfaces.

Set A: For LDEF flight
Set B: For time zero testing
Set C: For ground storage, post-flight testing

N93-28264

LDEF FIBER-COMPOSITE MATERIALS CHARACTERIZATION

C. J. Miglionico[1], C. Stein[1], R. E. Roybal[1], and L. E. Murr[2]

ABSTRACT

In this study we observed and compared degradation of a number of fiber/polymer composites located on the leading and trailing surfaces of LDEF where the atomic oxygen (AO) fluences ranged from 10^{22} to 10^{4} atoms/cm^2, respectively. While matrices of the composites on the leading edge generally exhibited considerable degradation and erosion-induced fragmentation, this "ashing" process was confined to the near surface regions because these degraded structures acted as a "protective blanket" for deeper-lying regions. This finding leads to the conclusion that simple surface coatings can significantly retard AO and other combinations of degrading phenomena in low-Earth orbit. Micrometeoroid and debris particle impacts were not a prominent feature on the fiber-composites studied and apparently do not contribute in a significant way to their degradation or alteration in low-Earth orbit.

---

[1] Space Environmental Interaction Branch, Phillips Laboratory, PL/VTSI, Kirtland Air Force Base, NM 87117

[2] Department of Metallurgical and Materials Engineering, The University of Texas at El Paso, El Paso, TX 79968

PRECEDING PAGE BLANK NOT FILMED

INTRODUCTION

Composites have played an important role in a host of space and aerospace materials systems and are currently one of the most promising materials areas not only in the context of advanced aerospace systems but also a wide range of commercial applications as well. Early re-entry ballistic missle components, especially nose cones and heat shields, relied upon composites and related fiber materials systems, and when the Long Duration Exposure Facility (LDEF) was conceived as a space materials test facility, numerous composite materials experiments were designed to examine the effects of low-Earth orbit on these contemporary as well as more advanced composites of that period (early 1980's). These included a range of medium-to-light weight polymer (epoxy) matrix/fiber composites, especially unidirectional, bidirectional composites and laminated graphite and glass fiber composites.

As shown in Fig. 1, LDEF was a 12-sided re-usable, hollow satellite about the size of a bus (4.6m x 9.2m). It weighed roughly 10^5 kg and contained some 10,000 specimens for test and analysis when deployed on orbit April 7, 1984 by the Shuttle Orbiter Challenger. When retrieved by the Shuttle Orbiter Columbia on January 12, 1990, LDEF's circular, non-geosynchronous, low-Earth orbit of 257 nautical miles (476 km) had decayed to roughly 180 nautical miles (333 km).

Composite samples to be described in this study were located either in row 9, bay D (D09) on the leading edge of the stabilized satellite, or in row 3, bay D (D03) on the trailing edge of the satellite. These distinctions, as illustrated in Fig. 2, were especially dramatic in the context of atomic oxygen (AO) fluence which was observed to vary from about 10^{22} atoms/cm^2 on the leading edge to about 10^4 atoms/cm^2 on the trailing edge.

In addition to the AO flux difference, the leading edge samples experienced a temperature difference of nearly 100°F over 34,000 orbital cycles. Exposure during these cycles included intense UV, X-ray, electron, proton, gamma ray, and cosmic radiations. Micrometeoroid impacts (nearly 1 billion over the 130 m^2 of LDEF surface) and other contaminating particles (more than a trillion over the surface) along with outgassing of a silicone-hydrocarbon film also influenced the surface structure and integrity of many test materials [1, 2].

ORIGINAL PAGE
BLACK AND WHITE PHOTOGRAPH

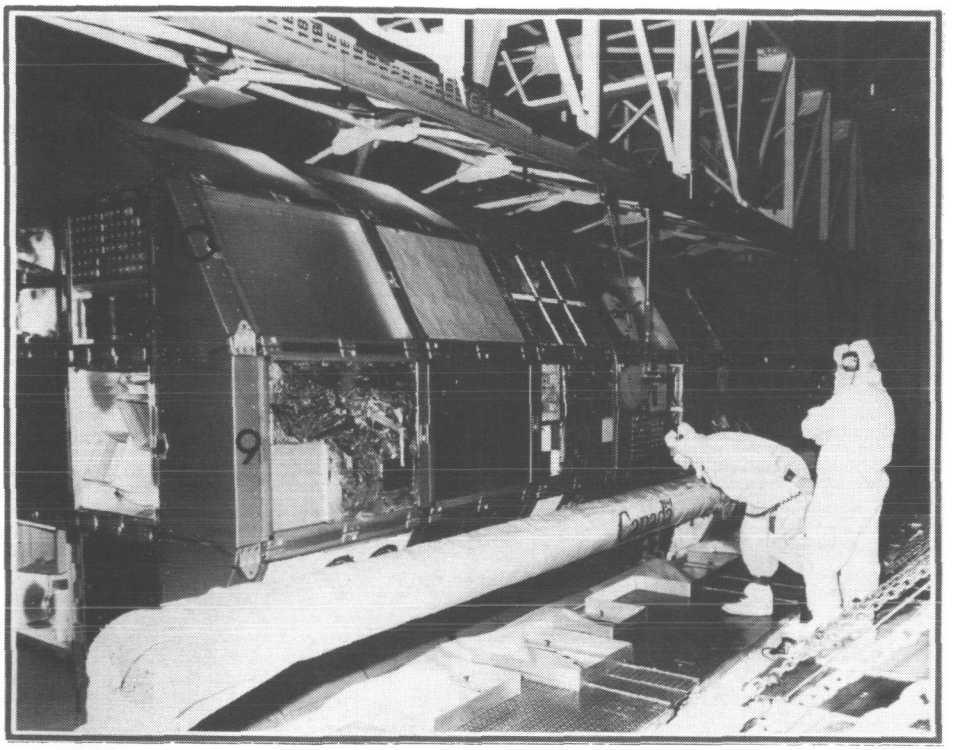

Figure 1. Long Duration Exposure Facility (LDEF) during post-recovery examination at Kennedy Space Center.

EXPERIMENTAL DETAILS

In this study we have examined representative fiber composites from both the leading and trailing edges of LDEF and compared them with control samples which were not flown on LDEF using optical metallography and scanning electron microscopy (SEM) techniques. Samples which were examined in this study included the following: graphite polyimide, graphite polysulphone, tape-wrapped carbon phenolic (a multi-directional carbon fiber weave in a phenolic binder) pyrocarb 431, and quartz phenolic.

RESULTS AND DISCUSSION

Graphite Polyimide - Figure 3 shows for comparison purposes, both leading and trailing edge examples of the graphite polyimide composite in the same relative orientations between corresponding bays (refer to

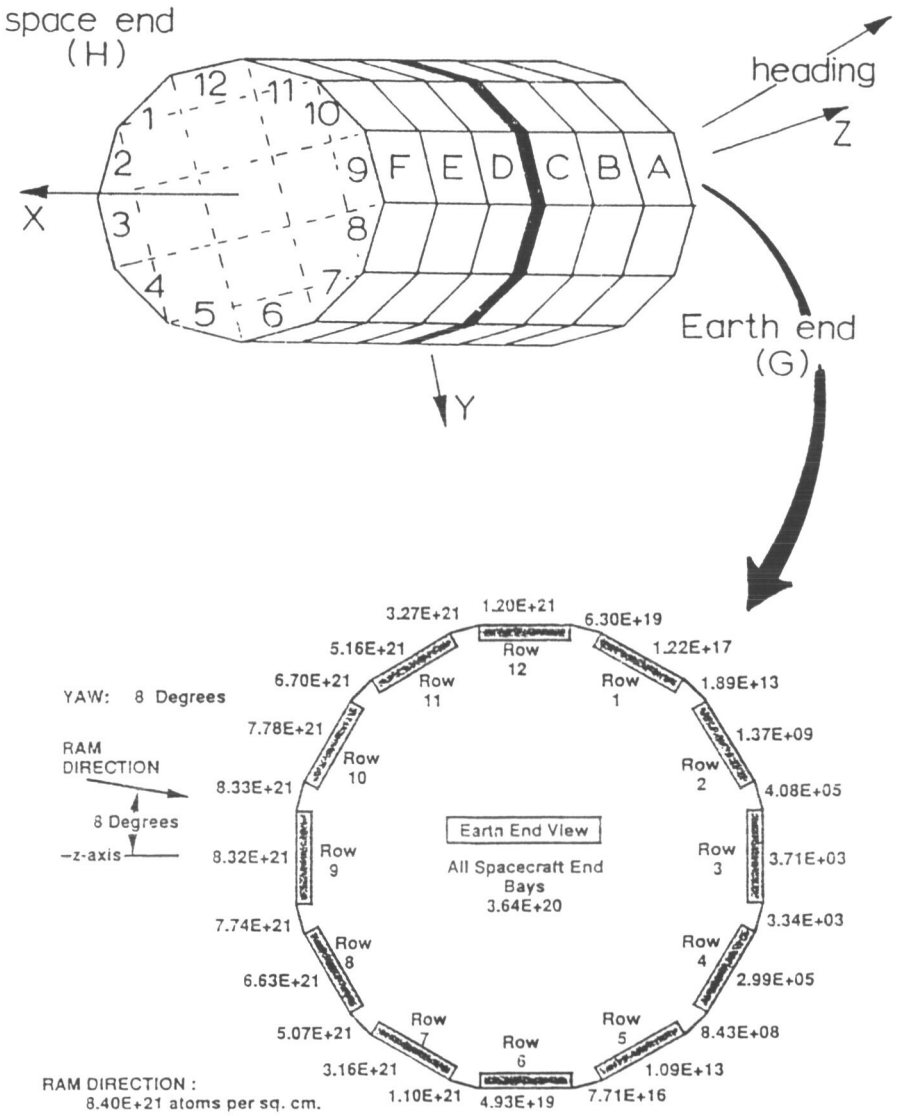

Figure 2. Schematic view of LDEF oriented as in Fig. 1 showing orientation and tray notations (top) and corresponding atomic oxygen fluences (bottom) (Courtesy of NASA).

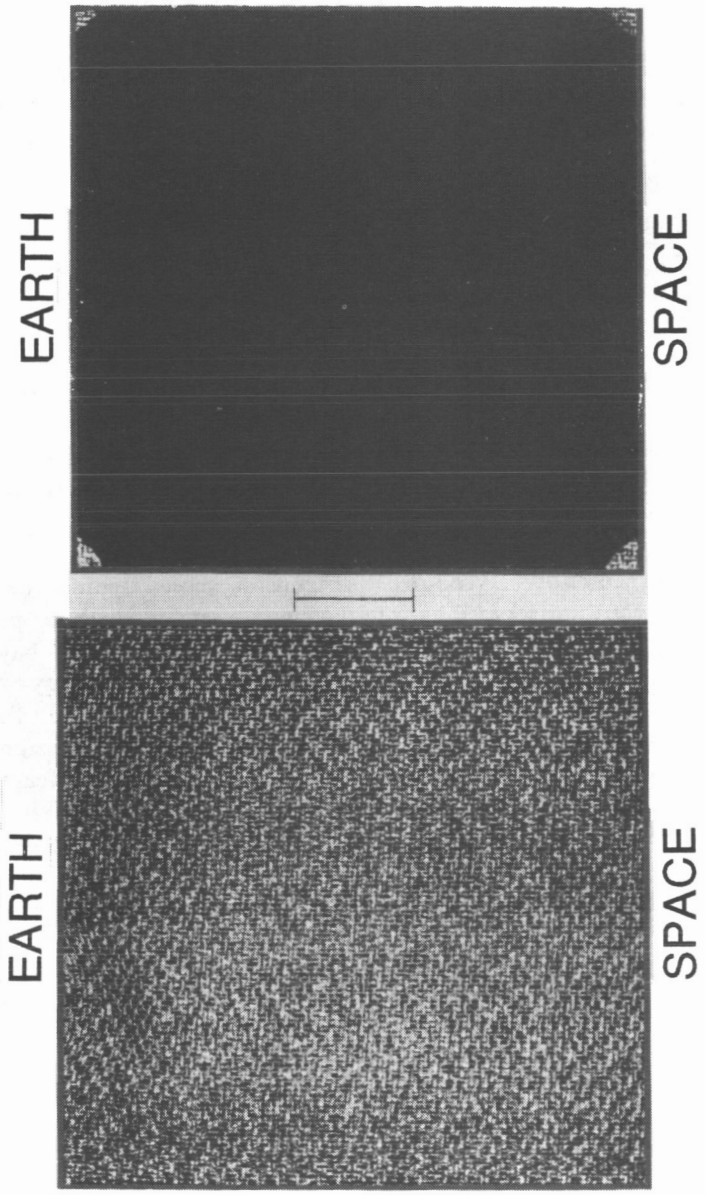

Figure 3. Leading (D09) (top) and trailing (D03) (bottom) edge samples of graphite-polyimide composite from LDEF. Note corners of leading edge sample protected by clamping washers appear similar to the trailing edge sample (marker corresponds to 1 cm).

Fig. 2(a)). While the weave (fiber) pattern degradation is not apparent in this comparative figure, the magnified views provided in Fig. 4 show that the leading edge degradation is much more severe than that experienced in the trailing edge.

Graphite Polysulphone - Figure 5 shows a similar pattern to that of Fig. 4 for leading-edge degradation in graphite polysulphone composite. In addition Fig. 5 shows a comparative view of a control sample (Fig. 5(c)) which suggests that while the trailing edge degradation was not very noticeable compared to that observed on the leading edge, there were some subtle changes which may be related to volatilization or related phenomena. Morphologies essentially identical to those shown in Fig. 3 were also observed on the leading and trailing edge graphite polysulphone samples and are therefore not reproduced here.

Tape-wrapped Carbon Phenolic - Figure 6 shows typical examples of light microscopy observations of the tape-wrapped carbon phenolic composite taken from the leading and trailing edge locations in bay D of LDEF. These views show the degradation and morphology on the leading edge to be essentially identical to that observed for the graphite polyimide shown in Figs. 3 and 4 and the graphite polysulphone shown in Fig. 5, as well. Although the surface features of Figs. 4 to 6 were observed at low magnifications, they are similar in appearance, leading us to conclude that the degradation mechanisms are essentially the same for each of these fiber composite systems.

Pyrocarb 431 - Figure 7 shows a low magnification view of the leading edge Pyrocarb 431 composite. It is interesting to note that a chalk number provided some protection against underlying degradation.

Figure 7(b) shows that areas under the chalk mark were maintained relatively undegraded, which attests to the ability to provide simple protective measures for polymers exposed in space in low-Earth orbit (LEO).

Three Dimensional Quartz Phenolic - In contrast to the other composites examined in this study, the quartz phenolic exhibited much less degradation as indicated in the comparative views reproduced in Figs. 8 and 9. Figure 9(a) also shows the interface between two groups of quartz fibers perpendicular to each other and shows little degradation in this (interface) region. Apparently considerably less

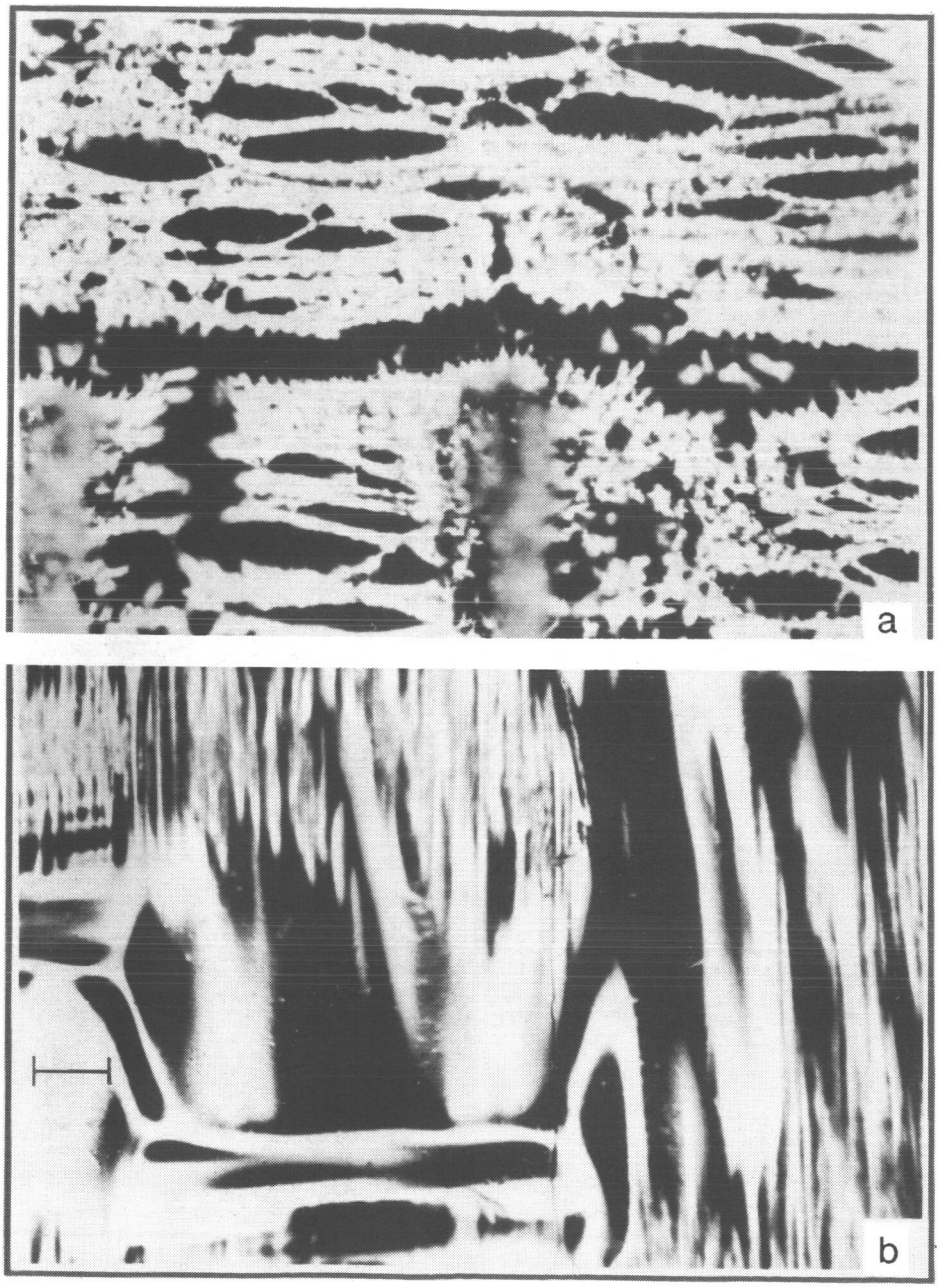

Figure 4. Magnified views (in the light microscope) of leading (a) and trailing (b) edge samples of graphite-polyimide on LDEF showing leading edge surface degradation. (Marker is 0.1 mm.)

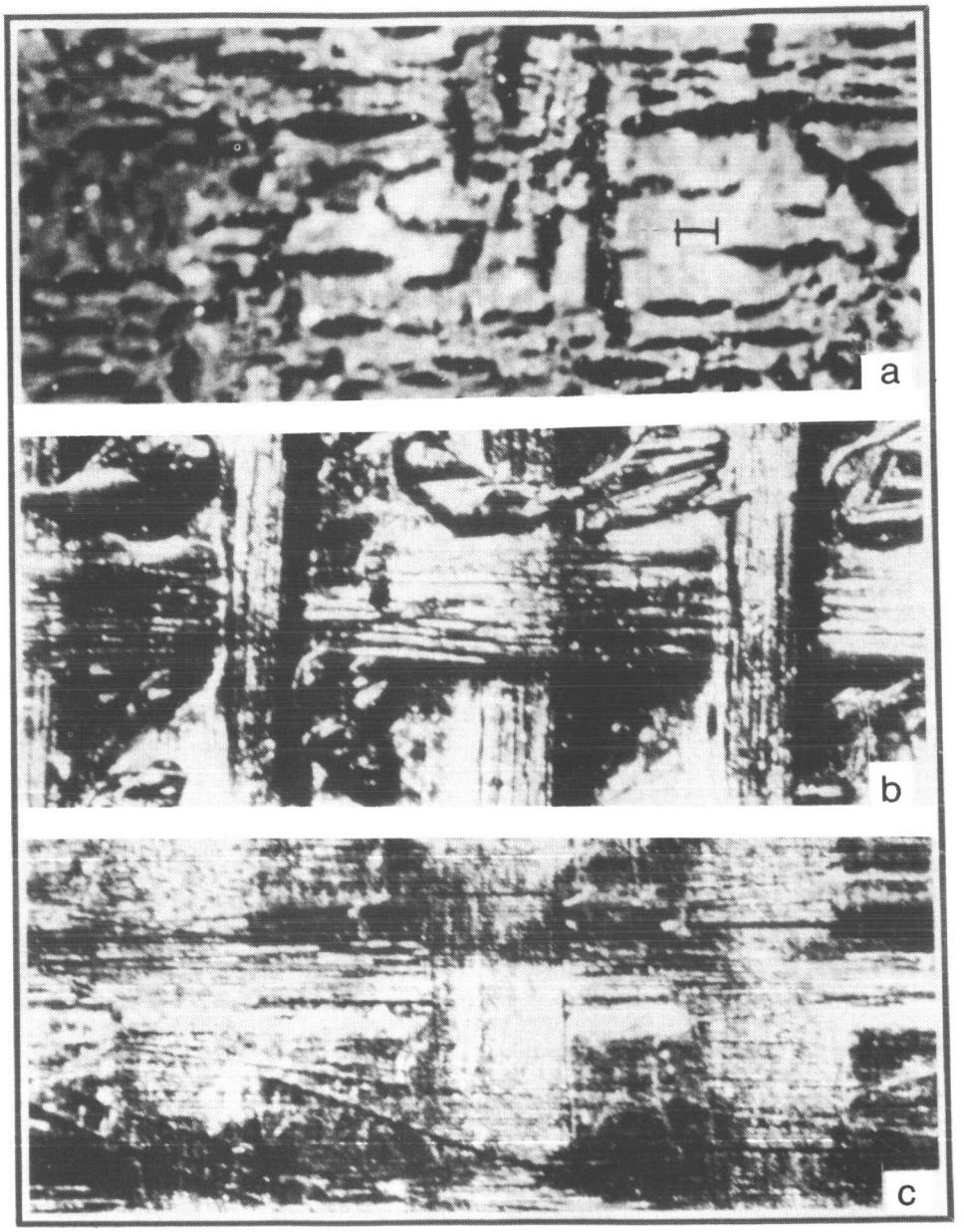

Figure 5. Comparison of light microscope views of graphite polysulphone composite. (a) Leading edge LDEF sample of graphite polysulphone. (b) Trailing edge LDEF sample. (c) Control sample not flown on LDEF. (Magnification marker corresponds to 0.1 mm).

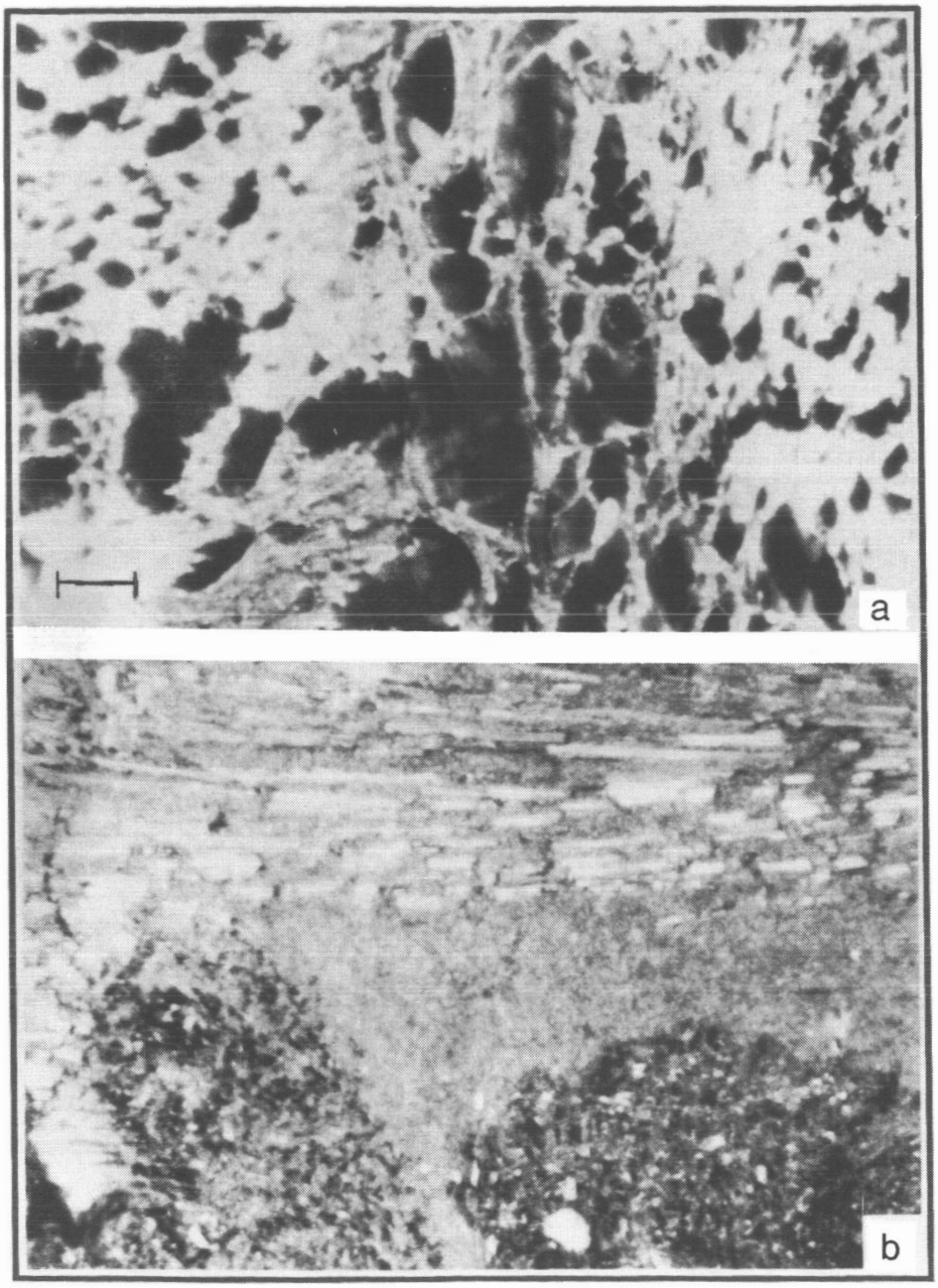

Figure 6. Leading (top) and trailing (bottom) edge views of tape-wrapped carbon phenolic on LDEF. (Marker is 0.1 mm).

C-3

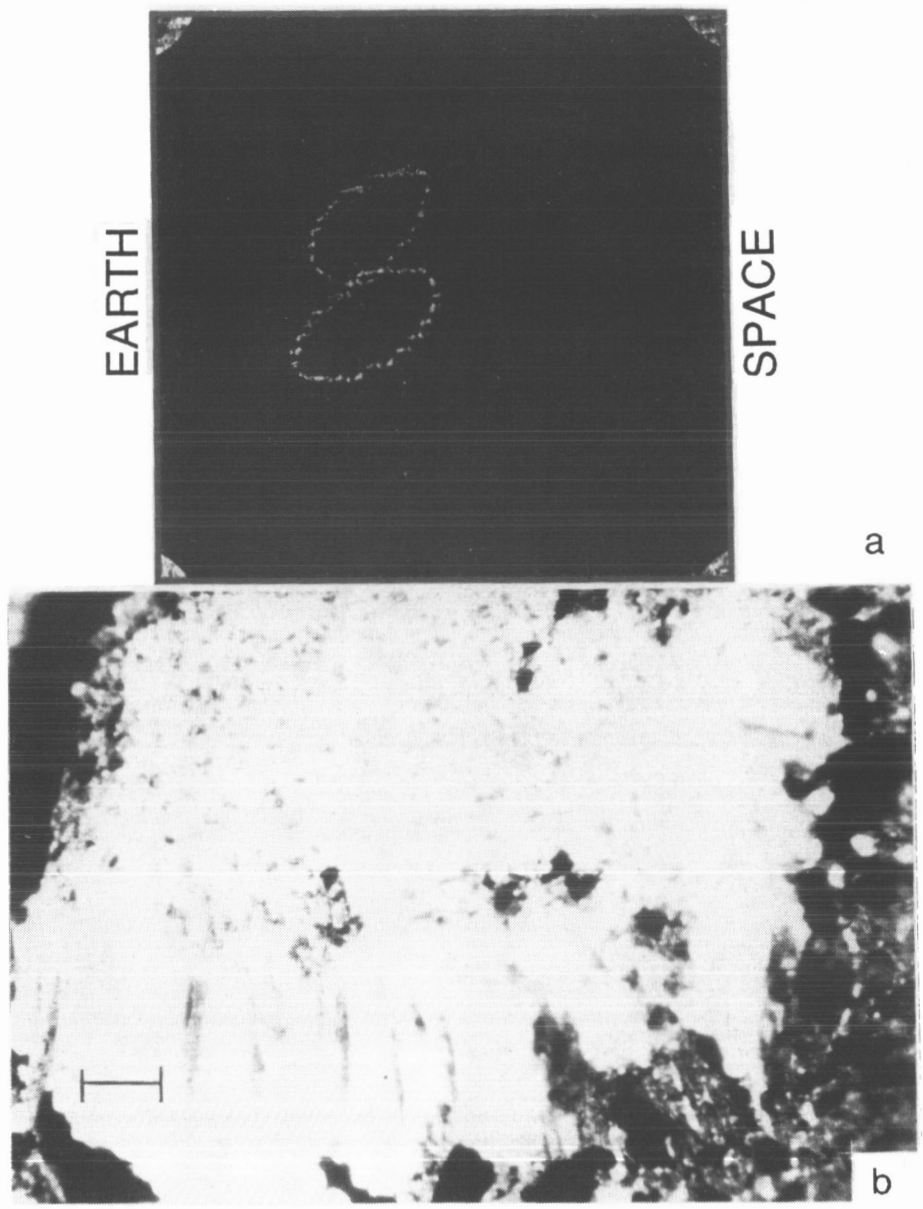

Figure 7. Comparative views of Pyrocarb 431 composite. (a) Low magnification view of leading edge sample (a). (b) Leading edge area under the chalk number shown in (a) is illustrated in (b). The chalk tends to protect the underlying regime from degradation. (Marker is in (b) 0.1 mm).

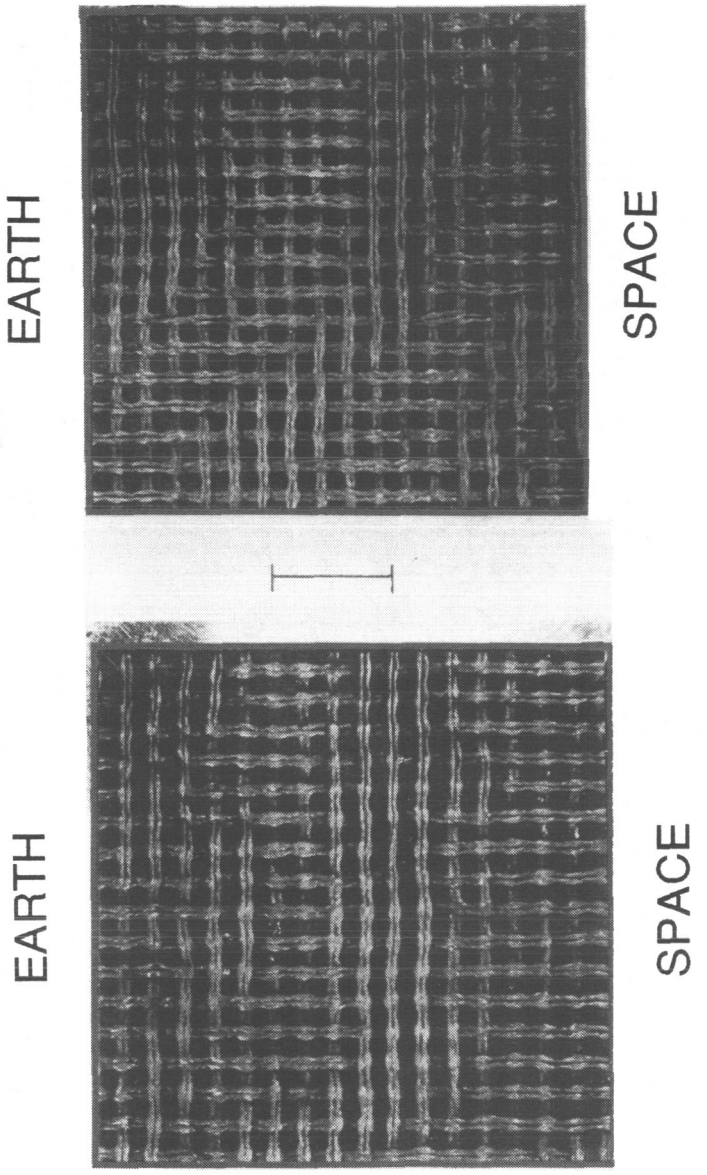

Fig. 8. Leading (top) and trailing (bottom) edge views of the 3-dimensional quartz phenolic composite on LDEF. (Marker is 1 cm).

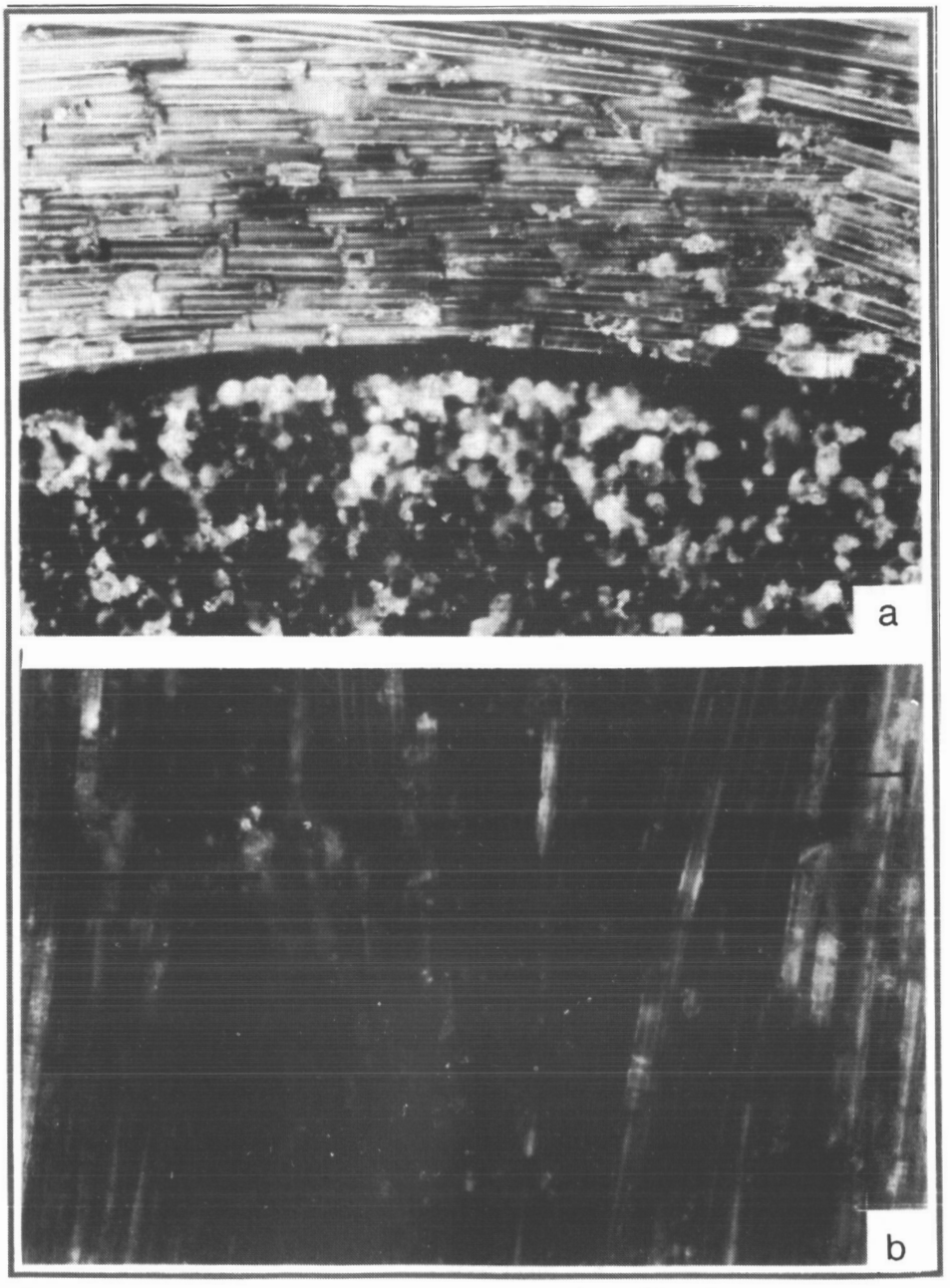

Figure 9. Magnified leading (a) and trailing (b) edge views of the quartz phenolic composite shown in Fig. 8. (Magnification markers equal 0.1 mm).

damage occurs in quartz phenolic composites in LEO than for the other composites examined (compare Figs. 4, 5, 6, and 9).

While the optical (light) microscope views shown in Fig. 9 do not exhibit any noticeable degradation of this composite, more detailed observations in the SEM reveal several degradation features especially in the phenolic (polymer) binder which are similar to other SEM observations for the other polymers. These features are illustrated in a series of SEM views reproduced in Fig. 10.

Surface Erosion Phenomena - The degradation of the polymer matrices in high AO fluences in LEO as illustrated for the leading edge LDEF composites has been discussed previously to be a consequence of polymer bond breaking and subsequent molecular fragmentation leading to erosion of material [3-6]. This phenomenon is particularly severe for certain polymer chain structures such as polyethylene, kapton [5], polyimide, and polysulphone studied here. This energetic AO erosion process (8 km/s orbital velocity produces 5 eV collision energy) is catalyzed and accelerated by UV radiation and altered in some cases by orbital thermal fluctuations and temperature localization which alters the eroded surfaces, creating a plethora of erosion-degradation structures (Fig. 10).

As noted earlier the AO-induced surface erosion, especially for carbon in polyimide and polysulfone binder matrices (Fig. 11), creates a surface region of molecular fragments and larger ash-like fragments. Like chalk marks on the surface (see Fig. 7), these fragments provide a protective regime that retards the erosion process and limits the degradation to a few microns of surface region at worst in polymer composites observed in this investigation.

Observations of Micrometeoroid Impact Phenomena - Because of the size of the fibers and the weave spacings it is often difficult to observe micrometeoroid or debris particle impact damage in fiber/polymer composites. This is because the cratering will cause melting or vaporization which can trap the particles (which are usually 1/5 the crater diameter) below the surface where it (the crater) would be unobservable. Carbon fiber composites, because of their melt/vapor features and fiber weave, can serve as an efficient absorber of impacting particle residue as well. These features are illustrated in Figs. 11 and 12. Figure 11 shows a large (0.1 mm) impact crater in a graphite polyimide which was probably a paint chip because of its Ti-Ca-Si composition. Figure 12 shows two examples of micrometeoroid impacts in the aluminum frame surrounding the leading edge quartz phenolic

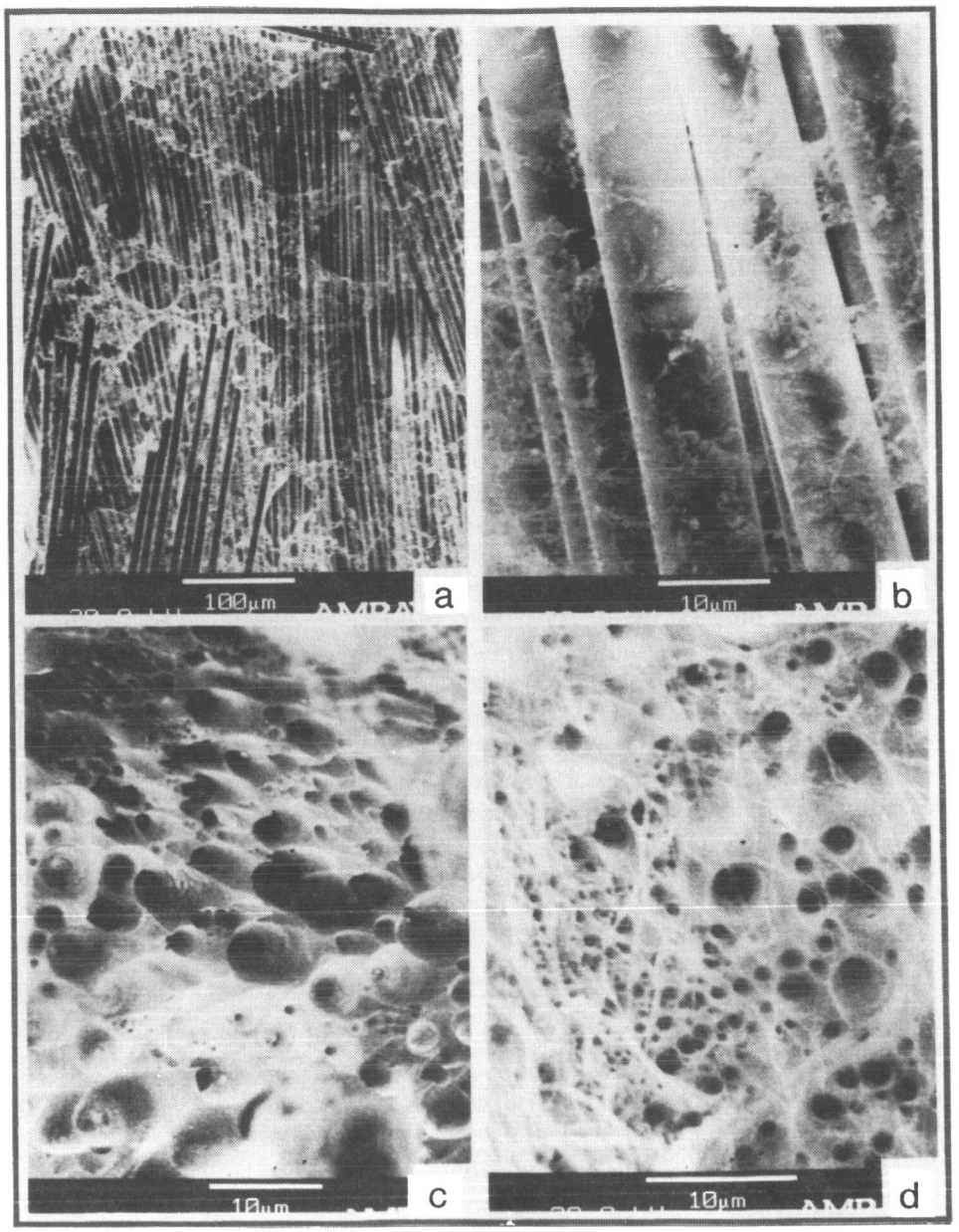

Figure 10. SEM views of phenolic degradation in quartz phenolic composites on the leading edge of LDEF. (a) Low magnification view showing filmy surface residue. (b) Magnified views of (a). (c) Protruding surface features. (d) Surface erosion pits presenting an inverse view of features in (c).

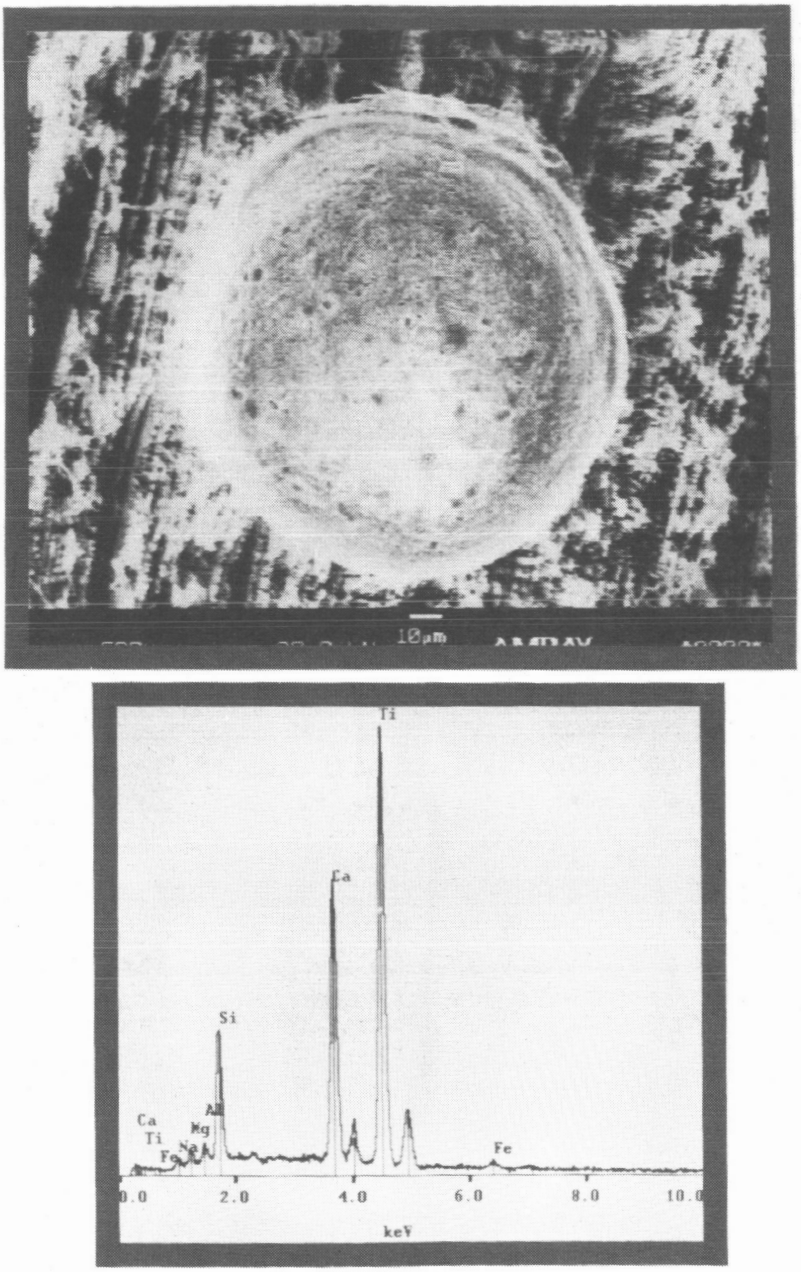

Figure 11. Impact crater in graphite poyimide composite (a) and corresponding energy-dispersive X-ray spectrum showing particle residue composition.

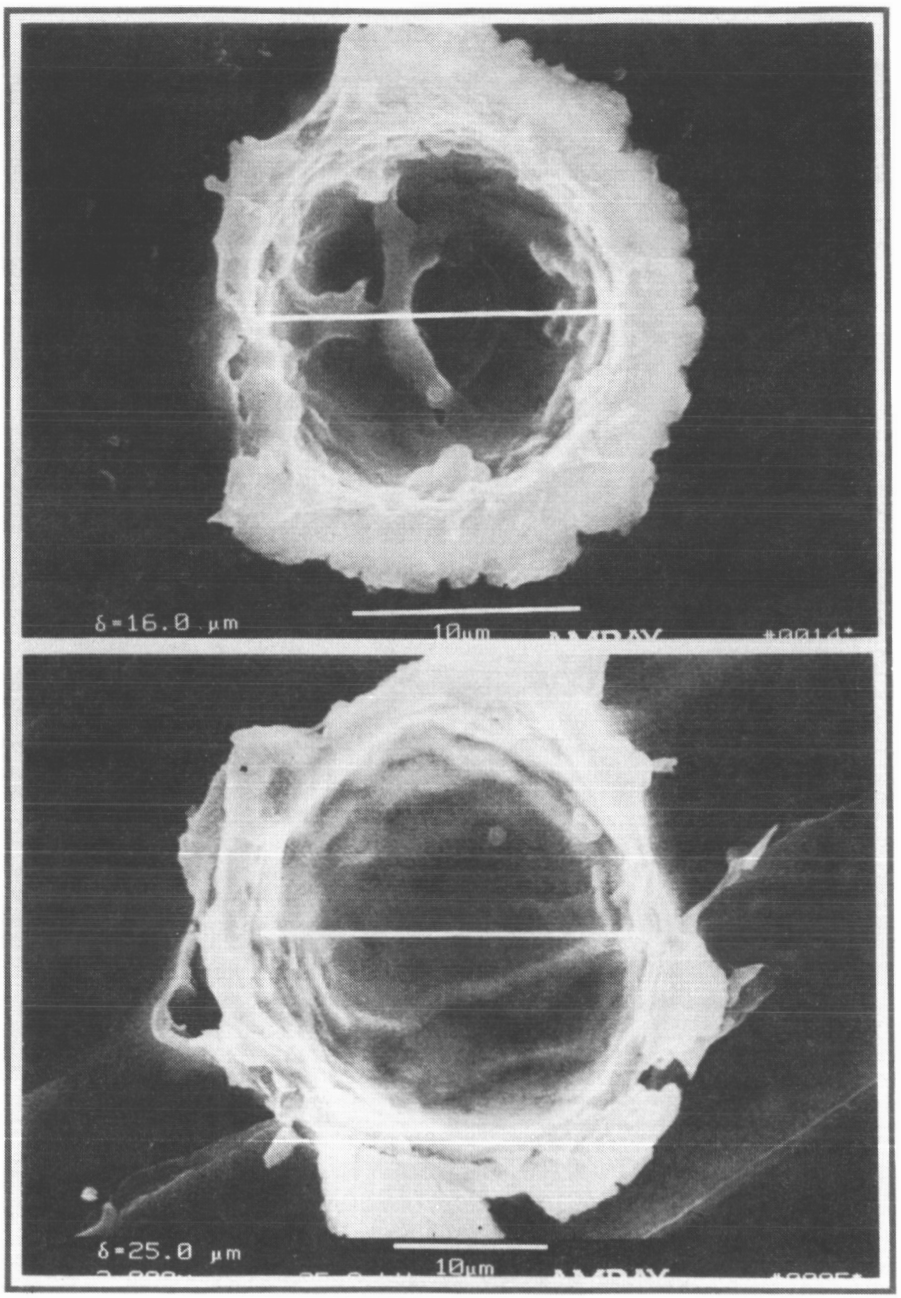

Figure 12. Examples of micrometeorite impact craters in aluminum frame surrounding the leading edge quartz phenolic sample in Fig. 8.

sample shown in Fig. 8. These are the more normal-appearing impact craters observed in metal surfaces [1, 7]. No similar observations were made in the quartz phenolic itself. This is also different from the microparticle impact damage in other composites such as the teflon-fiber glass woven beta cloth which exhibits considerable glass particle shedding and impact-induced glass fiber fragmentation [8].

SUMMARY AND CONCLUSIONS

Many matrices in fibers in polymeric composites are quite susceptible to the erosive effects of atomic oxygen (AO) in low-Earth orbit. These features were particularly notable in this study for polyimide and polysulphone matrices supporting graphite fibers, as well as phenolics. However, the ash-like erosion products which accumulate on the surfaces of these fiber composites act like a barrier to retard or prevent underlying erosion. Some systems, like quartz phenolic, exhibit less erosion as has been shown previously [4, 6]. The observations suggest that relatively simple coating schemes might be employed to significantly reduce AO erosion even for susceptible polymer composites.

Damage to polymer composites as a consequence of debris particles and micrometeoroids also seems to be less, in most instances, than in metallic surfaces and structural alloys, for example. This feature combined with relatively simple coating applications to reduce AO erosion could have important consequences for a number of polymer composite applications on spacecraft and space structures in low-Earth orbit. However, the synergistic effects of UV, electron irradiation, protons, etc. can certainly complicate specific situations.

ACKNOWLEDGMENTS

This research was supported by the Phillips Laboratory and related U.S. Air Force components, especially the Wright Patterson Air Force Base, Ohio. This work was also supported in part by a NASA-Johnson Space Center Research Grant (NAG 9-481).

REFERENCES

1) T. See, et al, "A Preliminary Report - Meteoroid and Debris Impact Features Documented on the Long Duration Exposure Facility", NASA-JSC Publication No. 24608, August, 1990.
2) C. Miglionico, C. Stein, and L. E. Murr, "Effects of Space Environment on Structural Materials: A Preliminary Study and Development of Materials Characterization Protocols", **Journal of Materials Science,** Vol. 26, p. 5134, 1991.
3) L. J. Leger and J. T. Visentine, "Protecting Spacecraft from Atomic Oxygen", **Aerospace America,** Vol. 24, p. 32, 1986.
4) S. L. Koontz, K. Albyn, and L. J. Leger, "Materials Selection for Long Life in Low Earth Orbit", **Journal of the IES,** March/April, p. 50, 1990.
5) N. J. Stevens, "Method for Estimating Atomic Oxygen Surface Erosion in Space Environments", **Journal of Spacecraft,** Vol. 27, p. 93, 1990.
6) V. Srinivasan and B. A. Banks, (Editors), Materials Degradation in Low Earth Orbit (LEO), The Minerals, Metals, & Materials Society of AIME, Warrendale, PA, 1990.
7) L. E. Murr, C-S. Niou, S. Quinones, and K. S. Murr, "Cracking Associated with Micrometeoroid Impact Craters in Anodized Aluminum Alloy Clamps on LDEF", **Scripta Metallurgica et Materialia,** Vol. 27, p. 101, 1992.
8) See "Beta Cloth Early Results Are Alert for Spaceflight Servicing", in **LDEF Spaceflight Environmental Effects Newsletter,** Vol. II, No. 6, p. 8, November 15, 1991.

N93-28265

SPACE ENVIRONMENTAL EFFECTS ON LDEF COMPOSITES: A LEADING EDGE COATED GRAPHITE EPOXY PANEL

Pete E. George
Boeing Defense and Space Group
Seattle, Washington 98124-2499 M/S 73-09
Phone: 206/234-2679, Fax: 206/237--0052

Harry W. Dursch
Boeing Defense and Space Group
Seattle, Washington 98124-2499 M/S 82-32
Phone: 206/773-0527, Fax: 206/773-4969

Sylvester G. Hill
Boeing Defense and Space Group
Seattle, Washington 98124-2499 M/S 82-32
Phone: 206/773-2767, Fax: 206/773-2767

SUMMARY

The electronics module cover for the leading edge (Row D 9) experiment M0003-8 was fabricated from T300 graphite/934 epoxy unidirectional prepreg tape in a $(0_2, \pm 45, 0_2, \pm 45, 90, 0)_S$ layup. This 11.75" x 16.75" panel was covered with thermal control coatings in three of the four quadrants with the fourth quadrant uncoated. The composite panel experienced different thermal cycling extremes in each quadrant due to the different optical properties of the coatings and bare composite. The panel also experienced ultraviolet (UV) and atomic oxygen (AO) attack as well as micrometeoroid and space debris impacts.

An AO reactivity of 0.99×10^{-24} cm^3/atom was calculated for the bare composite based on thickness loss. The white urethane thermal control coatings (A276 and BMS 10-60) prevented AO attack of the composite substrate. However, the black urethane thermal control coating (Z306) was severely eroded by AO, allowing some AO attack of the composite substrate. An interesting banding pattern on the AO eroded bare composite surface was investigated and found to match the dimensions of the graphite fiber tow widths as prepregged. Also, erosion depths were greater in the darker bands.

Five micrometeoroid/space debris impacts were cross sectioned to investigate possible structural damage as well as impact/AO interactions. Local crushing and delaminations were found to some extent in all of the impacts. No signs of coating undercutting were observed despite the extensive AO erosion patterns seen in the exposed composite material at the impact sites.

An extensive microcrack study was performed on the panel along with modeling of the thermal environment to estimate temperature extremes and thermal shock. The white coated composite substrate displayed almost no microcracking while the black coated and

bare composite showed extensive microcracking. Significant AO erosion was seen in many of the cracks in the bare composite.

INTRODUCTION

The Long Duration Exposure Facility (LDEF) was deployed on April 7, 1984 in low earth orbit (LEO) at an altitude of 482 kilometers. During the 5.8 year mission the LDEF experienced LEO environment conditions including atomic oxygen (AO), ultraviolet radiation (UV), thermal cycling, and micrometeorioid/space debris impacts. The LDEF was retrieved on January 12, 1990 from an altitude of 340 kilometers. The higher AO concentrations at lower altitudes resulted in most of the total AO fluence occurring late in the mission.

One of the experiments on board was M0003 "Space Environment Effects on Spacecraft Materials" from the Aerospace Corporation. As a sub set of the experiment the Boeing Defense and Space Group flew a number of organic composite specimens (M0003-8) most of which have been tested and the results presented elsewhere (refs. 1,2).

A portion of experiment M0003-8 flew on the leading edge of the LDEF at position D9 as shown in Figure 1. Included in this experiment was an electronics module cover fabricated from T300 graphite/934 epoxy. This panel, shown in Figure 2 in postflight condition, consisted of 20 plies layed up at $(0_2, \pm 45°, 0_2, \pm 45°, 90, 0)_S$ and autoclave cured at 350°F.

The panel was coated with thermal control coatings in three of the four quadrants. The white thermal control coatings (BMS 10-60 and A -276) contained a titanium dioxide pigment while the black coating (Z306) contained carbon. All the coatings had a polyurethane matrix. The fourth quadrant was left bare to allow direct exposure of the composite substrate. One inch diameter mounting washers located at the corners and along each side shielded the underlying composite and coating. These shielded areas are apparent in Figure 2 as circular areas in the corners and along the sides of the panel. The shielded areas provided control surfaces for erosion measurement. Figure 3 shows the three thermal control coatings along with the relative orientation of the panel to the spacecraft.

A summary of the environmental conditions for the composite panel is listed in Figure 4. The AO and UV exposure levels were among the highest of the experiment positions on LDEF (Refs. 3,4). Thermal cycling was predicted based on the pre and postflight optical properties of the coatings and pre and post flight properties of the bare composite along with exposure conditions and thermocouple data from an aluminum plate located beneath the composite panel. Thermal cycle modeling details are discussed in the microcrack study section of this paper.

OBJECTIVE

Based on lessons learned from investigation of the other organic composite specimens flown on M0003-8 a test plan was developed for the coated panel. AO erosion, micrometeoroid and debris impacts and thermal cycle induced microcracking were found to present the greatest threat to the performance of organic matrix composites in LEO. These environments impact dimensional stability, mechanical stiffness and strength, and optical properties of uncoated organic matrix composites.

Another LEO environmental effect worth investigation is outgassing effects on dimensional stability. These properties are best investigated by insitu measurement of dimensional change vs. LEO exposure time and conditions as performed by Tennyson (Ref. 5). The M0003-8 composite specimens were not strain gauged during flight and the outgassing-dimensional change relationship has been found to be reversible (Ref.5). Therefore those effects were not investigated here.

AO erosion appears to be the most detrimental environmental effect on uncoated organic composites. Quantification of the erosion level on the bare quadrant of the T300 graphite/934 epoxy panel was a top priority. Also, some interesting "band patterns" were apparent in the AO eroded surface of the bare composite. Measurements were made on the size and spacing of the bands in an attempt to determine their origin.

Micrometeoroid/debris impacts on the composite panel left visible signs of damage on the surface including removal of protective coatings. The majority of the visible impacts on the composite panel occurred in the white A276 coated quadrant. The five largest impacts in that quadrant were cross sectioned and polished for coating and substrate damage evaluation.

Three different thermal control coatings were applied to the composite panel prior to flight. The coatings provided different levels of protection against thermal shock based on their optical properties. The thermal cycling and thermal shock levels for the coated composite panel and bare composite panel areas were modeled based on available temperature data and the known optical and physical properties of the panel and coatings. This data was evaluated in conjunction with a detailed microcracking study to determine the possible existence of a thermal cycling/microcracking correlation. Polished sections containing microcracks were also examined for evidence of microcracking/AO erosion interaction.

ATOMIC OXYGEN EROSION

Test Method

AO erosion of the bare T300 graphite / 934 epoxy panel was measured by comparing the eroded surface to an adjacent area where the original surface was protected by a mounting washer. A Cyber Optics Cyberscan 2000 laser profilometer was used to measure the distance from the protected to the eroded surface. Line scans across the step were performed in six locations. A step size of 0.0005 inch was used with a 0.00003 inch depth resolution. The measured erosion depths were based on data outside a 0.030 inch buffer zone centered on the transition from protected to eroded surfaces. This eliminated any transition effects of possible shadowing from contributing to the erosion depth measurement.

Results

An average thickness loss of 0.00339" of composite material was measured. Using this material loss with the AO exposure conditions shown in Figure 3, a 0.99×10^{-24} cm^3/atom reactivity was calculated for the T300 graphite / 934 epoxy uncoated area. This value compares favorably with other reported reactivities for T300 graphite / 934 epoxy specimens flown on LDEF. The white coated quadrants did not experience any erosion of the composite substrate due to AO shielding by the AO stable titanium dioxide pigment.

The black coating was severely eroded as both the carbon pigment and the polyurethane matrix reacted with AO. Some initial attack of the substrate under the black Z306 coating was apparent.

Figure 5 is a 3-D plot of the data collected during a laser profilometry raster scan of a partially coated T300 graphite/934 epoxy panel segment. Data is plotted as a 0.0005" grid for the x-y plane and 0.001" line segments of various thicknesses for the z-direction (depth). The approximately 1 inch square area contains a circular region shielded from AO attack by a mounting washer on the surface. An A276 white polyurethane coating covers the rear left half of the panel segment.

There are three distinct height levels in this plot representing (from highest to lowest) the coating surface, the original uncoated composite surface (semicircular disk), and the AO eroded composite surface. The outline of the mounting washer can be seen on the coating surface where approximately 0.002" of coating was eroded beyond the washer protected area. On the uncoated composite half of the segment the washer protected area is easily detectable as a 0.003" step between the AO eroded surface and the original bare composite surface. The original coating thickness of 0.002" can be seen between the original uncoated composite (semicircular disk) surface and the coating surface.

Other visible features include a micrometeoroid or debris impact on the coated surface just to the left of the washer protected area and vertical spikes rising from the AO eroded composite surface due to particulate contaminate AO shielding.

Band Patterns

Just in front of the semicircular original uncoated composite surface shown in Figure 5 are some periodic height variations in the AO eroded composite surface. These variations correspond to a light and dark banding pattern that has also been reported for other leading edge exposed graphite/epoxy surfaces (Ref. 6). The light and dark bands were visible on the AO eroded bare graphite/epoxy surface as shown in Figure 6. Laser profilometery and physical measurements of the bands were taken to determine their width and height. The profilometry data revealed a height of approximately 0.0005" of the lighter bands over the darker bands. A width of 0.059 "$\pm$ 0.003" was measured for 10 separate bands indicating fairly uniform width from band to band. This width compares closely to the 0.056" average width for as prepregged T300/934 epoxy 3K graphite tows (18 tows or graphite fiber yarns per inch of T300/934 prepreg tape). Therefore the banding pattern shown on this panel is most likely due to a tow to tow material variation. The lighter color of the higher bands corresponds to a higher level of "ash" material as observed with optical microscopy. This "ash", which has been reported to contain sodium sulfate based on chemical analysis (Refs. 1 and 2), may have provided some shielding which would account for the reduced erosion of the lighter bands.

IMPACT CROSS SECTIONING

The five most prominent impact sites in the graphite/epoxy panel were cross sectioned to investigate coating and substrate damage. These impacts were all located in the A276 coated quadrant of the panel and had penetrated the coating, exposing the composite substrate. AO erosion of the exposed composite was visible with the unaided eye and its possible interactions with the impact geometry and damage were also investigated.

Sample Preparation

In order to preserve the impact damage and delicate AO erosion features including possible under cutting of the coating the impact sites were protected prior to rough trimming of the panel by placing a drop of low viscosity optical quality epoxy resin on their surfaces. The sites were under microscopic observation during this process and no flaking or movement of material other than some loose pigment particles from adjacent surfaces was seen.

After abrasive water jet trimming the preserved impacts were mounted in an epoxy casting for sectioning. The mounts were then trimmed using a liquid cooled abrasive cutting wheel to within approximately 0.1" of the impact. The remaining material was removed by polishing to reach the center line of the impact. Four of the impacts were sectioned in the 90° direction and one in the 0° direction.

Impact Observations

The polished cross sections were then examined at various magnifications using a Zeiss Axomat microscope with bright field illumination. Figures 7 through 11 are photomicrographs of the polished cross sections for impacts one through five respectively. These impacts have many of the same features along with some distinct dissimilarities. Four of the five impacts display an inverted hat shape (three very strongly). These four impacts (numbers 1,2,3 & 5) also display AO erosion features which are approximately 3 to 4 fiber diameters tall both on the "shoulders" and at the "base" of the hat (See Figure 12). Impact number four, which does not have the inverted hat shape, displays extensive crushing and displacement of material. Also, its erosion features are only one fiber diameter tall.

All impact sites displayed delaminations at the first ply orientation transition interface. Only the largest impact, #5, displayed deeper delaminations. Impact #5 also contains what appear to be fiber fractures below the base of the impact. These were initially thought to be polishing artifacts. However, after repolishing and observing using a differential interference contrast technique the fractures were still present and an indication of depth to the fractures visible (see Figure 13). No indications of coating undercutting by AO were visible.

MICROCRACKING STUDY

Thermal Modeling

The epoxy/graphite composite substrate experienced different thermal extremes and thermal shocks in the four quadrants based on the optical properties of the coatings. These cycles and extremes were estimated using LDEF environmental data (ref. 4), coating and composite physical and optical properties, and recorded flight data for temperature vs. time of an aluminum plate which was located beneath the coated panel. The results are shown graphically in Figure 14 as temperature vs. time for 2 cycles. As was expected, the thermal cycle shock and extremes were much greater for the Z306 black coated and uncoated composite quadrants than for the A276 and BMS 10-60 white coated composite quadrants.

Microcrack Density Measurements

Six specimens were taken from each quadrant at 0°, +45° and 90° (2 each) for cross sectional microcrack analysis. A total of 48 lineal inches of cross section, twelve from each

quadrant, were examined by optical microscopy at 200x magnification for microcrack location and density. A summary of the results is presented in Figure 15. The black coated and bare quadrants contained significant levels of microcracking while the white coated quadrants were relatively crack free. Most of the cracks that were found in the white coated specimens were located within close proximity to the black or bare area boundaries. The more extreme thermal environment experienced by the black coated and bare quadrants appears to have created thermal stress induced microcracking in those areas as well as in adjacent regions of the white coated quadrants.

Undoubtedly other factors came into play during microcrack formation. The panel was restrained by the mounting points possibly interfering or aggravating the thermal expansion or contraction of the panel. AO erosion, which may have provided possible crack initiation sites in the black and bare coated quadrants, basically removed one ply from the bare quadrant creating an unbalanced layup. Finally, the heating and cooling from direct and reflected solar radiation occurred on one side of the panel possibly creating a significant thermal gradient through the thickness of the panel. Indeed there is more cracking in the exposed outer three plies than the shielded inner three plies for all the quadrants. The white coatings did adequately minimize thermal stresses in their quadrants to effectively prevent substrate microcracking. However, due to the complexity of the thermal stresses experienced by the panel, extracting quantitative design data from these results would be challenging.

Microcrack-Atomic Oxygen Interaction

AO interaction with microcracks was observed in both bare and coated areas. Figure 16 shows a microcrack in the surface ply of the bare composite quadrant. The upper portion of the crack has been enlarged by AO attack. This interaction was found in two thirds of the observed surface ply cracks for the bare quadrant. Figure 17 shows similar interaction for a crack in the black coated quadrant. Note that AO attack has begun in the composite substrate in some regions where the coating has been completely eroded. As mentioned above the AO erosion may have also created crack initiation sites. The AO created sharp erosion troughs running parallel to the fiber direction.

AO-microcrack interaction was also observed for a crack in the A276 white coated region. Figure 18 shows a thermal cycle induced microcrack in the surface ply of the A276 coated quadrant. Careful observation reveals that the crack has propagated through the coating allowing limited AO attack of the substrate. The coating breach, which is visible with the unaided eye on the panel surface, was present during flight as evidenced by the signs of AO erosion in the crack. Crack propagation through the A276 coating was unexpected as the coating has a strain to failure of 30-50%. The limited AO erosion in the substrate microcrack suggests that propagation through the coating occurred later in the mission. The substrate crack which would have developed before most of the AO exposure may have created stresses in the coating which accelerated AO attack of the coating over the crack.

CONCLUSIONS

Atomic Oxygen Exposure

Response to low earth orbit atomic oxygen exposure varied for the different panel quadrants. The AO reactivity of the uncoated T300 graphite / 934 epoxy composite quadrant was measured to be $0.99 \times 10^{-24} cm^3$/atom. This value agrees favorably with

other reported AO reactivities for T300 / 934 flown on LDEF. The Z306 black urethane coating did not prevent AO attack of the graphite epoxy. Further exposure would have completely removed the coating, allowing unhindered attack of the substrate.

Both the A276 and BMS 10-60 white urethane coatings effectively protected the graphite/epoxy from attack. This is due to the AO resistant nature of the titanium dioxide pigment in these coatings. The only AO attack of the white coated composite substrates occurred where the coatings had been breached by either an impact or a surface microcrack propagating from the black coated or bare composite areas.

Light and dark bands were observed on the surface of the uncoated composite region. Using optical microscopy and profilometry the light bands were found to be approximately 0.005" taller than the dark bands and contained a higher level of "ash" giving them their lighter appearance. The band widths closely match the widths for as prepregged 3K T300 graphite/934 epoxy tows. Therefore, the banding appears to be a tow to tow material variation.

Cross sectional analysis of micrometeoroid/debris impact sites provided direct observation of the damage to the coating and composite substrate. Local delaminations and crushing were evident at all observed impact sights. The largest impact site had unexplained fiber damage in the form of fiber cracks running parallel to the direction of the impact. Four of the five impacts displayed an "inverted hat" shape and these four had similar size AO erosion features. The fifth impact did not have the inverted hat shape and had significantly smaller AO erosion features. This impact may have occured much later in the mission. The inverted hat shape may be due to coating removal around the impact site and/or accelerated AO erosion of crushed composite at the impact center. No signs of coating undercutting were observed at the impact sites.

The quadrants of the graphite/epoxy panel experienced significantly different thermal cycle/shock conditions. The A276 and BMS 10-60 white thermal control coatings effectively prevented microcracking of the composite substrate. The Z306 black urethane and uncoated quadrants experienced hotter thermal cycle extremes and greater thermal shock resulting in significant microcracking of the outer three laminate plies. AO interaction with cracks on the surface ply was observed in the form of crack enlargement. Surface ply cracks extended a short distance from the black coated and uncoated quadrants into the white coated quadrants. Evidence of initial AO attack was seen in one of these cracks indicating that crack propagation through the white coatings occurred during flight.

FUTURE WORK

The reduced AO erosion observed for the the lighter bands on the uncoated composite surface warrants further investigation. Tow to tow variables targeted for investigation include local resin content by cross sectional image analysis and carbon fiber sodium content, one of the elements present in the surface "ash" which has been identified as AO resistant sodium sulfate. These findings may help development of structural composites with inherent AO resistance.

The impact sites have only been examined in one cross sectional plane. Continued sectioning with quantitative geometry measurements will allow a 3-D picture of impact sites to be assembled from slices. This may yield further insights into impact damage and AO impact interactions.

The thermal cycling/microcracking results may offer the most useful information for space composite hardware designers. Adjustment of the thermal cycle calculations for the white coated regions will be necessary due to the temporary UV degradation of optical properties before AO bleaching occurred. CTE measurements of samples from the quadrants may reveal microcrack induced changes. Also, thermal cycling specimens from the white coated quadrants to the same extremes experienced by the black coated and bare quadrants followed by microcrack inspections will help verify the thermal modeling. Finally, incorporation of these results with additional ground based testing and existing work could lead to development of a comprehensive LEO exposure/microcracking model allowing refined prediction of mechanical properties.

ACKNOWLEDGMENTS

The authors would like to thank the Analytical Engineering, Physics, and Structures organizations along with members of the Nonmetallic Materials Technology group of Boeing Defense and Space Group for their assistance.

References

1. George, P.E. and Hill, S.G.; Results from Analysis of Boeing Composite Specimens Flown on LDEF Experiment M0003-8. First LDEF Post Retrieval Symposium, NASA CP-3134, Feb. 1992.

2. George, P.E.; Space Environmental Effects on LDEF Low Earth Orbit Exposed Graphite Reinforced Polymer Matrix Composites. LDEF Materials Workshop 1991, NASA CP-3162.

3. Bourassa, R.J.; and Gillis, J.R.; Atomic Oxygen Exposure of LDEF Experiment Trays. NASA Contractor Report No 189627. May 1992.

4. Bourassa, R.J.; and Gillis, J.R.; Solar Exposure of LDEF Experiment Trays NASA Contractor Report No. 189554. Feb. 1992.

5. Tennyson, R. et al; Preliminary Results From the LDEF UTIAS Composite Materials Experiment. First LDEF Post Retrieval Symposium NASA CP-3134, Feb. 1992.

6. Slemp, W. S. et al; Effects of LDEF Flight Exposure on Selected Polymer Matrix Composite Materials. First LDEF Post Retrieval Symposium, NASA CP-3134 Feb. 1992.

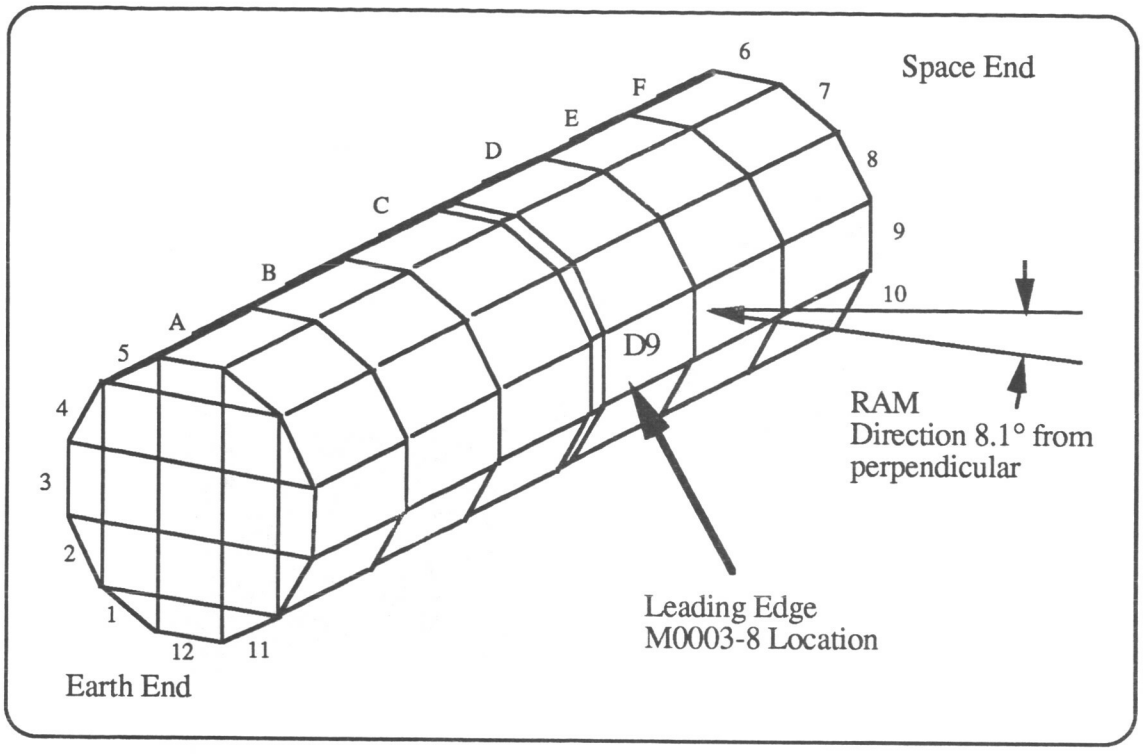

FIGURE I. - LEADING EDGE POSITION OF LDEF EXPERIMENT M0003-8

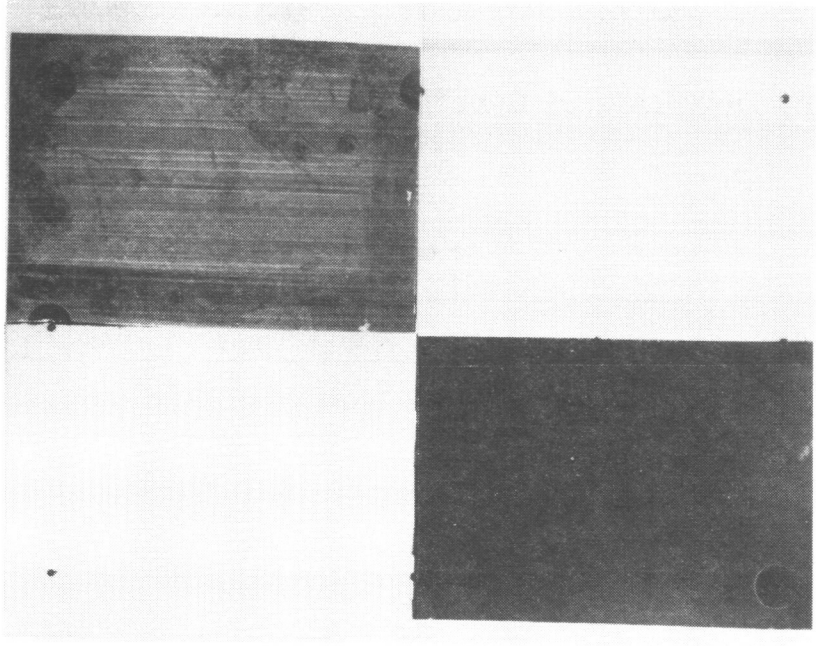

FIGURE II. - POST FLIGHT PHOTOGRAPH OF COATED T300 GRAPHITE/934 EPOXY TEST PANEL

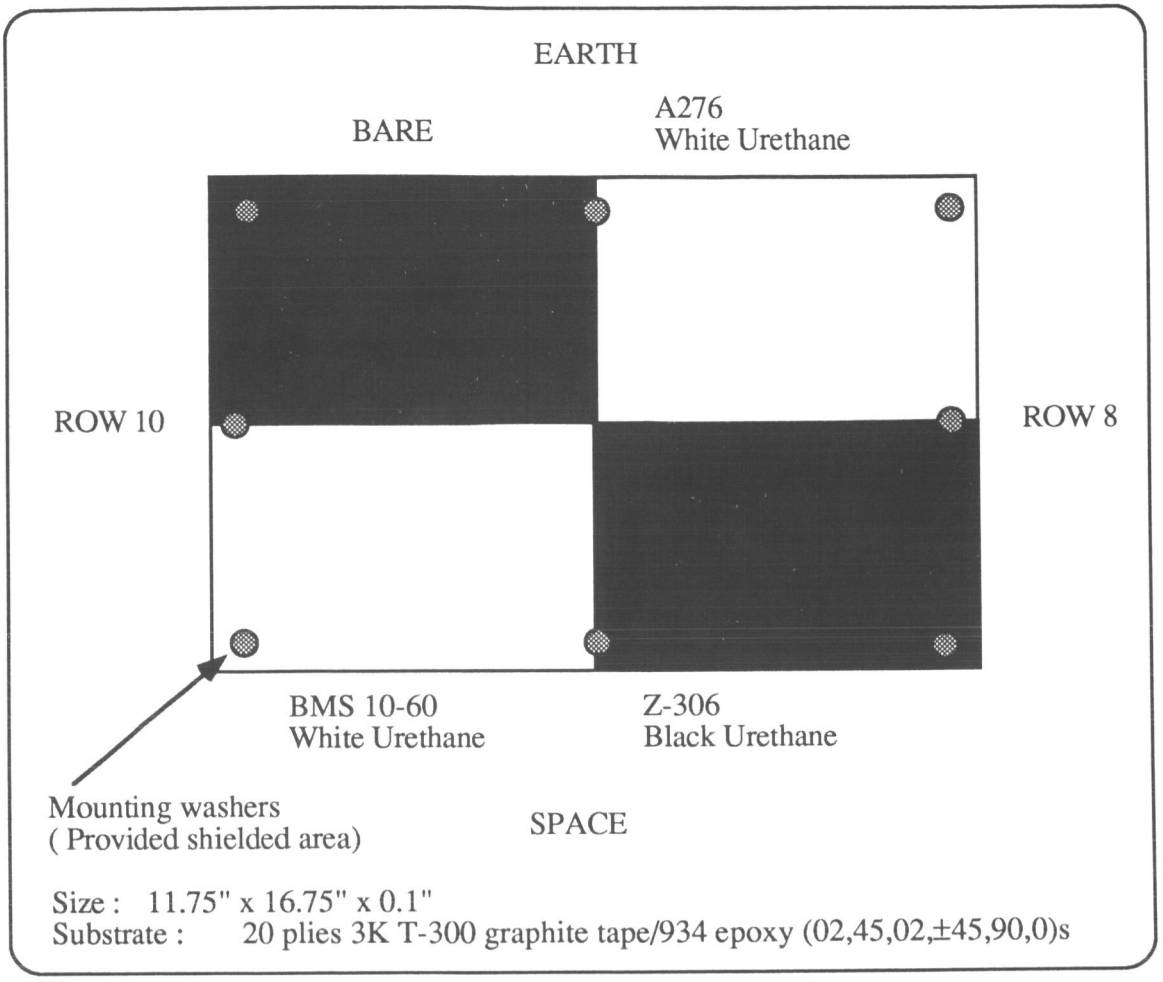

FIGURE III. - DIAGRAM OF COATED T300 GRAPHITE/934 EPOXY TEST PANEL

	LEADING EDGE TRAY POSITION D9			
COATING	Uncoated	Z-306 Black	A-276 White	BMS 10-60 White
ATOMIC OXYGEN EXPOSURE (Impacts / cm^2)	8.72×10^{21}			
INCIDENT SOLAR PLUS EARTH REFLECTED RADIATION (Equivalent solar hours)	11,200			
THERMAL CYCLING	-70° to 235°F	-75° to 205°F	-75° to 60°F	-75° to 60°F
(based on modeling and measurements)	34,000 CYCLES			

FIGURE IV - EXPOSURE CONDITIONS FOR M0003-8 COATED T300 GRAPHITE/934 EPOXY TEST PANEL

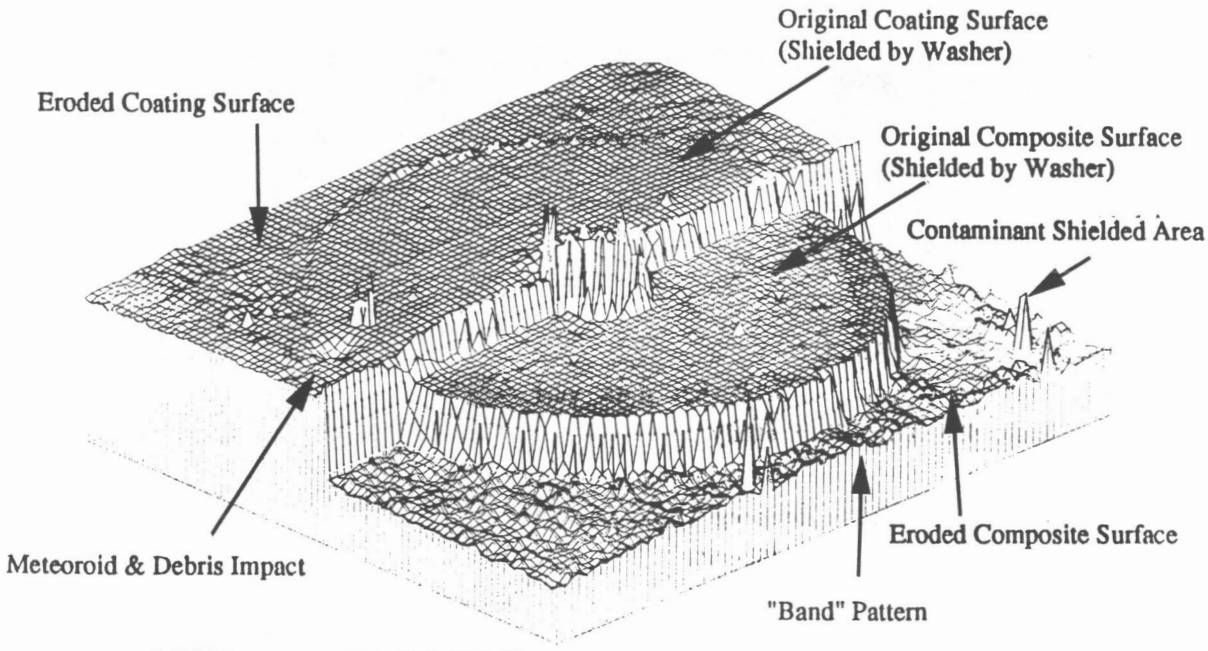

FIGURE V - LASER PROFILOMETRY RASTER SCAN OF WASHER REGION

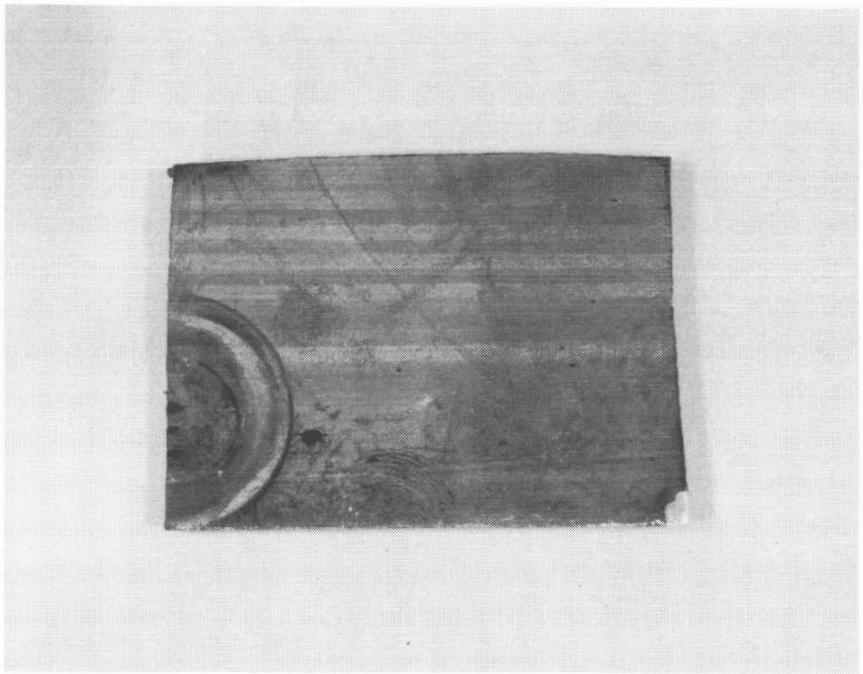

FIGURE VI - PHOTOGRAPH OF BAND PATTERN ON EXPOSED UNCOATED T300 GRAPHITE/934 EPOXY SURFACE

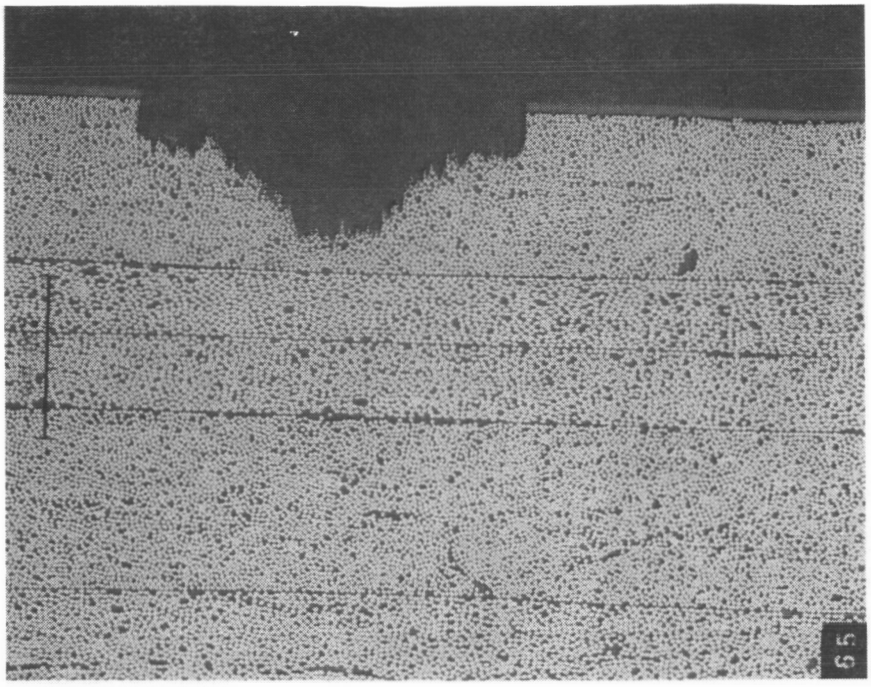

FIGURE VII - CROSS SECTIONAL PHOTOMICROGRAPH OF IMPACT #1 IN A-276 COATED T300/934

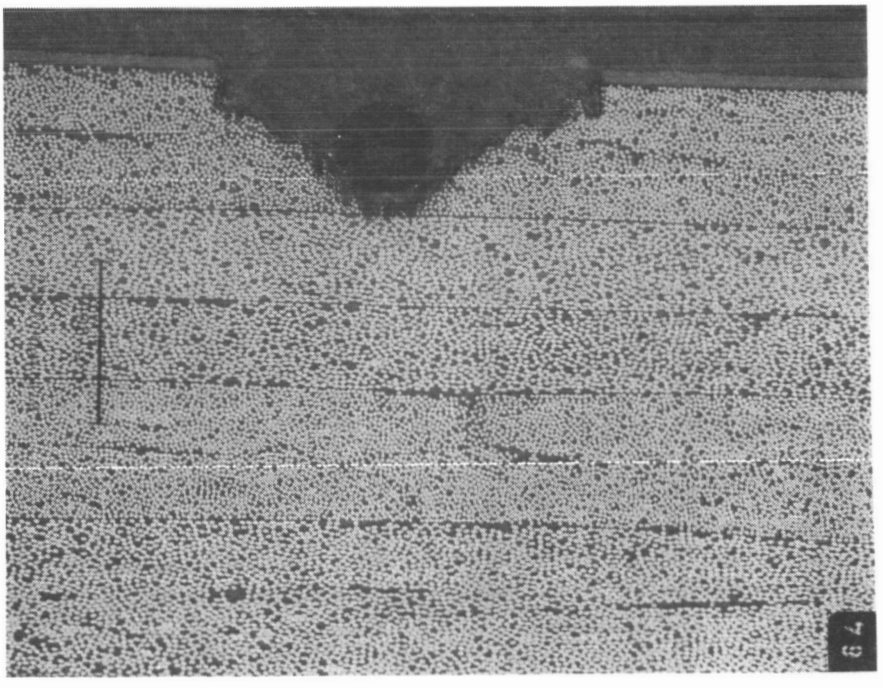

FIGURE VIII - CROSS SECTIONAL PHOTOMICROGRAPH OF IMPACT #2 IN A-276 COATED T300/934

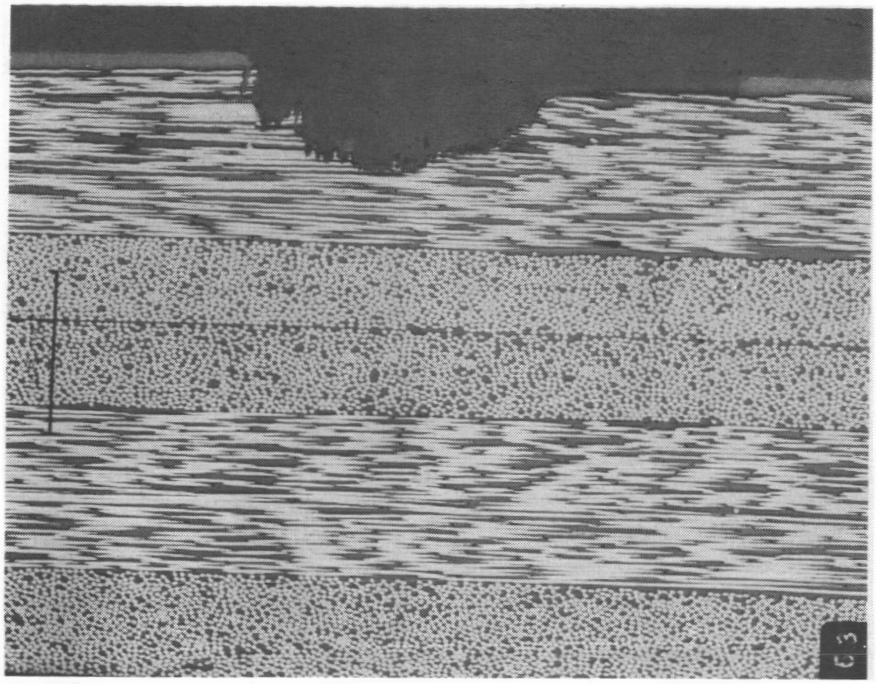

FIGURE IX - CROSS SECTIONAL PHOTOMICROGRAPH OF IMPACT #3 IN A-276 COATED T300/934

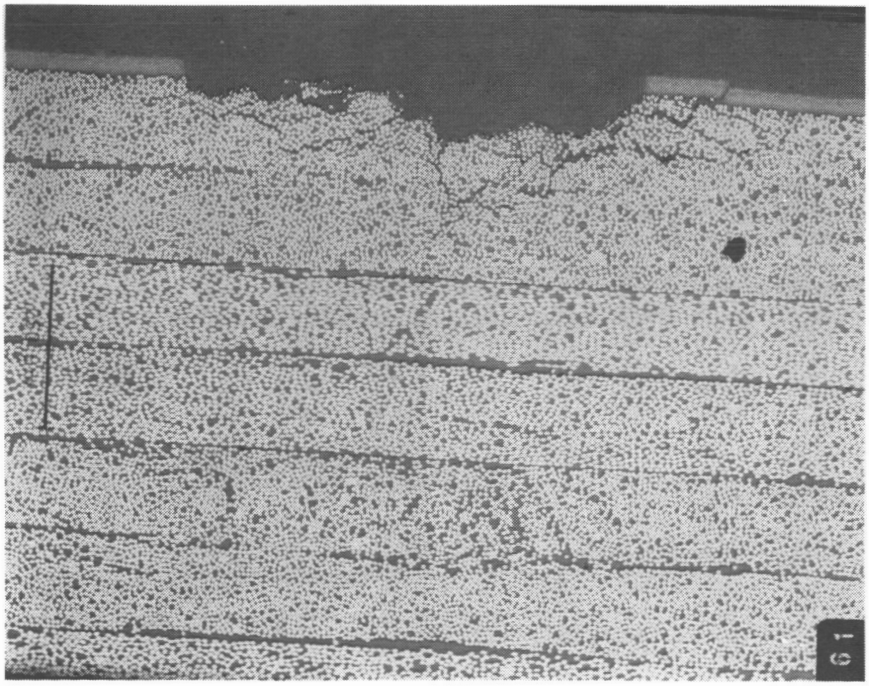

FIGURE X - CROSS SECTIONAL PHOTOMICROGRAPH OF IMPACT #4 IN A-276 COATED T300/934

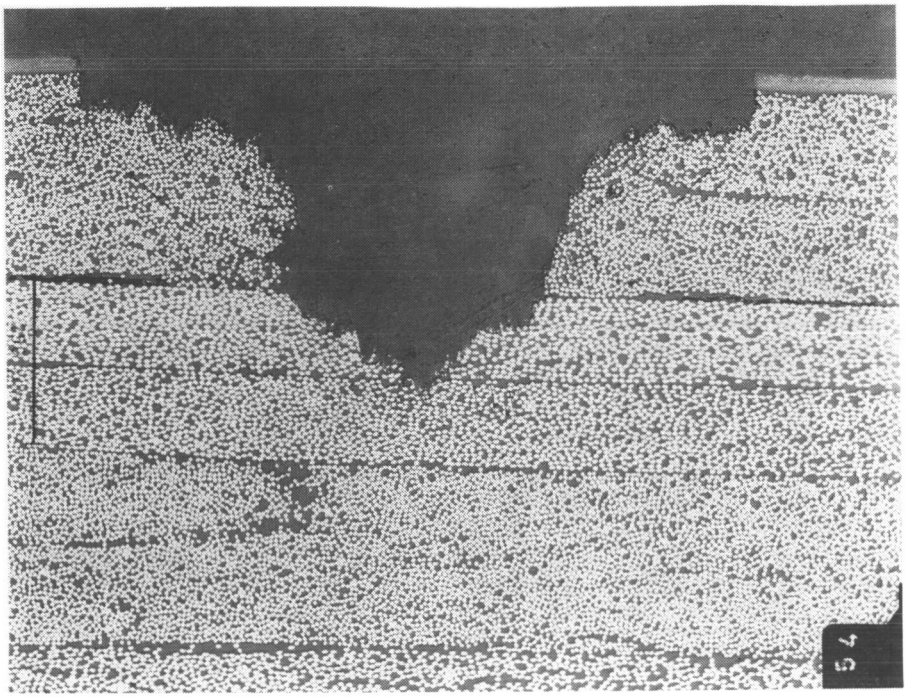

FIGURE XI - CROSS SECTIONAL PHOTOMICROGRAPH OF IMPACT #5 IN A-276 COATED T300/934

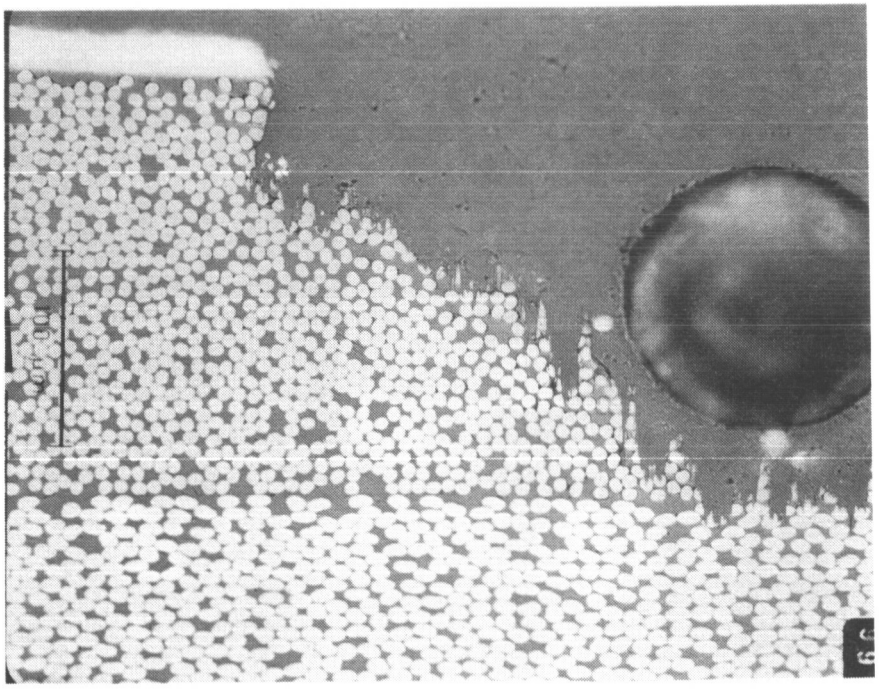

FIGURE XII - ATOMIC OXYGEN EROSION FEATURES OF IMPACT #2

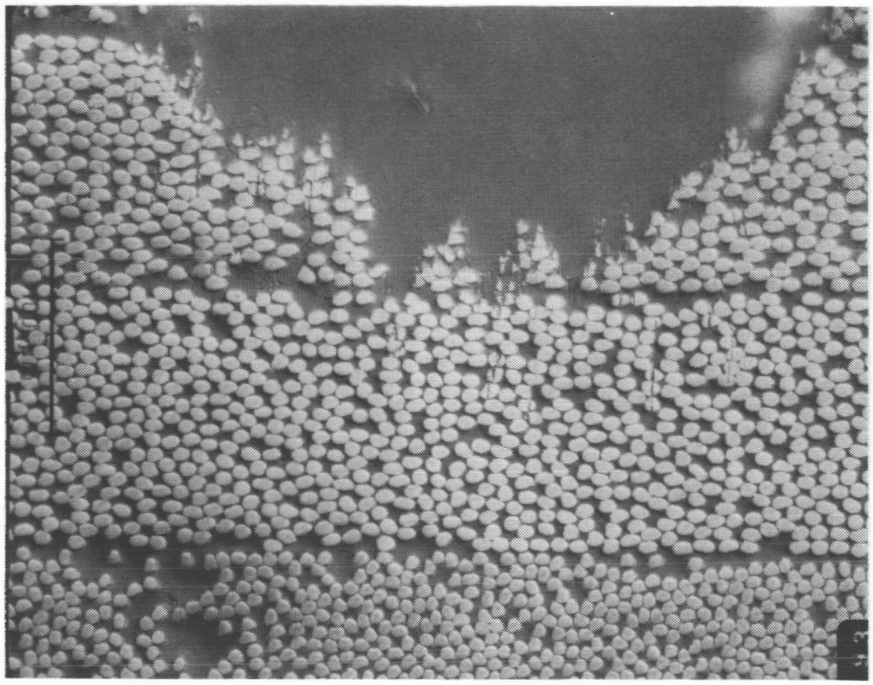

FIGURE XIII - DIFFERENTIAL INTERFERENCE CONTRAST PHOTOMICROGRAPH OF FIBER CRACKS IN IMPACT #5

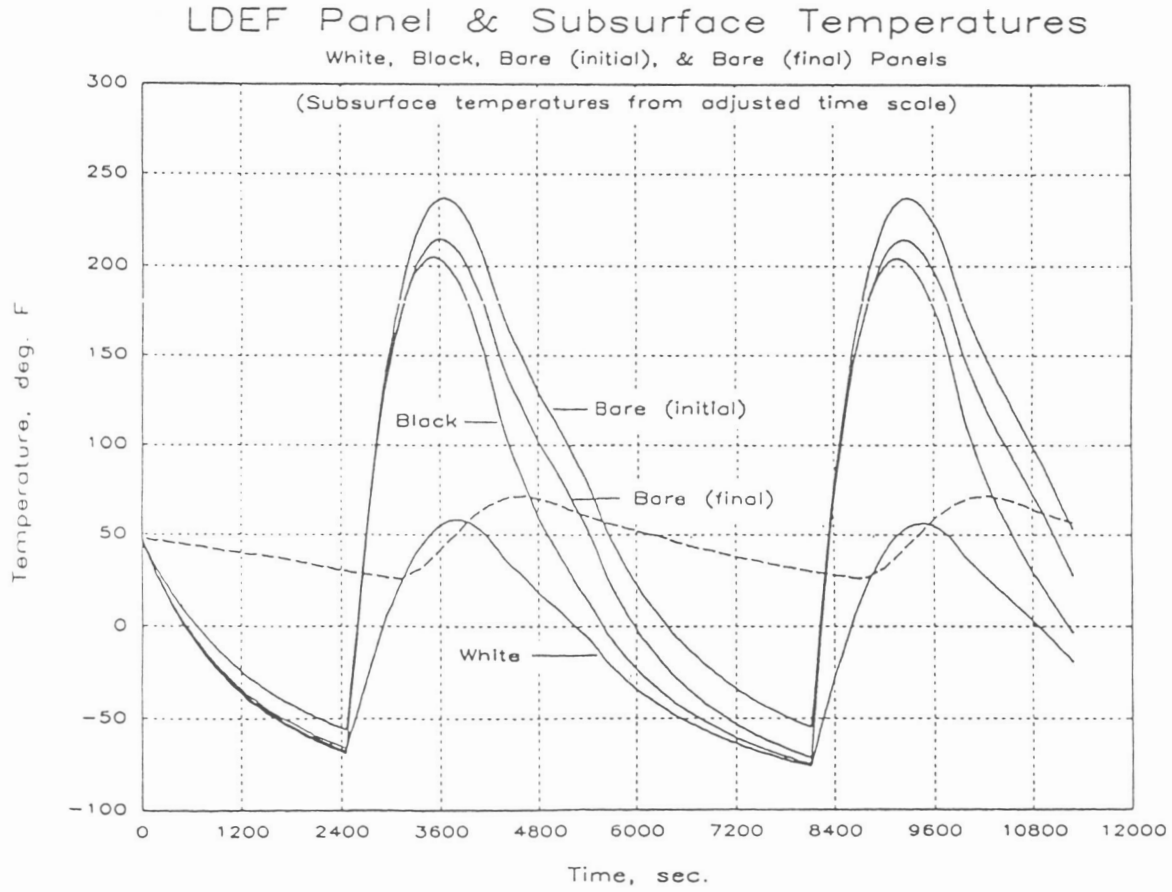

FIGURE XIV - RESULTS OF THERMAL CYCLE MODELING FOR LDEF EXPOSURE OF T300 GRAPHITE 934 EPOXY PANEL

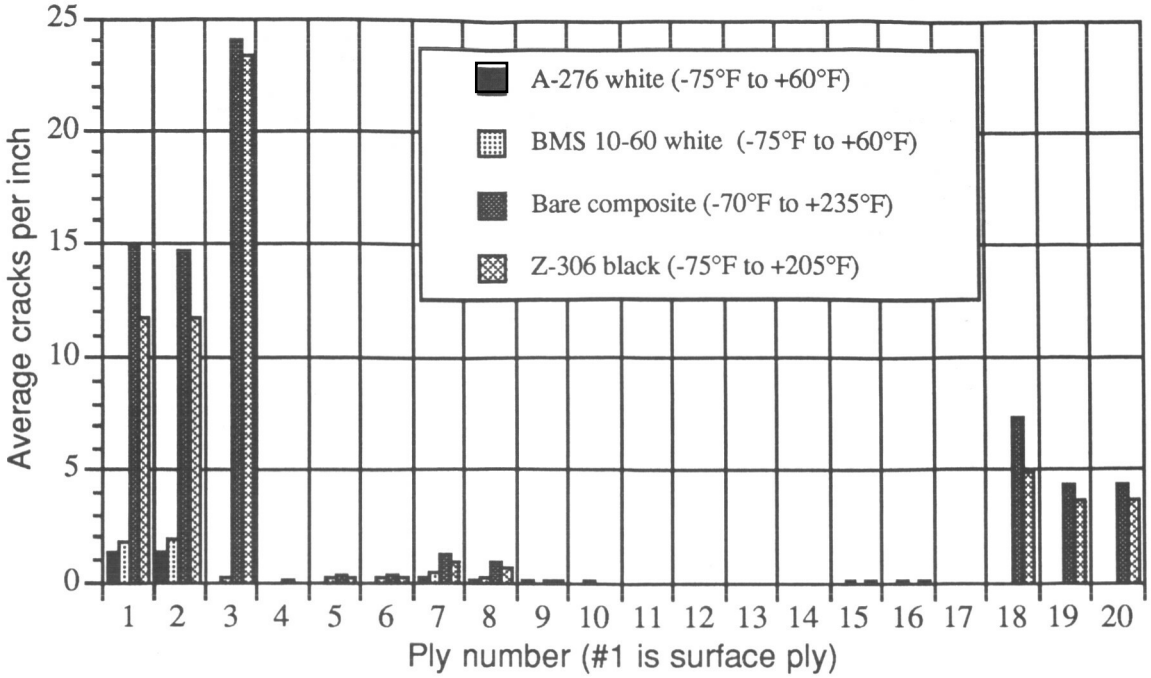

FIGURE XV - MICROCRACK DENSITY VS. PLY NUMBER FOR THE COATED AND UNCOATED COMPOSITE SUBSTRATES

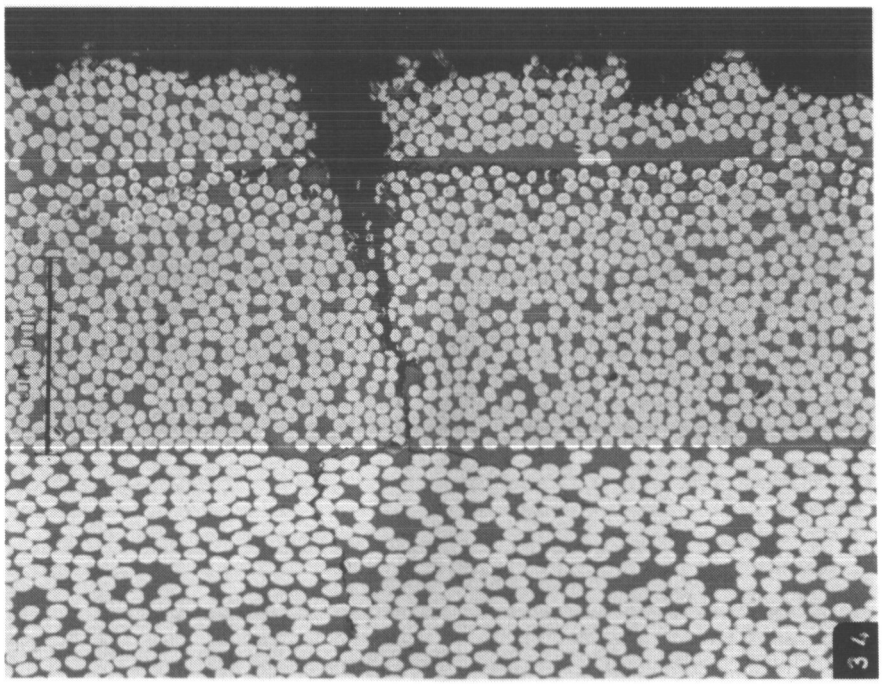

FIGURE XVI - CROSS SECTIONAL PHOTOMICROGRAPH OF MICROCRACK IN SURFACE PLY OF EXPOSED UNCOATED T300/934 PANEL QUADRANT

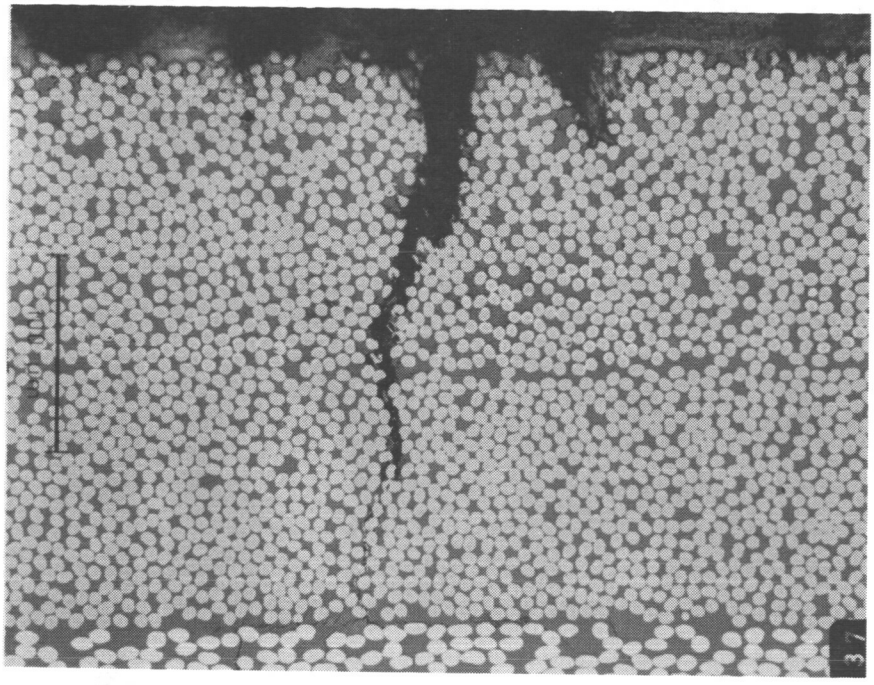

FIGURE XVII - CROSS SECTIONAL PHOTOMICROGRAPH OF MICROCRACK IN SURFACE PLY OF EXPOSED Z306 COATED T300/934 PANEL QUADRANT

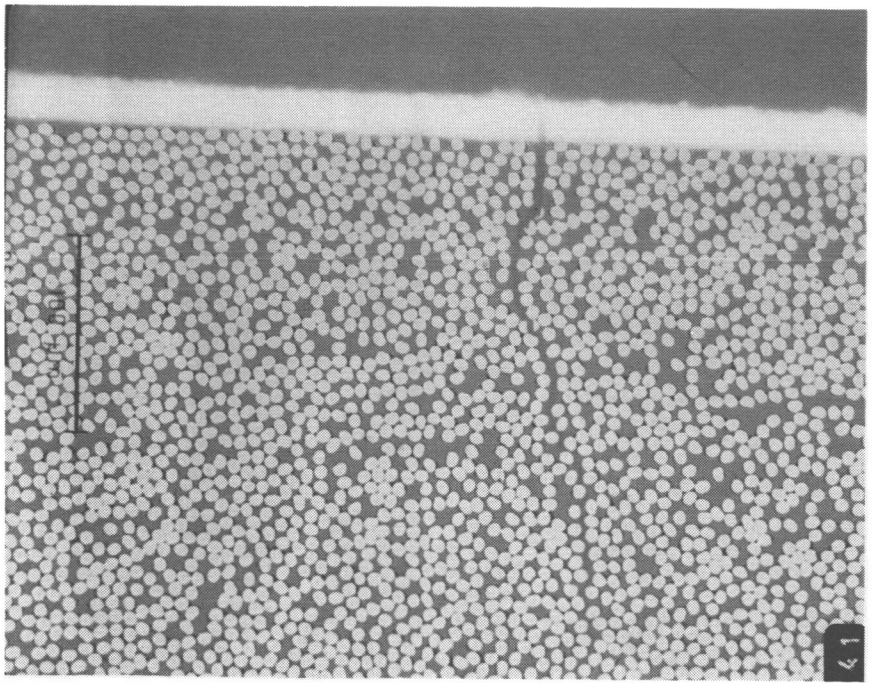

FIGURE XVIII - CROSS SECTIONAL PHOTOMICROGRAPH OF MICROCRACK IN SURFACE PLY OF EXPOSED A276 COATED T300/934 PANEL QUADRANT

N93-28266

THE EFFECTS OF LONG-DURATION SPACE EXPOSURE ON THE MECHANICAL PROPERTIES OF SOME CARBON-REINFORCED RESIN MATRIX COMPOSITES

Richard F. Vyhnal
Rockwell International-North American Aircraft
Tulsa, Oklahoma 74115
Phone: 918/835-3111, Ext. 2252, Fax: 918/834-7722

INTRODUCTION

LDEF Experiment A0175 involved the non-instrumented exposure of seven carbon-fiber-reinforced resin-matrix advanced composite panels contained in two trays - A7 and A1. These two trays were located, respectively, on the leading and trailing faces of LDEF, obliquely oriented to the RAM (Row 9) and WAKE (Row 3) directions, as shown in Figure 1. This figure also shows:

(a) The identity and location of the seven panels, which consisted of six flat laminates of the following material systems: carbon/epoxy (T300/934), carbon/bismaleimide (T300/F178), and carbon/polyimide (C6000/LARC-160 and C6000/PMR-15), plus one bonded honeycomb sandwich panel (T300/934 facesheets and Nomex core) patterned after the Space Shuttle payload bay door construction. These material systems were selected to represent a range of then-available matrix resins which, by virtue of their differing polymer chemistry, could conceivably exhibit differing susceptibility to the low-earth orbit (LEO) environment.

(b) The principal exposure conditions of the LDEF environment at these tray locations. Noteworthy to some of the observations to be discussed herein is the four-orders-of-magnitude difference in the atomic oxygen (AO) fluence, [1] which made a shallow incidence angle (~22°) to Tray A7, while Tray A1 on the trailing face was essentially shielded from AO exposure.

This evaluation focused on determining the individual and relative suitability of a variety of resin-matrix composite systems for long-term space structural applications. This was accomplished primarily by measuring and comparing a range of engineering mechanical properties on over 300 test coupons sectioned from the flight panels and from identical control panels, and tested at ambient and elevated temperatures. This testing was supported by limited physical characterization, involving visual examination of flight panel surface features, measurements of weight loss and warpage, and examination for changes in internal integrity (microcracking, delamination) by ultrasonic c-scan and polished cross-sections.

RESULTS

Visual Observations

Detailed results of a survey performed by The Meteroid and Debris Special Investigation Group (M&D SIG) at Kennedy Space Center on the number and size of micrometeroid and debris impact sites have been published previously [4] and are summarized briefly here. For this experiment, the survey found that the number of impact sites, both above and below a 0.5 mm threshold size, was roughly twice as high on Tray A7 on the leading face of LDEF as on Tray A1 on the trailing face. Seven of the largest impact features, including the largest site (2.3 x 0.7 mm) located on the PMR-15 laminate, were protected against contamination after the survey, subsequently excised from the panels, and submitted for further evaluation (in progress) by the M&D SIG.

PRECEDING PAGE BLANK NOT FILMED

A second visual observation was of a fine white powdery residue over the surfaces of all three panels from Tray A7, except for a narrow band on each adjacent to the aluminum retainer strip along the "leading edge" of this tray. This residue was assumed to be a product of the reaction of AO with the surface layer of matrix resin; the narrow band was merely a region which had been shadowed from the full AO flux by the retainer strip. No loose fibers were detected on the superficially eroded surfaces.

A final visual observation involved the differing appearance of yellow epoxy ink markings which had been applied to identify both flight and control panels. These markings on the trailing-face panels were noticeably discolored to a brownish tint, whereas those on the leading-face panels as well as on laboratory control panels retained their original bright yellow color. Similar observations have been reported by other LDEF investigators and interpreted [5] as being due to competing effects of ultraviolet radiation and atomic oxygen on the epoxy ink. The discoloration is attributed to the effect of ultraviolet radiation which was of similar intensity on both trays; however, the atomic oxygen flux, which was four orders of magnitude more intense on Tray A7, resulted in a continual erosion of the UV- discolored surface of the ink, thus maintaining its near-original coloration.

Weight Loss Determination

Following disassembly of the panels from their trays and a drying cycle to remove any moisture absorbed during the disassembly period (7-12 days at 250F, identical to that performed prior to preflight weighing), the panels were reweighed. As shown in Table 1, the laminates from the leading-face tray lost 14-to-17 grams, equivalent to approximately 1%, whereas those from the trailing-face lost 0-to-3 grams (0-to-0.4%). [The sandwich panel lost 12 grams which, after subtracting the weight of the 76 metallic fasteners, corresponds to 0.5%.]

The difference in weight change between leading- and trailing-face laminates is attributable to the observed AO erosion of the former. If all of the weight loss is assumed to be due to AO erosion of matrix resin (realistically, some fraction may be due to outgassing of volatile constituents), this is equivalent to an erosion depth of 40 microns.

Warpage Measurements

It is commonly observed in composites that even balanced, symmetric laminates cured on a flat surface exhibit some small degree of nonflatness which is a manifestation of the state of residual stress within the laminate. It was originally thought that any changes in this physical characteristic might be relatable to the exposure conditions, such as thermal cycling, or to other potential changes in the laminates due to exposure such as, perhaps, microcracking or one-sided surface attrition. Consequently, the flatness of the exposed panels was measured before and after exposure.

The panels were placed on a surface table, weighted down along one edge with the exposed surfaces up, and the deflection measured along the opposite edge at the midpoint and both corners. In the preflight measurements, all of the BMI and PI panels were concave upward; in the postflight measurements, they were still concave upward, although generally to a much lesser degree. The carbon/epoxy laminate and sandwich panel were both flat, both before and after exposure. As shown in Table 2, the remaining laminates exhibited a marked reduction in warpage following exposure, with the single exception of the cocured* BMI laminate which exhibited, on average, a slight increase in warpage.

---

*For a description of the terms "precured" and "cocured" , see the section on Mechanical Properties.

Evaluation of Laminate Quality

All flight panels were re-inspected following exposure by ultrasonic c-scan, which revealed no defects - such as delaminations or disbonds - which could be attributable to the exposure. Both the epoxy laminate and sandwich panel were completely free of any ultrasonic indications; the BMI laminates each exhibited overall sound quality with one or two small areas of porosity from the original as-cured condition. The PI laminates, however, exhibited substantial areas of porosity - both in the control and flight laminates - which must be attributed to non-optimized curing conditions for these materials. Accordingly, additional measurements of resin content, fiber volume, and void volume were performed which yielded results (Table 3) consistent with the c-scan observations, i.e., higher porosity levels in the PI laminates. More importantly, these measurements indicated lower fiber volume values than the customary 60% (nominal) level. These results raise a caution in comparing the mechanical properties results reported herein with those published elsewhere in the literature for these PI materials.

Cross-Sectional Examination of Panel Integrity

Small samples were sectioned from control and exposed panels and polished for examination of laminate integrity. A typical section through the epoxy sandwich panel is shown in Figure 2 which contains the exposed facesheet of the flight article and one or two Nomex core cell walls with adhesive fillets along the bondline. No differences were observed between pre- and postflight articles; there was no evidence of microcracking.

The postflight condition of the carbon/epoxy laminate is illustrated in Figure 3 which shows uniform microcracking through the thickness. In the single sample examined, the density of microcracks in the 8-ply stacks of unidirectional tape was identical on both sides of the laminate midplane (15 per inch) and the individual spacing varied from 0.04-to-0.11 inch. The original control laminate for this material was not available for examination; however, a newer laminate prepared by identical processing with the same layup sequence showed no evidence of microcracking in the as-cured condition.

Cross-sections of the BMI laminates in both pre- and postflight conditions are shown in Figure 4 (precured) and 5 (cocured). Both cure conditions exhibited similar levels of microcracking in the preflight condition and a notably higher density of cracks in the postflight condition. The results of measurement of the microcrack density at various layers through the thickness on a number of such specimens are summarized in Table 4. The results from specimen to specimen were quite consistent. It is noted that the midplane plies, which showed a low density relative to the surface plies in the preflight condition, exhibited a much higher density than the surface plies in the postflight condition, while the surface density also increased. This pattern held true for both cure conditions. No interpretation may be offered for this pattern of microcracking.

Cross-sections of the PI laminates in both pre- and postflight conditions are shown in Figure 6 (LARC 160) and 7 (PMR-15). As with the BMI samples, both materials exhibited similar microcrack densities in the preflight condition; however, there was no obvious increase in microcracking in the single postflight sample examined for each PI material (refer to Table 4).

During this examination it was also discovered that one 90° ply had been inadvertently omitted from the layup in the PMR-15 control, as noted in Figure 7; this fact comes into play in the interpretation of mechanical properties results discussed below. Also shown here in the postflight laminate is a localized area of porosity, which had been detected previously by ultrasonic inspection.

The development of, or increase in, microcracking in the flight panels is attributable to the thermal cycling experienced by all the panels during their exposure, which amounted to more than

30,000 cycles (orbits) over a maximum temperature range of 200 to -40°F. Also, an increase in microcrack density can provide an explanation for the reduction in warpage described above, since the cracking would tend to relieve cured-in residual stresses.

Mechanical Properties

All of the mechanical property test results are presented in Tables 5 and 6 and Figures 8 through 10. Each data point represents the high-average-low value of 5 replicas, unless otherwise noted in the table.

For the epoxy sandwich panel, flatwise tension and beam shear tests were used to evaluate the effect of exposure on, principally, the honeycomb core. In these tests, failure is expected to occur in the core (rather than in the adhesive bondline or the facesheet), and this was, in fact, observed for both the control and flight specimens. In general, wider scatter bands were observed for the flight specimens, although it should be noted that the control scatter bands were uncharacteristically small (a variation of $\pm$5% is not uncommon for these tests).

With regard to the flatwise tension test, there was essentially no difference noted in the room temperature results (less than 2% difference in average value), while the 350°F results showed a 17% lower value for the flight specimens. The beam shear test yielded just the reverse pattern of behavior, i.e., no difference at 350°F and a 6% lower value for the flight specimens at room temperature. Taken together, these tests are regarded as showing no unambiguous effect of the LDEF exposure on the honeycomb core strength.

The beam shear specimens were also instrumented with strain gages on the compression side, and the modulus values so determined are included in Table 5 . A 17% lower value was measured for the flight specimens at both temperatures. In itself, this result might be taken as evidence for some exposure-induced degradation in stiffness which could conceivably have been caused by thermal-cycling-induced breakdown of the fiber-matrix bond, for example. However, this possible interpretation must be tempered by other observed differences in modulus (discussed below) in which other flight specimens exhibited higher -- as well as lower -- moduli values.

Results of tension, compression, and rail shear testing are shown in Figure 9 for the BMI laminates which represented two different cure conditions. The "precured" laminate had been autoclave-cured at 350°F and 85 psi (per the prepreg manufacturer's specification) against a flat metal surface, whereas the "cocured" laminate was autoclave-cured against a layer of honeycomb core at a reduced pressure of 45 psi. This latter simulated a cure condition commonly employed in the production of sandwich structures, and it typically yields slightly reduced values for certain matrix-dependent mechanical properties due to the reduced consolidation pressure and the dimple-pattern which is transferred to the laminate from the honeycomb cell structure.

With regard to the 0°-tension and 90°-compression strength measurements, the differences between the mean strength values of control versus exposed materials are less than the individual scatter bands associated with these mean values. In some cases, the exposed material exhibits even a slightly higher strength value than the control, this despite the existence of a significantly higher density of microcracking in the former, as discussed previously.

With respect to moduli, the 0°-tensile moduli of all the exposed samples were curiously higher than those of the controls by anywhere from 1 to 22 percent, while the 90°-compressive moduli at 75°F were somewhat lower by 6 to 16 percent respectively for the precured and cocured materials. (Note: Compressive moduli were not measured at 450°F in the exposed samples due to the premature failure of elevated-temperature compression specimens of the control material at the point of contact with compressometer knife edges).

The lack of a consistent pattern of behavior in these property measurements precludes any inference as to the effect of microcracking, or any other exposure-related mechanism, on these properties.

The rail shear results are even more inconsistent and difficult to understand, inasmuch as the strength values measured for the exposed material are 40 to 60 percent higher than control values (measured in 1979), while the moduli values are comparable. Both sets of specimens - control and exposed - were examined to check for any apparent differences in failure mode, but all specimens exhibited valid and similar failures through the gage area. The comparable moduli values discount the possibility of incorrect chart-scale settings. The orientation of the specimens relative to the laminate 0° direction was confirmed to be the same (although in this regard, it is noted that rail shear strength should be insensitive to such an orientation mix-up). Similar standardized specimen preparation procedures, test fixtures, and test methods were used in both series of tests. There is simply no plausible explanation for this wide disparity in strength values.

With respect to the polyimide laminates, it is recalled that the fiber volume values for all the PI laminates were slightly-to-well below the generally targeted range of 60-65 percent (Table 3). For this reason, the mechanical properties measured for both PI materials in this study should not be considered to be representative of these material systems. Furthermore, the wide variation from laminate-to-laminate among the LARC-160 panels, in particular, makes any attempt to interpret differences in mechanical properties between control and exposed specimens rather meaningless. At least with the PMR-15 laminates, the physical properties and ultrasonic quality are not too dissimilar, so comparison of exposed and control values may be valid.

For the PMR-15 material, the mechanical properties of the control specimens were generally slightly higher than those of the exposed material by no more than 12 percent, which is not a large difference, especially considering the small sample populations (five replicates) being compared here. This trend is consistent with the somewhat better quality of the control laminate, as indicated by ultrasonic C-scans and the fiber volume measurements.

In a few cases, the control material exhibited lower values, namely 90° compression strength (7 percent) and modulus (38 percent) at 75°F and rail shear strength (6 percent) at 75°F. The former may be attributed in large part to the fact that the control laminate was missing one of the four 90° plies as noted previously, which would be expected to reduce its compression strength and modulus in this 90° direction relative to the exposed laminate. However, cursory analysis has indicated that the absence of one 90° ply should result in a slightly higher* rail shear strength (4 percent), rather than the measured 6 percent lower value, although again, this difference may not be significant.

It is further recalled that cross-sectional examination showed comparable levels of microcracking in both control and exposed PMR-15 samples and, moreover, that in the BMI laminates, higher microcrack densities after exposure were not reflected in any concomitant property reductions. In light of these considerations, the small differences between control and exposed PMR-15 samples noted here cannot reasonaby be tied to any exposure-related degradation, but rather to small-population data scatter and slight differences in as-cured laminate quality.

---

*Due to a disproportionate reduction in cross-sectional area relative to load-carrying contribution of the missing 90° ply.

SUMMARY AND CONCLUSIONS

The principal effects of almost six years exposure in a low-earth-orbit environment on the condition of several carbon-reinforced resin-matrix composites were: (1) superficial erosion of the resin-rich surface by atomic oxygen; and (2) the development, or increase in density, of microcracks through the thickness of the laminates.

Atomic oxygen erosion was visibly apparent as a powdery white residue on the laminates exposed to an oblique incidence (approximately 22°) of atomic oxygen on the leading face of LDEF. It is believed to be responsible for a slightly greater weight loss among these laminates (1 percent) as compared to laminates on LDEF's trailing face (0 to 0.5 percent) where the atomic oxygen fluence was four orders of magnitude less. However, the erosion was confined to the resin-rich surface; there was no evidence of fiber loss or loosening and no indication that such erosion was sufficient to have a detectable influence on composite physical characteristics (specific gravity, thickness, resin content) or mechanical properties.

The development of microcracking in laminates which contained no microcracks in the as-cured state (carbon/epoxy), and the increase in microcrack density in laminates which did exhibit some cracking in the as-cured state (BMI), are attributed to thermal cycling (more than 30,000 cycles) over a temperature range of -40 to 200°F due to varying solar exposure. This microcracking is believed to be responsible, in large part, for the relief of cured-in residual stresses manifested by the reduced warpage measured in the flight articles as compared to their preflight condition. However, the microcracking did not appear to be of sufficient magnitude to have a measurable effect on the mechanical properties measured in this study.

In the BMI laminates, which contained some microcracking in the as-cured condition (for both the precured and cocured conditions), a notable increase in microcrack density did not produce any measurable effect on strength or stiffness properties. The modest differences in properties that were observed for these materials appeared to be of a random nature, either higher or lower in the exposed material relative to baseline control material.

In the PI laminates which showed somewhat wider variations in mechanical properties (than the BMI) but not necessarily an increase in microcrack density, the observed variations are more readily attributable to differences in original as-cured laminate quality rather than to any exposure effect.

The epoxy sandwich panel exhibited generally comparable mechanical properties between exposed and control, indicating no measurable degradation of bondline or honeycomb core strength due to the exposure. The lone exception to this is a small reduction in facesheet compressive modulus, but the small number of replicas, the inherent scatter in such measurement, and the lack of any independent evidence of a mechanism to explain such a difference make this observation rather inconclusive.

The primary conclusion, therefore, from LDEF Experiment A0175 is that the structural performance of a range of resin-matrix composites was not measurably affected by the almost six-year exposure in low-earth-orbit. The observation of some evidence of atomic oxygen erosion of the resin matrix in these materials, together with the knowledge that AO erosion was much more pronounced in similar materials located on the leading edge of LDEF, confirm the need for some sort of protection for such materials intended for long-life LEO missions. Likewise, the evidence of increased microcracking provides a mechanism for structural degradation in these materials which could become significant under certain types of loading or longer periods of exposure.

References

1. Bourassa, R. J. and Gillis , J. R., Atomic Oxygen Exposure of LDEF Experiment Trays; NASA Contractor Report No. 189627, May 1992.

2. Bourassa, R. J. and Gillis, J. R.; Solar Exposure of LDEF Experiment Trays; NASA Contractor Report No. 189554, Feb. 1992.

3. Berrios, W. M. and Sampair, T. R.; LDEF Post-Flight Thermal Analysis Calculated Flight Temperature Data Package - Preliminary.

4. See, T. et al; Meteroid and Debris Impact Features Documented on The Long Duration Exposure Facility, A Preliminary Report, Publication No. 84, JSC No. 24608, August 1990.

5. LDEF Spaceflight Environment Effects Newsletter, Vol. 1, No. 3, May 15, 1990.

Table 1

COMPARISON OF PREFLIGHT AND POSTFLIGHT PANEL WEIGHTS

Panel Description	Dry Weight (grams)		% Change
	Preflight	Postflight	
Tray A1 (Trailing Face)			
T300/934 sandwich panel	2642	2630	-0.45
T300/934 laminate	753.0	749.9	-0.41
C6000/LARC 160 laminate	579.5	579.1	-0.07
C6000/LARC 160 laminate	566.5	566.9	+0.07
Tray A7 (Leading Face)			
T300/F178 laminate			
. precured at 85 psi	1318	1303	-1.14
. cocured at 45 psi	1341	1324	-1.27
C6000/PMR-15 laminate	1490	1476	-0.94

Table 2

COMPARISON OF PREFLIGHT AND POSTFLIGHT WARPAGE

Panel Description	Deflection (inches)*	
	Preflight	Postflight
T300/F178 precured at 85 psi	0.339 0.270 0.221 0.277	0.000 0.012 0.000 0.004
T300/F178 cocured at 45 psi	0.243 0.100 0.155 0.166	0.209 0.175 0.185 0.190
C6000/PMR-15	0.204 0.270 0.221 0.232	0.107 0.083 0.130 0.107
C6000/LARC 160	0.445 0.350 0.315 0.370	0.149 0.189 0.194 0.177
C6000/LARC 160	0.530 0.600 0.715 0.615	0.008 0.007 0.040 0.018

*Three values listed correspond to corner-midpoint-corner of freestanding edge of laminate with opposite edge held down against surface table.

Table 3

LAMINATE PHYSICAL PROPERTY MEASUREMENTS

LAMINATE	THICKNESS (INCH) MIN.	MAX.	SPECIFIC GRAVITY	RESIN CONTENT(%)	FIBER VOL. (%)	VOID[1] VOL. (%)
BMI						
Precured Control	.088	.097	1.59	31.3	62.3	-2.6
Precured Exposed	.089	.095	1.59	31.4	61.8	-2.8
Cocured Control	.088	.097	1.56	33.7	59.1	-1.7
Cocured Exposed	.093	.098	1.57	34.0	59.3	-2.4
LARC-160						
Control (LD 3-1)	.090	.108	1.38	42.5	44.8	10.3
Control (LD 3-4)	.080	.087	1.54	37.4	54.3	1.5
Control (LD 3-6)	.078	.090	1.56	35.7	56.6	0.6
Exposed (LD 3-3)	.074	.092	1.55	37.6	54.5	0.8
Exposed (LD 3-5)	.080	.095	1.53	41.0	51.0	0.9
PMR-15						
Control	.100	.106	1.55	44.0	49.0	-1.5
Exposed	.105	.114	1.52	45.1	47.2	0.0

[1] "Void Volume" is a calculated value which typically yields a negative value (physically meaningless) for good quality laminates. Positive values are an indication of abnormally high porosity content.

Table 4

SUMMARY OF MICROCRACKING EXAMINATION

		No. of Microcracks per Inch in Indicated Plies								
	SAMPLE I.D.	O_2	(±45)	90_2	(∓45)	O_2	(∓45)	90_2	(±45)	O_2
BMI CONTROL										
Precured	A1	10.7		-		4.0		-		14.7
	A2	11.1		-		3.7		-		9.3
	A3	9.3		-		3.7		-		13.0
Cocured	B1	9.5		-		3.2		-		17.2
	B2	-		2.0		-		6.0		-
	B3	10.9		-		4.3		-		17.4
	B4	10.9		-		4.3		-		17.4
	B5	-		2.3		-		0.0		-
	B6	-		2.3		-		1.1		-
Average		10.4		2.2		3.9		2.4		14.8
BMI EXPOSED										
Precured	C1	16.0		-		34.0		-		18.1
Cocured	D1	19.0		-		46.6		-		20.7
	D2	15.9		-		38.6		-		15.9
Average		17.0		-		39.7		-		18.2
POLYIMIDE										
LARC-160 Control	E1	19.4		-		(No 0° plies		-		14.6
LARC-160 Exposed	F1	17.6		-		at midplane)		-		16.5
PMR-15 Control	G1	6.0		-		(No 0° plies		-		7.1
PMR-15 Exposed	H1	10.6		-		at midplane)		-		8.5

Table 5

SUMMARY OF MECHANICAL TEST RESULTS FOR T300/934 EPOXY HONEYCOMB SANDWICH PANEL

PROPERTY	CONTROL RT	CONTROL 350F	EXPOSED RT	EXPOSED 350F
FWT STRENGTH (PSI)	343	271	338 (6)*	225 (6)
(as % of "Control")			98.8	83.1
SANDWICH BEAM CORE SHEAR TRANSVERSE STRENGTH (PSI)	85.9	68.0	80.7	67.2
(as % of "Control")			94.0	98.8
SANDWICH BEAM FACESHEET COMPRESSIVE MODULUS (MSI)	13.6	13.7	11.3	11.5
(as % of "Control")			83.3	83.7

*Five replicates per test unless indicated otherwise in ( ).

Table 6

MECHANICAL TEST RESULTS FOR BISMALEIMIDE AND POLYIMIDE LAMINATES

Property	C=Control E=Exposed	T300/F178 BMI				Polyimide			
		Precured		Cocured		LARC 160		PMR 15	
		75°F	450°F	75°F	450°F	75°F	550°F	75°F	550°F
0° Tensile Strength F_{tu} (ksi)	C	66.5	71.7 (3)*	68.4	67.1 (2)	69.8 (6)	62.4 (6)	65.2	50.5 (6)
	E	71.1	71.4	61.7	65.4 (6)	66.0 (6)	49.3 (6)	57.1 (6)	45.8 (6)
0° Tensile Modulus E_t (msi)	C	7.9	7.8 (3)	7.6	8.2 (3)	7.1 (6)	[1]	6.0	[1]
	E	8.2	9.5	7.7	9.1 (6)	6.7 (6)	[1]	5.4 (6)	[1]
90° Compressive Strength F_{cu} (ksi)	C	48.7 (3)	40.9 (3)	47.1 (3)	38.3 (3)	60.4	48.2	50.2 (6)	37.2 (6)
	E	47.4	42.0 (6)	46.2	40.3 (6)	52.9	31.7	53.5 (6)	34.3 (6)
90° Compressive Modulus E_c (msi)	C	6.1 (3)	6.2 (3)	6.2 (3)	6.6 (3)	—	[1]	3.4 (6)	[1]
	E	5.7	[1]	5.2	[1]	4.8	[1]	4.7 (6)	[1]
Rail Shear Strength F_{su} (ksi)	C	27.9 (2)	22.3 (1)	24.8 (2)	19.4 (1)	35.7 (4)	24.1 (2)	26.6 (2)	27.0 (2)
	E	38.7	31.9	35.5	31.0	34.2 (4)	29.9 (4)	28.3 (2)	25.9 (2)
Rail Shear Modulus E_s (msi)	C	2.3 (2)	2.4 (1)	2.0 (2)	3.0 (1)	2.2 (4)	2.0 (2)	2.1 (2)	2.3 (2)
	E	2.1	2.4	2.1	2.4	2.0 (4)	2.3 (4)	1.9 (2)	2.0 (2)

* Five replicates per test unless indicated otherwise in ( ).

[1] Compressive modulus was not measured on these specimens to avoid causing premature failure at compressometer knife edges (which was observed to occur in the previous testing of control specimens)

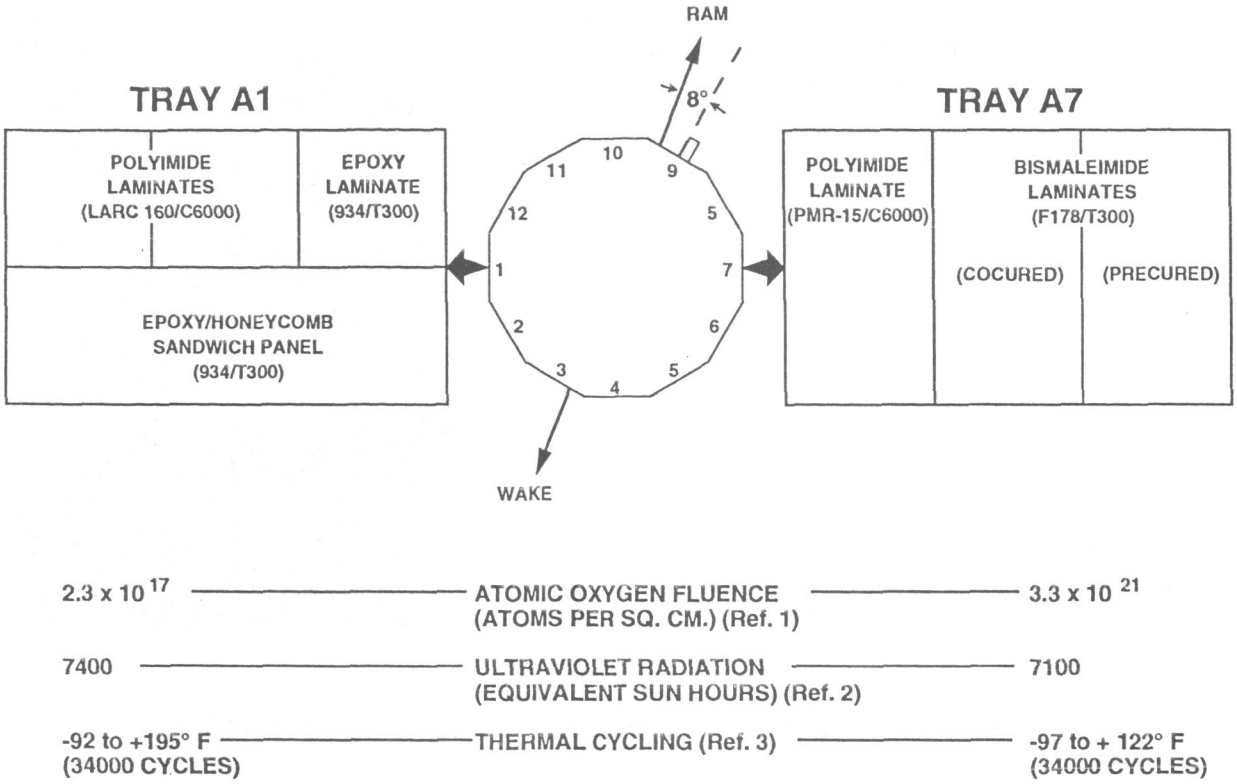

Figure 1. Composite Systems and Exposure Conditions

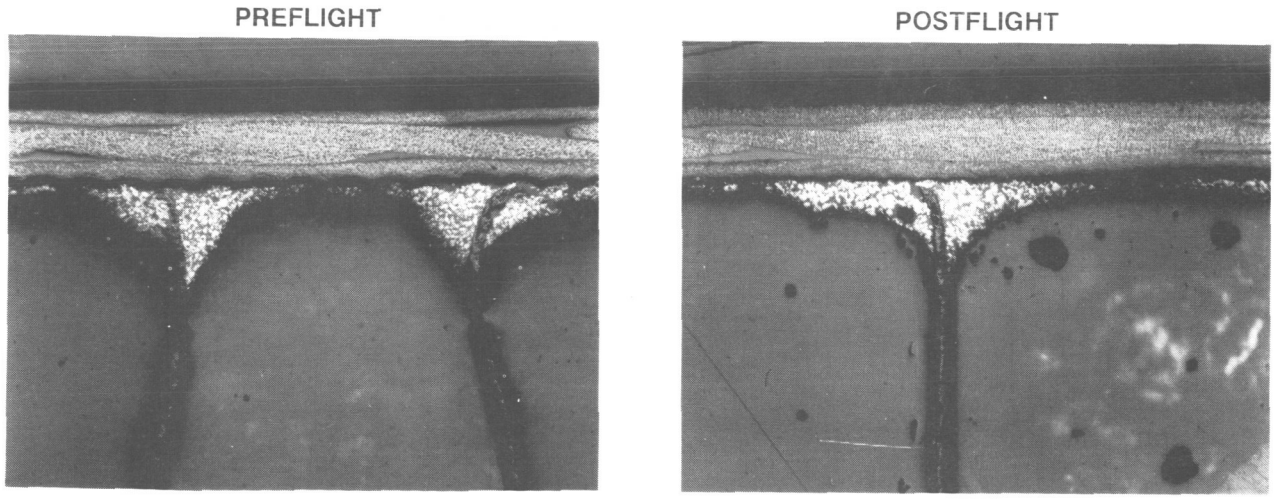

Figure 2. Polished Cross-Section of Honeycomb Sandwich Panel

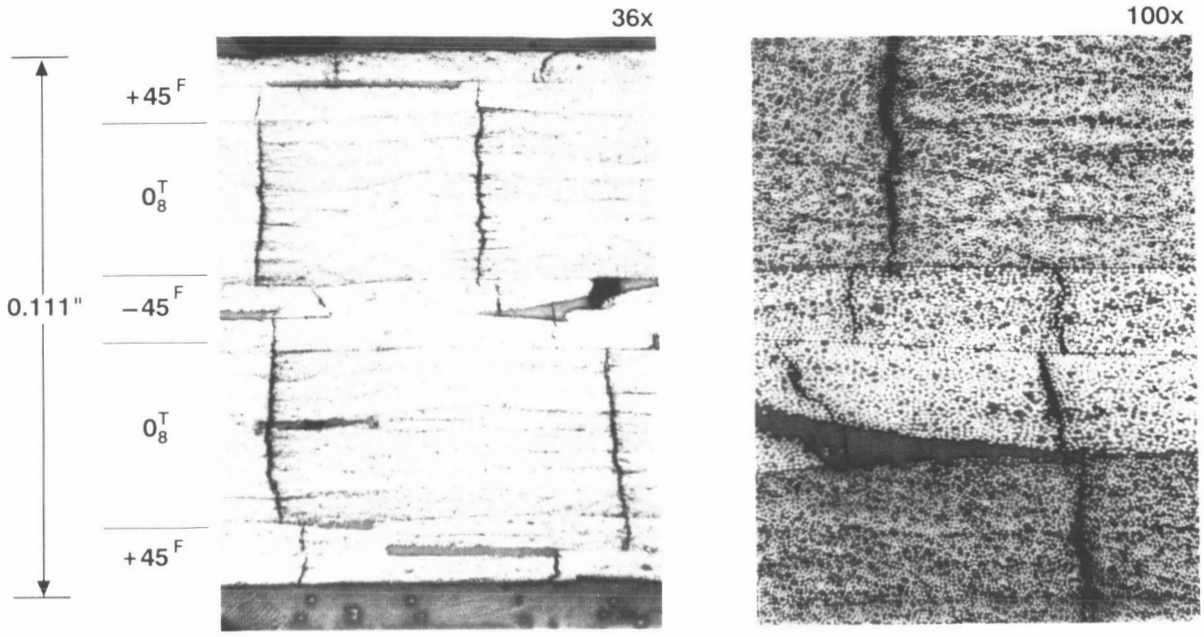

Figure 3. Polished Cross-Section of Postflight Epoxy Laminate, Showing Microcracking

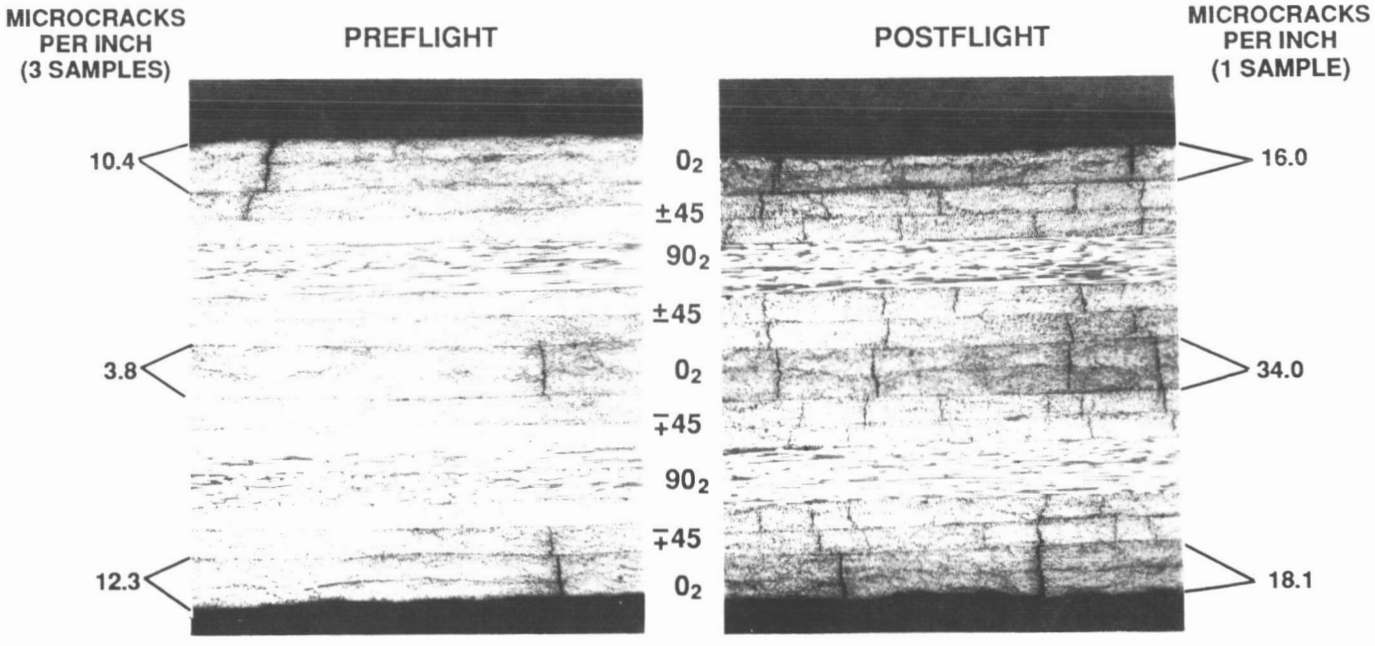

Figure 4. Polished Cross-Sections of Precured Bismaleimide Laminates, Showing Increase in Microcrack Density

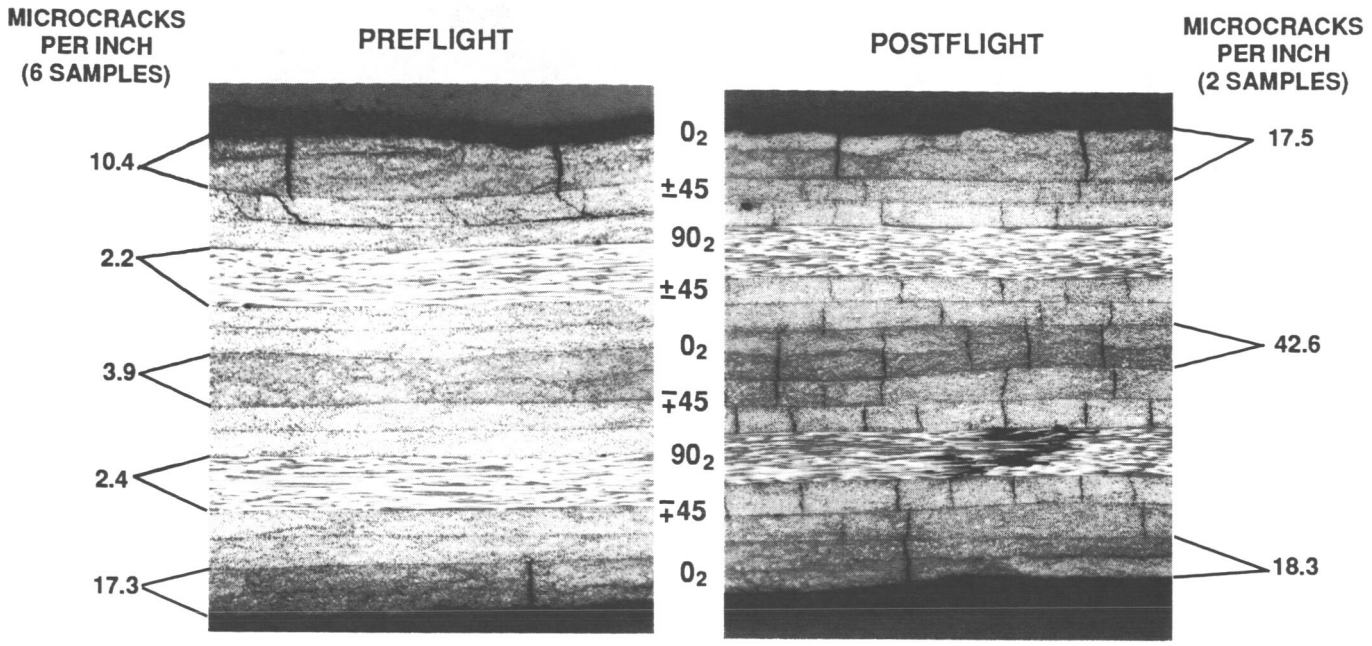

Figure 5. Polished Cross-Sections of Cocured Bismaleimide Laminates, Showing Increase in Microcrack Density

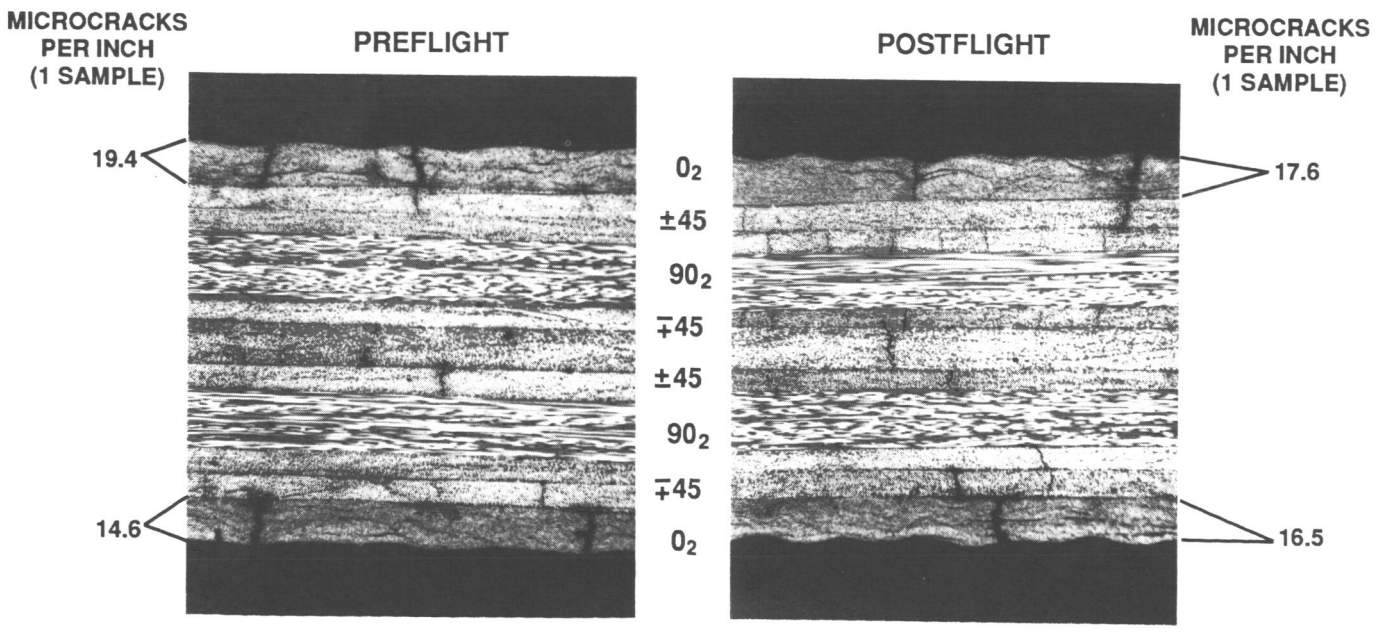

Figure 6. Polished Cross-Sections of LARC 160 Polyimide Laminates, Showing Comparable Microcrack Densities

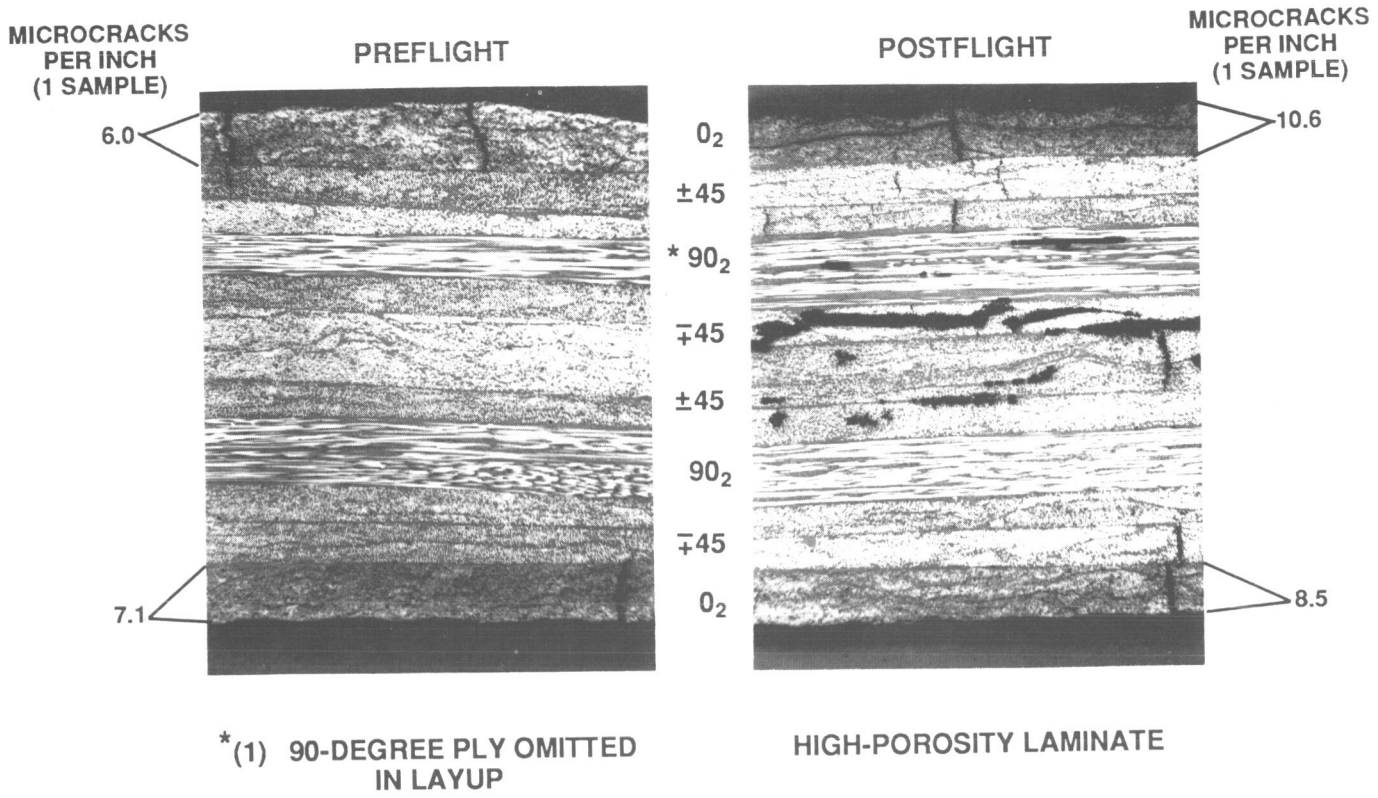

Figure 7. Polished Cross-Sections of PMR-15 Polyimide Laminates, Showing Microcrack Density, Missing 90° Ply (*), and Cured-In Porosity

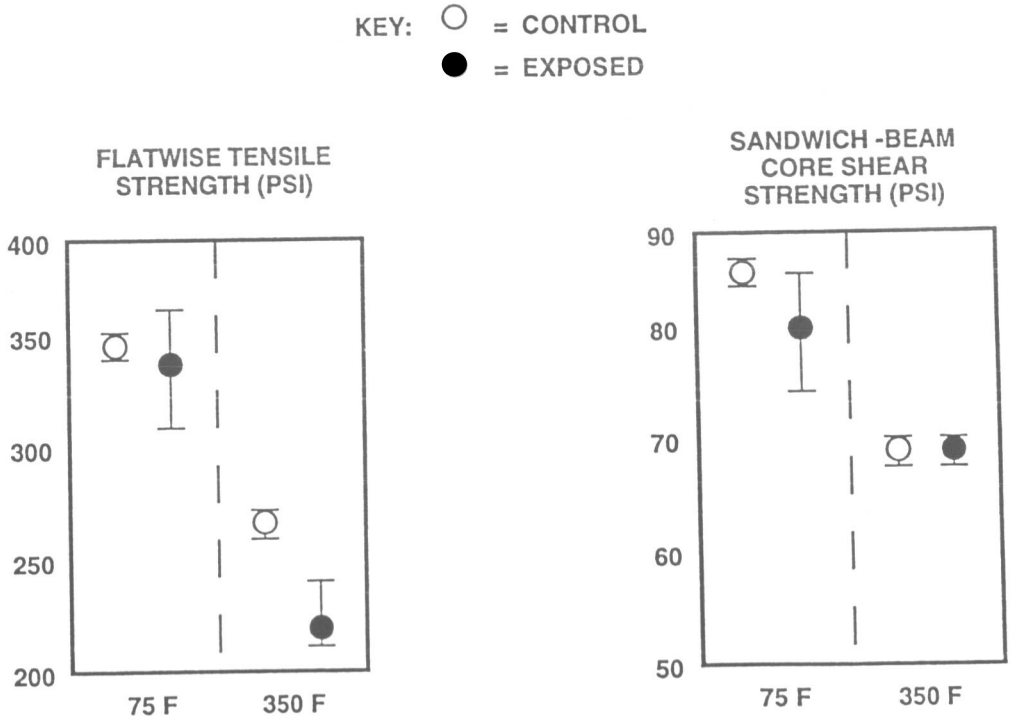

Figure 8. Mechanical Test Results for Epoxy Sandwich Panel

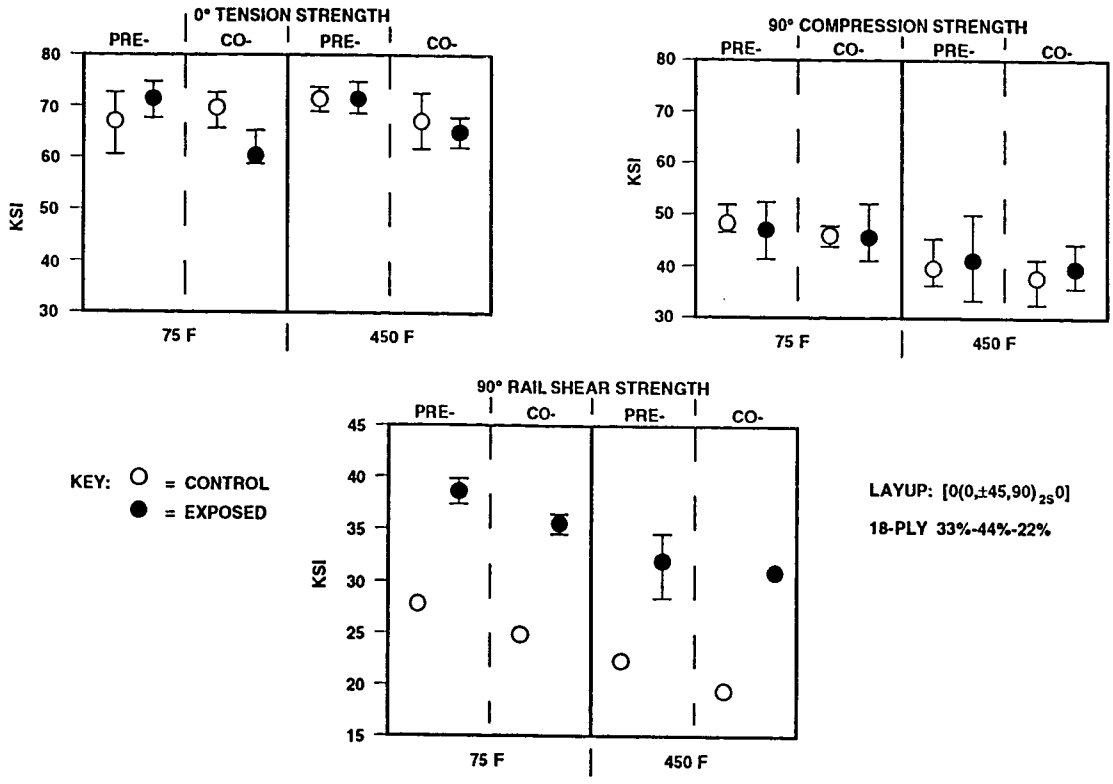

Figure 9. Mechanical Test Results for Precured and Cocured Bismaleimide Laminates

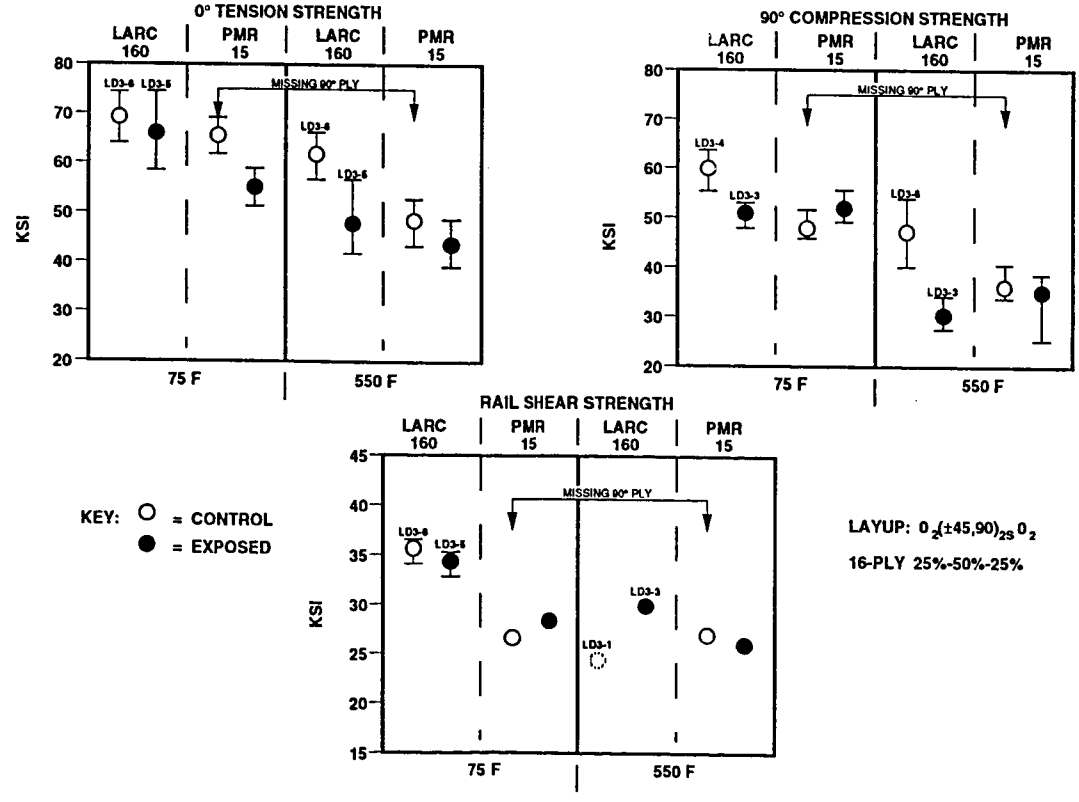

Figure 10. Mechanical Test Results for LARC 160 and PMR-15 Polyimide Laminates

N93-28267

AN XPS STUDY OF SPACE-EXPOSED POLYIMIDE FILM

Myung Lee, William Rooney, and James Whiteside

Grumman Corporate Research Center
Bethpage, New York 11714
Phone: (516)575-2354; Fax:(516)575-7716

SUMMARY

X-ray photoelectron spectroscopy was used to assess changes induced in the surface chemistry of Kapton H (Du Pont Trademark) polyimide strips exposed to the low Earth orbit environment at the space-end of the LDEF satellite on Experiment A0133. Results from flight specimens are compared to material cut from the same lot and stored at room temperature under standard atmospheric conditions. One notable difference was a nearly two-fold increase in surface oxygen (atom-percent composition) for specimens exposed to the direct space environment as compared to controls. In addition, space exposed specimens contained distinct silicon peaks (2p 103.2 eV and 2s 154.2 eV) in their spectra. These peaks were absent in control spectra. It is likely that the increase in oxygen is associated with the silicon. This is in agreement with reports of widespread silicon contamination throughout the LDEF satellite.

INTRODUCTION

Initial studies of Kapton H (Du Pont Trademark) polyimide film exposed to the low Earth orbit (LEO) space experiment on LDEF Experiment A0133 revealed no significant differences in bulk physical-chemical properties when compared to either ground or space control specimens despite the fact that space exposed specimens suffered significant weathering with surface erosions of approximately 8.0 um (1). It has been proposed that the primary mechanism of polyimide degradation in LEO involves the interaction with high velocity atomic oxygen. Damage induced by atomic oxygen is largely localized at the surface of the polyimide and it is likely that the surface is continually refreshed by a sputtering type mechanism. Therefore, techniques that measure primarily bulk physical-chemical properties are unlikely to have the sensitivity to detect changes localized at the surface.

X-ray photoelectron spectroscopy (XPS) has been used to detect changes induced in the surface chemical composition of polyimide films exposed to reactive oxygen atmospheres. Egitto and coworkers (2) observed an increase in the relative amount of high binding energy peaks in the carbon 1s spectrum of a polyimide exposed to a pure oxygen plasma in an Earth based reactor. A report by Golub et al. (3) describes an increase in surface oxygen concentration for polyimide specimens that had been exposed to

PRECEDING PAGE BLANK NOT FILMED

oxygen in either an earth based rf plasma reactor or LEO space environment for a short duration (ca. 40 hrs) during shuttle mission STS-8.

In this communication we report results from an XPS study of Kapton H polyimide films exposed to the LEO for approximately 5.8 years during the LDEF mission.

METHODS

Kapton H polyimide sheets with a thickness of 127 um (5 mil) were obtained from Du Pont. Three unique specimen groups were analyzed. Two groups were recovered from the LDEF satellite (space end, bay H row 7) and one group remained in storage at room temperature under Earth ambient atmosphere. Of the two groups recovered from the LDEF satellite, one group had direct exposure to the LEO space environment and the other was protected from the direct space exposure by 0.32 cm butted aluminum plate. We shall refer to the former as space exposed and the latter as space control specimens. The material that remained on Earth will be referred to as ground control. The LDEF experiment A0133 module and specimens have been described in detail elsewhere (1).

Prior to XPS all specimens were placed in a room temperature trichloroethylene ultrasonic bath for ten minutes to remove labile surface contaminants. Following the ultrasonic bath the specimens were dried in a stream of nitrogen gas and placed in the XPS chamber for analysis. The chamber was evacuated to a base pressure of 2×10^{-10} torr. All spectra were acquired on a Leybold AG XPS spectrometer at room temperature using a non-monochromatic Mg K-alpha (1253.6 eV) x-ray as the excitation source produced by a power supply operating at 12 kV and 10 mA. Survey spectra were acquired from 0-1260 eV for qualitative analysis. Semi-quantitative analysis was performed on elemental scans obtained over the energy ranges of 95-160 eV, 274-296 eV, 396-406, and 520-540 eV for silicon, carbon, nitrogen and oxygen, respectively. Peaks were fitted using software provided by Leybold AG with relative intensities determined using photoemission sensitivity factors provided by the manufacturer.

RESULTS

Representative XPS survey spectra obtained from ground control, space control, and space exposed specimens are presented in panels a, b, and c of Figure 1. All three specimens contain carbon, nitrogen and oxygen as the principal constituents at the surface. The XPS 1s peaks of these constituents appear in Figure 1 at about 285 eV, 400 eV and 533 eV, respectively. Auger peaks associated with oxygen (KVV1, ca. 748 eV and KVV2, ca. 769 eV) and carbon (KLL, ca. 995 eV) also are apparent. A striking observation is the appearance of peaks at about 103.2 and 154.2 eV in spectra obtained from space exposed specimens; peaks that are not present in either ground or space control spectra. We assign these peaks to silicon $2p_{1/2}$ and 2s, respectively. Also evident is an increase in the relative intensity of the oxygen peak in the spectrum of the space exposed specimen (Figure 1c) compared to spectra obtained from controls. The peak at about 230 eV in Figure 1b (indicated by asterisk) is from Mo substrate.

Additional chemical information can be obtained through spectral deconvolution of peaks obtained during individual elemental scans. The two silicon peaks of the space samples were baseline resolved and each could be well fitted with a single component. Likewise, the single nitrogen peak of all specimens was well fitted with a single component. This is in contrast to the carbon and oxygen peaks of all specimens that exhibited substantial fine structure and required peak deconvolution. The results of

spectral deconvolutions were used to extract semiquantitative surface composition. The chemical information from the XPS elemental scans for ground control and space exposed specimens is collected in Table 1. The binding energy data for both specimen groups has been referenced to carbon 1s (C-C) at 284.6 eV. The values in parenthesis in Table 1 represent elemental fractional contributions.

DISCUSSION

Parameter extraction from XPS spectra yields information on electronic binding energies and intensities. Binding energy provides information on chemical state and peak intensity provides information on stoichiometry. The binding energies extracted from the ground control specimen were within 0.2 eV of values reported by other workers (2,3). The space exposed specimens had binding energies that were consistently shifted to higher values, typically by 0.5 eV, relative to the ground control specimen. This could be due to differences in surface charging between the samples since the values in Table 1 were not chemical shift referenced. We have data that demonstrates differences in the surface charging profiles for these three specimen groups (4). However, referencing to carbon 1s at 284.6 eV, as has been done in Table 1, brings all binding energies into excellent agreement with previous reports.

The composition of the ground control polyimide determined from XPS is in fair agreement with expected values. However, consistent differences between measured and expected values were obtained. In particular, carbon and nitrogen were deficient by six and two atom percent, respectively. Oxygen, on the other hand, was in excess by about seven atom percent. Assuming that sensitivity factors provided by the manufacturer are correct for the XPS spectrometer, differences could be attributed to non-ideal surface stoichiometry possibly including strongly adsorbed H_2O. As expected three carbon peaks, two oxygen peaks and a single nitrogen peak were extracted from the XPS spectra obtained from all polyimide specimens. The ratios of intensities obtained from the various sub-peaks of ground control specimens are essentially in agreement with values reported by other workers (2,3).

In comparison to the control specimens the space exposed specimens had a greatly enriched surface concentration of oxygen as determined from XPS. It is likely that the increase in oxygen for the space exposed specimens is associated with silicon containing surface contaminants deposited during the LDEF mission, since silicon peaks were always observed in XPS spectra of space exposed specimens showing greatly increased oxygen. Furthermore, the binding energy of the silicon ($2p_{1/2}$ 103.5 eV and 2s 154.5 eV) indicates direct silicon-oxygen chemical bonding apparently very similar to SiO_2 or a silcon sub-oxide (5). This is in agreement with the binding energy of Si deposited on Kapton at the leading edge of the LDEF satellite as reported by Young and coworkers (6). It is interesting to note that an XPS spectrum obtained from a space exposed region that was shielded from the atomic oxygen showed only a trace of silicon (spectrum not shown). Infrared and EDS data from our lab (1) and from others (7) indicates that in addition to silicon, organics are also present in the surface contaminants. However, it does appear that most of the increased oxygen is associated with silicon. Assuming an SiO_2 stoichiometry most of the 15-20 atom percent increase in oxygen can be accounted for with a 7-10 atom percent of silicon. In addition, the ratio of carbon sub-peaks to total carbon does not change appreciably between ground control and space exposed specimens. The contaminants have been attributed to satellite outgassing followed by condensation and activation in the energetically (uv, AO, e-, etc.) rich LEO environment. It is interesting to note that these contaminants were not removed by trichloroethylene in the ultrasonic bath and appear to be strongly associated with the Kapton surface.

ACKNOWLEDGMENTS

Dr. Richard DeIasi directed the design and integration of Experiment A0133. We thank Jerry DeCarlo for assisting in the collection and processing of XPS data.

REFERENCES

1. Whiteside, J.B.; Giangano, D.; Heuer, R.L.; Kamykowski, E.; Kesselman, M.; Rooney, W.D.; Schulte,R.; and Stauber, M.: LDEF Conference Proceedings, Kissimee Florida, June 1991

2. Egitto, F.D.; Emmi, F.; Horwath, R.S.; and Vukanovic, V.: *Journal of Vacuum Science Technology B* 3 893 (1985)

3. Golub, M.A.; Wydeven, T.; and Cormia, R.D: *Polymer Communications* 29 285 (1988)

4. Walters, W.S: private communication (1991)

5. Briggs, D; and Seah, M.P., eds: *Practical Surface Analysis 2nd Edition Volume 1: Auger and Photoelectron Spectroscopy* Wiley, 1990

6. Young, P. R.; Slemp, W.S.; Witte, Jr., W.G.; and Shen, J.Y.: 36th International SAMPE San Diego CA, April 15-18 1991

7. Young, P. R.; Slemp, W.S.; and Gautreux, C.R.: 37th International SAMPE Anaheim CA, March 9-12 1992

FIGURE LEGENDS

Figure 1. XPS survey spectra for ground control, space control and space exposed Kapton specimens. The asterisk in panel **b** (ca. 230 eV) indicates contamination by Mo substrate.

Table 1. Summary of XPS Results

	ground control		space exposed	
	B.E. (eV)	atom %	B.E. (eV)	atom %
Si 2s			154.3	8.8
C 1s	284.6	28.1(0.40)	284.6	20.1(0.40)
	285.7	34.1(0.48)	285.6	24.6(0.50)
	288.6	8.2(0.12)	288.6	5.0(0.10)
subtotal		*70.3(1.00)*		*49.7(1.00)*
N 1s	400.7	4.9	400.7	0.82
O 1s	532.4	17.4(0.70)	532.5	17.2(0.42)
	533.7	7.3(0.30)	533.3	23.6(0.58)
subtotal		*24.7(1.00)*		*40.8(1.00)*

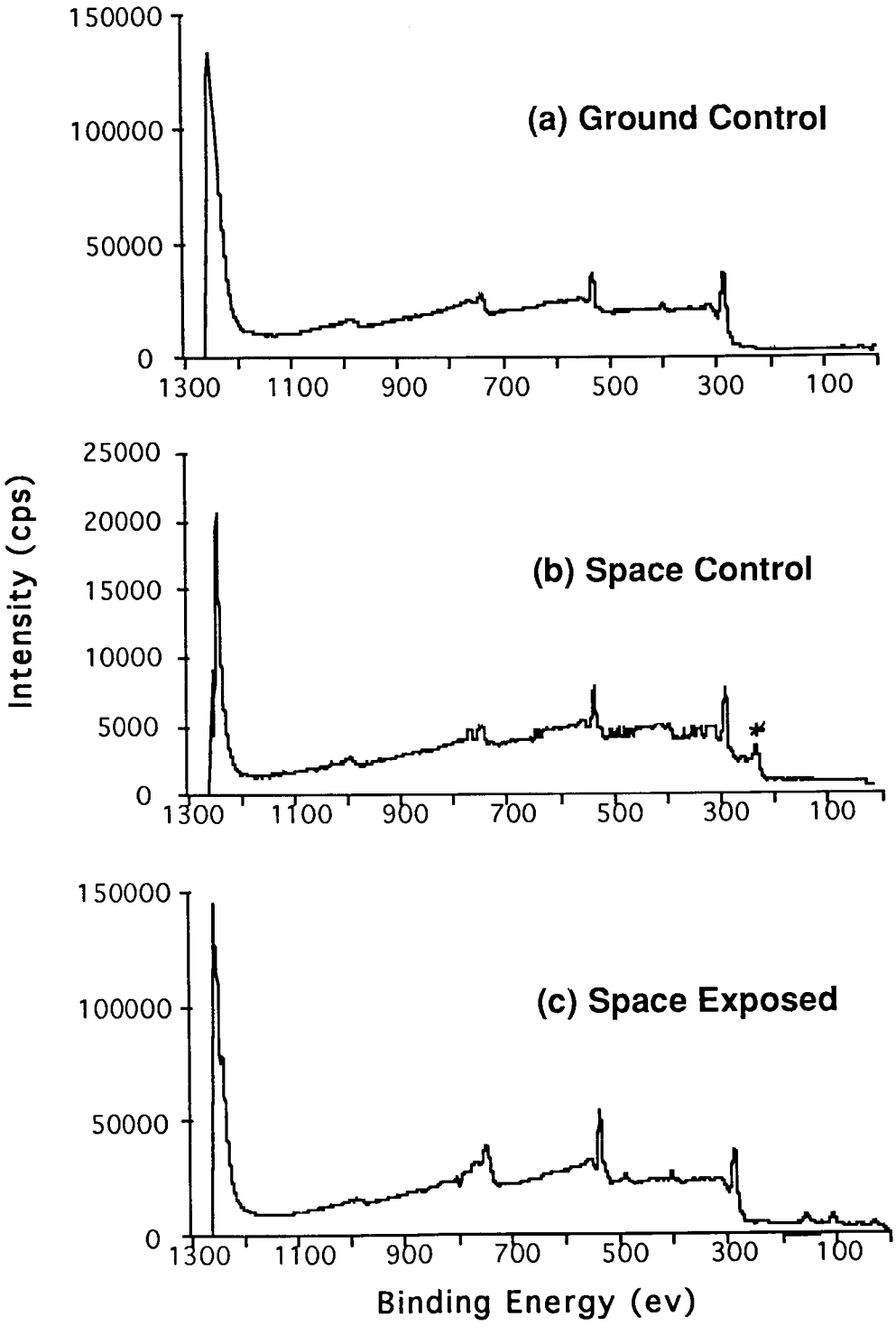

Figure 1. XPS survey spectra for ground control, space control and space exposed Kapton specimens

N93-28268

SURFACE ANALYSES OF COMPOSITES EXPOSED TO THE SPACE ENVIRONMENT ON LDEF *

Joseph J. Mallon, Joseph C. Uht, and Carol S. Hemminger
The Aerospace Corporation
2350 E. El Segundo Blvd.
El Segundo, CA 90245
Phone: 310/336-1619, Fax: 310/336-5846

ABSTRACT

We have conducted a series of surface analyses on carbon fiber/poly(arylacetylene) (PAA) matrix composites that were exposed to the space environment on the Long Duration Exposure Facility (LDEF) satellite. These composite panels were arranged in pairs on both the leading edge and trailing edge of LDEF. None of the composites were catastrophically damaged by nearly six years of exposure to the space environment. Composites on the leading edge exhibited from 25 to 125 μm of surface erosion, but trailing edge panels exhibited no physical appearance changes due to exposure. Scanning electron microscopy (SEM) was used to show that the erosion morphology on the leading edge samples was dominated by crevasses parallel to the fibers with triangular cross sections 10 to 100 μm in depth. The edges of the crevasses were well defined and penetrated through both matrix and fiber. The data suggest that the carbon fibers are playing an important role in crevasse initiation and/or enlargement, and in the overall erosion rate of the composite. X-ray photoelectron spectroscopy (XPS) and energy dispersive X-ray spectroscopy (EDS) results showed contamination from in-flight sources of silicone.

INTRODUCTION

LDEF experiment M0003, Space Environment Effects on Spacecraft Materials, consisted of 19 subexperiments and was flown as part of the materials, coatings, and thermal systems experimental category (ref. 1). The overall objective of this experiment was to obtain data concerning structure and property changes in materials that had been exposed to the space environment and to understand the reasons for these changes. Subexperiment MOOO3-16, Advanced Composite Materials, included three pairs of carbon fiber/poly(arylacetylene) (PAA) composite panels. Composites are principally used in space as structural components, so the effects of the space environment on the mechanical and physical properties of the composites flown on LDEF is of great interest to the design community. In this paper, we will report on the surface analyses of the carbon fiber/PAA composite samples as determined by optical microscopy, scanning electron microscopy (SEM), energy dispersive X-ray (EDS) spectroscopy, and X-ray photoelectron spectroscopy (XPS). Surface morphology changes due to space environment exposure and in-flight surface contamination will be discussed.

EXPERIMENTAL

Samples

The three composites selected for the experiment were carbon-fabric-reinforced poly(arylacetylene) (PAA) materials that were under development at The Aerospace Corporation in 1984 as replacements for more traditional composites such as carbon/epoxy. PAA is a hydrophobic matrix made by the

* This work was supported by Air Force Space Systems Division contract F04701-88-C-0089.

polycyclotrimerization reaction of m-diethynylbenzene (DEB) (refs. 2-7). The cyclotrimerization of DEB is shown in Fig.1; further cyclotrimerization of available ethynyl groups results in products with increasing molecular weight. One of the PAA composites contained an additional component, poly(phenylquinoxiline) (PPQ), which was added to increase the toughness of the PAA matrix.

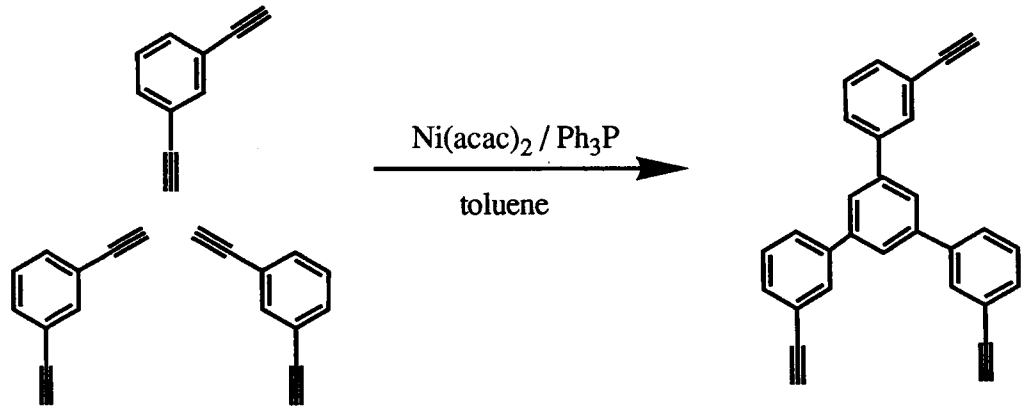

Figure 1. Cyclotrimerization reaction of diethynylbenzene (DEB).

The carbon fabric, designated T300, was from Ferro Corporation. HA-43 is a commercial version of PAA that was supplied by Hercules, Inc. PAA for panel B was prepared in toluene solution from m-diethynylbenzene and 1,4-diphenylbutadiyne in a manner analogous to that of Jabloner (ref. 2). PPQ for the panel C was prepared in m-cresol by the condensation reaction of bis-benzil and 3,3',4,4'-tetraaminobiphenyl (see Ref. 8 for details). The prepreg plys were prepared by impregnation of the carbon fabric with a toluene solution of the resin, followed by drying in air to evaporate the solvent. Formulation of the composite panels, which measured 3.8 cm x 8.8 cm x 0.3 cm, was as follows:

Panel A, HA-43/T300. Thirteen prepreg plys of HA-43/T300 were laid up and cured in a press at 3.4 x 10^6 Pa (500 psi) and 177°C for three hours, then allowed to cool to room temperature. Resin content of the panel was about 37 wt%. The panel was cut to provide leading and trailing edge samples designated L-A and T-A, respectively.

Panel B, PAA/T300. Thirteen prepreg plys of PAA/T300 were laid up and cured in a press at 3.4 x 10^6 Pa (500 psi) and 177°C for three hours, then allowed to cool to room temperature. Resin content of the panel was about 22 wt%. The panel was cut to provide leading and trailing edge samples designated L-B and T-B, respectively.

Panel C, HA-43, PPQ blend/T300. A resin mixture consisting of 86 g of dry HA-43, 86 g of dry PPQ, 2300 g of chloroform, 207 g of 1,1,1-trichloroethane, and 22 g of m-cresol was prepared to make the prepreg plys. Thirteen prepreg plys were laid up and cured in a press at 6.9 x 10^6 Pa (1000 psi) and 250°C for six hours, then allowed to cool to room temperature. Resin content of the panel was about 33 wt%. The panel was cut to provide leading and trailing edge samples designated L-C and T-C, respectively.

The leading edge panels were located on Bay D of Row 9, and the trailing edge panels were located on Bay D of Row 3. Row 9 received about 8.7 x 10^{21} atoms/cm^2 of atomic oxygen fluence (ref. 9) and 11,200 equivalent sun hours of radiation exposure (ref. 10), Row 3, about 1.3 x 10^{17} atoms/cm^2 and 11,100 equivalent sun hours. The difference in atomic oxygen exposure between Row 9 and Row 3 was more than 4 orders of magnitude, but there was essentially no difference in radiation exposure. The side of the panel that was subjected to the space environment will be referred to as the "exposed" face, and the reverse side of the panel that was mounted flat against LDEF will be referred to as the "backside." The

backside of each panel functions as a convenient control for the exposed side since laboratory control samples were not available.

On-orbit photography of the samples by the crew of the space shuttle Columbia showed that the samples were intact and relatively undamaged. After examination and photography at Kennedy Space Center, the experiment trays were flown to Aerospace and deintegrated by Aerospace personnel. Deintegration and the initial, cursory examination of individual samples were performed in a class 10,000 clean room. The samples were then packaged into individual, closed boxes for storage between experiments.

Scanning Electron Microscopy/Energy Dispersive X-Ray Spectroscopy

Analyses were performed on the front and back surfaces of the three pairs of composites samples. Each sample was studied as received. No sample preparation was necessary except pump-down at high vacuum for about 24 hours before introduction to the SEM (due to the large size of these samples). A JEOL 840 SEM with an EDAX 9900 EDS system was used for this study. Electron micrographs were acquired using accelerating voltages ranging from 5 to 25 kV. EDS data were acquired using an accelerating voltage of 15 kV, which allowed for the acquisition of the lower atomic number elements such as carbon and oxygen while still exciting X-ray fluorescence from heavier elements.

X-Ray Photoelectron Spectroscopy

Preparation for surface analysis by XPS involved cutting a segment approximately 1.5 cm x 1.5 cm from one end of each composite sample. This was necessary because the original panels were too large to be accommodated by the VG Scientific ESCALAB MKII instument used for the analyses. A dry cut of the samples minimized surface contamination from the sample preparation step. Each sample was mounted on top of a stub using four Ta foil tabs that were spot welded around the stub periphery. During analysis of each exposed surface, the backside was in contact only with the top 1.3 cm diameter rim of the stub. This minimized surface contact contamination of the backsides, so that each sample could be remounted for the comparative analysis of the backside.

The Al Kα source was chosen for X-ray irradiation. Survey scans from 0 to 1100 eV binding energy were acquired to qualitatively determine the sample surface composition. High resolution elemental scans were subsequently run to obtain semiquantitative elemental analyses from peak area measurements and chemical state information from the details of binding energy and shape. Measured peak areas for all detected elements were corrected by elemental sensitivity factors before normalization to give surface mole percent. The quantitation error on a relative basis is $\leq$10% for components >1 mole %. Large uncertainties in the relative elemental sensitivity factors can introduce absolute errors of a factor of 2 or even greater. All elements of the periodic table except H and He can be detected by XPS. The detection limit is about 0.1 surface mole %, but spectral overlaps between large peaks and small peaks can make it impossible to detect minor components. Scanning electron beam imaging, used to set up the sample surface analysis area, helped avoid analysis of sample edge areas that were masked from line-of-sight exposure to the space environment by the mounting hardware.

Cross Sections

After examination by XPS, the 1.5 cm x 1.5 cm samples were embedded in epoxy, cut, and polished so that the cross section of the sample could be examined by optical microscopy and SEM. The

samples were evaporatively coated with several hundred angstoms of carbon before SEM analysis. Average erosion depth measurements were made from the cross-section micrographs.

RESULTS AND DISCUSSION

Microscopy

The initial visual and light microscopy examinations of the samples showed that none of the composites had been catastrophically damaged by nearly six years of exposure to the space environment. The effect of the large difference in atomic oxygen exposure between the leading and trailing edges is illustrated in Fig. 2, which shows SEM micrographs of L-A and T-A. In both of the micrographs, the right-hand side of the sample was masked from the effects of the space environment by the mounting hardware. In Fig. 2, the lack of surface charging on the exposed area of L-A relative to the masked area and relative to T-A in the SEM chamber demonstrates that the nonconductive matrix at the surface of the leading edge samples was removed by atomic oxygen erosion. In each sample pair, we found that the exposed area of the leading edge sample had little or no surface charging, indicating that the conductive carbon fibers were exposed. The trailing edge samples had extensive surface charging and were difficult to image because the nonconductive matrix had not been removed by erosion.

The erosion process resulted in a morphology on all the leading edge samples that is best visualized by examining the micrograph of the surface and of the cross-sectioned samples. Figure 2 shows that a leading edge exposed surface is characterized by large crevasses that have developed predominantly parallel to the long axis of the fibers. This emphasizes the weave pattern of the carbon fiber tows in the fabric. However, the surface SEM micrographs do not clearly elucidate the condition of the remaining exposed fibers, even at higher magnification, as seen in Fig. 3. The optical micrograph cross section of the L-A surface shown in Fig. 4a highlights the "peak and valley" morphology associated with crevasse development on the exposed surface. Note that crevasses parallel to the cut of the cross section may not be seen. The area on the left side of the optical micrograph, where the sample was masked, shows the relatively smooth preflight condition of the surface. Higher magnification SEM micrographs of the L-C cross section are shown in Figs. 5-6. They show that the crevasses traversed both fibers and matrix, and most appeared to have steep sides and a well-defined tip. The crevasses ranged from 10 to 100 μm in depth, and no undercutting of the matrix relative to the fibers was apparent along the sides of the crevasses.

At this point, it may be useful to distinguish between "cracks" and "crevasses." Cracks form when two previously united sections of the composite become separated. There is no net loss of material during crack formation. The cracks observed in the samples were probably caused by thermal stresses during molding or during flight. In contrast, crevasses resulted from removal of fiber and matrix material, and were characterized by sharp triangular cross sections. Crevasses were completely absent on trailing edge sample surfaces, suggesting that they developed on leading edge surfaces as a result of atomic oxygen erosion. Figure 5 shows a section of L-C that contains both a surface crack and surface crevasses. The crack is narrow, uniform in width, and extends further into the sample interior than the wider, triangular crevasses. Note that the intersection of the crack with the surface did not cause a crevasse to form. In general, we found no correlation between the location of cracks and crevasses, and, as seen in Fig.5, crevasses were more numerous than cracks.

It was estimated from the cross-section optical micrographs that the erosion depth on L-A and on L-C was about 125 μm. The measurements were taken at the left side of the micrographs (see Fig. 4), where there is an edge between the masked and exposed areas of the surface. Individual crevasses reflect erosion depths less than or greater than the value at the edge. The optical micrograph of L-B, shown in Fig. 4b, showed features similar to those in the micrographs of L-A and L-C. However, the average depth of erosion from Fig. 4b appeared to be 25 to 50 μm, and was difficult to measure because of the

curvature of the surface. For comparison, reactive polymers, such as Kapton and Mylar, were eroded to a relatively uniform depth of about 220 μm by the atomic oxygen fluence received on Row 9 (ref. 11). We hypothesize that the decreased erosion of the composites relative to polymers is probably best understood in terms of a two-step erosion process. In the first step, the outer layer of organic matrix was removed at roughly the same rate as other reactive polymers. In the second step, when the carbon fibers became exposed, a lower reaction efficiency for the fibers led to a lower overall (bulk) erosion rate, and contributed to the development of the highly irregular surface morphology. Carbon fabric/organic matrix composites with epoxy, polyimide, and polysulfone matrices were reported to have leading edge erosion values near the masked edge of 50 μm, 75 μm, and 50 μm, respectively (ref. 12), measured from cross section optical micrographs. Maxium crevasse depths of 80 μm were reported for the epoxy and polysulfone matrices, and 120 μm for polyimide matrices.

The addition of PPQ to the HA-43 matrix did not have an obvious effect on the erosion rate or pattern of erosion for L-C relative to L-A. L-B, however, was eroded only 20 to 40% as deeply as the other two composites, as seen by comparing Fig. 4b to 4a. Examination of L-B at high magnification, as seen in Fig. 7, revealed well-defined crevasses comparable to those on L-A and L-C in appearance, but on average less enlarged. The panel for samples L-B and T-B, fabricated using PAA prepared in our laboratory, had the lowest resin content (about 40% lower than the other two panels). In this case, the lower reaction efficiency of the fibers relative to the organic matrix would contribute to the lower erosion rate observed for L-B. With so few samples, it can only be noted at this point that resin content and/or the details of resin composition/fabrication may play an important role in the overall composite erosion rate.

Atomic oxygen exposure of epoxy-resin-embedded fibers on shuttle mission STS-8 resulted in much faster removal of epoxy from between the fibers than erosion of the fibers themselves (ref. 13). Nothing observed on the STS-8 samples led to a prediction that atomic oxygen erosion of composite surfaces would cause the highly defined crevasses observed on the LDEF-exposed composites. From STS-8 results, we would have predicted an erosion process that preferentially removed matrix, perhaps with significant undercutting of the matrix around fibers from atomic oxygen scatter in the eroded areas. The sharpness of the crevasse tips shown penetrating into the fibers in Fig. 6 was unexpected. Unlike the LDEF samples, the exposed fibers on STS-8 were metallographically prepared in the transverse direction; it is possible that fiber orientation plays an important role in the erosion process. On a macroscopic level, examination of the eroded composite surfaces showed a definite pattern correlated with fiber direction. This indicates that the carbon fibers are playing a crucial role in crevasse initiation and/or enlargement since a more uniform erosion pattern would be predicted, such as observed for graphite (ref. 13), or Teflon (ref. 14), if there were no differences in rate or mechanism between the atomic oxygen erosion of fibers and matrix. The possible role of preflight and on-flight contamination in crevasse initiation and enlargement is unknown at this time.

From these results, it seems clear that it is very difficult to predict the erosion morphology of composites from information obtained on relatively short shuttle missions. LDEF was subjected to thousands of thermal cycles, much higher levels of UV radiation, and a much higher atomic oxygen fluence than the samples that were exposed on shuttle mission STS-8. The relative importance of each of these factors and combinations thereof is presently unknown.

Energy Dispersive X-Ray Spectroscopy

At 15 kV, X-ray information for EDS surface composition determination comes from a depth of ≤ 1 μm. The EDS data showed that all of the composites flown on LDEF were contaminated with Si and O. Low levels of Cl and Cu were also present on most of the analyzed samples. Other minor contaminants detected on one or more surfaces included Ca, Al, S, P, Mg, Ni, Fe, and Ti. In each case, the O concentration was higher on the exposed face than on the backside face, and higher on the leading edge exposed surface than on the trailing edge exposed surface, as seen in Fig. 8a. EDS data are not readily quantified for the low atomic number elements, such as C and O. Therefore, comparison of relative

surface concentrations has been approximated for these composite samples by using elemental peak heights (arbitrary units) after setting all of the carbon peaks to the same height. This should be a valid approximation since carbon from the fabric and organic matrix is the dominant component in the volume analyzed (SEM analysis of the sample cross sections and XPS analyses do not show thick contaminant overlayers on the exposed surfaces). It is seen in Fig. 8b that the silicon concentration was higher on the leading edge exposed surfaces than on the trailing edge exposed surfaces or any of the backside surfaces. The exposed surface of L-B had higher silicon and oxygen concentrations than the exposed surfaces of L-A and L-C, which is consistent with the lower extent of erosion on L-B observed in the micrographs.

a. EDS relative oxygen signals.

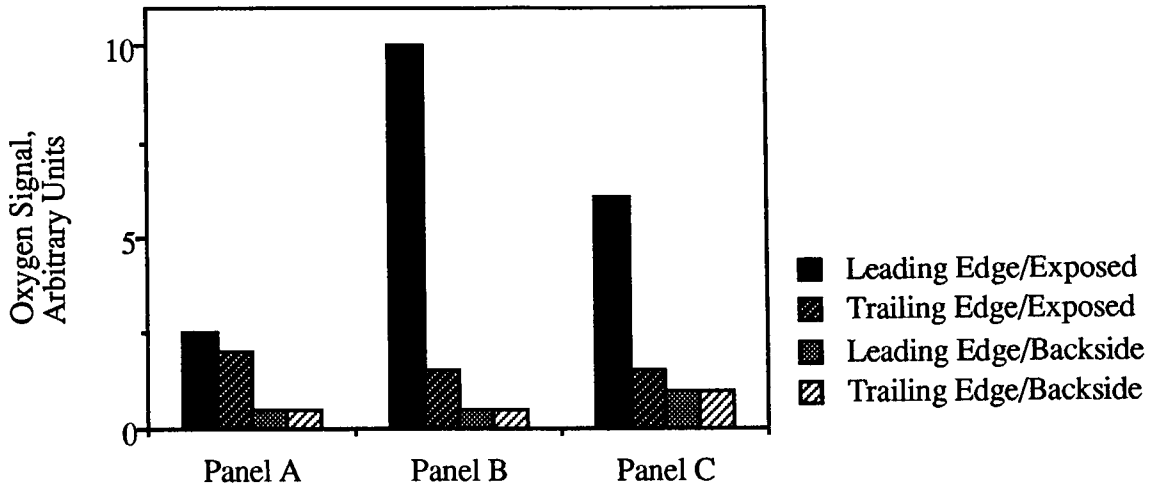

b. EDS relative silicon signals.

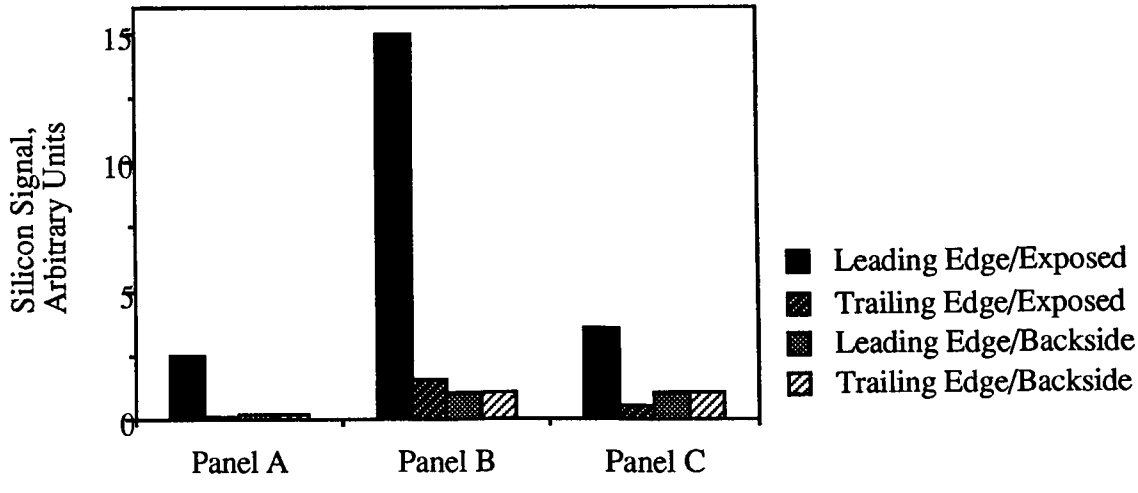

Figure 8. EDS surface composition of samples compared as a function of exposure.

X-Ray Photoelectron Spectroscopy

The XPS surface composition results are tabulated in Table I. The experimental depth of analysis was about 50 to 100 Å. Since this depth is roughly 1% of the depth probed by EDS analysis, XPS is much more sensitive to surface contaminants and less sensitive to bulk compositional differences.

Table I. XPS Data for LDEF Fiber/Organic Matrix Composites

Sample ID	Sample Surface	Surface Mole %, Normalized[a]												
		C	O	Si	N	F	S	Cl	Cu	Zn	Ni	Sn	Na	P
L-A	Exposed	45	42	10	2		0.6		0.3					
	Exposed	44	44	8	1	0.4	0.5	tr	2	0.3				
	Backside	71	20	2	2	3	0.1	0.1	1	tr				
T-A	Exposed	51	36	6	2	3	tr	0.1	3	0.2		0.1		
	Backside	66	26	2	1	3	0.2	0.1	1					
L-B	Exposed	17	59	19	0.6	nd	0.3	0.1	2	tr	1		nd	0.3
	Backside	59	31	3	2	2	0.2	0.2	2	nd			1	nd
T-B	Exposed	45	23	4	0.9	25	0.1	0.1	1	0.1			0.1	
	Exposed	46	27	3	1	19	0.1	0.2	2	0.2			1	
	Backside	70	22	2	1	3	0.1	0.2	0.7	nd			0.2	nd
L-C	Exposed	61	31	3	3	0.1	0.5	nd	0.3	nd		0.4	0.3	0.6
	Backside	67	23	4	2	3	0.1	0.2	2	nd		nd	0.1	nd
T-C	Exposed	47	39	7	2	0.4	0.2	0.4	5	0.4		tr	0.1	nd
	Backside	65	24	4	1	0.3	nd	0.3	1	0.2		tr	nd	nd
Release Cloth		39	4	0.7		56								

[a]tr = trace.
nd = not detected in elemental scan.
blank = not detected in survey scan and no elemental scan acquired.

Examination of the data in Table I shows that the surface composition of the fiber/organic matrix composites is complex, but the major surface contaminants are silicon and oxygen. For five of the six samples, the exposed vs. backside surface comparison reveals significantly higher silicon on the exposed surfaces. The concentration of silicon ranged from 3 to 19 mole % on the exposed surfaces, and from 2 to 4 mole % on the backsides. The backsides have probably accumulated some surface contamination on flight (ref. 15). The exposed surface oxygen concentration on each of the samples is higher and the carbon concentration is lower relative to the backside surface. The decrease in carbon concentration on the exposed surfaces is due to attenuation of the carbon fabric/organic matrix signals by contaminant buildup.

The predominant surface species of Si on the exposed surfaces was SiO_2, based on a measured binding energy for the Si2p peaks of about 103.5 eV. The silicon detected on the sample backsides was predominantly from silicone or mixed silicone/silicate/silica, based on a measured binding energy for the Si2p peaks of $\leq$103.0 eV. SiO_2 is generally accepted to be a degradation product from silicones outgassed

from materials on LDEF such as RTV silicones (ref. 16). Atomic oxygen reactions and UV radiation damage could cause degradation of silicones. It is probable that the return flux from atmospheric backscatter, i.e., collisions with residual atmosphere such as atomic oxygen, resulted in enhanced deposition of silicones and other contaminants on the leading edge flight surfaces relative to the trailing edge. The exposed surface of L-B had higher silicon and oxygen concentrations than the exposed surfaces of L-A and L-C, which is consistent with the lower extent of erosion observed in the micrograph of L-B. It is not known what role the buildup of contamination layers may have had on crevasse initiation and enlargement during atomic oxygen erosion of the leading edge surfaces.

A significant fraction of the surface carbon detected may be due to contamination residues from outgassed silicones or hydrocarbons, but XPS did not differentiate contamination from the composite surface components in this complex system. The inability to discriminate between deposited carbon contamination and the composite matrix also makes it impossible with these data to assess chemical changes induced in the composite surfaces by space environment exposure. XPS analysis of contamination on a variety of materials from LDEF (ref. 15) showed that in general the silicon contamination levels were higher on the leading edge surfaces than on the trailing edge surfaces, and that the trailing edge deposits contained a higher percentage of carbon than the leading edge deposits. It was hypothesized in ref. 16 that atomic oxygen reactions volatilized carbon from the leading edge surface residues, leaving predominantly SiO_2. The XPS analyses, however, did not conclusively show different relative total thicknesses of flight-deposited contamination for leading and trailing edge surfaces. The data were consistent with a contaminant film that has an average thickness of 50 to 100 Å. The contaminant overlayer is probably patchy, with significant areas covered by less than 100 Å, and other areas by greater than 100Å of molecular film.

A major concentration of degraded fluorocarbon (as indicated by about 20 mole % F) was detected on the exposed surface of sample T-B. At least minor concentrations were observed on all but one sample surface. The observed fluorine contamination levels on other LDEF surfaces analyzed by XPS, including paints, Kapton, and aluminum alloy composites, have been <1 mole %. It is probable that some of the carbon/organic matrix composite surfaces have high residual fluorocarbon residue from the release cloth used in their fabrication. The surface composition of a sample of release cloth is included at the bottom of Table I.

The minor surface contaminants detected on the composite surfaces included N, S, Cl, and Cu on most of the analyzed surfaces and Zn, Ni, Sn, Na, and P on one or more surfaces. For all contaminants except silicon and oxygen, the exposed surface is not consistently different from the backside. Preflight contamination of this type is normal for complex materials and is considered the most significant source for the minor contaminants. The exposed flight surfaces were not contaminated with detectable levels of ^{7}Be as measured by XPS or EDS. The detected concentrations of ^{7}Be on other LDEF exposed surfaces were about 1-10 parts per billion (ref. 17), well below the detection limits of XPS and EDS.

CONCLUSIONS

None of the composites were catastrophically damaged by nearly six years of exposure to the space environment. The trailing edge samples exhibited no physical appearance changes due to exposure. Composites on the leading edge were eroded to a depth from 25 to 125 μm. More quantitative measures of the erosion level were difficult because of the irregularity of the erosion process. The erosion morphology was dominated by crevasses parallel to the fibers with triangular cross sections 10-100 μm in depth. The location of the crevasses was not correlated with the location of surface cracks. The edges of the crevasses were well defined and penetrated through both matrix and fiber. No preferential removal of the matrix relative to the fibers was apparent along the sides in the crevasse enlargement pattern. At the present time, we do not know the mechanism for the formation of the crevasses. However, the data suggest that the carbon fibers are playing an important role in crevasse initiation and/or enlargement, and in the overall

erosion rate. The available data did not lead to a conclusion that there are differences in erosion behavior between matrix types, but resin content and/or the details of resin composition/fabrication may play a role in determining the overall composite erosion rate.

It is difficult to predict long-term atomic oxygen erosion morphology of composite materials from erosion data obtained on short shuttle missions. A better understanding of other factors, such as thermal cycling and UV exposure, that may influence erosion is necessary to improve the accuracy of these predictions.

Major on-flight contamination from silicones was observed, as evidenced by higher levels of silicon and oxygen detected on the exposed surfaces than on the backsides. Silicon and oxygen contamination levels were higher on the leading edge surfaces than on the trailing edge surfaces. It is probable that the return flux associated with atmospheric backscatter resulted in enhanced deposition of silicones and other contaminants on the leading edge flight surfaces. The exposed surface of PAA/T300 had higher silicon and oxygen concentrations than the exposed surfaces of HA-43/T300 and HA-43, PPQ blend/T300, which is consistent with the lower extent of erosion observed on PAA/T300. The role of contamination in crevasse initiation and enlargement is unknown at this time. Good agreement was seen between EDS and XPS data on major contaminants, with minor differences explained by the difference in depth probed by the two techniques. The presence of a wide range of minor contaminants, probably due to preflight contamination, was also observed.

ACKNOWLEDGMENTS

This experiment was initially conceived by Dr. James Gee, Camille Gaulin, and Clark Williams. The LDEF deintegration effort was performed by Sandra Gyetvay, Laana Fishman, and Dr. Michael Meshishnek, with funding from the Space Test Program (administered by the Air Force SSD/CLP). The initial examination and photography of the composite samples were performed by Sandra Gyetvay, Laana Fishman, and Dr. Michael Meshishnek, with funding from SDIO/TNK under the Space Environment Effects (SEE) Program, administered by Wright Laboratory Materials Directorate. The authors would like to credit Mr. Ca Su with the preparation of the cross-section samples. We would also like to thank Dr. Sherrie Zacharius, Dr. Howard Katzman, Dr. Gary Steckel, Dr. Gerald Rellick, and Dr. Wayne Stuckey for helpful suggestions and comments. This work was supported by the Wright Laboratory Materials Directorate and by The Aerospace Corporation Mission Oriented Investigation and Experimentation program.

REFERENCES

1. Schall, P.: Space Environment Effects on Spacecraft Materials (M0003). *The Long Duration Exposure Facility (LDEF). Mission 1 Experiments,* NASA SP-473, 1984, pp. 44-48.

2. Jabloner, H.: Poly(arylacetylene) Molding Compositions. U. S. Patent No. 4,070,333, 1978.

3. Whitesides, G. M.; and Neenan, T. X.: Synthesis of High Carbon Materials from Acetylenic Precursors. Preparation of Aromatic Monomers Bearing Multiple Ethynyl Groups. *J. Org. Chem.*, vol. 53, no. 11, 1988, pp. 2489-2496.

4. Barry, W. T.; Gaulin, C. A.; and Kobayshi, R. W.: Review of Polyarylacetylene Matrices for Thin-Walled Composites. The Aerospace Corporation, El Segundo CA, TR-0089(4935-06)-1, Sept. 1989.

5. Katzman, H. A.: Polyarylacetylene Resin Composites. The Aerospace Corporation, El Segundo CA, TR-0090(5935-06)-1, April 1990.

6. Zaldivar, R. J.; Rellick, G. S.; and Yang, J. M.: Processing Effects on the Mechanical Behavior of Polyarylacetylene-Derived C-C. *Sampe J.*, vol. 27, no.5, 1991, pp. 29-36.

7. Zaldivar, R. J.; Kobayashi, R. W.; Rellick, G. S.; and Yang, J. M.: Carborane-Catalyzed Graphitization in Poly(arylacetylene)-Derived Carbon-Carbon Composites. *Carbon*, vol. 29, no. 8, 1991, p. 1145-1153.

8. Hergenrother, P. M.: Polyphenyl Quinoxilines: Synthesis, Characterization, and Mechanical Properties. *J. Appl. Polym. Sci.*, vol. 18, 1974, pp. 1779-1791.

9. Bourassa, R. J.; and Gillis, J. R.: Atomic Oxygen Exposure of LDEF Experiment Trays. NASA CR-189627, May 1992.

10. Bourassa, R. J.; and Gillis, J. R.: Solar Exposure of LDEF Experiment Trays. NASA CR-189554, Feb. 1992.

11. Gregory, J. C.: Atomic Oxygen Erosion Yields of LDEF Materials. Presented at the LDEF Materials Workshop '91, Hampton VA, Nov. 1991.

12. George, P. E.; and Hill, S. G.: Results from Analysis of Boeing Composite Specimens Flown on LDEF Experiment M0003. *NASA/SDIO Space Environmental Effects on Materials Workshop*, NASA CP-3035, Part 2, June, 1988, pp. 1115-1141.

13. Meshishnek, M. J.; Stuckey, W. K.; Evangelides, J. S.; Feldman, L. A.; Peterson, R. V.; Arnold, G. S.; and Peplinski, D. R.: Effects on Advanced Materials: Results of the STS-8 EOIM Experiment. The Aerospace Corporation, El Segundo, CA, TR-0086(6935-05)-2, July 1987.

14. Hemminger, C. S.; Stuckey, W. K.; and Uht, J. C.: Space Environmental Effects on Silvered Teflon Thermal Control Surfaces. *LDEF--69 Months in Space. First Post-Retrieval Symposium*, NASA CP-3134, Part 2, June, 1991, pp. 831-845.

15. Hemminger, C. S.: Surface Contamination on LDEF Exposed Materials. Presented at the LDEF Materials Workshop '91, Hampton VA, Nov. 1991.

16. Crutcher, E. R.; and Warner, K. J.: Molecular Films Associated with LDEF. *LDEF--69 Months in Space. First Post-Retrieval Symposium*, NASA CP-3134, Part 1, June, 1991, pp. 155-177.

17. Fishman, G. J.; Harmon, B. A.; Gregory, J. C.; Parnell, T. A.; Peters, P.; Phillips, G. W.; King, S. E.; August, R. V.; Ritter, J. C.; Cutchin, J. H.; Haskins, P. S.; McKisson, J. E.; Ely, D. W.; Weisenberger, A. G.; Piercey, R. B.; and Dybler, T.: Observation of ^{7}Be on the Surface of LDEF Spacecraft. *Nature*, vol. 349, no. 6311, 1991, pp. 678-80.

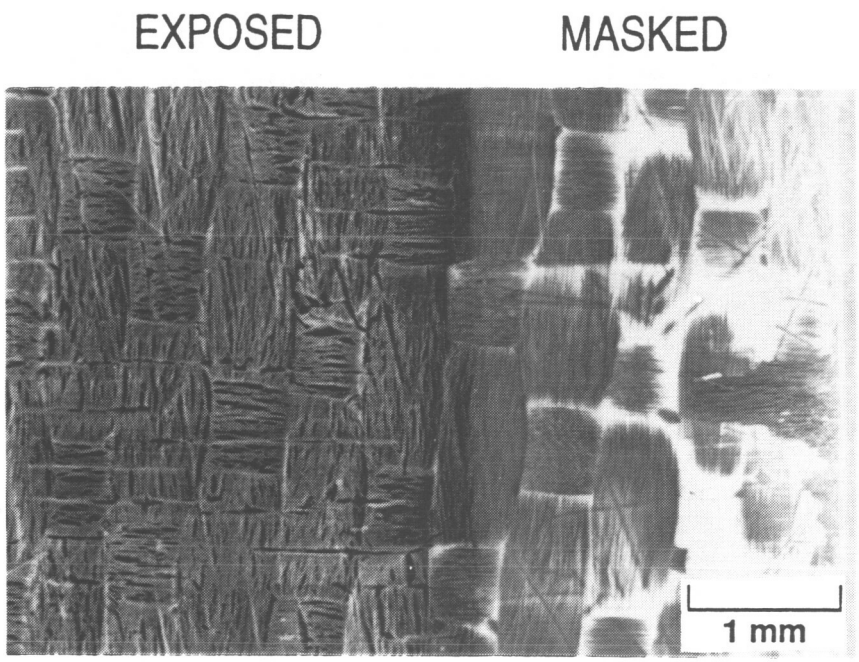

(a)

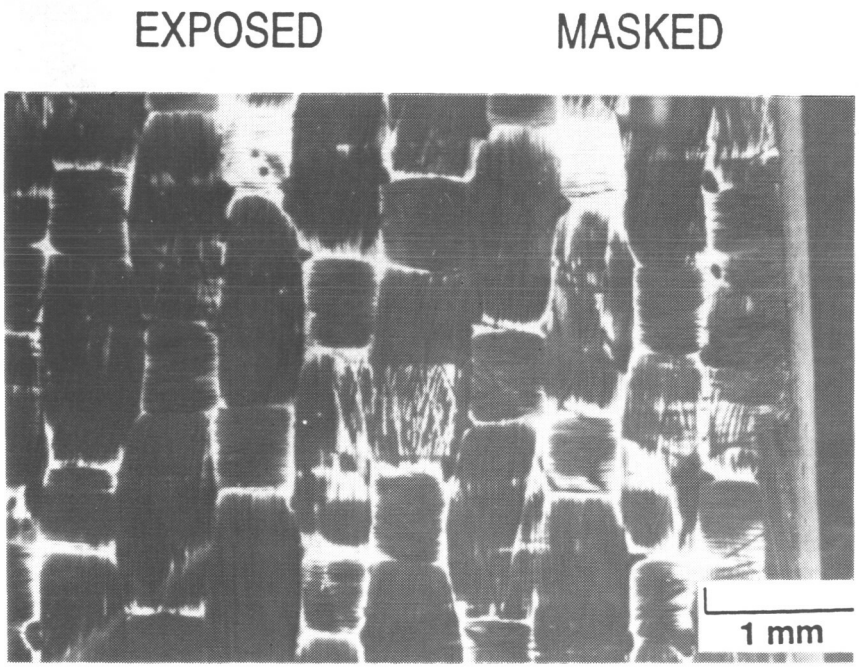

(b)

Figure 2. Difference in surface erosion of samples after leading and trailing edge exposure. (a) SEM of sample L-A surface; (b) SEM of sample T-A surface.

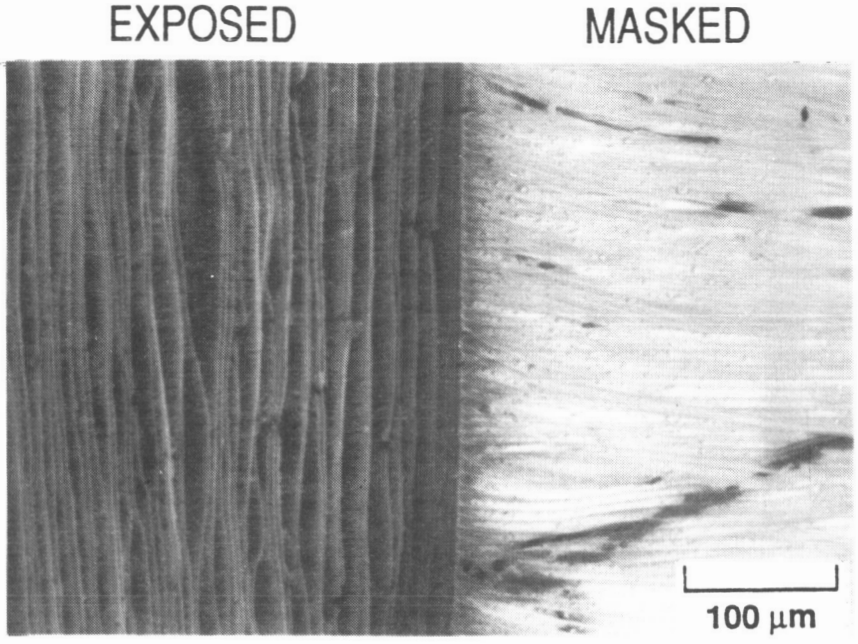

Figure 3. SEM micrograph of L-C surface showing details of exposed and masked areas.

(a)

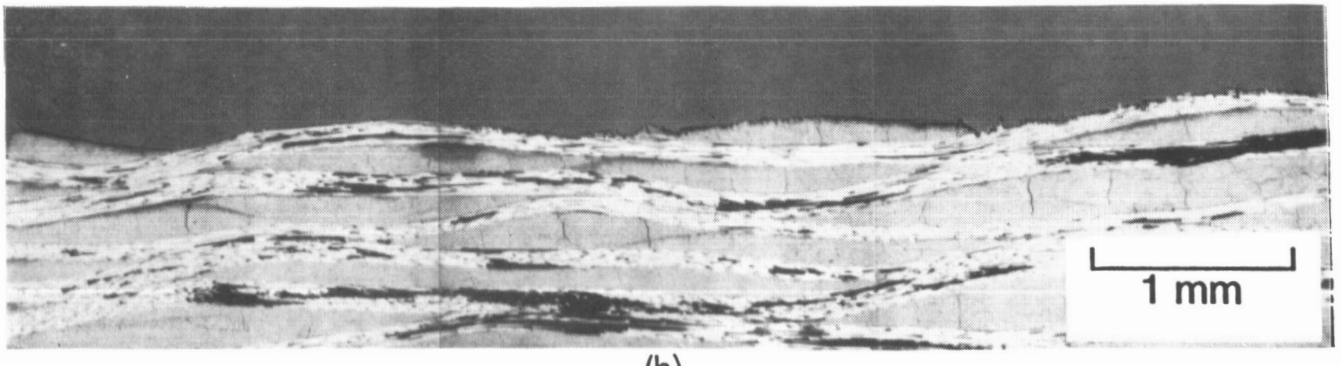

(b)

Figure 4. Optical micrographs of (a) L-A cross section and (b) L-B cross section.

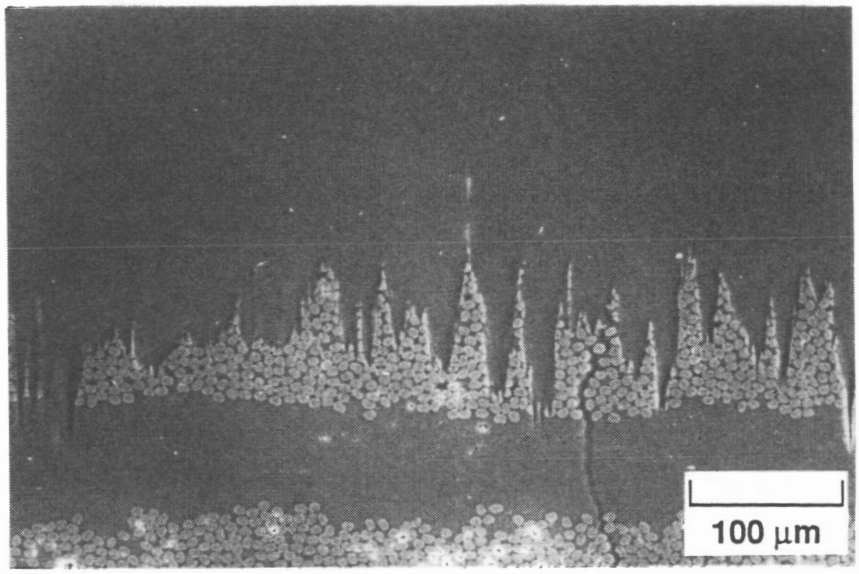

Figure 5. SEM micrograph of L-C cross section contrasting surface crack with surface crevasses .

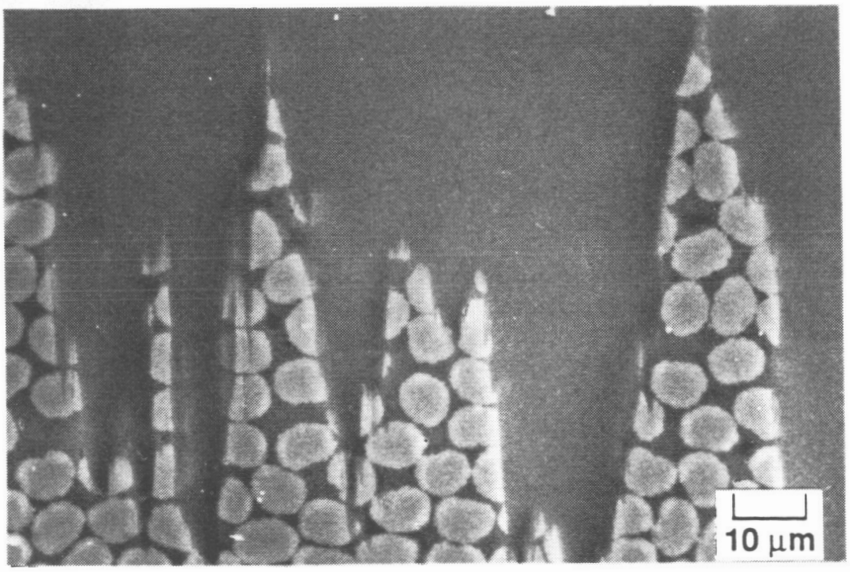

Figure 6. SEM micrograph of detail of L-C cross section.

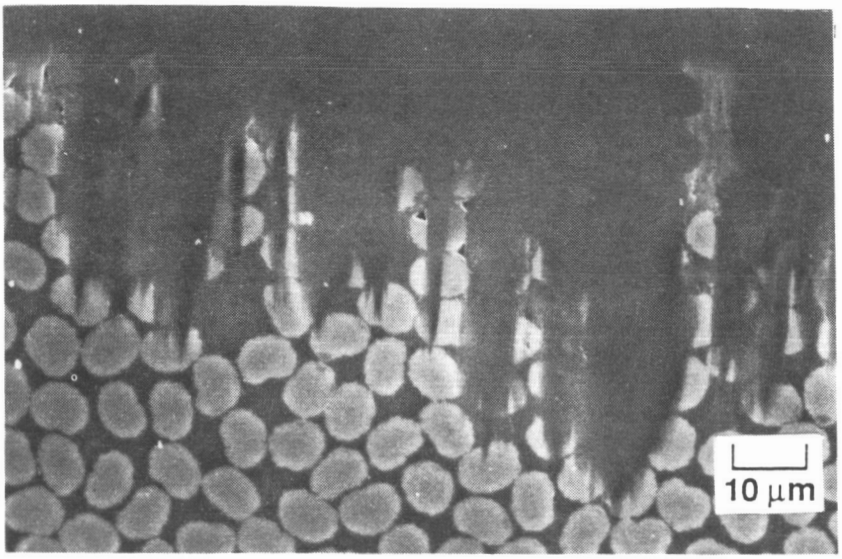

Figure 7. SEM micrograph of detail of L-B cross section.

N93-28269

THERMAL EXPANSION BEHAVIOR OF LDEF METAL MATRIX COMPOSITES

Tuyen D. Le
Mechanics and Materials Technology Center
The Aerospace Corporation
P.O. Box 92957
Los Angeles, CA 90009
Phone: 310/336-7864, Fax: 310/336-5846

Gary.L. Steckel
Mechanics and Materials Technology Center
The Aerospace Corporation
P.O. Box 92957
Los Angeles, CA 90009
Phone: 310/336-7116, Fax: 310/336-7055

SUMMARY

The thermal expansion behavior of LDEF metal matrix composite materials was studied by (1) analyzing the flight data that was recorded on orbit to determine the effects of orbital time and heating/cooling rates on the performance of the composite materials, and (2) characterizing and comparing the thermal expansion behavior of post-flight LDEF and lab-control samples. The flight data revealed that structures in space are subjected to non-uniform temperature distributions, and thermal conductivity of a material is an important factor in establishing a uniform temperature distribution and avoiding thermal distortion. The flight and laboratory data showed that both Gr/Al and Gr/Mg composites were stabilized after prolonged thermal cycling on orbit. However, Gr/Al composites showed more stable thermal expansion behavior than Gr/Mg composites and offer advantages for space structures particularly where very tight thermal stability requirements in addition to high material performance must be met. .

INTRODUCTION

The Advanced Composites Experiment is a sub-experiment of LDEF Experiment M0003, "Space Environmental Effects on Spacecraft Materials." The sub-experiment is a joint effort between government and industry, with Air Force Wright Laboratory, Flight Dynamics Laboratory, and the Aerospace Corporation, Mechanics & Materials Technology Center acting as experimenters.

In our first paper, presented at The First LDEF Post-Retrieval Symposium, we examined the microstructure and discussed the effects of atomic oxygen erosion, micrometeoroid bombardment, surface contamination on physical morphology, and surface damage of composite materials (Ref. 1). Besides these factors, in low earth orbit, the materials are also subjected to thermal cycling effects due to alternating eclipse and sun exposure. The materials experience transient heating/cooling in addition to thermal gradients. The effects of this environment on the thermal expansion behavior of composite materials needed to be characterized and documented. Therefore, the present analysis evaluates the thermal expansion behavior of post-flight composite materials compared with lab-control samples. In this analysis, temperature change vs. time, dimensional change vs. temperature, coefficients of thermal expansion (CTE), and thermal hysteresis are considered in predicting the dimensional stability experienced by the metal matrix composite materials in the space environment.

The analysis was done in two parts: (1) analysis of the flight data that was recorded on orbit to determine the effects of orbital time and heating/cooling rates on the performance of the composite materials, and (2) the characterization and comparison of the thermal expansion behavior of post-flight LDEF and lab-control samples. This study, combined with the results previously reported (Ref. 1), completes a full evaluation of all factors affecting composite materials in the LDEF space environment. This allows us to evaluate possible synergistic effects of long term space exposure that cannot be studied on earth.

MATERIALS AND EXPERIMENTAL PROCEDURE

The experiment includes a wide variety of metal matrix composites (MMC). The materials selected for this study are shown in Table I. The "Material Description" column first specifies the type of fibers and then the materials for the matrices and face sheets. The MMC's are primarily continuous graphite fiber-reinforced aluminum and magnesium alloys. They are either single-ply or multi-ply composites with different ply angles. In each group, typical procedures were followed to produce five (5) sets of samples: leading-edge (LE) exposures, trailing-edge (TE) exposures, LE controls, TE controls, and lab-control samples. The lab-control samples were stored in vacuum on earth. The locations of flight samples on LDEF were Bay D, Row 4 on the TE and Bay D, Row 7 on the LE. It is worth noting here that the LDEF samples were mounted such that there was no clamping force on them, i.e. the samples were free to expand or contract in their slots. The sample cassettes were thermally decoupled from the LDEF to minimize effects of the structure on the temperature excursions. The LE and TE controls were mounted on the back side of cassettes, facing inward, not directly exposed to the space environment. However, they were expected to be subjected to thermal excursions similar to those experienced by the exposed samples. The samples were 3.5 in. long X 0.5 in. wide X 0.031 in. thick strips. One or more samples from the top two classes of Gr/Al composites listed in Table I and the MG3-MG6 group of Gr/Mg composites were instrumented with thermistors and strain gages (SG) to monitor the thermal cycles and thermal strains during orbiting. It should be noted that the SG and thermistors were only mounted on the back side of LE and TE exposures, and not directly exposed to the thermal radiation in space. This was done to avoid any possible damage caused by atomic oxygen erosion, UV radiation, or micrometeoroid bombardment on these sensors. The strain gages were mounted to measure the change in dimension along the direction parallel to the fibers. The data acquisition system was set up to record temperature and strains during the duration of an orbit once every 107 hrs. (approximately 78 orbits.) Data were collected every three minutes during the selected orbit. For the record, the first set of data was collected after approximately 44 hours on orbit, and the last set was recorded after approximately 14 months into the flight. No data were recorded during the unplanned final 4.5 years of the mission.

In the flight data analysis, typical thermal expansion curves were selected at the beginning, middle, and the end of the recording time. These durations are approximately 40, 5K, and 10K hours (1, 208, 416 days) after being placed in orbit. These curves were

all selected over the same range of temperature for the purpose of comparisons. The thermal cycles of each type of material were also analyzed to determine the heating and cooling rates.

The absolute values of linear thermal expansion in composite materials are extremely small, particularly in the direction parallel to the fibers. This requires the use of a highly specialized, sensitive, stable, high resolution apparatus like a laser interferometer. In this study, the Michelson Laser Interferometer of The Aerospace Corporation was used to characterize the thermal behavior of LDEF post-flight and lab-control samples. This technique provides in-situ, direct, and continuous measurements of thermal expansion/contraction through a thermal cycle without recourse to a comparative standard. It also allows very small changes in dimension (on the order of 1μ-strain or less) to be resolved. This technique has been described in detail elsewhere (Refs. 2, 3). Before mounting on the interferometer, the ends of each strip sample were slightly ground to a dome shape. This was done to avoid the effects of thermal distortion in the face sheet at the ends of the sample that could cause error in the measurements. A chromel-alumel thermocouple was mounted on each side of the sample to monitor the temperature change. In all cases, thermal cycling was carried out by heating the sample first from room temperature (RT) to the hot end of the cycle, and then cooling down to the cold end and heating back up to RT. The heating/cooling rate was limited to ~1°C/min. to ensure thermal equilibrium throughout the sample. Again, for the purpose of comparison with the flight data, the samples were thermally cycled over the same range of temperature that was derived from the flight data analysis.

RESULTS AND DISCUSSION

In this section, the flight data analyses are presented first, followed by the results obtained using the laser interferometer. It should be noted that all thermal expansion curves are plotted on coordinates of the same dimensions to provide consistency for comparisons.

Gr/Al Composites

Figures 1 and 2 show the change in dimension vs. temperature of P55/6061/6061 and GY70/201/2024 composites mounted on LE and TE respectively. Figure 1 shows the thermal expansion behavior of P55/6061/6061 composites after 40, 5K, and 10K hours in orbit. It is clearly seen that generally the behavior was fairly linear with only a small hysteresis. During the entire duration of orbiting or at least for the first 10 thousand hours (approximately 6,150 cycles), the behavior of this material showed little change. The curves consistently conformed to the same shape with the same total change of length. A similar behavior was observed for the GY70/201/2024 composites, except that this material showed more thermal hysteresis, particularly in the TE sample, Fig. 2. However, in all cases, the total changes in dimension and the slopes remained constant during the entire time of recording. When the LE and TE curves for either of these Gr/Al composites were compared, it was noted that the total dimensional changes in the TE samples were smaller than for the LE samples, even though the temperature span was about the same.

The thermal cycles of LE and TE Gr/Al samples were also analyzed. The results showed a consistent shape of the temperature/time plots for either LE or TE for both types of Gr/Al composites. The typical cycles are shown in Figs. 3(a) and (b) for the GY70/201/2024 composites. The only differences between samples were the starting point and the end of the cycle that obviously depended on when the data were recorded. In both cases, it is seen that the samples did not have constant heating/cooling rates throughout a cycle. As seen in Fig. 3(a), the samples on the LE heated very rapidly at a rate of ~15°F/min. when the heating cycle started. The heating rate slowed down when the temperature approached the hot end. Initial cooling was just as fast as initial heating, but again the rate slowed down to ~ 1-2°F/min. when approaching the cold end. However, an important point to be noted here is that the heating and cooling rates were twice as high in the LE than TE samples. It is also noted that the hot end of the TE thermal cycle was sharper than for the LE; the dwell time for the transition from heating to cooling of the TE samples was much less than for the LE, causing an abrupt, sharp drop in temperature on the TE.

Figure 4 shows the change in dimension vs. temperature of single-ply P100/EZ33A/AZ31B mounted on the LE and TE, respectively. These curves again were plotted for thermal cycles selected at the beginning, middle, and the end of the recording time. It is clearly seen that the thermal behavior plotted from flight data are completely different from the normal response for this material. Instead of expanding and contracting upon heating and cooling as shown for the Gr/Al composites, these materials expanded and then slowly contracted with increasing temperature and vice versa upon cooling, forming convex curves. This anomalous behavior was further investigated and will be explained later when the change in temperature and the corresponding change in dimension vs. time for each individual curve are examined.

In comparing the LE and TE samples, the thermal behavior was very similar in that the curves followed the same pattern. The dimensional change was observed to continually change as a function of the number of thermal cycles. The curves shifted upward indicating that the samples were getting longer with time until stability was attained. Significant shifting occurred in the first five thousand hours of flight, but minimal shifting occurred between the 5K and 10K hour curves. It should be noted that during the first 40 hours of flight after the LDEF was released, no data were recorded. Therefore, for the first 27 cycles, it is possible that the behavior of the samples was very unstable. Apparently the dimensions were reduced from the initial SG reading of 0.0 μ-strain to a minimal value during the first few cycles and then increased with additional cycles until the final, stable dimensions were attained. It can be seen in Fig. 4 for the TE sample that the data recorded at 40 hrs. shows more scatter as compared to the LE, indicating that the TE sample was more unstable after 40 hrs of flight. The 5K and 10K hour curves are smooth, and the data fall consistently along the same path. This indicates that after a certain number of thermal cycles, the Gr/Mg composites stabilized and behaved quite consistently.

Figure 5 shows a typical thermal cycle and the corresponding dimensional change for the Gr/Al composites plotted vs. time. This plot shows the normal behavior of Gr/Al composites which expand and contract with heating and cooling throughout the cycle. The rates of change in dimension were consistent with the rates of change of temperature. When the same curves were plotted for Gr/Mg composites, anomalous behavior was observed as shown in Fig. 6 . As the cycle started, temperature increased slowly and the sample expanded as expected. However, as the heating rate rapidly increased, the sample

contracted instead of expanding. The sample kept contracting until the hot end point was reached. Upon cooling, at first the temperature dropped very rapidly and the sample expanded instead of contracting. As the cooling rate slowed down, the sample started contracting as originally expected. Two factors are used in explaining this unusual phenomenon. First, in the original set-up of the experiment, the SG and thermistors were mounted on the back side of the sample. They were not directly exposed to radiation, which is the heating source. Second, the thermal conductivity of Gr/Al composites is significantly greater than Gr/Mg due to the much higher matrix conductivity of the Al matrix alloy compared to the Mg alloy (1104 vs. 408 Btu-in/ hr. ft °F). When the exposed surface of the Gr/Mg samples was heated or cooled slowly (in this case at the rate of 1.5°F/min. or less), thermal equilibrium was maintained throughout the sample leading to normal behavior. However, when just leaving or entering the shadow, the samples were heated or cooled at a much faster rate (10°F/min.). Due to the low thermal conductivity of the Gr/Mg, a steep thermal gradient existed through the thickness. A larger temperature gradient existed between exposed front-surface and back-side surface in the Gr/Mg composite materials than for Gr/Al. Upon heating, the exposed surface was therefore much hotter and consequently expanded faster than the back surface, causing sample bending and inducing compression in the back surface leading to negative SG readings. These bending deformations give the erroneous indication that the sample has a negative CTE. Similar arguments apply for the fast cooling condition, the exposed surface cooled faster making the sample bend the other way. This time the bending induced tension on the back side and led to expanding readings by the SG, again implying that the sample had a negative CTE. Consequently, the anomalous behavior of the Gr/Mg composites resulted from the nature of the space exposure and the experiment design and was not an inherent characteristic of the materials themselves. The temperature versus time plots for the Gr/Mg composites mounted on LE and TE showed the same features as observed for Gr/Al composites, except that the heating and cooling rates were higher than for Gr/Al (20 and 10°F/min. as compared to 15 and 7°F/min.). This again might be attributed to the combined effects of low thermal conductivity and differences in solar absorptance and emissivity of Gr/Mg composites.

From the results of flight data analysis, it is clearly shown that in a space environment, the temperature distribution in a structure is not uniform. Nonuniform temperatures arise from radiant heating on one side of a structure as typically occurs in a geostationary satellite or by transient heating/cooling as in the LDEF structure placed in a day-night low earth orbit with alternating eclipse and sun exposure. Depending on the

location, as in this case LE or TE, materials are subjected to widely different temperature ranges and heating/cooling rates. The disparity of the temperature range and rates of heating/cooling lead to a differential total change in dimensions that could eventually lead to thermal distortion. In low thermal conductivity materials like Gr/Mg or Gr/Epoxy composites, the thermal gradient effects on distortion are more severe. Therefore, besides the thermal expansion behavior (CTE and thermal hysteresis), thermal conductivity must be considered in predicting the structural stability of a material in the space environment.

Laser Interferometer Data Analysis

Gr/Al Composites

The flight samples with mounted strain gages and thermistors selected for flight data analysis were subsequently used in the lab to characterize the post-flight thermal expansion behavior. These samples as well as lab-control samples of the same material were characterized with the laser interferometer over the same ranges of temperature derived from flight data. The thermal expansion curves of single-ply GY70/201/2024 are shown in Figs. 7 to 10. Fig. 7 shows the comparison between thermal expansion curves of LE and TE samples. The LE curve illustrates linear, stable behavior with zero hysteresis. The upper half of the TE curve did not retrace along the same path upon cooling resulting in a residual thermal strain of about 20 μ-strain that caused a permanent offset when the cycle was completed at RT. The offset that occurred in the TE samples is not readily explainable. However, the overall behavior was linear and stable with small hysteresis. Fig. 8 compares the thermal expansion curve of a lab-control sample with the LE sample. In the lab-control sample, the change in specimen length upon heating from RT to the hot end of the cycle was not recovered on cooling back to RT, i.e., upon cooling the dimensional change did not retrace the same path as heating. Further cooling from RT to the cold end and heating back up to RT also did not result in recovery of the total length change. A residual thermal strain was induced such that a thermal strain hysteresis was formed with permanent offset at RT of ~ 10 μ-strain. The lab-control sample shows a small, open thermal hysteresis loop of about 20 μ-strain wide. The results indicated that after a certain number of thermal cycles in space, strain hardening in the matrix stabilized the composites, reducing thermal hysteresis for subsequent thermal cycles.

The P55/6061/6061 composites showed basically the same behavior; therefore, the results are not shown here. The post-flight samples behaved elastically over the entire temperature range with no hysteresis. The lab-control sample behavior was stable and linear with a very small hysteresis of about 5 μ-strain. The very small hysteresis demonstrates that the high yield strength of 6061 matrix probably delays the plasticity of the matrix to broader temperature ranges than encountered in low earth orbits. The average CTE for all Gr/Al composite samples determined over the entire temperature range is listed in Table II. It may be seen that the CTE of both composite materials was apparently unaffected by the extended space exposure. These results indicate that the LDEF space environment has little effect on the thermal behavior of Gr/Al. Thermal cycling in orbit stabilized the Gr/Al composites, eliminating thermal hysteresis after a number of cycles.

In order to simulate the thermal cycling conditions experienced by a satellite in a geosynchronous orbit, additional measurements were made on the lab-control and flight samples over the temperature range of ±250°F. These measurements were performed at Composite Optics, Inc., San Diego, CA. The results are shown in Figs. 9 to 12. In these experiments, two continuous thermal cycles were performed. For each cycle, the samples were first cooled from RT to -250°F, heated up to + 250°F, and then cooled to RT. As shown in Fig. 9, the behavior of the lab-control sample was not as linear as in the narrower temperature range. At temperatures near both extremes, the behavior deviated from linearity due to the plasticity in the matrix, leading to the formation of an open hysteresis loop. It is noted that the hysteresis of the second cycle is larger than that of the first cycle (100 μ-strain and 50 μ-strain respectively). It is not well understood why upon cooling for the second cycle, the matrix yielded at a higher temperature than for the first cycle leading to the formation of a larger loop. From our experience, in the first few cycles, the behavior of composite materials can be quite erratic and unpredictable, until the materials stabilize and behave more predictably. As shown in Fig 10, the LE sample was cycled over the same temperature range. It is seen that for both cycles, the flight sample expanded and contracted along the same linear path and was hysteresis-free. This indicates that after the excessive thermal cycling on LDEF, the material was very stable even over a much wider temperature range.

The thermal expansion behavior of the 4-ply/±20° lab-control and LE samples are shown in Figs. 11 and 12. Both samples showed non-linear response with a larger thermal hysteresis loop for the second cycle. The overall response shown is characteristic of angle ply laminates. The average CTE is lower compared to unidirectional, single ply composites

because of the interaction between plies and a higher volume fraction of fibers in the 4-ply composites. However, the hysteresis loop is wider due to the existence of interply stresses. After extensive thermal cycling in orbit, the CTE of the post flight sample is about the same as of the lab-control sample. The thermal hysteresis of the post-flight sample is slightly larger (150 to 120 μ-strain). Additional post-flight measurements need to be made on another LE or TE sample over the LDEF temperature range to better indicate the effect of prolonged thermal cycling on the hysteresis for this composite. However, it can be deduced from Figs. 11 and 12 that, over the LDEF temperature range, the thermal behavior would be linear with only a small thermal hysteresis loop. Microstructure examination of both lab-control and post-flight samples revealed no cracking, delamination, or debonding.

Gr/Mg Composites

Figure 13 shows thermal behavior of P100/EZ33A/AZ31B post-flight and lab-control samples. It is clearly seen that the lab-control sample was very unstable. The behavior was non-linear with a large residual thermal strain at RT of ~ 280 μ-strain. The large residual strain of the material in the as-fabricated condition is typical of the MMC, and is caused by yielding of the matrix, in this case, upon cooling to the cold end of the cycle. The composite behavior near the cold end of the cycle was dominated by the expansion of the fibers causing yielding in the matrix. This leads to an increase in dimension and consequently an open loop with large permanent offset at RT. The thermal expansion behavior of post-flight samples showed that the amount of permanent offset and the magnitude of thermal hysteresis over the temperature range decreased remarkably after thermal cycling. The implication of the results is that extensive thermal cycling had a large effect on stabilizing the behavior of these materials. However, the thermal expansion behavior remained non-linear and the thermal hysteresis could not be cycled out as in the case of Gr/Al composites even after nearly 30K cycles. These data indicate that the EZ33A Mg alloy, unlike the high strength 6061 and 201 Al alloys, was not effectively strain-hardened by thermal cycling, which would have increased the yield strength and minimized strain hysteresis over the LDEF temperature range. It should be noted however that the total dimensional change and average CTE of the Gr/Mg composites are smaller than those of the Gr/Al composites. This is due to the low elastic modulus of the Mg alloys (6.5 Msi) and the high modulus, low CTE P100 fiber. The CTEs are near-zero and similar for both LE and TE samples within the error range of the experiment.

It should be noted that P100/EZ33A/AZ31B composites are an obsolete system. During the initial sample preparation stage for LDEF these were the only Gr/Mg composites being produced. It was later learned that P100/EZ33A/AZ31B composites had inherently low strength properties due to interaction between the rare earth elements in the EZ33A matrix alloy and the P100 fibers. This interaction may also affect the matrix and limit its work hardening so that hysteresis in the thermal expansion curves cannot be eliminated. Shortly before the M0003 trays were shipped to NASA before launch, several P100/EZ33A/AZ31B composites were replaced by P100/AZ91C/AZ61A Gr/Mg composites. This system subsequently became the most commonly produced Gr/Mg composites. None of the P100/AZ91C/AZ61A composites were instrumented with thermistors or strain gages because of their late addition to the experiment.

The Gr/Mg composite materials were also tested over a wider range of temperatures to simulate the conditions of higher orbits. The results of LE and lab-control single-ply and 4-ply P100/AZ91C/AZ61A laminates are shown in Figs. 14 to 16. Figs. 14 and 15 show that the behavior of both lab-control and post-flight LE was unstable, non-linear, had large, thermal hysteresis and residual strains. The post-flight LE shows better stability with smaller residual strain as compared to the lab-control. It is noted that, for both cases, the average length of the sample decreased with cycling. Again, however, the overall CTE was quite low and near-zero. The behavior of the Gr/Mg composites in this study is quite different from the results of other experiments (Refs. 2, 4, and 5). This observation again demonstrates that characterizing the thermal response of MMC can be complicated by secondary effects such as the processing procedure. Variations in the residual stresses existing in "as-fabricated" composites, for example, can have a dominant effect on the thermal response of MMC.

Figure 16 shows the response of 4-ply laminates over the same range of temperatures. It can be seen that the performances of multi-ply laminates differ considerably from the unidirectional single-ply composites. The 4-ply lab-control and LE samples show a closed thermal hysteresis loop with magnitude of about 100 μ-strain. The lab-control and post-flight samples have nearly identical curves. This indicates that the behavior of multi-ply laminates was originally quite stable, and extensive thermal cycling over the LDEF temperature range did not have much effect on their behavior over ±250°F. The thermal expansion was characteristically non-linear due to interply stresses. The total change in dimension was relatively small, about 50 μ-strain. The overall CTE is near-zero (0.071×10^{-6}/°F) over the test temperature range. Here again, as for the Gr/Al composites,

the P100/AZ91C/AZ61A composites should also be evaluated post-flight over the LDEF temperature range. This will give a better indication of the stabilizing effect of the LDEF thermal cycling.

CONCLUSIONS

In this study, the thermal expansion behavior of MMC was fully evaluated to determine the synergistic effects of space environment such as high vacuum, solar radiation, atomic oxygen exposure, and micrometeoroid bombardment on these materials. The results obtained for these materials are very valuable for assessing their performance for space structures requiring low-CTE materials.

Gr/Al composites showed a stable, linear thermal expansion behavior with near-zero thermal hysteresis over the LDEF temperature range. Prolonged thermal cycling on LDEF also stabilized the thermal expansion of Gr/Al over wider temperature ranges. In contrast, Gr/Mg composites, even after extensive cycling during orbiting, showed non-linear, unstable behavior with significant hysteresis. However, the hysteresis was significantly reduced as compared to the as-fabricated samples. The thermal expansion data on Gr/Mg composites indicated that near-zero CTE over the application temperature range can be obtained and maintained on-orbit.

The flight data revealed that in the space environment, the temperature distribution in a structure is often time varying or non-uniform due to radiant heating. For a satellite like LDEF in a low earth orbit with alternating eclipse and sun exposure, the data showed that the materials experienced thermal cycling over different temperature extremes with different heating/cooling rates depending on the location of samples on the satellite. In a thermal cycle, the heating/cooling rates could vary from 0°F/min. to 20°F/min. when LDEF was going in or out of the earth's shadow. On the LE, the rates were almost double those on the TE. Two things were learned as a consequence of this phenomenon: first, the differential heating/cooling rates caused a difference in the total changes in dimension between LE and TE samples over the same temperature range as observed in Gr/Al composites, and second, thermal bending was observed on Gr/Mg composite materials due to their low thermal conductivity as compared to Gr/Al composites. The flight data also implied that structures in space are always subjected to non-uniform temperature distributions and thermal

conductivity of a material is an important factor in establishing a uniform temperature distribution. Therefore, besides CTE and thermal hysteresis, thermal conductivity of a material must be considered to predict structural stability in the space environment. The application of Gr/Al composites offers advantages for space structures particularly where very tight thermal stability requirements in addition to high material performances are to be met. Gr/Al composites offer better thermal conductivity than Gr/Mg or Gr/Polymer composites, and also have lower susceptibility to space environmental effects as compared to Gr/Polymer composites (Refs. 6-8).

REFERENCES

1. G.L. Steckel and T.D. Le, "M0003-10: LDEF Advanced Composites Experiment" *LDEF First Post-Retrieval Symposium*, Kissimmee, FL, June 2-8, 1991, NASA CP-3134, pp. 1041-1053.

2. S.S. Tompkins, "Techniques for Measurement of the Thermal Expansion of Advanced Composite Materials" STP 1032, ASTM, Sparks, NV, 1988, pp.54-67.

3. E.G. Wolff and S.A. Eselun, "Double Michelson Interferometer for Contactless Thermal Expansion Measurement" *Proceeding of SPIE*, Vol. 192, Interferometry, 1979, pp. 204-208.

4. J.R. Strife and V.C. Nardone, "Thermal Expansion Behavior of Graphite Reinforced Metals" *Sixth Metal Matrix Composites Technology Conference*, Monterey, CA 1985, pp. 21-27.

5. K.W. Buesking, J.J. Kibler, B. Coffenberry, and C-F. Yen, "Advanced Composite Materials Evaluations" *MSC Technical Progress Report on NSWC*, Contract No. N60921-86-C-0236, Jan. 1987.

6. P.E. George and S.G. Hill, "Results from Analysis of Boeing Composite Specimens Flown on LDEF Experiment M0003," *LDEF First Post-Retrieval Symposium*, Kissimmee, FL, June 2-8, 1991, NASA CP-3134, pp. 1115-1141.

7. W.S. Slemp, P.R. Young, W.G. Witte, Jr., and J.Y. Shen, "Effects of LDEF Flight Exposure on Selected Polymer Matrix Resin Composite Materials," *LDEF First Post-Retrieval Symposium, Kissimmee*, FL, June 2-8, 1991, NASA CP-3134, pp. 1149-1162.

8. G.L. Steckel, T. Cookson, and C. Blair, "Polymer Matrix Composites on LDEF Experiments M0003-9 & 10," *Proceedings of LDEF Materials Workshops '91*, NASA CP-3162, pp. 515-542.

TABLE I

Aerospace Material Number	Material Description	Flight Data	Laser Interferometer Data
AL3-AL6	GY70/201/2024 (1 PLY)	LE & TE	LE, TE, and Lab-Control
AL12 & AL14	P55/6061/6061 (1 PLY)	LE & TE	LE, TE, and Lab-Control
AL33	P100/201/2024 (4 PLY/±20°S)		LE, TE, and Lab-Control
MG3 - MG6	P100/EZ33A/AZ31B (1 PLY)	LE & TE	LE, TE, and Lab-Control
MG9	P100/AZ91C/AZ61A (1 PLY)		LE and Lab-Control
MG10	P100/AZ91C/AZ61A (4 PLY/±10°S)		LE and Lab-Control

TABLE II

CTE of Gr/Al Composites (x 10^{-6}/°F)

Materials	Lab-Control	LE	TE
GY70/201/2024 (1 Ply)	3.5	3.2	3.8
P55/6061/6061 (1 Ply)	3.0	3.3	3.5

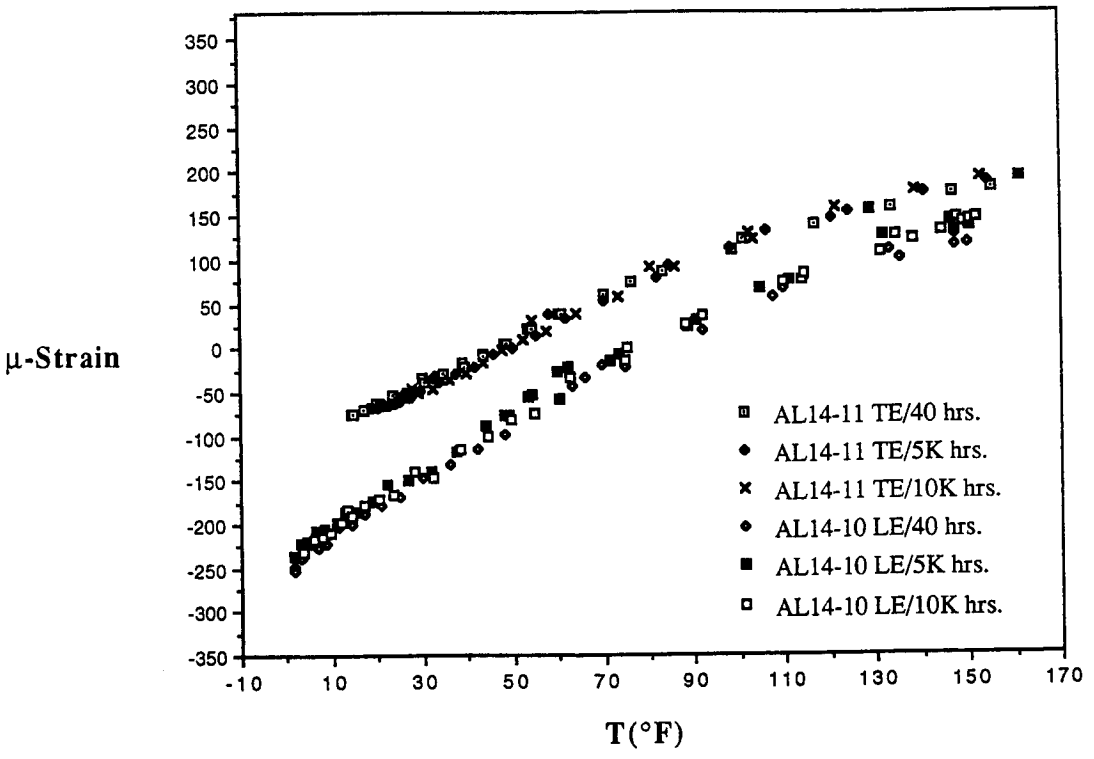

Fig. 1. Flight data showing the change in dimension vs. T of P55/6061/6061 Gr/Al composites

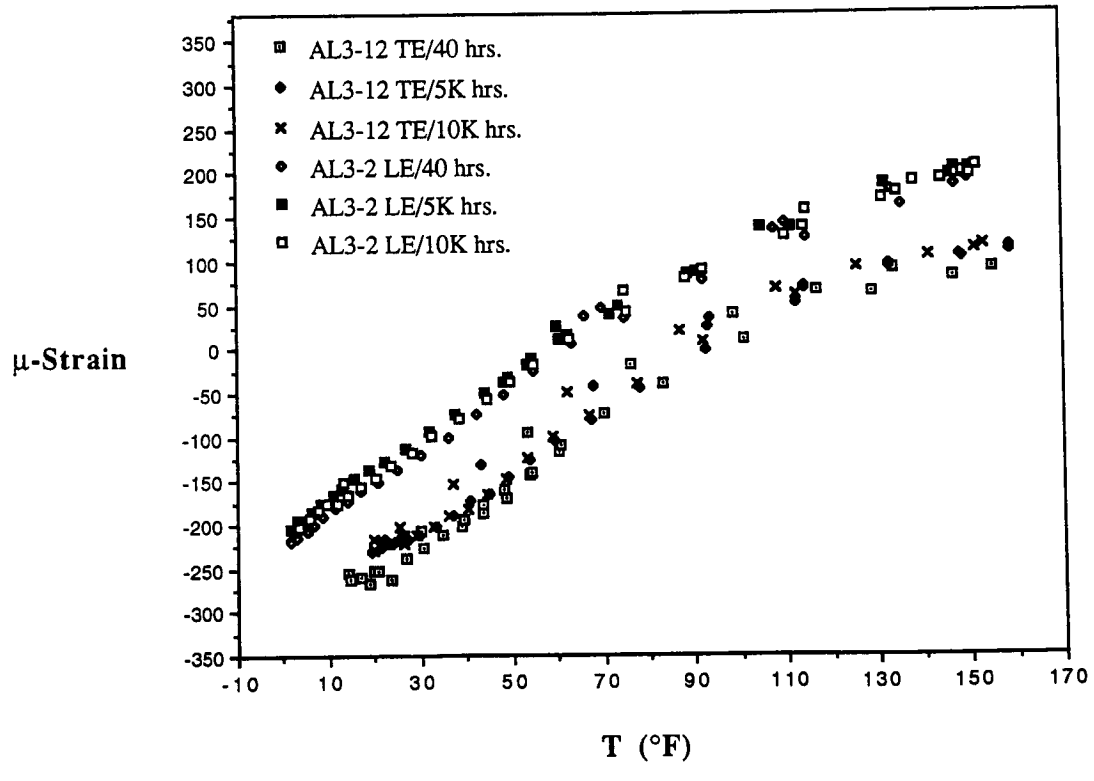

Fig. 2. Flight data showing the change in dimension vs. T of GY70/201/2024 Gr/Al composites.

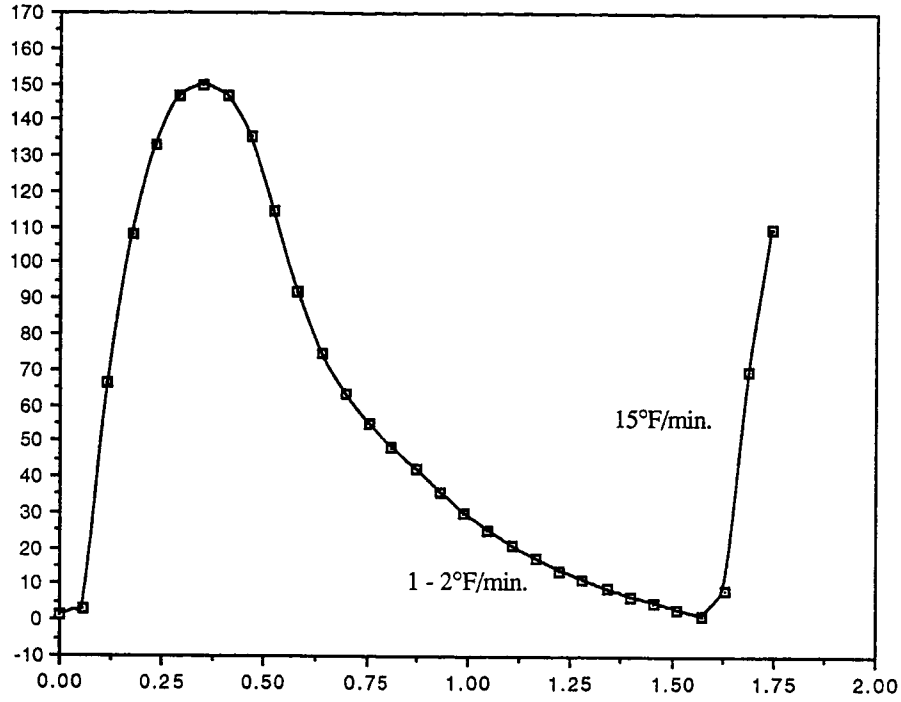

(a) LE

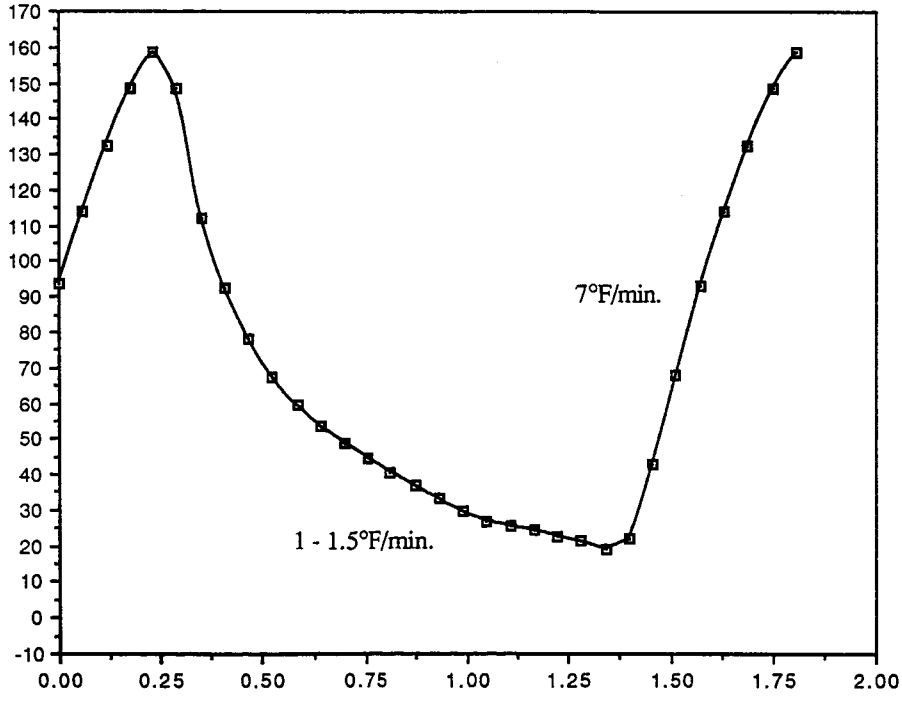

Fig. 3(b). TE

Fig. 3. Flight data showing the change in T vs. time in a single cycle of Gr/Al composites, (a) LE and (b) TE.

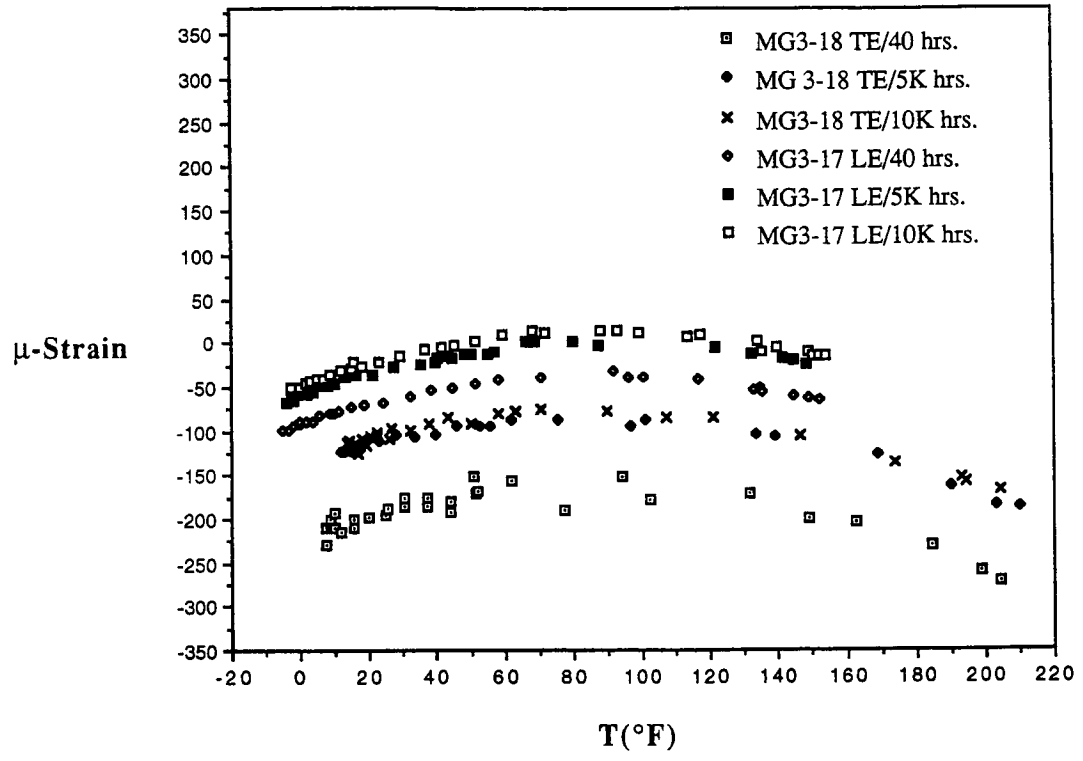

Fig. 4. Flight data showing the change in dimension vs. T of P100/EZ33A/AZ31B Gr/Mg composites.

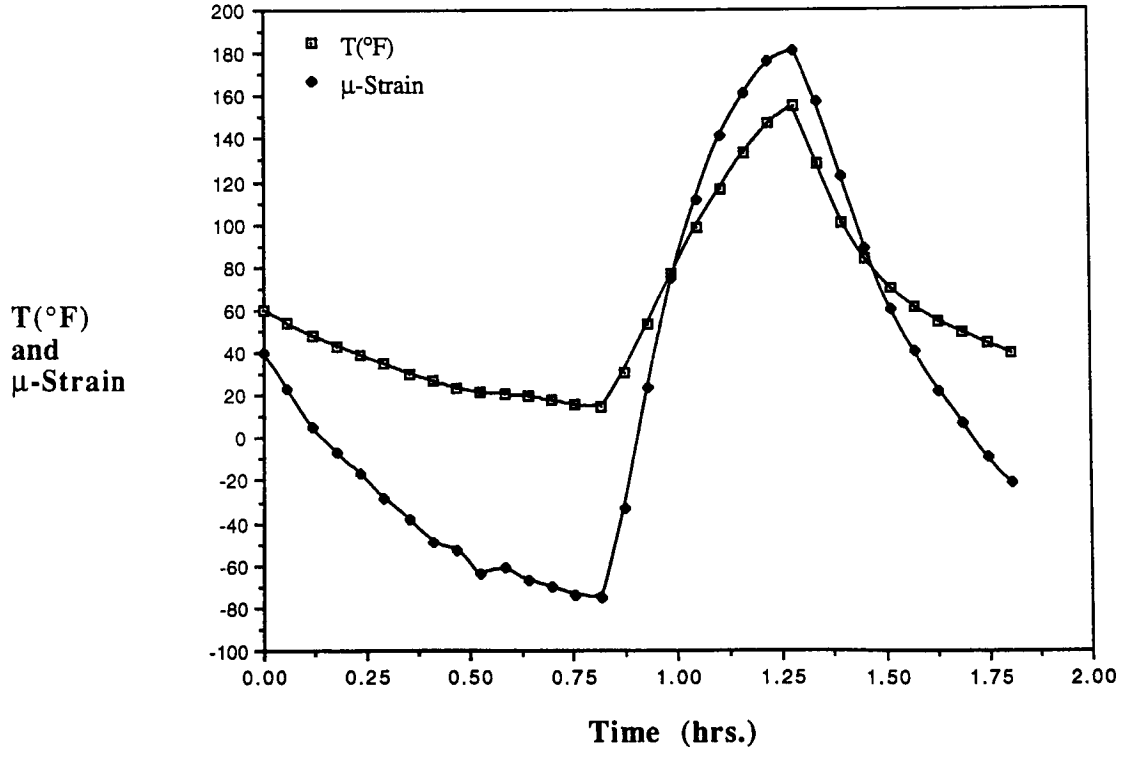

Fig. 5. Flight data showing the change in dimension and temperature vs. time in a thermal cycle of P55/6061/6061 composite.

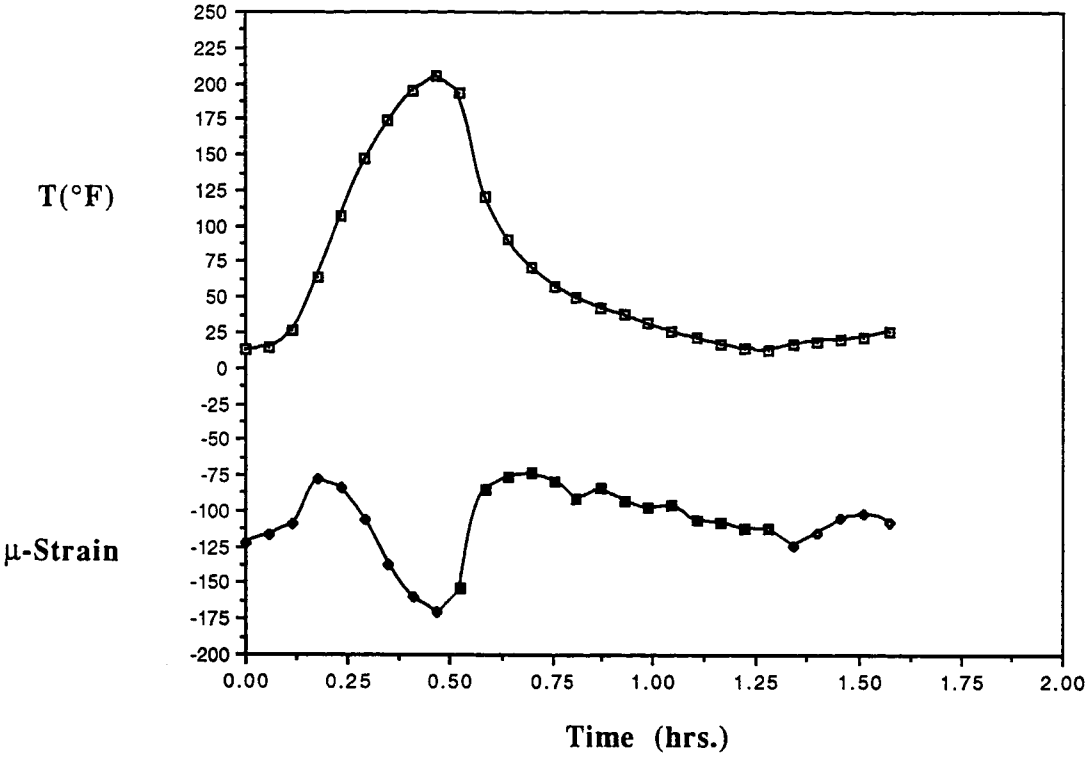

Fig. 6. Flight data showing the change in dimension and temperature vs. time in a single thermal cycle of P100/EZ33A/AZ31B Gr/Mg composites.

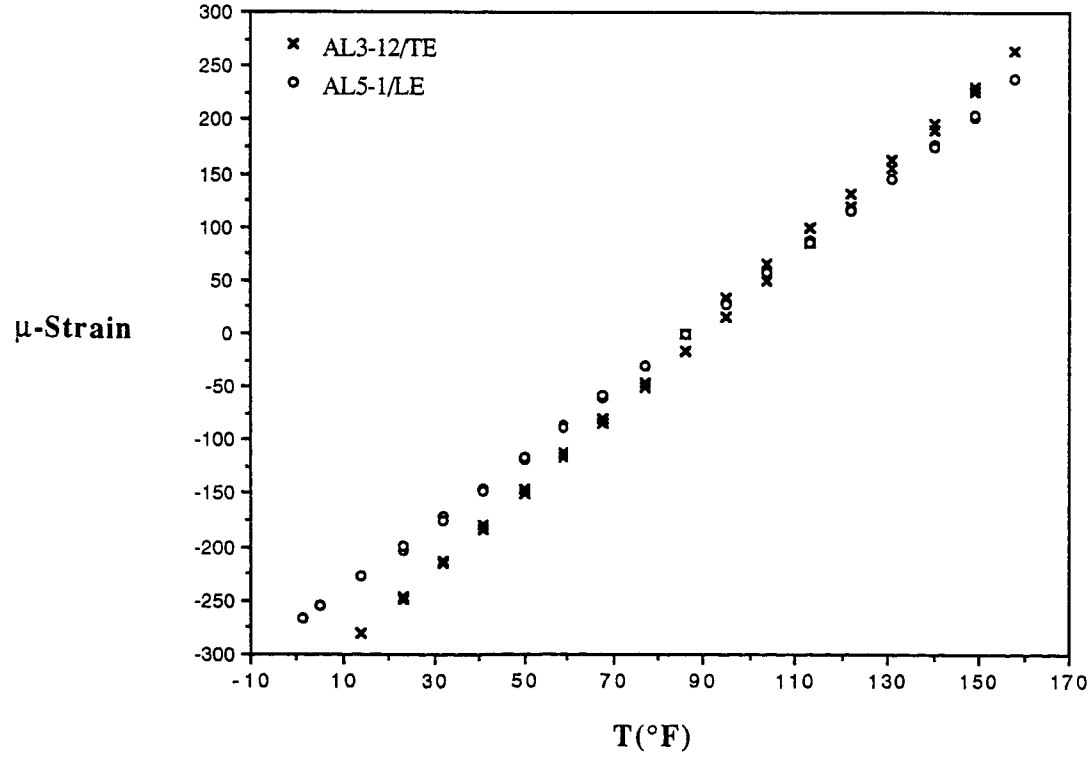

Fig. 7. Thermal expansion curves of the LE and TE sample of GY70/201/2024 Gr/Al composites determined by laser interferometry.

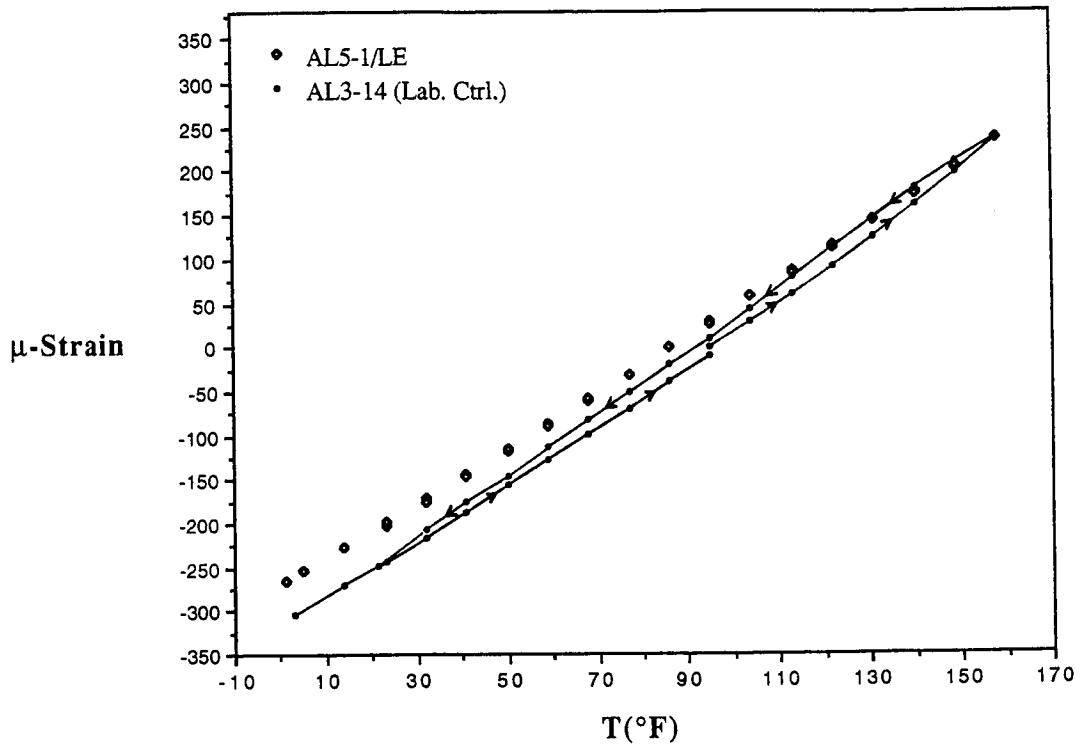

Fig. 8. Thermal expansion curves of lab. control and LE of GY70/201/2024 Gr/Al composites determined by laser interferometry.

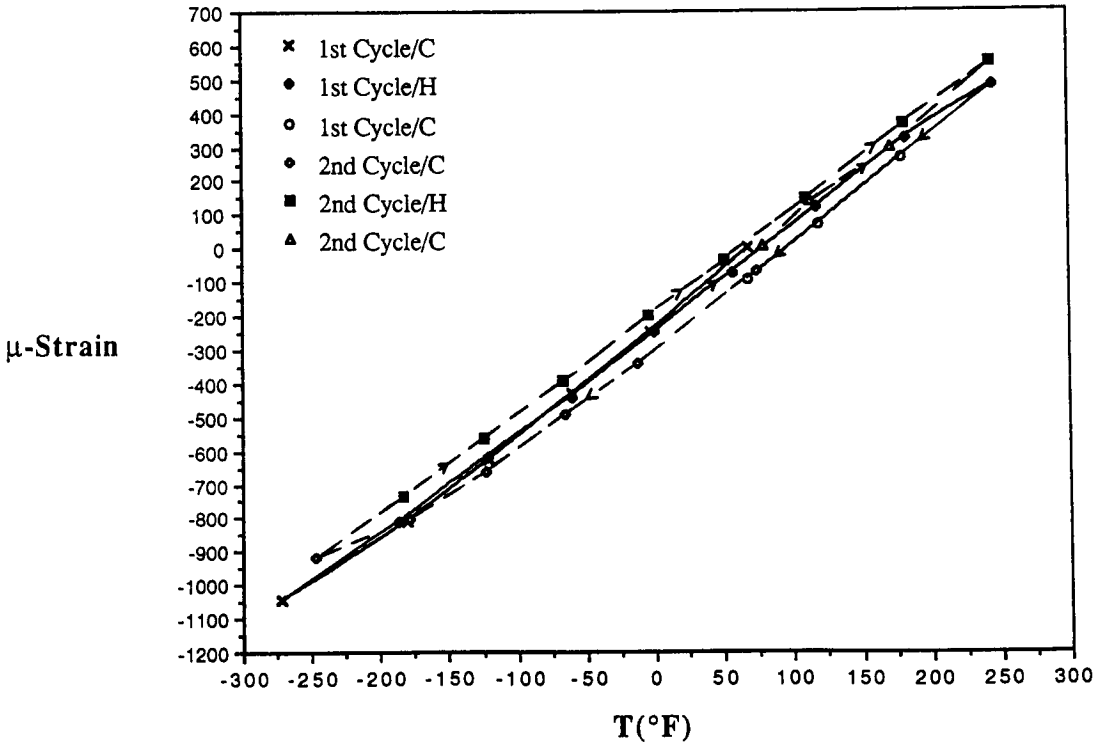

Fig. 9. Thermal expansion curves of the lab. control sample of GY70/201/2024 Gr/Al composites determined by laser interferometry.

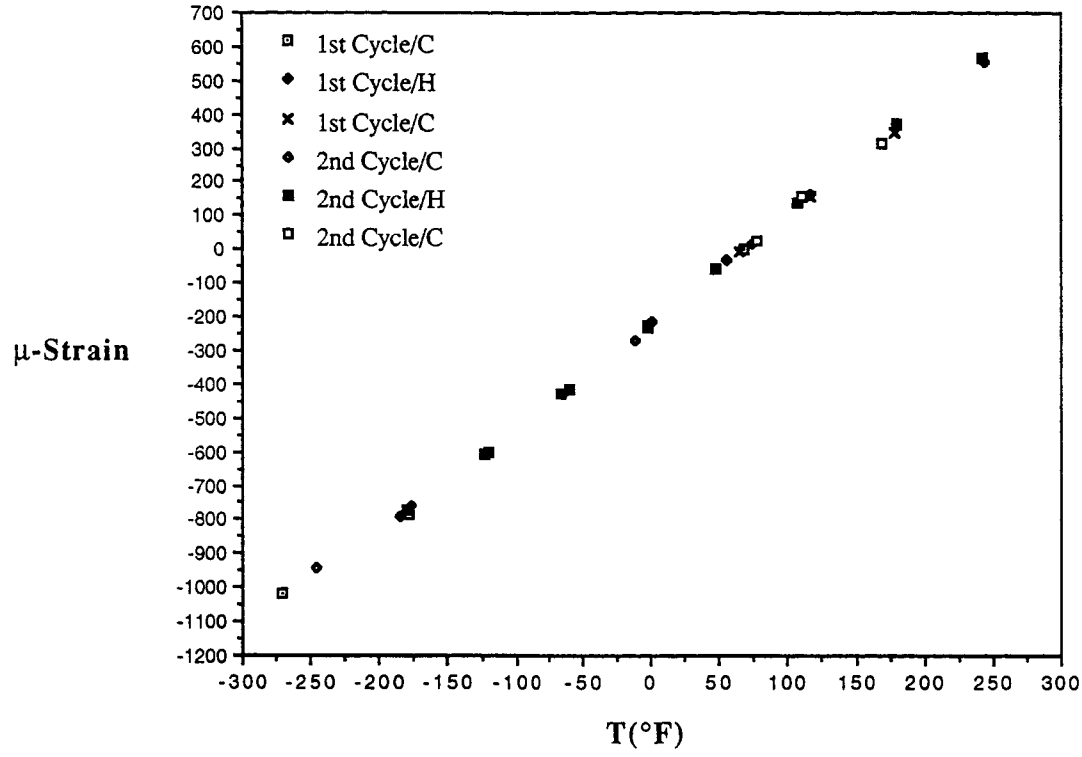

Fig. 10. Thermal expansion curves of the LE sample of GY70/201/2024 Gr/Al composites determined by laser interferometry.

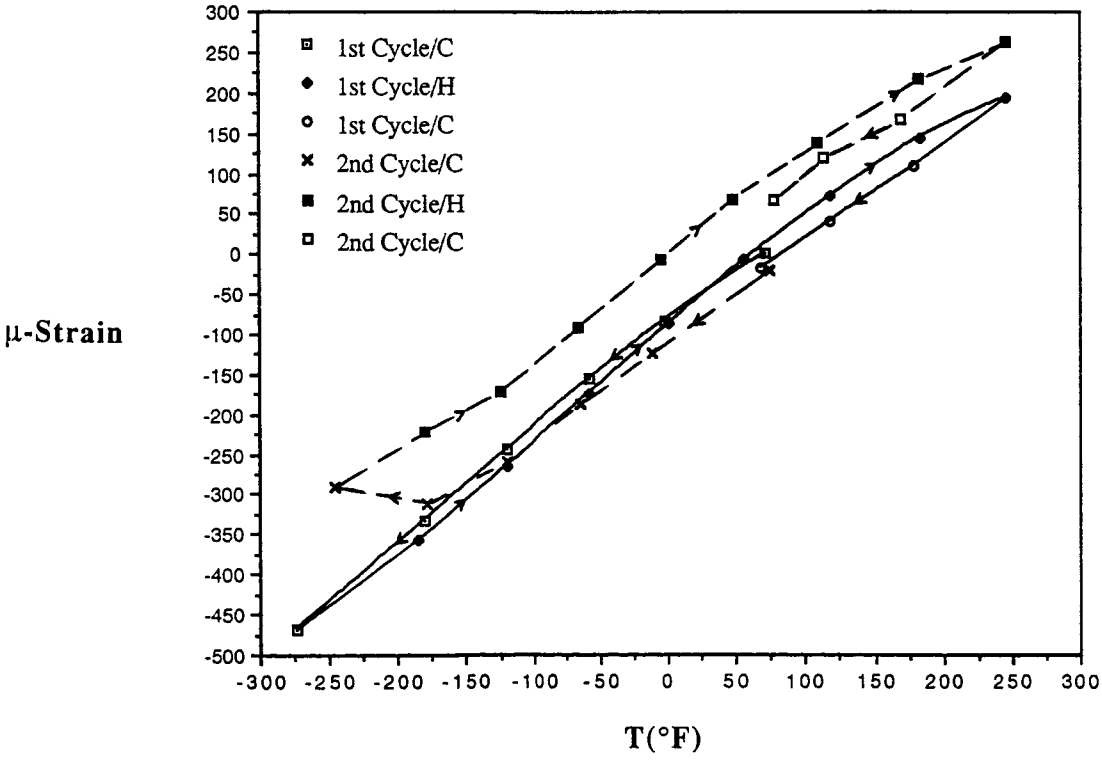

Fig. 11. Thermal expansion curves of the lab. control sample of P100/201/2024 (4-ply) Gr/Al composites determined by laser interferometry.

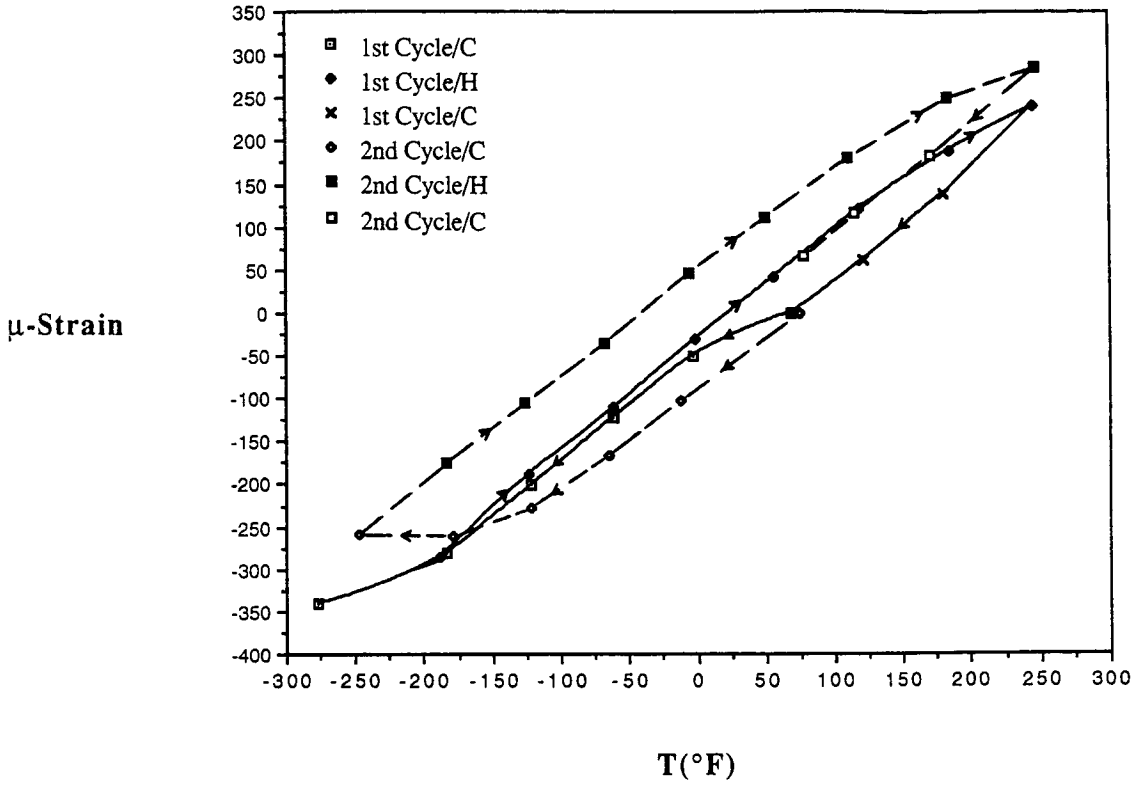

Fig. 12. Thermal expansion curves of the LE sample of P100/201/2024 (4 ply) Gr/Al composites determined by laser interferometry.

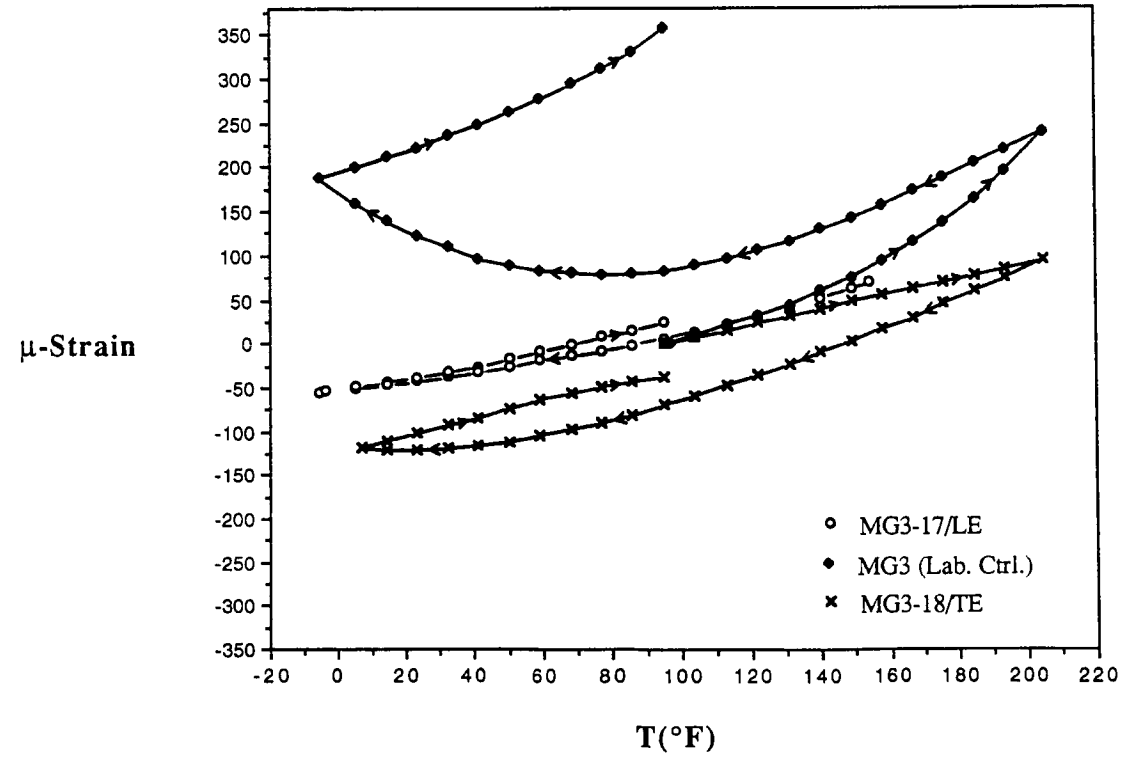

Fig. 13. Thermal expansion curves of the LE, TE, and lab. control sample of P100/EZ33A/AZ31B Gr/Mg composites determined by laser interferometry.

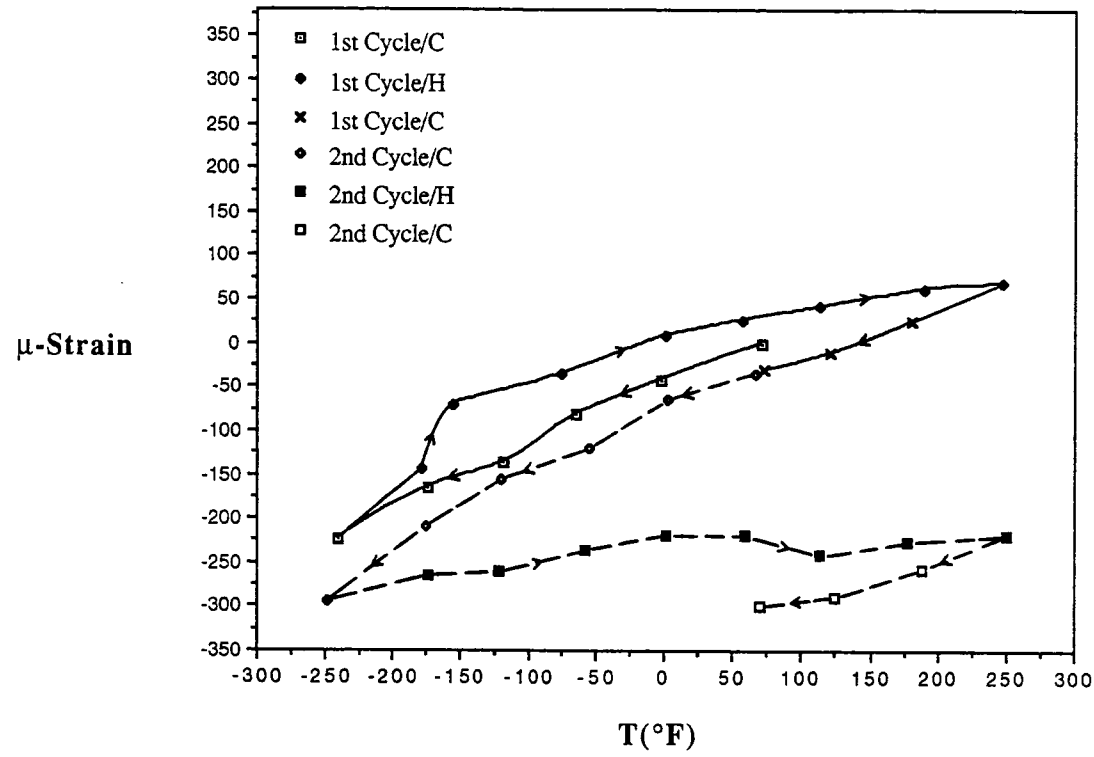

Fig. 14. Thermal expansion curves of the lab. control sample of P100/AZ91C/AZ61A Gr/Mg composites determined by laser interferometry.

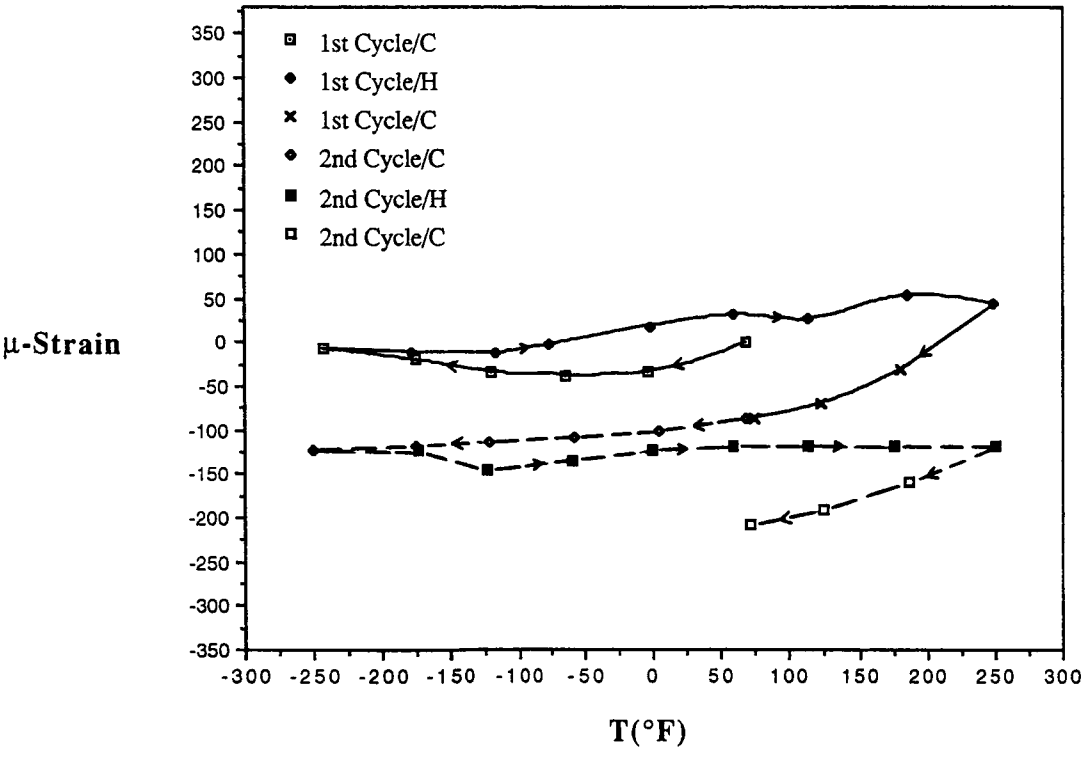

Fig. 15. Thermal expansion curves of the LE sample of P100/AZ91C/AZ61A Gr/Mg composites determined by laser interferometry.

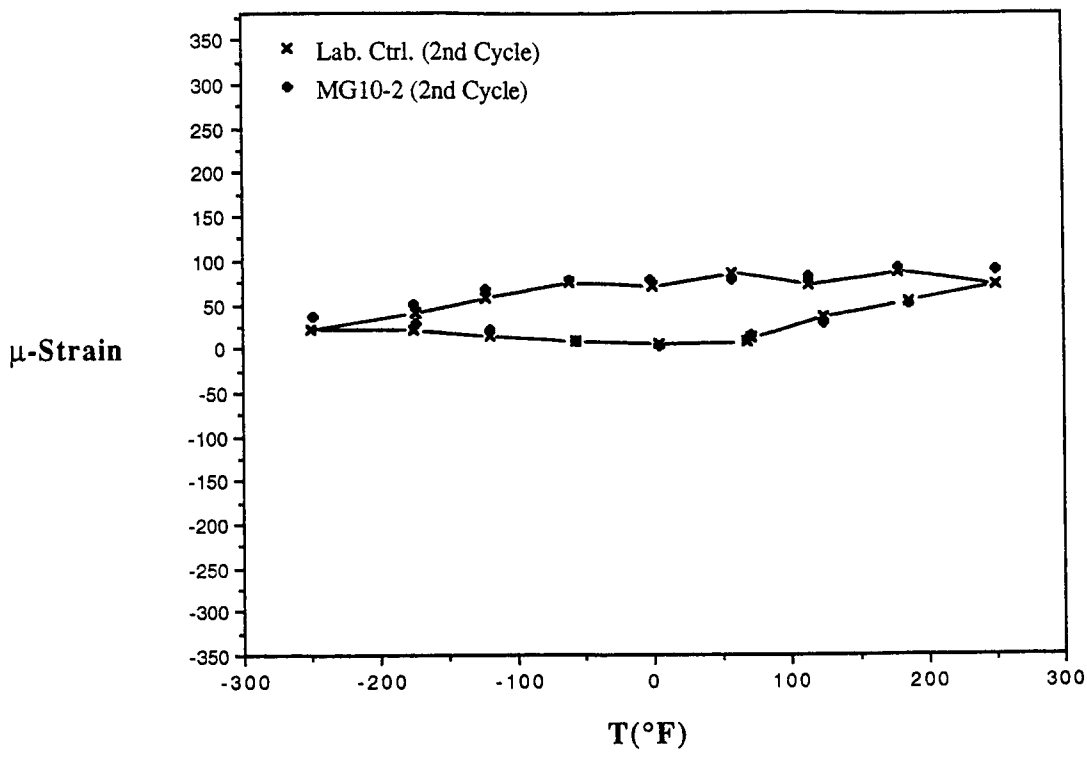

Fig. 16. Thermal expansion curves of the lab. control and LE sample of P100/AZ91C/AZ61A (4 ply) Gr/Mg composites determined by laser interferometry.

N93-28270

SPECTRAL INFRARED HEMISPHERICAL REFLECTANCE MEASUREMENTS FOR LDEF TRAY CLAMPS

B. K. Cromwell
Sverdrup Technology Inc., AEDC Group
Arnold Air Force Base, TN 37389
Phone: 615/454-3478, FAX: 615/454-4913

Capt. S. D. Shepherd
USAF, Directorate of Technology
Arnold Air Force Base, TN 37389
Phone: 615/454-6517, FAX: 615/454-3559

C. W. Pender
Sverdrup Technology Inc., AEDC Group
Arnold Air Force Base, TN 37389
Phone: 615/454-4649, FAX: 615/454-4913

B. E. Wood
Calspan Corporation/AEDC Operations
Arnold Air Force Base, TN 37389
Phone: 615/454-7719, FAX: 615/454-6348

SUMMARY

This paper describes infrared hemispherical reflectance measurements that were made on 58 chromic acid anodized tray clamps from LDEF. The measurements were made using a hemiellipsoidal mirror reflectometer with interferometer for wavelengths between 2-15 μm. The tray clamps investigated were from locations about the entire spacecraft and provided the opportunity for comparing the effects of atomic oxygen at each location. Our results indicate there was essentially no dependence on atomic oxygen fluence for the surfaces studied, but there did appear to be a slight dependence on solar radiation exposure. The reflectances of the front sides of the tray clamps consistently were slightly higher than for the protected rear tray clamp surfaces.

INTRODUCTION

The Long Duration Exposure Facility (LDEF) spent 5 years and 10 months in space. The experiments and materials on board have provided a wealth of data for determining long-term effects of space on materials. Many measurements have been made on the various

samples and surfaces returned to determine sources and effects of the contaminants that were experienced.

The measurements described herein were funded through the Office of the Secretary of Defense Central Test and Evaluation Investment Program - Project on Space Systems Aging Study (DD29) and Wright Laboratory Project DB72 for Surface Effects of Contamination.

This paper describes measurements that were made on 58 chromic acid anodized tray clamps removed from LDEF that were used for maintaining the experiments in place. Spectral infrared reflectance measurements were made for the clamps that were located in various positions about the spacecraft. These clamps were located externally and were used to hold the experiments in place. The reflectances of the front surfaces of the clamps were measured to determine the variation in surface contaminant with satellite location. Reflectance measurements of the rear surfaces for the clamps were made to provide a clean reference surface of the same material that was not externally exposed to space. Changes in reflectance of the tray clamps have been compared to atomic oxygen fluences (atoms/cm^2) incident at those locations. No correlation was observed. A decrease in infrared absorption for absorption bands near 2.9 and 6.2 μm was observed for the surfaces exposed to space, indicating that there was some surface change in the outer layer of the chromic acid anodized material. In all of the surfaces measured no evidence of contamination was observed from the spectral reflectance measurements made, and none of the samples showed evidence of the brown so-called "nicotine" stain that has been seen so prominently in other experiments.

Total emittance values (for an angle of 15 deg from the surface normal) were calculated for both the exposed (front side) and unexposed (back side) tray clamp surfaces. Only small differences (average of about 1 percent) were observed. The surface exposed to space generally exhibited an overall decrease in emittance (reflectance increase) as compared to the back side (shielded) of the tray clamp. The average change in emittance of the clamps located on the space end of the satellite was about a factor of 2 greater than the average for the other locations. The space end received the greatest amount of solar flux. It appears that for these clamps the solar incident flux had a greater effect on the emittance than did the atomic oxygen fluence.

REFLECTANCE MEASUREMENTS DESCRIPTION

It wasn't known beforehand whether the samples would reflect specularly or diffusely. Therefore, a technique for measuring combined specular and diffuse components was employed. An ellipsoidal mirror reflectometer approximately 12 in. in diameter (Ref. 1) was used for making the hemispherical reflectance measurements (Fig. 1). The reflectance measurement technique was improved through the use of a Fourier transform scanning (FTS) interferometer which allowed reflectance measurements to be made in a more timely fashion than was accomplished in Ref. 1 (Fig. 2). The ellipsoidal mirror is ground such that the two foci are located on the major axis (y axis in Fig. 1) and are separated by 2 in. At one focus, a blackbody is located to provide the diffuse hemispherical radiance. This radiation is collected by the hemiellipsoidal mirror and is focused at the second ellipsoid focus where the sample is located. The radiation emitted by the blackbody (temperature = 350°C) is chopped at a rate of approximately 0.5 Hz. The slow chopping rate allows the interferometer to scan the radiation reflected and emitted from the sample while the chopper is in the open position and only the emitted radiation from the sample when the chopper is in the closed position. By subtracting these two values, a

signal is obtained that is proportional to the sample reflected radiation. The interferometer views the sample through a hole in the mirror which is centered at an angle of 15 deg from the sample normal. After the reflected radiation from the test sample is measured, the tray clamp is then replaced with a gold mirror (reflectance ~ 0.98) and the measurements repeated. The tray clamp reflectance is determined by ratioing the sample signal to that obtained for the gold reference mirror since its reflectance is near unity.

The Fourier transform spectrometer used was a Block Model 197RS Michelson-type interferometer. The resolution used was 8 cm^{-1}. The FTS scan rate was synchronized with the chopper such that 20 scans were recorded for the chopper in the open position and then 20 scans when the chopper was in the closed position. The Fourier transform was executed after all of the 20 scans were coadded for each case. Measurements were made for both the tray clamp and the gold reference surface and the output values at each wavelength were ratioed to obtain the tray clamp spectral reflectance.

DESCRIPTION OF SAMPLES AND LDEF LOCATIONS

The samples consisted of 58 tray clamps which were taken from more than 700 total clamps on LDEF. The clamps were made of chromic acid anodized (CAA) aluminum. Measurements on other tray clamps have been previously investigated (Refs. 2-5). The locations of the samples on LDEF that were investigated in this study are listed in Table 1 and are shown in Fig. 3 for both forward and rear views of the LDEF satellite. In Fig. 3 the locations of the tray clamps used in this study are indicated by the dots at the various bay and row locations. In Table 1 the sample locations on the trailing edge (Rows 1-4) are listed. Similarly, rows 5-6 and 11-12 are grouped for the side locations, and rows 7-10 list the samples in the forward moving (ram) direction. Samples on the earth end of the satellite (Bay G) and for the space viewing end (Bay H) are also shown. The locations given in Table 1 are grouped in the same manner as for the reflectance data, which will be shown later.

RESULTS

Reflectance measurements were made on the LDEF tray clamps after they had been retrieved from space. Measurements were made on the front surface (exposed to space) and back surface (shielded from space effects) for each tray clamp. The reflectance data are shown in Figs. 4-10. The data have been grouped to include data from relatively high atomic oxygen incidence rate (Fig. 4) for all bay locations in rows 7-10, the lowest atomic oxygen rates (Fig. 5) for all bays in rows 1-4, for intermediate atomic oxygen rates for bays in rows 5,6 (Fig. 6) and in rows 11-12, (Fig. 7), and for trays located on the earth (G bay) and space (H bay) ends (Figs. 8-9). The atomic oxygen fluences are those provided in Ref. 3 (also presented in Table 2). The atomic oxygen fluence levels for rows 1-4 varied from 1.13E+03 up to 2.27E+17; for rows 5-6, 11-12 the levels varied from 3.73E+12 up to 5.43E+21; for rows 7-10, the levels varied from 1.12E+21 up to 8.74E+21; and for the earth and space ends, the levels were 3.05E+20 and 4.27E+20, respectively. There is some overlap in fluence levels between the 5-6, 11-12 category and the 7-10 category.

All reflectance curves for the 58 samples front and rear surfaces exhibited essentially the same spectral features which evidently are a result of the anodizing process. The major absorption band is located at 2.9 to 3.0 μm, and the depth of this band varied considerably

from clamp to clamp for both exposed and shielded surfaces. A weak absorption band is sometimes seen at 3.4 um and a relatively strong band appears in the 6.1- to 6.2-μm region. A shoulder in the reflectance curves is seen centered at approximately 9.0 μm and is followed by a broad spectral feature centered about 10.8 to 11.0 μm. The spectral feature at 4.3 um should be ignored, since this is caused by the variation in CO_2 concentration in the radiation path from measurement to measurement.

Figure 10 shows direct comparisons of the front and back surfaces for samples F02-1, D07-4, C06-7, and B12-1 which were typical samples from the trailing edge, side edges, and leading edge, respectively. Similarly, Fig. 11 shows comparisons of front and back sides of samples taken from the earth (Bay G) and space (H) viewing ends of LDEF. In comparing the results between the front surfaces and back surfaces for the same tray clamp, the major differences are seen in the depths of the absorption bands located in the vicinity of 6.1 μm. This band is believed to be a C=O band, which is a carbonyl band. In nearly all cases, the depth of this band is less for the front surface than for the rear surface. This indicates that the source for this absorption band is being removed as a result of its location on an exterior surface. This may be due to a reduction in the anodize film layer thickness as suggested in Ref. 2, or some form of bleaching mechanism. One interesting point is that there is no observable difference seen between the front and rear surface when the four categories of atomic oxygen fluences are considered. Even for the lowest atomic oxygen fluence levels, rows 1-4, (down by at least 16 orders of magnitude) it is seen that the 6.1-μm band has been reduced on the front surface. The C-H hydrocarbon band at 3.4 μm similarly is observed to be eliminated or reduced in intensity for the front surfaces, as compared to the rear surfaces. Again, this is observed for all row categories regardless of atomic oxygen fluence level.

The surfaces that showed the most spectral structure are the rear (or shielded) tray clamp surfaces indicating that essentially all of the spectral features seen were due to the anodizing process used in preparing the clamps. No evidence was seen on the external surfaces of the clamps of space-deposited silicones or hydrocarbon contaminants. Visually, all of the clamps appeared the same for both front (exposed) and rear (shielded) surfaces. None of the so-called "nicotine" brown stain or other forms of contaminant reported in Ref. 4-5 was observed on any of the clamps.

Effect of Space Exposure on Tray Clamp Emittance

To determine emittance effects, the total (wavelengths) emittance, $E(\theta = 15°)$ was determined for an incidence or view angle (θ) of 15 deg. The spectral emittance values (E_λ) were determined by subtracting the spectral reflectivity values from one, since $E_\lambda(\theta = 15°) = A_\lambda(\theta = 15°)$ where $A_\lambda(\theta = 15°)$ is the spectral absorptivity.

$$E_\lambda(\theta = 15°) = A_\lambda(\theta = 15°) = 1 - R_\lambda(\theta = 15°) \tag{1}$$

The spectral emittances measured were used with the blackbody emission curve for a temperature of 300 K, $B_\lambda(T = 300\ K)$ to determine the total emittance for each of the 58 samples, both front and rear surfaces. The expression used for calculating emittance is

$$E(\theta = 15°) = \frac{\int_{2.5}^{15.0} E_\lambda(\theta = 15°)\, B_\lambda(T = 300\ K)\, d\lambda}{\int_{2.5}^{15.0} B_\lambda(T = 300\ K)\, d\lambda} \tag{2}$$

The emittance values determined for all the surfaces measured are shown in Table 2 and are presented in **order of decreasing atomic oxygen fluence**. The atomic oxygen and sun exposure levels were taken from Ref. 6. By averaging all the emittance values for both front and back surfaces, it was found that the exposed surface emittance, at 15 deg from the surface normal, was 0.185 and the rear (shielded) surface was 0.197. This yields an average difference of (0.012) in emittance between front and back surfaces. In the LDEF Interim Report (Ref. 3) it is reported that only slight changes were observed in the ratio of the solar absorptance to surface emittance (a/e). At that time it was unknown if the changes were due to contamination or surface erosion. From the results of this investigation it would appear the change in a/e ratio is due more to surface change than deposition of contaminants. The changes observed indicate that the space-exposed surface reflectances of the clamps are increased, thereby decreasing the surface emittances. This, then, would cause an increase in the a/e ratios. This behavior, in principle, is consistent with the findings of Ref. 2 which reported a/e increases from 1 to 6 percent, depending on the clamp location. They reported that the largest change in a/e was observed on the space end (H bay).

The average change in emittance is calculated for each of the four atomic oxygen ranges presented in Table 2. There were 20 samples in the predominantly forward moving direction (Rows 7-12) where the atomic oxygen fluence was greater than 1×10^{21} atoms/cm2 and 15 samples on the predominantly trailing rows (1-6) where the AO fluence varied between 9×10^{4} and 3.9×10^{19}. The other sample locations were 11 on the space end (H bay) and 12 on the earth end (G bay) where the AO fluence was on the order of 10^{20}. The change in average emittance between front and rear surfaces for the space end clamps is seen to be 0.022, which is about double that for the entire spacecraft. The space end also received the greatest amount of sunlight (see Table 2) and apparently the sunlight affected the tray clamp emittances more than did the atomic oxygen. This trend was also observed in Ref. 2. However, the reflectance/emittance measurement uncertainty for the present study was $\pm$ 1 percent, which means the changes measured may not be statistically significant.

SUMMARY

Hemispherical infrared (2.5 to 15.0 μm) reflectance measurements have been made on 58 LDEF tray clamps after retrieval from 5 years and 10 months in space. These clamps were located externally and were used to hold the experiments in place. The reflectances of the front surfaces of the clamps were measured to determine the variation in surface contaminant with satellite location. Reflectance measurements of the rear surfaces for the clamps were made to provide a clean reference surface of the same material but not externally exposed to space. The reflectance measurements were made using a scanning interferometer with an ellipsoidal mirror reflectometer.

The results of this investigation show only slight differences between the exposed surfaces of the tray clamps and the shielded surfaces. Some evidence of surface cleaning was observed with absorption band intensities at 2.9 and 6.1 being reduced for the exposed surfaces. This cleaning didn't appear to be a strong function of the surface location relative to the ram direction and hence appeared to be independent of atomic oxygen fluence level.

Total emittances were determined for the individual tray clamp surfaces for a temperature of 300 K. The average emittance for the surfaces exposed to space was 0.185 and was 0.197 for the side that was shielded from space. This indicated a slight "cleaning" of the clamps exposed to space. The average difference in emittance for the front and rear

surfaces was −0.012 and agrees with the findings of Ref. 2. This change in emittance may have been a stronger function of sunlight hours than atomic oxygen exposure.

Overall, the relatively small changes observed in infrared reflectance and emittance of the chromic acid anodized aluminum surfaces for the 5 years + in space should be pleasing to designers who are considering the use of similar material for the Space Station Freedom.

REFERENCES

1. Wood, B. E., Pipes, J. G., Smith, A. M., and Roux, J. A., "Hemi-ellipsoidal mirror infrared reflectometer: development and operation," Applied Optics, Vol. 15, No. 4, April 1976, pp. 940-950.

2. Plagemann, Walter L., "Space Environmental Effects on the Integrity of Chromic Acid Anodized Coatings", NASA CP-3134 (Part 2), "LDEF -- 69 Months in Space", 1991, pp. 1023-1040.

3. Systems Special Investigation Group, Long Duration Exposure Facility, Interim Report, January 1991.

4. LDEF Materials Special Investigation Group (Bland Stein - Chairman), "Preliminary Report on LDEF-Related Contaminants," August 1990.

5. Crutcher, E.R. and Warner, K. J., "Molecular Films Associated With LDEF," NASA CP-3134 (Part 1), "LDEF -- 69 Months in Space," First Post-Retrieval Symposium, 1991, pp. 155-177.

6. Bourassa, Roger J., Gillis, James R., and Rousslang, K. W., "Atomic Oxygen and Ultraviolet Radiation Mission Total Exposures for LDEF Experiments," NASA Report Number 3134 - Part 2, "LDEF -- 69 Months in Space," First Post-Retrieval Symposium, 1991, pp. 643-662.

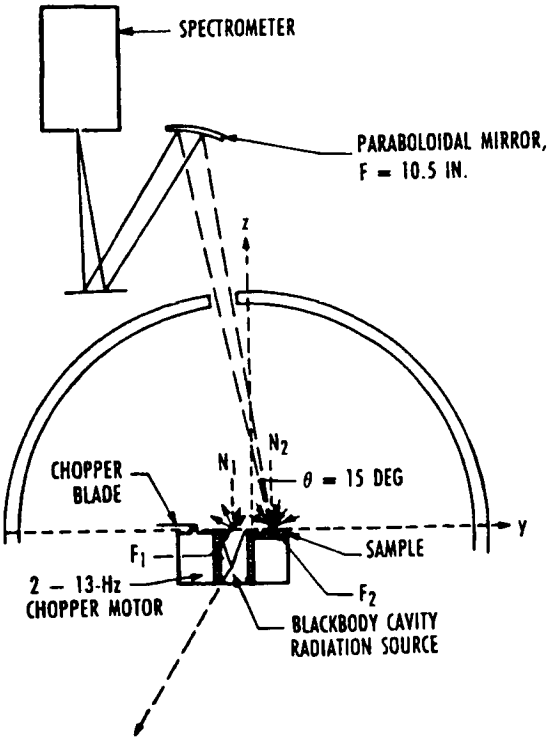

Figure 1. Experimental arrangement of hemiellipsoidal mirror reflectometer.

C-4

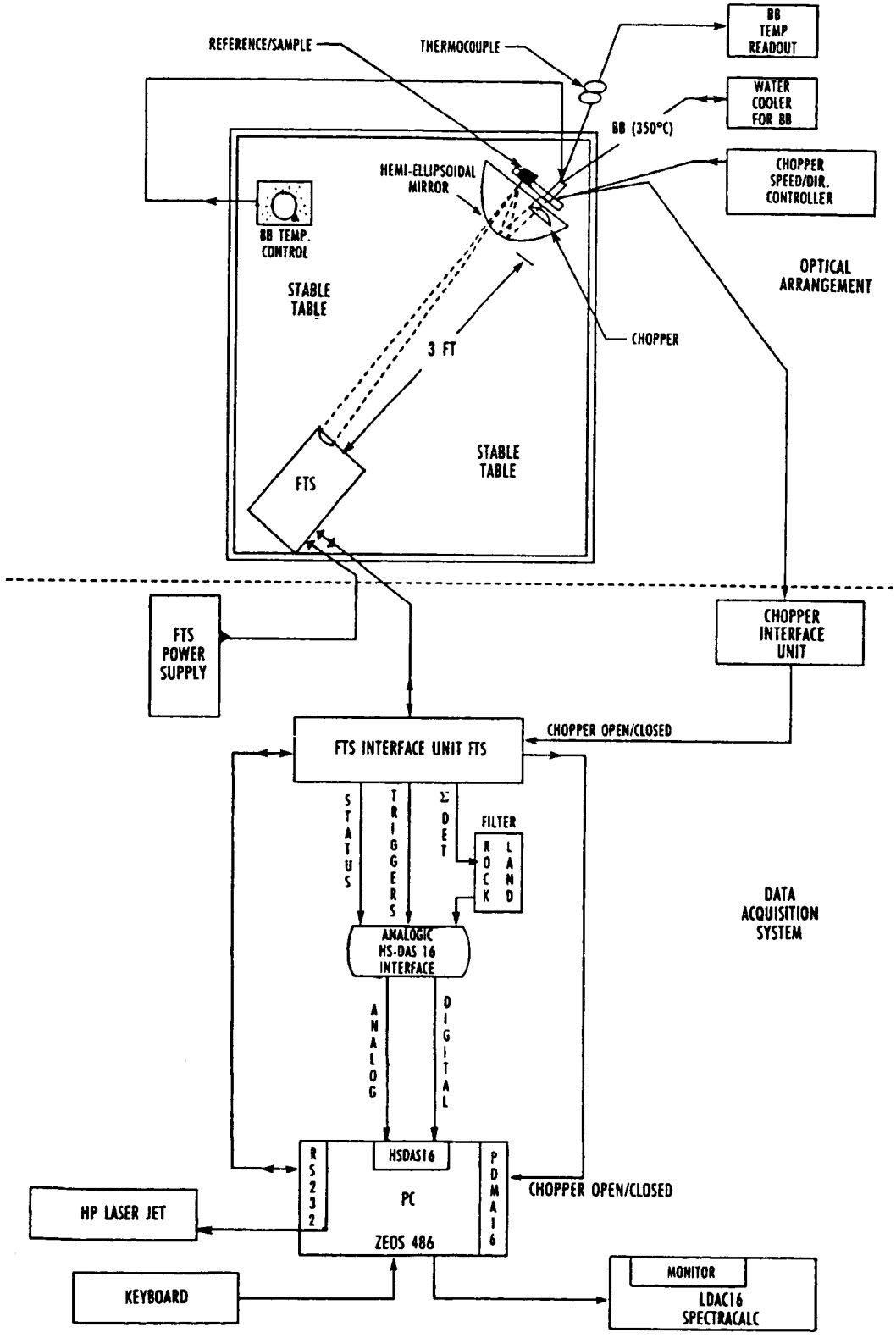

Figure 2. FTS interferometer interfaced with hemiellipsoidal mirror reflectometer.

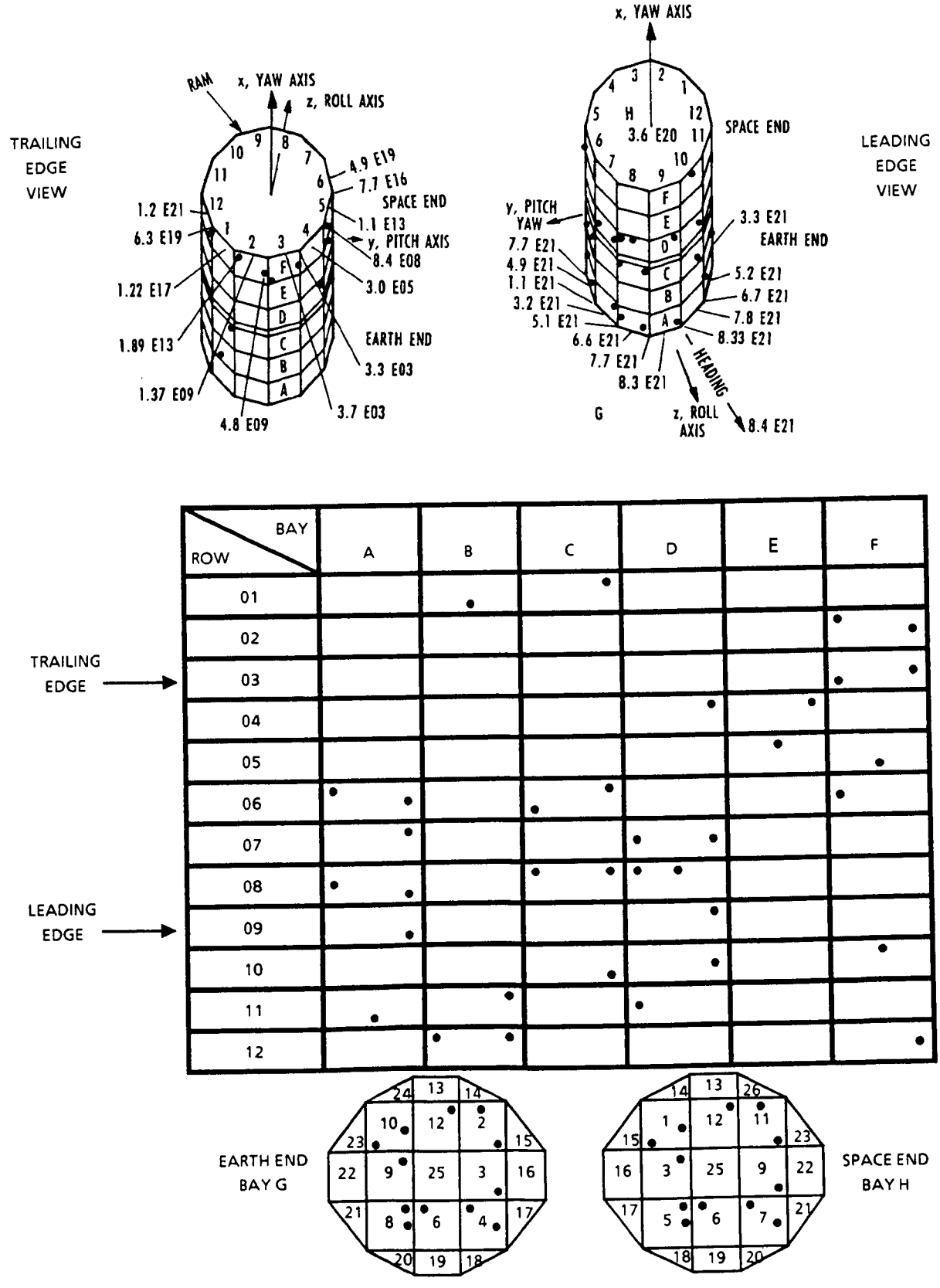

Figure 3. Location of LDEF tray clamps.

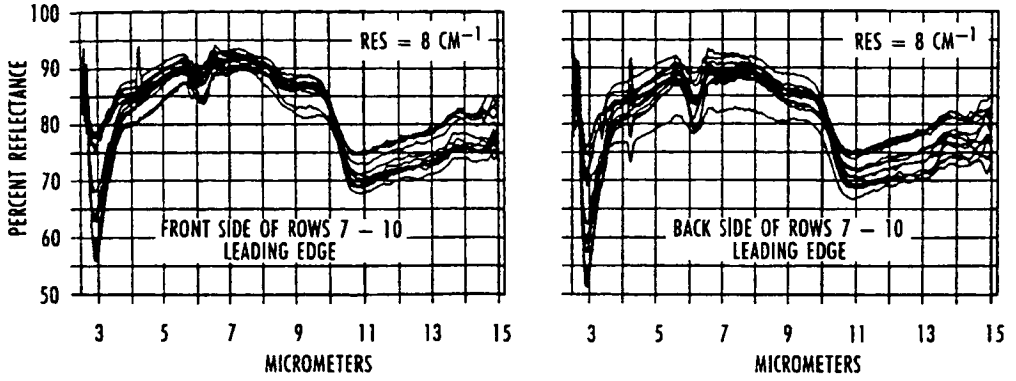

Figure 4. Tray clamp spectral reflectance, rows 7 - 10.

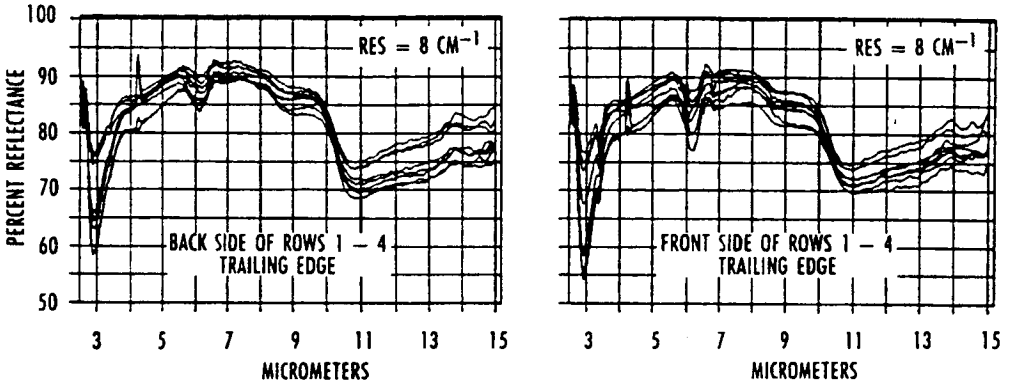

Figure 5. Tray clamp spectral reflectance, rows 1 - 4.

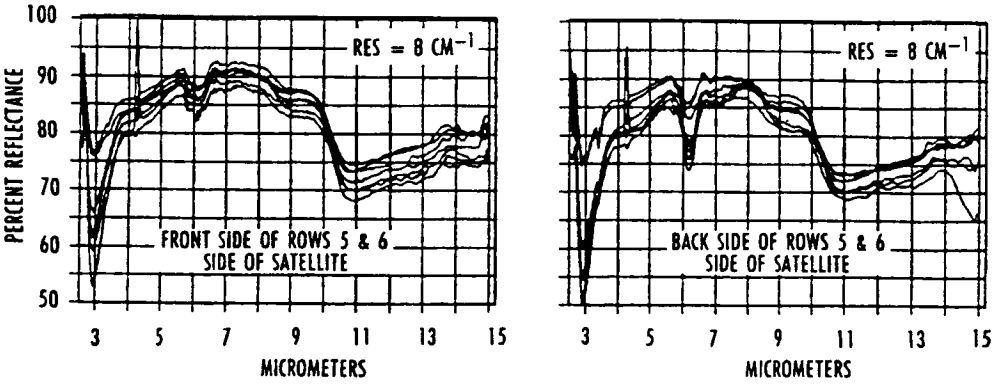

Figure 6. Tray clamp spectral reflectance, rows 5 - 6.

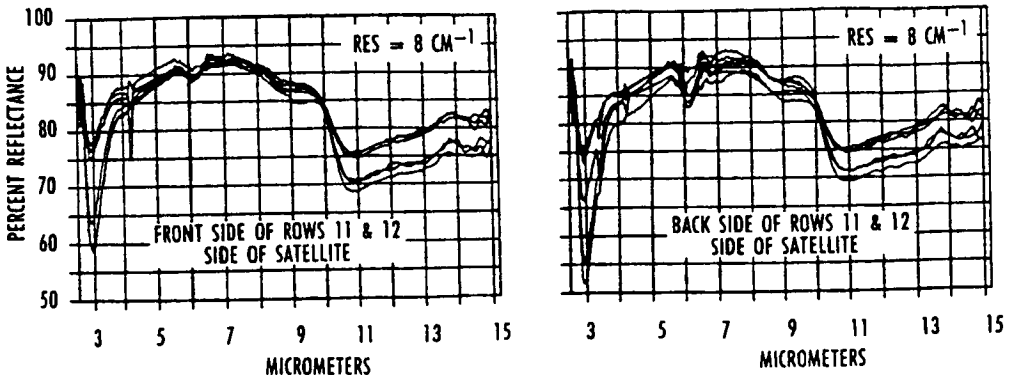

Figure 7. Tray clamp spectral reflectance, rows 11 - 12.

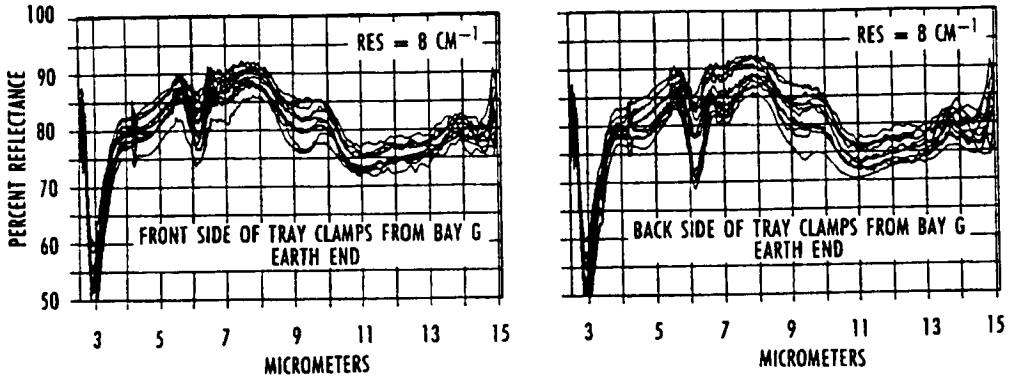

Figure 8. Tray clamp spectral reflectance, earth end.

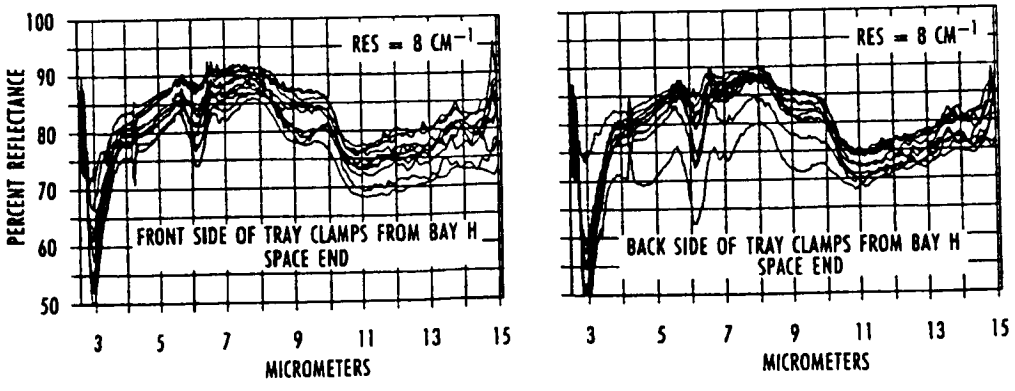

Figure 9. Tray clamp spectral reflectance, space end.

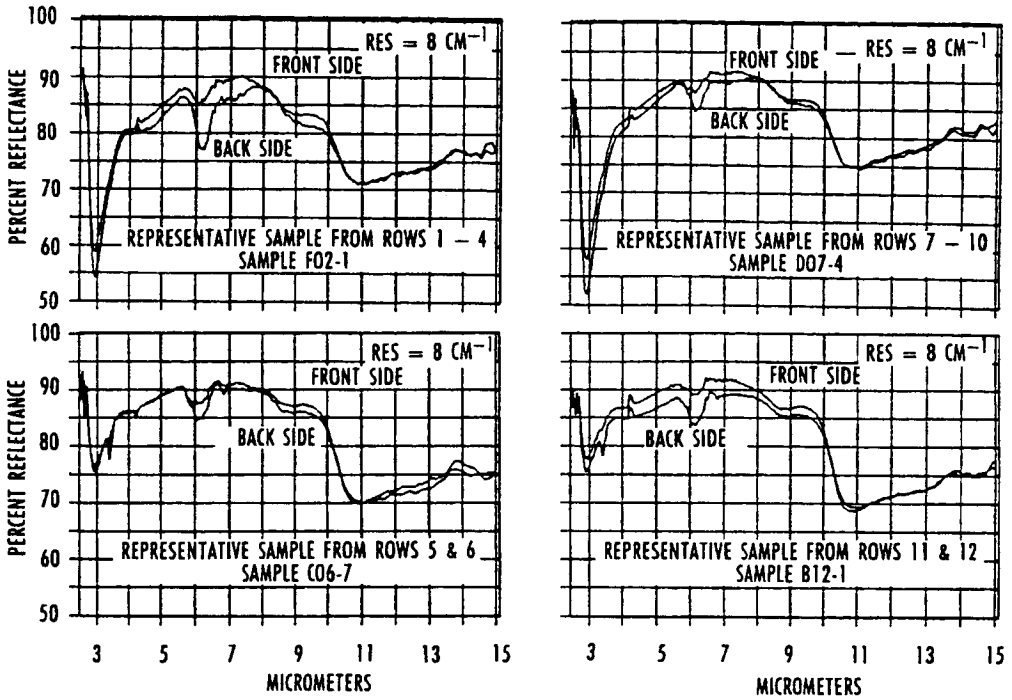

Figure 10. Comparisons of front and back surfaces for tray clamps located on leading edge, trailing edge, and sides of LDEF.

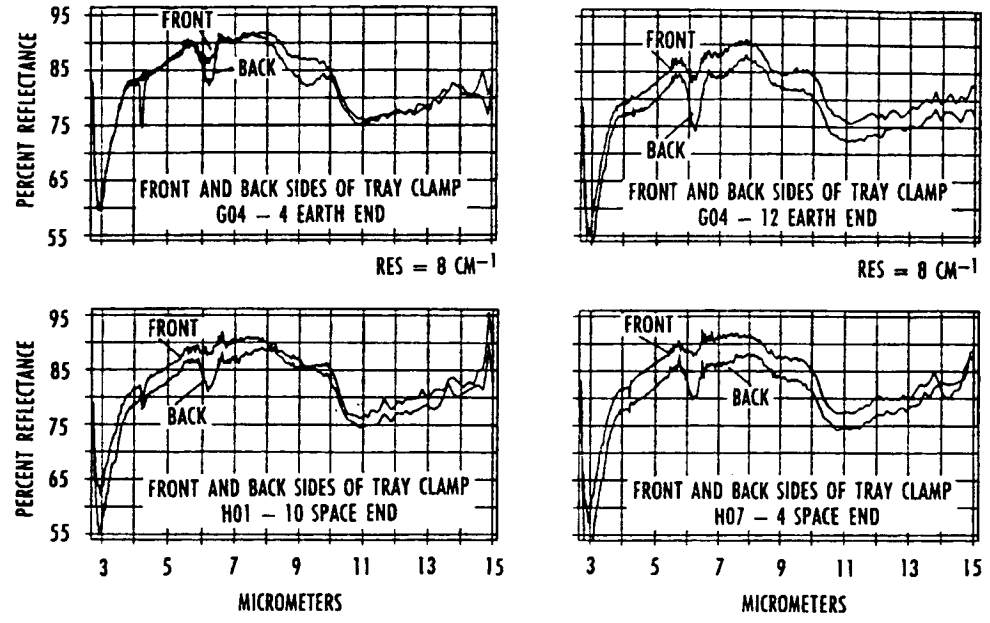

Figure 11. Comparisons of front and back surfaces for tray clamps located on space and earth viewing ends of LDEF.

Table 1. Locations of LDEF Tray Clamps

ROW 1-4	ROWS 5-6, 11-12	ROW 7-10	EARTH END	SPACE END
B01-6	A06-1	A07-3	G02-2	H01-5
C01-3	A06-4	A08-5	G02-7	H01-10
D04-3	A11-6	A08-8	G04-4	H03-4
E04-3	B11-3	A09-5	G04-10	H05-3
F02-1	B12-1	C08-1	G04-12	H05-5
F02-4	B12-3	C08-3	G06-3	H06-1
F03-4	C06-3	C10-5	G06-6	H07-1
F03-7	C06-7	D07-4	G08-3	H07-4
	D11-8	D07-8	G08-11	H09-7
	E05-2	D08-1	G10-1	H11-2
	F05-6	D08-2	G10-8	H12-4
	F06-8	D09-3	G12-7	
	F12-4	D10-4		
		F10-2		

Table 2. Total Emittance Values of LDEF Tray Clamps at 300 K and Atomic Oxygen Fluence (atoms/cm^2) Levels and Equivalent Sun Hours (Listed in order of Atomic Oxygen Fluence)

SAMPLE NO.	EMITTANCE FRONT	EMITTANCE BACK	EMITTANCE DIFF. (f-b)	AO FLUENCE*	SUN HOURS*
ROWS 7-12					
A09-5	0.208	0.205	+ 0.003	8.72E21	11,200
D09-3	0.205	0.203	+ 0.002	8.72E21	11,200
C10-5	0.194	0.199	– 0.005	8.17E21	10,700
D10-4	0.162	0.170	– 0.008	8.17E21	10,700
F10-2	0.172	0.166	+ 0.006	8.17E21	10,700
A08-5	0.204	0.199	+ 0.005	6.93E21	9,400
A08-8	0.161	0.170	– 0.009	6.93E21	9,400
C08-1	0.182	0.245	– 0.063	6.93E21	9,400
C08-3	0.173	0.172	+ 0.001	6.93E21	9,400
D08-1	0.198	0.211	– 0.013	6.93E21	9,400
D08-2	0.162	0.175	– 0.013	6.93E21	9,400
A11-6	0.158	0.166	– 0.008	5.43E21	8,500
B11-3	0.180	0.184	– 0.004	5.43E21	8,500
D11-8	0.165	0.181	– 0.016	5.43E21	8,500
A07-3	0.189	0.212	– 0.023	3.28E21	7,100
D07-4	0.165	0.172	– 0.007	3.28E21	7,100
D07-8	0.173	0.200	– 0.027	3.28E21	7,100
B12-1	0.194	0.203	– 0.009	1.28E21	6,800
B12-3	0.185	0.179	+ 0.006	1.28E21	6,800
F12-4	0.162	0.171	– 0.009	1.28E21	6,800
			AVG. – 0.01		
SPACE END					
H01-5	0.159	0.182	– 0.023	4.27E20	14,500
H01-10	0.158	0.180	– 0.022	4.27E20	14,500
H03-4	0.203	0.272	– 0.069	4.27E20	14,500
H05-3	0.200	0.210	– 0.010	4.27E20	14,500
H05-5	0.208	0.243	– 0.035	4.27E20	14,500
H06-1	0.208	0.208	0	4.27E20	14,500
H07-1	0.187	0.187	+ 0.003	4.27E20	14,500
H07-4	0.153	0.153	– 0.033	4.27E20	14,500
H09-7	0.215	0.215	+ 0.014	4.27E20	14,500
H11-2	0.190	0.190	0	4.27E20	14,500
H12-4	0.169	0.169	– 0.064	4.27E20	14,500
			AVG. – 0.022		

NOTES: *Ref. 6 — Bourassa and Gillis

Table 2. Concluded.

SAMPLE NO.	EMITTANCE FRONT	EMITTANCE BACK	EMITTANCE DIFF. (f-b)	AO FLUENCE*	SUN HOURS*
EARTH END					
A09-5	0.197	0.193	+ 0.004	3.05E20	4,500
D09-3	0.171	0.159	– 0.012	3.05E20	4,500
C10-5	0.174	0.164	+ 0.010	3.05E20	4,500
D10-4	0.194	0.194	0	3.05E20	4,500
F10-2	0.175	0.210	– 0.035	3.05E20	4,500
A08-5	0.217	0.241	– 0.024	3.05E20	4,500
A08-8	0.178	0.188	– 0.010	3.05E20	4,500
C08-1	0.164	0.159	+ 0.005	3.05E20	4,500
C08-3	0.222	0.215	+ 0.007	3.05E20	4,500
D08-1	0.208	0.218	– 0.010	3.05E20	4,500
D08-2	0.198	0.213	– 0.015	3.05E20	4,500
A11-6	0.212	0.216	– 0.004	3.05E20	4,500
			AVG. – 0.01		
ROW S1-6					
A06-1	0.211	0.231	– 0.020	3.89E19	14,500
A06-4	0.182	0.201	– 0.019	3.89E19	14,500
C06-3	0.207	0.193	+ 0.014	3.89E19	14,500
C06-7	0.190	0.198	– 0.008	3.89E19	14,500
F06-8	0.164	0.192	– 0.028	3.89E19	14,500
B01-6	0.156	0.207	– 0.051	2.27E17	14,500
C01-3	0.187	0.189	– 0.002	2.27E17	14,500
F02-1	0.200	0.211	– 0.011	1.54E17	14,500
F02-4	0.166	0.178	– 0.012	1.54E17	14,500
F03-4	0.170	0.163	+ 0.007	1.32E17	14,500
F03-7	0.196	0.198	– 0.002	1.32E17	14,500
E05-2	0.170	0.191	– 0.021	3.73E12	14,500
F05-6	0.188	0.204	– 0.016	3.73E12	14,500
D04-3	0.204	0.205	– 0.001	9.32E04	14,500
E04-3	0.201	0.205	– 0.004	9.32E04	14,500
			AVG. – 0.01		
AVERAGE	**0.185**	**0.197**	**– 0.012**		

NOTES: *Ref. 6 — Bourassa and Gillis

N93-28271

SURFACE CHARACTERIZATION OF SELECTED LDEF TRAY CLAMPS

T.F. Cromer, H.L. Grammer and J. P. Wightman
Virginia Polytechnic Institute and State University
Department of Chemistry
Blacksburg, VA 24061
Phone: 703/231-5854 Fax: 703/231-3971

P.R. Young and W.S. Slemp
NASA Langley Research Center
Hampton, VA 23665-5225
Phone: 804/864-4265 Fax: 804/864-8312

SUMMARY

The surface characterization of chromic acid anodized 6061-T6 aluminum alloy tray clamps has shown differences in surface chemistry depending upon the position on the LDEF. Water contact angle results showed no changes in wettability of the tray clamps. The overall surface topography of the control, trailing edge(E3) and leading edge(D9) samples was similar. The thickness of the aluminum oxide layer for all samples determined by Auger depth profiling was less than one micron. XPS analysis of the tray clamps showed significant differences in the surface composition. Carbon and silicon containing compounds were the primary contaminants detected.

INTRODUCTION

One of the tasks of the MSIG (Materials Special Investigation Group) is the detailed analysis of the chromic acid anodized 6061-T6 aluminum alloy tray clamps. These tray clamps were located at regular intervals over the entire LDEF frame and were exposed to varying amounts of atomic oxygen and vacuum ultraviolet radiation.

A detailed study of the relatively small but statistically significant changes in the optical properties of 228 anodized clamps has been reported [1]. However, there has been no systematic study reported of the effect of low-earth orbit (LEO) environment on the surface chemistry of these clamps.

The objective of this work was to document changes in the surface chemistry of tray clamps taken from different locations on LDEF. Surface characterization of the anodized aluminum clamps using contact angle measurements, scanning electron microscopy (SEM), energy dispersive spectroscopy (EDS), Auger electron spectroscopy (AES), and x-ray photoelectron spectroscopy (XPS) is reported.

EXPERIMENTAL

The surface analytical techniques used in the characterization of the surface of the seven anodized aluminum tray clamps (control and six flight) are described below. Tray clamps were cut manually to prevent heating of the sample as well as possible contamination of the surface when cutting. Typical sample sizes were 13mm x 13mm. Surface characterization techniques were used in the following order due to the nondestructive/destructive aspects of the analyses: XPS, SEM/EDS and AES. Water contact angle measurements were made to evaluate the wettability of the aluminum surface using a Rame-Hart 100-00115 NRL goniometer equipped with a video monitor. Different samples were used for the contact angle measurements.

Surface topography was examined by scanning electron microscopy using an ISI-SX-40 microscope operating at 20kV beam voltage. Near surface/bulk (1-5mm) elemental analysis was performed using a Tracor Northern energy dispersive spectrometer. Auger electron spectroscopy-depth profiling was performed on a Perkin-Elmer PHI-610 spectrometer operating at an electron beam voltage/current of 3kv/0.05mA and an argon ion beam voltage/current of 4kV/20mA. X-ray photoelectron spectroscopy was performed utilizing a Perkin-Elmer PHI 5400 spectrometer equipped with a Mg Ka X-ray source (1253.6eV), operating at 15kV/120mA.

The flight samples were located at the following positions on the LDEF: E3 (trailing edge), B4 (near trailing edge), D7 (near leading edge), D9 (leading edge), H9 (space end), and G2 (earth end).

RESULTS/DISCUSSION

Contact Angle

Water contact angle measurements were used to evaluate the wettability of the clamp surface. The results are listed in Table I. An average water contact angle of 62° was calculated for the seven samples independent of location. The high water contact angles on the clamps are indicative of low energy surfaces such as polymers [2]. A near zero contact angle would be expected for a clean anodized aluminum surface [3]. As shown by the results, no changes in wettability of the clamps were observed due to exposure to the low-earth orbit environment.

Scanning Electron Microscopy/Energy Dispersive Spectroscopy

SEM photomicrographs of the control, leading (D9) and trailing (E3) edge samples are shown in Figure 1. The overall surface topography of the three samples is similar. No significant change in the surface topography was evident for the leading compared to the trailing edge samples.

Energy dispersive spectroscopy(EDS) is a near surface/bulk elemental analysis technique. The EDS results for the tray clamps are listed in Table II. An average composition of fifty-two weight percent aluminum and forty-eight weight percent oxygen was determined for the three samples. These results are consistent with the calculated weight percent of aluminum(53%) and oxygen(47%) for Al_2O_3. Aluminum and oxygen were the only elements detected by EDS in the sampling depth of 1-5mm.

Auger Electron Spectroscopy

Auger depth profiling was used to determine the thickness of the oxide layer on five of the clamps. The depth profile of the space end (H9) sample is shown in Figure 2 which is representative of the other samples. The thickness of the aluminum oxide layer was calculated at the time when the oxygen and aluminum signals cross. Aluminum with an oxide layer of known thickness was used as a standard to determine the sputtering rate. Aluminum oxide thickness values are listed in Table III. The average thickness of 0.82 mm is consistent with the results of Plagemann [1] who concluded from SEM measurements that the oxide thickness was <1mm. The range in oxide thickness from 0.6 to 1.0 mm for the trailing edge (E3) and space end (H9) samples respectively can not be attributed to the LEO environment but in fact may be a result of variation in the anodization conditions.

X-Ray Photoelectron Spectroscopy

The XPS results shown in Table IV for the LDEF tray clamps are reported as binding energy (B.E.) in eV and atomic concentration (A.C.) in %. All photopeaks were referenced to the C 1s photopeak taken at 285.0 eV. The largest amount (53%) of carbon-containing organic contamination was detected on the control sample. However, significant quantities of this same contamination were found on all the LDEF tray clamps. There is no discernible correlation of the surface atomic concentration of carbon with clamp position. This carbon contamination as determined by XPS is indicative of a hydrophobic surface and is consistent with the high water contact angles determined on the same surfaces (see Table I). If the control surface were clean, the expected atomic concentration of aluminum and oxygen for a 1mm aluminum oxide (Al_2O_3) surface layer would be 40% and 60% respectively; and, the O/Al atomic concentration ratio would be 1.5. The fact that the atomic concentration of aluminum is only 11% is prima facie evidence that an ultra-thin layer of carbon-containing organic contamination covers the aluminum oxide surface. The thickness of these contamination layers cannot be more than 5 nm otherwise no aluminum signal would have been detected. The fact that the O/Al ratio is nearly 3 also suggests that this contamination layer contains oxygen in addition to carbon. It is recognized that some of the excess oxygen is probably associated with the silicon which was also detected on the control sample. The sources of the small quantities of nitrogen, sulfur and sodium detected on the control sample were not identified.

It is noteworthy that the silicon content of all flight samples exceeded that of the control sample form 4 to 16 times. Thus, these XPS results further support the case for extensive silicon contamination of the LDEF clamps [4]. Again, there was no discernible correlation of the surface atomic concentration of silicon with clamp position. On the other hand, there was definitive shift in the binding energy of silicon on the clamps (D7, D9, H9,G2) which received a higher atomic oxygen fluence compared to those clamps (E3, B4, control) receiving a lower atomic oxygen fluence. This definitive shift in binding energy of $1.1_8 \pm 0.1_7$ correlates to a change in the state of silicon contamination. The organo-silicon (lower B.E.) material contained in the contamination on the clamps subjected to a higher atomic oxygen fluence was converted to an inorganic-silicon (higher B.E.) or silicate type material. Such an effect of atomic oxygen on organo-silicon material has been noted previously [5].

The fluorine contamination detected on all the flight samples is in the form of inorganic fluorine (fluoride) with a binding energy of 686 eV. In contrast, the binding energy of fluorine in a fluoropolymer is approximately 689 eV. The fluorine contamination present in the ion

form may be a result of the degradation effects of vacuum ultraviolet radiation on the carbon-fluorine bonds of fluoropolymers such as fluoroethylene propylene copolymer (FEP) on the backside of the satellite.

Trace amounts of sulfur, nitrogen and sodium contamination were present on the majority of the flight samples as well as the control. The source of the contamination may be a result of preflight or post flight handling.

ACKNOWLEDGEMENTS

The authors (T.F.C., H.L.G. and J.P.W.) acknowledge the support of this research under NASA Grant NAG-1-1186.

REFERENCES

[1] Walter L. Plagemann: *Space Environmental Effects on the Integrity of Chromic Acid Anodized Coatings.* LDEF 69 Months in Space First Post-Retrieval Symposium, NASA CP-3134, Part 2, p. 1023-1040, Jan. 1992.

[2] M. Yekta-Fard and A.B. Ponter, *J. Adhesion Sci. Technol.*, 6, 253 (1992).

[3] William C. Wake, *Adhesion and the Formulation of Adhesives* (Applied Science Publishers, NY 1982) p. 52.

[4] E.R. Crutcher and K.J. Warner: *Molecular Films Associated with LDEF.* LDEF 69 Months in Space First Post-Retrieval Symposium, NASA CP-3134, Part 1, p. 155-177, Jan. 1992.

[5] B.A. Bank, Joyce A. Dever, Linda Gebauer and Carol M. Hill: *Atomic Oxygen Interactions with FEP Teflon and Silicones on LDEF.* LDEF 69 Months in Space First Post-Retrieval Symposium, NASA CP-3134, Part 2, p. 801-816, Jan. 1992.

TABLE I

WATER CONTACT ANGLES ON LDEF TRAY CLAMPS

SAMPLE LOCATION	θw
Control	61°
E3	64°
B4	66°
D7	63°
D9	66°
H9	63°
G2	54°

TABLE II

ENERGY DISPERSIVE ANALYSIS OF LDEF TRAY CLAMPS

SAMPLE	ALUMINUM (wt%)	OXYGEN (wt%)
Control	54.	46.
E3	53.	46.
D9	49.	50.

TABLE III

THICKNESS OF OXIDE LAYER ON LDEF TRAY CLAMPS

SAMPLE	τ(nm)
Control	785
E3	1005
D9	865
H9	765
G2	665

TABLE IV

XPS ANALYSIS OF LDEF TRAY CLAMPS

	SAMPLES						
PHOTOPEAKS	Control	E3	B4	D7	D9	H9	G2
C1s A.C. (%)	53.2	27.8	28.0	16.5	20.7	16.6	30.0
B.E. (eV)	285.0	285.0	285.0	285.0	285.0	285.0	285.0
Al2p	11.4	17.6	15.8	17.0	4.9	15.8	8.2
	74.6	74.7	74.6	74.6	74.8	74.6	74.7
O1s	31.0	46.8	47.2	53.4	51.1	52.4	43.5
	532.2	532.3	533.1	532.4	533.0	532.5	532.6
Si2p	1.4	6.0	6.1	10.5	22.6	11.0	13.1
	102.2	102.1	102.2	103.2	103.6	103.3	103.4
N1s	1.8	0.6	1.3	0.3	--	0.3	1.4
	399.9	400.2	400.2	400.6		400.1	400.4
S2p	0.6	0.3	0.4	0.3	--	0.9	--
	169.0	169.5	169.6	169.6		169.5	
Na1s	0.7	0.6	0.7	0.7	--	1.4	1.5
	1072.2	1072.8	1073.0	1072.8		1072.9	1072.7
F1s	--	0.3	0.5	1.5	0.7	1.5	2.4
		686.3	686.4	686.1	686.5	686.5	686.6

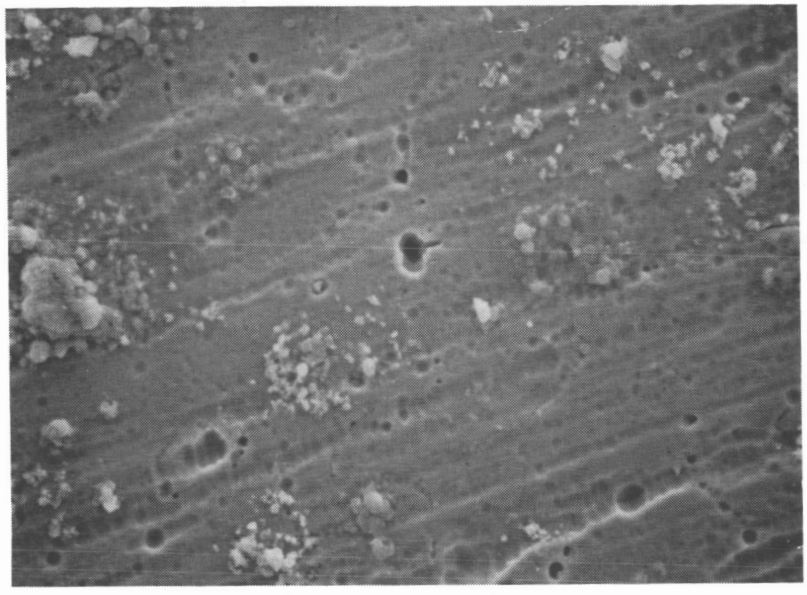

CONTROL 0.5 KX

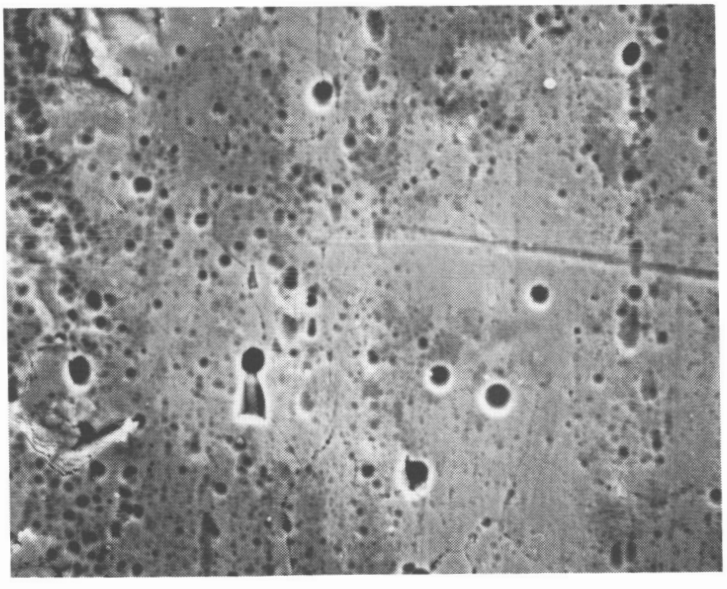

E3 0.5 KX

FIGURE 1: SEM PHOTOMICROGRAPHS OF LDEF TRAY CLAMPS.

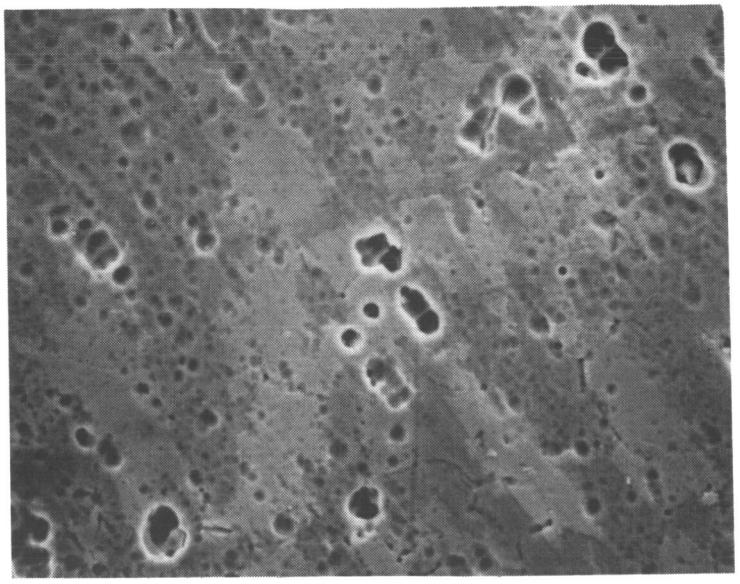

D9 0.5 KX

FIGURE 1: CONCLUDED.

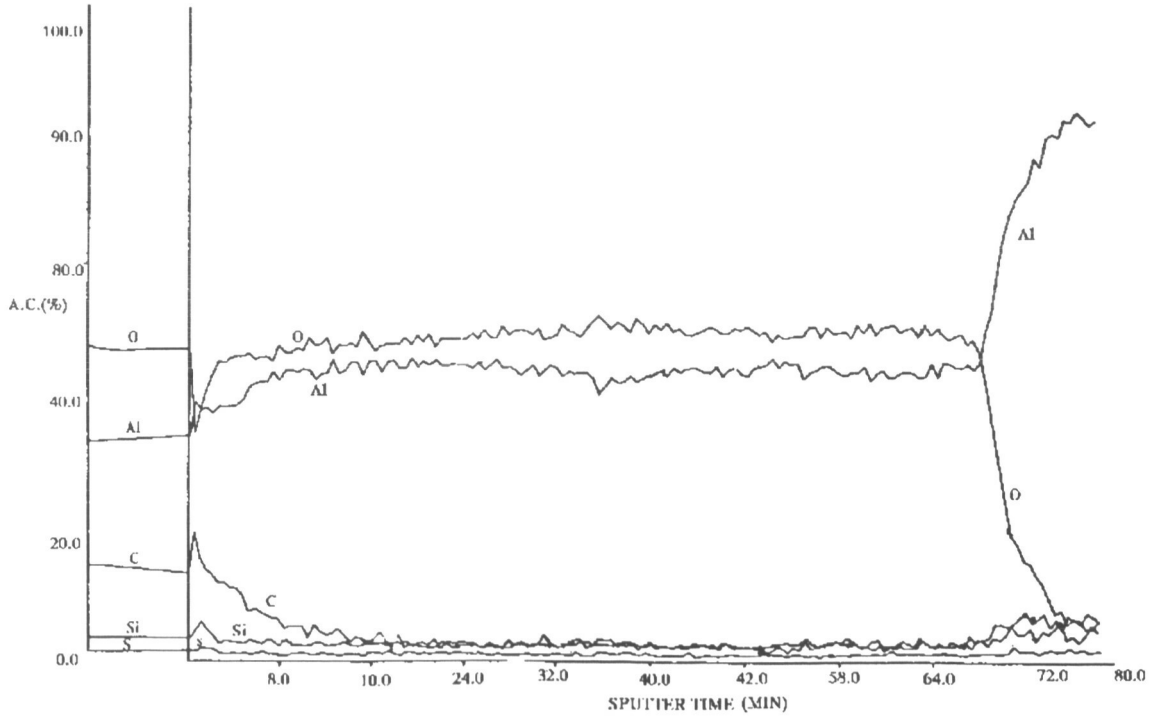

FIGURE 2: AUGER DEPTH PROFILE OF LDEF TRAY CLAMPS.

N93-28272

CONTAMINATION ON LDEF: SOURCES, DISTRIBUTION, AND HISTORY

Gary Pippin and Russ Crutcher
Boeing Defense & Space Group
Seattle, WA 98124-2499
Phone: 206/773-2846, Fax: 206/773-4946

In this paper we present an introduction to contamination effects observed on the Long Duration Exposure Facility (ref 1). The activities reported here are part of Boeing's obligation to the LDEF Materials Special Investigation Group (ref 2).

The contamination films and particles had minimal influence on the thermal performance of the LDEF. Some specific areas did have large changes in optical properties. Films also interfered with recession rate determination by reacting with the oxygen or physically shielding underlying material. Generally, contaminant films lessen the measured recession rate relative to "clean" surfaces. On orbit generation of particles may be an issue for sensitive optics. Deposition on lenses may lead to artifacts on photographic images or cause sensors to respond inappropriately. Particles in the line of sight of sensors can cause stray light to be scattered into sensors. Particles also represent a hazard for mechanisms in that they can physically block and/or increase friction or wear on moving surfaces.

LDEF carried a rather complex mixture of samples and support hardware into orbit(ref. 3) The experiments were assembled under a variety of conditions and time constraints and stored for up to five years before launch. The structure itself was so large that it could not be baked after the interior was painted with chemglaze Z-306 polyurethane based black paint. Any analysis of the effects of molecular and particulate contamination must account for a complex array of sources, wide variation in processes over time, and extreme variation in environment from ground to launch to flight. Surface conditions at certain locations on LDEF were established by outgassing of molecular species from particular materials onto adjacent surfaces, followed by alteration of those species due to exposure to atomic oxygen and/or solar radiation.

Venting during ascent and prior to development was the initial opportunity for large scale mass transfer of volatile species. Distinct layers of materials in selected areas is evidence of short term variation in outgassing rates as LDEF traversed the earth shadow during each orbit. Over the long term the rate may be altered as the materials degrade under exposure to the space environment. Solar ultraviolet radiation(UV), and in leading edge locations, atomic oxygen exposure, affect the long term state of the outgassed deposits.

The environmental exposures also varied over time with short wavelength radiation intensity about 50% to 100% greater at the end of the mission relative to the start. The relative increase was even greater for certain wavelengths. A majority of the oxygen exposure occurring in the last six months.

Figure 1 is a schematic mission time line to define the types of exposure. Time periods 1,6,8, and 10 are ground environments, and 3 and 4 are deployment from, and retrieval by, the shuttle. The mission may be usefully divided into three categories of contamination exposure periods. First, the preflight exposures include all the ground based processing, which created particles and films which were subsequently carried into orbit. Second, the on-orbit exposure, venting, outgassing and deposition, and subsequent degradation produced new particles and films whose composition varied with time. Third, the post flight environments included additional particulate deposition, moisture absorption, and molecular

film formation. Events during the first two periods must be evaluated for their effects on spacecraft performance. The third time period, post flight exposure, is not typical for payloads because most spacecraft are not retrieved. Therefore contamination from this time period must be viewed simply as an artifact to be factored out of analysis of material performance in flight.

Contamination sources can be grouped according to particulates, and two types of molecular sources, carbon based films and silicone based films. Particulate sources include fibers, pollen, dust, manufacturing debris and salt deposits from ground operations and exposures. While individual items certainly caused profound effects on a local microscopic scale, particulate sources did not have a significant effect on the overall thermal control performance of the satellite and its systems. The level of surface particulate contamination was extensive enough to be of concern for spacecraft with optical sensors.

Sources of carbon based molecular films include paint solvents, polymeric thin films, and organic composite materials, which outgassed on-orbit, as well as organic dust and solvent present during manufacturing, or used for cleaning, such as cetyl alcohol used a lubricant for bolts and alcohols used to wipe down surfaces.

Potential silicone based film sources include as manufactured coating on support hardware, adhesive materials, coatings on test specimens, solar cells, paints, and the orbiter.

The final disposition of contaminant films was determined by the specific on-orbit conditions at each location. Two types of competing processes are occurring. Removal is possible by thermal cycling and/or oxidation to volatile species. Simultaneously, fixing of selected contaminant species in place by UV induced bond rupture, and crosslinking between polymer chains, oxidation to non volatile species.

The end of mission surface products which remain are thermodynamically stable, non-volatile materials or species which are physically trapped by silica coatings formed by oxidation of outgassed siloxanes. The trapped species have likely undergone change due to UV subsequent to deposition onto the exposed surfaces.

There were major differences in environmental effects creating contaminants on-orbit. Leading edge exposure conditions caused certain materials to deteriorate and/or fail, creating a number of particle sources. Trailing edge conditions allow creation of thin films as materials outgassed and redeposited, but exposure to solar UV did not lead to catastrophic failure of any materials.

Figure 2 shows examples of surface contamination on tray A2. At the top of the photo is skin tissue, identified under a microscope by its cellular structure, and which was deposited subsequent to recovery. The lower right location is skin tissue which was exposed to space, as evidenced by the outgassing patterns around the location. The lower left corner shows a weld sphere from a manufacturing process. Figure 3 shows layering of contaminant films from Tray C-12. This pattern is indicative of thermal cycling causing intermittent deposition and likely occurred early in the mission.

A brown discoloration was observed in many locations on external aluminum surfaces. This film was formed by relatively complex processes. Outgassed organic molecules deposit on the surface where they were degraded by solar UV permanently fixed to the surface and further crosslinked and polymerized. For leading edge surfaces silicones co-deposited with the organics were oxidized to silica and trap underlying organic molecules, which then darken over time due to the solar UV Heat from thermal cycling may also accelerate degradation for part of each orbit.

Figure 4 shows shadow patterns forming the silhouettes of nuts and bolts from an interior location on LDEF. This shadowing is due to external environmental factors effecting molecular fixing, and not localized outgassing. The edges of the "shadow" patterns are quite distinct and well aligned with one another.

The areas not protected by the bolts appear to have lightened rather uniformly, probably due to intermittent UV exposure through a small opening on the opposite side of the spacecraft. Figure 5 shows a NASA photo taken in SAEF 2 during deintegration. This is the corner of trays A9 and A10, the longeron and tray clamps between and part of the black coated cover plate for the earth end of the LDEF. The black covered plates are slightly raised relative to the structure. Dark brown deposits can be seen on the aluminum structure next to the black plate. This was a vent path from the interior of LDEF and shows that volatile species form the interior can be directed parallel to the exterior surfaces. This plot shows deposition only near the vents because there surfaces are essentially oriented into the ram direction and have been "cleaned" by atomic oxygen. Figure 6 shows an on-orbit photo with large scale deposition of molecular contaminants clearly visible in tray E12. Darkened areas are visible around each electrical feed through and in particular corrosion of the tray.

However, while significant areas do have a substantially increased absorptance, the overall absorptance to emittance ratio on this satellite is only slightly influenced by the contaminant films. This is because the large majority of the surface of this satellite is anodized aluminum, which showed only slight changes in a/e, and silverized FEP, which was virtually unchanged.

Figure 7 is an on-orbit photo of tray D8 and part of tray D9 taken by NASA astronauts during retrieval of LDEF. The lower portion of the photograph shows a considerable amount of particulate debris spread over tray D9, created as the hardware from one of the experiments on this tray failed and lost its mechanical integrity. Tray D8 shows no visual evidence of migration of these particles from D9 even though this tray is in close proximity. The distribution pattern of this contamination and any anomalies it may have caused in the analysis of the nearby specimens must be inferred from the on-orbit photos. Re-entry turbulence removed this loose debris and distributed some of the very small pieces of aluminum all around the spacecraft.

Images from NASA's video downlink have been examined and image enhanced using a computer. Figure 8 shows one frame from the downlink and individual debris particles are seen in the LDEF wake. These particles are visible on the video as they reflect sunlight in the direction of the camera, then disappear as they rotate, and then reappear on a later frame. This debris has collected in the wake of LDEF. No particles were visible on the ram side. Individual particles may be moving away from the LDEF structure at very low relative velocities, taking weeks or months to leave the vicinity of the spacecraft, until they trail LDEF by such a distance that they are back in the ambient environment.

Net momentum changes due to impact with the ambient environment would be away from the satellite direction of motion and once in the wake there would be no additional impacts to further change the velocity. This condition was only being observed during the short period of time before recovery, so long term changes were not seen. In addition, effects due to electrostatic charging have not been considered and details of processes by which the particles left the location of the material failure and moved around the spacecraft are completely unknown. Figure 9 shows results from computer enhancement of the particle images. The left side of the figure shows one frame and the right half shows the sum of several frames with the background averaged out of the box in the center. Only images which persist for several frames appear in the enhanced image. Enhanced video shows many

more particles are present than are seen in any individual frames. The significance of these particles being present is that they are a significant potential source of interference to experiments done with a wake shield facility and could interfere with optical sensors or telescopes observing either the earth or other objects of interest to astronomers. It is particularly relevant for space station, which will fly in a series of constant orientations.

Long term outgassing of materials is subject to many influences, local temperature cycles, geometry of hardware around the source, and orientation of the source with respect to environmental factors. Even space qualified materials can outgas significant total amounts of material. Materials which are rated as vacuum stable may in fact break down very slowly, but at a relatively constant rate, and have an essentially infinite outgassing time. Outgassed material has complex interactions with the environment and it is the changes subsequent to material deposition on a surface which dominate the surface conditions. For organic contaminants, oxygen atoms can clean surfaces by producing volatile reaction products.

LDEF contamination was extensive but very site specific. Films deposited were essentially from line of sight sources with slight enhancement for specific geometries due to scattered species.

This work was carried out under direction from NASA Langley Research Center under contract NAS1-19247 as part of Boeing's responsibilities to the LDEF Materials Special Investigation Group.

References

1. See papers from section on LDEF mission and induced environments in NASA CP 3134, LDEF-69 Months in Space, First Post-Retreival Symposium, Part 1, A.S. Levine, ed., Jan. 1992.

2. NASA CP-3162, LDEF Materials Workshop '91, Parts 1 and 2, B.A. Stein and P.R. Young, eds., Sept. 1992.

3. NASA SP-473 The Long Duration Exposure Facility. See also articles from references 1 and 2.

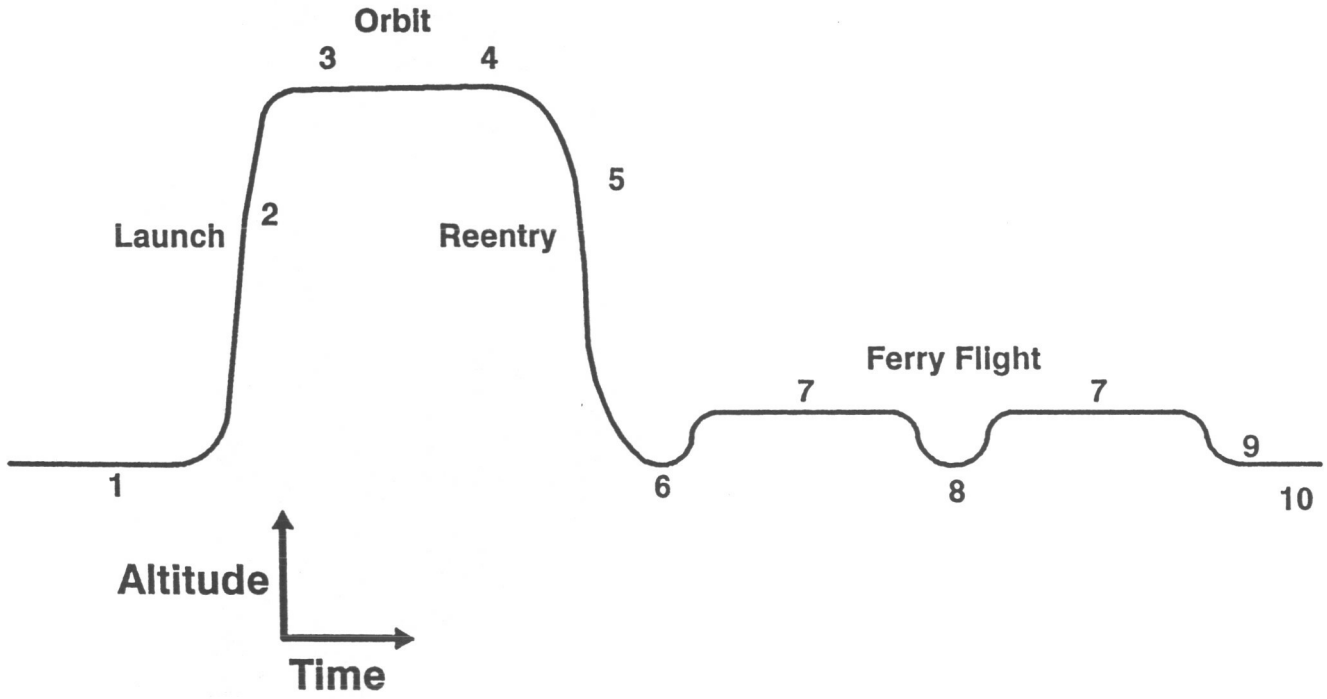

Figure 1. LDEF Contamination Exposure History

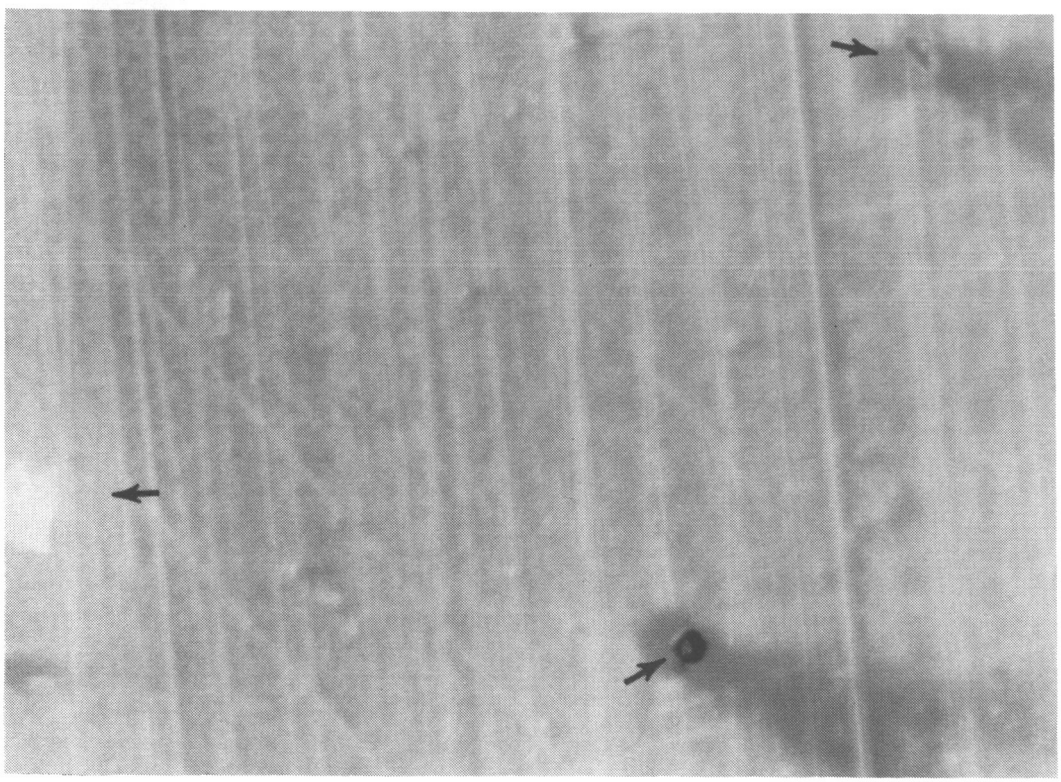

Figure 2. Particulate Contamination Examples on LDEF

Figure 3. Layered Contaminant Films from Tray C12
(Color version of black and white photograph shown on page 1247.)

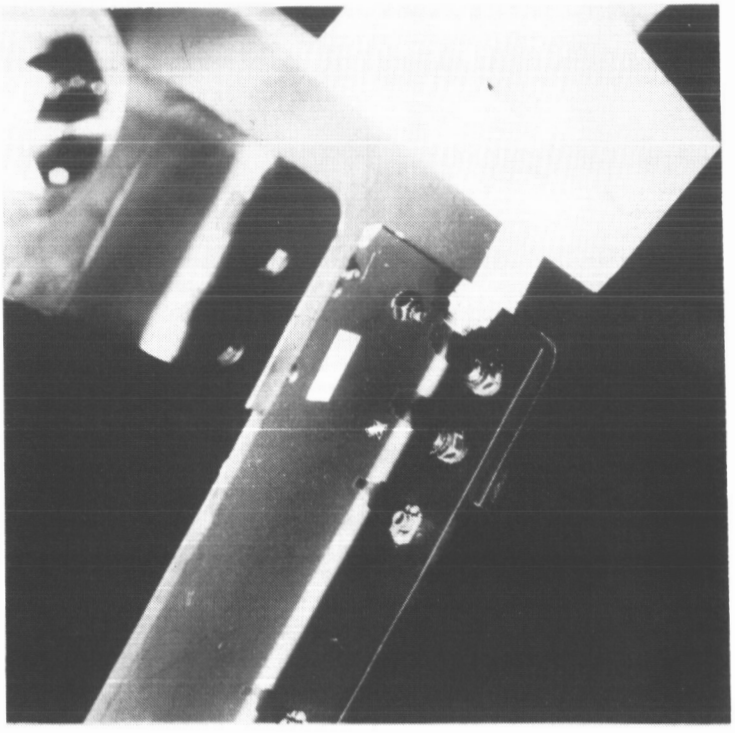

Figure 4. Shadowing from External Environmental Factors at LDEF Interior Locations

ORIGINAL PAGE
BLACK AND WHITE PHOTOGRAPH

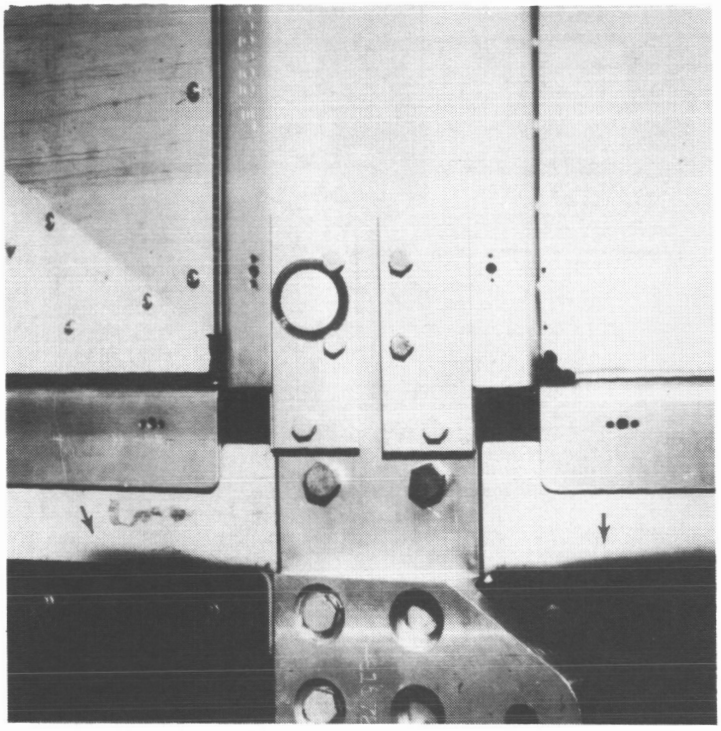

Figure 5. Outgassed Material on LDEF Structure Near Vents from Interior
(Color version of black and white photograph shown on page 1247.)

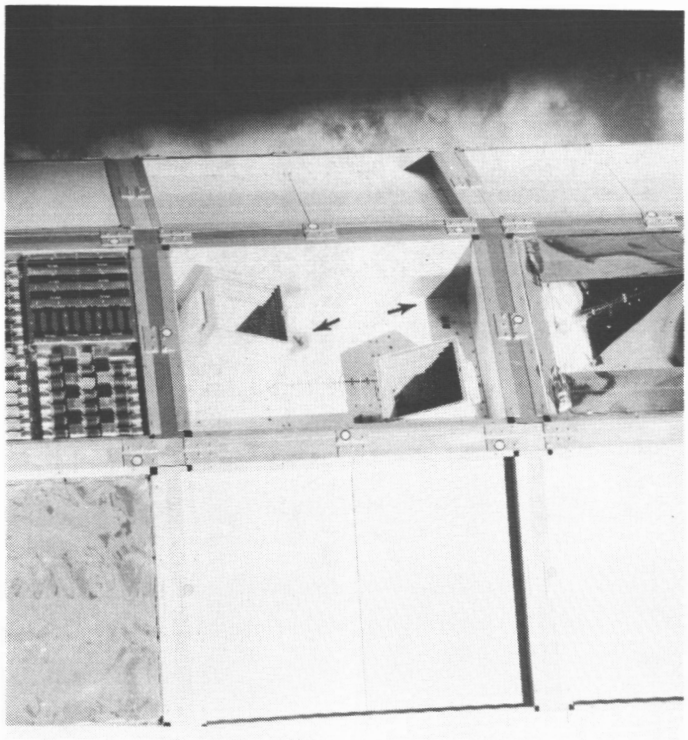

Figure 6. On-Orbit Photo of Tray E12 Showing Molecular Contamination Patterns

ORIGINAL PAGE
BLACK AND WHITE PHOTOGRAPH

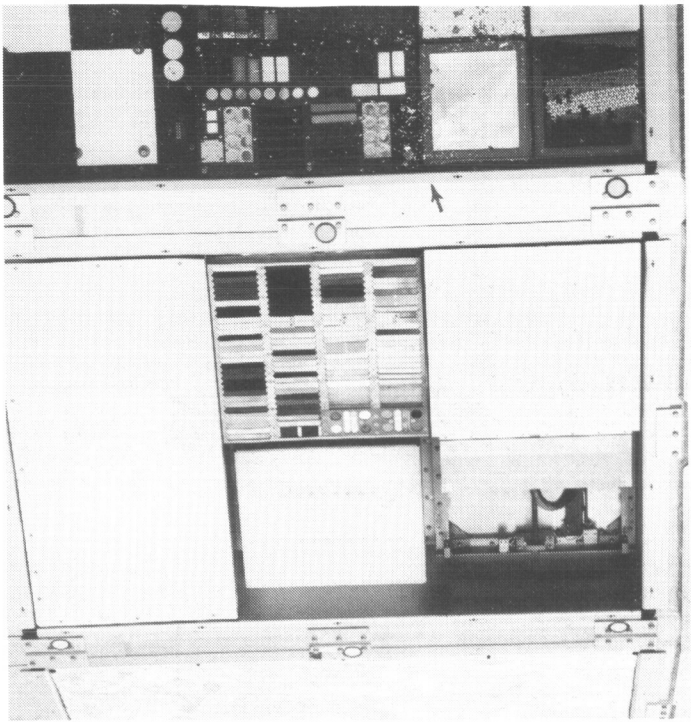

Figure 7. On-Orbit Photo of Trays D8 and D9(partial) Showing Particulate Debris from Degraded Hardware

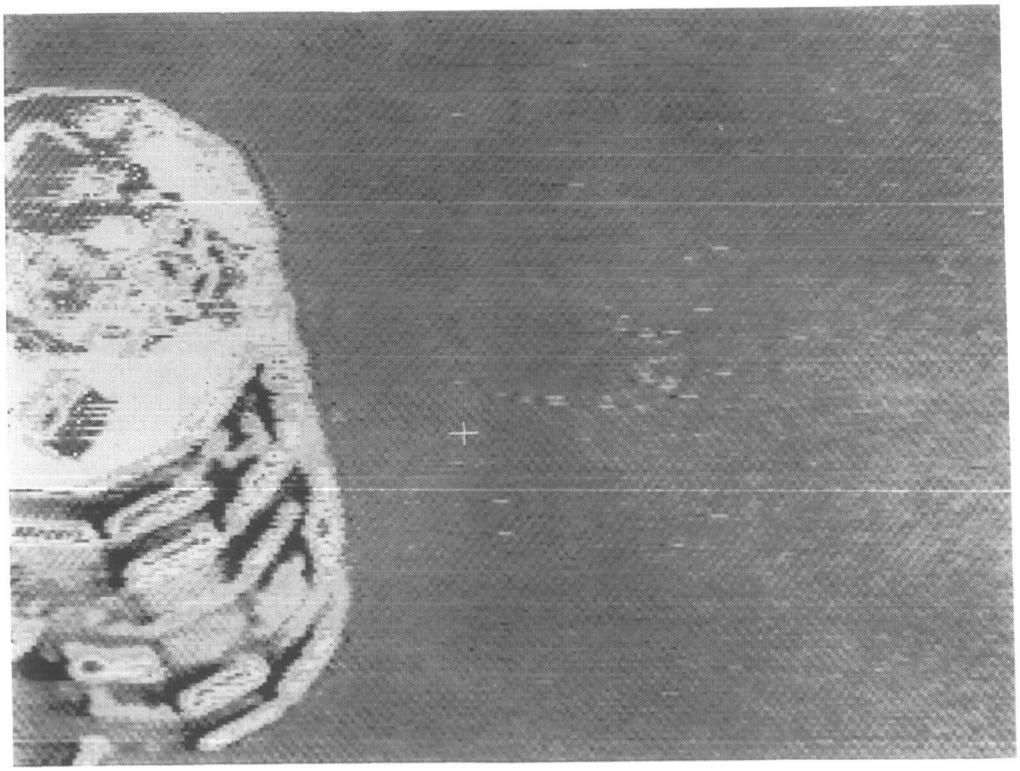

Figure 8. Image made from one Frame of NASA Video Downlink During LDEF Recovery. Particles Observed in LDEF Wake are Visible

ORIGINAL PAGE
BLACK AND WHITE PHOTOGRAPH

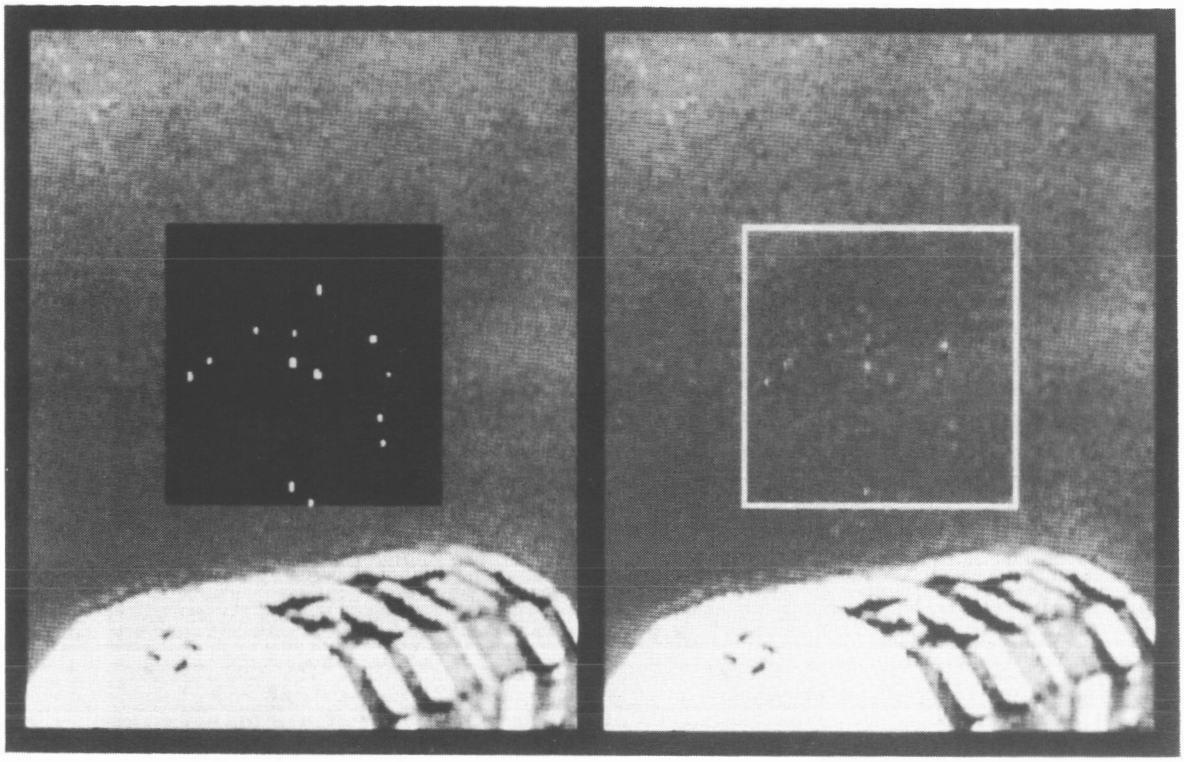

Figure 9 Computer Enhancement of Particle Images. Image with Dark Background in Center is Computer Enhanced Average of Several Frames

ORIGINAL PAGE
BLACK AND WHITE PHOTOGRAPH

N93-28273

CONTAMINATION MEASUREMENTS ON EXPERIMENT M0003

Eugene N. Borson
F. Barry Sinsheimer

The Aerospace Corporation
El Segundo, CA 90245-4691
Phone: 310/336-6943-310/336-7395; Fax: 310/336-5846

ABSTRACT

The contamination monitors on the M0003 experiment consisted of passive sample collectors to measure molecular and particulate deposition. The collectors were placed in the leading and trailing edge trays of M0003. The objective was to quantify the contaminants and determine how contamination affected the other materials in the trays. Duplicate collectors were placed inside the vacuum canisters that provided protection from the launch, ascent, deployment, and recovery environments.

The sample collectors and the analyses performed are listed below:

Sample Collector Material	Measurement Technique	Quantity Measured
Low Scatter, Black Glass Mirror	Light Scatter	Optical Effects of Particles
Aluminized, Fused Silica Mirror, Front Surface	Scanning Electron Microscopy (SEM), Electron Dispersive X-Ray (EDX)	Particle Numbers, Sizes & Composition
Low Scatter, Nickel Mirror	SEM/EDX	Particle Numbers, Sizes & Composition
Low Scatter, Gold Coated Nickel Mirrors	SEM/EDX	Particle Numbers, Sizes & Composition
Gold on Copper Mirror	SEM/EDX	Particle Numbers, Sizes & Composition
KRS-5 & Zinc Selenide Multiple Internal Reflectance Elements	Infrared Spectroscopy	Composition of Molecular Deposits
Aluminized, Fused Silica Mirror, Second Surface	Spectral Reflectance	Solar Absorptance

Analyses of the samples show small quantities of molecular deposition on both the leading and trailing edge trays. Silicone deposits are negligible. The aluminized fused silica, second surface mirrors showed small changes in solar absorptances. This is consistent with the small quantities of molecular deposits deduced from the FTIR measurements. The conclusions that can be made are as follows:

1) Molecular contamination from local sources in the SSD-802 trays was small.
2) Return flux of LDEF outgassed products to the leading edge was small or consisted of hydrocarbons that were removed by atomic oxygen in the atmosphere.
3) In contrast to some other LDEF experiments, negligible silicone deposition was observed.
4) Silicone contamination from the Shuttle Orbiter during launch and deployment or recovery was negligible.

The paper will also present the results of particle deposition, light scatter, and a micrometeoroid (or debris) impact.
This work was performed under contract F04701-88-C-0089 with the Air Force Space Systems Division, AFSC, El Segundo, California

PRECEDING PAGE BLANK NOT FILMED

N93-28274

OPTICAL CHARACTERIZATION OF LDEF CONTAMINANT FILM

Brian K. Blakkolb and Lorraine E. Ryan
TRW Electronic Systems Group
Redondo Beach CA 90278
(310) 813-9200, FAX (310) 812-8768

Howard S. Bowen and Thomas J. Kosic
HUGHES Electro-Optical & Data Systems Group
El Segundo CA 90245
(310) 616-9819, FAX (310) 616-5987

EXTENDED ABSTRACT

Dark brown molecular film deposits were found at numerous locations on the LDEF and have been documented in great detail by several investigators.[1,2,3,4] The exact deposition mechanism for these deposits is as yet unknown, although direct and scattered atomic oxygen, and solar radiation interacting with materials outgassing products have all been implicated in the formation process. Specimens of the brown molecular film were taken from below the flange of the experimental tray located at position D10 on the LDEF. The tray was one of two, comprising the same experiment, the other being located on the wake facing side of the LDEF satellite at position B4 (see Figure 1†). Having access to both trays, we were able to directly compare the effect that orientation with respect to the atomic oxygen flux vector had on the formation of the brown molecular film deposits.

The film is thickest on surfaces facing toward the exterior, i.e. the tray corner, as can be seen by comparing the lee and wake aspects of the rivets. The patterns appear to be aligned not with the velocity vector but with the corner of the tray suggesting that flux to the surface is due to scattered atomic oxygen rather than direct ram impingement. The role of scattered flux is further supported by more faint plume patterns (unfortunately not readily visible from the photograph in Figure 1) on the sides of the tray. The angle of these plumes is strongly aligned with the ram direction but the outline of the deposit implies that incident atoms are scattered by collisions with the edges of the opening resulting in a directed, but diffuse, flux of atomic oxygen to the surface.

Spectral reflectance measurements in the 2 to 10 micron (4000 to 1000 wavenumbers) spectral range are presented for the film in the "as deposited" condition and for the free standing film in Figures 2a and 2b. The material was analyzed by FTIR (Fourier Transform Infrared) microspectroscopy using gold as the reference standard. The "as deposited" specimen was on an aluminum rivet taken from beneath the tray flange while the free film was obtained by chipping some of the material from the rivet. The transmission spectrum over the 2 to 10 micron range for the free film is presented in Figure 3. This spectrum appears to be essentially the same as that presented by Crutcher et.al. (ref.2) for films formed at vent sites which faced into the ram direction and suggested to originate from urethanes and silicones used on the LDEF. Banks et.al. (ref.4) state that silicones, when exposed to atomic oxygen, release polymeric scission fragments which deposit on surfaces and form a glassy, dark contaminant layer upon further atomic oxygen exposure and solar irradiation.

† Atomic oxygen fluence distribution diagram from: Kinard, W.H., Martin, G.D, "LDEF Space Environments Overview," pg 54, Proceedings of the First LDEF Post-Retrieval Symposium, NASA CP-3134, 1992.

PRECEDING PAGE BLANK NOT FILMED

Examination of the film specimens via scanning electron microscopy (SEM) showed the films to be between 22 to 24 μm thick and reveled a layered structure composed of light and dark bands which are visible in Figure 4. These layers suggest a cyclic deposition mechanism related to the periodic variation of solar illumination and temperature seen around each orbit. The micrographs also show that the layers decrease in thickness going from the inner to the outer surface which is consistent with a decrease in the flux of materials outgassing species over the length of the mission. It is unclear, however, what gives rise to the light and dark bands, although density or compositional variations between the layers could manifest in this way when viewed via SEM. Electron Spectroscopy for Chemical Analysis (ESCA) probe examination of the film found it to be substantially the same composition down to the probed depth of 50 Å (Table 1).

Table 1. ESCA Probe Survey of Molecular Film

Element	Depth 0 Å	15 Å	50 Å
Carbon	72%	73%	74%
Oxygen	23%	15%	15%
Silicon	2%	4%	5%
Other	3%	8%	7%

1 Crutcher, E. R., Nishimura, L.S., Warner, W.J, Wascher, W.W., "Qualification of Contaminants Associated With LDEF," First LDEF Post-Retrieval Symposium, pp. 141-154, NASA CP-3134, 1992.

2 Crutcher, E.R., Warner, W.J, "Molecular Films Associated with LDEF," First LDEF Post-Retrieval Symposium, pp. 155-177, NASA CP-3134, 1992.

3 Harvey, G.A., "Organic Contamination of LDEF," First LDEF Post-Retrieval Symposium, pp. 179-196, NASA CP-3134, 1992.

4 Banks, B.A., Gebauer, L., Hill, C. M., "Atomic Oxygen Interactions With FEP Teflon and Silicones on LDEF," First LDEF Post-Retrieval Symposium, pp. 801-815, NASA CP-3134, 1992.

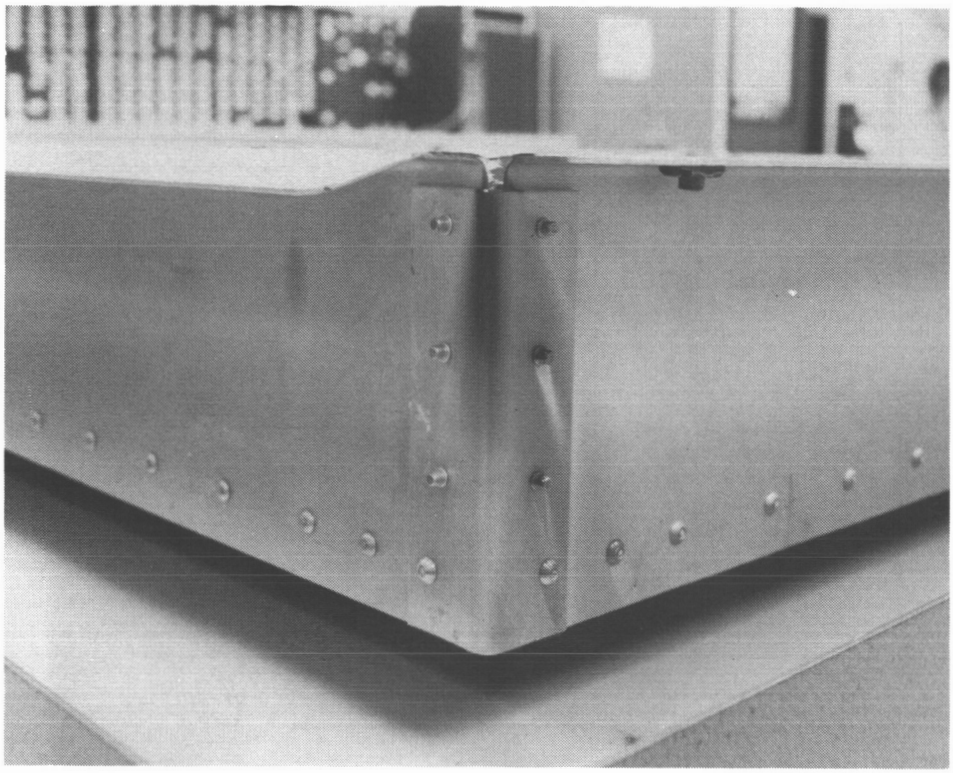

Figure 1a. Molecular film deposit below the mounting flange of experimental tray located at D10. Edge between Rows 9 and 10 pictured. RAM flow, left to right.

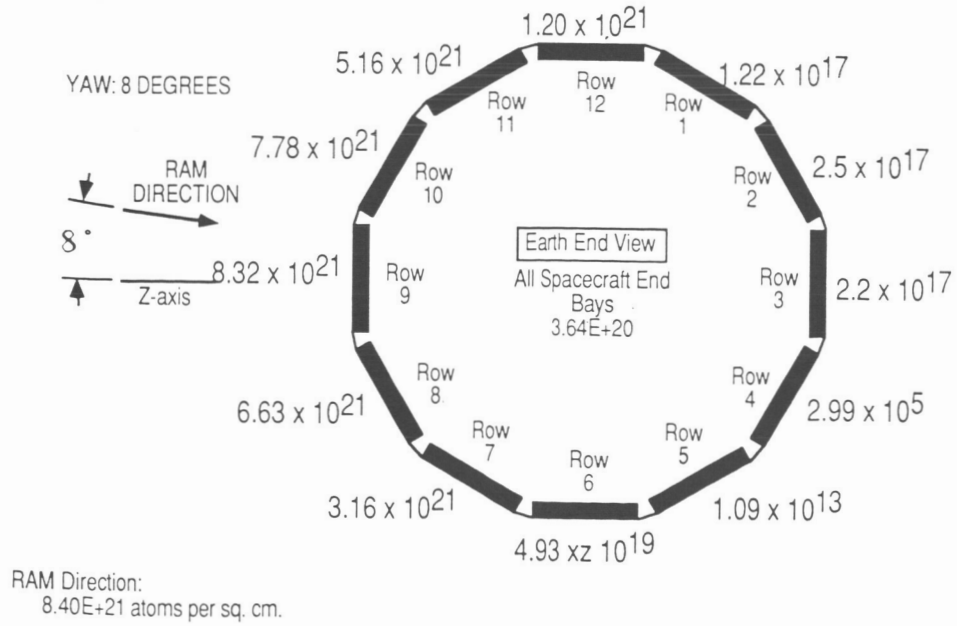

Figure 1b. Calculated distribution of atomic oxygen fluence on each of the LDEF surfaces. Note Rows 10 and 4.

ORIGINAL PAGE
BLACK AND WHITE PHOTOGRAPH

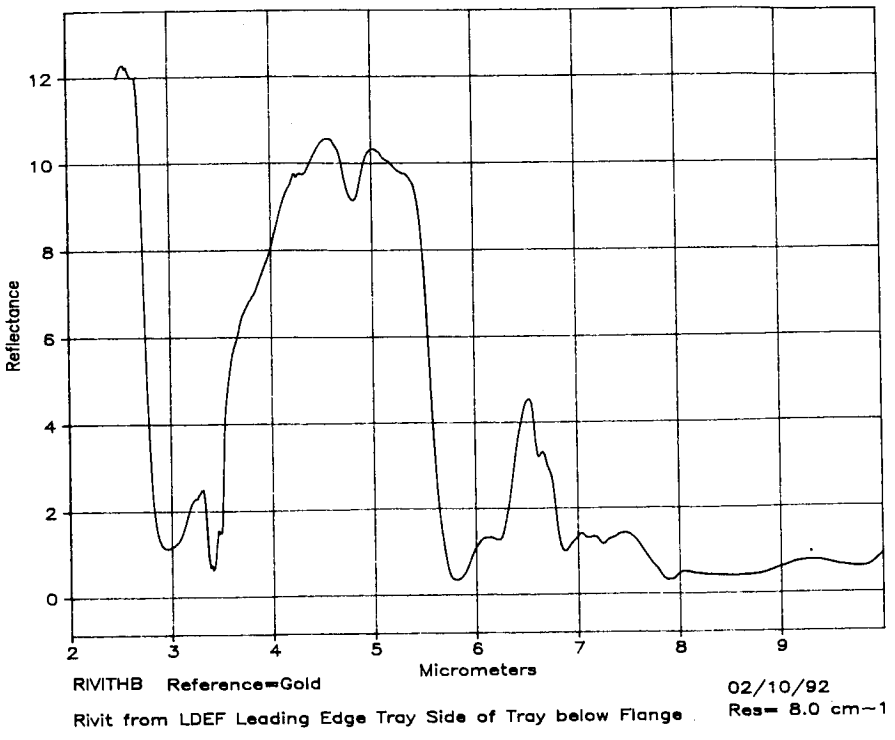

Figure 2a

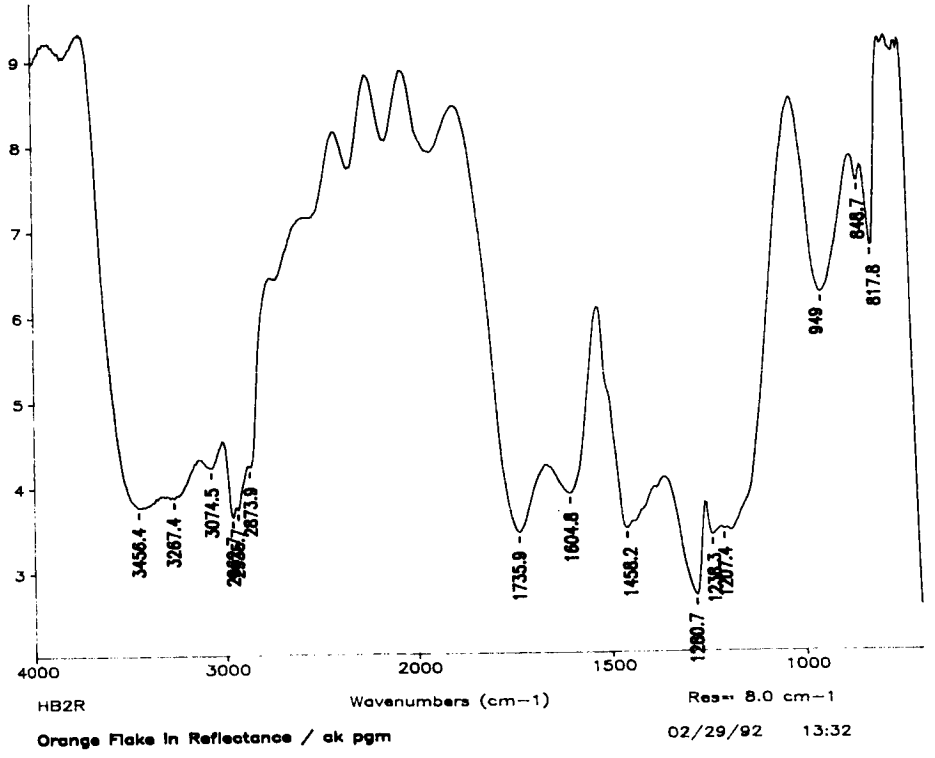

Figure 2b

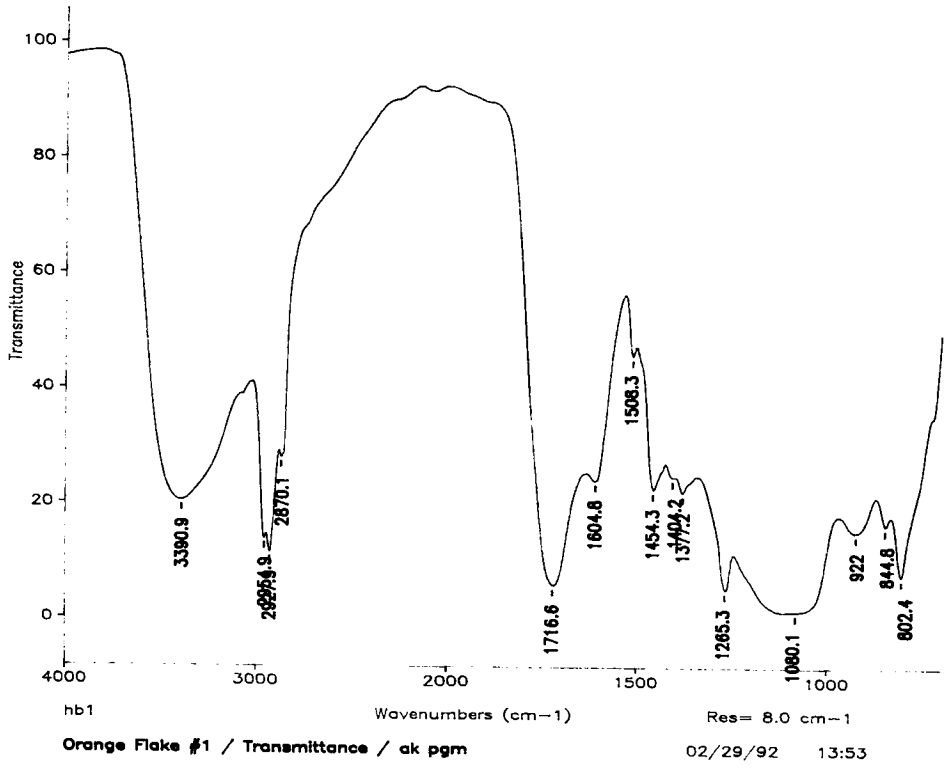
100
80
60
40
20
0
Transmittance
3390.9
2954.9
2870.1
1716.6
1604.8
1508.3
1454.3
1265.3
1080.1
922
844.8
802.4
4000
3000
2000
1500
1000
hb1
Wavenumbers (cm−1)
Res= 8.0 cm−1
Orange Flake #1 / Transmittance / ak pgm
02/29/92 13:53

Figure 3

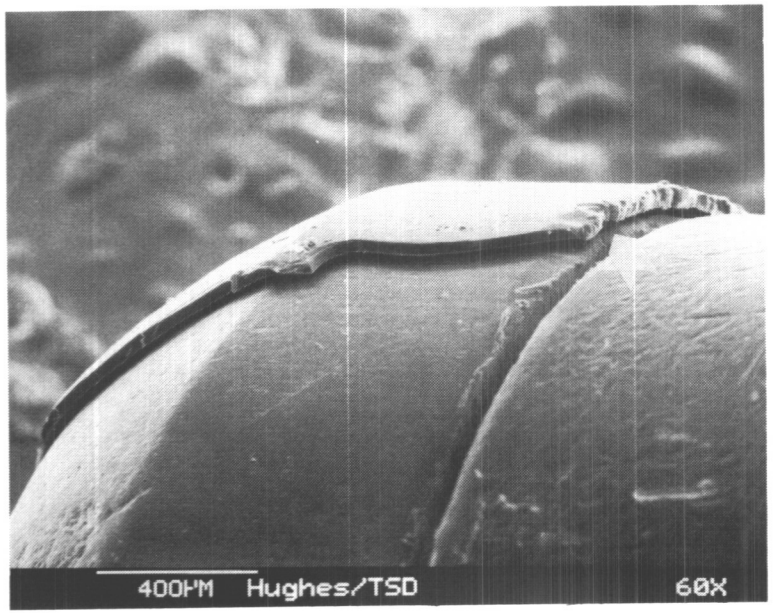

(a)

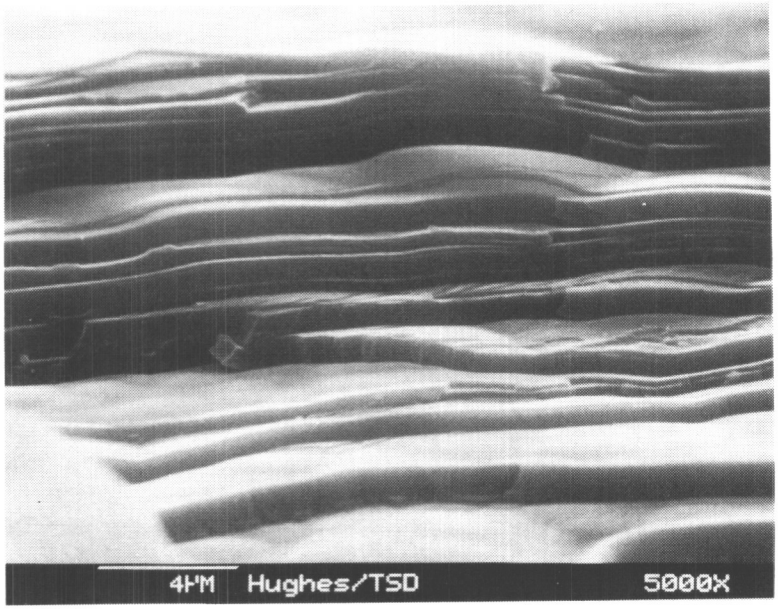

(b)

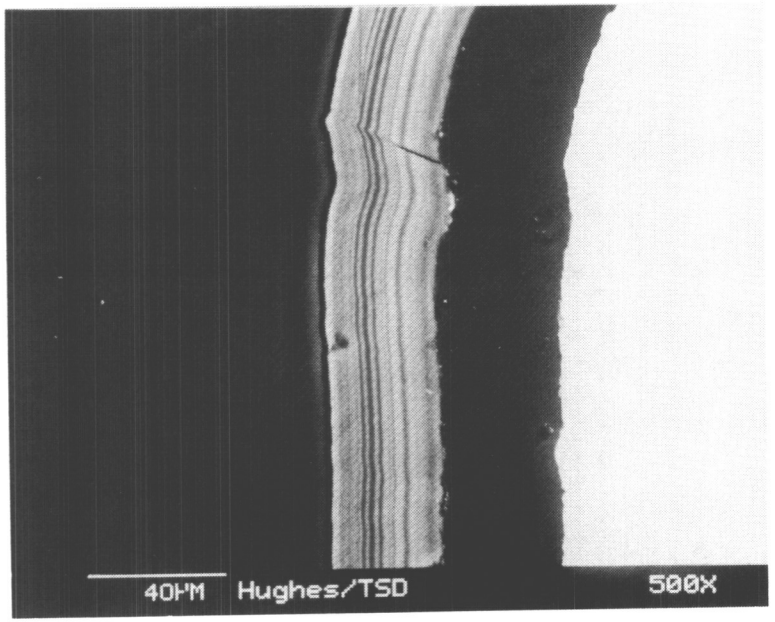

(c)

Figure 4. Molecular film deposit on D10 tray

4a. Molecular film on tray rivet.

4b. Layering of film indicating cyclic deposition.

4c. Light and dark bands through film cross section.

N93-28275

EVALUATION OF SEALS, LUBRICANTS, AND ADHESIVES USED ON LDEF

Harry Dursch
Bruce Keough
Gary Pippin

Boeing Defense & Space Group
Seattle, WA 98124
Phone: 206/773-0527, FAX 206/773-4946

SUMMARY

A wide variety of seals, lubricants, and adhesives were used on the Long Duration Exposure Facility (LDEF). This paper discusses the results, to date, of the Systems Special Investigation Group (SIG) and the Materials SIG investigation into the effect of the long term low Earth orbit (LEO) exposure on these materials. Results of this investigation show that if the material was shielded from exposure to LDEF's external environment, the 69 month exposure to LEO had minimal effect on the material. However, if the material was on LDEF's exterior surface, a variety of events occurred ranging from no material change, to changes in mechanical or physical properties, to complete disappearance of the material.

The results presented in this paper are from the following sources: 1) Visual examinations and/or testing of materials performed by various LDEF experimenters, 2) Testing done at Boeing in support of the Materials or Systems SIG investigations, 3) Testing done at Boeing on Boeing hardware flown on LDEF.

LUBRICANTS AND GREASES

A variety of lubricants and greases were flown on LDEF. With the exception of three lubricant systems flown as specimens in experiment M0003, all lubricants were components of functioning hardware, not the primary item of the experimenter's investigation. Table 1 identifies the lubricants flown on LDEF, where they were located, and a brief summary of their performances. The following paragraphs discuss findings for each of the identified lubricants. The majority of the lubricants were shielded from direct exposure to space and performed their design function as anticipated. However, a MoS_2 dry film lubricant exposed to the trailing edge environment completely disappeared.

Cetyl alcohol and a molybdenum disulfide (MoS_2) dry film lubricant were used on nut plate assemblies on experiment A0175. Nut plates were coated

with either MoS_2 or cetyl alcohol. During post-flight disassembly, severe difficulties were encountered with seizure and thread stripping of the nut plates that had been coated with cetyl alcohol. Examples of this are shown in Figure 1. Post-flight inspection of the fasteners installed into nutplates with MoS_2 dry film lubricant showed no damage to the threads and nominal removal torques. Fasteners installed into nutplates using only cetyl alcohol sustained substantial damage to the fasteners and nutplates. Post-flight FTIR examination of the nutplates found no remaining traces of cetyl alcohol.

MIL-L-23398 air-cured MoS_2 lubricant was used on several components on each of the five NASA provided Environmental Exposure Control Canisters (EECC). The EECC's were located on rows 9 (leading edge), 8, 4, 3 (trailing edge), and 2. The lubricant was applied to the Belleville washers, drive shafts, and linkages (see Figure 2). Portions of the Belleville washers and drive shafts were exposed to the external environment. Visual examination of the EECC located on the trailing edge revealed no evidence of abnormal wear or coating degradation on the surfaces not exposed to UV. Portions of the drive shaft exposed to UV exhibited slight discoloration. Further testing is planned.

VacKote 18.07 and 21207, both made by Ball Aerospace, were used on carousel components of experiment S0069. VacKote 18.07 is a polyimide bonded MoS_2 that is sprayed on to the substrate and then cured at elevated temperatures (1 hour at 590F or 50 hours at 300F). This lubricant meets current NASA outgassing requirements. The 21207 is thin pure MoS_2 that contains no binder or glue. It is applied by high velocity impingement. Its primary use is in reduction of rolling friction (it possesses poor properties for sliding friction applications). The only post-flight evaluation of either lubricant has been a system functional test of the overall experiment. The system performance was unchanged. To date, no post-flight examination of either lubricant has been performed.

Dow Corning Molykote Z was used on Experiment A0138-10. No results have been reported.

Tungsten disulfide (WS_2) dry film lubricant was used as the lubricant on both the rigidize sensing and flight-releasable grapple shafts. This lubricant was used to ensure successful release of the grapple from the RMS during initiation of the active experiments, deployment, and retrieval of LDEF. The grapples performed as designed. The tray containing the grapple used for deployment and retrieval was located 122 degrees to ram and saw an atomic oxygen exposure of 22E+17 atoms/cm^2. However, because the shaft extended 3 to 4 inches beyond the LDEF surface, portions of the shaft (and the Teflon tip) were exposed to a much greater fluence. During post-flight analysis at Johnson Space Center, samples of WS_2 were removed from both grapple shafts for SEM and EDX analysis. This analysis showed the bulk lubricant to be intact with no discernible difference between the lubricant exposed on the ram surfaces of the shafts and the lubricant exposed on the trailing edges. No surface analysis was performed. To date, the tribological properties of the WS_2 have not been determined.

Apiezon H was used as a heat sink grease on experiment A0076, Cascade Variable Conductance Heat Pipe. The grease was not exposed to atomic oxygen or UV. To determine the effect of extended vacuum on the grease, a sample was tested for outgassing in accordance with NASA SP-R-0022A. The LDEF sample had considerably higher total mass loss than the control sample, but the volatile condensible material was similar. It was postulated that this was due to the LDEF sample picking up moisture between satellite retrieval and sample test. Therefore, a series of tests were performed to determine the propensity of Apiezon H to absorb atmospheric moisture. A thin film of the grease was exposed to 100% humidity at room temperature prior to testing. The absorbed moisture caused a total mass loss similar to the difference between the LDEF sample and the control sample. Chemical analysis of the grease indicates that both the grease and the condensible material from the volatility test match those of a control sample. This implies that changes noted in the LDEF material were caused by storage on earth, not by exposure to LEO.

Apiezon L was used on experiment A0180, as a lubricant during fastener installation. To date, it has not been examined.

Apiezon T was used on experiment M0001 as a lubricant for installation of a large O-ring in a flange seal. Examination of the lubricant/O-ring by optical microscopy revealed some slight separation of the oil from the filler. Infrared spectroscopy of the lubricant showed no changes from the control. The O-ring was entirely wetted with the oil and showed no evidence of attack. Post-flight examination of the flange revealed migration of the Apiezon T onto the flange. This migration was not quantified.

Ball Brothers lubricant 44177 was used to lubricate the thrust washer on the five EECC's. A nearby bracket was found to have a diffraction pattern due to the out-gassing of the volatile component of the lubricant as shown in Figure 2. Although the 44177 is still used on previously designed spacecraft, Ball Brothers no longer recommends it for new design.

Castrol Braycote 601 was used to lubricate the four drive shafts which opened and closed the clam shells (canisters) of experiment A0187-1, Chemistry of Micrometeoroids. The drive shafts were located on the exterior surface of tray A3 (trailing edge) but saw minimal direct exposure to UV as the clam shells shielded the drive shafts. Due to the trailing edge location, the 601 saw very minimal atomic oxygen. The lubricant had picked up a black color, as yet not identified, but thought to be some form of contamination. Castrol (manufacturer of Braycote) examined the Braycote 601 with the following results. Infrared and thermogravimetric analysis did not indicate any degradation of the base oil or thickener. Differential infrared analysis of the LDEF Braycote 601 showed it to be virtually identical to new 601. Thermal gravimetric analysis results of the flight sample are very similar to those of a control sample. A slight difference was observed but is likely due to traces of moisture and contamination. No significant change in the temperature at which

decomposition begins or in the relative levels of base oil to thickener was observed, indicating that the Braycote was unchanged.

Dow Corning 340 heat sink compound was used on two LDEF experiments, A0133 and M0001. The heat sink compound in both experiments performed as expected, transferring heat from one surface to another. Neither application exposed the Dow Corning 340 to UV or to atomic oxygen. The infrared spectra of a sample of Dow Corning 340 from experiment M0001 were unchanged compared to that of a control sample.

Dow Corning 1102, used on Experiment S1001, Low Temperature Heat Pipe, is an obsolete heat sink compound that was composed of 85% mineral oil, 10% Bentonite, 3% MoS_2, and 3 percent acetone. Post-flight visual examination of the material showed no change from the initial condition.

Exxon Andok C was used in Experiment S0069, Thermal Control Surfaces Experiment. No results have been reported.

Mobil Grease 28 was used on the NASA provided magnetic tape modules (MTM). The MTMs contained the cassette tape that recorded on-orbit data. The MTMs were tested and compared to pre-flight measurements. No significant changes were noted. The MTMs were not disassembled so no grease analysis has been performed. No change in the grease was expected as it was in a sealed enclosure backfilled with an inert atmosphere.

Vespel bushings were used in experiments A0147, A0187, and S1002. None of the bushings were exposed to UV or to atomic oxygen. All Vespel bushings performed as expected.

The following three paragraphs describe the results from testing of experiment specimens that were flown as part of a Boeing materials experiment located on the exterior surface of a trailing edge tray (tray D3). These were the only lubricants flown on LDEF that were experiment specimens. All other lubricants were components of a functioning experiment.

DuPont Vespel 21 - Optical and EDX comparison of the flight specimens with control specimens showed no differences. A friction test was performed (in a standard test lab environment) to determine if any changes occurred in lubricity. Four specimens were tested, two flight specimens and two control specimens. The results, shown in Figure 3, verify that the exposure did not degrade the Vespel 21.

Everlube 620 - Post-flight visual inspection of the sample showed that none of the lubricant remained on the test specimen substrates (Figure 4). EDX examination of the surface showed only traces of the MoS_2 remaining in the bottom of the machining grooves of the substrate. The binder, a modified phenolic, was apparently decomposed by exposure to UV and then offgassed (evaporated). This led to the MoS_2 becoming separated from the stainless steel substrate. This was a failure of the lubricant system, not the lubricant.

Rod end bearings - The bearings were tested at their manufacturer, New Hampshire Ball Bearings, to original specifications. All original test requirements were met including dynamic testing. One of the tests involved removing the PTFE-coated Nomex liner from the bearing body. The force required to remove the liner was similar to virgin bearings. Inspection of the Nomex/PTFE liner showed no degradation. The exterior surfaces of the bearing bodies were cadmium plated in accordance with QQ-P-35, Class 2, Type II. The Type II designation requires that the parts receive a chromate conversion coating after plating. The conversion coating, which was an iridescent yellow brown color, exhibited signs of degradation. Post-flight visual inspection of the bearing bodies showed that the conversion coating had become more transparent. However, this change was not uniform over the exterior surfaces of the three bearing bodies. We speculate that, as has been observed with the aluminum conversion coatings used on LDEF, the hexavalent chromium in the conversion coating has been reduced to trivalent with the associated loss of color. No changes in the cadmium plating were noted.

SEALS

A variety of seals were used on LDEF, all of them as components of various experiments. These were generally O-rings, although sheet rubber was also used as a seal. In addition, materials that are commonly used for seals were used as cushioning pads. These materials performed as designed, sustaining little or no degradation caused by long term exposure to LEO. The only failure was the ethylene propylene O-rings on Experiment S0069 used to seal the lithium carbon monofluoride (LiCF) batteries. This failure was caused by long term exposure to the LiCF electrolyte (dimethyl sulfite) which caused a compression set to occur in the O-ring. This same phenomenon occurred on ground stored batteries; therefore, this failure is not attributed to space exposure. The performances of these elastomeric materials, listed in Table 2, are discussed in the following paragraphs.

Butyl O-rings were used in face seals on experiment P0004, Seeds in Space Experiment. Because the O-rings were sandwiched between metal surfaces, their exposure was limited to vacuum and thermal cycling. The O-rings were apparently installed without lubricant and sustained some scuff marks and pinching upon installation. Accurate post flight weights of each seed container were taken and compared to preflight values. The results showed no change in weight. This means that the O-rings performed as designed by preventing any desorption of moisture in space (7% of a seed's weight is moisture). There was no evidence of space-induced degradation and the performance of the O-ring seal was as predicted.

The butyl seal used to ensure vacuum inside of the three A0138 canisters underwent post-flight characterization. The seal was bonded to one of the face-plates of the canisters. In the closed position a compression force was

exerted on the canister to apply the necessary sealing force between canister halves. When the canisters were in the open position (10 months), the seals were protected from direct exposure to trailing edge environment by an aluminum shield. Tests reveal a slight increase in hardness (4%) but the seals were still in good working order and efficiently adhered to the canisters.

Ethylene propylene (EP) O-rings were used to seal the lithium batteries on experiment S0069, Thermal Control Surfaces Experiment. These seals failed due to excessive compression set of the O-rings. The temperatures seen by the batteries, 13 to 27^0 C, were well within the limits of EP O-ring capabilities. Therefore, failure has been attributed to attack of the O-ring by the battery electrolyte, dimethyl sulfite.

Ethylene propylene diene monomer rubber (EPDM) and acrylonitrile butadiene rubber (NBR) were tested in experiment P0005, Space Aging of Solid Rocket Materials, which was located on the interior of LDEF. As shown in Figure 5, both elastomers exhibited slight changes in strength, modulus and ultimate elongation.

Silicone rubber was used as a cushioning gasket between the sunscreen and the tray in experiment S0050, Investigation of the Effects on Active Optical System Components. Portions of the gasket were exposed through holes in the sunscreen. Since the experiment was on the trailing side of LDEF (row 5), the gasket saw UV, but not atomic oxygen. The exposed areas of the gasket were slightly darkened but did not show any other signs of degradation. The hardness of the gasket was the same in exposed and unexposed areas, and all material was very pliable. Although control specimens were not available, tensile strength and elongation were determined and found to be within the range of other silicone elastomers.

Silicone rubber was also used as a cushioning pad between a metal clamp and some optical fibers in experiment M0004, Space Environment Effects on Fiber Optics Systems. The rubber was mostly shielded, but some edges were exposed to UV and atomic oxygen. The rubber remained pliable and free of cracks. Some darkening of the rubber was observed in the exposed areas.

A large number of Viton O-rings were used on LDEF. Post flight examination showed that the ones examined were in nominal condition. No Viton O-ring seals failed to maintain a seal. None of the Viton O-rings were exposed to UV or to atomic oxygen.

A group of Viton washers was used to pad the quartz crystal oscillators in experiment A0189. The washers were apparently dinked out of sheet stock as a fabric texture was apparent on the flat surfaces. Many of the washers had indentations on one or both of the contacting surface, indicating compression set. No further analysis is planned because the original compression is unknown.

A metal "V" seal was used to seal the pressure valve in the EECC's. The seal was made of Inconel 750 and had a currently unknown finish. It was sealing the stainless steel valve to an aluminum surface. There was no evidence of coldwelding between the valve, the seal, and the mating aluminum surface contacting an aluminum surface.

ADHESIVES

A variety of adhesives and adhesive-like materials were flown on LDEF. These included epoxies and silicones, conformal coatings and potting compounds, and several tapes and transfer films. Six different adhesive systems were evaluated using lap shear specimens exposed to leading and trailing edge experiments. All other materials were used in assembly of the various experiments flown on LDEF. Typically, these adhesives were shielded from exposure to the external spacecraft environment. The various materials are listed in Tables 3 through 6.

In most experiments, the adhesives were of secondary interest and were only investigated by visual examination and a "Did they fail?" criteria. Because of this role, most adhesive applications had only a few specimens, not enough for statistical data generation. Often, no control samples were kept, and documentation of what was used was occasionally sketchy. With few exceptions, the adhesives performed as expected, that is they held the hardware together. Several experimenters noted that the adhesives had darkened in areas that were exposed to UV. The remainder of this section will document the additional information available on the performance of these materials along with the status of their evaluation.

One of the most obvious adhesive failures on LDEF was on experiment M0003, Space Environment Effects on Spacecraft Materials. In this experiment, four solar cells deposited onto an alumina substrate were bonded to an aluminum mounting plate using an unfilled low viscosity epoxy, Shell Epon 828. On-orbit photographs showed that all four solar cells were no longer bonded to LDEF. No adhesive remained on the cell mounting plates on the leading edge tray but some remained on the mounting plates located on the trailing edge. This indicates that the bond failed at the solar cell interface, and then the adhesive was attacked by atomic oxygen. Epon 828 was used successfully on other experiments so no conclusions have been drawn as to the failure mode. Possibilities include surface contamination prior to bonding, excessive thermal cycling and high loads due to different thermal expansion coefficients between the solar cell substrate and the aluminum mounting plate.

Another adhesive failure occurred on 8 of the 12 polymeric lap shear specimens flown on LDEF's leading and trailing edges. This experiment, M0003-5, included the exposure of 32 - 1"x6" polymeric film strips. The ends of all 32 strips were wrapped around and then bonded to the backside of the mounting plate using a clear RTV silicone (thought to be Dow Corning DC 93-

500). All 64 of these shielded bonds survived the mission intact. 12 of the 32 strips were silverized Teflon foils bonded to aluminized Kapton using the following three different adhesive systems. The adherend for all 12 specimens was the Inconel on the backside of the silverized Teflon and the Kapton.

- RTV 560 plus 12% graphite. RTV 560 is a two part room temperature cure silicone and the graphite is used to increase the electrical conductivity through the bond. Four specimens were located on the leading edge and four specimens were located on the trailing edge. All eight lap shear specimens had become debonded during the mission. Visual examination showed that it was an adhesive failure.
- EC 57C which is a two part conductive epoxy. One specimen was located on the leading edge and one specimen was on the trailing edge. Both bonds were intact.
- Y966, a pressure sensitive acrylic adhesive, was also evaluated. As with the EC 57C, one specimen was located on the leading edge and one specimen was on the trailing edge. Both bonds were intact.

Control specimens exist for all three adhesive systems and the experimenter reports that future plans include testing of both the intact and control specimens.

One other adhesive failed on LDEF. Four out of 40 strain gauges bonded to composite parts on experiment M0003 debonded. The strain gauges, made by Micromeasurements, were bonded to the composites with Micromeasurements MBond 600 and were cured at 200°F. The substrates were graphite-epoxy (1), graphite-polyimide (1), and graphite-polysulfone (2). The strain gauges which were mounted on the shielded side of the specimens saw no atomic oxygen or UV. The specimens saw thermal cycles of -40 to 176°F. The composite substrate had the rough texture of the bleeder cloth used to lay up the specimens. No sanding was done to smooth the surfaces prior to bonding. It is thought that the failures were due to a combination of the thermal cycling and poor surface preparation.

EC 2216 (BMS 5-92) and AF 143 (BMS 5-104), epoxy adhesive lap shear specimens, were flown on the trailing edge. The EC 2216 is a room temperature cure system and the AF 143 is a 350F cure system. Both titanium-composite and composite-composite adherends were evaluated. Composite adherends were T300/934 graphite/epoxy. The lap shear specimens were mounted such that one surface was facing out towards space. Visual examination of the specimens showed the exposed bondline to have become dark brown when compared to the shielded bondline on the backside of the specimens. Five specimens for each of the two epoxy systems were flown (three Ti-composite and two composite-composite specimens for the AF 143 and two Ti-composite and three composite-composite specimens for the EC 2216). The results of post-flight testing are shown in Figure 6. The shear stress values increased 6.8 to 27.8 percent over preflight values. The preflight specimens were tested in 1978. No control specimens exist. The reason for the increase in strength compared to pre-flight values is speculated to be related to continued cure advancement.

A third epoxy system, Hysol EA 9628 250F cure, was also evaluated on LDEF using T300/934 composite lap shear specimens. Three specimens were located on the leading edge and three specimens were on the trailing edge. All six specimens were mounted so one flat surface was facing towards space. The pre-flight measurements were made in 1978 and no control samples exist. The results, shown in the bottom graph of Figure 6, show a decrease in shear strength for all flight specimens when compared to pre-flight measurements and a decrease for the trailing edge specimens (UV only) compared to the leading edge specimens (UV and atomic oxygen). The reason for the difference between leading and trailing edges is unknown as the vast majority of the adhesive is between the mating surfaces and, therefore, shielded from the detrimental effects of the atomic oxygen and UV.

Prior to determination of shear stresses of the above specimens, the epoxy fillets around the edges of the lap shear joints underwent FTIR analysis. This testing was performed to determine if the exposed portion of the adhesive had undergone any physical changes. Comparison of infrared spectra of the shielded Hysol EA 9628 fillets to fillets exposed to UV or UV/atomic oxygen showed the following:

- Absence of the dicyandiamide catalyst from the six shielded fillets that underwent FTIR. Several of the fillets then had their exterior surface scrapped away to exposed new, fresh surfaces. These surfaces then underwent FTIR. Similar results were found with no catalyst identified on these fresh surfaces. The absence of the catalyst is an expected result for thoroughly cured epoxy systems.
- The presence of catalyst on almost all exposed leading and trailing edge fillets. Several of these fillets had their exterior surface scrapped away with the newly exposed surfaces undergoing FTIR. Catalyst was also found to exist in similar quantities. The reason the dicyandiamide catalyst is present on the exposed specimens is most likely due to chemical bonds being broken by the long term exposure to UV. This caused the regeneration or reappearance of the catalyst (or a material with a very similar structure).

Dow Corning 6-1104 silicone adhesive was used to bond velcro to the thermal blankets on the sixteen trays that comprised experiment A0178, A High Resolution Study of Ultra-Heavy Cosmic Ray Nuclei. The bond between the velcro and the blanket performed very well. No degradation of the adhesive was noted.

3M tape 92 ST, a Kapton tape with a silicone adhesive, was flown on experiment A0054, Space Plasma High Voltage Drainage. Peel strength of tape 0.787 inch wide bonded to aluminum was 1.3 pounds on a leading edge tray, 1.2 pounds on a trailing edge tray, and 0.9 pounds for a fresh, unflown tape.

3M tape X-1181, a copper foil tape with a conductive adhesive, was used as grounding straps for the silver/Teflon blankets. The grounding straps were constructed by plying two layers of tape, the adhesives together, with an area of adhesive remaining on each end. A peel test was performed on a sample of the

ground strap and compared to a control sample of a freshly constructed strap made from the same roll of tape. All samples had a peel strength of 3.5 to 3.9 pounds per inch. No difference was found between space hardware and ground hardware.

3M tape Y966, an acrylic transfer tape, was used in experiment A0054. The tape was used to bond vapor deposited aluminum (VDA) Kapton film to the aluminum trays. The tape was tested using a 90 degree peel test similar to ASTM D1000 except that tape width was 0.4 inches. Tape from the leading edge tray had a 4.5 pound peel strength while tape from the trailing edge tray had a 3.5 pound peel strength. A ground control specimen made from a different lot of material had a peel strength of 1.4 pounds. The differences may be attributable to tape variations from batch to batch, additional "cure" of the space exposed tape, and experimental variation. Comparison of the failure mode of the tapes from the leading and trailing edge trays showed significant variation. On the trailing edge tray approximately 75 percent of the adhesive stuck to the VDA Kapton while on the leading edge, 85 percent of the adhesive stuck to the aluminum tray and pulled the VDA from the Kapton film.

3M tape Y966 on a silverized FEP film was also used to hold the thermal blankets to the tray frame on experiment M0001. The blankets apparently shrunk in flight causing the blankets to detach from the frame (Figure 7). Portions of the tape were attached to both the blanket and to the frame, having failed across the width of the tape in tension. The film and Y966 remained pliable. Attempts to fail the tape to frame joint in shear were unsuccessful even though a load of roughly 100 pounds was applied to a piece of tape less than a quarter inch wide. The tape was then tested in peel. The Y966 bonded to the aluminum and to the silver on the film well enough to cause delamination of the silver from the film.

3M tape Y8437, a VDA Mylar tape, was used as a coating on the viscous damper shroud, a fiberglass epoxy structure. The tape used on LDEF had a 90 degree peel strength of approximately 4 pounds per inch. After the LDEF tape had been removed, a new piece of the same type of tape (different batch and manufacture time) was applied to the shroud. This tape had a peel strength of only 0.5 pounds per inch. Apparently, the adhesive on the tape sets up with time to give increased adhesion. Space did not appear to have any adverse effect on the tape.

CONCLUSIONS

A wide variety of lubricants, adhesives, and seals were flown on LDEF. The vast majority of materials flown were not part of the experimenter's initial objectives, but because of LDEF's extended mission, the interest in the performance of these materials was greatly enhanced. Therefore, the Materials and Systems SIG conducted an investigation into the post-flight condition of these materials. This involved documenting what had flown, developing

standard test plans for experimenters to use, "inspiring" the experimenters to perform testing on these materials, testing materials at Boeing facilities, and documenting and collating the findings.

One of the two primary conclusions of this investigation was that if the material was shielded from direct or indirect exposure to atomic oxygen and/or UV radiation, the materials returned in nominal condition. The only exception to this was outgassing of the material. While the outgassing proved to have no effect on the material's ability to function as design, in several cases it did contribute to the overall molecular contamination that was throughout LDEF. The other primary conclusion was that if the material is exposed to the exterior spacecraft environment, a thorough knowledge of both the microenvironment that the material will see and how that material will interact with that microenvironment is essential.

TABLE 1 - LUBRICANTS AND GREASES		
MATERIAL - DESCRIPTION	LOCATION	FINDINGS (5/92)
Cetyl alcohol	A1 & A7	Used on nut plates, no traces remain
MoS_2	A1 & A7	Used on nut plates, appears to be nominal
MoS_2 - Air cured dry film lubricant (MIL-L-23398)	EECCs (shielded and exposed)	No apparent visual change, further testing required
MoS_2 - chemically deposited	B3	Degraded
Ball Aerospace 21207 - MoS_2	A9 (shielded)	System test results nominal, lubricant not evaluated
Ball Aerospace VacKote 18.07 - MoS_2 with polyimide binder	A9 (shielded)	System test results nominal, lubricant not evaluated
Molykote Z - MoS_2	B3 (shielded)	Not tested
WS_2 (tungsten disulfide)	Grapples	Bulk properties unchanged, no difference between leading and trailing edge
Apiezon H - petroleum based thermal grease	F9 (shielded)	Outgassing tests showed no change
Apiezon L - petroleum based lubricant	D12	Not tested
Apiezon T - petroleum based lubricant	H3 & H12 (space end)	Slight separation of oil from filler, some migration
Ball Brothers 44177 - Hydrocarbon oil with lead naphthanate and clay thickener	EECCs (shielded)	Not tested, extensive offgassing
Castrol Braycote 601 - PTFE filled perfluoronated polyether lubricant	A3	Extensive testing, to date results show no change
Dow Corning 340 - Silicone heat sink compound	Shielded	IR spectra unchanged
Dow Corning 1102 - Mineral oil based heat sink compound	Shielded	Appearance unchanged
Exxon Andok C - Petroleum grease	Shielded	System test results nominal, lubricant not evaluated
Mobil Grease 28 - Silicone grease	MTMs (shielded)	System test results nominal, lubricant not evaluated
DuPont Vespel bushings - polyimide	Various	Appearance unchanged
DuPont Vespel 21 - Graphite filled polyimide	D3	Optical, EDX, and friction tests showed no change
E/M Lubricants Everlube 620C - MoS_2 with modified phenolic binder	D3	Complete binder failure, only minimal traces remained
Rod end bearings with PTFE coated Nomex liner	D3	Extensive testing showed no changes

Table 2 - SEALS		
ELASTOMERIC PARTS	EXPERIMENT	COMMENTS
Butyl O-ring	P0004	1,4
Butyl rubber seal	A0138	1,4
EP O-ring	S0069	4
EPDM rubber	P0005	1,4
NBR rubber	P0005	1,4
Neoprene gasket	A0139	
Nitrile O-ring	M0006	
Silicone gasket	S0050	1,2,4
Silicone pad	M0004	1,2,4
Viton O-ring	A0015, A0134, A0138-2, A0139, A0180, M0001, M0002, P0005, S0010, S0069	1,4
Viton washer	A0189	1,4
Metal "V" washer	EECC's	1,4

Key to Comments:

1: Performed as expected, 2: Discolored where exposed to UV, 4: Results discussed in this paper

Table 3 - SILICONE ADHESIVES			
VENDOR	PRODUCT	EXPERIMENT	COMMENTS
Dennison	Densil Silicone PSA	A0076	1
Dow Corning	6-1104	A0187, P0005, A0178	1,4
	43-117	A0171	1,3
	93-500	A0171	1,3
		S1002	
		M0003-5	1,4
	RTV 3140	S1001	1
General Electric	RTV 560 + 12% graphite	M0003-5	4
	RTV 566	A0076	1
		A0171	1,3
		S0014	1
		S1002	
	RTV 567	A0054	1
	RTV 655	A0171	1,3
	SR 585 PSA	A0076	1

Key to Comments:

1: Performed as expected, 2: Discolored where exposed to UV, 3: Further testing is planned, 4: Results discussed in this paper

Table 4 - EPOXY ADHESIVES			
VENDOR	PRODUCT	EXPERIMENT	COMMENTS
Ciba Ceigy	Araldite AV 100/HV 100	A0056, A0139	
	Araldite AV 138/HV 998	A0023, A0056, A0138-1, S1002	
	Araldite AV 138/HW 2951	A0138-1	
	Araldite AW 136/HY 994	M0002	
	Araldite AW 2101/HW 2951	A0138-1	
	Araldite MY 750/HY 956	A0056	
Crest	3135/7111	A0180	1,2,3
Emerson & Cuming	Eccobond 55	A0056,A0139	
		A0147	1
		S1004	1,2
	Eccobond 55 + 10% Ecosil	S1002	
	Eccobond 56C	A0076	1
		A0171	1,3
		S0069	1
	Eccobond 56C + Ag powder	S1002	
	Eccobond 57C	M0003-5	1,4
Epoxy Technology	Epo-Tec 301	A0147	1
		S0014	1
	Epo-Tec 331	M0004	1
Furane	Epi-Bond 104	S0014	1
Hysol	EA 934	A0180	1,2,3
		M0004	1
		S1001	1
	EA 956	A0054	1
	EA 9210/109519	M0004	1
	EA 9628	M0003-8	1,2,4
Micromeasurements	MBond 600	M0003	4
Rome & Haas	K-14	A0171	1,3
	N-580	A0171	1,3
Shell	Epon 828	A0056	
		A0180	1,2,3
		P0003	1
		S1001	1
		M0003-8	4
3M	AF-143	M0003-8	1,2,4
	EC 2216	A0076,A0138-1, A0178	
		M0003-8	1,2,4
		S1005	1
		Viscous Damper	1
Varian	Torrseal	M0006	

Key to Comments - 1: Performed as expected, 2: Discolored where exposed to UV, 3: Further testing is planned, 4: Results discussed in this paper

Table 5 - CONFORMAL COATINGS AND POTTING COMPOUNDS			
VENDOR	PRODUCT	EXPERIMENT	COMMENTS
Conap	CE-1155	A0201 P0005	1
Dow Corning	Sylgard 182	S1001	1
	Sylgard 186	S1001	1
Emerson & Cuming	Stycast 1090	A0056	
	Stycast 2850	P0003	1
	Stycast 3050	S0069	1
General Electric	RTV 411/511	S0014	1
Products Research	PR 1535	A0038	
	PR 1568	A0201	
Thiokel	Solithane 112	A0178	
	Solithane 113	A0038, A0178, A0187-2, S0001, S1001, S1002	
3M	Scotchcast 280	A0139	

Key to Comments - 1: Performed as expected,

Table 6 - TAPES AND OTHER MATERIALS			
VENDOR	PRODUCT	EXPERIMENT	COMMENTS
Emerson & Cuming	Eccoshield PST-C	M0003	
Loctite		A0119, A0138-1	
Mystic Tapes	7355	M0001	1
		P0003	1
3M	5	A0139	
	56	S0069	1,4
	74	S0069	1
	92 ST	A0054	1,4
	433	A0076	1
	X-1181	A0178	1,4
		M0001	
	Y966	A0054	1,4
		M0003-5	1,4
		S0069	1
		M0001	4
	Y8437	A0076	1
		Viscous Damper	1,4
	Polyester Hot Melt Adhesive	A0133	1,3

Key to Comments:

1: Performed as expected, 3: Further testing planned, 4: Results discussed in this paper

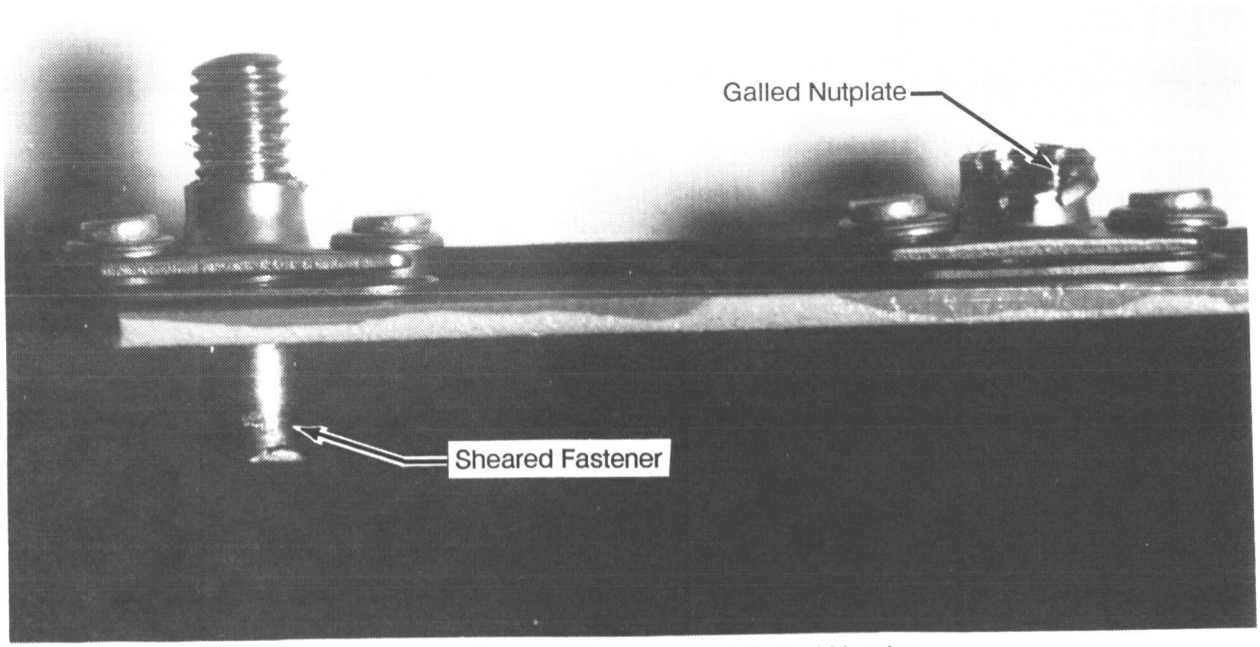

Figure 1. Sheared Fastener and Galled Nutplate

ORIGINAL PAGE
BLACK AND WHITE PHOTOGRAPH

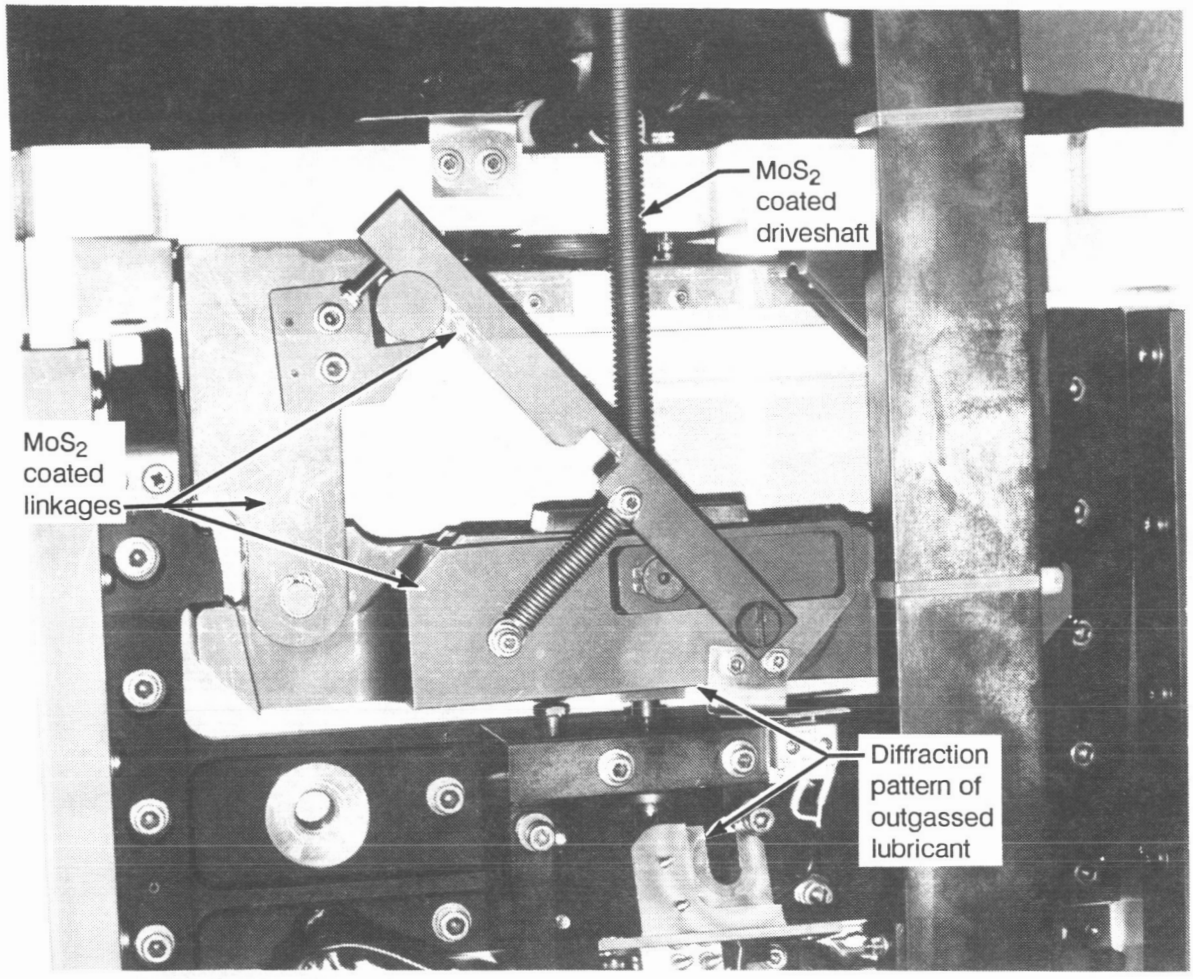

Figure 2. Lubricant Outgassing Patterns

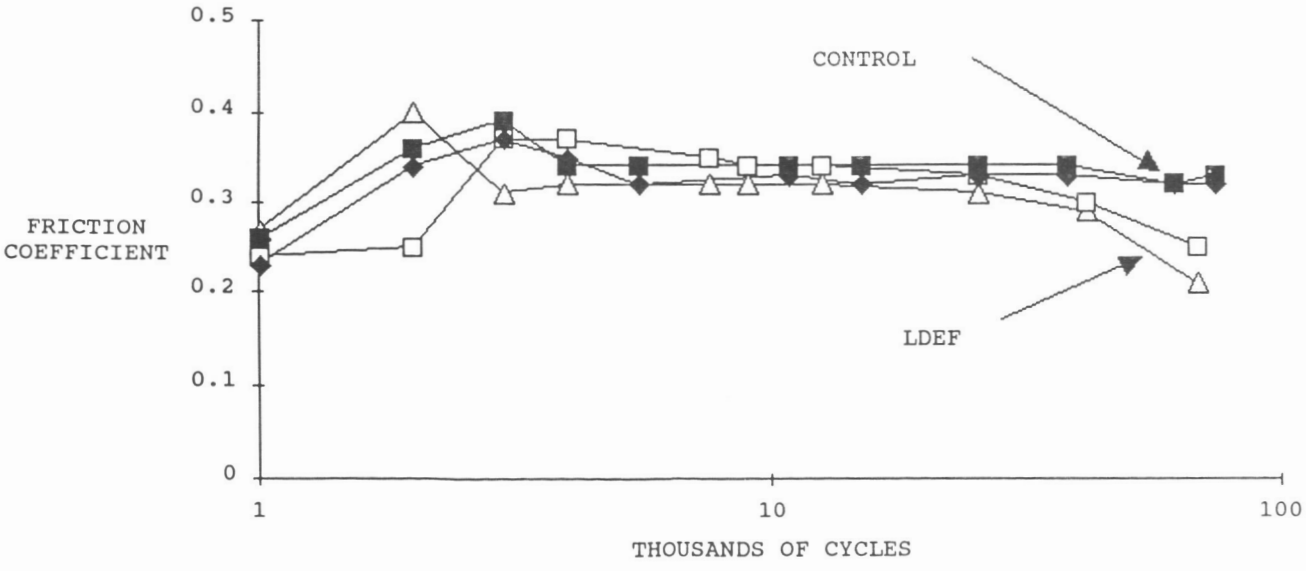

Figure 3. Friction Coefficient of Vespel 21

ORIGINAL PAGE
BLACK AND WHITE PHOTOGRAPH

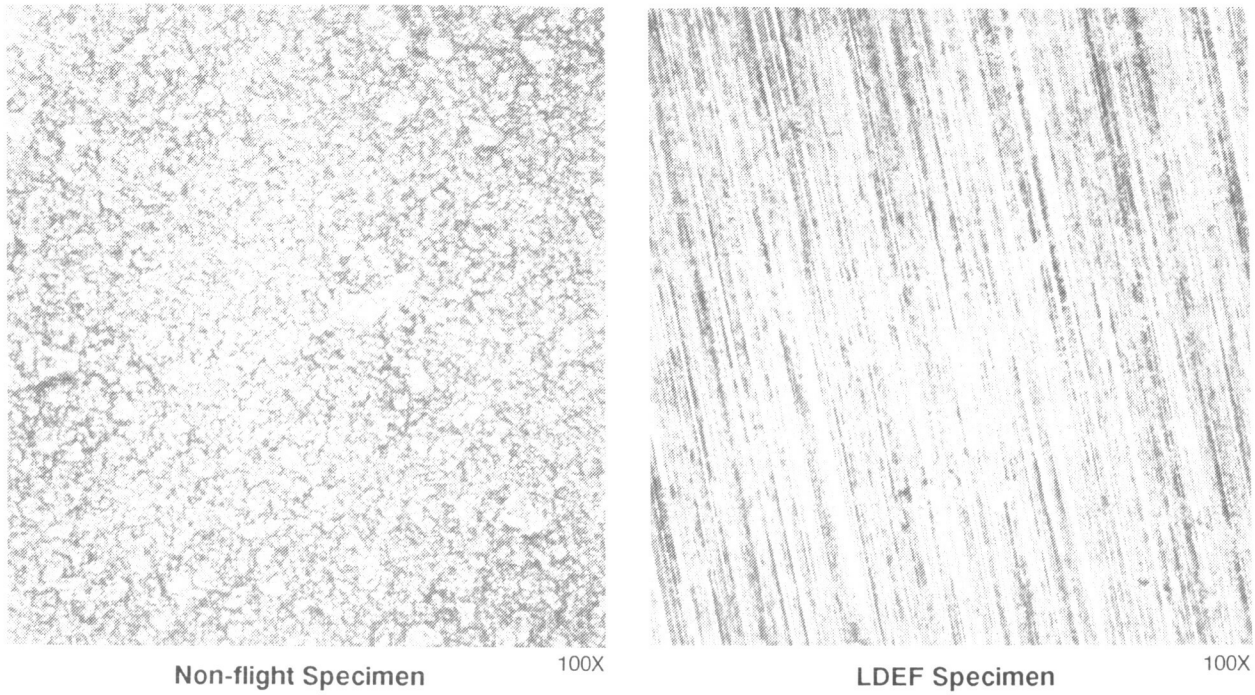

Figure 4. Everlube 620C Lubricant

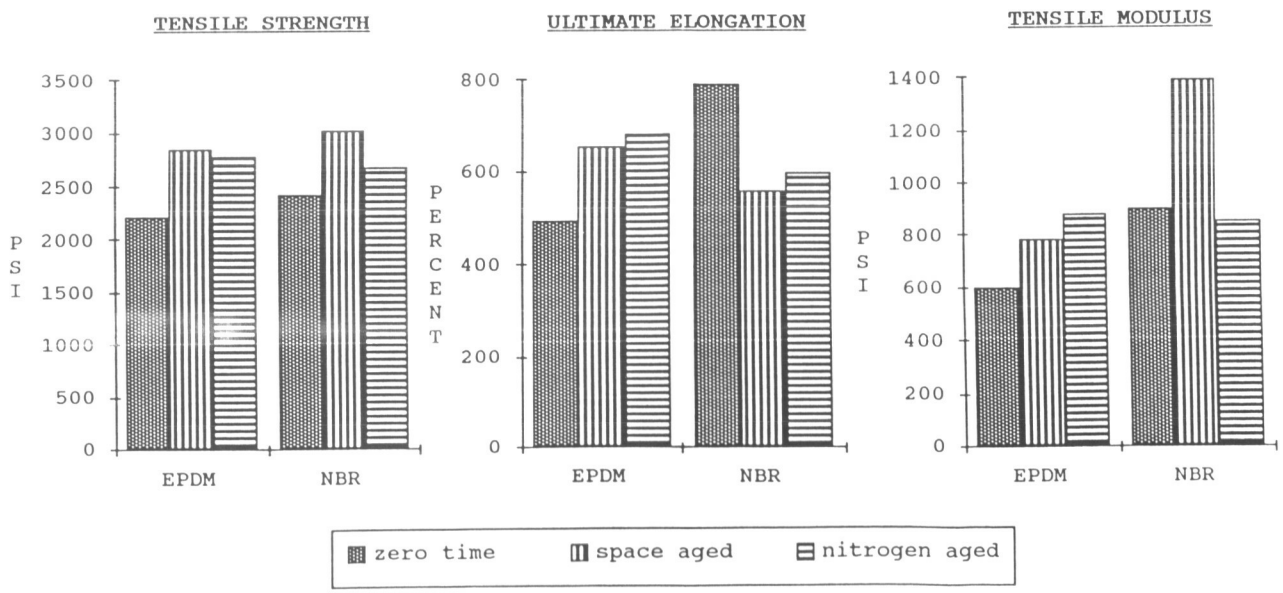

Figure 5. Mechanical Properties of EPDM and NBR

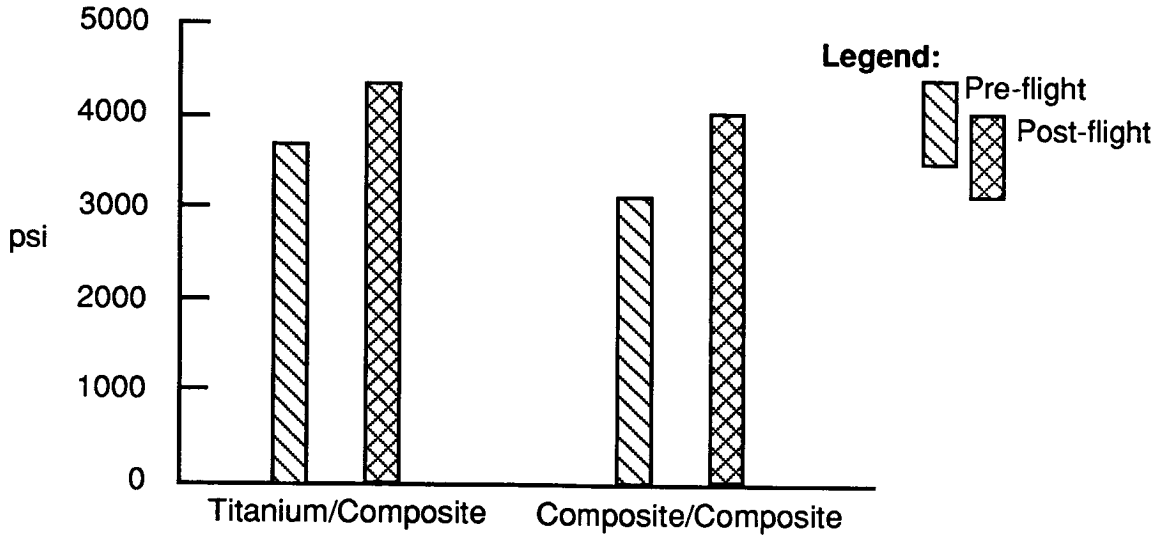

- 3M EC 2216 R.T. cure epoxy adhesive (BMS 5-109)
- Trailing edge

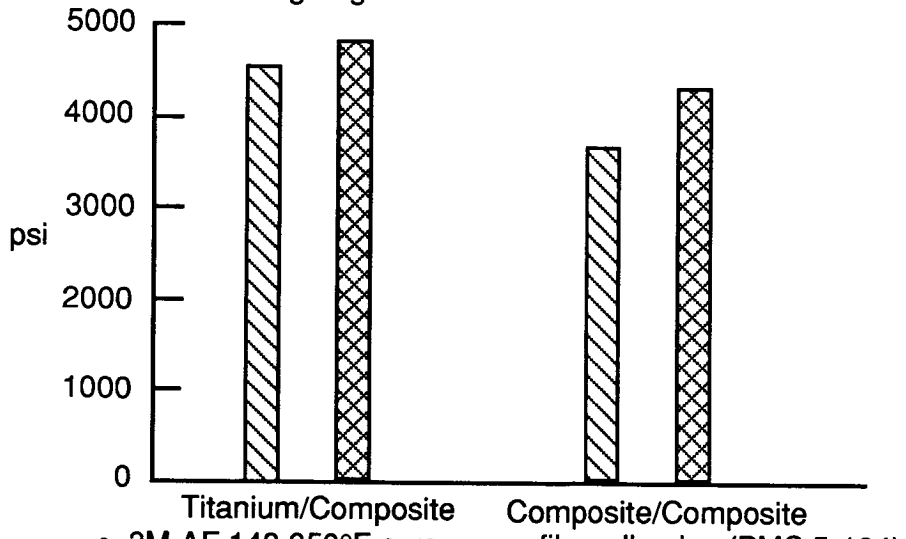

- 3M AF 143 350°F cure epoxy film adhesive (BMS 5-104)
- Trailing edge

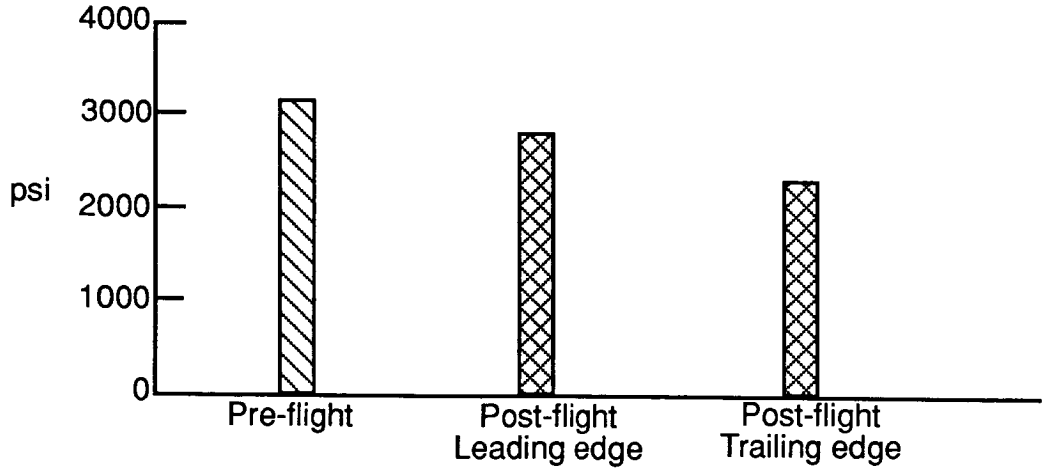

- T300/934 composite lap shear specimens
- Hysol EA 9628 250°F cure epoxy tape adhesive

Figure 6. Lap Shear Testing of Epoxy Adhesives Flown on LDEF

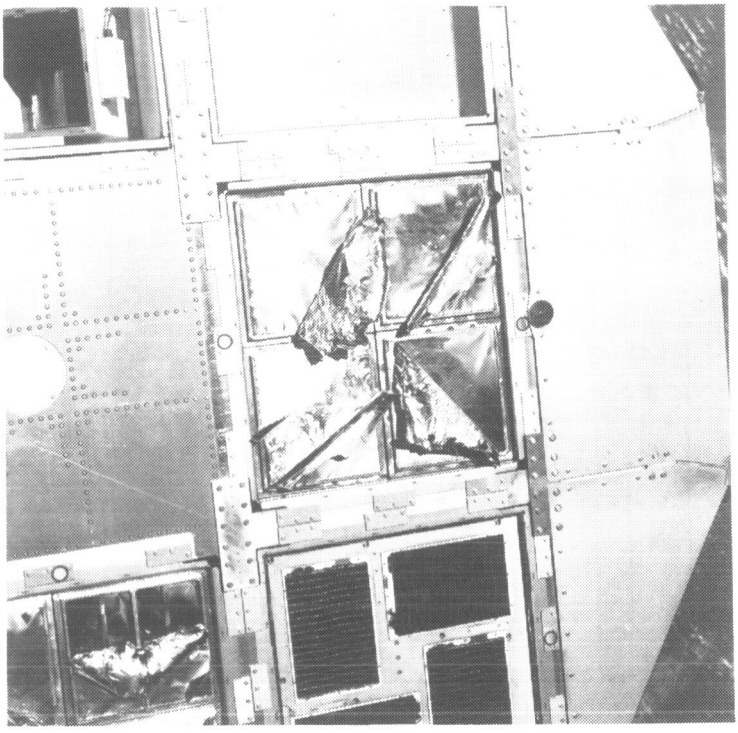

Figure 7. Loose Silverized Teflon Thermal Blankets

N93-28276

THE CONTINUING MATERIALS ANALYSIS OF THE THERMAL CONTROL SURFACES EXPERIMENT (S0069)

Donald R. Wilkes, Edgar R. Miller
AZ Technology, Inc.
3322 Memorial Parkway SW, Suite 93
Huntsville, AL 35801
Phone: 205/880-7481, Fax: 205/880-7483

James M. Zwiener, Richard J. Mell
NASA/Marshall Space Flight Center
Marshall Space Flight Center, AL 35812
Phone: 205/544-2528, 205/544-7329

SUMMARY

The long term effects of the natural and induced space environment on spacecraft surfaces are critically important to future spacecraft--including Space Station Freedom. The damaging constituents of this environment include thermal vacuum, solar ultraviolet radiation, atomic oxygen, particulate radiation, and the spacecraft induced environment. The behavior of materials and coatings in the space environment continues to be a limiting technology for spacecraft and experiments. The Thermal Control Surfaces Experiment (TCSE) was flown on the National Aeronautics and Space Administration (NASA) Long Duration Exposure Facility (LDEF) to study these environmental effects on surfaces--particularly on thermal control surfaces.

The TCSE was a comprehensive experiment that combined in-space measurements with extensive pre- and post-flight analyses of thermal control surfaces to determine the effects of exposure to the low Earth orbit space environment. The TCSE is the first space experiment to directly measure the total hemispherical reflectance of thermal control surfaces in the same way they are routinely measured in the laboratory.

This paper describes the trend analyses of selected coatings performed as part of the continuing post-flight analysis of the TCSE. A brief description of the TCSE and its mission on LDEF will be presented. There are several publications available that describe the TCSE, it's mission on LDEF, and initial results in greater detail. These are listed in the TCSE Bibliography at the end of this paper.

Experiment Description

The basic objective of the TCSE on the LDEF was to determine the effects of the near-Earth orbital environment and the LDEF induced environment on spacecraft thermal control surfaces. To accomplish this objective, the TCSE exposed selected material samples to the space environment and used in-flight and post-flight measurements of their thermo-optical properties to determine the effects of this exposure.

The TCSE was a completely self-contained experiment package, providing its own power, data system, reflectometer, and pre-programmed controller for automatically exposing, monitoring, and measuring the sample materials (See Figure 1). The primary TCSE in-space measurement was total hemispherical reflectance as a function of wavelength from 250 to 2500 nm using a scanning integrating sphere reflectometer. The measurements were repeated at preprogrammed intervals until battery power depletion.

The LDEF with the TCSE on board was placed in low earth orbit by the Shuttle Challenger on April 7, 1984. LDEF was retrieved by the Shuttle on January 12, 1990 after 5 years 10 months in space. The LDEF was gravity-gradient stabilized and mass loaded so that one end of LDEF always pointed at the earth and one side pointed into the velocity vector or RAM direction. The TCSE was located on the leading edge (row 9) of LDEF and at the earth end of this row (position A9). In this configuration, the TCSE faced the RAM direction. This LDEF/TCSE orientation and mission duration provided the following exposure environment for the TCSE:

Total space exposure	5 years 10 months
Atomic oxygen fluence[1] atoms/cm^2	8.0×10^{21} atoms/cm^2
Solar UV exposure[2]	1.0×10^4 ESH
Thermal cycles	3.3×10^4 cycles
Radiation (at surface)[3]	3.0×10^5 rads

The TCSE operated for the first 584 days of the LDEF mission before its batteries were depleted. Although the flight recorder malfunctioned, data were recovered for the last 421 days of this operational period. The recovered data included eleven sets of reflectometry data. The battery power was fully expended while the sample carousel was being rotated leaving the carousel in a partially open position. Figure 2 is a photograph taken during the LDEF retrieval operations showing the final position of the carousel. This carousel position permitted exposure of 35 of the samples for the complete LDEF

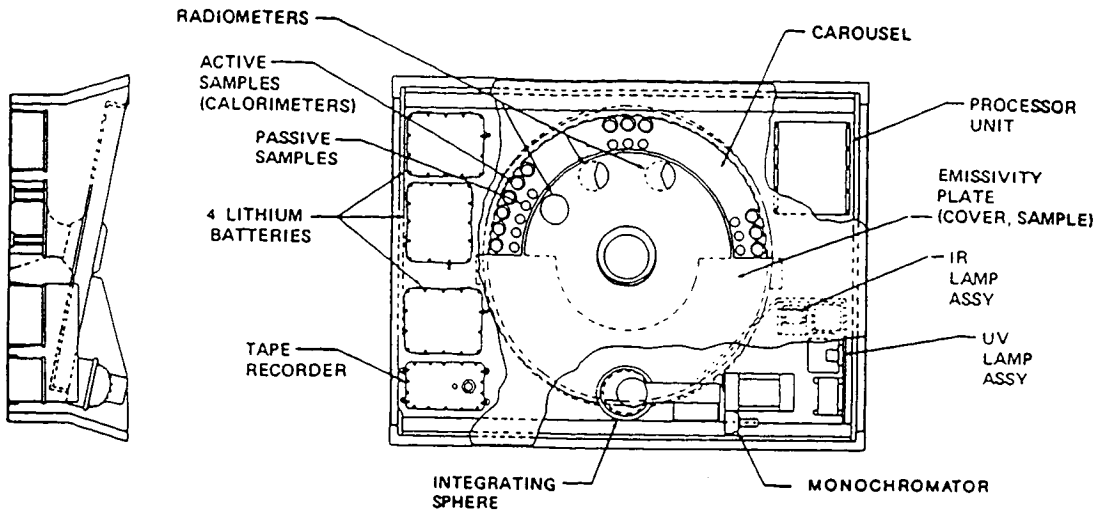

Figure 1. TCSE Assembly

mission (69.2 months), while 14 samples were exposed for only 19.5 months and protected from the space environment for the subsequent four years.

The test materials chosen for the TCSE mission comprised the thermal control surfaces of the greatest current interest (in 1983) to NASA, MSFC and the thermophysics community. The samples flown on the TCSE mission were:

- A276 Polyurethane White Paint
- A276/OI650 Clear Silicone Overcoat
- A276/RTV670 Clear Silicone Overcoat
- S13G/LO Inorganic White Paint
- Z93 Inorganic White Paint
- YB71 Inorganic White Paint
- YB71 over Z93
- Chromic Acid Anodize
- Silver/FEP Teflon (2 mil)
- Silver/FEP Teflon (5 mil)
- Silver/FEP Teflon (5 mil Diffuse)
- White Tedlar
- D111 Inorganic Black Paint
- Z302 Polyurethane Black Paint
- Z302/OI650 Clear Silicone Overcoat
- Z302/RTV670 Clear Silicone Overcoat

Note: Teflon and Tedlar are trademarks of Dupont.

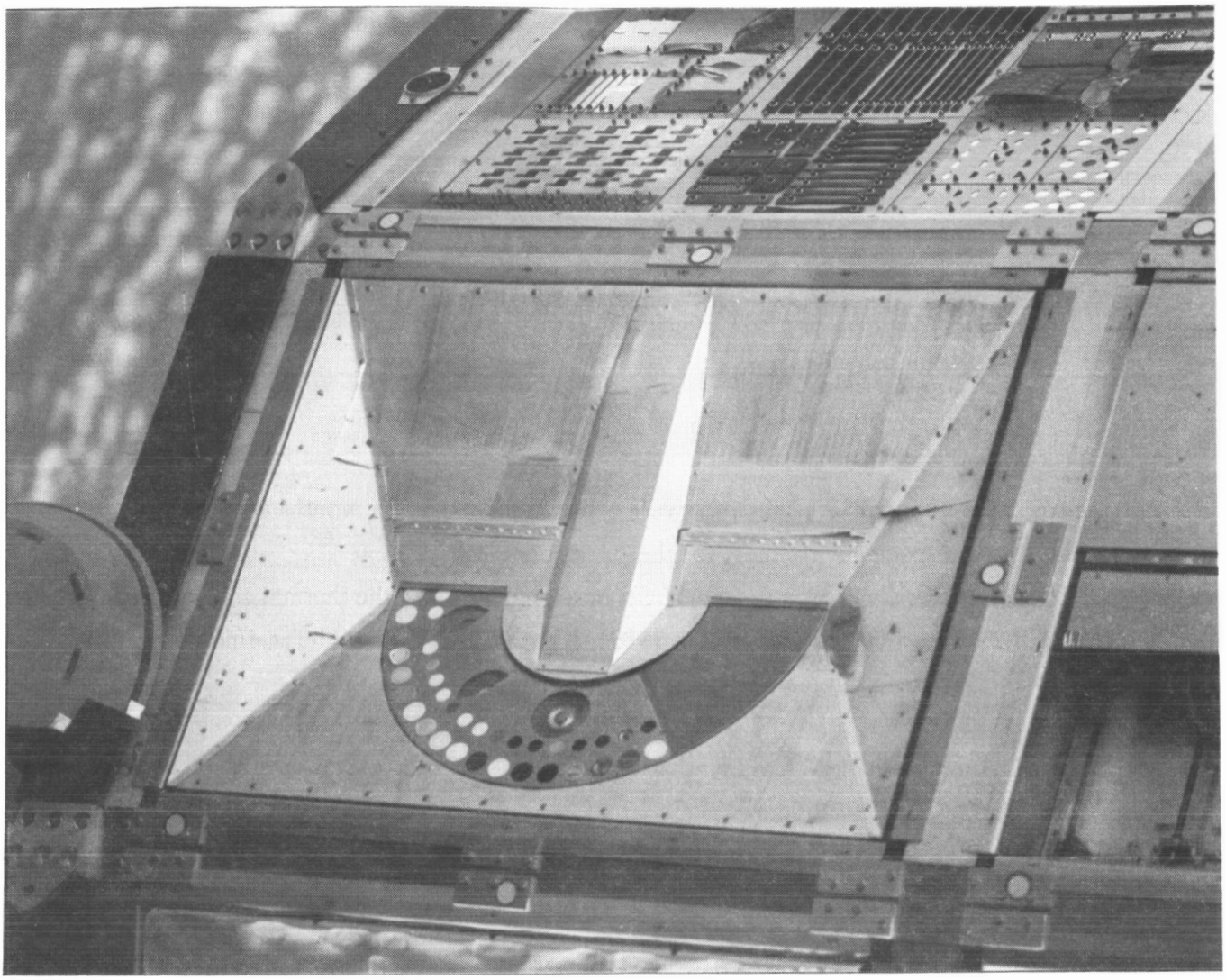

Figure 2. Photograph of LDEF Retrieval

Degradation Trend Analysis

The increasing duration of space missions requires significant extrapolation of flight and ground simulation data to provide predictions of end-of-life properties for thermal control surfaces. This is particularly true for NASA programs such as the 30 year lifetime Space Station Freedom, AXAF and the Hubble Space Telescope. The in-space optical measurements performed by the TCSE offer the unique opportunity to perform a trend analysis on the performance of materials in the space environment.

Trend analysis of flight data provides the potential to develop an empirical prediction model for some of the thermal control surfaces. For material research, trend analysis of the TCSE flight data can provide some insight into the damage mechanisms of space exposure.

The initial trend analysis for the TCSE samples has been limited to those materials that were not significantly eroded by the atomic oxygen (AO) environment. The performance of several materials on the LDEF mission was dominated by AO effects. This is particularly true for unprotected A276 and Tedlar where the AO eroded away the surface layers faster than they were degraded by Solar UV. This resulted in a fresh surface with unchanged or slightly improved optical properties. These coatings on the LDEF trailing edge suffered severe degradation of solar reflectance.

Preliminary analyses have been performed on the following five materials:

- Z93 White paint
- S13G/LO White Paint
- Chromic Acid Anodize
- A276 White Paint/RTV670 Clear Overcoat
- A276 White Paint/OI650 Clear Overcoat

These analyses were performed on the solar absorptance (α_S) values calculated from detailed spectral reflectance data taken in space and in ground pre-flight and post-flight measurements. Several standard regression analyses were tried including polynominal, exponential, logarithmic and power. In all cases the power regression analysis provided a better fit of the experimental data. The power regression line takes the form:

$$\alpha_S = \varepsilon(a + b \ln(t))$$

Figures 3 through 7 show the results of the regression analysis on the five materials.

For Z93 there appear to be at least two mechanisms affecting the Z93 solar absorptance for the LDEF mission (see Figure 3). The first is an improvement (decrease) in α_s typical of silicate coatings in thermal vacuum. This improvement is normally associated with loss of water from the ceramic matrix. In ground simulation tests this process takes a much shorter time than the TCSE flight data suggests. This slower loss of water may be due to the cold temperature of the TCSE Z93 sample mounted on a thermally isolated calorimeter. The temperature of the Z93 sample ranged from approximately -55°C to + 6°C but remained well below 0°C most of the time.

The short term improvement is dominant for the first year of exposure after which a long term degradation becomes dominant. The log/log plot of the Z93 data and the regression analysis projects a 30 year end-of-life value of $\alpha_s = 0.185$. This predicted value is statistically a most likely value and not a worse case value.

An analysis of the S13G optical data also suggests more than one damage mechanism. The power regression analysis shown in Figure 4 of the S13G data (except for the pre-flight point) provides a good fit of the data. Degradation from competing mechanisms appears different during the first six months of exposure compared to the last twelve months. The regression model predicts a 30 year end-of-life value of 0.61 for S13G/LO.

There were two thick chromic acid anodize samples on the TCSE active sample array. Solar absorptance values for the two samples tracked closely for the early part of the LDEF mission as shown by the TCSE in-space data shown in Figure 5. When the TCSE batteries were exhausted (at 19.5 months) the sample carousel stopped at a position where one of the samples was protected from further direct environmental exposure for the remaining duration of the LDEF mission. For the protected sample the post-flight α_s is plotted at the 19.5 month point. The anodize sample that was exposed for the entire mission had a mottled, washed out appearance suggesting a different damage mechanism occurring late in the mission. This is in contrast to the post-flight data that shows only a small degradation. In-flight data during the complete LDEF mission would have explained this ambiguity. This data is an excellent example of how misleading only pre- and post-flight data can be.

The regression analysis provides a good fit of the anodize sample data and predicts 30 year end-of-life α_s values of 0.82 and 0.76. As the predicted values approach $\alpha_s = 1.0$, the power regression model should fail, so these values may be somewhat high.

There were two samples of Chemglaze A276 polyurethane white paint with AO protective overcoats flown on TCSE. The protective overcoats were RTV670 and OI650. The regression analysis of the A276/RTV670 data shown in Figure 6 provides a good fit. However the power regression analysis of the A276/OI650 data provides a poor fit of the flight and post-flight measurements. This suggests a different degradation mechanism or combination of mechanisms for this coating; thus, it is not a surprising result considering the combining of completely different materials and the complexity of the environment.

These preliminary results from the trend analysis offer the potential of an empirical performance prediction model for some thermal control surfaces. Care must be exercised in use of empirical models in general and especially from this preliminary study. Log/log plots of experimental data can be misleading but are useful to examine the possibility of trends and the potential of an empirical model.

This analysis was performed on solar absorptance data. Solar absorptance is not a basic material property but an integrated value calculated using spectral reflectance data. This analysis will be extended to the detailed spectral reflectance data which should provide more insight into damage mechanisms for these materials.

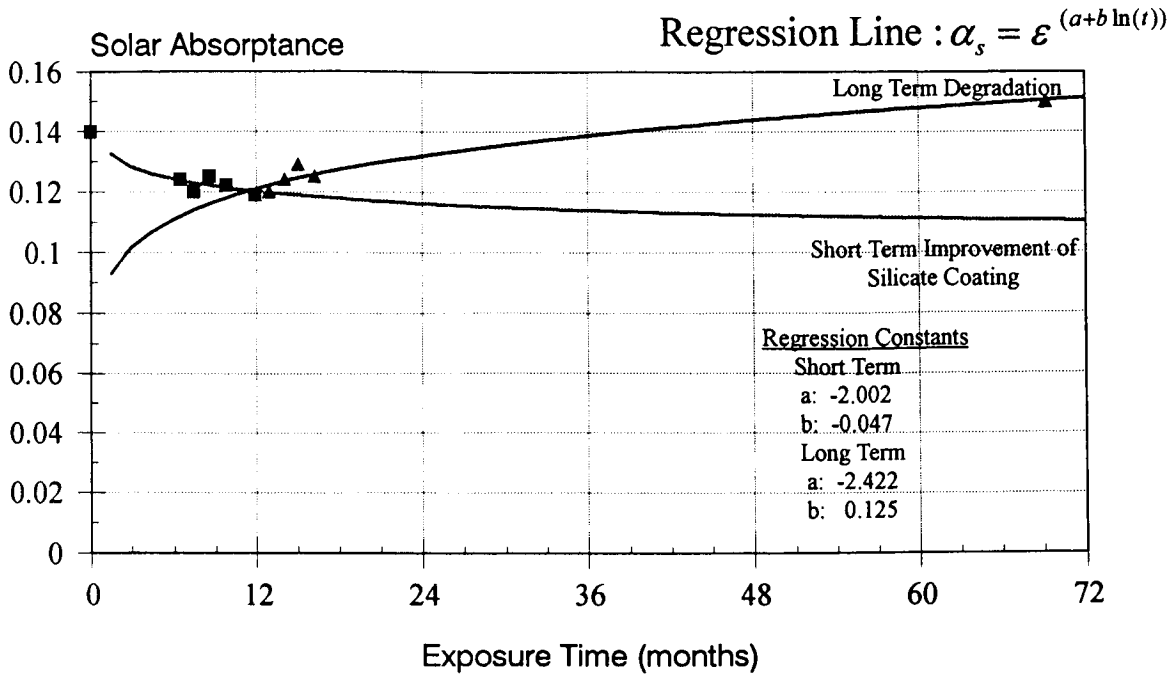

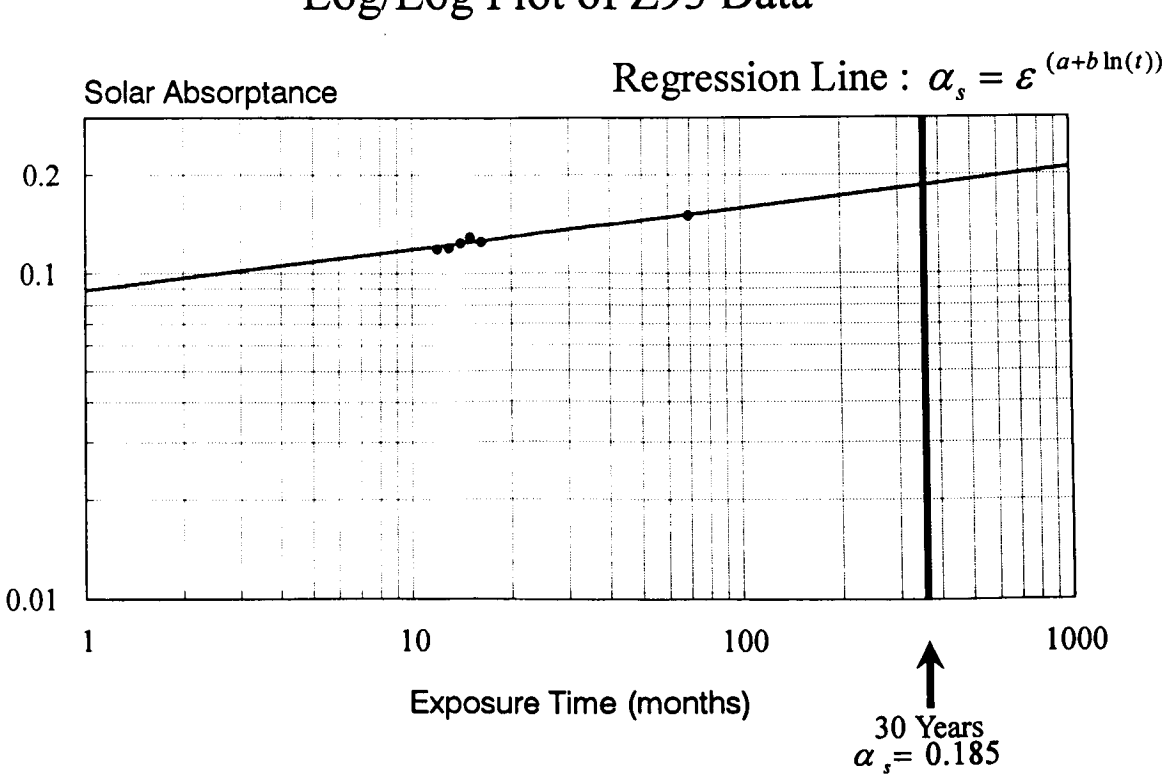

Figure 3. Degradation Rate Study of Z93

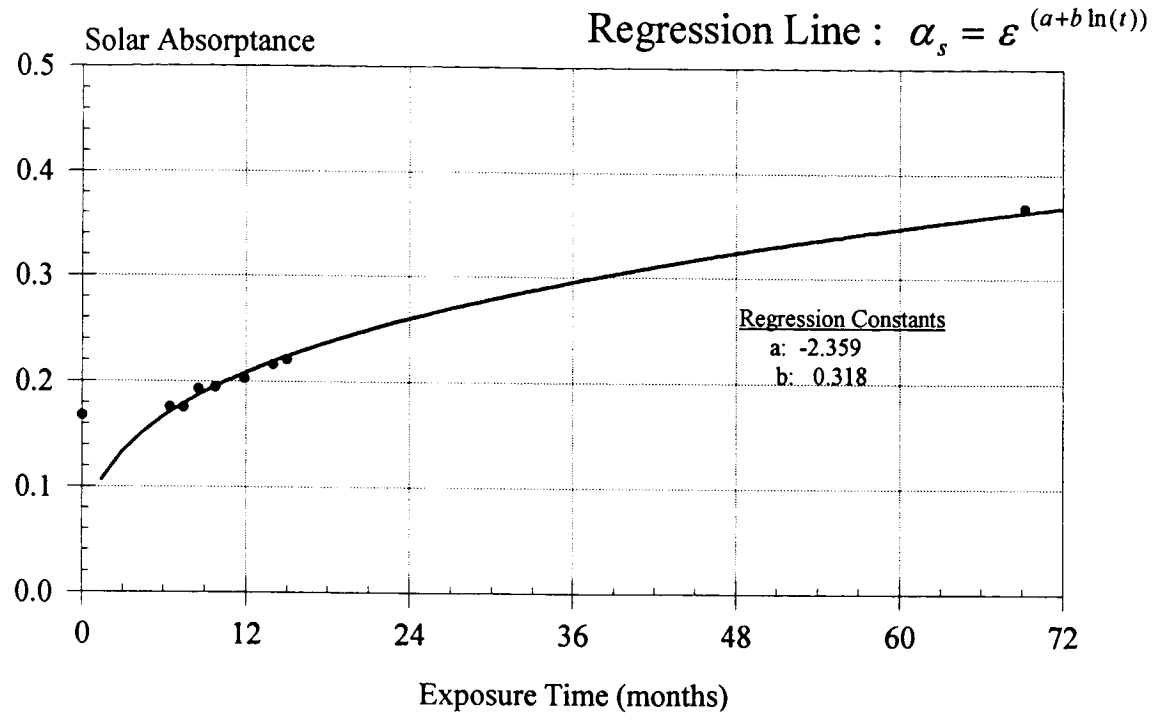

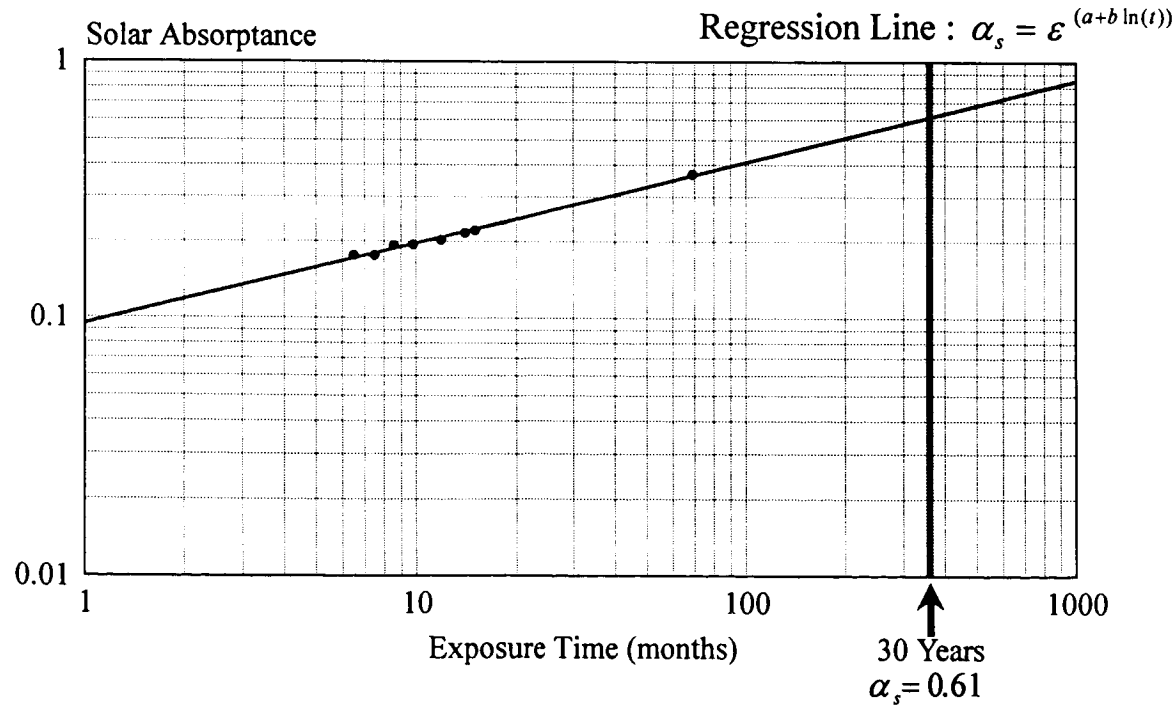

Figure 4. Degradation Rate Study of S13G/LO

Power Regression Analysis of Chromic Acid Anodize

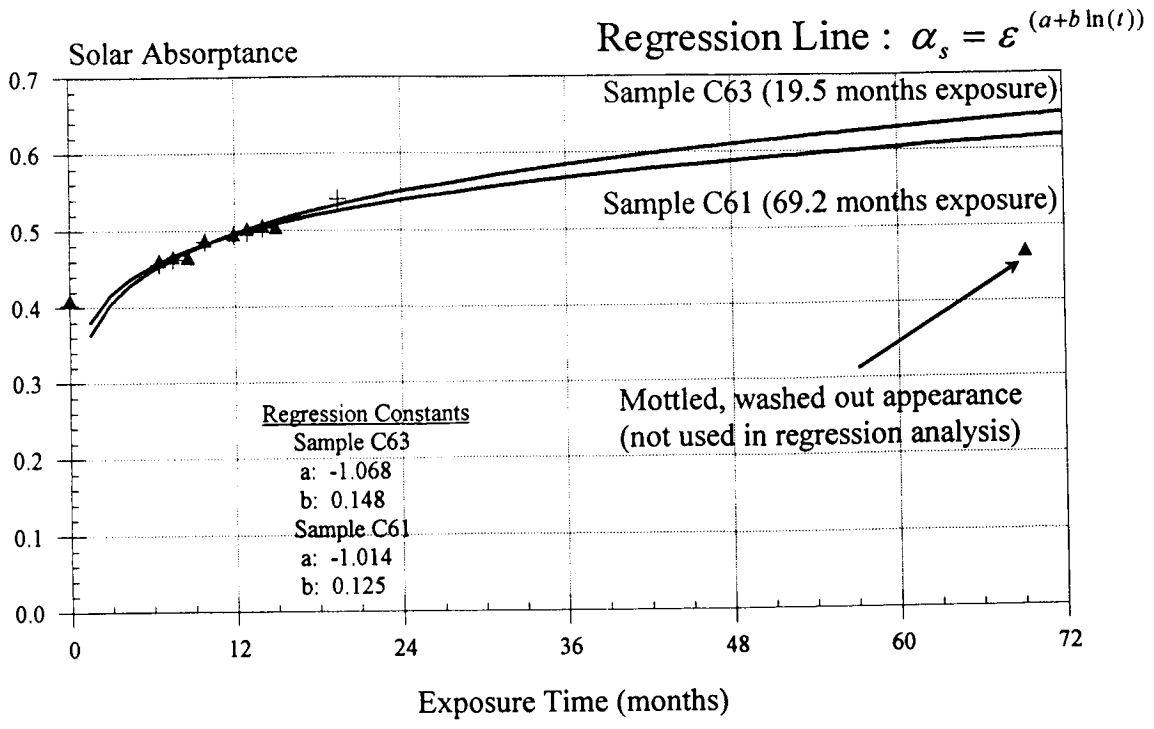

Log/Log Plot of Chromic Acid Anodize Data

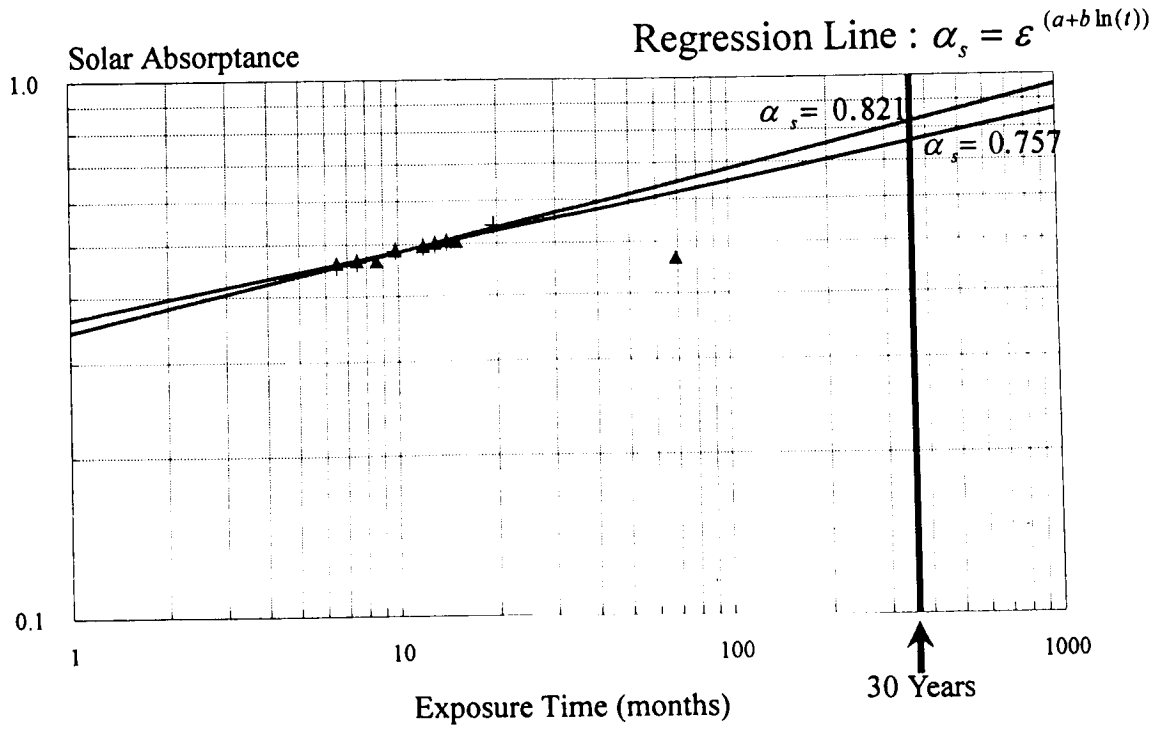

Figure 5. Degradation Rate Study of Chromic Acid Anodize

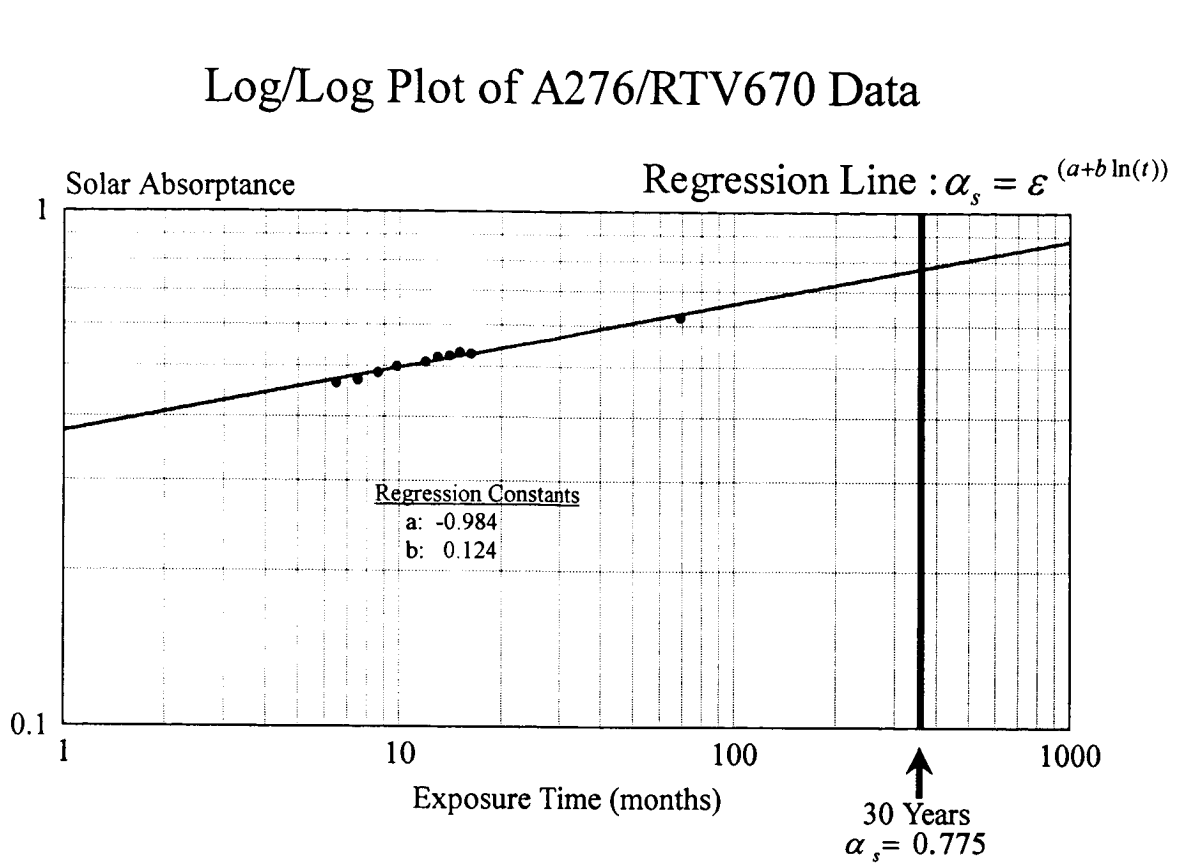

Figure 6. Degradation Rate Study of A276/RTV670 Data

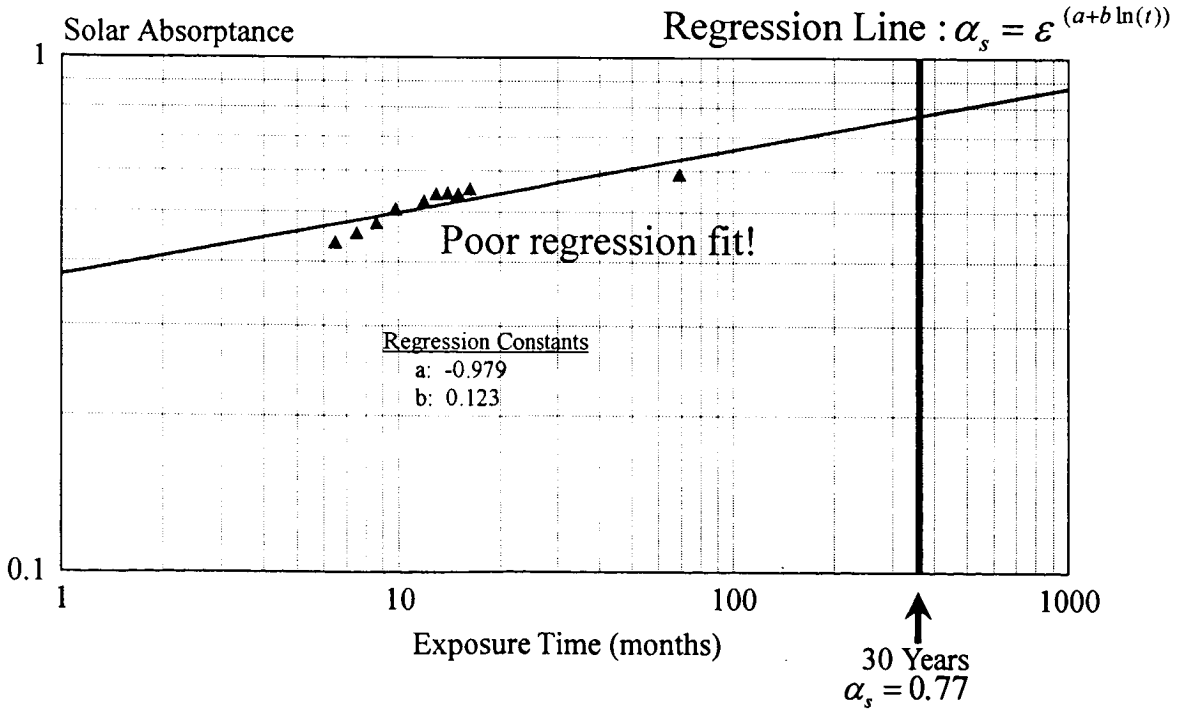

Figure 7. Degradation Rate Study of A276/OI650 Data

References

[1] Bourassa, R.J. and Gillis, J.R.; "Atomic Oxygen Flux and Fluence Calculation for Long Duration Exposure Facility (LDEF) Supporting Data", Contract NAS1-18224, January 1991.

[2] Berrios, W.M.; "Long Duration Exposure Facility Post-Flight Thermal Analysis, Orbital/Thermal Environment Data Package," NASA LaRC, Hampton, VA, October 3, 1990.

[3] Benton, E.V. and Heinrich, W.; "Ionizing Radiation Exposure of LDEF", University of San Francisco Report USF-TR-77, August 1990.

TCSE BIBLIOGRAPHY

Wilkes, Zwiener, "LDEF Thermal Control Surfaces Experiment", AIAA Space Programs and Technology, Huntsville, AL, September 1990.

Wilkes, Hummer, "LDEF TCSE (S0069) Post-Flight System Functional Check-out", Final Test Report, Contract HJ-3234, AZ Technology Report No. 90-2-107-1, February 1991.

Wilkes, Hummer, Brown, "Measurement and Analysis of LDEF/TCSE Flight Samples", Contract HK-7879, AZ Technology Report No. 90-2-107-1, February 1991.

Wilkes, Hummer, "Thermal Control Surfaces Experiment Initial Flight Data Analysis", Final Contract Report NAS8-38689, June 1991.

Wilkes, Zwiener, "Initial Materials Evaluation of the Thermal Control Surfaces Experiment (S0069)", First LDEF Post-Retrieval Symposium, Orlando, FL, June 1991

Zwiener, Wilkes, et al, "Unusual Material Effects Observed on the Thermal Control Surfaces Experiment (S0069)", First LDEF Post-Retrieval Symposium, Orlando, FL, June, 1991

Wilkes, Zwiener, et al, "Thermal Control Surfaces on the MSFC LDEF Experiments", LDEF Materials Workshop, Hampton, VA, November 1991

Zwiener, Wilkes, et al, "Fluorescence of Thermal Control Coatings on Experiment S0069 and AO114", LDEF Materials Workshop, Hampton, VA, November 1991

Wilkes, Zwiener, "The Thermal Control Surfaces Experiment (TCSE) on LDEF", AIAA 92-2166, AIAA Coatings Technologies for Aerospace Systems Specialist Conference, Dallas, TX, April, 1992.

Zwiener, Wilkes, et al, "Fluorescence Measurements of the Thermal Control Coatings on LDEF Experiments S0069 and A0114", Second LDEF Post-Retrieval Symposium in San Diego, California, NASA CP-3194, 1993.

N93-28277

THERMAL CONTROL PAINTS ON LDEF: RESULTS OF M0003 SUB-EXPERIMENT 18

C. H. Jaggers
M. J. Meshishnek
J. M. Coggi

The Aerospace Corporation
Mechanics and Materials Technology Center
El Segundo, CA 90245
Phone: 310/336-8680, Fax: 310/336-1636

ABSTRACT

Several thermal control paints were flown on LDEF, including the white paints Chemglaze A276, S13GLO, and YB-71, and the black paint D-111. The effects of low earth orbit, which includes those induced by UV radiation and atomic oxygen, varied significantly with each paint and its location on LDEF. For example, samples of Chemglaze A276 located on the trailing edge of LDEF darkened significantly due to UV-induced degradation of the paint's binder, while leading edge samples remained white but exhibited severe atomic oxygen erosion of the binder. Although the response of S13GLO to low earth orbit is much more complicated, it also exhibited greater darkening on trailing edge samples as compared to leading edge samples. In contrast, YB-71 and D-111 remained relatively stable and showed minimal degradation.

This paper examines the performance of these paints as determined by changes in their optical and physical properties, including solar absorptance as well as surface chemical changes and changes in surface morphology. It will also provide a correlation of these optical and physical property changes to the physical phenomena that occurred in these materials during the LDEF mission.

INTRODUCTION

The Long Duration Exposure Facility (LDEF) was initiated in 1976 as an exposure facility for various materials to the low earth orbit environment. The 30-ft long, 14-ft diameter spacecraft consisted of 57 experiments and was placed in a 255 nautical mile orbit by the Space Shuttle Challenger on April 7, 1984[1] for almost six years. It was returned to earth on January 20, 1990.

Spacecraft in low earth orbit (LEO), such as LDEF, are exposed to an environment that includes UV radiation, atomic oxygen, electrons, protons, thermal cycling, and micrometeoroids and debris. However, compared to synchronous orbits, the fluxes of electrons and protons are small and the effects are therefore minor in comparison to atomic oxygen and UV irradiation effects.[2] The spacecraft encountered an apparent flux of atomic oxygen of 10^{15} atoms/cm^2-sec with a kinetic energy of approximately 5 eV due to the average orbital velocity of 8 km/sec through the static low earth atomosphere.[3] However, the entire LDEF spacecraft was not exposed to the same atomic oxygen flux. The leading edge (LE) of the spacecraft, which is nearly perpendicular to the velocity vector (~8° off normal), receives a much higher flux than the trailing edge.[4] Consequently, leading edge samples on LDEF were exposed to an atomic oxygen fluence of as much as 8.74×10^{21} atoms/cm^2, while trailing edge samples were exposed to an atomic oxygen fluence

PRECEDING PAGE BLANK NOT FILMED

as low as 1.13×10^3 atoms/cm^2.[5-6] This difference allows the comparison of the synergistic effects of UV radiation and atomic oxygen exposure on leading edge samples to UV radiation exposure on the trailing edge samples.

The materials experiment M0003 was designed, built, and integrated by the Aerospace Corporation Mechanics and Materials Technology Center as principal investigator and was designed to study the effects of the space environment on current and developmental spacecraft materials. The M0003 subexperiment 18, one of a collection of 8 subexperiments from the Aerospace Corporation Laboratories, consists of 12 samples located on trays D9 (LE) and D3 (TE). These samples included two white thermal control paints, S13GLO (four samples; two on LE, two on TE) and YB-71 (LE, TE), and the black thermal control paint, D-111 (LE, TE). In addition, we were able to section additional samples from the signal conditioning unit (SCU) covers (painted with S13GLO) and the Experiment Power and Data System (EPDS) sunshields (painted with Chemglaze A276, another white thermal control paint) from trays D8 (LE) and D4 (TE) which provided us with numerous samples for destructive analyses. Initial results from this experiment have been previously reported.[7]

A summary of the solar absorptances for the thermal control paints are listed in Table 1. Chemglaze A276 and S13GLO, which are both white thermal control paints with organic binders, exhibited large increases of their solar absorptance on the trailing edge, while the leading edge either decreased slightly (Chemglaze A276) or showed a moderate increase (S13GLO). In contrast, YB-71 and D-111 contain inorganic binders and exhibited little degradation. This paper therefore focuses on the effects of low earth orbit on Chemglaze A276 and S13GLO.

BACKGROUND

Chemglaze A276

Chemglaze A276 is a white thermal control paint manufactured by Lord Corporation that incorporates a titanium dioxide pigment in a polyurethane binder. This paint was used on LDEF as a thermal control coating on the Experiment Power and Data System (EPDS) sunshields; these covers were used to protect data system instrumentation for other experiments. These covers were located on the leading edge (row 8) and trailing edge (row 4) of the spacecraft; row 8 is located 30° from the perpendicular of the atomic oxygen vector, and row 4 is located 30° from the perpendicular of the wake region. Consequently, these trays were exposed to different levels of UV radiation and atomic oxygen; samples from row 8 (referred to as leading edge samples) were exposed to 9400 equivalent sun hours of UV radiation and an atomic oxygen fluence of 6.93×10^{21} atoms/cm^2, while samples from row 4 (referred to as trailing edge samples) was exposed to 10,400 equivalent sun hours of UV radiation and an atomic oxygen fluence of 9.32×10^4 atoms/cm^2.[5-6]

Experiments from Shuttle missions STS-5 and STS-8 demonstrated the effects of atomic oxygen exposure on material degradation.[8-11] Whitaker reported the effects of atomic oxygen on several paints from the STS-5 mission, including Chemglaze A276.[12] Based on SEM results, she noted that the Chemglaze A276 developed a porous surface, probably due to the atomic oxygen reacting with the polyurethane binder. However, the total atomic oxygen fluence incident on the samples was only 9.9×10^{19} atoms/cm^2, which is significantly less than the fluence that the leading edge of LDEF received. Additionally, the limited duration of the STS-5 Space Shuttle flight did not permit the evaluation of long-term UV radiation effects.

Other LDEF investigators have reported the effects of atomic oxygen and UV radiation on Chemglaze A276. Pippin[13] reported that the polyurethane binder was eroded by atomic oxygen, leaving the white pigment exposed. Wilkes and Hummer[14] also reported that A276 exposed to atomic oxygen remained white, while samples on the leading edge of LDEF that had protective overcoatings and therefore only received UV radiation exhibited the same UV darkening effects.

The effects of UV radiation on the optical properties of titanium dioxide have been investigated previously.[15] The reflectance spectra of titanium dioxide degrades significantly more in the visible than the IR region, but almost completely recovers to the pre-irradiation values after exposure to an oxidizing atmosphere. This suggests that any UV induced damage to the Chemglaze A276 pigment could recover upon return of the LDEF spacecraft to earth or on interaction with atomic oxygen.

S13GLO

S13GLO is a white thermal control paint manufactured by IITRI that incorporates a zinc oxide pigment in a methyl silicone binder. The ZnO pigment is encapsulated with potassium silicate for increased stability in the space environment. Our samples consist of two leading edge and two trailing edge samples (trays D9 and D3) plus samples sectioned from the leading and trailing edge signal conditioning unit covers (trays D8 and D4). Consequently, we were able to access many samples for destructive laboratory evaluations.

Zinc oxide was originally thought to be one of the most stable white pigments to UV irradiation in vacuum.[16] However, in 1965 serious doubts arose due to discrepancies between ground-based and in-flight experiments.[17-18] As a result, it was determined that the original zinc oxide-based silicone coatings (S-13) were not as stable as first predicted. This instability has been attributed to the formation of an easily bleachable (by oxygen) infrared absorption band (~700-2800 nm).[19] This damage was not observed by post-exposure reflectance measurements performed in air, since exposure to the atmosphere resulted in a rapid and complete recovery of the UV-induced damage.[20]

Since the ultraviolet-induced infrared absorption band develops rapidly in zinc oxide and is easily reversed upon exposure to oxygen, it has been suggested that the infrared phenomenon is not related to bulk phenomena but is associated with the photodesorption of oxygen. Gilligan[19] explained the infrared optical behavior of ZnO on the basis of a free-carrier absorption mechanism. Absorbed photons create electron-hole pairs in a "depletion zone" with the holes discharging adsorbed oxygen from the surface of the pigment particles. The zinc oxide pigments therefore becomes electron rich with the electrons accumulating in the infrared-active conduction band, resulting in an increase in the infrared absorption.

The methyl silicone binder itself does not offer an effective barrier to photodesorption reaction on the surface of zinc oxide since it does not "wet" the pigment particles. Consequently, a method was developed to reactively encapsulate the zinc oxide pigment particles with potassium silicate to provide stability to the surface. Studies have shown that the reactively-encapsulated zinc oxide pigment greatly reduces UV-induced infrared degradation.[21]

There is additional UV-induced degradation observed in the S13GLO paint system due to degradation of the silicone binder. When exposed to ultraviolet radiation, the methyl silicone binder exhibits induced ultraviolet-visible absorption. Only a portion of this damage observed in S13GLO recovered upon exposure to oxygen[21-22], indicating that the degradation is not limited to bleachable surface defects but may be the result of bulk polymer degradation.[21] Gaseous products have been observed to evolve during exposure of a methyl silicone/TiO_2 paint system to UV radiation in vacuum and are primarily hydrocarbon molecules. These hydrocarbon molecules are a result of bulk degradation of the methyl silicone binder.[23]

Previous atomic oxygen experiments on Shuttle missions STS-5 and STS-8 did not reveal any noticeable degradation to S13GLO.[12] Solar absorptivity and scanning electron microscope (SEM) photographs did not indicate any atomic oxygen erosion of the surface of S13GLO.

EXPERIMENTAL

Samples of Chemglaze A276 and S13GLO from LDEF were studied to determine the effects of atomic oxygen and UV radiation on these materials. Both leading and trailing edge samples were compared to control samples, since the atomic oxygen fluence varied significantly with location on LDEF. Optical properties, surface morphologies, and surface chemistry were investigated.

Changes in the optical properties of the materials, especially solar absorptance, is the primary indication of degradation after exposure to atomic oxygen and UV radiation. Optical measurements of the samples were obtained using a Perkin-Elmer Lambda 9 UV/VIS/NIR spectrophotometer. The diffuse reflectance spectra between 250 and 2500 nm were used to calculate the solar absorptances of each sample. This information allowed us to quantify the change in performance of these thermal control coatings.

Atomic oxygen erosion of these materials was a concern, based on previous studies.[12-14] The surface morphologies of the samples were compared using a JEOL JSM-840 Scanning Electron Microscope (SEM). It was necessary to coat the samples with carbon prior to analysis since they were non-conducting. The results allowed us to compare the effects of the atomic oxygen impingement on the surface of the leading edge samples.

Changes in surface composition and structure were investigated using X-ray Photoelectron Spectroscopy (XPS), Energy Dispersive X-ray Analysis (EDAX), and Fourier-Transform Infrared Analysis (FTIR). A VG ESCALAB MK II multiprobe instrument was used for XPS analysis, which yielded surface elemental compositional information. Additional elemental analysis of the surface was obtained by EDAX using instrumentation located on the SEM. Structural information, in addition to limited chemical compositional information, was given by FTIR; the FTIR analysis was performed by the diffuse reflectance method using a Nicolet MX-1 infrared spectrometer. These three analytical techniques complemented each other and aided in our investigation of the degradation mechanisms of these coatings.

The degradation mechanisms were also investigated by UV exposure of leading edge and reference samples, performed in a space environmental effects chamber in the Mechanics and Materials Technology Center at Aerospace. UV irradiation was performed in vacuum (~5×10^{-8} torr) using a 1000 W xenon-mercury lamp (spectral output >230 nm) passing through a water filter and a fused silica window. The samples were exposed for 10 days at a rate of 2-3 times the output of the sun over the UV range of 200-400 nm (the xenon-mercury lamp has a spectral output comparable to the sun at wavelengths above 230 nm but is significantly less than the sun below 230 nm). This flux resulted in a total fluence of approximately 480-720 equivalent solar hours, depending upon their location on the sample table.

RESULTS

Chemglaze A276

Samples of Chemglaze A276 used in this study were sectioned from the EPDS sunshield covers. The reference samples were sectioned from aluminum panels provided by Rockwell Corporation that were prepared after LDEF was returned to earth. Variations in surface preparation, pigment particle size, and paint thickness[24] can lead to inherent differences between the LDEF samples and our reference sample; therefore, any conclusions based on a comparison to the reference material should be made cautiously.

The effects of low earth orbit on Chemglaze A276 can be seen in Figure 1. The difference in appearance of the samples is significant; the trailing edge sample has darkened considerably, while the leading edge sample has remained white. These differences are also shown in the reflectance spectra in Figure 2 and the calculated solar absorptances in Table 1. The solar absorptance of the trailing edge sample increased significantly during the LDEF mission. Since the trailing edge of the spacecraft was exposed to predominately UV radiation with limited atomic oxygen exposure, the observed degradation was assumed to be UV-induced. Similarly, preliminary observations indicated that the synergistic effects of atomic oxygen and UV radiation resulted in the leading edge sample of Chemglaze A276 remaining white.

Leading Edge

Although it appears from Figure 1 that the optical properties of the leading edge samples remained unchanged during the mission, optical measurements show that its solar absorptance actually decreased. Inspection of the SEM photographs in Figure 3 show the effects of atomic oxygen on the surface of the leading edge samples. The polyurethane binder has been eroded away by the atomic oxygen, leaving a surface of titanium dioxide pigment particles. Sample analysis using EDAX confirm that the surface of the leading edge sample is titanium-rich. EDAX shows a much stronger carbon signal for the trailing edge sample, which is attributed to the organic polyurethane binder (Figures 4-5).

The increase in the leading edge solar absorptance can be explained if we consider the refractive indices of the individual components. For the pristine paint, the titanium dioxide pigment particles are embedded in the polyurethane binder. After atomic oxygen exposure, the binder has been eroded from the surface leaving the pigment particles primarily surrounded by air. Scattering in paints is proportional to

$$\frac{(n_1-n_2)^2}{(n_1+n_2)^2} \qquad \text{(Eqn. 1)}$$

where n_1 is the refractive index of the pigment and n_2 is the refractive index of the medium around it.[24] For titanium dioxide, $n_1 \sim 2.7$, while the refractive index for the polyurethane binder, n_2, is >1.0. Therefore, when the binder is eroded from the surface leaving only pigment particles surrounded by air, where $n_2(\text{air})=1$, the scatter increases. Increased scattering decreases the depth of penetration of the light into the sample, thereby reducing the number of absorption events and reducing the coating's solar absorption. Lowrance and Cox[25] discuss the decrease in solar absorptance obtained by eliminating the binder in a pigmented coating and directly sintering the pigment particles together.

Trailing Edge

The major difference between the surfaces of the leading and trailing edge samples is the erosion of the polyurethane binder from the leading edge sample; the surface of the trailing edge sample still contains binder. An obvious difference is the glossy appearance of the TE sample compared to the chalky LE sample, indicating the changes in paint composition. Combined with the knowledge that the trailing edge of LDEF was exposed to primarily UV radiation, it is most likely that the increase in solar absorptance of the trailing edge is due to UV degradation of the polyurethane binder. Previous investigators have shown that exposure of polyurethanes to ultraviolet radiation results in autoxidization of the urethane chains to a quinone-imide structure. A consequence of these chemical changes is a deeping color from colorless to yellow to amber, and on extensive exposures even to a brown.[26] These results are consistent with our observations of the Chemglaze A276 samples from LDEF, as well as those by other LDEF investigators.[27-29]

By exposing leading edge samples that had surfaces that were eroded by atomic oxygen causing binder loss and were therefore pigment-rich, such as leading edge samples, and previously unexposed virgin paint, we were able to show that the degradation does indeed occur in the binder. A rather interesting sample is shown in Figure 6. This sample is from the leading edge of the spacecraft; the opening in the sample is a bolt hole. The area adjacent to this hole was shielded from atomic oxygen impingement by the bolt head, and therefore still contains binder on the surface. The rest of the sample surface, however, is predominantly titanium dioxide pigment. As the photographs show, the area immediately adjacent to the hole has darkened after the laboratory UV exposure, while the rest of the sample is unaffected. Pre- and post-irradiation solar absorptances of the samples, listed in Table 1, clearly show that the samples that are affected by the UV radiation are those that contain binder on the surface. The solar absorptance of the leading edge sample remained fairly constant during UV irradiation, while a virgin paint sample darkened considerably.

S13GLO

Initial observations showed considerable differences between leading and trailing edge samples, as shown in Figures 7 and 8. Both sets of samples did degrade in the space environment, as evident by comparison of the exposed sample regions to the masked regions under the mounting hardware. As with Chemglaze A276, the optical properties of the trailing edge samples degraded more severely than the leading edge samples; the trailing edge discolored significantly from white to brown, while the leading edge samples appeared slightly off-white to tan in color.

The solar absorptances of the two samples, calculated from reflectance spectra obtained in our laboratory (see Figure 9), confirm that the trailing edge samples darkened much more than the leading edge samples. The solar absorptance of the trailing edge has increased threefold from an initial value of 0.15 (see Table 1). The leading edge has also degraded, but its solar absorptance has only increased to 0.23. Almost all of the degradation occurs in the visible and ultraviolet wavelengths, with very little degradation occurring above 1200 nm. The absorption peaks above 1200 nm have been identified as methyl silicone (binder) absorption peaks and are present in leading edge, trailing edge, and control samples.

Unlike Chemglaze A276, we do not observe any gross difference in the surface morphologies of S13GLO leading and trailing edge samples. Scanning electron microscopy (SEM) photographs of the leading and trailing edge surfaces are shown in Figures 10 and 11. At high magnification (5000X) the surface morphologies of the leading and trailing edge samples appear similar. At lower magnification (100X), however, we see evidence for two different cracking networks on the leading edge, while only one cracking network appears on the trailing edge. Also, the degree of cracking, or cracking density, appears to

be much greater on the leading edge. The nature of these cracking networks is not well understood, although elemental mapping with EDAX indicates that the cracks are rich in silicon and depleted in zinc.

Surface analysis of S13GLO using XPS indicates that oxidation of both the leading and trailing edge sample surfaces has occurred relative to the control sample, as shown in Table 2. The change in O:Si ratio, combined with a Si2p binding energy shift, strongly supports a change from silicone to silica as the predominant surface species on the LDEF samples. It is interesting to note that the O:Si ratio for both the leading and trailing edge samples has increased to roughly the same values, even though the atomic oxygen fluence on the surfaces varied by sixteen orders of magnitude. Surface carbon has been "lost" relative to O and Si, particularly on the leading edge, probably due to the replacement of methyl groups with oxygen in the methyl silicone binder. The amount of carbon lost, however, is related to the atomic oxygen fluence as indicated by the C:Si ratio of the samples. Erosion of surface layers of silicone binder is also consistent with increased K and Zn signals on both leading and trailing edge paint.

Significant levels of N, S, Cl, Na and F were detected as contaminants by XPS on all the LDEF samples, including S13GLO. As table 2 indicates, the contaminant levels were slightly higher on the trailing edge samples. However, the contamination most likely did not contribute significantly to the observed degradation of the optical properties of the S13GLO samples. Optical contamination monitors flown on the M0003 experiment indicated small changes in solar absorptance due to contamination consistent with our assertion that the darkening is not related significantly to contamination but is in fact UV-induced degradation.[7] Additionally, we have been able to cause darkening similar to the observed degradation of S13GLO using ultraviolet (UV) and vacuum ultraviolet (VUV) irradiation on uncontaminated laboratory samples, as discussed elsewhere in this paper.

Additional evidence for surface oxidation and loss of methyl groups can be seen in the IR spectra in Figure 12. The control sample exhibits absorption peaks characteristic of the methyl silicone binder.[30] However, the IR spectra of both leading and trailing edge samples differ from the control sample in similar details. In particular, the asymmetric Si-O-Si stretch in methyl silicone, represented by absorption peaks at 1066 and 977 cm^{-1}, has broadened significantly and shifted to ~1200-1300 cm^{-1}. This broader absorption peak is characteristic of the formation of silica.[31] Also, the absorption peaks associated with the asymmetric $-CH_3$ stretch (2965 cm^{-1}), the symmetric $-CH_3$ stretch (2906 cm^{-1}), and the asymmetric $-CH_3$ deformation (1410 cm^{-1}) in methyl silicone have decreased significantly in the LDEF samples, indicating a loss of methyl groups.

Ultraviolet Radiation Effects

Changes in the reflectance spectra of both the leading and trailing edge samples occurs in the region that is normally associated with degradation of methyl silicone, while little change is observed in the region of the spectra associated with the degradation of zinc oxide. When exposed to ultraviolet radiation, methyl silicone shows ultraviolet-visible damage[21-22]. In contrast, zinc oxide exhibits damage in the infrared wavelengths[18-19]. Even though silicate coatings on zinc oxide greatly reduce UV-induced degradation, it is possible that some degradation of the zinc oxide pigment did occur during the LDEF mission and that the bleachable nature of these defects resulted in their recovery before the reflectance measurements were made[20], in-flight reflectance measurements of S13GLO samples on LDEF show that the majority of damage does indeed occur in the ultraviolet-visible wavelengths[32], which is characteristic of binder degradation. Therefore, the change in the reflectance spectra of both the leading and trailing edge samples is typical of UV-induced degradation of the methyl silicone binder while there is little evidence to support degradation of the zinc oxide pigment.

Testing of the individual components in our laboratory indicates that UV-induced damage to the methyl silicone binder is the most likely cause of the degradation to the S13GLO samples. When exposed to UV radiation, only the methyl silicone sample exhibited degradation, while encapsulated zinc oxide pellets remained stable. Samples of S13GLO prepared in our laboratory exhibited an increase in solar absorptance less than 0.04.

Atomic Oxygen Effects

Since both the leading and trailing edge samples received similar amounts of ultraviolet radiation, it is interesting to note that the trailing edge samples showed a much greater increase in solar absorptance. The role of atomic oxygen must therefore be considered. The leading edge surface was subjected to an atomic oxygen fluence several orders of magnitude greater than the trailing edge surface, which may have resulted in chemical and physical differences between the two surfaces.

Surface analyses of the LDEF samples clearly indicates that significant changes occured in the methyl silicone binders on both leading and trailing edge samples. The loss of methyl groups, accompanied by an increase in the O:Si ratio, is consistent with an oxidation of methyl silicone to silica. Although the leading edge surface was exposed to significant amounts of atomic oxygen, it is interesting to note that samples of S13GLO sectioned from the trailing edge SCU cover on tray D4 also exhibited surface oxidation, even though the reported atomic oxygen fluence of 9.32×10^4 atoms/cm^2 is significantly less than the amount necessary for one monolayer of coverage (~10^{15} atoms/cm^2, based on our calculations). The implications of this observation, however, are not fully understood.

The surface oxidation of the methyl silicone binder resulted in changes to the surface morphology of the LDEF samples. The exposure of S13GLO to atomic oxygen resulted in a chemical change (oxidation) of the methyl silicone binder. At high magnification, the surface appears intact since the binder has not been removed from the surface. However, at lower magnifications the changes become apparent. The surface has developed a cracking network, the extent of which is related to the degree of oxidation as indicated by the atomic oxygen fluence. The most likely explanation is that the cracks developed due to a density change as a result of the oxidation of the methyl silicone binder to silica.

It is not clear why the leading edge paint surface shows less degradation than the trailing edge paint surface, although atomic oxygen exposure almost certainly plays a role. One theory is that spalling of the degraded S13GLO surface occurred on the leading edge due to surface oxidation and cracking, thereby exposing a fresh surface. However, this mechanism has not been reproduced in the laboratory and is still under investigation.

SUMMARY

Our investigation of Chemglaze A276 shows that severe degradation occurs due to UV radiation and atomic oxygen interactions. The polyurethane binder in Chemglaze A276 is easily and severely degraded by UV radiation, resulting in a large increase in the material's solar absorptance. Our simulated UV exposure represented only 5-8% of the total exposure that the paints on LDEF actually received, but the degradation of the Chemglaze A276 solar absorptance was obvious. In fact, for this test we did not include the vacuum ultraviolet (VUV) radiation at the shorter wavelengths, which has been shown to result in a greater rate of degradation for some polymer systems.[33-36] Additional simulations are in progress.

The polyurethane binder of Chemglaze A276 is also susceptible to atomic oxygen erosion, which creates a surface that is predominantly titanium dioxide pigment. The degree of atomic oxygen erosion depends on the location of the material in relation to the velocity vector in the low earth orbit. Although the thermal control properties of the surface are not deleteriously affected, the surface has lost its physical integrity and is easily damaged upon contact.

Chemglaze A276 is not recommended as a white thermal control paint for spacecraft that require any significant mission lifetimes due to its susceptibility to UV degradation and atomic oxygen erosion. Ultraviolet radiation causes a significant increase in the material's solar absorption, while atomic oxygen erosion of the binder results in a fragmented surface and could cause particulate contamination to other areas of the spacecraft. Its low cost and ease of application, however, make it much more desirable for boosters and upper stage rockets that do not require long mission lifetimes.

The increase in solar absorptance of S13GLO is due to UV-induced damage of the methyl silicone binder on both the leading and trailing edge samples; based on our reflectance data, there is no evidence of damage to the encapsulated zinc oxide pigment. This damage is not bleachable and does not recover upon exposure to air, even after one year. Both the leading and trailing edge surfaces show oxidation of the methyl silicone binder to silica, which is accompanied by a loss of methyl groups and a formation of a cracking network on the surface. The extent of this cracking network depends largely on the atomic oxygen fluence that the surface received. However, unlike A276 there was no preferential removal of the binder by atomic oxygen from the leading edge surface.

CURRENT WORK

We are continuing our investigation of atomic oxygen interactions with Chemglaze A276 and S13GLO by participating in EOIM III, scheduled to be flown on the Space Shuttle in late 1992. Trailing edge samples of A276 and S13GLO that were previously flown on LDEF have been included in the sample complement. Pre- and post-test analyses will allow us to study the atomic oxygen effects on these materials and to determine the role of atomic oxygen in the observed degradation of these materials in low-earth orbit.

Laboratory simulations of low-earth orbit, consisting of UV radiation and atomic oxygen, are continuing. Our facilities in the Mechanics and Materials Technology Center at The Aerospace Corporation allow us to study the effects of UV radiation on unflown and previously flown materials. Atomic oxygen experiments are scheduled for Los Alamos this year; additional atomic oxygen simulations may be performed in facilities at the Aerospace Corporation.

Our investigations are currently expanding to include the YB-71 and D-111 thermal control paints that were originally flown as part of this sample complement.

ACKNOWLEDGEMENTS

The authors would like to express their sincere appreciation to Col. M. Obal of the Strategic Defense Initiative Organization/TNI, Materials and Structures program, and Dr. W. Ward and Lt. M. Jones, Wright Laboratory/Materials Directorate, for funding a portion of this work as part of the SDIO/TNI/M+S Space Environmental Effects program.

Our efforts would not be successful without the assistance and expertise of many people at The Aerospace Corporation. We would like to thank D.A. Brose and J.C. Uht for SEM photographs and EDAX surface analysis measurements; L. Fishman for deintegration and initial documentation of the LDEF samples; S.R. Gyetvay for quick-look reports, photographs, and assistance in the analysis of our data; C.S. Hemminger for XPS surface analysis measurements and interpretations; and G.A. To for IR analysis. In addition, we would like to thank Mike Dyott of Rockwell for providing samples of unflown Chemglaze A276 for analysis.

REFERENCES

1. Long Duration Facility Deployed Successfully. *Aviation Week and Space Technology*, April 16, 1984, p. 20.
2. Outlaw, R.A. and Brock, F.J.: Orbiting Molecular-Beam Laboratory. *Vac. Sci. Technol.*, Vol. 14, no. 6, 1977, pp. 1269-1275.
3. Arnold, G.S. and Peplinski, D.R.: Reaction of High-Velocity Atomic Oxygen with Carbon. *AIAA Journal*, Vol. 24, no. 4, 1986, pp. 673-677.
4. Oran, W.A. and Naumann, R.J.: Utilization of the Vacuum Developed in the Wake Zone of Space Vehicles in the LDEF Class. *J. Vac. Sci. Technol.*, Vol. 14, no. 6, 1977, pp. 1276-1278.
5. Bourassa, R.J. and Gillis, J.R.: Atomic Oxygen Exposure of LDEF Experiment Trays. NASA Contractor Report 189627, May 1992.
6. Bourassa, R. and Pippin, G.: Induced Environment Characterized, Effects Summarized. *LDEF Spaceflight Environmental Effects Newsletter*, Vol. 2, no. 3, June 15, 1991, pp. 6-7.
7. Meshishnek, M.J., Gyetvay, S.R., and Jaggers, C.H.: Long Duration Exposure Facility Experiment M0003 Deintegration/Findings and Impacts. *Proceedings of the LDEF First Post-Retrieval Symposium*, NASA Conference Publication 3134, Part 2, pp. 1073-1107, Jan. 1992.
8. Leger, L.J., Spiker, I.K., Kuminecz, J.F., and Visentine, J.T.: STS Flight 5 LEO Effects Experiments - Background Description and Thin Film Results. AIAA-83-2631-CP, October 1983.
9. Leger, L.J., Visentine, J.F. and Kuminecz, J.F.: Low Earth Orbit Atomic Oxygen Effects on Surfaces. AIAA-84-0548, January 1984.
10. Visentine, J.T., Leger, L.J., Kuminecz, J.F., and Spiker, I.K.: STS-8 Atomic Oxygen Effects Experiments. Paper presented at AIAA 23rd Aerospace Sciences Meeting, Reno, NV, January 1985.
11. Green, B.D., Caledonia, G.E., and Wilderson, T.D.: The Shuttle Environment: Gases, Particulates and Glow. *J. Spacecraft and Rockets*, Vol. 22, no. 5, 1985, pp. 500-511.
12. Whitaker, A.F.: LEO Atomic Oxygen Effects on Spacecraft Materials - STS-5 Results. NASA-TM-86463, August 1984.
13. Pippin, G., *LDEF Spaceflight Environmental Effects Newsletter*, Vol. 1, no. 8, January 23, 1991, pp. 10-11.
14. Wilkes, D.R. and Hummer, L.L.: Thermal Control Surfaces Experiment Initial Flight Data Analysis Final Report. AZ Technology Report No. 90-1-100-2, June 1991.
15. Firle, T.E. and Flanagan, T.M.: Mechanisms of Degradation of Polymeric Thermal Control Coatings: Part II. Effects of Radiation on Selected Pigments. AFML-TR-68-334, Part II, March 1970.
16. Zerlaut, G.A., Harada, Y. and Tompkins, E.H.: Ultraviolet Irradiation of White Spacecraft Coatings in Vacuum. *Symposium of Thermal Radiation of Solids*, NASA-SP-55, Washington, D.C., 1965.

17. Pearson, B.D. Jr.: Preliminary Results from the Ames Emissivity Experiment on OSO-II. *Progress in Astronautics and Aeronautics*, Vol. 18, Academic Press, New York, 1966, pp. 459-472.
18. Schafer, C.F. and Bannister, T.C.: Peagasus Thermal Control Coatings Experiment. AIAA-66-419, June, 1966.
19. Gilligan, J.E.: The Induced Optical Properites of Zinc Oxide. AIAA-67-214, January 1967.
20. MacMillan, H.F., Sklensky, A.F. and McKellar, L.A.: Apparatus for Spectral Bidirectional Reflectance Measurements During Ultraviolet Irradiation in Vacuum. *Thermophysics and Temperature Control of Spacecraft and Entry Vehicles*, Academic Press, New York, 1966, pp. 129- 149.
21. Mell, R.J. and Harada, Y.: Space Stable Thermal Control Coatings. AFWAL-TR-87-4010, May 1987.
22. Gilligan, J.E. and Zerlaut, G.A.: The Space Environment Stability Problem in White Pigment Coatings. *Institute of Environmental Science, Technical Meeting, Proceedings*, Vol. 17, 1971, pp. 447-457.
23. Choate, J.S., Johnson, S.W., and Mongold, V.L.: Analysis of Products Evolved From Selected Thermal Control Coating Materials During Ultraviolet Radiation in Vacuum. AIAA-69-640, June, 1969.
24. Lambourne, R., ed.: *Paints and Surface Coatings: Theory and Practice*. John Wiley and Sons, New York, 1987, pp. 622-643.
25. Lowrance, D.T. and Cox, R.L.: Fundamental Studies of the Stability of Thermal Control Coatings. AIAA-65-136, January 1965.
26. Schollenberger, C.S. and Stewart, F.D.: Thermoplastic Urethane Structure and Ultraviolet Stability. *J. Elastoplastics*, Vol. 4, pp. 294-331.
27. Wilkes, D.R. and Zwiener, J.M.: Initial Materials Evaluation of the Thermal Control Surfaces Experiment (S0069). *Proceedings of the LDEF First Post-Retrieval Symposium*, NASA Conference Publication 3134, Part 2, pp. 899-917, Jan. 1992.
28. Sampair, T.R. and Berrios, W.M.: Effects of Low Earth Orbit Environment on the Long Duration Exposure Facility Thermal Control Coatings. *Proceedings of the LDEF First Post-Retrieval Symposium*, NASA Conference Publication 3134, Part 2, pp. 935-944, Jan. 1992.
29. Golden, J.L.: Results of Examination of the A276 White and Z306 Black Thermal Control Paint Disks Flown on LDEF. *Proceedings of the LDEF First Post-Retrieval Symposium*, NASA Conference Publication 3134, Part 2, pp. 975-987, Jan. 1992.
30. Smith, A.L., ed.: *Analysis of Silicones*. Robert E. Krieger Pub. Co., Malabar, FL, 1983, p. 260.
31. *The Infrared Spectra Handbook of Inorganic Compounds*. Sadtler Research Laboratories, Philadelphia, PA, 1984, p.149.
32. Wilkes, D.R. and Hummer, L.L.: Thermal Control Surfaces Experiment Initial Flight Data Analysis Final Report. AZ Tech.-90-1-200-2, June 1991, pp. 89-92.
33. Bass, J.A.: Ultraviolet Radiation Effects on the Infrared Damage Rate of a Thermal Control Coating. NASA TN-D-6686, May 1972.
34. Arvensen, J.C.: Spectral Dependence of Ultraviolet-Induced Degradation of Coatings for Spacecraft Thermal Control. AIAA-67-340, April 1967.
35. Streed, E.R. and Arvensen, J.C.: A Review of the Status of Spacecraft Thermal Control Materials. Paper presented at 11th National SAMPE Symposium, St. Louis, MO, April 1967.
36. Swofford, D.D., Johnson, S.W. and Mangold, V.L.: The Effects of Extreme Ultraviolet on the Optical Properties of Thermal Control Coatings. AIAA-68-783, June 1968.

Table I. Summary of Solar Absorptances and UV/Atomic Oxygen Fluences

Sample	Location	Solar Absorptance	UV (Sun-hrs)	Atomic Oxygen (atoms/cm^2)
S13GLO	Control	0.147	-------	-------
	D9 (LE)	0.232	11,100	8.72×10^{21}
	D9 (LE)	0.228	11,100	8.72×10^{21}
	D3 (TE)	0.458	11,100	1.32×10^{17}
	D3 (TE)	0.473	11,100	1.32×10^{17}
	D8 (LE-SCU)	0.257	9,400	6.93×10^{17}
	D4 (TE-SCU)	0.496	10,400	9.32×10^{4}
A276	Reference	0.282	-------	-------
	D8 (LE-SS)	0.228	9,400	6.93×10^{17}
	D4 (TE-SS)	0.552	10,400	9.32×10^{4}
ZOT	Control	0.130(est)	-------	-------
	D9 (LE)	0.182	11,100	8.72×10^{21}
	D3 (TE)	0.182	11,100	1.32×10^{17}
D111	Control	0.971	-------	-------
	D9 (LE)	0.933	11,100	8.72×10^{21}
	D3 (TE)	0.968	11,100	1.32×10^{17}

TE = trailing edge; LE = leading edge; SS = sun shield cover; SCU = signal conditioning unit cover

Table II. XPS Analysis of S13GLO Samples

Sample	Surface Mole % (Normalized)										Ratio	
	C	O	Si	K	Zn	N	S	Cl	Na	F	O:Si	C:Si
Control	44	30	26	0.2	nd	nd	nd	nd	nd	nd	1.15	1.69
LE(D9)	12	56	27	1	0.5	2	0.3	0.5	0.3	0.1	2.07	0.44
LE(D9)	13	56	27	1	0.5	2	0.2	0.5	0.3	0.1	2.07	0.62
TE(D3)	28	46	21	0.8	0.3	2	0.4	0.4	0.7	0.5	2.19	1.33
TE(D3)	27	47	21	1	0.2	2	0.4	0.4	0.8	0.4	2.24	1.29
TE(D4-SCU)	33	43	19	0.6	0.3	2.2	0.5	0.4	0.5	0.4	2.26	1.74
TE(D4-SCU)	34	41	21	0.6	0.4	1.9	0.6	0.4	0.3	0.2	1.95	1.62

ORIGINAL PAGE
BLACK AND WHITE PHOTOGRAPH

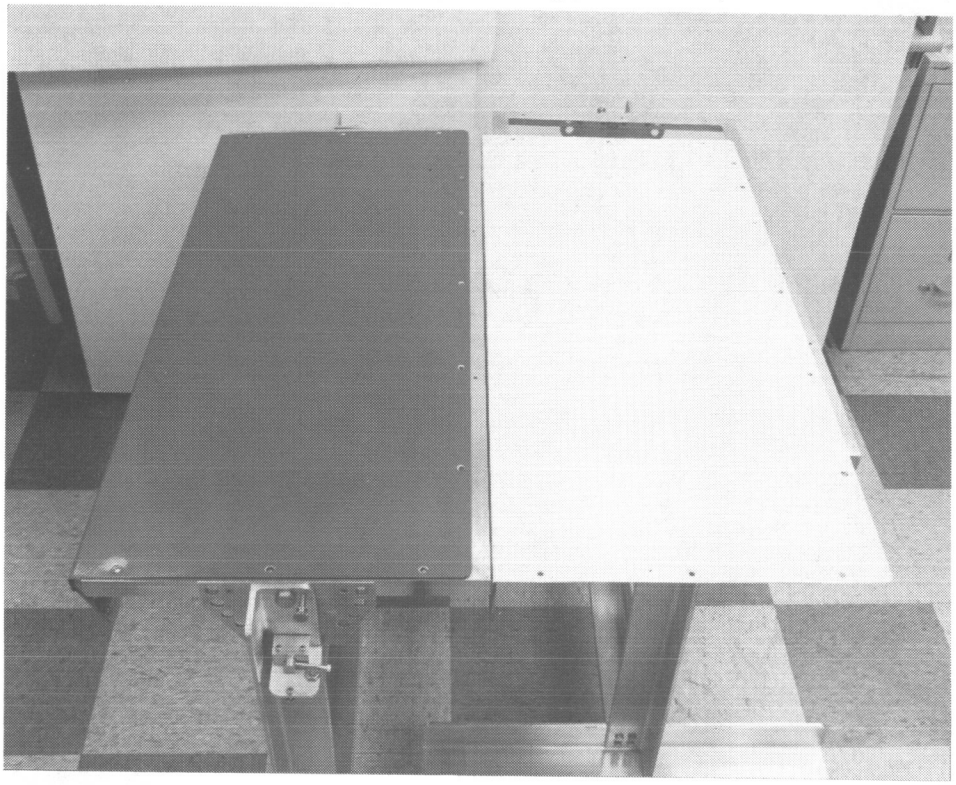

Figure 1. Chemglaze A276-painted sunshields flown on D4 (TE) on left and D8 (LE) on right.

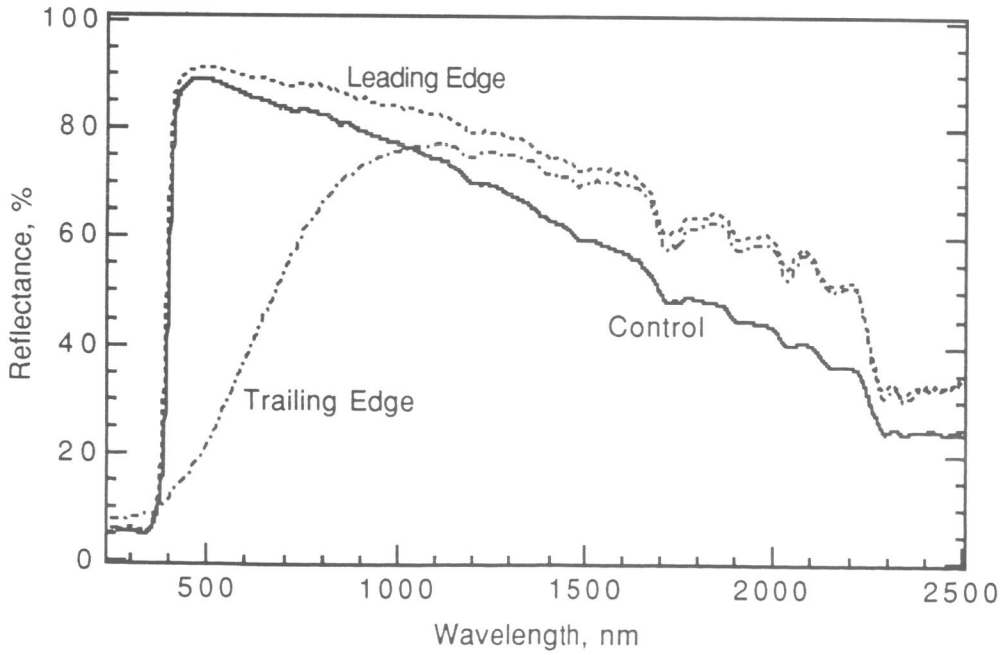

Figure 2. Reflectance spectra of Chemglaze A276 used as a white thermal control paint on the sun shields located on trays D8 (leading edge) and D4 (trailing edge) of LDEF.

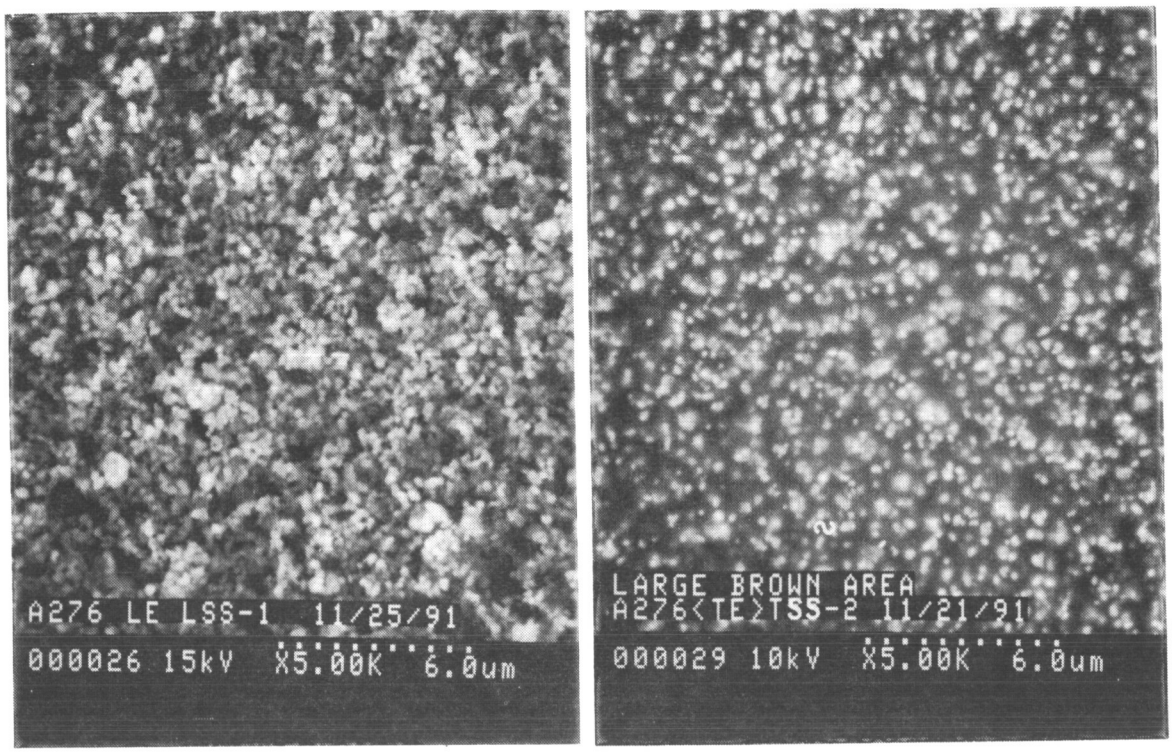

LEADING EDGE TRAILING EDGE

Figure 3. SEM photographs of surface of Chemglaze A276 paint exposed on LE (left) and TE (right).

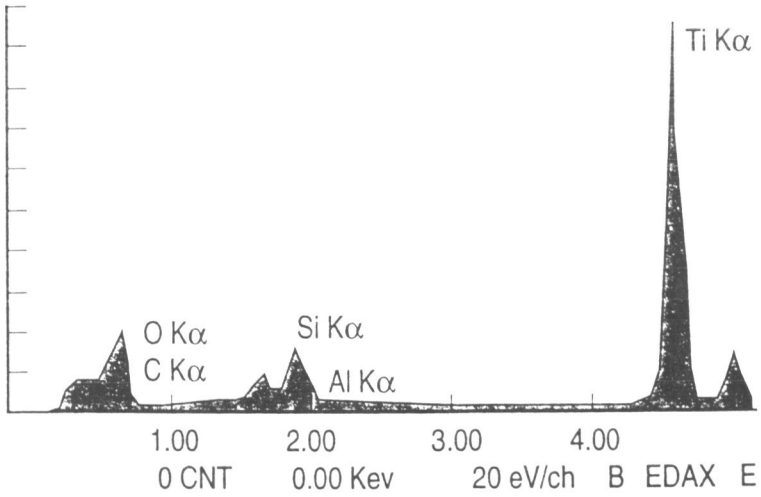

Figure 4. EDAX measurement of Chemglaze A276 leading edge surface.

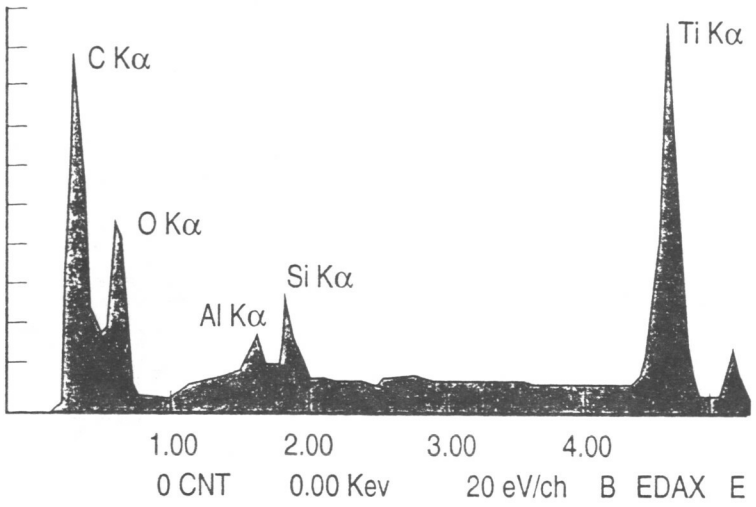

Figure 5. EDAX measurement of Chemglaze A276 trailing edge surface.

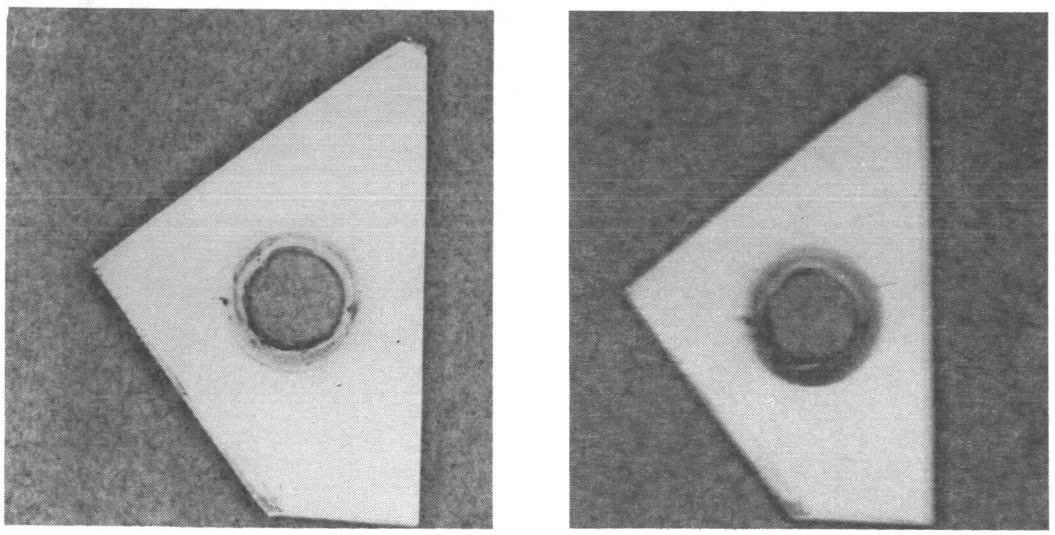

Figure 6. Response of protected Chemglaze A276 to UV radiation.

ORIGINAL PAGE
BLACK AND WHITE PHOTOGRAPH

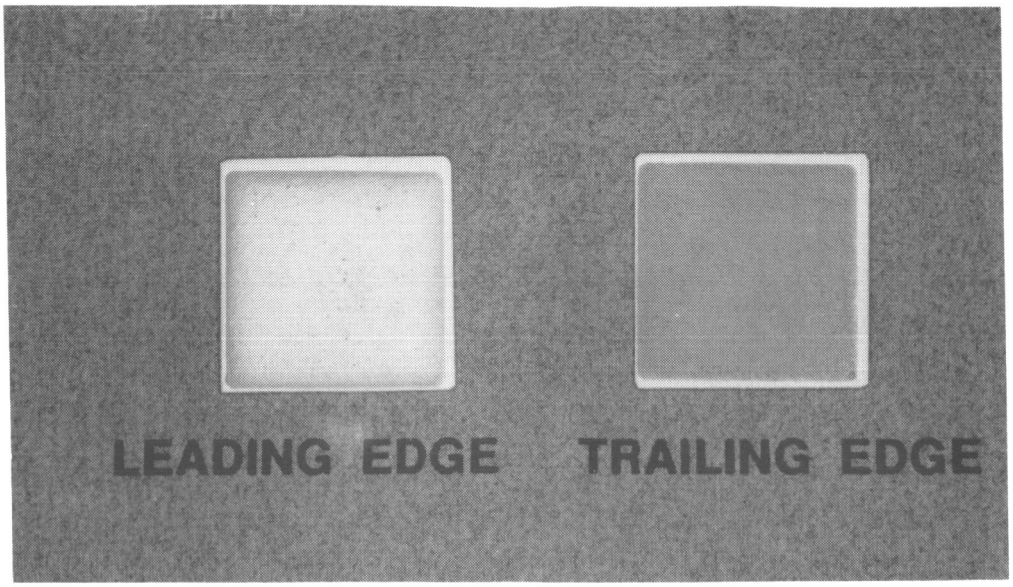

Figure 7. Comparison of S13GLO test samples from trays D9 (LE) on left and D3 (TE) on right.

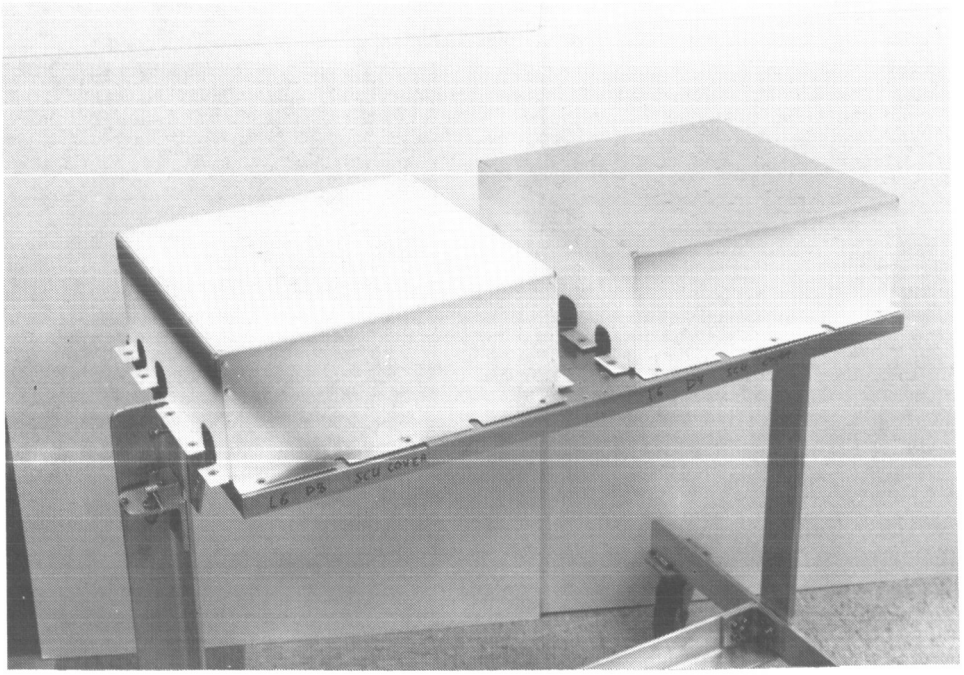

Figure 8. Signal conditioning unit (SCU) covers showing dramatic differences in damage from LE (left) to TE (right).

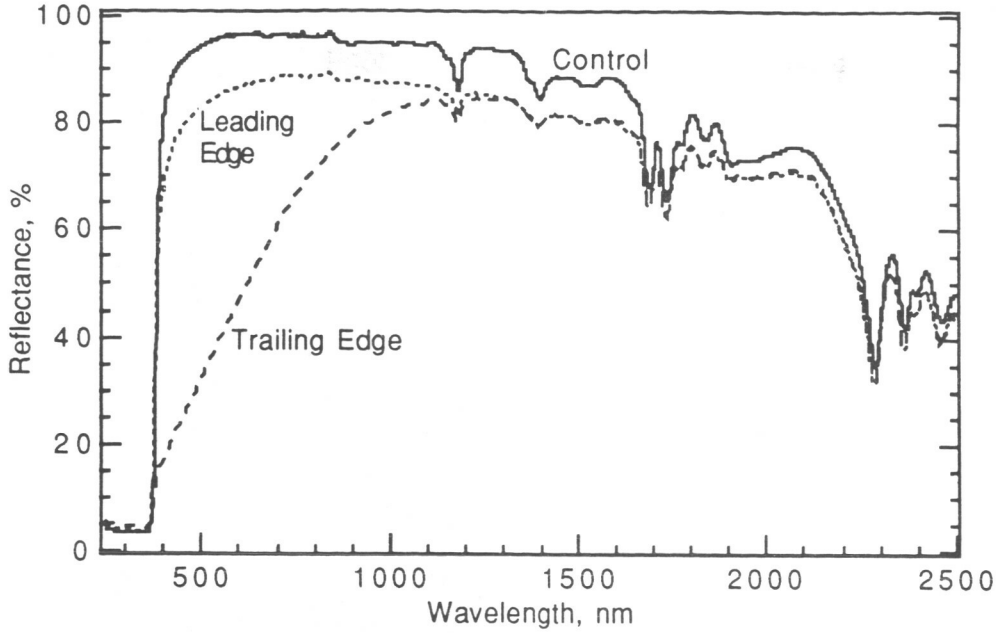

Figure 9. Reflectance spectra of S13GLO test samples from trays D9 (LE) and D3 (TE).

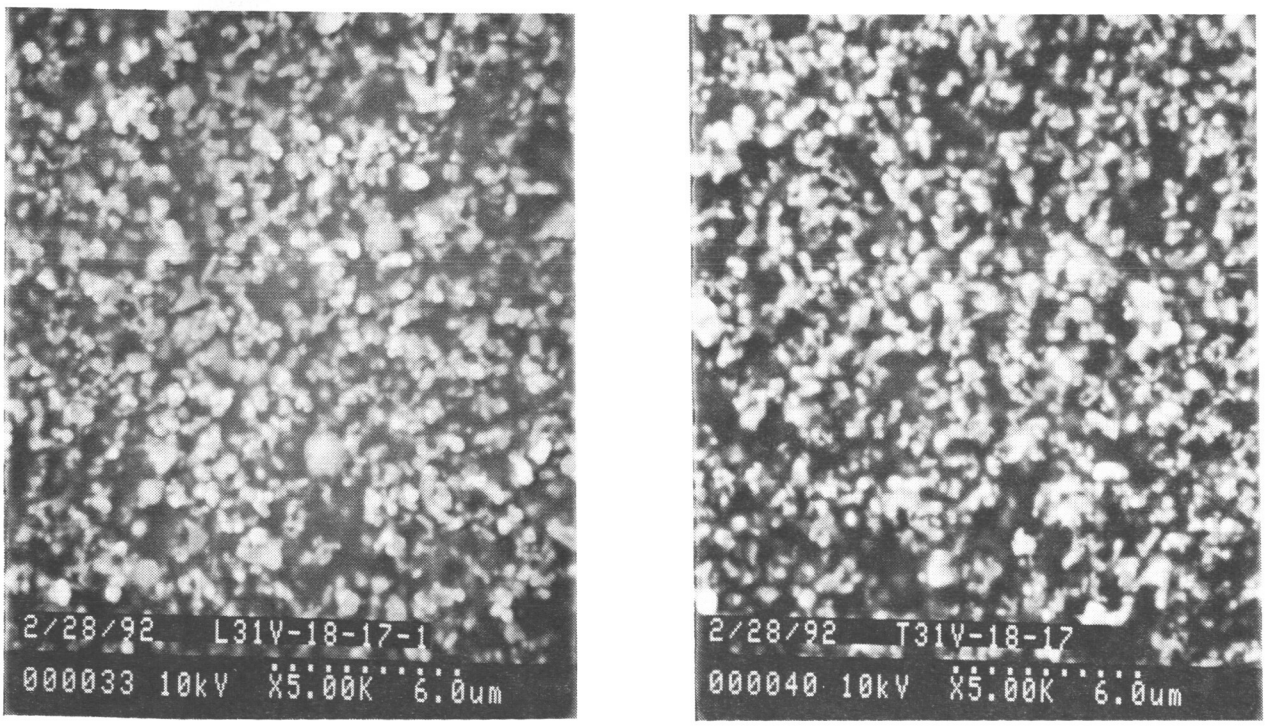

LEADING EDGE

TRAILING EDGE

Figure 10. SEM photographs of surfaces of S13GLO on LE (left) and TE (right) at 5000X.

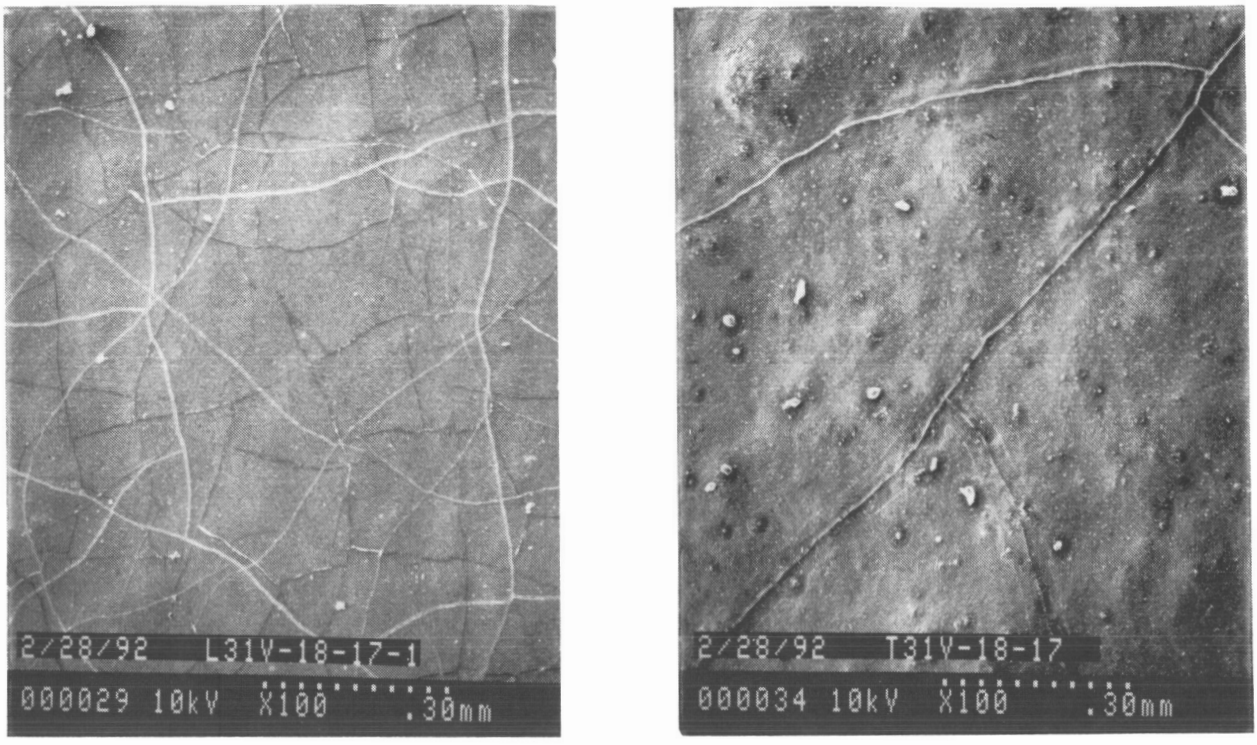

Figure 11. SEM photographs of surfaces of S13GLO on LE (left) and TE (right) at 100X.

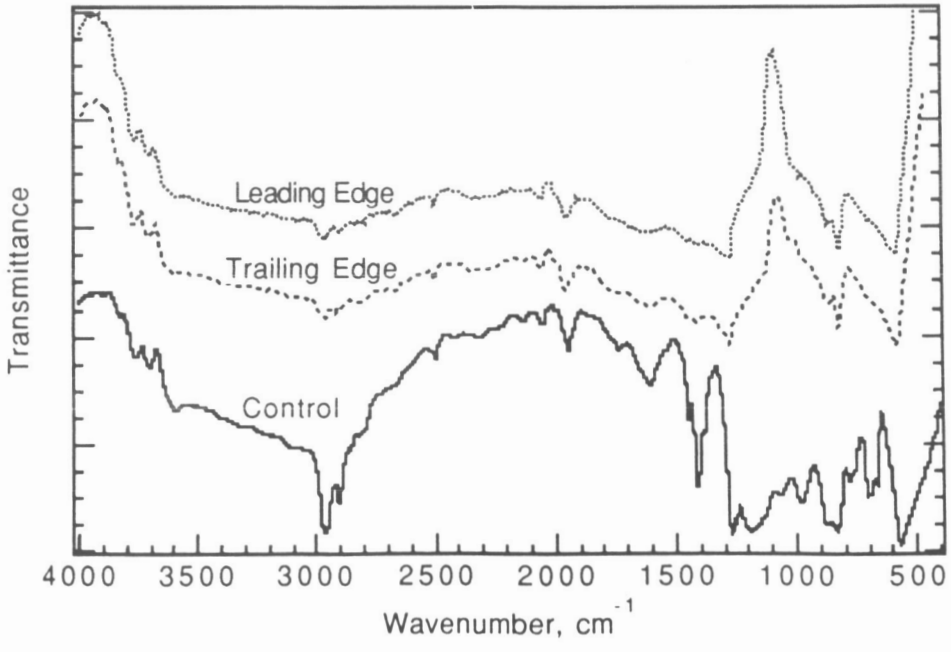

Figure 12. IR spectra of S13GLO samples from D9 (LE) and D3 (TE).

N93-28278

LDEF THERMAL CONTROL COATINGS POST-FLIGHT ANALYSIS

Wayne S. Slemp and Philip R. Young
NASA Langley Research Center
Hampton, VA 23681-0001

EXTENDED ABSTRACT

The NASA Long Duration Exposure Facility (LDEF) provided a unique flight opportunity for conducting experiments in space and return of these experiments to Earth for laboratory evaluation (1). This paper reports the results of one of these experiments, S0010, Exposure of Spacecraft Coatings, in which selected spacecraft thermal control coatings were exposed to the low-Earth orbital (LEO) environment on LDEF.

Figure 1 is a preflight photograph of the LDEF tray which housed this and another experiment. This experiment was located in Tray B on Row 9, which was the leading edge of LDEF. A compilation of the Row 9 exposure conditions for the 5-year 9-month orbital lifetime of LDEF is summarized in Table I. The canister shown open on the left side figure 1 was opened for 10 months, early in the LDEF mission. This allowed flight data to be obtained for 10-month and 5-year 9-month exposures on the selected coating specimens. The objective of this experiment is to evaluate the response of thermal control coatings to LEO exposure, which includes atomic oxygen, ultraviolet and particulate radiation, meteoroid and debris, vacuum, and temperature cycling.

Table II lists the coatings in this experiment, and Table III presents the solar absorptance and total normal emittance of a selected group of these coatings for preflight, 10-month exposure, and the full 5-year 9-month exposure. The mass loss data for the 10-month exposure of these coatings is presented in Table IV. Typical thicknesses of the optical solar reflectors (OSR), metallized FEP Teflon, and the paint coatings ranged from 1.3×10^{-2} cm to 2×10^{-2} cm. The anodized and sputtered coatings were much thinner, ranging from 3×10^{-4} cm to 3×10^{-3} cm for the anodized to 1×10^{-5} cm to 2.5×10^{-5} cm for the sputtered multi-layered coatings.

X-ray Photoelectron Spectroscopy (XPS) and Energy Dispersive X-ray (EDS) studies of these coatings indicate that a silicone molecular contamination film was deposited on the specimens during LDEF flight. Such contamination films were also identified in other experiments on LDEF (2-5). Since these silicones are typically converted to a silicate when exposed to atomic oxygen (6), they are not easily removed from the surface of coatings. This contamination may influence the mass loss and optical property data generated by this experiment.

These results show that the chromic acid anodized aluminum and the YB-71 (zinc orthotitinate/ potassium silicate) white paint have extremely stable optical properties when exposed in the LEO environment. Similar results were found in references 7 and 8. The silvered FEP Teflon retained its initial solar absorptance after 5.8 years of exposure, although the surface roughness increased and the FEP Teflon thickness decreased by 0.0011 inches. In the case of the S-13GLO (treated zinc oxide/silicone), exposure to air (oxygen) after UV exposure is known to "bleach" the reflectance degradation caused by the UV exposure. It is therefore surprising that the S-13GLO exhibited a 25-percent increase in solar absorptance in this study and in reference 9, although subjected to atomic oxygen in space and oxygen from air upon return to Earth.

REFERENCES

1. Clark, Lenwood G.; Kinard, William H.; Carter, David J., Jr.; and Jones, James L., Jr. (Editors): The Long Duration Exposure Facility (LDEF). NASA SP-473.

2. Crutcher, E. R.; and Warner, K. J.: Molecular Films Associated with LDEF. In LDEF-69 Months in Space, NASA Conference Publication 3134 (Arlene Levine, Editor), Part 1, 1991, p. 155.

3. Harvey, G. A.: Organic Contamination of LDEF. In LDEF-69 Months in Space, NASA Conference Publication 3134 (Arlene Levine, Editor), Part 1, 1991, p. 179.

4. Crutcher, Russ: Materials SIG Quantification and Characterization of Surface Contaminants. In LDEF Materials Workshop '91 (Bland A. Stein and Philip R. Young, Compilers), NASA Conference Publication 3162, Part 1, 1992, p. 95.

5. Hemminger, Carol S.: Surface Contamination on LDEF Exposed Materials. In LDEF Materials Workshop '91 (Bland A. Stein and Philip R. Young, Compilers), NASA Conference Publication 3162, Part 1, 1992, p. 159.

6. Harvey, Gale A.: Silizane to Silica. Second LDEF Post-Retrieval Symposium, NASA Conference Publication 3194, 1993.

7. Golden, Johnny L.: Anodized Aluminum on LDEF: A Current Status of Measurements. In LDEF Materials Workshop '91 (Bland A. Stein, and Philip R. Young, Compilers). NASA Conference Publication 3162, Part 1, 1992, p. 211.

8. Stein, Bland A.: LDEF Materials: An Overview of the Interim Findings. In LDEF Materials Workshop '91 (Bland A. Stein, and Philip R. Young, Compilers). NASA Conference Publication 3162, Part 1, 1992, p. 1.

9. Hurley, C. J.: Long Duration Exposure Facility Experiment M0003-5: Thermal Control Materials. In LDEF-69 Months in Space, NASA Conference Publication 3134 (A. Levine, Editor), Part 2, 1991, p. 961.

TABLE 1. EXPOSURE CONDITIONS FOR TRAY B ON ROW 9

- Atomic oxygen
  8.99×10^{21} atoms/cm^2
- UV radiation
  100-400 nm; 11,000 hrs
- Particulate radiation
  e^- and p^+: 2.5×10^5 rad surface fluence
  Cosmic: <10 rads
- Micrometeoroid and debris
  734 impact craters <0.5 mm
  74 impact craters >0.5 mm
- Vacuum
  1.33×10^{-4} - 1.33 x 10-5 N/m^2 (10^{-6} - 10^{-7} torr)
- Thermal cycles
  ~34,000 cycles: -29 to 71°C, ±11°
  (-20 to 160°F, ±20°)
- Altitude
  4.72×10^5 - 3.33×10^5 m (255-180 nautical miles)
- Orbital inclination
  28.5°

TABLE II. THERMAL CONTROL COATINGS IN EXPERIMENT S0010.

TYPE	COMPOSITION	SUBSTRATE
Second-surface mirrors	Quartz/Ag Quartz/Al FEP Teflon/Ag FEP Teflon/Al	Al Al Al Al
Black paints	Chemglaze, Z-306	Al
White paints	Zinc oxide-silicone, S-13GLO Zinc orthotitinate-silicate, YB-71 Chemglaze, A-276	Al Al Al
Anodized	Chromic acid, high emissivity Chromic acid, medium emissivity Chromic acid, low emissivity	Al Al Al
Sputtered	Al Al/Ni SiO_2/Ni SiO_2/Al/Ni SiO_2/Cr	Graphite-epoxy Graphite-epoxy Graphite-epoxy Graphite-epoxy Graphite-epoxy

TABLE III. OPTICAL PROPERTY CHANGES OF COATINGS EXPOSED IN EXPERIMENT S0010 ON LDEF.

Coating	Preflight		10 Months Exposure		5.8 Years Exposure	
	α_s	ε_{TN}	α_s	ε_{TN}	α_s	ε_{TN}
Thin Anodized AL	.295 .288	0.16 0.18	.299 ---	0.17 ---	--- .296	--- 0.19
Mid-Range Anodized AL	.292 .306	0.43 0.45	.287 ---	0.43 ---	--- .311	--- 0.46
Thick Anodized AL	.330 .341	0.71 0.75	.337 ---	0.71 ---	--- .354	--- 0.74
A276 White Paint	.229 .243	0.89 0.91	.237 ---	0.90 ---	--- .259	--- 0.88
S-13GLO White Paint	.158 .163	0.90 0.90	.182 ---	0.89 ---	--- .206	--- 0.89
YB-71 White Paint	.121 .128	0.91 0.90	.123 ---	0.91 ---	--- .125	--- 0.90
Z-306 Black Paint	.926 .922	0.91 0.92	.911 ---	0.91 ---	--- .902	--- 0.91
Silvered FEP Teflon	.069 .070	0.80 0.80	.068 ---	0.80 ---	--- .073	--- 0.78

TABLE IV. MASS LOSS OF COATINGS IN LDEF EXPERIMENT S0010

Test Material Description	Mass Loss/cm^2 AO Fluence[(a)]
1. Quartz/Aluminum 0SR	0 x 10^{-20}
2. Quartz/Silver OSR	.01
3. 1034C/N:/SiO_2	.05
4. 1034C/N:/AL/SiO_2	.06
5. YB-71 on Aluminum	.15
6. S-13GLO on Aluminum	.19
7. A276 on Aluminum	.23
8. Z306 on Aluminum	.26

(a) Fluence = 2.6 x 10^{20} atoms/cm^2

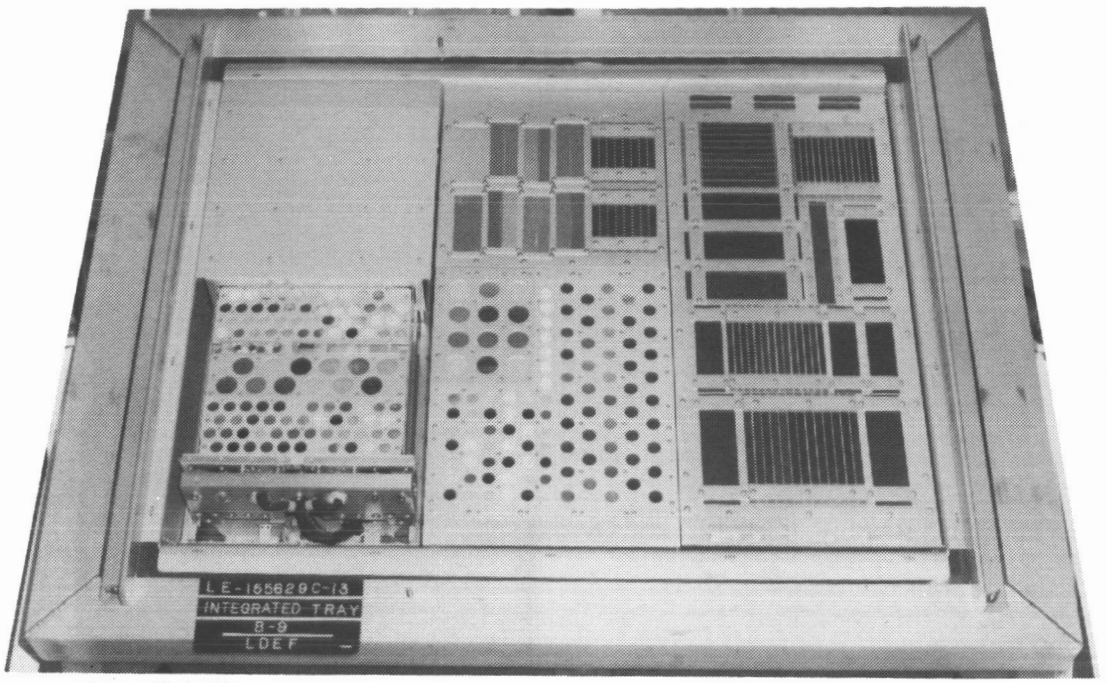

Figure 1. Langley materials exposure experiments in LDEF Tray B on Row 9.

N93-28279

SELECTED RESULTS FOR LDEF THERMAL CONTROL COATINGS

Johnny L. Golden
Boeing Defense & Space Group
PO Box 3999 M/S 82-32
Seattle, WA 98214-2499
Phone: (206) 773-2055, FAX: (206) 773-4946

SUMMARY

Several different thermal control coatings have been analyzed as part of LDEF Materials Special Investigation Group activity and as part of the Space Environment Effects on Spacecraft Materials Experiment M0003. This paper presents a brief discussion of the results obtained for these materials.

INTRODUCTION

Several thermal control coatings have been analyzed through activities supporting the Long Duration Exposure Facility (LDEF) Materials Special Investigation Group (MSIG), and as investigators on LDEF subexperiment M0003-8. The materials to be discussed here are polyurethane paints (specifically the Chemglaze A276, A971, and Z306 coatings), black chromium plate, chromate conversion coating on aluminum, and chromic acid anodize on aluminum.

The Z306 black and A276 white polyurethane coatings were applied to a graphite epoxy composite panel on experiment M0003-8. This experiment was located on tray D9, with the coatings subsequently exposed to 8.7×10^{21} oxygen atoms / cm^2 and to 11,200 equivalent sun hours (ESH) of ultraviolet (UV) radiation (ref. 1). Further description of the graphite epoxy panel and its changes due to environmental exposure are reported elsewhere in this conference publication (ref.2).

The A971 yellow polyurethane coating specimen was a trunnion scuff plate, located between trays C3 and D3 on the LDEF center ring frame. The A971 coating was exposed to 1.3×10^{17} O atoms/cm^2 and to 11,100 ESH of UV radiation (ref. 1).

The black chromium plate was from a solar absorber panel, which acted as the heat source for the Cascade Variable Conductance Heat Pipe Experiment A0076. This specimen, located on tray F9, was exposed to 8.7×10^{21} AO atoms / cm^2 and to 11,200 ESH of UV radiation (ref. 1).

PRECEDING PAGE BLANK NOT FILMED

C-5

The chromate conversion coating on aluminum involved specimens taken from a 6061-T6 aluminum panel used on experiment M0003 as a mounting plate for composite test specimens. The panel was located on tray D3 and was generally exposed to 1.3 x 10^{17} AO atoms/cm^2 and 11,100 ESH of UV radiation (ref. 1). Areas of the panel were, however, partially protected from exposure to these environmental conditions due to the specimens located above its surface. The aluminum panel was not intended as an experimental surface, and so did not have baseline optical properties measured prior to integration into LDEF.

The chromic acid anodized aluminum data was from measurements made on 156 of the LDEF tray clamps, taken from all possible exposure locations on the LDEF structure. The substrate material was 6061-T6, and the clamps were treated by NASA LaRC using a variable anodic process to achieve specific values of solar absorptance and thermal emittance (ref. 3). An initial report on the analysis of the chromic acid anodized tray clamps is available (ref. 4).

RESULTS AND DISCUSSION

Z306 Black Polyurethane

The Z306 polyurethane paint was almost completely eroded away from the composite substrate to which it was applied. The red coloration characteristic of the primer pigment was visible and significant erosion into the composite substrate was observed (ref. 2). Attempts to obtain SEM images of the surface were unsuccessful due to excessive charging, despite having applied three coatings of conductive metal. Based on the specified coating thickness used for the Z306 coating (there were no 'protected' areas of the Z306 on the composite panel to use for an initial surface reference) and the near complete removal of the coating, the erosion rate is estimated to be at least 5 x 10^{-25} cm^3/O atom.

The optical properties of the Z306 coated specimen were measured. The solar absorptance was measured to be 0.93, which is only a 0.02 unit reduction from the initial absorptance of 0.95 for the coating. This was somewhat of a surprising result considering the amount of red primer pigment readily visible on the surface. The thermal emittance was measured as 0.94, which is an increase of 0.04 apparently due to the roughening and diffuse character of the eroded surface.

A971 Yellow Polyurethane

Optical properties have been analyzed for the A971 yellow coating. Solar absorptance was measured to be 0.58, which is about 0.10 higher than what is expected from vendor literature. It is interesting that the absorptance of this particular A971 coating is comparable to that measured for A276 white polyurethane paint exposed to the same environmental conditions. The thermal emittance was measured as 0.87, essentially no change from what is expected for a gloss polyurethane paint without atomic oxygen exposure and consistent with observations for comparably exposed A276 white polyurethane paint.

Black Chromium Plate

Initial analyses for the black chromium plated absorber panel on Experiment A0076 have been reported (ref.5). The panel was observed on-orbit to have a section of the surface covered by a flap of aluminum foil, the flap being a result of atomic oxygen degradation of the experiment's thermal blanket. During deintegration, it was observed that the foil flap had been lost, and that the area which had been covered at the time of retrieval was a tan color. The original color of the panel was a very diffuse black, as can still be observed on protected areas of the panel. The panel surface which was exposed to the space environment for the full mission was observed to be a very dark blue (slate blue), see figure 1.

The optical properties of the various areas on the absorber panel were measured as depicted in figure 2. Emittance was not affected by any of the environmental exposures to the panel. The solar absorptance was reduced slightly on the exposed blue area and was significantly reduced in the tan area.

Contamination was observed to be significant around the periphery of the exposed portion of the panel, with silicon a major component. But there was not an apparent correlation between contamination and the tan discoloration area. SEM imaging of the surfaces also did not seem to provide a clear cause for the different optical properties observed. Based on preliminary Auger emission profiles, it appeared that the tan area on the panel had oxidized relative to both the unexposed black and exposed blue surfaces. It was hypothesized that the discoloration was induced by a thermal effect, caused by the close proximity of the bare aluminum foil flap. The premise for this hypothesis was that the foil flap, with high α/ε ratio and very low thermal mass, became significantly hotter than the absorber panel and accelerated the atomic oxygen driven oxidation of the chromium plated surface (ref. 5).

To test the heating effect hypothesis, one and two dimensional thermal modelling analyses were performed with the plate and foil flap system. The results indicated that

the foil flap, though experiencing 300°F thermal cycles, could not have heated the absorber panel under it to a temperature higher than that achieved by the exposed surface.

With the heating effect hypothesis discredited, surface analysis was again tried in order to illuminate the differences between the blue and tan areas on the absorber panel. Figure 3 is an ESCA surface survey of the iridescent or 'rainbow' area in one corner of the exposed area. Most notable in this survey are the high levels of oxygen, silicon, and carbon, indicative of silicone contamination. Figure 4 is an ESCA survey of the exposed blue area, where the silicon levels are significant but much less than that observed the corners of the exposed area. Figure 5 is a survey of the tan area, which appears to have lower silicon levels than the exposed blue area.

Elemental Auger profiles for the blue and tan areas are shown in figures 6 and 7. The blue area in figure 6 indicates initially chromium and oxygen, changing to mostly chromium metal with sputtering just as the nickel underplate begins to become apparent. The data from figure 6 is consistent with what is expected for both this system and for the unexposed original black surface. The tan area profile in figure 7 was unexpected. Note the scale on the y-axis is 10% of that in figure 6. It appears that the tan area is much thicker and more completely oxidized than the blue area. A consistent picture for this particular coating and the changes it exhibits has not been achieved; the analysis is continuing.

Chromate Conversion Coating on Aluminum

The chromate conversion coating was only partially exposed to the LDEF environment of tray D3. The surface still had the characteristic iridescence observed for chromate conversion coatings. Optical properties of the surface were measured even though there were no initial readings of the surface taken prior to LDEF integration. The solar absorptance of the surface varied between 0.55 and 0.57, which is about 0.1 higher than what has been typical for chromated conversion coatings measured at Boeing. In lieu of what has been observed on other surfaces on the trailing edge of LDEF, it is likely that this darkening of the coating is due to contaminant deposition. The emittance of the surface was measured at between 0.09 and 0.11, which is certainly in the expected range from Boeing experience.

The chromate conversion coating was also analyzed by X-ray absorption spectroscopy (XAS), to determine the amount and oxidation state of the chromium in the coating. XAS indicated that of the chromium in the coating, only 4% was as hexavalent chromium. This appears to be a significant depletion of Cr (VI) when compared to the 24% level typically observed by XAS in fresh chromate conversion coatings.

Hexavalent chromium depletion in conversion coatings is generally associated with a reduction in the corrosion resistance afforded to the aluminum substrate. Therefore,

three 3" x 5" samples of the M0003 chromate conversion coated panel were subjected to the salt spray corrosion test (ASTM B117) for seven days, as is customary for evaluating fresh conversion coatings on aluminum from aerospace processing. The M0003 chromate conversion coating passed the corrosion resistance test, with no pitting observed on any of the three samples. The salt spray result was, therefore, contrary to what was expected from the XAS results. It is possible that the UV-fixed contaminant layer provided some degree of protection to the test specimens during the salt spray test. But because the specimens did "wet" completely in the salt spray test, it is more likely that the conversion coating itself provided a continuous protective barrier, reducing the need for the corrosion inhibition provided by the hexavalent chromium ion.

Chromic Acid Anodize

The results obtained for LDEF tray clamps treated with chromic acid anodize are shown in table 1. The standard deviations for the populations indicate that the results from one environmental condition to another essentially overlap, with slight indication of absorptance increase for the surfaces not subject to significant levels of atomic oxygen. However, even with this slight increase in absorptance, the results indicate that the optical properties of chromic acid anodize are quite stable in the low earth orbit environment.

A276 White Polyurethane

The A276 paint on composite (Experiment M0003, Tray D9) had areas protected from atomic oxygen erosion, where washers were used in the attachment of the panel to support structure. The atomic oxygen eroded the polyurethane portion of the paint in exposed areas, leaving behind a loose agglomeration of paint pigment particles. We were curious to know how deep the atomic oxygen was able to penetrate into this network of pigment particles, or how deep the exposed paint was damaged from a physical integrity perspective.

Specimens from the composite panel were taken from around the protected attachment areas, and the loose pigment on those specimens was removed by rag wiping. The specimens were then measured using laser profilometry. Height profiles from two different areas along the protected-to-unprotected interface are shown in figures 8 and 9. The figure 8 profile was taken perpendicular to the LDEF axis along the surface toward row 10. The LDEF yaw offset gave the incident atomic oxygen direct access to the paint at the washer interface, yielding a steep erosion profile. Figure 9 was also taken perpendicular to the LDEF axis, but along the surface toward row 8 (180° from figure 8). Here the yaw offset allowed the washer to shield the paint from atomic oxygen erosion at the interface, yielding a tapered erosion profile. The total erosion depth measured using these two profiles, plus four additional measurements, indicated atomic oxygen attack

into the A276 paint surface to a depth of about 10μm (0.0004 inch). Correlation has not been established between the depth of attack and the pigment layer porous structure (0.2μm TiO_2 particles, 1-2μm talc particles, 40.6 volume percent solids). It is not certain that this measured erosion depth is the limit for which atomic oxygen can penetrate into the A276 pigment layer. However, it seems likely that this must be the penetration limit based on the tortuous path atomic oxygen would have to follow in order to continue reacting with the paint resin layer.

The UV degradation of A276 paint on LDEF has been discussed previously (ref. 6). A276 on surfaces not exposed to atomic oxygen has exhibited a sharp increase in solar absorptance with UV exposure. Attempts made to locate ground-based test data for comparison with the LDEF results were essentially unsuccessful. Literature data for numerous white coatings (including A276) have been found, but these reports are typically limited to less than 1000 ESH total UV exposure, due to the moderate UV source intensities that must be used. Another limitation is that ground-based test results are from in-situ reflectance measurements, because of the recognized recovery effect that occurs when short-term UV exposure test specimens come in contact with air. The precise extent of reflectance recovery that may have occurred with the LDEF A276 paint specimens is unknown. The present levels of discoloration in the A276 coating have been determined to be due to degradation of the polyurethane resin portion of the coating, a degradation which cannot "recover".

For engineering purposes, it is essential to establish accelerated test criteria which can be used to predict performance life in a cost effective and timely manner. It was for this reason that comparison of the LDEF A276 results to ground-based UV exposure results was attempted. Failing this, a more controversial approach was made in applying the concept of radiation equivalence. Recent measurements have been made at Boeing Combined Radiation Effects Test Center (CRETC) on the A276 paint, concerning the effects of proton/electron radiation on solar absorptance.[1] A276 was irradiated with 40 keV protons and electrons, simultaneously and in roughly equal fluences to prevent sample charging. Significant degradation in solar absorptance was observed in-situ as a function of radiation fluence. For the purposes of trend comparison, the radiation fluence which produced a solar absorptance reading of 0.52 was arbitrarily equated with a LDEF UV exposure of 8300 ESH. All other particulate radiation fluence levels were scaled from this point. The scaled data set was then compared to the results for A276 white paint data from the LDEF tray clamps, as is shown in figure 10. The trends in the data are significantly similar. The comparison of these two sets of measurements is made here partly as a curiosity. But this comparison is made principally to stimulate thought on the concept of radiation equivalence for materials testing, recognizing the significant impact such an approach could have on long-term performance life prediction.

---

[1]L. Fogdall and M. Wilkinson, Boeing Defense & Space Group, personal communication of results to be published.

REFERENCES

1. R. J. Bourassa: Atomic Oxygen And Ultraviolet Radiation Mission Total Exposures For LDEF Experiments. Second LDEF Post-Retrieval Symposium, NASA CP-3194, 1993.

2. P. George: Results From Analysis of Boeing Composite Specimens Flown on LDEF Experiment M003. Second LDEF Post-Retrieval Symposium, NASA CP-3194, 1993.

3. R. J. Duckett and C. S. Gilliland: Variable Anodic Thermal Control Coating on Aluminum, AIAA-83-1492. AIAA 18th Thermophysics Conference. June, 1983.

4. W. L. Plagemann: Space Environmental Effects On The Integrity Of Chromic Acid Anodized Coatings. First LDEF Post-Retrieval Symposium, NASA CP-3134, 1992.

5. J. L. Golden: Changes In Oxidation State Of Chromium During LDEF Exposure. LDEF Materials Workshop '91, NASA CP-3162, 1992.

6. J. L. Golden: Results Of Examination Of The A276 White And Z306 Black Thermal Control Paint Disks Flown On LDEF. First LDEF Post-Retrieval Symposium, NASA CP-3134, 1992.

Measurements On Flight Tray Clamps					Data From AIAA-83-1492	Measurements On Unused Clamps
Unexposed	Exposed-Leading	Exposed-Trailing	Exposed - Space	Exposed - Earth		
$\alpha = 0.34$ 0.01	$\alpha = 0.33$ 0.01	$\alpha = 0.35$ 0.02	$\alpha = 0.35$ 0.02	$\alpha = 0.35$ 0.01	$\alpha = 0.32$	$\alpha = 0.36$
$\varepsilon = 0.16$ 0.01	$\varepsilon = 0.15$ 0.01	$\varepsilon = 0.15$ 0.01	$\varepsilon = 0.16$ 0.02	$\varepsilon = 0.17$ 0.01	$\varepsilon = 0.16$	$\varepsilon = 0.18$
$\alpha/\varepsilon = 2.1$	$\alpha/\varepsilon = 2.2$	$\alpha/\varepsilon = 2.3$	$\alpha/\varepsilon = 2.2$	$\alpha/\varepsilon = 2.1$	$\alpha/\varepsilon = 2.0$	$\alpha/\varepsilon = 2.0$

Note: Second Value Is Standard Deviation

Table 1. Averages of optical property measurements for groups of anodized tray clamps.

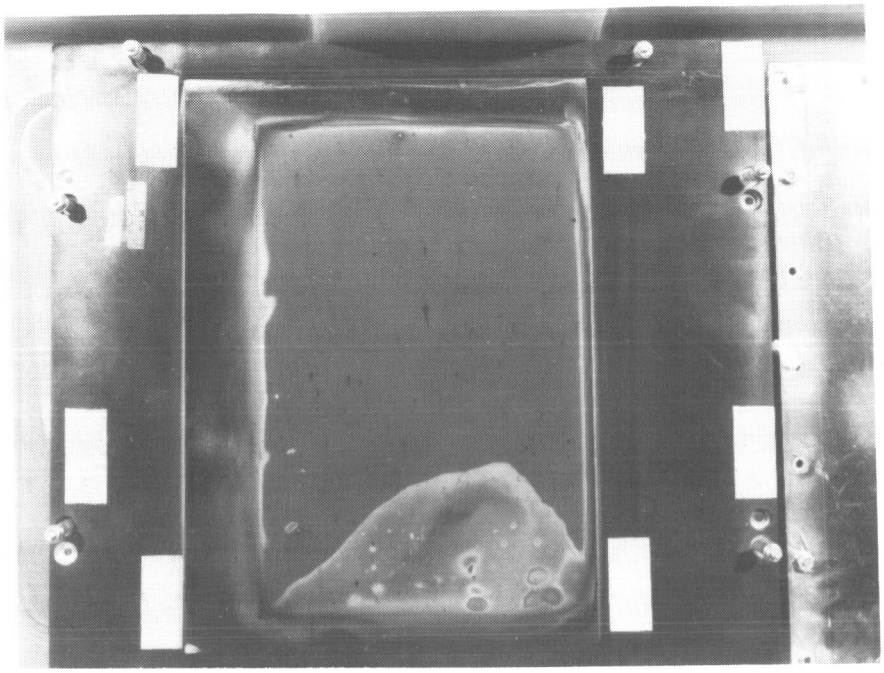

Figure 1. Photograph of black chromium plated solar absorber panel, experiment A0076, tray F9. (Color photograph is shown on page 1248.)

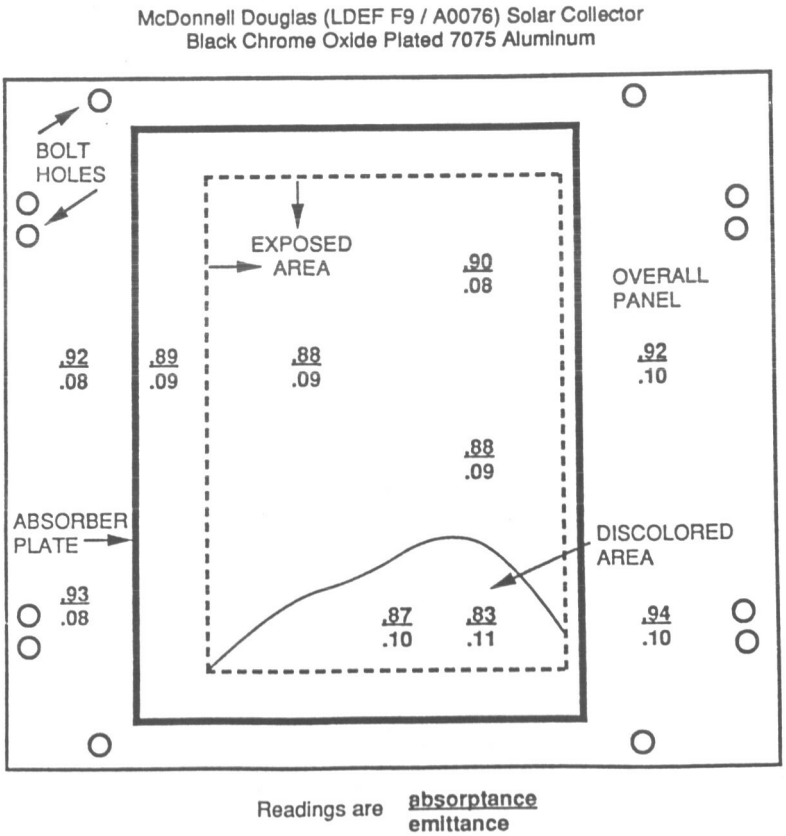

Figure 2. Optical properties of the black chromium plated solar absorber panel.

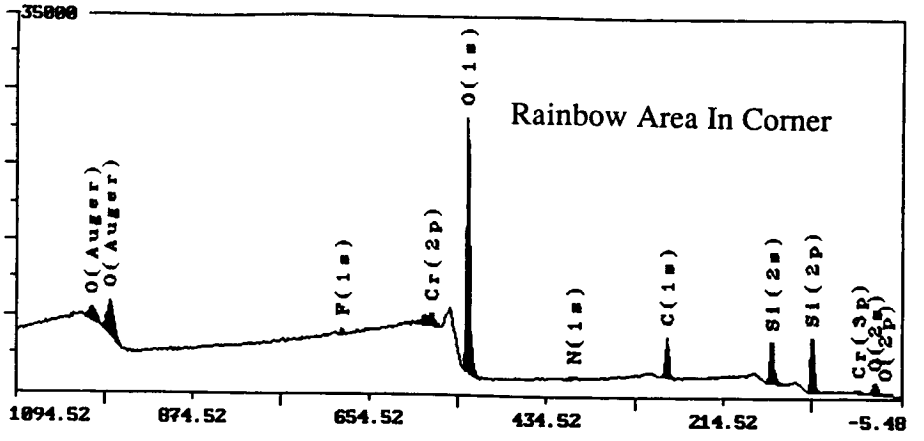

Surface Composition Table Summary

Element	Binding Energy	atom %
F (1s)	688.78	0.72 %
Cr (2p)	578.06	1.75 %
O (1s)	532.87	51.70 %
N (1s)	401.12	1.32 %
C (1s)	285.00	20.59 %
Si (2s)	153.69	23.93 %
Total Percent		100.00 %

Figure 3. ESCA survey of a rainbow colored area on the black chromium plated solar absorber panel

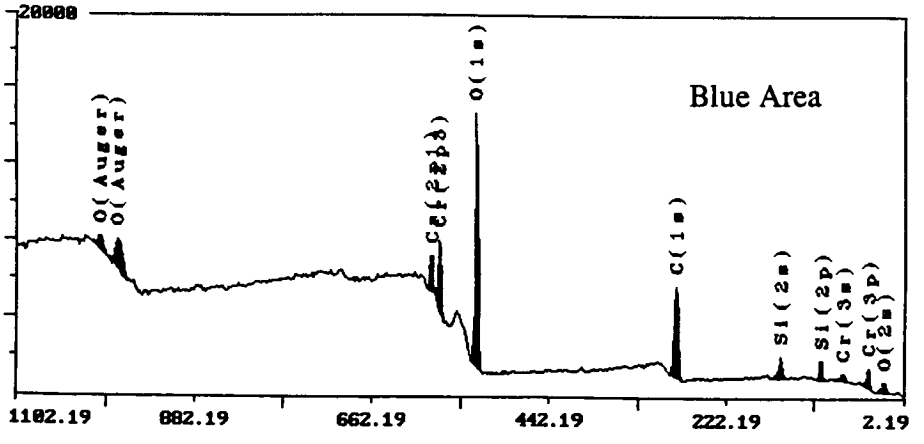

Surface Composition Table Summary

Element	Binding Energy	atom %
Cr (2p3)	578.50	4.16 %
O (1s)	532.68	44.02 %
C (1s)	285.00	43.05 %
Si (2s)	154.37	8.78 %
Total Percent		100.00 %

Figure 4. ESCA survey of a blue colored area on the black chromium plated solar absorber panel

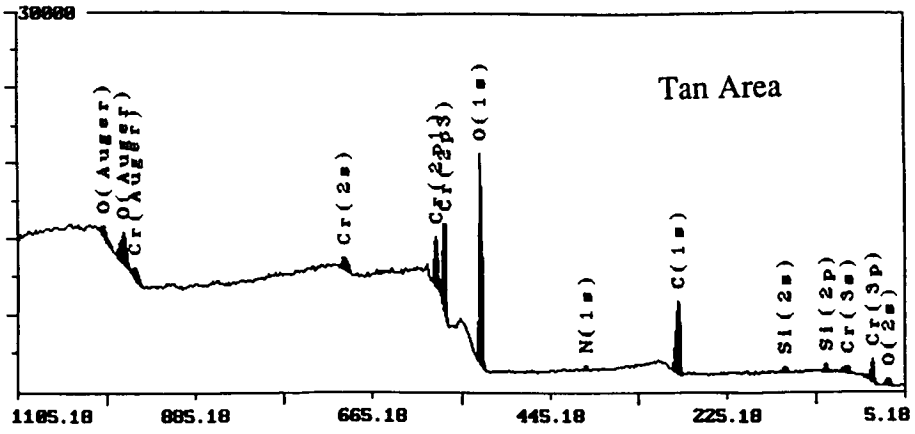

Surface Composition Table Summary

Element	Binding Energy	atom %
Cr (2p3)	577.16	6.29 %
O (1s)	531.82	43.19 %
N (1s)	400.04	0.80 %
C (1s)	285.00	45.14 %
Si (2p)	101.58	4.58 %
Total Percent		100.00 %

Figure 5. ESCA survey of a tan colored area on the black chromium plated solar absorber panel

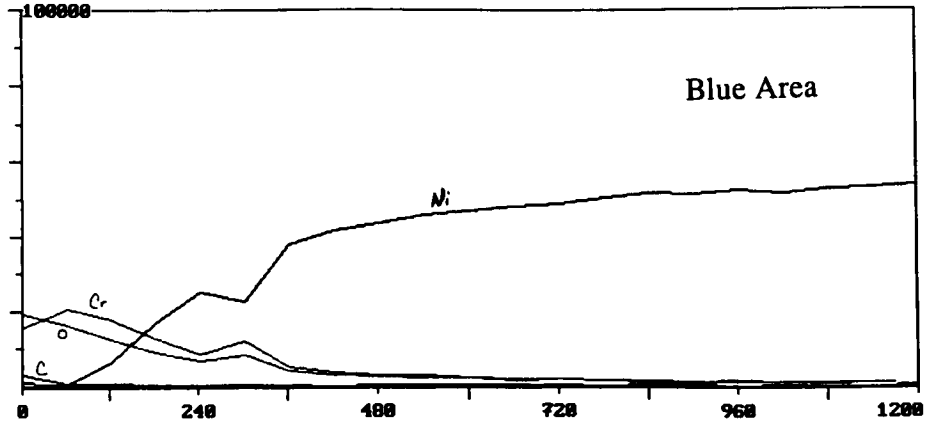

Figure 6. Auger profile of blue area on the black chromium plated solar absorber panel.

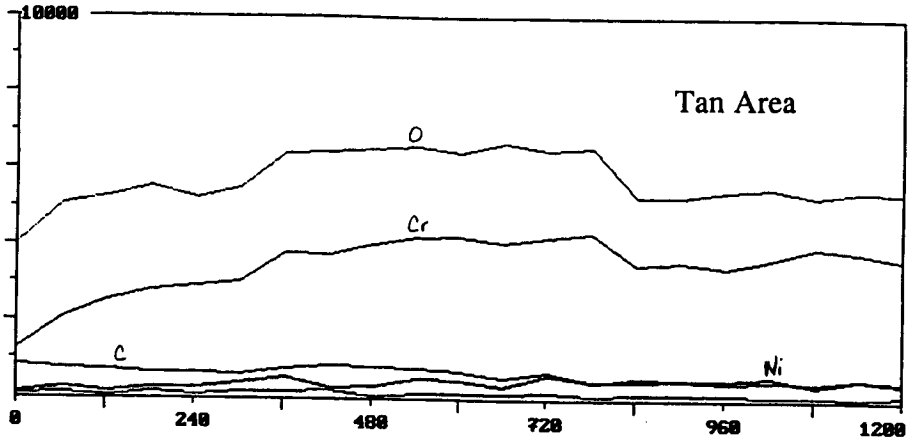

Figure 7. Auger profile of tan area on the black chromium plated solar absorber panel.

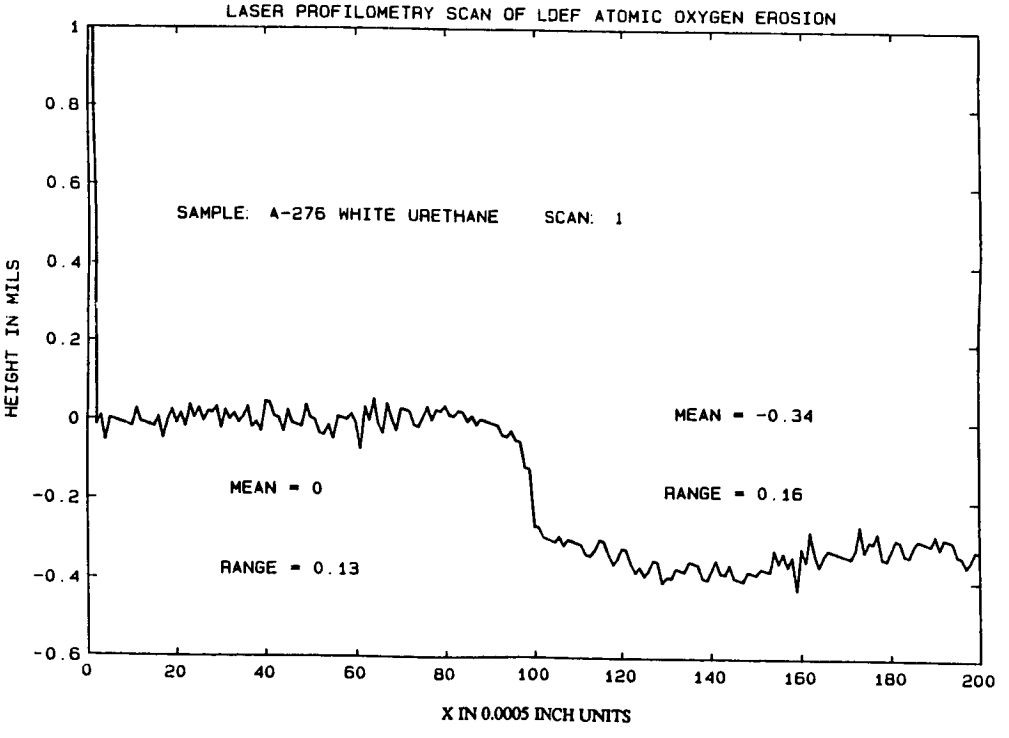

Figure 8. Laser profilometry of A276 white paint on tray D9 at a protected/unprotected interface towards row 10.

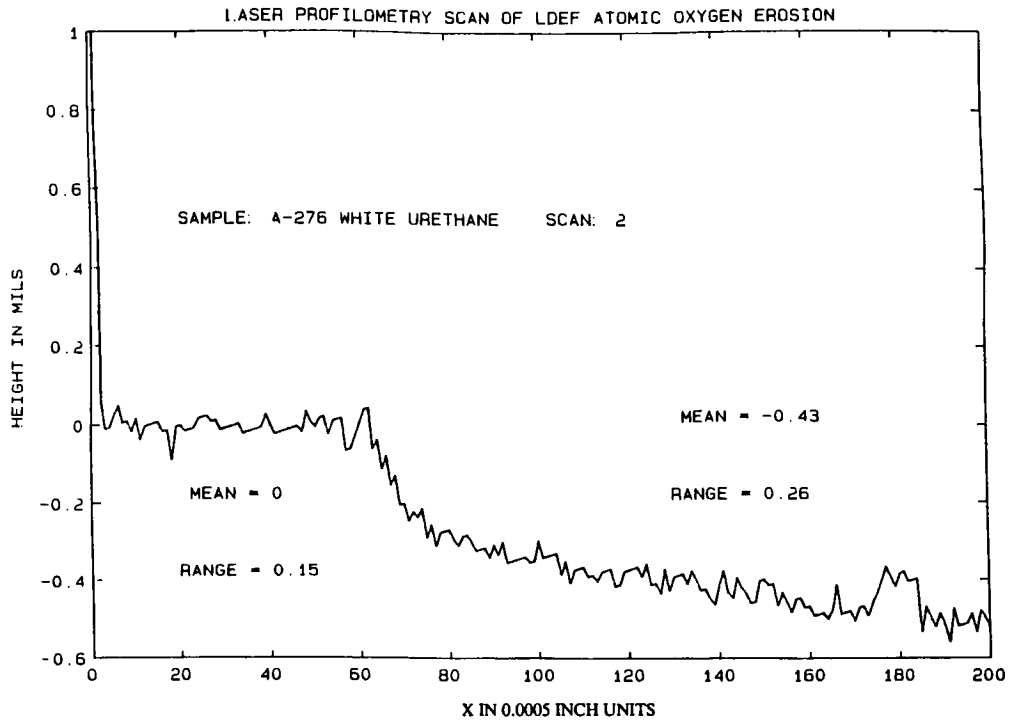

Figure 9. Laser profilometry of A276 white paint on tray D9 at a protected/unprotected interface towards row 8.

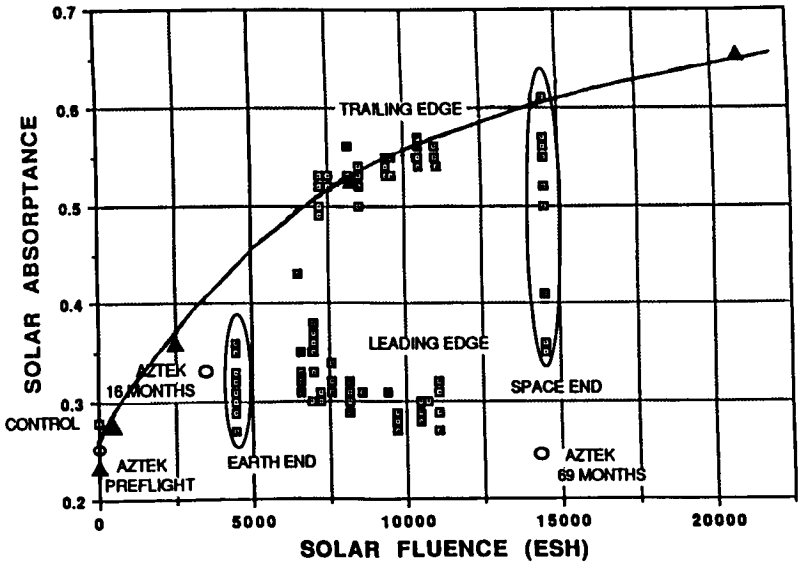

▲ 40 keV Electron + Protons

Fluence (per cm^2)	Scaled ESH	Absorptance
0	0	0.23
1×10^{14}	420	0.27
6×10^{14}	2500	0.36
2×10^{15}	8300	0.52
5×10^{15}	20800	0.66

Figure 10. Comparison of LDEF results with ground-based radiation test result from Boeing CRETC for A276 white paint.

N93-28280

FLUORESCENCE MEASUREMENTS OF THE THERMAL CONTROL EXPERIMENTS COATINGS ON LDEF S0069 AND A0114

J.M. Zwiener, R.J. Mell, P.N. Peters
NASA/Marshall Space Flight Center
Huntsville, AL 35812
Phone: 205/544-2528 Fax: 205/544-0212

J.C. Gregory
University of Alabama - Huntsville
Huntsville, AL 35899
Phone: 205/895-6028; Fax: 205/895-6349

D.R. Wilkes, E.R. Miller
AZ Technology, Inc.
3322 Memorial Parkway SW, Suite 93
Huntsville, AL 35801
Phone: 205/880-7481; Fax: 205/880-7483

SUMMARY

Fluorescence measurements have been made on the thermal control coatings from the LDEF S0069, Thermal Control Surfaces Experiment (TCSE); and the A0114, Interaction of Atomic Oxygen with Material Surfaces in Low Earth Orbit. Fluorescence was observed in two types of thermal control coatings and is attributed to pigments or binders. In addition, fluorescence measurement on the silver Teflon* from the front cover of TCSE led to confirmation of damage (cracking) to the metal layers during application.

INTRODUCTION

When the TCSE experiment was inspected upon its return to the laboratory, one technique employed was the use of an ultraviolet source ("black light") to look for fluorescing contaminants such as cloth fibers and oils or greases. It was obvious, when compared with similar unexposed materials and with sample controls, that changes had occurred in the visible fluorescent brightness of the thermal control samples and of the TCSE experiment hardware itself (Figure 1). The fluorescence was so striking in some cases, such as the black urethane based coating Z302, that it was decided to try to obtain quantitative measurements of the changes. The goals were to try to characterize the various types of coatings in terms of their fluorescent properties and to possibly learn if the observed changes could further elucidate effects of exposure to the space environment.

Measurement Equipment and Set-ups

Absolute fluorescence measurements were made using the following experiment set up and calibration procedure.

*Teflon is a trademark of Dupont

A Beckman DK-2 Spectrophotometer using its 1P28 photo multiplier tube mounted in the spectroradiometric position was used to detect any fluorescent behavior from the samples. Fluorescence was induced by irradiating the sample, mounted at 45° to the optical beam, in line with the sample entrance port of the spectrophotometer (Figure 2). For these measurements, a one kw mercury-xenon lamp with a Schoeffel monochromator was used. It was found that use of the strong peak of 280 nm was convenient. Overall, the illuminating band was from 265 to 290 nm with the monochromator slits set at 1.5 mm. Measurements of output with this set up using a molectron radiometer indicated an irradiance level of 0.5 m2/cm2 at the sample (equivalent to about 1 sun in this band). To provide a calibration of the DK-2 spectrophotometer, a one kw quartz-halogen tungsten Standard of Total and Spectral Irradiance (Model 200H) supplied by Optronics Laboratories (traceable to NIST), was used in place of the Hg-Xe source (Figure 3). A 99% diffuse reflectance standard (from Labsphere, Inc. SRS-99-010-6561A) was placed at the sample location. Since this non-fluorescing standard provided essentially Lambertian reflectance of a known irradiance level, a calibration of the DK-2 as a system was made over its sensitive wavelengths (~300-650 nm). For ZnO pigmented coatings, it was also determined that the fluorescent energy is proportional to irradiance, over a factor of 5.5; and that there was no detectable change in fluorescent wavelength peaks for irradiance bands of 265 to 290 nm, 295 to 320 nm, and 310 to 340 nm. Other coatings were not tested in this manner, but probably would behave similarly.

Fluorescence Measurements

Two types of thermal control coating samples were found to exhibit rather strong fluorescence. These were: 1) coatings that used urethane as a binder and, 2) coatings that used ZnO as a pigment. In addition, there were variations of the above coatings with a thin overcoat of silicone to test the feasibility of an additional protective layer against the deleterious effects of atomic oxygen (AO) bombardment at orbital velocities. Controls for the TCSE experiment were maintained in covered containers in a limited-access steel cabinet.

Other TCSE thermal control coatings samples that were measured and found not to have significant fluorescence were Z306 (a urethane based black paint), YB71 (silicate), and D111 (silicate). A white Tedlar* flight sample did not fluoresce, while a laboratory specimen exhibited very weak fluorescence peaks at about 420 to 440 nm. Also measured, were silver Teflon samples cut from the front cover of TCSE. Similar materials that were unexposed to the space environment were used for comparison.

Figures 4 and 5 allow comparison of the flight and control fluorescent spectra of Z302 and A276 urethane based coatings. The similarity in the control spectra from 400-575 nm is likely attributable to the fluorescence characteristics of the polyurethane binder. However, the spectra for the flight exposed sample of Z302 is somewhat unique in that the magnitude and band width of the fluorescence is less than most of the other polyurethane samples. This may be due to the erosion of the sample by AO and/or as a natural frequency shift of the material caused by exposure to the LEO environment. Fluorescence data is not available for Z302, exposed in the RAM direction for 5.8 years, since it was completely eroded.

The similarities shown in the spectra of Z302 and A276 with a OI650 silicone overcoat are even more striking (Figures 6 and 7). These figures tend to illustrate that the polyurethane samples, both Z302 and A276, overcoated with OI650 and then exposed to the flight environment fluoresce very similar to one another. In addition, the similarities between the overcoated and neat A276 polyurethane coatings fluorescence spectra are shown in Figures 5 and 7. The OI650 overcoated control samples have enhanced ultraviolet fluorescence attributable to the overcoat itself. This effect is not present in the flight exposed samples and, in fact, there is no fluorescence evidence that the overcoat is still present. The similarity in exposed A276 (neat and overcoated) spectra may be due to extensive crosslinking of the silane polymer on the surface. The crosslinking of the polymer modified the electronic and molecular structure and may have more effectively bonded the available electrons. The result is the electrons could no longer be excited to a

*Tedlar is a trademark of Dupont

higher, unstable energy level when exposed to UV irradiation and therefore the overcoat no longer fluoresced, but the fluorescence of the A276 was transmitted through the overcoat. Further evidence that crosslinking of the silane overcoat is a likely explanation for this phenomenon is that visual inspection of the surface of the overcoated samples shows significant cracking. This can be the result of the hardening and embrittlement of the polymer from increasing crosslinking based on optical properties measurements[1]. The overcoat has served its purpose to protect the Z302 from eroding.

The ZnO pigmented Z93 and S13GLO coatings show remarkably similar fluorescence spectra for the control samples as well as those that were protected by an aluminum cover during flight (Figures 8-13). The spectra from the exposed samples generally appear similar, with unexplained weaker fluorescence on the TCSE P7, 5.8 years exposure S13GLO sample (figure 9) and on AO114 Wake mounted S13GLO sample (Figure 13). Especially, the Wake mounted sample shows a weak fluorescence and the absence of the 380 mm peak.

From Figure 8, Z93 spectra for 1.6 and 5.8 years exposure are shown, providing evidence that the change occurring is not linear with time and that the 380 and 520 nm fluorescence change rates may be different.

The slight fluorescent glow noticed on the TCSE front cover was measured and is shown in Figure 14. Measurements on non-flight Teflon failed to produce any detectable fluorescence. However, measurements of the 3M 966 high temperature acrylic adhesive used to apply the silver Teflon produced fluorescence that, like the silicone overcoat, extended into the ultraviolet (Figure 15). Upon exposure to strong ultraviolet for various periods of time, the spectra shifted toward the visible region during the first short exposure and did not continue to shift significantly, but fluorescence intensity continued to grow in this band.

Discussion and Summary

It is clear that the fluorescence of the urethane based paints is produced by the urethane binder itself and not the various pigments. Hill[2] has correlated laser-induced fluorescence (LIF) with tensile strength of several polyurethane based materials. He also found LIF changes in LDEF Tray Clamps samples of A276 and Z306 supplied to him by Boeing[3]. It is not apparent if the specific LIF changes detected in the thermal control coatings are the same as polyurethane/tensile strength LIF changes. Hill attributes the latter to "complex molecular and intermolecular relationships (such as cross-linking, scission, oxidation) that are altered during degradation."[2] Silicone overcoated urethane paints, although severely cracked and sometimes peeling seem to provide protection from atomic oxygen erosion. From the measurements, not only does the initial enhanced ultraviolet fluorescence disappear after space exposure, but the resulting spectra closely matches that of the urethane paints without the silicone. If polyurethanes are to continue to be used in the space environment, it is necessary to better understand the degradation mechanisms involved. Fluorescence may prove to be a useful tool in this understanding as well as in the valuation of the condition of polyurethane based materials.

The coatings containing ZnO (S13G/LO and Z93) exhibited fluorescent spectra apparently dominated by ZnO. Nicoll[4] showed that the ultraviolet (~380 nm) band wavelength peak shifts with wavelength toward the visible at about 0.12 nm/°C (Figure 16). This shift seems to correlate with the fundamental absorption edge shift. There is no shift in the visible band, but its intensity decreases with temperature. Kroeger[5] attributes this visible fluorescence (~520 nm) in ZnO to the presence of oxygen vacancies, that is, a non-stoichiometric zinc rich condition. It is tempting to attribute the reduction seen in this band for the LDEF S13G/LO and Z93 to the reaction of ZnO with atomic oxygen. Streed[6] shows, in ground chamber tests, that fluorescence reduction in this band may be caused by ultraviolet and/or proton irradiation. Perhaps, in space, the reaction is indeed proceeding toward a stoichiometric mixture aided by the presence of zinc and oxygen in the lattice reacting as a result of exposure to the various high-energy environments.

Fluorescence of silver Teflon (TCSE front cover) is attributed to the microcracking that occurred during installation. The matching spectra of ultraviolet irradiated adhesive used to apply the silver Teflon leaves little doubt of the source of the flight material fluorescence and also is an example of fluorescence as an additional analytical tool available to materials researchers and technologists.

REFERENCES

1. Wilkes, D.R., et. al., Thermal Control Surfaces on the MSFC & LDEF Experiments, LDEF Materials Workshop, Hampton, VA, November, 1991.

2. Hill, R.H. Jr., Feuer, H.O. Jr., Laser-Induced Fluorescence Inspection of Polyurethane, Proceedings of the 17th Symposium on Nondestructive Evaluation, April 17-20, 1989, San Antonio, TX.

3. Hill, R.H. Jr., Laser-Induced Fluorescence of Space-Exposed Polyurethane, Southwest Research Institute Report 15-9682, April 6, 1992.

4. Nicoll, F.H., Temperature Dependence of Emission Bands of ZnO Phosphors, Journal of the Optical Society of America, Vol. 39, 1948.

5. Kroeger, Vink, et. al., The Origin of Fluorescence in Self-Activated ZnS, CdS, and ZnO, Journal of Chemical Physics, Vol. 22, No. 2, p. 250, 1954.

6. Streed, E.R., Experimental Study of the Combined Space Environment Effects on ZnO/Potassium Silicate, Thermophysics of Spacecraft and Planetary Bodies, ed. by G. Heller, 1967.

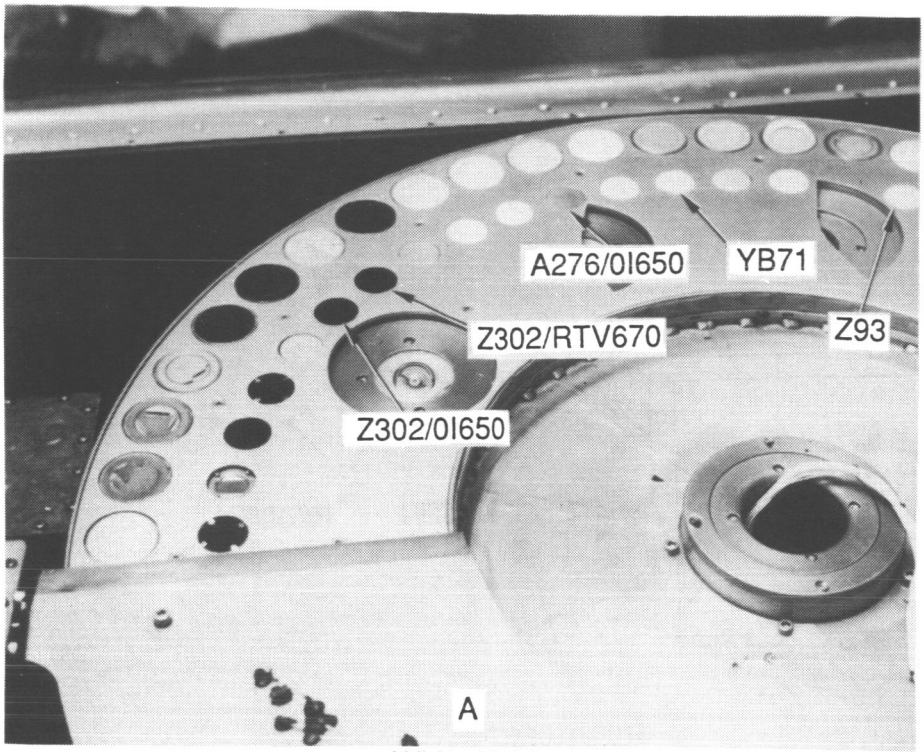

White Light

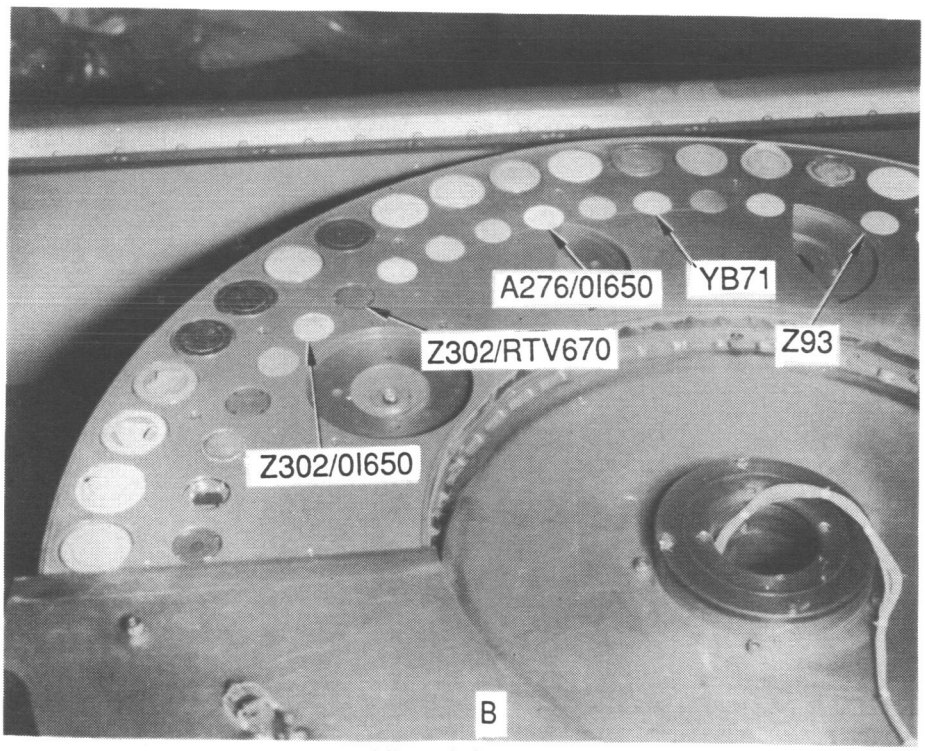

Ultraviolet Light

Figure 1. Fluorescence of Thermal Control Coatings Comparison of Samples Under White and Ultraviolet Light.

ORIGINAL PAGE
BLACK AND WHITE PHOTOGRAPH

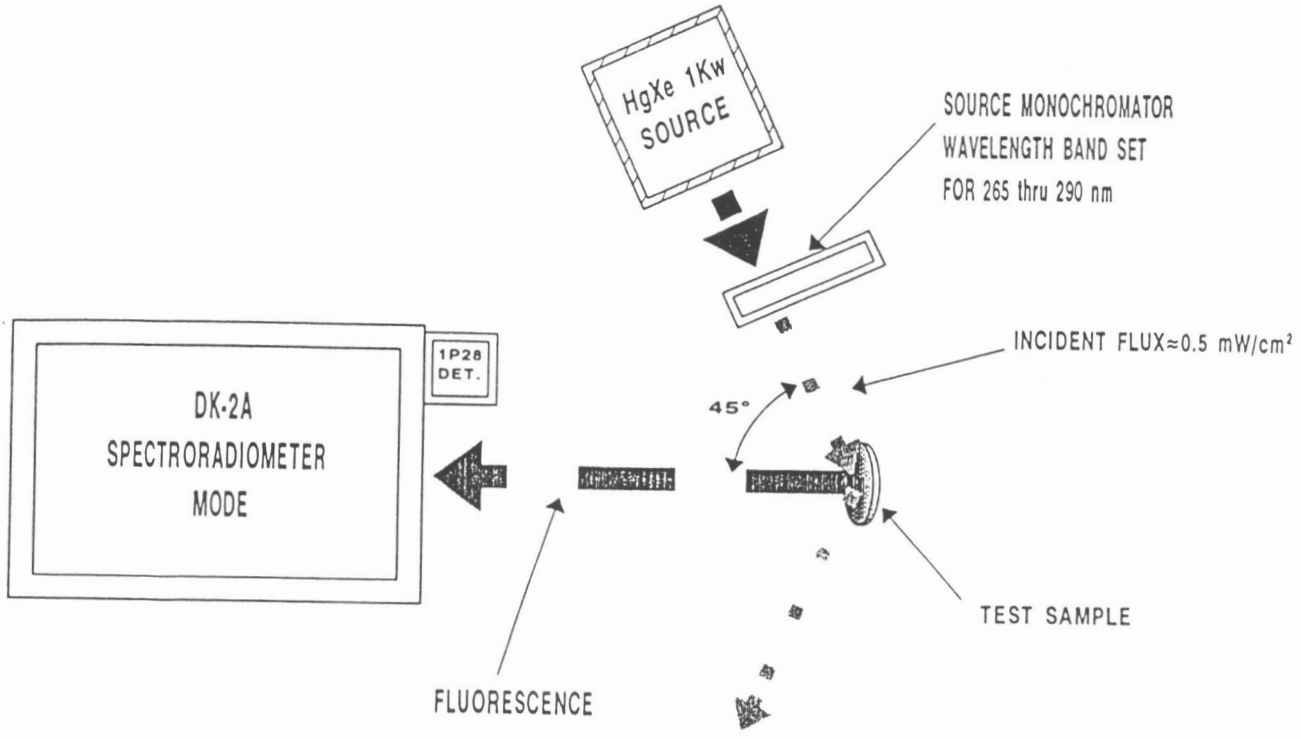

Figure 2. Schematic of Fluorescence Measurement.

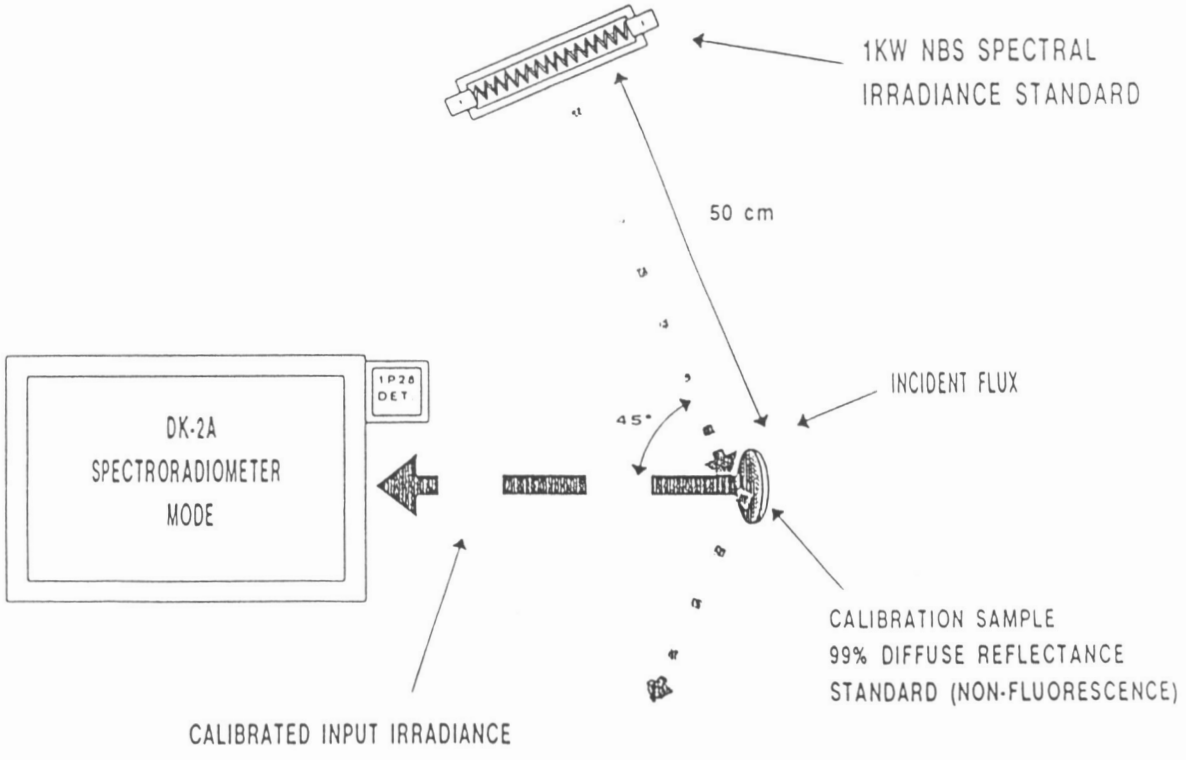

Figure 3. Schematic of Calibration Setup for Fluorescence Measurements.

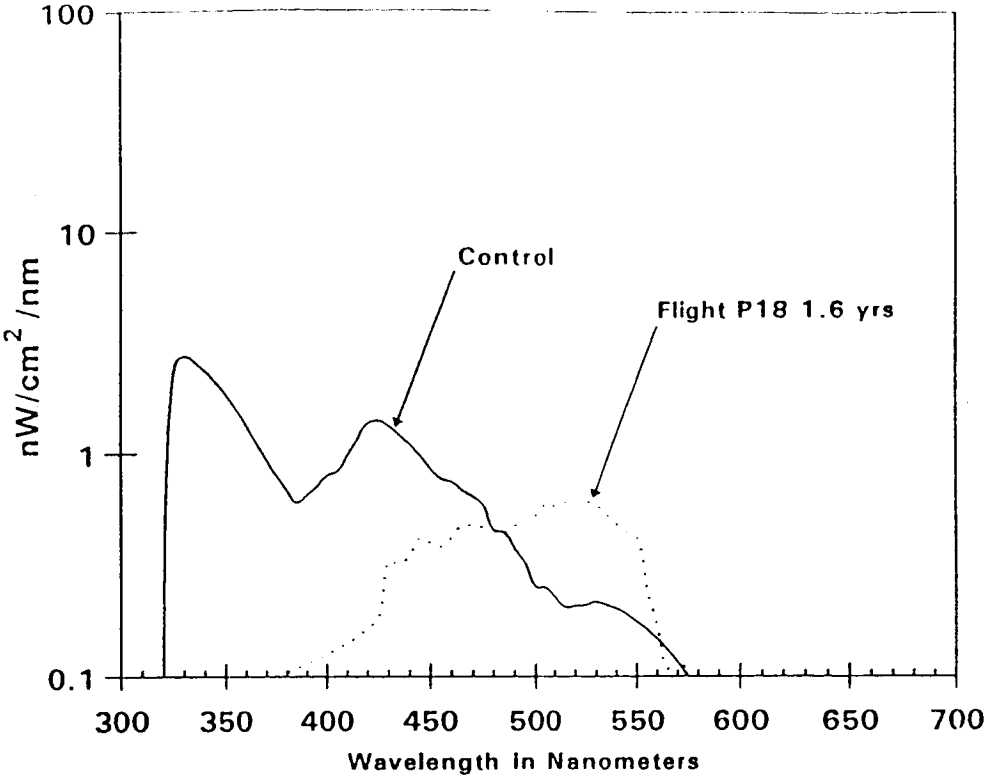

Figure 4. Fluorescence Spectra of Z302.
Thermal Control Surfaces Experiment S0069

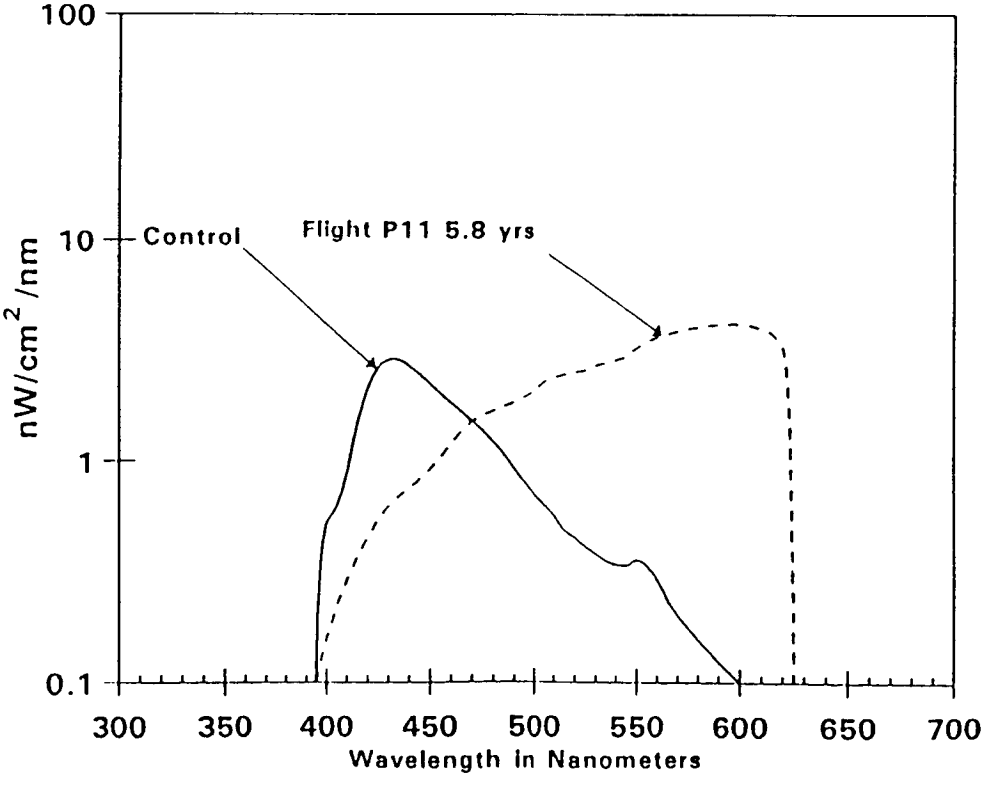

Figure 5. Fluorescence Spectra of A276.
Thermal Control Surfaces Experiment S0069

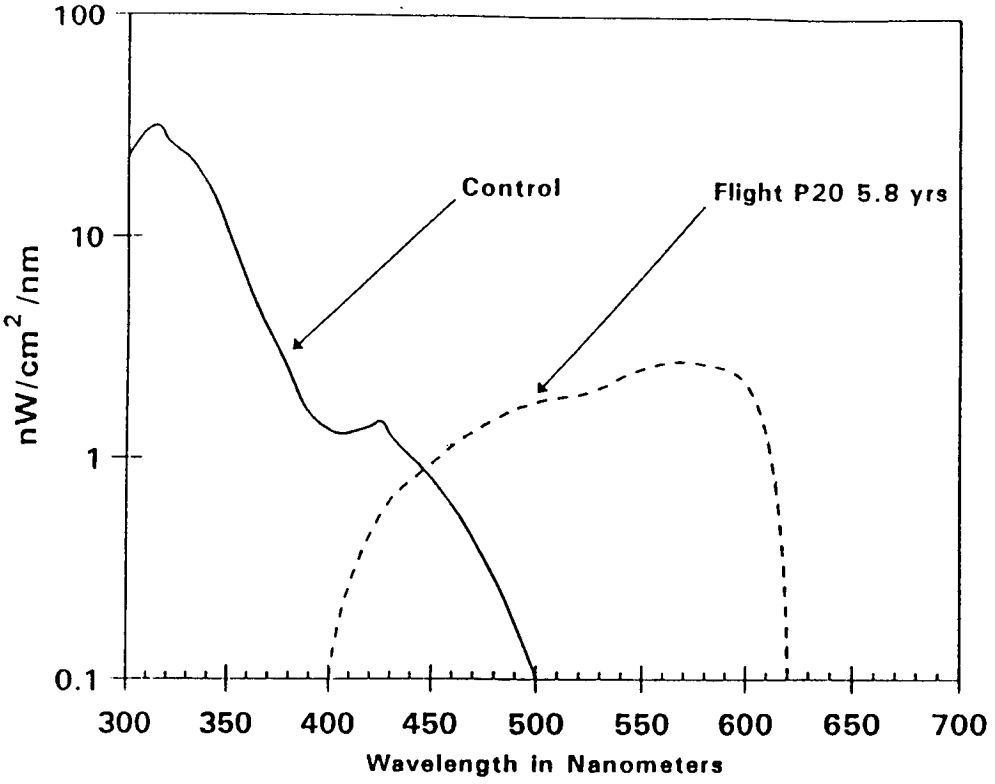

Figure 6. Fluorescence Spectra of Z302 with OI650 Overcoat. Thermal Control Surfaces Experiment S0069

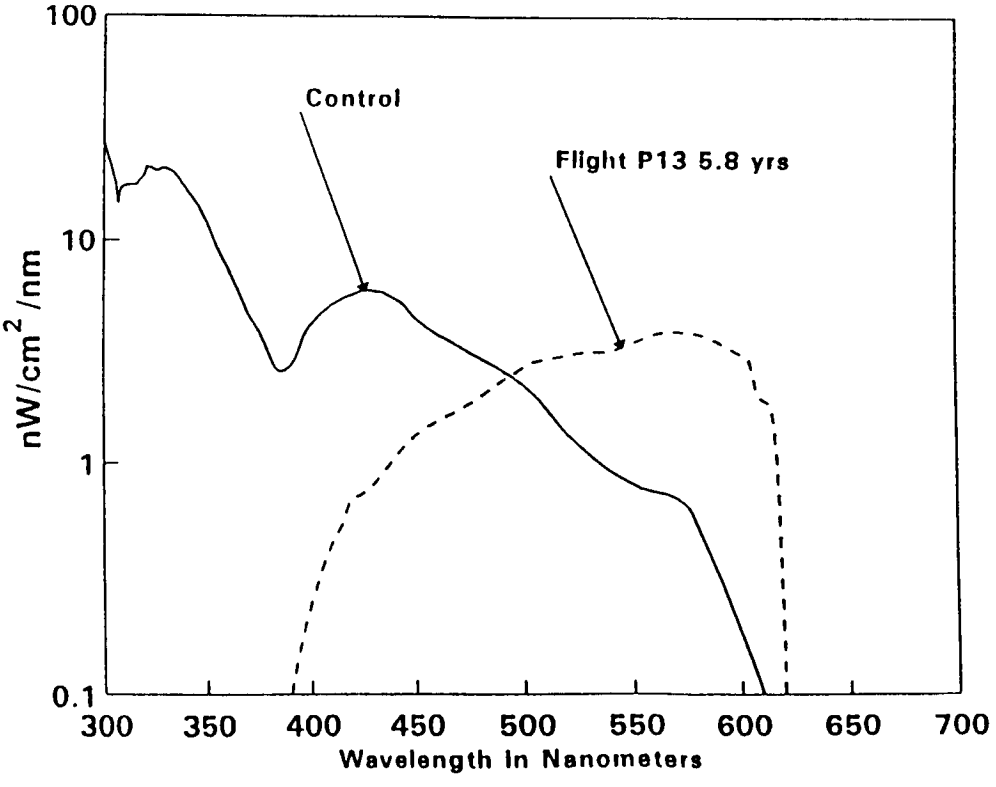

Figure 7. Fluorescence Spectra of A276 with OI650 Overcoat. Thermal Control Surfaces Experiment S0069

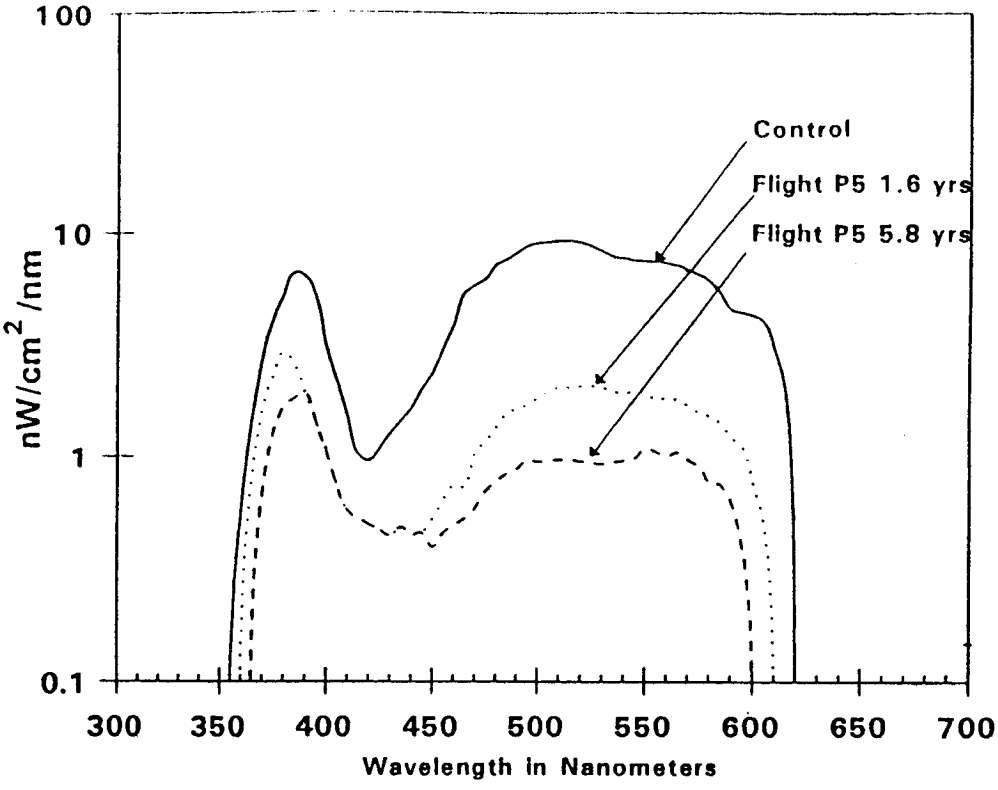

Figure 8. Fluorescence Spectra of Z93.
Thermal Control Surfaces Experiment S0069

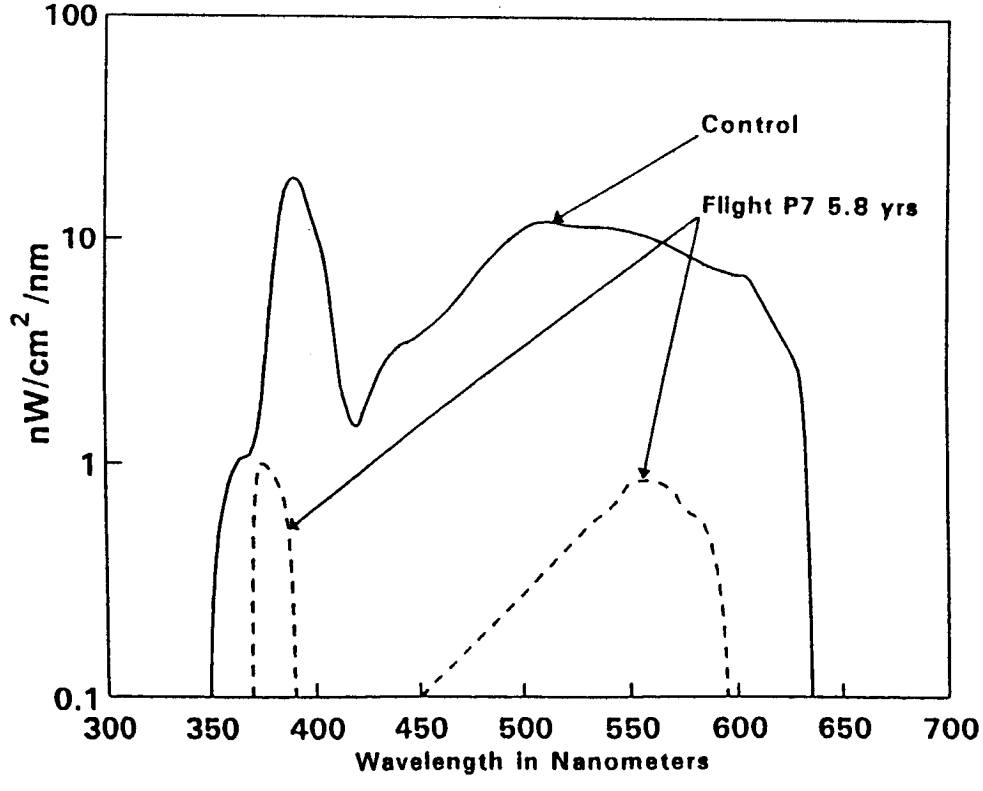

Figure 9. Fluorescence Spectra of S13G/LO.
Thermal Control Surfaces Experiment S0069

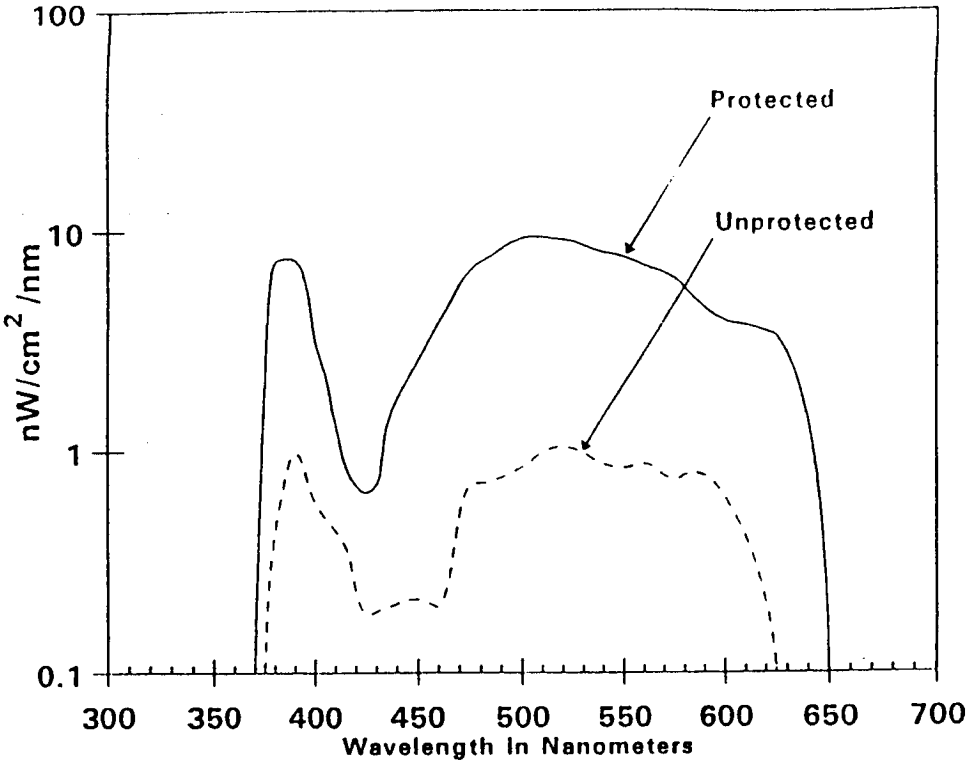

Figure 10. Fluorescence Spectra of Z93 (RAM).
Interaction of AO with Material Surfaces in LEO AO114

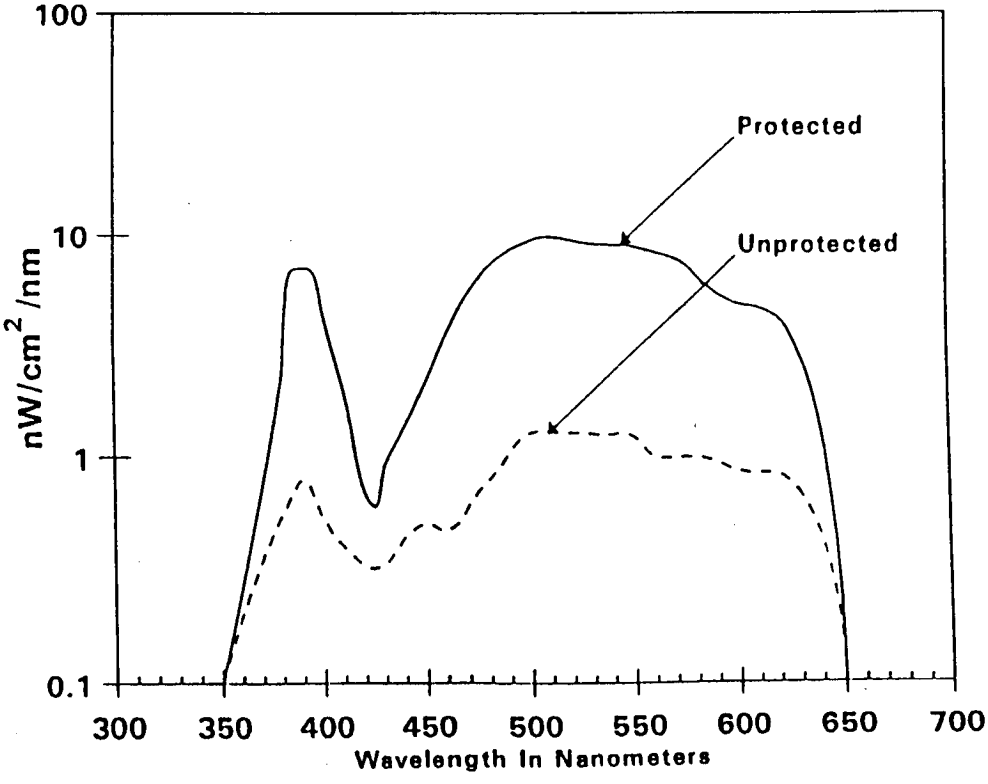

Figure 11. Fluorescence Spectra of Z93 (WAKE)
Interaction of AO with Material Surfaces in LEO AO114

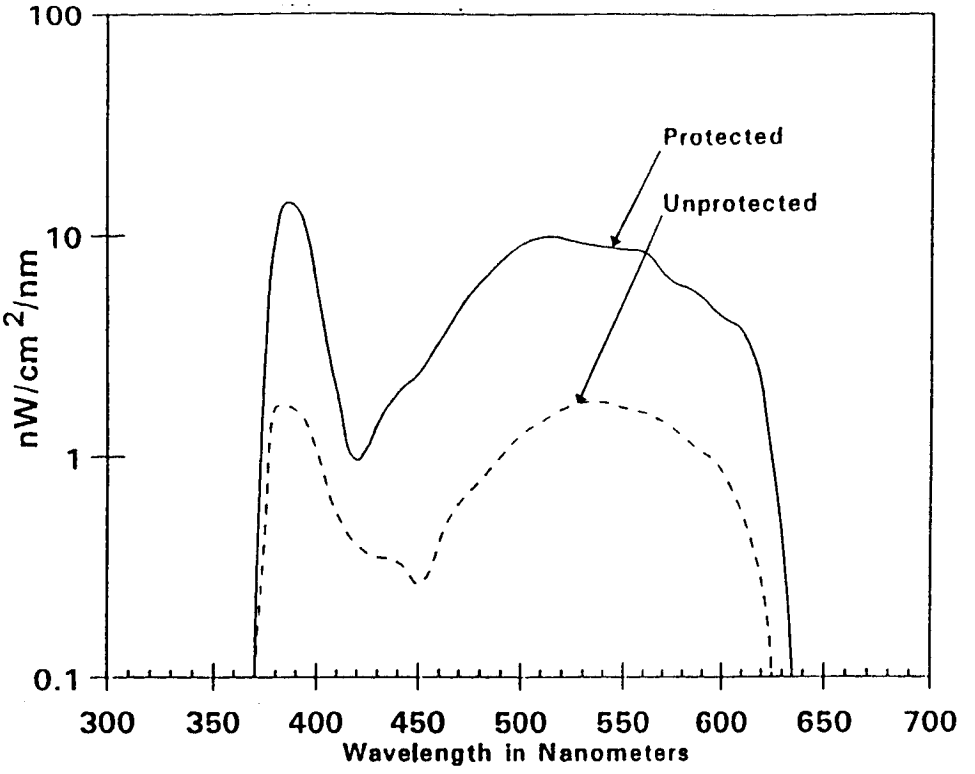

Figure 12. Fluorescence Spectra of S13G/LO (RAM). Interaction of AO with Material Surfaces in LEO AO114

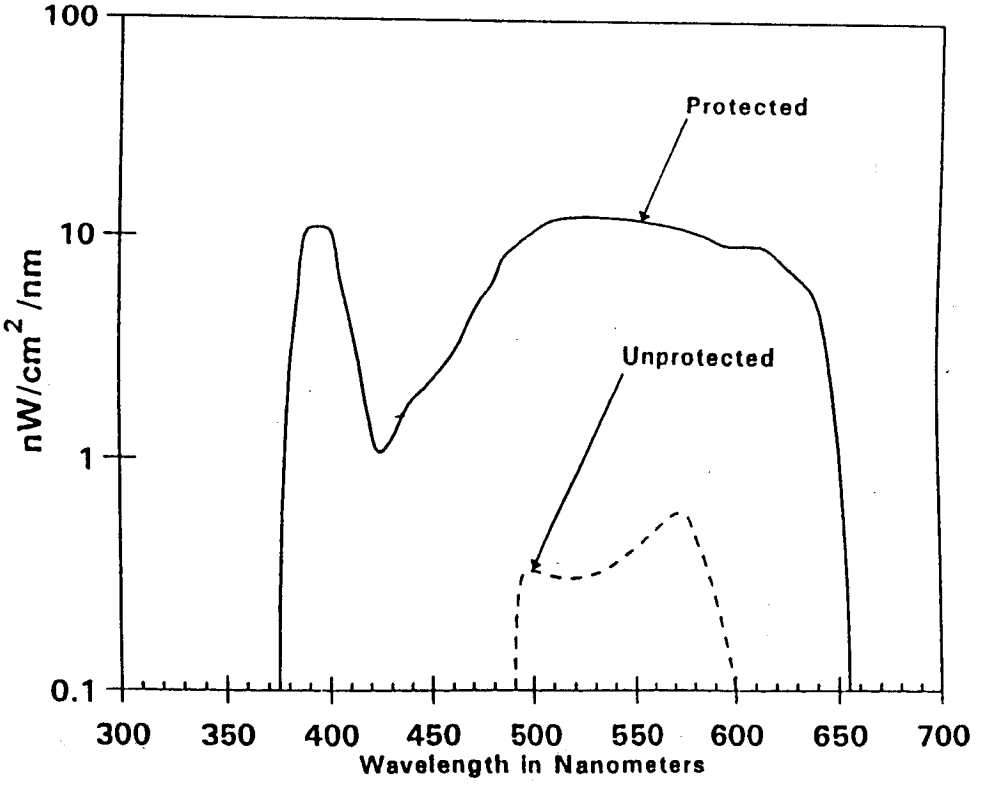

Figure 13. Fluorescence Spectra of S13G/LO (WAKE) Interaction of AO with Material Surfaces in LEO AO114

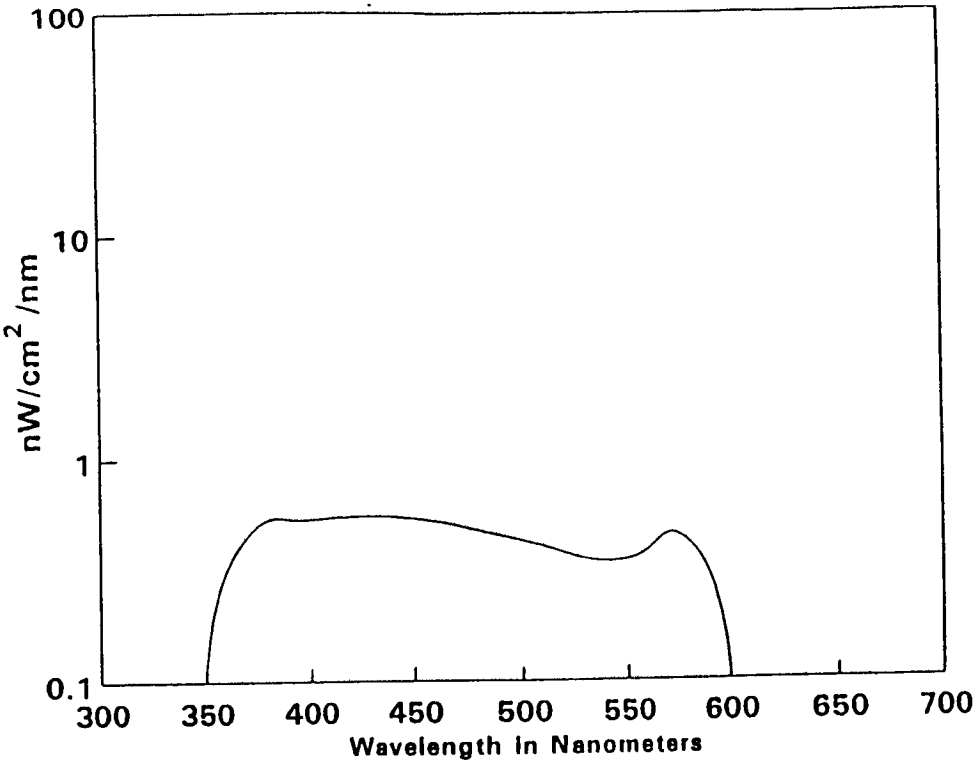

Figure 14. Fluorescence Spectra of Front Cover Silver Teflon. Thermal Control Surfaces Experiment S0069

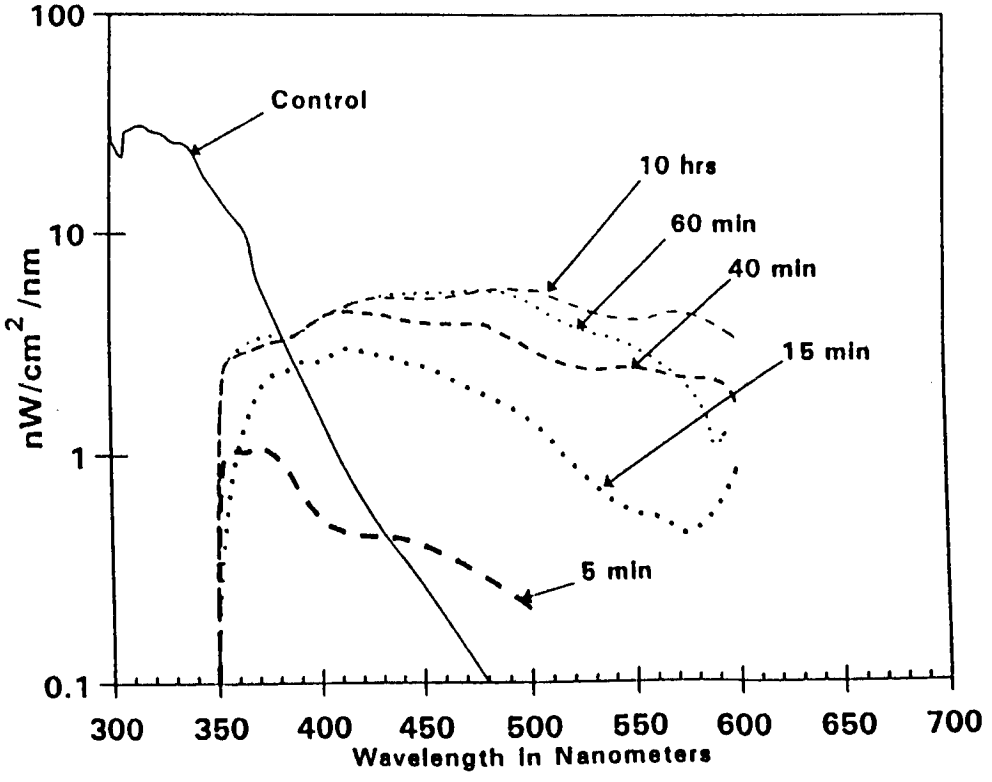

Figure 15. Fluorescence Spectra of Adhesive 966 After UV Exposure. Thermal Control Surfaces Experiment S0069

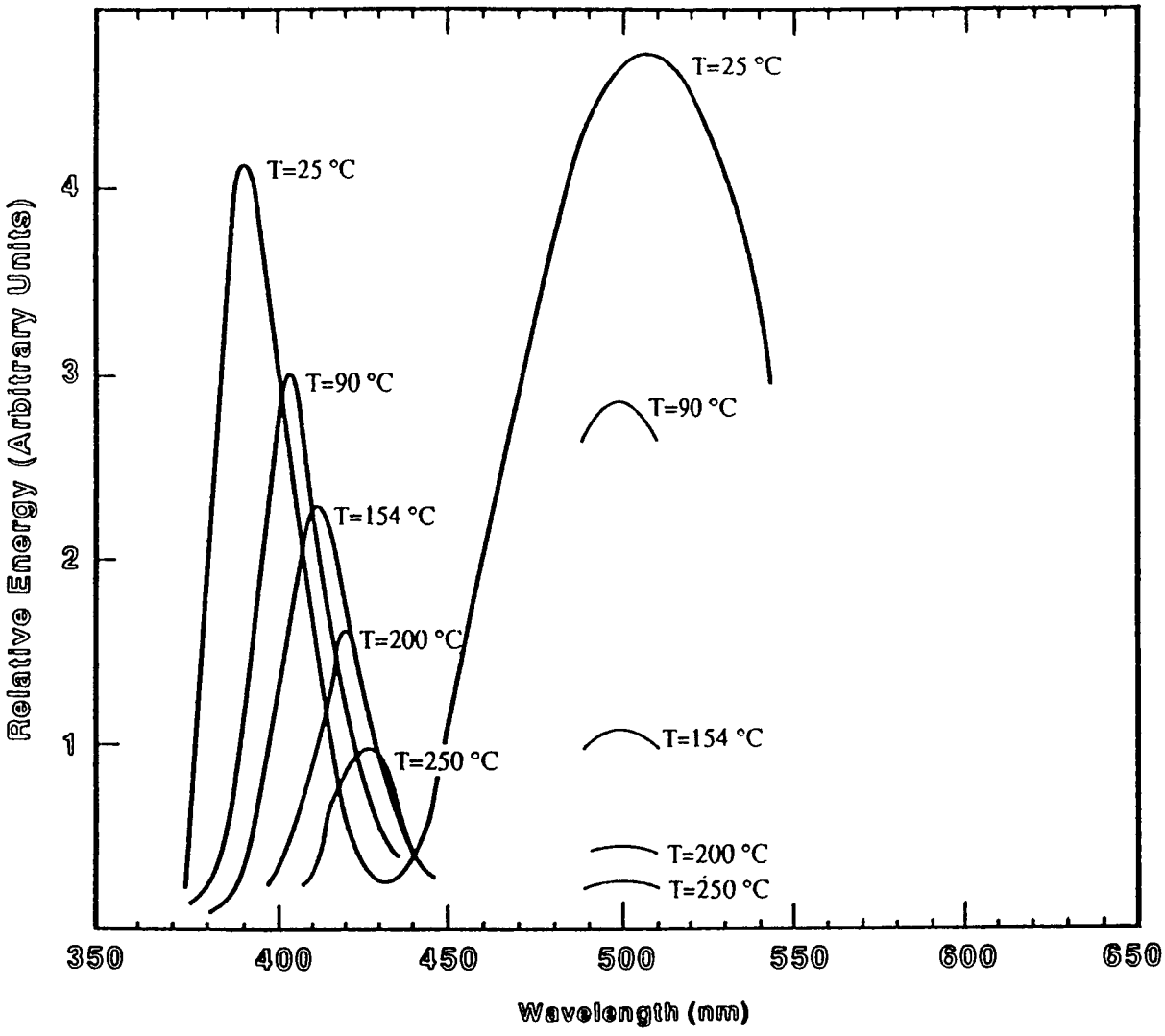

Relative energy emitted by hex, ZnO: [Zn] phosphor as a function of wavelength for different temperatures. Emission produced by a high current density electron beam, 100 MA focused and scanning a 3-in. × 4-in. television pattern at 20 kV.

Refer: Nicoll, F.H.; J.Opt. Soc. Amer. 38, 817 (1948).

[Reprinted with permission of the Journal of the Optical Society of America.]

Figure 16. Fluorescence ZnO.

N93-28281

ATOMIC OXYGEN EFFECTS ON LDEF EXPERIMENT AO171

Ann F. Whitaker
Rachel R. Kamenetzky
Miria M. Finckenor
Joseph K. Norwood
NASA Marshall Space Flight Center
MSFC, AL 35812
Phone: 205/544-2510, Fax: 205/544-0212

INTRODUCTION

The Solar Array Materials Passive LDEF Experiment (SAMPLE), AO171, contained in total approximately 100 materials and materials processes with a 300 specimen complement. With the exception of experiment solar cell and solar cell modules, all test specimens were weighed before flight, thus allowing an accurate determination of mass loss as a result of space exposure. Since almost all of the test specimens were thermal vacuum baked before flight, the mass loss sustained can be attributed principally to atomic oxygen attack. This paper documents the atomic oxygen effects observed and measured in five classes of materials. The atomic oxygen reactivity values generated for these materials are compared to those values derived for the same materials from exposures on short term shuttle flights. An assessment of the utility of predicting long term atomic oxygen effects from short term exposures is given.

This experiment was located on Row 8 position A which allowed all experiment materials to be exposed to an atomic oxygen fluence of 6.93×10^{21} atoms/cm^2 as a result of being positioned 38 degrees off the RAM direction.

Composites

Table I summarizes the atomic oxygen erosion data for three carbon fiber and one glass fiber composite systems. A comparison of flight and control carbon fiber composites, figure 1, shows a darker, more diffuse surface as a result of flight exposure. Profilometer traces across the protected area of the bolt hole attachment points onto the exposed region of the flight specimen, figure 2, were used to generate thickness loss. Fiber bundles were easily discernible in the patterns of the traces. On a microscopic level, peak type structures characteristic of orbital atomic oxygen attack and "ash" material are observable on the exposed surfaces as is a protected "mesa" area, figure 3. Thickness losses measured on the flight specimens were consistent with their measured mass loss. Composite matrix erosion was greater than that of the carbon fibers and was most pronounced for the polysulfone P1700 system. Atomic oxygen reactivity values generally averaged 1×10^{-24} cm^3/atom with the exception of the "S" glass epoxy composites which tend to become self protecting. Reactivity values generated from short term shuttle exposures yield twice the LDEF values noted here. A reasonable explanation is that high fluences accumulated through long

PRECEDING PAGE BLANK NOT FILMED

exposures readily erode the as-prepared matrix rich composite surfaces so that the fiber rich bulk region receives comparatively higher exposure. Reactivity values for high fluence exposed or long term exposed composites are thus more characteristic of the carbon fiber than the more reactive matrix material. As a result, long term prediction of erosion of carbon fiber composites should be based on carbon reactivity to give a more realistic measure of material loss. Short term exposures will yield erosion rates much too high for these materials.

Table I. AO171 Composites - Atomic Oxygen Erosion Rates

Composite Materials (No. of Specimens)	Avg. Thickness Loss (mils)	Atomic Oxygen Reactivity 10^{-24} cm^3/atom	Comments
* HMF 322/P1700/+/- 45°(5)	2.5 to 6.2*	0.92 to 2.3	On AO171: Matls. (1-5) "blacker, i.e. more diffuse. "S" glass epoxy much darker probably from UV effects. Fibers evident in materials (1-6). Material (7) shows unexplained corrugated features on Al tape. Shuttle Flights: Graphite/epoxy reactivity 2 to 2.6 x 10^{-24} cm^3/atom
* HMS/934/0° (5)	2.5**	0.920	
* HMS/934/90° (6)	2.700	1.0	
• P75S/934/90° (6)	2.700	1.0	
* P75S/934/0° (5)	2.800	1.0	
* "S" Glass-epoxy (3)	0.36***	0.130	
* Thermal Control * Aluminized Taped "S" Glass-epoxy (3)	Indeterminate	---	

* Matrix erosion much greater than fiber

** Average of rates from 2 ends of sample; contamination likely on forward end

*** Fibers uneroded and become protective after initial matrix mass loss

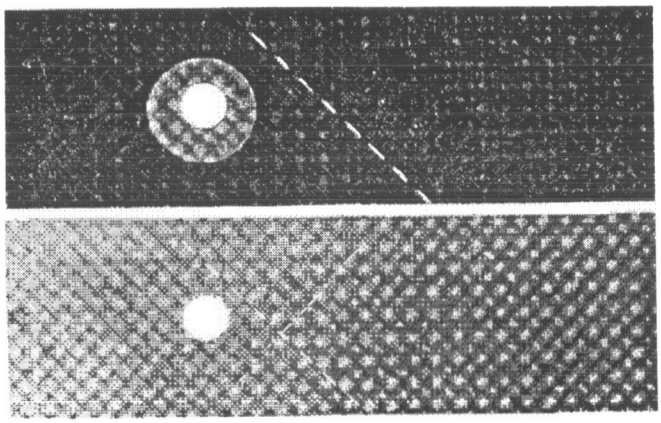

Figure 1. AO171 Carbon fiber composite flight (top) and control (bottom) specimens.

Paints

Table II contains absorptivity data and mass loss data for eight paints flown on LDEF compared with similar data obtained from short term shuttle flights. Control values of absorptivity were generated either on the sample flown or on control samples in the batch from

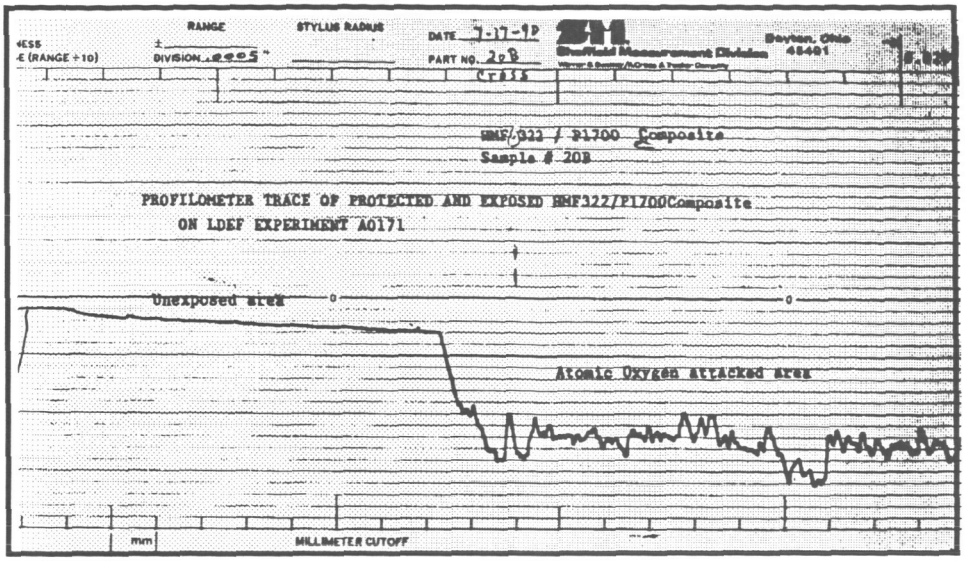

Figure 2. AO171 Carbon fiber profilometer trace.

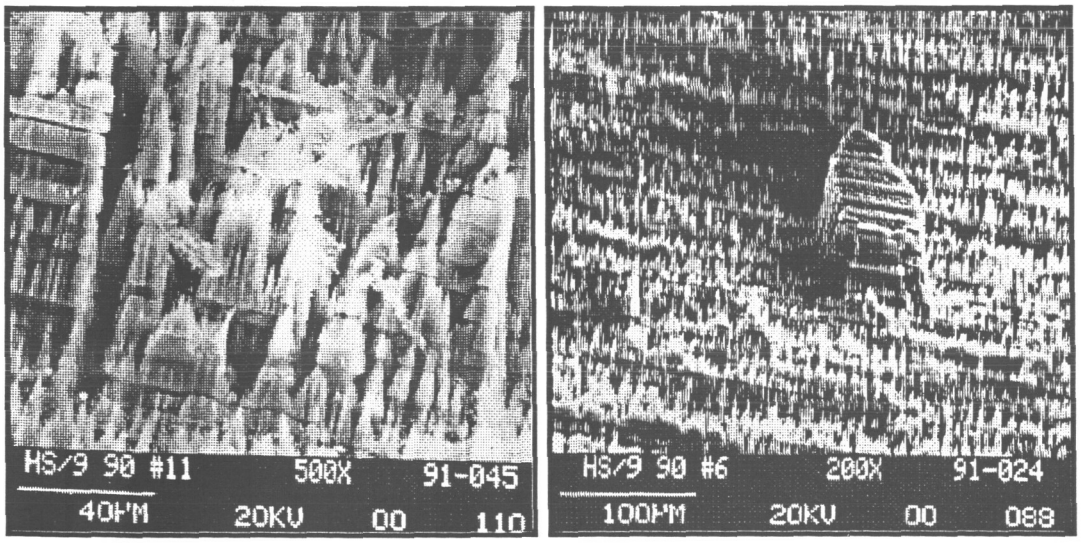

Figure 3. SEM photos of exposed carbon fiber composites showing peak type surface structure and "ash" material at 500x (left) and a protected "mesa" on the exposed surface at 200x (right).

which the flight samples were taken. With the exception of the Z302 black, all the paints that flew were optically diffuse. The trend for paints which do not drastically change color is to decrease in solar absorptivity, α_s, as a result of long term orbital atomic oxygen exposure whereas an increase in α_s is observed after similar short exposures. Under these short exposures to atomic oxygen, the surfaces of these diffuse paints increase in diffuseness but also have an accompanying increase in α_s. With long exposures in this environment, the colorless or lighter colored paint pigments are

Table II. Comparison of AO171 Flight Experiment and Shuttle Short Term Shuttle Paint Property Data

Paints	α_s Control	$\Delta\alpha_s$		Reactivity (mg/atom)	
		LDEF AO171	Shuttle Flight	LDEF AO171	Shuttle Flight
Z306 Black Diffuse	0.990	-0.010	-0.020	2.3×10^{-22}	1.0×10^{-21}
Z302 Black Specular	0.97 - 0.99	~ 0	0.040	5.7×10^{-22}	5.8×10^{-21}
Z853 Yellow Diffuse	0.41 - 0.49	-0.070	0.040	1.4×10^{-22}	0.90×10^{-21}
A276 White Diffuse	0.24 - 0.28	-0.050	~ 0	1.4×10^{-22}	1.0×10^{-21}
401-C10 Black Diffuse	0.98 - 0.99	3.7 ± 1.0	1.5 ± 0.5	1.6×10^{-22}	0.86×10^{-21}
Tiodized K17 White	0.38	0.030	Unavailable	Unavailable	No Data
Tiodized K17 Black	0.96	-0.15	Unavailable	Unavailable	No Data
S13GLO Diffuse White	0.19	0.14	1.1 ± 2	Negligible	Negligible

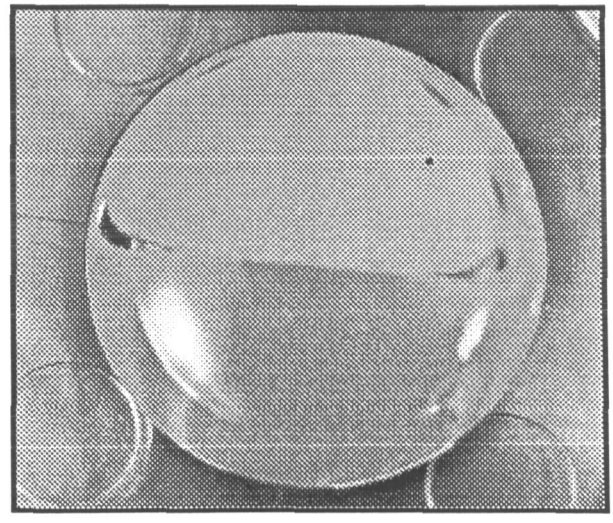

Figure 4. Post-flight photo of Z853 paint specimen shows a distinct contrast between the protected sample area and the lighter color exposed sample region.

exposed and have a greater influence on optical properties providing some increased reflectivity and a corresponding decrease in α_s. This increase in the reflectivity is observable in the Z853 yellow paint, figure 4, where the exposed area is lighter in color. Coincidentally, this specimen has sustained a micrometeoroid impact in the exposed area. The changes in optical properties for the

Tiodized paints are accounted for by the fact that the samples have lost their characteristic colors. The S13GLO white paint, which resisted atomic oxygen attack but darkened with exposure, doubled in absorptivity due probably from ultraviolet irradiation.

All the paints except S13GLO lost mass as a result of atomic oxygen exposure. The reactivity values for short and long term exposures are given in terms of milligrams per incident atomic oxygen atom rather than the conventional reactivity unit. These paints are diffuse implying the presence of inert components which do not erode, so thickness loss is not as sensitive a measure of atomic oxygen reactivity as is mass loss. As expected, the short term and long term reactivities are nonlinear so long term reactivities cannot be predicted from short exposures. With increased exposures more inert material is exposed, thus providing increased self shielding which results in

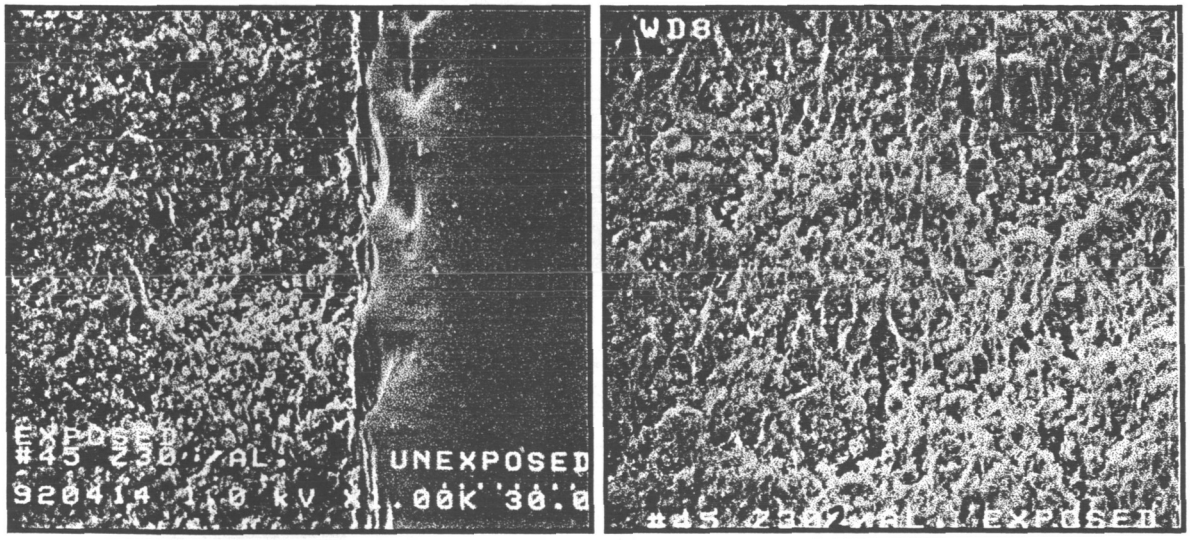

Figure 5. Micrographs of Z302 black paint showing the exposed/protected interface (left) and the "ash" material (right).

apparent decreased reaction to incident atomic oxygen. The benefit derived is that the paint will survive longer than predicted from short exposures. An eroded and controlled area on Z302 black is shown in figure 5 as is a microphotograph of the "ash" material which characteristically appears on orbital atomic oxygen exposed materials that contain black carbon.

Polymers

Polymers from Experiment AO171 whose reactivity values have been calculated from thickness decreases or mass loss are contained in table III with similar data generated from short shuttle exposures. These polymers consisted of thin films of white Tedlar, TFE Teflon washers, Polysulfone contained in carbon fiber composites and bulk samples of Halar, PEEK and RTV-511 and Kevlar 29 and 49 in woven fabrics. Mass loss due to atomic oxygen erosion in RTV-511 could

not be separated from vacuum outgassing so no reactivity value was generated for that material. Thin films of 5 mil Kapton, 1 mil black Kapton and 0.5 mil FEP Teflon were eroded away as a result of the 5.8 years of exposure.

White Tedlar contains self-shielding particles so that a residual film of Tedlar remained after exposure. These particles served to prevent a linear erosion of Tedlar with atomic oxygen fluence. No short term erosion data were available for this material for comparison. Profilometer traces across exposed and protected areas were used to determine atomic oxygen erosion of 40 TFE Teflon washers in order to generate TFE reactivity. This data is compared in table III to FEP Teflon data from LDEF Experiment S0069. This comparative analysis shows a definitive atomic oxygen erosion difference between TFE and FEP Teflon which short term exposure data could not previously resolve.

Kevlar 29 and 49 reactivity values on AO171 were based on thickness measurements of woven fabrics, and Kevlar 29 data from shuttle flight STS-8 was based on mass loss sustained from a woven tether. These data show a distinct difference in the response between Kevlar 49 and 29. Variability of sample configuration and method of determination of reactivity in the short term

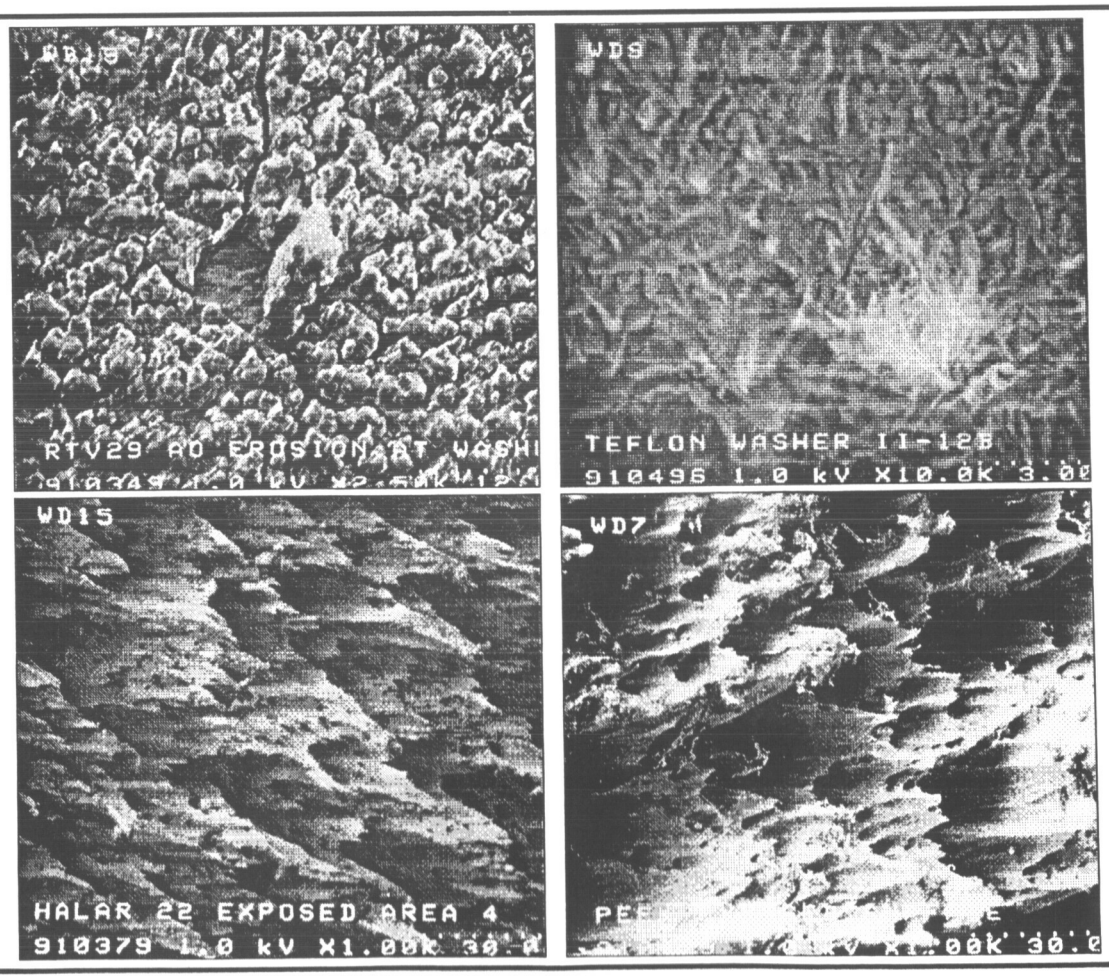

Figure 6. SEM photographs of AO171 exposed polymers (clockwise from top left) RTV 511, TFE Teflon, PEEK, and Halar.

STS-8 exposure and AO171 exposure for Kevlar 29 leave considerable uncertainty in the data. Kevlar 49 whose reactivity is higher is a more stressed material than is Kevlar 29, suggesting a connection between stress and atomic oxygen reactivity. Reactivity values for PEEK and Halar were derived from mass loss. Surface morphologies for selected exposed polymers from Experiment AO171 are shown in figure 6.

Atomic oxygen reactivity values for Experiment AO171 polymers are consistent with thermodynamic considerations and the effects of varying reactive constituents in materials. Polymers such as Polysulfone and Halar that represent pure polymers (i.e. polymers containing no components that erode at different rates) appear to erode linearly with atomic oxygen fluence, so long term thickness changes due to atomic oxygen attack in these materials can be predicted from short exposure data for these pure polymers.

Table III. Comparison of Atomic Oxygen Effects on Polymers from Experiment AO171 and Short Term Shuttle Flights

Polymer	Reactivity (10^{-24} cm^3/atom)		Comments
	AO171	Shuttle Flights	
White Tedlar	0.29	----	Inert particles retarded erosion
TFE Teflon	0.20	< 0.05 (estimated)	
FEP Teflon	0.35	< 0.05 (estimated)	Data from SOO69
PEEK	2.3	3.7 ± 1.0	Shuttle tested material was thin film with low emittance
Halar	2.1	2.0	
Kevlar 29	1.5 ±0.5	1.1 ± 2	Shuttle data based on STS-8 tether mass loss
Kevlar 49	4.0	---	
Polysulfone	2.3	2.4	

Metals

The metals complement of experiment AO171 consisted of various copper and silver ribbon materials, miscellaneous metallic specimens, and 1" diameter bulk metals including materials which readily oxidize and which resist oxidation in the atomic oxygen environment. A series of alloys containing various ratios of aluminum, chromium and nickel in the as-received and preoxidized condition were also flown. Cold rolled silver ribbon both thermally heat sunk to the experiment base and thermally isolated configured with and without a stress loop completed the metal samples reported on here. Data generated from the analyses of these materials are contained in table IV.

Macroscopic oxidation effects were observed in silver and copper. The orbital oxidation effects observed in copper have not been previously reported, partly because the effect in copper was not anticipated. Some fine structure is observable on the flight exposed copper surface of figure 7. The microstructure for the different silver samples is shown in figure 8. The silver oxide scaling on the cold rolled ribbon has been seen previously but the fine grained oxide

structures from the disk samples have not been previously observed. Most of the metals flown on this experiment were not finely polished so the microphotographs show large features which are machine marks from the sample preparation process. The atomic oxygen effects in the other metals appear to be minimal. With the exception of some of the silver samples, the metals were well heat sunk to the less than 100°F experiment structure. It is well known that temperature plays a strong role in oxidation phenomena, and the low temperatures to which these heat sunk metals were subjected would not be expected to accelerate oxidation.

All the metals reported on gained weight as a result of being exposed to orbital atomic oxygen. Reactivity values based on linear effects were reported for these materials even though it is known that metals oxidize nonlinearly. This was done in order to give a comparative measure of the observed effects. With the exception of silver, the magnitude of reactivity numbers was less than 1×10^{-26} cm^3/atom for the conditions experienced on AO171. Accommodation numbers presented are given in terms of atomic oxygen atoms reacted ratioed to the incident atoms. These calculations based on the mass increase show that, with the exception of stressed, thermally isolated silver, less than 10 atoms per 10^4 incident are reacted. The basic assumption for these accommodation numbers is that the mass increase resulted from the formation of the most thermodynamically favorable oxide. The presence of some of these oxides is yet to be confirmed. The reactivity and accommodation values for the cold rolled, stressed, and thermally isolated silver are an order of magnitude greater than that of the same material which had no additionally applied stress and was heat sunk to the structure. These results suggest that the atomic oxygen effects are more dependent on temperature and microstructure than on total incident atomic oxygen.

Table IV. LDEF AO171 Metals Data

Metal	Reactivity ($10^{-26}cm^3$/atom)	Accommodation of AO per 10^4 Incident Atoms	Comments
Copper	0.87	3.6	Accommodation strongly dependent on temperature and stress, numbers are tentative pending confirmation of oxide identity.
Molybdenum	0.14	2.8	
Tungsten	0.044	~ 1.0	
HOS 875	0.29	2.5	
Pre-Ox HOS 875	TBD	TBD	
Tophet 30	0.55	5.0	
Ni-Cr-Al-Zr Alloy	TBD	TBD	
Pre-Ox Ni-Cr-Al-Zr	---	---	
Tantalum	0.60	8.3	
Titanium 75A	0.39	4.4	
Mg AZ31B	0.45	2.0	
Niobium	0.14	2.0	
Silver disk-fine grain	2.9	8.4	
Silver - cold rolled ribbon in stress loop	27.5	80.0	

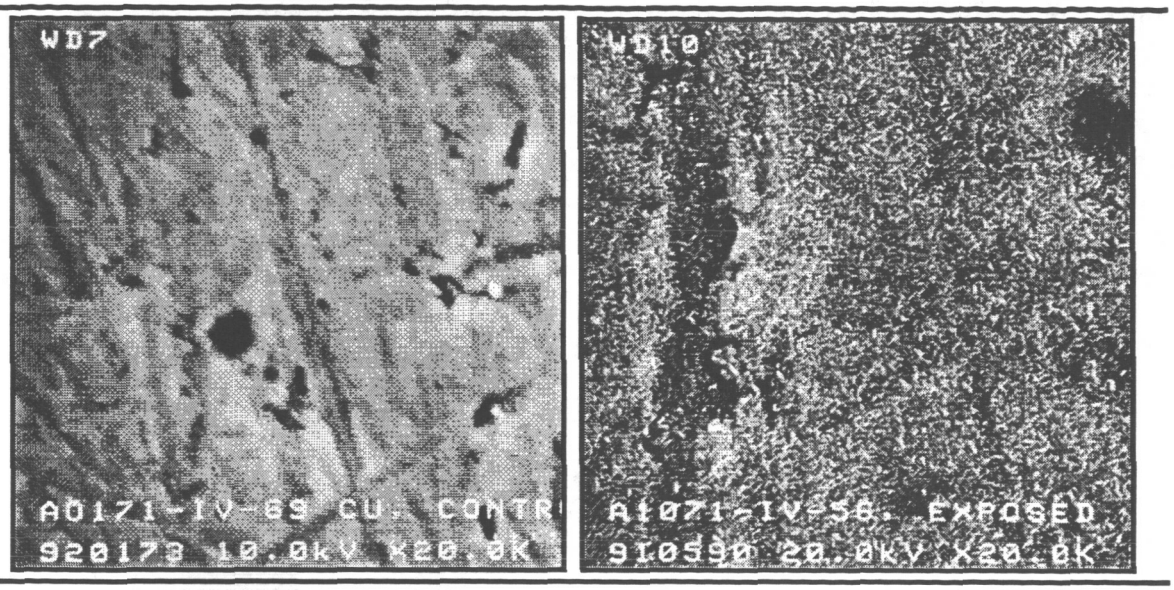

Figure 7. Microphotographs of LDEF AO171 copper sample protected surface (left) and exposed surface (right).

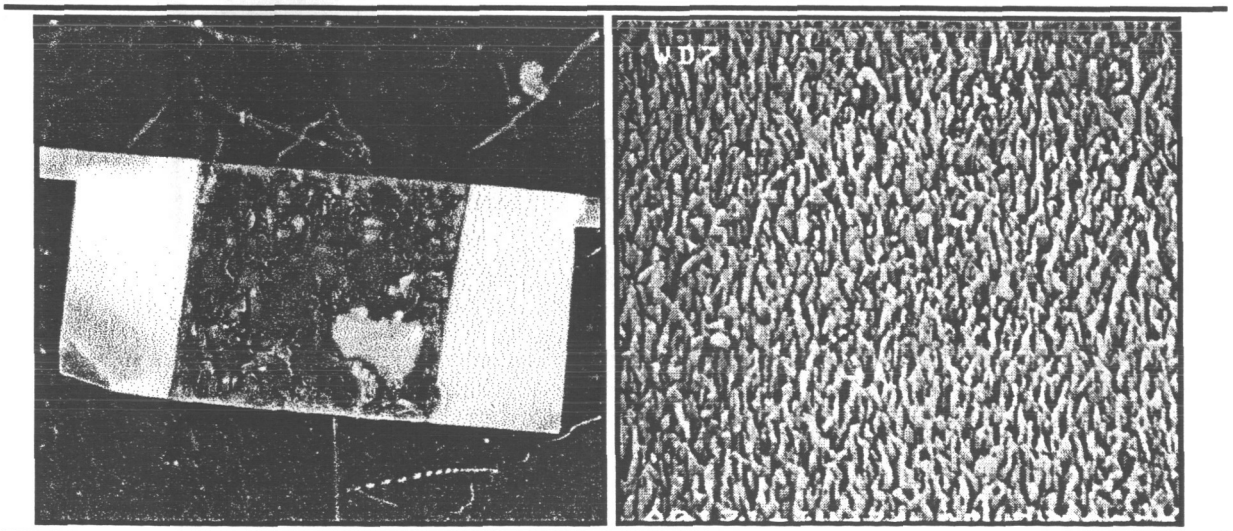

Figure 8. Photograph of LDEF AO171 silver interconnect (left) and SEM photograph of bulk silver exposed surface (right).

Glassy Ceramics

Approximately thirty silver and aluminum solar reflectors with thin coatings of various glassy ceramics were flown on this experiment. A large group of these reflector samples were configured with one-half of the sample exposed and the other half covered. Small decreases in reflectivity were noted in these samples but no contamination was present to account for these reflectivity decreases. Precision angstrometer traces were made on all the samples, and it was noted

that a decrease in film height occurred in the exposed areas. Selected samples were examined with low energy Rutherford backscattering which revealed that a densification of the film materials had occurred in the exposed region. A conversion of SiO to SiO_2 was identified. The results of these measurements are presented here under atomic oxygen effects. However, several factors can bring about the densification of these materials and it remains to be proven that the effects noted are the result of atomic oxygen attack. Table V provides a listing of these effects for the various solar reflectors. Decreases in thickness of these materials range up to 160 angstroms. For applications of these materials where the total coating thickness is 1000 to 1300 angstroms, the percentage change is considerable and the effect can be substantial for space optics. Reactivity values for these materials are based on the assumption that the observed effects result from atomic oxygen attack range from 0.4 to 2.3 x 10^{-28} cm^3/atom.

Table V. Property Changes in AO171 Glassy Ceramics

Coating/Solar Reflector	Change in Solar Reflectance (%)	Decrease in Film Thickness (Å)	Comments
SiO_2 / Ag	- < 1	40	No changes observed for *shuttle flight* exposures. On LDEF SiO-SiO_2, increase in film density noted. Defects observed on all reflectors except SiO_2/Al, small decreases in R_s measured. Reactivity ranges from 0.4 to 2.3 x 10^{-28} cm^3/atom for these materials.
SiO_2 / Al	- < 1	50	
SiO-SiO_2 / Enhanced Al	-2	125	
SiO / Al	-1.5	150	
MgF_2-Sapphire/Enhanced Al	+1.5	25	
MgF_2-Sapphire/Ag	-5 to -10	150	
Dielectric / Ag Alloy	-1 to -5	160	

SUMMARY

Table VI contains a summary of the atomic oxygen effects on five classes of materials exposed on LDEF experiment AO171. Unfilled polymers constitute the materials class in which long term erosion is predictable from short term exposures. The reaction of the remaining classes of materials appears to be considerably more complex so that prediction of long term effects must be based on factors other than thickness reduction.

Table VI. Summary of Long Term Atomic Oxygen Effects on AO171 Materials

Material	Atomic Oxygen Effects
Composites	Erosion from carbon fiber composites can be predicted from carbon reactivity. Glass fiber composites become self protecting.
Paints	Diffuse paints erode non-linearly.
Polymers	Unfilled polymers react linearly with atomic oxygen.
Metals	Reaction is non-linear and strongly dependent on temperature, stress and microstructure; accommodation on the order of less than 10 atoms per 10^4 incident.
Glassy Ceramics	Densification accompanied by a decrease of less than a few hundred angstroms results from space exposure.

Bibliography

1. Kamenetzky, R. R. and Whitaker, A. F.,"Performance of Thermal Control Tape in the Protection of Composite Materials to Space Environmental Exposure", NASA TM-103582.

2. Whitaker, Ann F. and Young, Leighton E., "An Overview of the First Results on the Solar Array Passive LDEF Experiment (SAMPLE), AO171", First LDEF Post-Retrieval Symposium, Orlando, Fl., June, 1991.

3. Whitaker, Ann F., Finckenor, Miria M., and Kamenetzky, Rachel R., "Property Changes Induced by the Space Environment in Polymeric Materials on LDEF", AIAA 30th Aerospace Sciences Meeting, Reno, NV, January, 1992.

4. Whitaker, Ann F., "Selected Results for Metals from LDEF Experiment AO171", LDEF Materials Workshop '91", NASA/Langley Research Center, Hampton, Va., November, 1991.

N93-28282

MONTE CARLO MODELING OF ATOMIC OXYGEN ATTACK OF POLYMERS WITH PROTECTIVE COATINGS ON LDEF

Bruce A. Banks
Kim K. de Groh
Bruce M. Auer
NASA Lewis Research Center
Cleveland, Ohio 44135
Phone: (216) 433-2308 Fax: (216) 433-6106

Linda Gebauer
Jonathan L. Edwards
Cleveland State University
Cleveland, Ohio 44115
Phone: (216) 433-2310 Fax: (216) 433-6106

SUMMARY

Characterization of the behavior of atomic oxygen interaction with materials on the Long Duration Exposure Facility (LDEF) assists in understanding of the mechanisms involved. Thus the reliability of predicting in-space durability of materials based on ground laboratory testing should be improved. A computational model which simulates atomic oxygen interaction with protected polymers has been developed using Monte Carlo techniques. Through the use of an assumed mechanistic behavior of atomic oxygen interaction based on in-space atomic oxygen erosion of unprotected polymers and ground laboratory atomic oxygen interaction with protected polymers, prediction of atomic oxygen interaction with protected polymers on LDEF has been accomplished. However, the results of these predictions are not consistent with the observed LDEF results at defect sites in protected polymers. Improved agreement between observed LDEF results and predicted Monte Carlo modeling can be achieved by modifying of the atomic oxygen interactive assumptions used in the model. LDEF atomic oxygen undercutting results, modeling assumptions, and implications are presented.

INTRODUCTION

Low-Earth-orbital (LEO) atomic oxygen interaction with unprotected and protected polymers has been investigated at low atomic oxygen fluences (approximately 10^{20} atoms/cm^2) in space. Results of these in-space tests have provided useful information concerning the erosion yield of unprotected polymers, and the benefits of atomic oxygen protective coatings for low fluence exposures (refs. 1-5). However, no high fluence data exists for protected polymers in LEO other than that generated from a few specimens on LDEF. Although the atomic oxygen protection can be evaluated and erosion yield measurements can be obtained from low

PRECEDING PAGE BLANK NOT FILMED

fluence LEO results, this information does not allow confident projection of protected material performance at high fluences, which is needed for long-term LEO missions such as Space Station Freedom (SSF). The inability to project long-term performance of protected polymers based on short-term data is due to the lack of understanding of how scattered atomic oxygen interacts in undercut cavities at defect sites in protective coatings. The data obtained from protected polymers on LDEF provided a unique opportunity to quantify effects of scattered atomic oxygen in undercut cavities at defect sites in protective coatings. Knowledge of the degree of thermal accommodation and erosion yield of thermally accommodated atomic oxygen can potentially be derived by comparing actual LDEF undercut cavity profiles with the Monte Carlo space model and the results of ground-based laboratory testing.

MATERIALS, METHODS, AND PROCEDURE

The procedure used in this investigation consists of an assessment of the validity of mechanistic assumptions used for Monte Carlo modeling of atomic oxygen interaction based on ground laboratory and in-space atomic oxygen exposure of both protected and unprotected polymers.

Ground Laboratory Atomic Oxygen Exposure

Characterization of atomic oxygen interaction with polymers at defect sites in protective coatings has been accomplished using 1300Å-thick SiO_X ($1.9<X<2.0$) protective coatings, sputter-deposited on Kapton HN polyimide. Samples were exposed to atomic oxygen in RF plasma ashers (SPI plasma prep II) with air as the working gas. Effects of atomic oxygen undercutting at defect sites in protective coatings were then characterized by scanning electron microscopy before and after removal of the SiO_X thin films over the undercut cavities. Removal of the SiO_X films was accomplished by adhesive tape peelings, which successfully removed the protected SiO_X coating where it was free-standing over undercut defect sites (ref. 6).

In-Space LDEF Atomic Oxygen Exposure

Three types of atomic oxygen protected materials, exposed on the leading edge (row 9) of LDEF, were evaluated by scanning electron microscopy in an effort to obtain atomic oxygen undercutting profiles at defect sites in the protective coatings. Table I describes the protected materials. The aluminized Kapton sample was part of the second layer of a multilayer insulation blanket. The top layer consisted of a sheet of 0.127 mm thick Kapton H, aluminized on the unexposed side only (ref. 7). As a result of atomic oxygen removal of Kapton from the sheet lying above this sample, it was exposed to less than the full leading edge LDEF atomic oxygen fluence. Removal of the aluminum film was accomplished using dilute HC1 to enable scanning electron microscopy examination.

Two carbon fiber epoxy composite samples with protective coatings were analyzed after LDEF exposure on row 9. The protective coating from one carbon fiber epoxy composite sample consisted of < 1000Å of Al_2O_3. The second carbon fiber epoxy composite sample had a protective coating of 400Å of aluminum on top of 800Å of chromium.

Monte Carlo Computational Model

A Monte Carlo computational model was developed to predict atomic oxygen undercutting of polymers at the sites of defects in their protective coatings under a variety of environments including LEO and ashers. The model was based on a combination of known and estimated atomic oxygen interaction mechanisms resulting from ground laboratory tests of atomic oxygen undercutting at defect sites in protective coatings and in-space erosion of unprotected polymeric materials (refs. 8-11). The computational model is intended to replicate the effects of atomic oxygen interaction with SiO_x-protected polyimide Kapton at defect sites in the protected Kapton. The Kapton is modeled as an array of square cells for which the behavior of simulated atomic oxygen atoms impinging on each cell is prescribed by a series of assumptions listed below:

1. The model is two-dimensional with atomic oxygen trajectories confined to a plane which simulates the cross-sectional view of a crack or scratch defect in the protective coating.
2. Reaction probability of atomic oxygen with Kapton is proportional to:
   a. $(\text{energy})^{0.68}$.
   b. the square root of the cosine of the angle between the surface normal and the arrival direction.
3. Reaction probability at normal incidence is equal to:
   a. 0.1380 for space (first impact).
   b. 0.0098 for space (≥ second impact).
   c. 0.0392 for plasma ashers (first impact).
   d. 0.0098 for plasma ashers (≥ second impact).
   e. 0.0490 for plasma ashers and space at Kapton/protective coating interface.
4. Atomic oxygen thermally accommodates upon first impact with surfaces, resulting in reduced reaction probability.
5. Atomic oxygen does not react with protective coatings, nor combines and remains atomic after impacting protective coatings.
6. Unreacted atomic oxygen leaves surfaces in a cosine ejection distribution.
7. Arrival direction of space atomic oxygen is angularly distributed because of the high temperature Maxwellian distribution.
8. Arrival direction of ground laboratory plasma asher atomic oxygen is isotropically distributed.

Several of the above assumptions concerning probability of atomic oxygen reaction after the first impact, energy of the scattered atomic oxygen, and ejection distribution of unreacted atomic oxygen, were optimized to produce good agreement with RF plasma asher results of

atomic oxygen undercutting, without having knowledge of in-space undercutting results. In this paper, atomic oxygen undercutting results from LDEF were used to examine the validity of these assumptions and were used to propose improved assumptions by comparison of predicted LDEF results (based on the previously described assumptions) with the actual LDEF results.

RESULTS AND DISCUSSION

Atomic oxygen undercutting of the LDEF aluminized Kapton multilayer insulation was found to produce undercut cavities which were up to a factor of 2.5-16.6 wider than the width of the aluminized film crack defects (ref. 7). The shape of the undercut cavities shown in figure 1 is rather broad, and would be expected, with isotropic arrival of atomic oxygen, but hardly expected for directed arrival of atomic oxygen. It is probable that the remains of the aluminization of the bottom side of the outermost multilayer insulation blanket contributed to scattering of arriving atomic oxygen which produced arrival trajectories atypical of most unobstructed surfaces on LDEF (ref. 7). As a result, no effort was made to compare the results from this sample with Monte Carlo model undercutting predictions.

Figure 2 is a scanning electron micrograph showing LDEF results of exposure of a T-300 carbon fiber - 934 epoxy composite with a < 1000Å-thick Al_2O_3 protective coating. As can be seen by the micrograph, the atomic oxygen protective coating is extremely thin, poorly attached to the substrate, and proliferated with defects, resulting in lack of clear definition of the undercut region for any specific defect site. As a result, no effort was made to compare the results of this sample with Monte Carlo predictions.

Figure 3 is a photograph of the T-300 carbon fiber - 934 epoxy composite sample with an aluminum and chromium protective coating after LDEF exposure. As can be seen in figure 3, the exposed area is a circular region with a slightly darker appearance. In addition, a micrometeoroid or debris impact crater can be seen as a black spot in the upper right section of the photo. The surface texture of the composite sample is highly-quilted as a result of the carbon fiber fabric. This highly irregular surface contributed greatly to the occurrence of defects in the protective coating (ref. 12). Figure 4 is a scanning electron micrograph of a typical defect site prior to and after adhesive tape removal of the aluminum and chromium protective coatings. As can be seen in figure 4, the undercut cavity diameter or width is significantly larger than the respective protective coating defect. Figure 5a and 5b are scanning electron micrographs of a similar defect whose geometry allowed a sufficiently inclined picture to be taken to examine the profile of the crack undercut cavity. Based on similar scanning electron micrographs, a representative undercut cavity profile for crack defects was identified, and is shown in figure 6. Measurement of the area of the undercut cavity shown in figure 6, given the row 9 LDEF atomic oxygen fluence of 8.72×10^{21} atoms/cm^2, results in an effective erosion yield under the defect site of 2.46×10^{-24} cm^3/atom. This erosion yield is approximately twice that of unprotected graphite epoxy based on previous LEO evaluation of carbon fiber epoxy composites (ref. 5). The higher effective erosion yield for atomic oxygen entering defects, compared to atomic oxygen impinging upon unprotected material, is thought to be due to the partial trapping of atomic oxygen within the undercut cavity, which results in multiple opportunities for it to react with the underlying organic material.

Many cracks developed at a 45° angle to the weave pattern. These cracks were more frequently observed in the area exposed to the LEO environment. This implies that some of the cracks may not have been present at the beginning of the in-space exposure, and may therefore have a lower fluence exposure to the underlying composite than others.

A comparison between the observed undercut cavity shown in figure 6, and the Monte Carlo model predicted undercut cavity, required proportioning the undercut-width-to-undercut-cavity-depth ratio so that it would be the same for both the LDEF observed profile and the Monte Carlo predicted profile. This was possible because the Monte Carlo predicted profile was found to vary only in size, but not in shape, once the undercut cavity depth became several times the undercut width. Figure 7 shows an overlay of the observed LDEF undercut profile previously shown in figure 6 and the Monte Carlo model predicted profile based on the previously described Monte Carlo assumptions. As can be seen in figure 7, the width of the Monte Carlo predicted undercut profile is much wider than that experimentally observed. Thus, one must question which assumptions are incorrect in the Monte Carlo model, and how they should be changed to more correctly predict what has been experimentally observed.

Although the Monte Carlo model assumes Kapton as the eroded material, and the actual LDEF material was carbon fiber-epoxy, which has been reported to have a lower erosion yield, the differences in erosion yield are not expected to be sufficient to resolve the differences between observed and predicted results. Reducing the Monte Carlo erosion yield would predominantly only slow down the rate of the development of the undercut cavity and not necessarily the depth-to-width ratio. This is partially based on reference 4, where the reaction probability of carbon is reported to be quite similar to that of Kapton, even though carbon's erosion yield is lower (ref. 4). Perhaps the weakest assumption for the Monte Carlo model is the five times higher reaction probability at the protective coating interface. This assumption was used successfully to predict chamfered undercut cavities for ground laboratory plasma asher results, but it lacks strong mechanistic justification. If one assumes that the Kapton at the interface has the same reaction probability as the bulk, then the chamfer is eliminated, thus producing an undercut cavity closer to the observed space results, but still too wide. The width of the undercut cavity is caused by erosion from scattered atomic oxygen. If one assumes a lower reaction probability for scattered atomic oxygen, then the undercut cavity width predicted by the Monte Carlo model should be smaller. If one assumes that the atomic oxygen thermally accommodates upon impact resulting in 0.04 eV (300 Kelvin) energy atoms, the reaction probability is proportional to the 0.68 power of the oxygen atom energy, and the reaction probability is 0.138 at 4.5 eV (ref. 13), then a reaction probability of 0.006 is predicted for thermally accommodated atomic oxygen. If one assumes that the reaction probability has an Arrhenius relationship, where the activation energy is 0.38 eV as postulated in reference 14, then a reaction probability of 7.7×10^{-6} is predicted for thermally accommodated atomic oxygen. Because a reaction probability of thermally accommodated atomic oxygen of 0.006 was thought to be insufficient to reduce the predicted width of the undercut cavity to match the observed results, atomic oxygen reaction probabilities of 0.0031 and 7.77×10^{-6} were evaluated as shown in figures 8a and 8b. As can be seen by comparison of figures 8a and 8b, the reaction probability of 0.0031 for atomic oxygen reacting with the composite after the first impact produces an undercut cavity profile much closer to that which is experimentally observed than the much lower reaction probability shown in figure 8b. Thus, based on figure 8, one can

conclude that the reaction probability of thermally accommodated atomic oxygen should be less than or equal to 0.003.

There may be other Monte Carlo assumptions which produce undercut profiles which approximate the observed LDEF results such as the degree to which energetic atomic oxygen arriving at 4.5 eV thermally accommodates upon its first impact. If one assumes that only a portion of the atomic oxygen thermally accommodates upon first impact, then higher reaction probabilities of more energetic scattered atomic oxygen will result, thus widening the undercut cavity in comparison to figure 8b. Figure 9 compares the observed LDEF undercut cavity profile and the Monte Carlo predicted profile for atomic oxygen, which is assumed to have only a 50% probability of accommodation upon each impact and the same low reaction probability as figure 8b for thermally accommodated atomic oxygen. The fraction of atoms which did not accommodate, and also did not react, were assumed to specularly scatter, retaining their initial energy. The fraction of atoms which did accommodate were assumed to scatter in a cosine distribution with thermally accommodated energies. As can be seen in figure 9, energetic scattering of atomic oxygen significantly widens the undercut cavity profile, even if the thermally accommodated reaction probability is negligible. Thus, it is quite possible that partial accommodation of atomic oxygen could occur upon first impact, provided that the fully accommodated atomic oxygen has a very low reaction probability.

CONCLUSION

A comparison was made between a Monte Carlo predicted undercut cavity profile for cracks in protected carbon fiber epoxy composite materials with experimentally observed results from an LDEF row 9 exposure to an atomic oxygen fluence of 8.72×10^{21} atoms/cm^2. These results indicate that the atomic oxygen erosion yield under defect sites in protective coatings on carbon fiber epoxy composites is 2.5×10^{-24} cm^3/atom, which is approximately twice that which is observed for unprotected carbon fiber epoxy composites. Monte Carlo modeling assumptions which result in predictions that replicate ground laboratory plasma asher results do not accurately predict LDEF results. Based on the LDEF results, several mechanistic assumptions used in the Monte Carlo modeling should be altered to produce in-space predictions which more accurately reflect experimentally observed results. The reaction probability of atomic oxygen with polymeric material at the interface between the protective coating and the polymer appears to be the same as for the bulk materials. The atomic oxygen reaction probability for thermally accommodated atomic oxygen is probably not greater than 0.003. The atomic oxygen may not fully accommodate upon first impact with organic materials, thus scattering with sufficient energy to significantly contribute to undercutting.

ACKNOWLEDGEMENTS

The authors gratefully acknowledge the assistance of Phillip Young and Wayne Slemp of the NASA Langley Research Center for kindly providing the samples of LDEF materials used for this paper.

REFERENCES

1. L.J. Leger, "Oxygen Atom Reaction with Shuttle Materials at Orbital Altitudes," NASA TM-58246, 1982.

2. J.T. Visentine, L.J. Leger, J.F. Kuminecz, and I.K. Spiker, "STS-8 Atomic Oxygen Effects Experiment," AIAA Paper 85-0415, AIAA 23rd Aerospace Sciences Meeting, Reno, Nevada, January 14-17, 1985.

3. B.A. Banks, M.J. Mirtich, S.K. Rutledge, D.M. Swec, and H.K. Nahra, "Ion Beam Sputter-Deposited Thin Film Coatings for the Protection of Spacecraft Polymers in Low Earth Orbit," NASA TM-87051, paper presented at the 23rd Aerospace Sciences Meeting, Reno, Nevada, January 14-17, 1985.

4. D.E. Brinza, "Proceedings of the NASA Workshop on Atomic Oxygen Effects," JPL Publication 87-14 (June 1, 1987), Pasadena, California, November 10-11, 1986.

5. B.A. Banks and S.K. Rutledge, "Low Earth Orbital Atomic Oxygen Simulation for Materials Durability Evaluation," proceedings of the 4th European Symposium on Spacecraft Materials in a Space Environment, CERT, Toulouse, France, September 6-9, 1988.

6. B.A. Banks, S.K. Rutledge, L. Gebauer, and C. LaMoreaux, "SiO_X Coatings for Atomic Oxygen Protection of Polyimide Kapton in Low Earth Orbit," AIAA Paper 92-2151 proceedings of the Coatings Technology for Aerospace Systems Materials Specialists Conference, Dallas, Texas, April 16-17, 1992.

7. K.K. de Groh and B.A. Banks, "Atomic Oxygen Undercutting of LDEF Aluminized-Kapton Multilayer Insulation," proceedings of the First LDEF Post-Retrieval Symposium, NASA CP-3134, Kissimmee, Florida, June 2-8, 1991.

8. B.A. Banks, S.K. Rutledge, B.M. Auer, and F. DiFilippo, "Atomic Oxygen Undercutting of Defects on SiO_2 Protected Polyimide Solar Array Blankets," Published in Materials Degradation in Low Earth Orbit (LEO), edited by V. Srinivasan and B.A. Banks (The Minerals, Metals, and Materials Society), pp. 15-33, 1990.

9. B.A. Banks, B.M. Auer, S.K. Rutledge, and C. Hill, " Atomic Oxygen Interaction with Solar Array Blankets at Protective Coating Defect Sites," paper presented at the 4th Annual Workshop on Space Operations, Automation, and Robotics (SOAR '90), Albuquerque, New Mexico, June 26-29, 1990.

10. B.A. Banks, S.K. Rutledge, K.K. de Groh, B.M. Auer, M.J. Mirtich, L. Gebauer, C. Hill, and R. Lebed, "LDEF Spacecraft, Ground Laboratory, and Computational Modeling Implications on Space Station Freedom's Solar Array Materials and Surfaces Durability," proceedings of the IEEE Photovoltaic Specialists Conference, Las Vegas, Nevada, October 7-11, 1991.

11. B.A. Banks, B.M. Auer, S.K. Rutledge, L. Gebauer, and E.A. Sechkar, "Monte Carlo Modeling of Atomic Oxygen Interaction with Protected Polymers for Projection of Materials Durability in Low Earth Orbit," proceedings of the MRS Spring Meeting '92, San Francisco, California, April 27-May 1, 1992.

12. K.K. de Groh, T. Dever, and W. Quinn, "The Effect of Leveling Coatings on the Atomic Oxygen Durability of Solar Concentrator Surfaces," proceedings of the 8th International Conference on Thin Films (ICTF-8) and the 17th International Conference on Metallurgical Coatings (ICMC-17), San Diego, California, April 2-6, 1990.

13. D.C. Ferguson, "The Energy Dependence of Surface Morphology of Kapton Degradation Under Atomic Oxygen Bombardment," paper presented at the 13th Space Simulation Conference, Orlando, Florida, October 8-11, 1984.

14. S. Koontz, K. Albyn, and L.J. Leger, "Atomic Oxygen Testing with Thermal Atom Systems: A Critical Evaluation," Journal of Spacecraft and Rockets, Vol. 28, No. 3, May-June, 1991.

Table I. LDEF Samples Evaluated Having Atomic Oxygen Protective Coating

SUBSTRATE	ATOMIC OXYGEN PROTECTIVE COATING
0.0076 mm thick Kapton H	1000Å thick aluminum on both surfaces
0.41 mm thick T300 carbon fiber - 934 epoxy composite	<1000Å thick Al_2O_3
0.64 mm thick T300 carbon fiber - 934 epoxy composite	400Å thick aluminum over 800Å of chromium

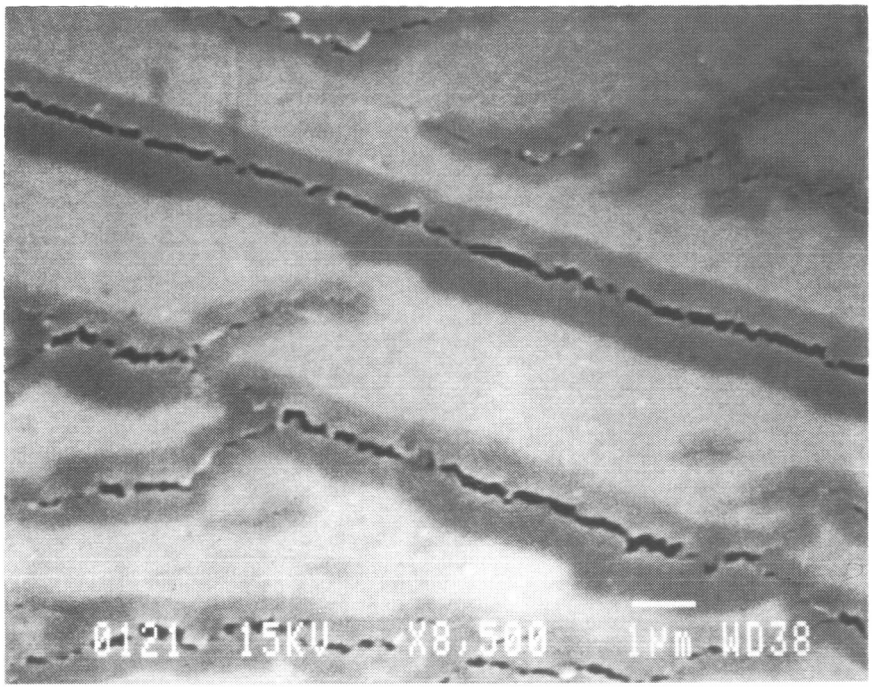

1a. With aluminum.

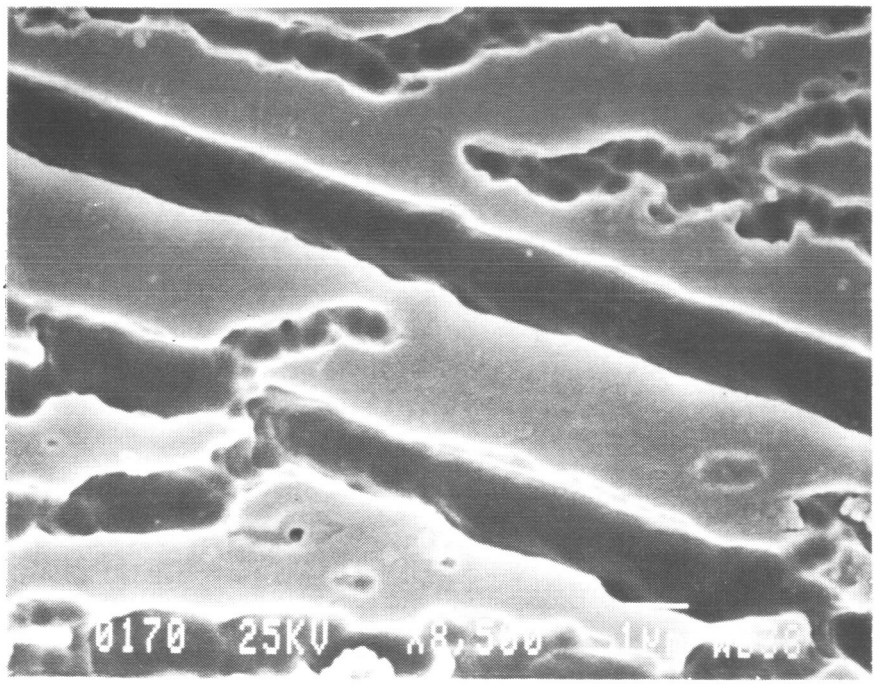

1b. Aluminum chemically removed.

Figure 1. Atomic oxygen undercutting of LDEF aluminized Kapton multilayer insulation at cracks in the aluminum film.

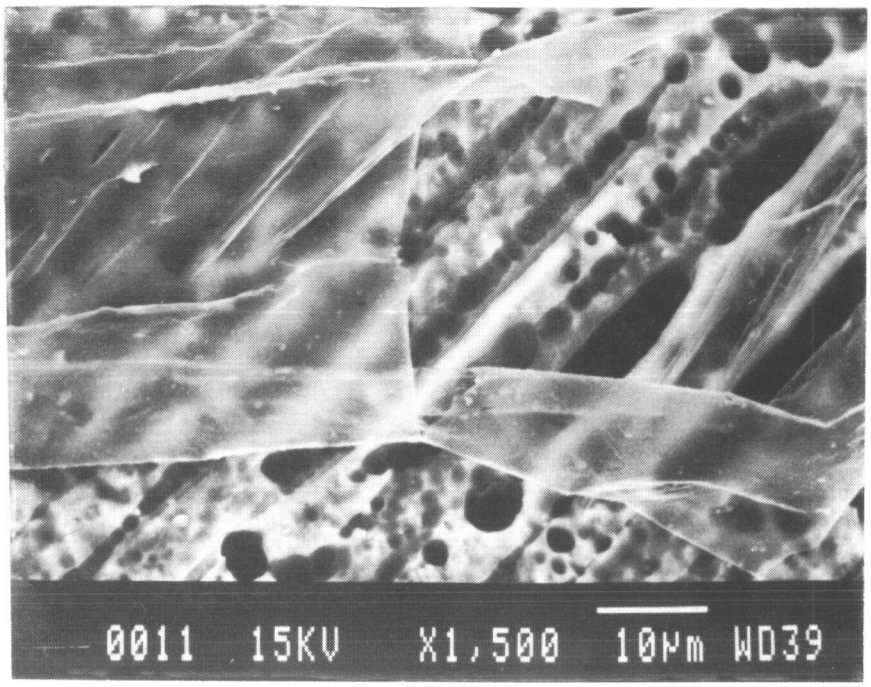

Figure 2. Scanning electron micrograph of < 1000Å-thick SiO_X T-300 carbon fiber - 934 epoxy composite after LDEF exposure to an atomic oxygen fluence of 8.72 x 10^{21} atoms/cm^2.

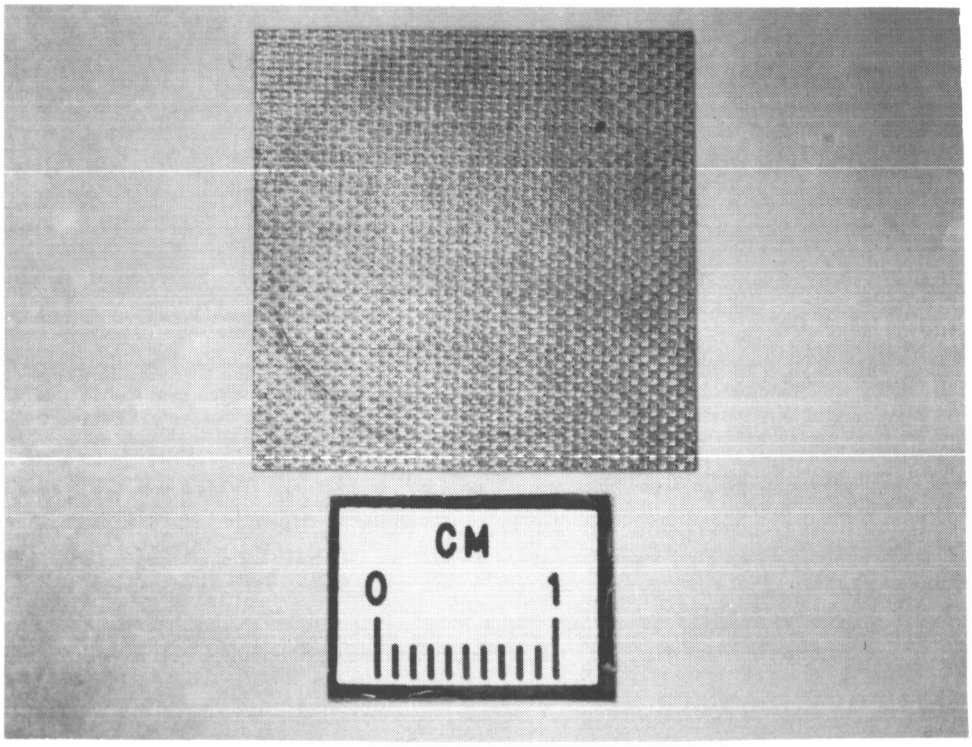

Figure 3. Photograph of 400Å Al/800Å Cr coated T-300 carbon fiber - 934 epoxy composite after LDEF exposure to an atomic oxygen fluence of 8.72 x 10^{21} atoms/cm^2.

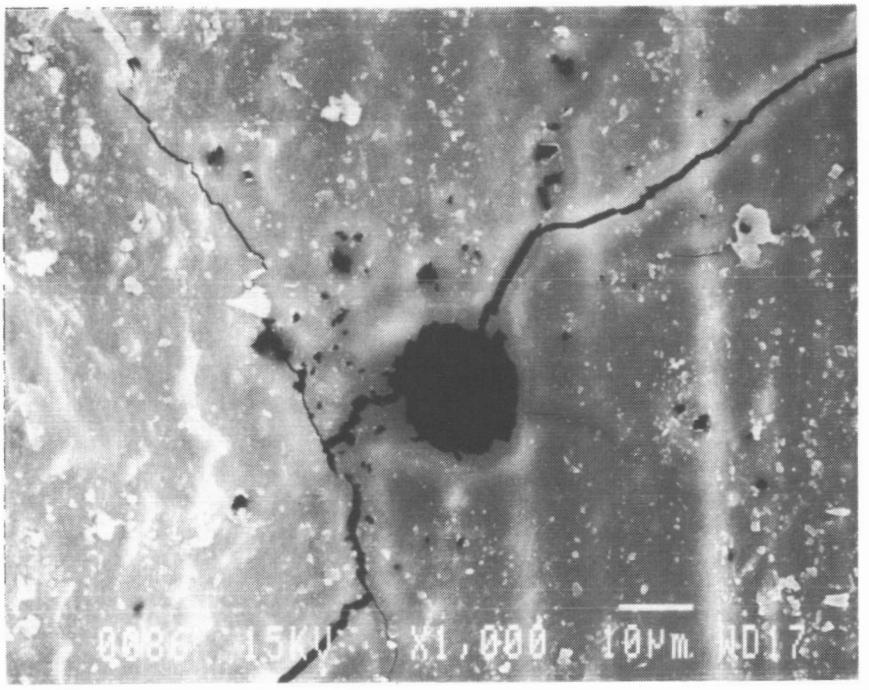

4a. Prior to removal of aluminum/chromium protective coating.

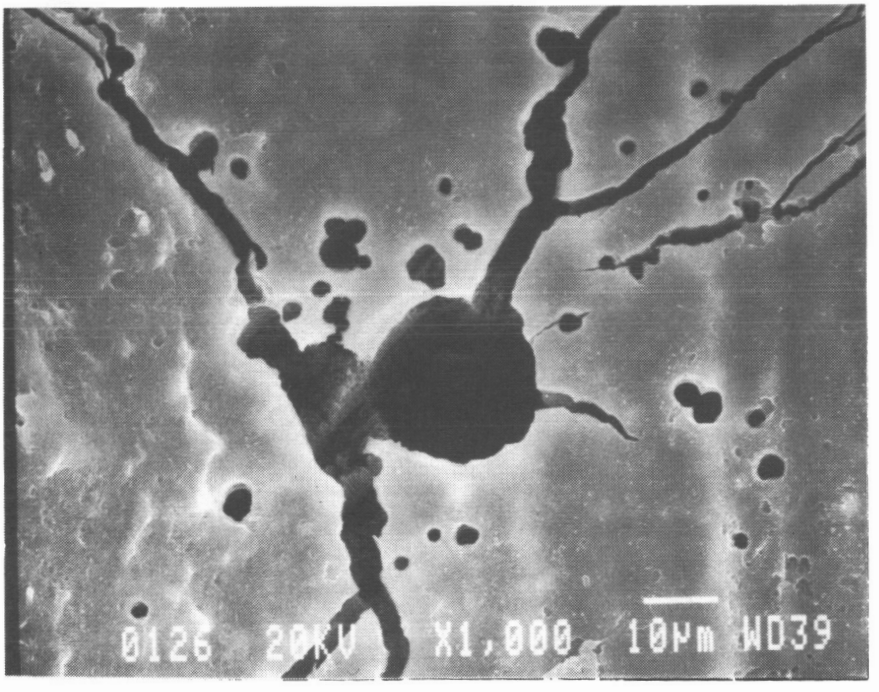

4b. After removal of aluminum/chromium protective coating.

Figure 4. Scanning electron micrograph of aluminum/chromium coated T-300 carbon fiber - 934 epoxy composite after LDEF exposure.

5a. Low magnification

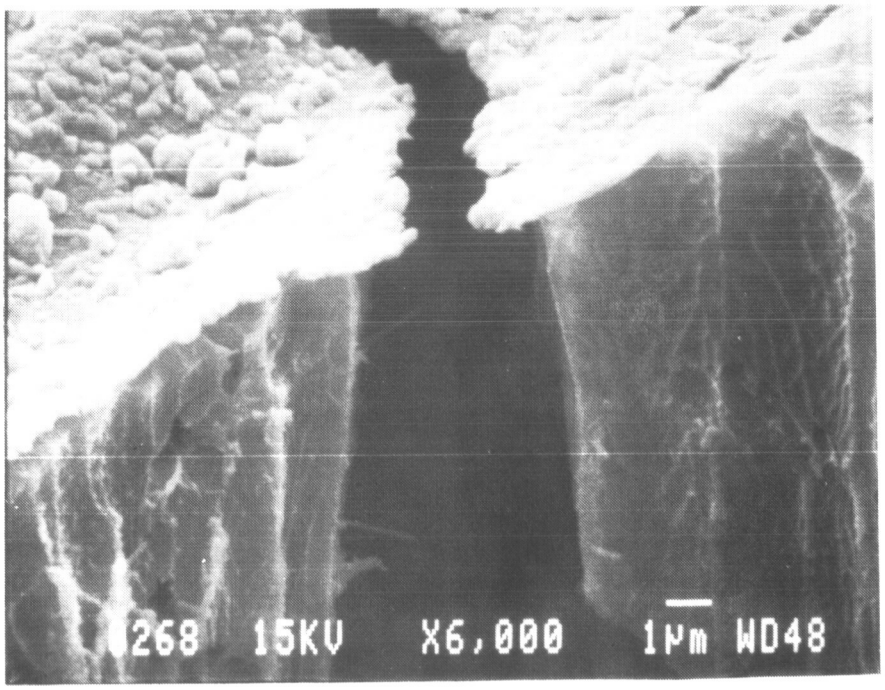

5b. High magnification

Figure 5. Scanning electron micrograph of aluminum/chromium coated T-300 carbon fiber - 934 epoxy composite after LDEF exposure showing crack undercut cavity profile.

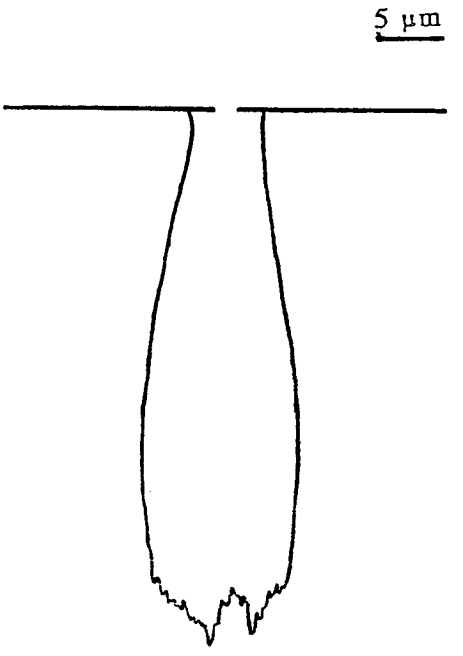

Figure 6. Crack defect undercut cavity profile based on scanning electron micrographs similar to figure 5.

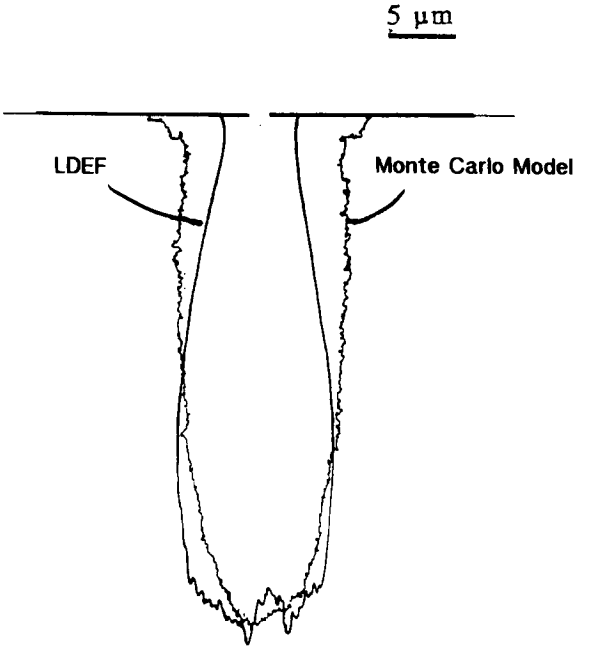

Figure 7. Comparison of LDEF undercut cavity profile and Monte Carlo predicted profile based on atomic oxygen: 100% accommodation, reaction probability of 0.0098 for greater than or equal to second impact, and reaction probability of 0.0490 at the protective coating interface.

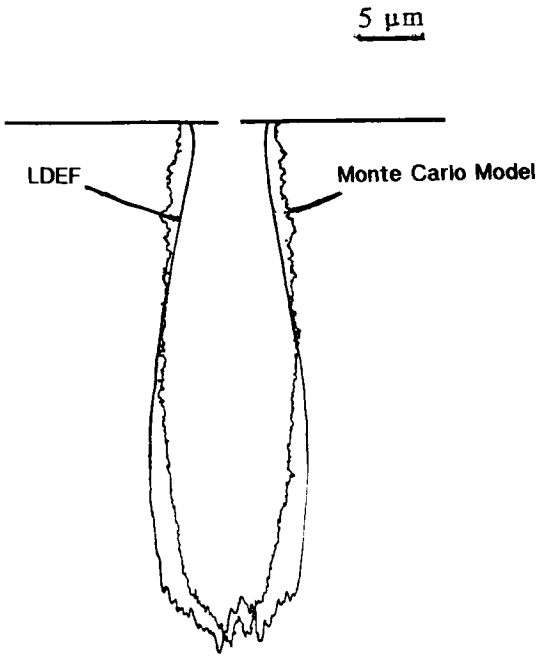

8a. Reaction probability of 0.0031 for ≥ second impact.

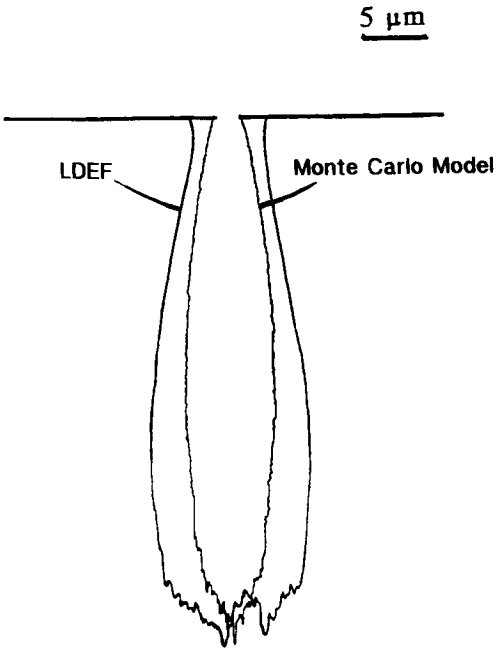

8b. Reaction probability of 7.77×10^{-6} for ≥ second impact.

Figure 8. Comparison of LDEF undercut cavity profiles and Monte Carlo predicted profiles based on atomic oxygen: 100% accommodation and reaction probability at the protective coating interface equal to the bulk.

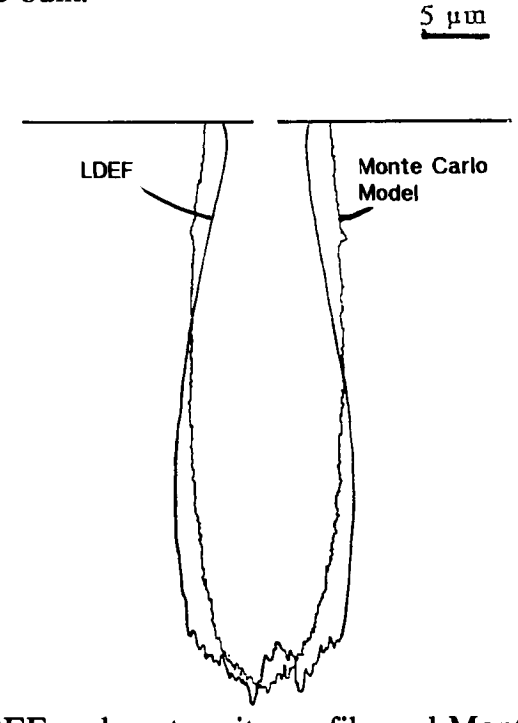

Figure 9. Comparison of LDEF undercut cavity profile and Monte Carlo predicted profile based on atomic oxygen: 50% accommodation, reaction probability of 7.77×10^{-6} for ≥ second impact, and reaction probability at the protective coating interface equal to the bulk.

N93-28283

SECOND LDEF POST-RETRIEVAL SYMPOSIUM

INTERIM RESULTS OF EXPERIMENT A0034

Roger C. Linton
Rachel R. Kamenetzky
NASA Marshall Space Flight Center
MSFC, AL 35812
Phone: 205/544-2526, Fax: 205/544-0212

INTRODUCTION

Thermal control coatings and contaminant collector mirrors were exposed on the leading and trailing edge modules of LDEF experiment A0034 to provide a basis of comparison for investigating the role of atomic oxygen in the stimulation of volatile outgassing products. The exposure of identical thermal coatings on both the leading and trailing edges of the LDEF and the additional modified exposure of identical coatings under glass windows and metallic covers in each of the flight modules provided multiple combinations of space environmental exposure to the coatings and the contaminant collector mirrors. Investigations have been made to evaluate the effects of the natural space and the induced environments on the thermal coatings and the collector mirrors to differentiate the sources of observed material degradation.

Two identical flight units were fabricated for the LDEF mission, each of which included twenty-five thermal control coatings mounted in isolated compartments, each with an adjacent contaminant collector mirror mounted on the wall. The covers of the flight units included apertures for each compartment, exposing the thermal coatings directly to the space environment. Six of these compartments were sealed with ultraviolet-grade transmitting quartz windows and four other compartments were sealed with aluminum covers. One module of this passive LDEF experiment, occupying one-sixth of a full tray, was mounted in Tray C9 (leading edge), while the other identical module was mounted in Tray C3 (trailing edge).

Each of the flight units of this experiment included multiple specimens of S13G, S13G-LO, Z93, and YB-71 (zinc orthotitanate) thermal control coatings. The leading edge (C9) flight unit contained, additionally, specimens of the polyurethane-based coatings A276 and Z306. Each flight unit also included some compartments with uncoated substrates (aluminum) substituting for a thermal coating as one more level of control for evaluating contamination effects. Each thermal control coating mounted in its individual compartment under an open aperture was directly exposed to the space environment, including atomic oxygen, while the adjacent collector mirrors on the side walls of the compartments were only indirectly exposed to the natural space environment by reflection or scattering from the thermal coatings or aluminum plates at the base of the

compartment.

The apertures proved significant in limiting the cumulative exposure of the specimens to solar ultraviolet radiation during the extended periods of the LDEF mission when the apertures shadowed the underlying coatings from oblique incidence solar radiation. Visible darkening, fluorescence changes, and changes in solar absorptance of sensitive thermal control coatings exposed under quartz windows on the leading edge unit and exposed directly or under quartz windows on the trailing edge unit indicate levels of incident solar radiation substantially less than that observed for similar coatings exposed without limiting apertures on other LDEF experiments. The apertures did not limit the incidence of atomic oxygen on the leading edge coatings, although the re-directed flux of oxygen atoms to the adjacent collector mirrors was dependent on the relative degree of accommodation associated with the various thermal coating materials.

Post-Flight Observations

Post-flight visual observations of the thermal control coatings indicated that only three leading edge specimens were significantly changed in appearance as a result of the exposure. These included one of the S13G coatings exposed under an "open" aperture with anomalous (by contrast with neighboring S13G specimens) reddish hued darkening, a darkened A276 specimen exposed under a quartz window, and the darker, more diffusively reflecting Z306 specimen (compared to the one exposed under a quartz window) exposed through an "open" aperture. Trailing edge exposure produced contrasting darkening of all RTV resin-bonded S13G and S13G-LO specimens; the Z93 and YB-71 specimens from both the leading and trailing edges were only slightly changed in appearance. These visual observations were confirmed by measurements of diffuse spectral reflectance (Varian/Cary 2300) for determination of solar absorptance and measurements of infrared thermal emittance with a Gier-Dunkle DB-100 portable reflectometer. These measurements were summarized and discussed in a previous publication (references 1, 2). It is assumed that the relatively unchanged optical properties of the leading edge S13G and S13G-LO specimens are a result of atomic oxygen bleaching of the damage induced by solar radiation, recognizing the relatively lower levels of solar radiation incident on the coatings in compartments with restricted fields-of-view.

The extent of reaction and induced changes in the exposed coating materials have been investigated with combinations of optical and surface profiling measurements. For each of the coating specimens, the diffuse spectral reflectance, optical scattering (BRDF), and surface morphology profiling (TalySurf) have been used to compare the effects of leading and trailing edge exposure.

For the polyurethane-based Chemglaze Z306 coatings exposed on the leading edge, the results indicate increased coating roughness and, consequently, solar absorptance, as a result of material erosion induced by atomic oxygen. Two specimens of Chemglaze Z306 paint were included in the leading edge module. These included the specimen exposed to atomic oxygen through an open aperture (#01-44) and the other exposed under a sealed quartz window (#01-14). Visual observations of a "blacker", more diffuse appearance for the Z306 coating exposed through

an open aperture are confirmed by the measurements of spectral diffuse reflectance (Figure 1) and the comparative profiles of light scattering provided by the BRDF measurements (Figure 2). The more specular profile, through 70 degrees angle of incidence, of the BRDF associated with the Z306 specimen exposed under a window (#01-14) in Figure 2 is characteristic of freshly prepared and unexposed Chemglaze Z306 and contrasts strikingly with the Lambertian profile of the atomic oxygen-exposed specimen (#01-44). These optical indications of increased surface roughening in the specimen exposed to atomic oxygen have been quantified by stylus profiling with the TalySurf profilometer (Figure 3). The two TalySurf profiles in Figure 3 correspond to 20 mm length traces across the surface of the Z306 specimen exposed through an open aperture ("O") and the windowed specimen ("W"), quantifying the increased roughness of the specimen exposed to atomic oxygen (PRg(rms) = 2.36 (#01-44) compared to PRg(rms) = 1.64 (#01-14).

Preliminary results of BRDF and TalySurf profiling measurements on the zinc oxide (S13G, S13G-LO, Z93) and zinc orthotitanate (YB-71) white thermal control coatings indicate that the changes in surface roughness induced by the space exposure are subtle, if not indistinguishable. The overlapping curves of cosine corrected BRDF dependence, through 70 degrees angle of incidence, for Z93 specimens exposed through open apertures from both the leading (#01-24) and trailing (#02-22) edges (Figure 4) are typical of the measured dependencies for these four types of coatings. Comparing the cosine corrected BRDF dependency of an exposed Z93 coating specimen to that of a laboratory diffuse standard (Figure 5), the results show that the Z93 specimen is more Lambertian than the standard itself. TalySurf profiles of these Z93 specimens indicate, unlike the overlapping BRDF profiles, that there are significant and systematic differences in surface roughness of leading edge Z93 coatings compared to trailing edge coatings of Z93 (Figure 6). These differences, for Z93 specimens of all types of exposure from the leading and trailing edges, are summarized in Figure 7. The bar-chart format differentiating TalySurf Group A scans from Group B scans refers to the pattern of dual scans on each coating specimen, the second scan done in a direction normal to the first scan. Since the leading edge "Control" Z93 trace differed in magnitude as well as the "window" exposure specimen (#01-52) and the "open" exposure specimen (#01-24) from any of the trailing edge traces in magnitude, the systematic differences in traces from the opposing module specimens probably indicate batch processed differences. The pattern of TalySurf traces for another of the zinc oxide pigmented paints (S13G-LO) gives evidence of a similar pattern, though significantly reduced in magnitude of difference (Figure 8). The investigation of induced surface roughness of the flight thermal control coatings is continuing.

Fluorescence Observations

Fluorescent emission from the thermal control coatings was detected during inspection of the flight hardware and specimens with black-light illumination. Closer inspection revealed systematic patterns of stimulated and quenched fluorescence in the coatings as a result of the space exposure. The determining environmental factors are apparently atomic oxygen and solar ultraviolet radiation.

Changes in fluorescence as a result of the space exposure were strongly material dependent. The three species of white thermal control coatings formulated with zinc oxide as the pigment

(S13G, S13G-LO, and Z93) all exhibit an intrinsic yellow coloration under black-light illumination which was quenched or suppressed as a result of space exposure on both the leading and trailing edges of the LDEF. In contrast, specimens of the polyurethane-based paints A276 and Z306 provided evidence of both stimulated and quenched fluorescence behavior as a result of the space exposure. The YB-71 (zinc orthotitanate) coatings were not obviously affected under black-light illumination as a result of the space exposure.

These changes in fluorescence as a result of the space exposure were found to be influenced by the type and degree of exposure. Comparison of fluorescent coloration for specimens from the leading and trailing edges and for specimens exposed "open", under windows, or "closed" provides insight into the mechanisms of interaction and the relationships to degree of exposure. These observations show that the quenching of fluorescence in the zinc oxide pigmented coatings, as detected by changes in the yellow coloration under black-light illumination, is found in specimens from both the leading and trailing edges and, to a significantly lesser degree, from specimens exposed under quartz windows. The stimulated orange fluorescence in the A276 specimen exposed under a quartz window has apparently been extinguished in the specimens exposed under an open aperture. A small peripheral area of the A276 specimen exposed under an open aperture exhibits the stimulated orange glow observed in the specimen exposed under a quartz window; this peripheral area corresponds to that portion of the A276 specimen shielded from atomic oxygen on the leading edge by the aperture and the documented 8 degree offset in RAM angle of attack for atomic oxygen.

The general observations of black-light illuminated fluorescence and the changes induced by the LDEF exposure were previously discussed (reference 1). The results are being quantified by measurement with an SLM Model SPF-500C spectrofluorometer. These types of measurements, for the flight S13G coatings, are summarized in Figures 9 and 10 for the comparison of effects for leading and trailing edge exposure on coatings exposed under open, windowed, and closed apertures. The quenching (suppressing) of the observed yellow fluorescence is apparently duplicated in the other more narrow wavelength bands, particularly for the strong ultraviolet band centered at 360 nanometers. Solar ultraviolet radiation transmitted through the quartz windows induced the same pattern of quenching as exposure through open apertures, though diminished in effect in relation to the spectral transmittance of the (contaminated) windows. The role of solar uv radiation in quenching zinc oxide pigmented coating fluorescence is clear. Subsequent laboratory testing, however, has shown that the role of atomic oxygen in producing the same effect is, for some materials, similar in nature and degree of effect. Measurements of the fluorescent emission from a conductive white paint (NS43C) exposed to thermal energy atomic oxygen at MSFC and a beam of 5 eV neutral atomic oxygen at the Princeton Plasma Physics Laboratory (PPPL) indicate similar patterns of quenching (Figure 11). The principal difference in the fluorescence quenching of this coating (similar in composition to Z93) and that of the flight S13G coatings is the more pronounced quenching of the ultraviolet band. Similar testing with the polyurethane based coatings has shown that the threshold level of uv radiation required to stimulate fluorescence in these coatings is very low (< 100 ESH), that the visible (black-light illuminated) coloration is strongly dependent on duration of exposure, and that the coloration fades rapidly (but does not disappear) following air exposure. These investigations are continuing with the objective of determining the mechanisms of interaction.

Collector Mirror Degradation

The original experimental approach to determining the role of atomic oxygen in the stimulation of volatile outgassing products anticipated differences in the optical degradation of contaminant collector mirrors adjacent to thermal control coatings exposed on the leading edge compared to mirrors adjacent to identical coatings exposed on the trailing edge. Comparative measurements of spectral reflectance of these mirrors indicated that the larger changes in optical properties were associated with mirrors adjacent to thermal coatings on the leading edge exposed under open apertures to atomic oxygen (reference 1). These increased levels of optical degradation are one indication of increased (stimulated) outgassing induced by atomic oxygen exposure of associated coatings exposed under open apertures. However, an alternative source of mirror degradation is interaction with the natural space environment.

Most of the collector mirrors were silicon monoxide overcoated aluminum thin films on quartz substrates. Each module also included, in selected compartments, thin film mirrors of silver and osmium as indicators of atomic oxygen exposure and thin film mirrors of gold and magnesium fluoride overcoated aluminum as indicators of the effects of alternative materials for contaminant "sticking" probability. Post-flight inspection of these substitute collector mirrors indicated that a measurable and relatively significant flux of re-directed atomic oxygen was incident on the mirrors of the leading edge module and, to a lesser extent, the trailing edge module as well (Figure 12). This was inferred from the total oxidation and virtually complete removal of the leading edge silver and osmium films and the partial oxidation of the counterpart silver and osmium mirrors on the trailing edge (reference 1). A perceptible difference in the visible appearance of the gold mirrors from the leading and trailing edge modules was also noted. An estimated fluence of atomic oxygen to the collector mirrors (10^{20} max) was inferred from the reactivities of silver and osmium and the observed film thickness losses (ibid).

Atomic oxygen exposure of the collector mirrors could be expected to have two effects. Contaminants deposited on the mirrors as a result of underlying thermal control coating outgassing would be subject to chemical conversion and potential re-volatilization and removal. The silicon monoxide overcoating itself would be subject to oxidation and subsequent conversion of optical properties. Although few of the collector mirrors from either flight module were conclusively visibly contaminated, the changes in optical properties of several mirrors were substantial. It has been previously stated that the more substantial changes in mirror optical properties were associated with mirrors adjacent to thermal coatings exposed directly to atomic oxygen through open apertures. Indications that these effects are attributable to atomic oxygen interactions with the collector mirrors have been found with additional analysis of the mirrors using ESCA, ellipsometry, and TalySurf profiling techniques.

Mirror coating thickness measurements using a Gaertner Model L119 ellipsometer indicate a systematic change in thickness (or optical properties) for the silicon monoxide overcoated aluminum collector mirrors located adjacent to thermal control coatings exposed through open apertures on the leading edge (Figure 13). The ellipsometer measurements shown in Figure 13 are based on a thin film configuration assuming only light (632.8 nm.) interaction with an opaque aluminum substrate and a film of silicon monoxide. Attempts to include an assumed top layer of

contamination were unsuccessful in producing systematic results. The collector mirrors with the most substantial indicated thickness change were located adjacent to source coatings of widely different outgassing potential: Z93, A276, Z306, a blank aluminum substrate plate, and one of the "open" S13G coating samples.

Attempts to determine the chemical composition of contaminant films on the collector mirrors by Fourier Transform Infrared Reflectance (FTIR) analyses were unsuccessful. The quantity (thickness) of contamination was apparently less than the sensitivity of the technique. Some compositional information was obtained through the use of Electron Spectroscopy for Chemical Analysis (ESCA) on selected collector mirrors. Results obtained to date are summarized in Figure 14 for carbon, silicon, and oxygen atomic concentration compartment on the leading edge. These results indicate the presence of silicon dioxide at the surface for nearly all of the mirrors. The degree (depth) of conversion of silicon monoxide to silicon dioxide has not been determined. These ESCA results also indicate that the lowest carbon concentrations are associated with the collector mirrors found, by ellipsometry, to have the more substantial indicated thickness change, namely the ones exposed to Z93, A276, Z306, and the blank aluminum coating substrate through "open" apertures on the leading edge. If the atomic concentration of carbon on the surface of the collector mirrors is assumed to be one indicator of contamination, then the ESCA results indicate the possibility of atomic oxygen "cleaning" of some of the mirrors exposed to contamination in compartments with "open" apertures on the leading edge. These ESCA results also provide evidence that the collector mirrors that were found to have the greater change in spectral reflectance were also found to be relatively free of contamination (as indicated by carbon concentration). It is possible, then, that the changes in optical properties of these mirrors were induced by accelerated oxidation during the leading edge exposure.

Another indication of oxidation of the silicon monoxide collector mirrors was obtained using a TalySurf stylus profiling analyzer. These profiles of surface morphology were obtained by scanning with the stylus from the exposed center area of the mirrors to the unexposed outer rim where the mirrors were protected from exposure. The results of TalySurf scanning on a collector mirror exposed to a blank aluminum coating substrate in an "open" compartment on the leading edge are provided in Figure 15. This TalySurf profile of collector mirror CM 01-45 indicates a decrease in thickness of the silicon monoxide of approximately 200 Angstroms in the exposed center area compared to the protected outer rim. Since the oxidation of silicon monoxide would be expected to lead to silicon dioxide (increasing "x" in SiOx), and silicon dioxide is more dense, the compaction of SiO converted to SiO2 would be expected to lead to such a thickness decrease.

Interim Conclusions

Preliminary analysis of optical degradation for the contaminant collector mirrors of this experiment indicated a systematic pattern of change. Mirrors that were located adjacent to thermal control coatings exposed to atomic oxygen under open apertures on the leading edge were systematically more severely degraded at ultraviolet wavelengths than the other mirrors. This evidence of stimulated outgassing has been shown to be tenuous as a result of evidence of atomic oxygen effects as another possible source of change in mirror optical properties. More direct

means of quantifying collector mirror oxidation as a result of natural environmental exposure, including ESCA/Auger depth profiling, are being investigated.

Thermal control coating stability to the space environment has been clearly differentiated by material and exposure in the compilation of coating optical properties. Despite obvious erosion in the Z306 black absorber coating exposed to atomic oxygen on the leading edge, the changes in solar absorptance and emittance are relatively small, indicating, as expected, a small improvement in light absorbing properties. The A276 white coating exposed to atomic oxygen was relatively unchanged in diffuse reflectance despite complete erosion by atomic oxygen of the polyurethane binder. Severe degradation of the A276 coating exposed under a severely contaminated window confirms the relatively minimal level of solar uv radiation required for darkening of this coating.

For the zinc oxide pigmented and zinc orthotitanate coatings, only the S13G and S13G-LO specimens exposed on the trailing edge were found to be visibly darkened (with one exception). BRDF measurements indicate that the intrinsic diffuseness of these coatings is not significantly affected by the exposure. Surface morphology profiling (TalySurf) of these coatings indicated differences in surface roughness that are presently not subject to systematic relation to exposure and, as indicated for Z93 coatings, may be more indicative of batch processing variations. The fluorescence observations and measurements clearly reveal interaction with the space environment for all of the exposed coatings. These investigations of the effects of exposure on the flight coatings, mirrors, and windows are continuing in conjunction with associated laboratory simulated exposure testing of similar materials.

Acknowledgement

The authors appreciate the contributions of Dr. James Hadaway, Dr. Ganesh Raiker, and Mr. Rob Connatser of UAH. Ellipsometer data were contributed by Mr. John Reynolds (EH12).

References

1. Linton, R.C., Kamenetzky, R.R., Reynolds, J.M., and Burris, C.L., "LDEF Experiment A0034: Atomic Oxygen Stimulated Outgassing", NASA Conference Publication 3134, Part 2, June, 1991.

2. Linton, R.C., "Effects of Space Exposure on Thermal Control Coatings", AIAA 92-0795, Reno, Nevada, January 6-9, 1992.

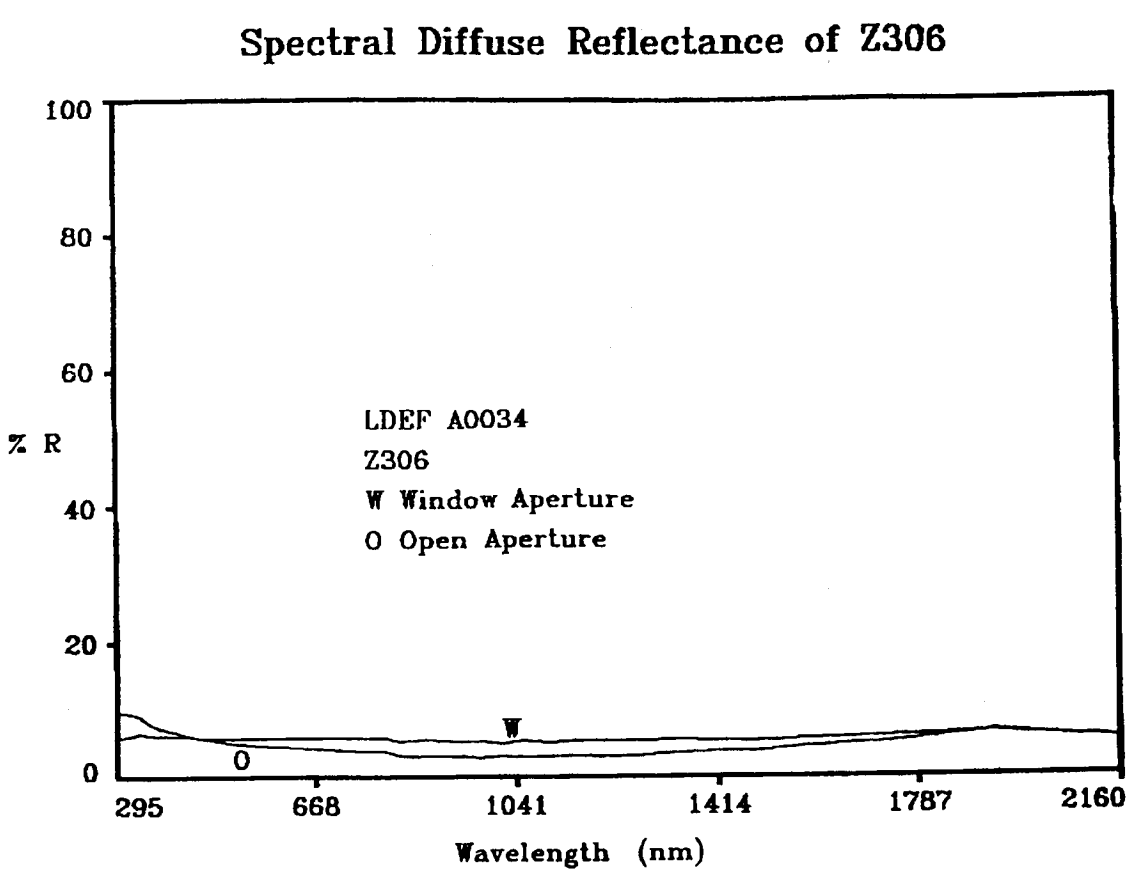

FIGURE 1

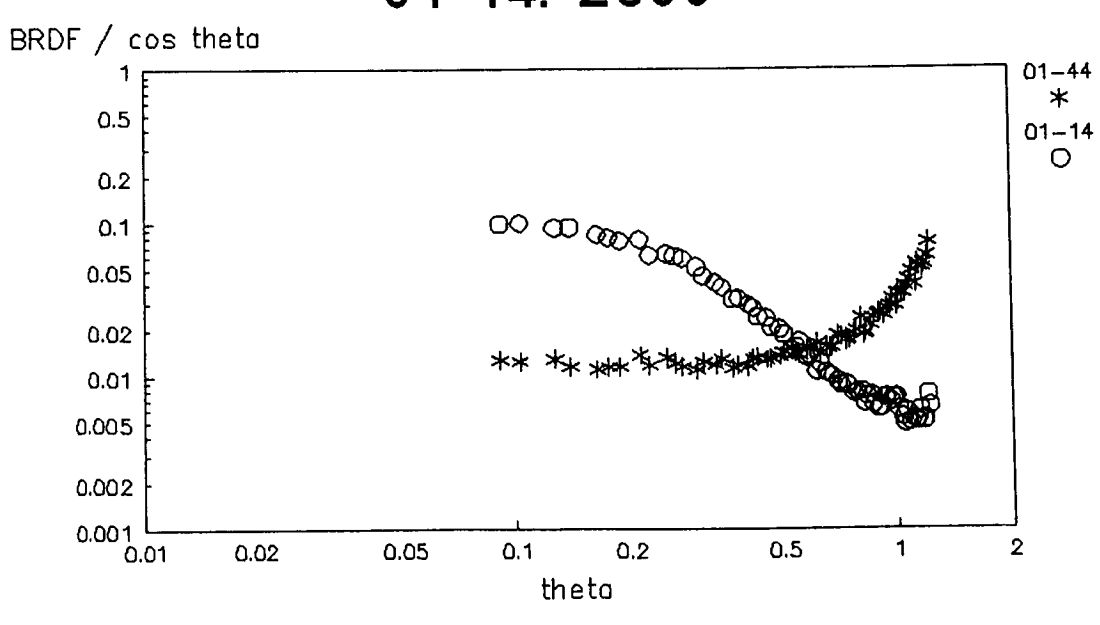

FIGURE 2 BRDF OF Z306 COATINGS

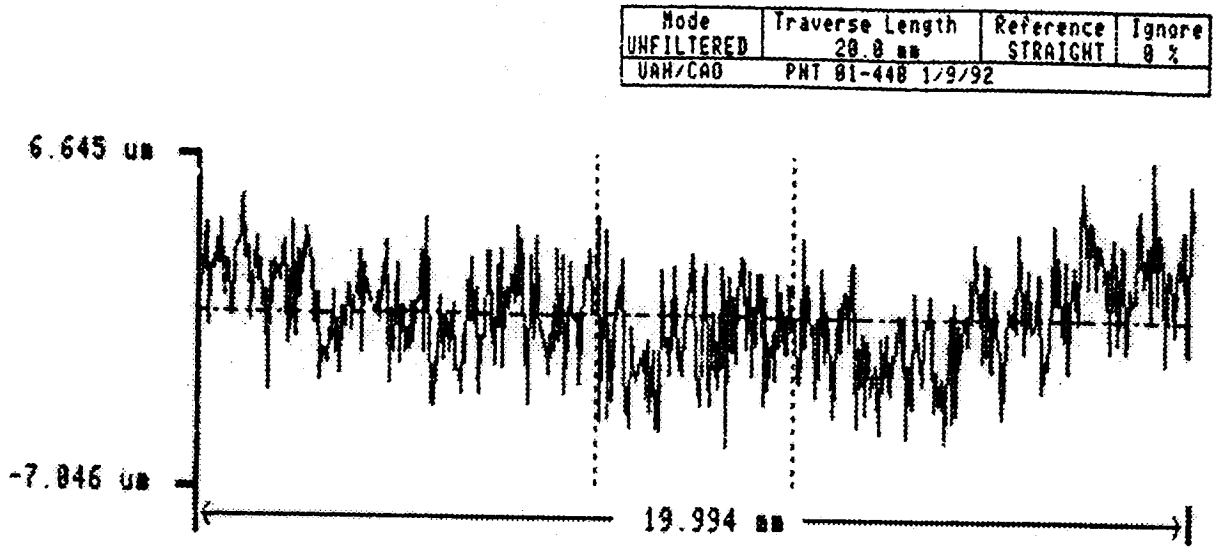

Peak To Valley = 13.691 um

Z-306 (O) Leading Edge

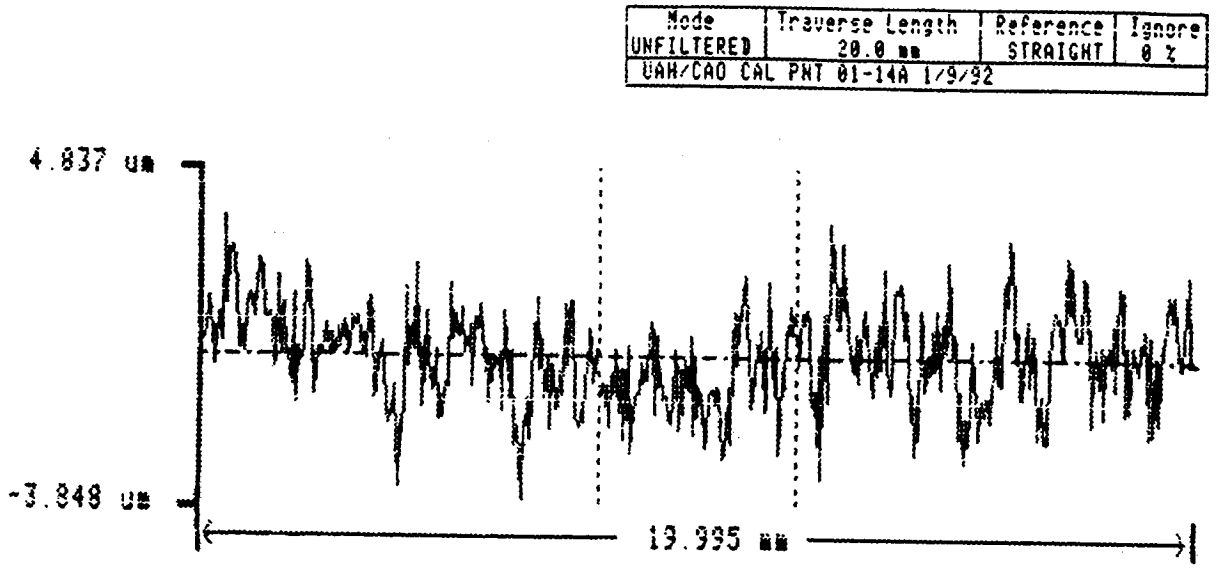

Peak To Valley = 8.685 um

Z-306 (W) Leading Edge

Talysurf Profiles of Z-306 - Experiment A0034

FIGURE 3

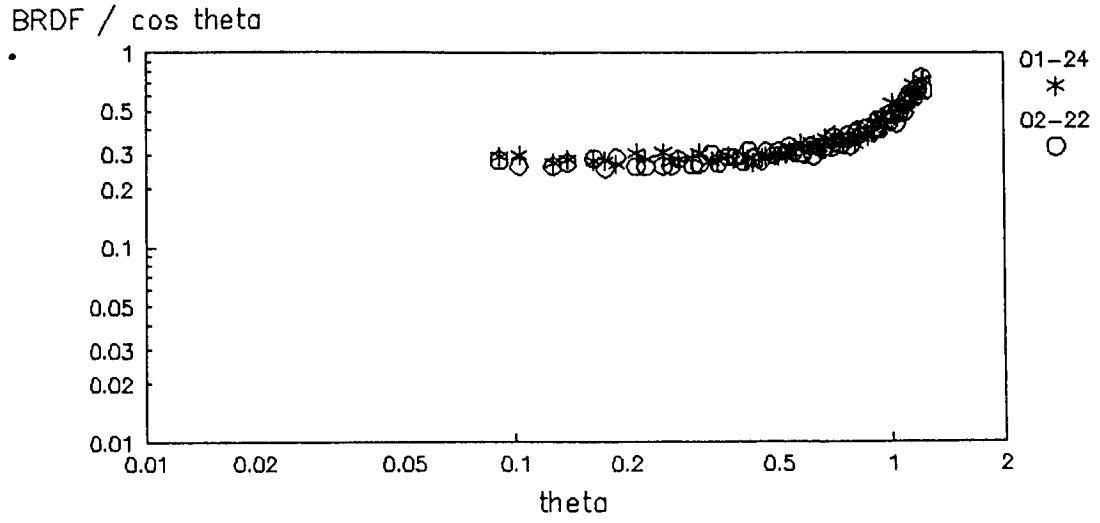

FIGURE 4 BRDF OF Z93 COATINGS FROM LEADING AND TRAILING EDGES

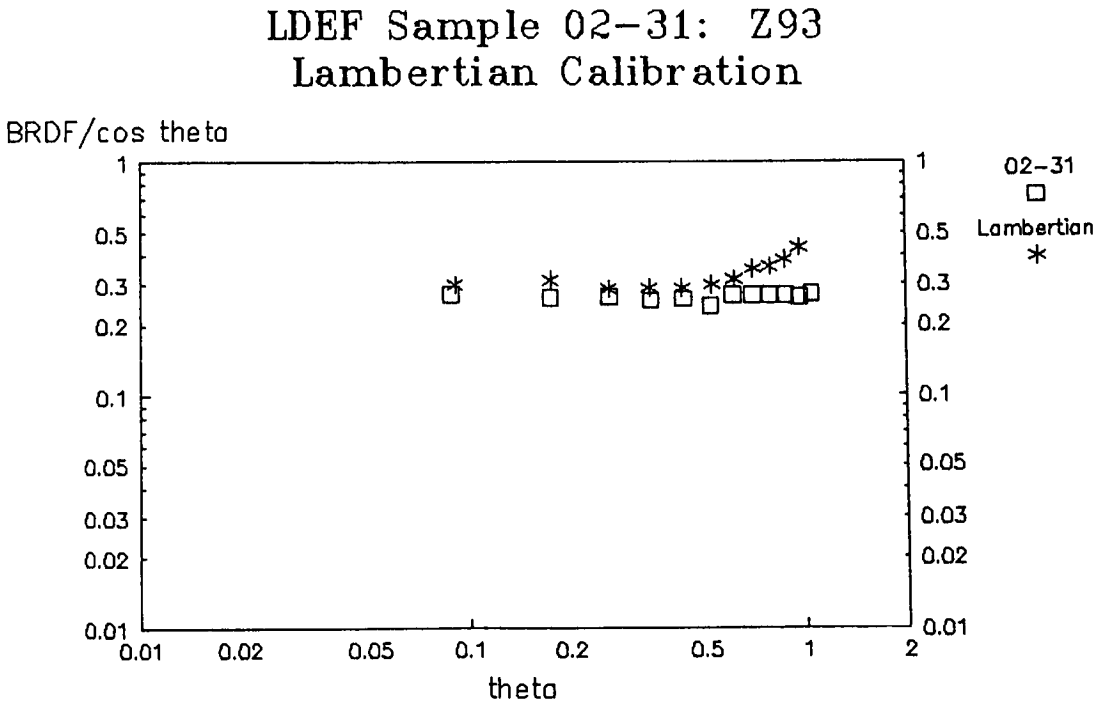

FIGURE 5 BRDF OF Z93 COATINGS AND LAMBERTIAN STANDARD

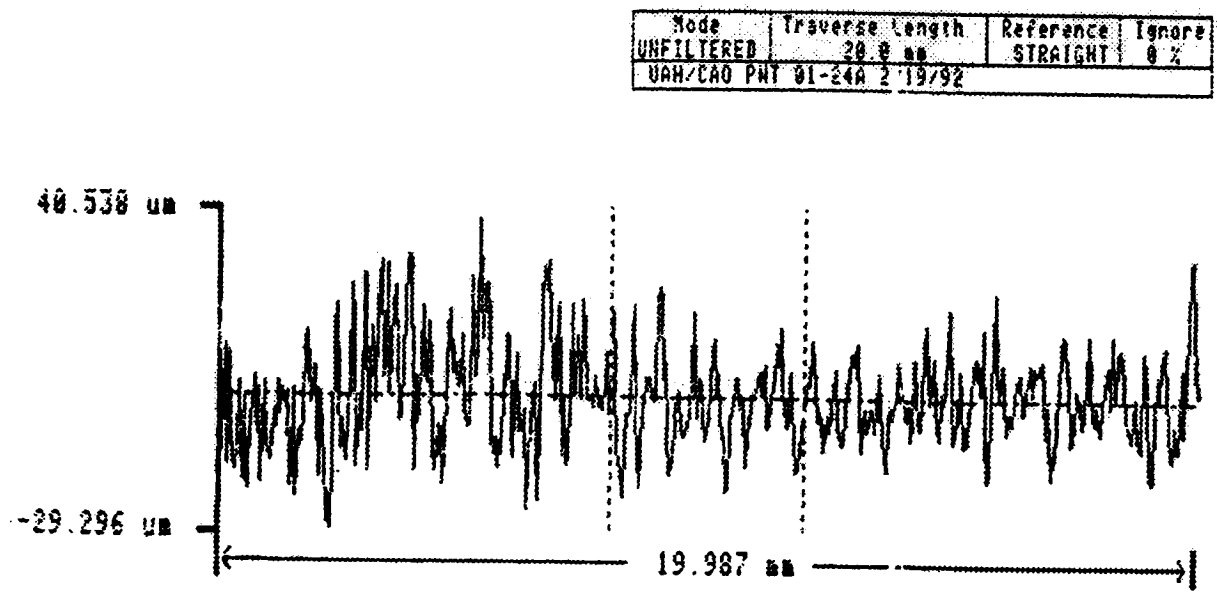

Peak To Valley = 69.834 um

Z-93 - Leading Edge

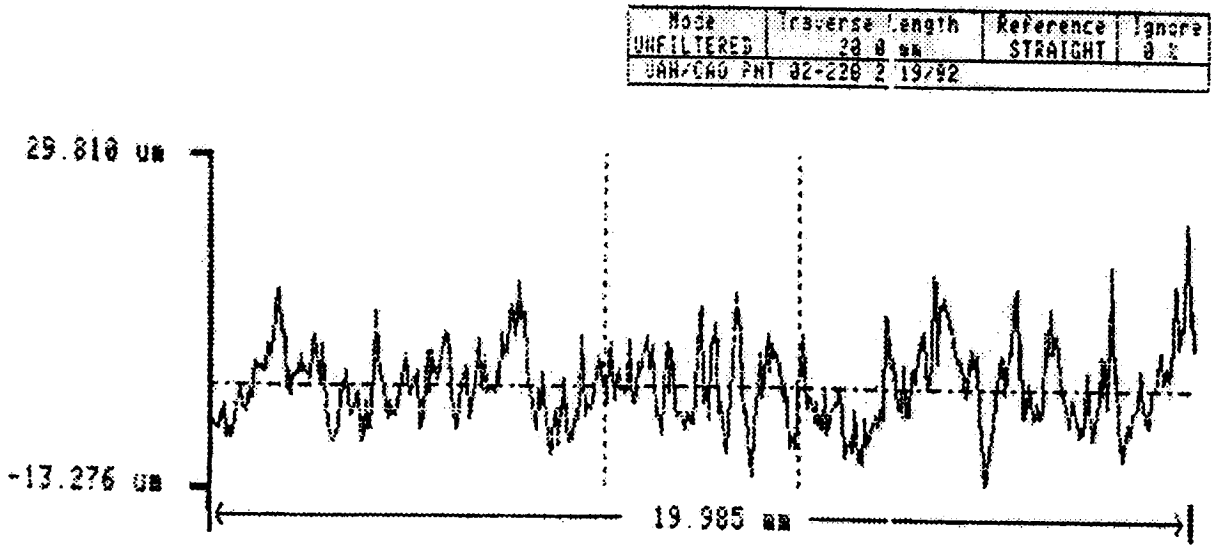

Peak To Valley = 43.085 um

Z-93 -Trailing Edge

Talysurf profiles of Z93 - Experiment A0034

FIGURE 6

Z-93 TALYSURF SUMMARY

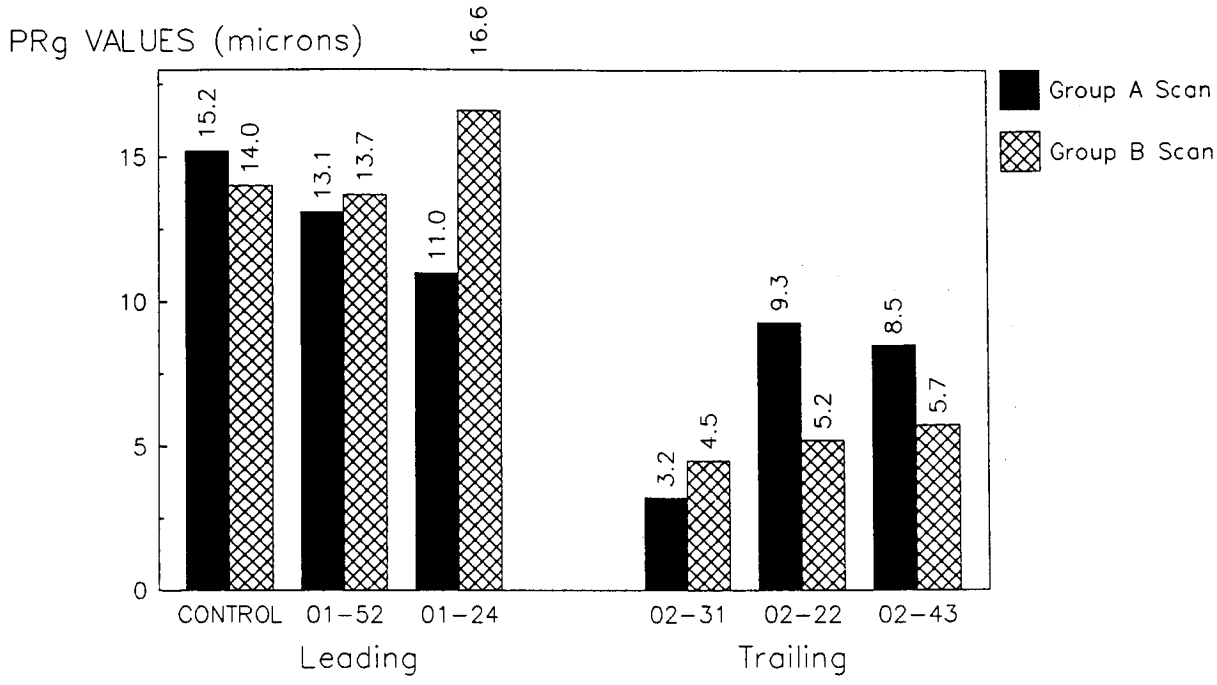

FIGURE 7

S-13G-LO TALYSURF SUMMARY

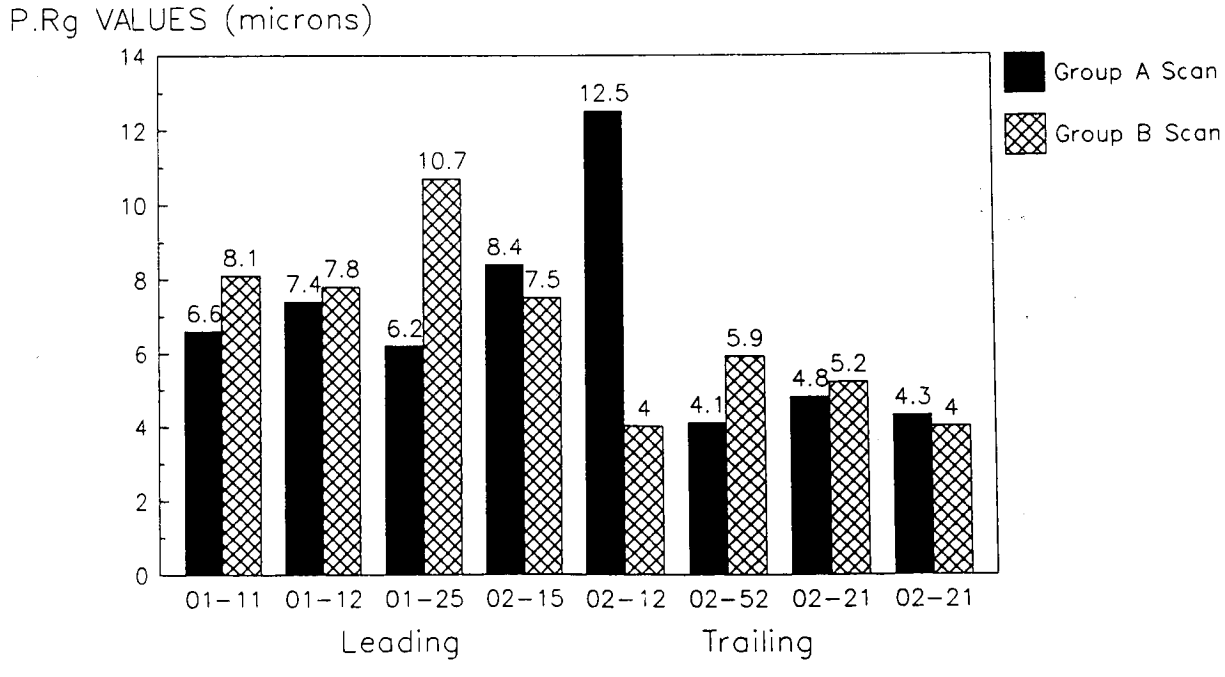

FIGURE 8

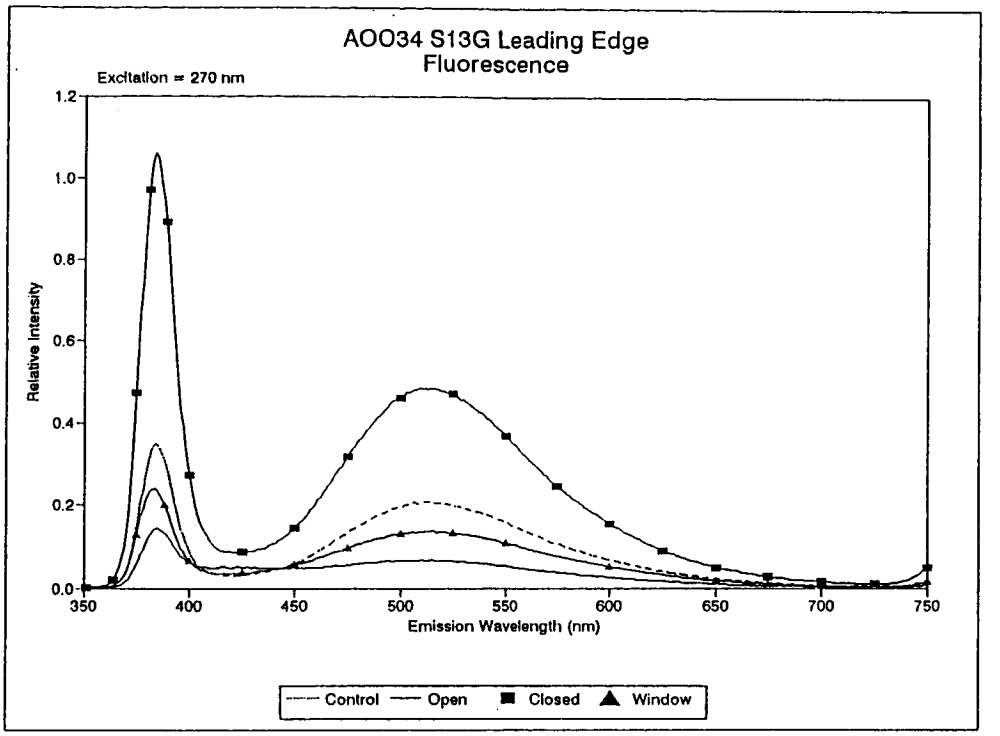

FIGURE 9

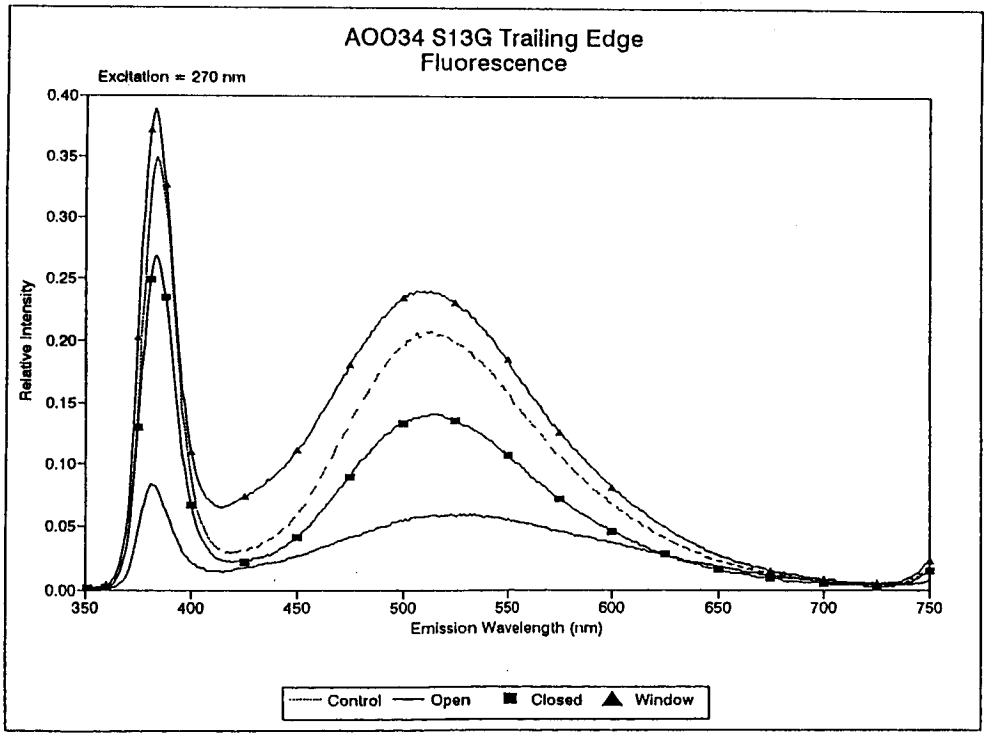

FIGURE 10

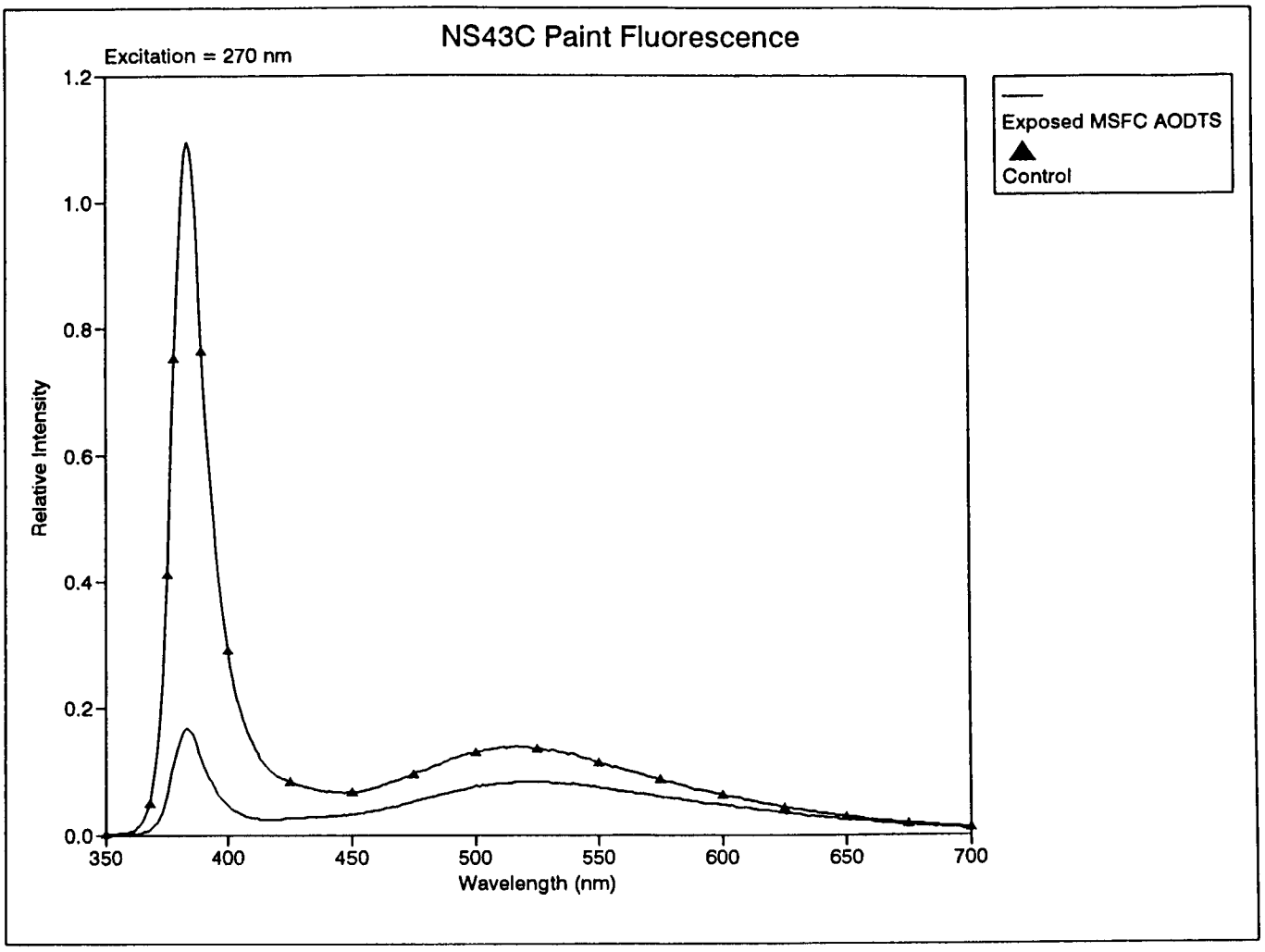

FIGURE 11 FLUORESCENCE OF NS43C EXPOSED TO ATOMIC OXYGEN

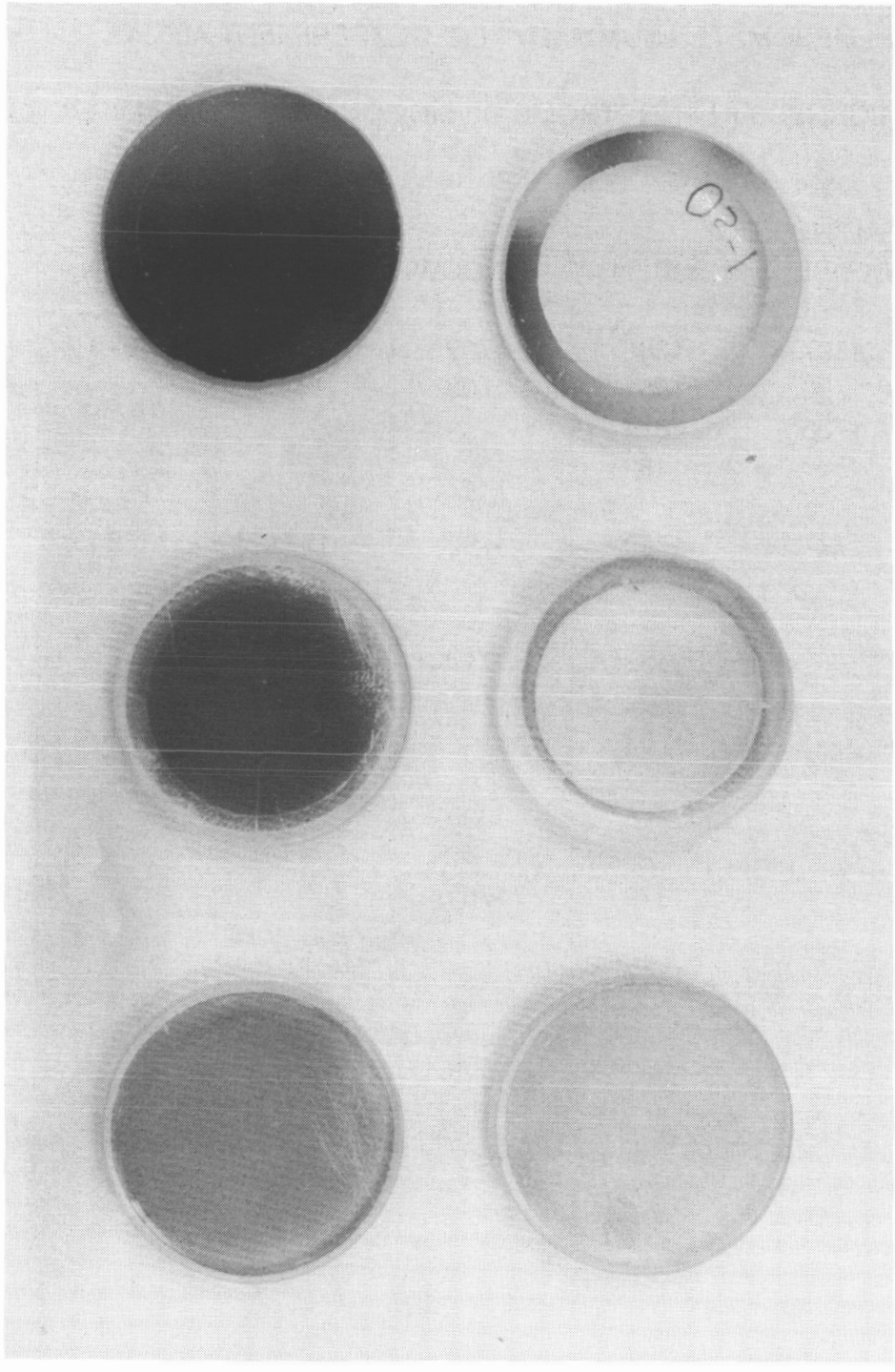

FIGURE 12 POST-FLIGHT APPEARANCE OF OSMIUM, SILVER, AND GOLD MIRRORS FROM A0034 LEADING AND TRAILING EDGES

ELLIPSOMETER SUMMARY - LDEF EXPERIMENT A0034

THICKNESS IN ANGSTROMS OF SiOx ON COLLECTOR MIRRORS

SOURCE TCC	LEADING EDGE			TRAILING EDGE		
	CLOSED	OPEN	WINDOW	CLOSED	OPEN	WINDOW
S13G	1897 1780 1733	1685 1661 1674 1482	1702 1708	1663	1670	1730 1764
S13G-LO	1777	1790	1782	1771	1694	1739 1764
Z93		1438	1712	1758		
YB-71		1703		1762	1691	1678
Z306		1428	1820			
A276		1379	1764			
Al PLATE		1447				

FIGURE 13

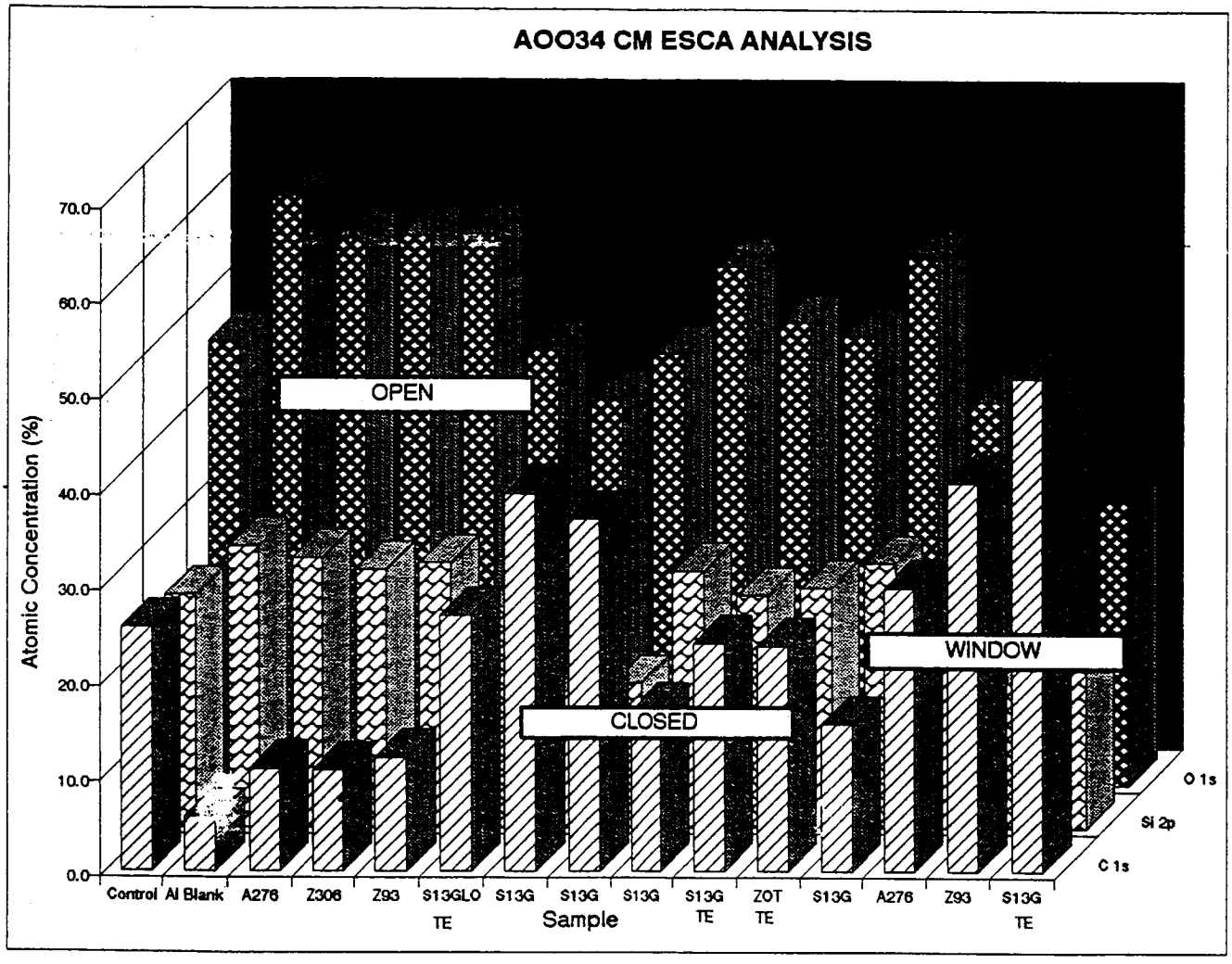

FIGURE 14 ESCA RESULTS FOR EXPERIMENT A0034 COLLECTOR MIRRORS

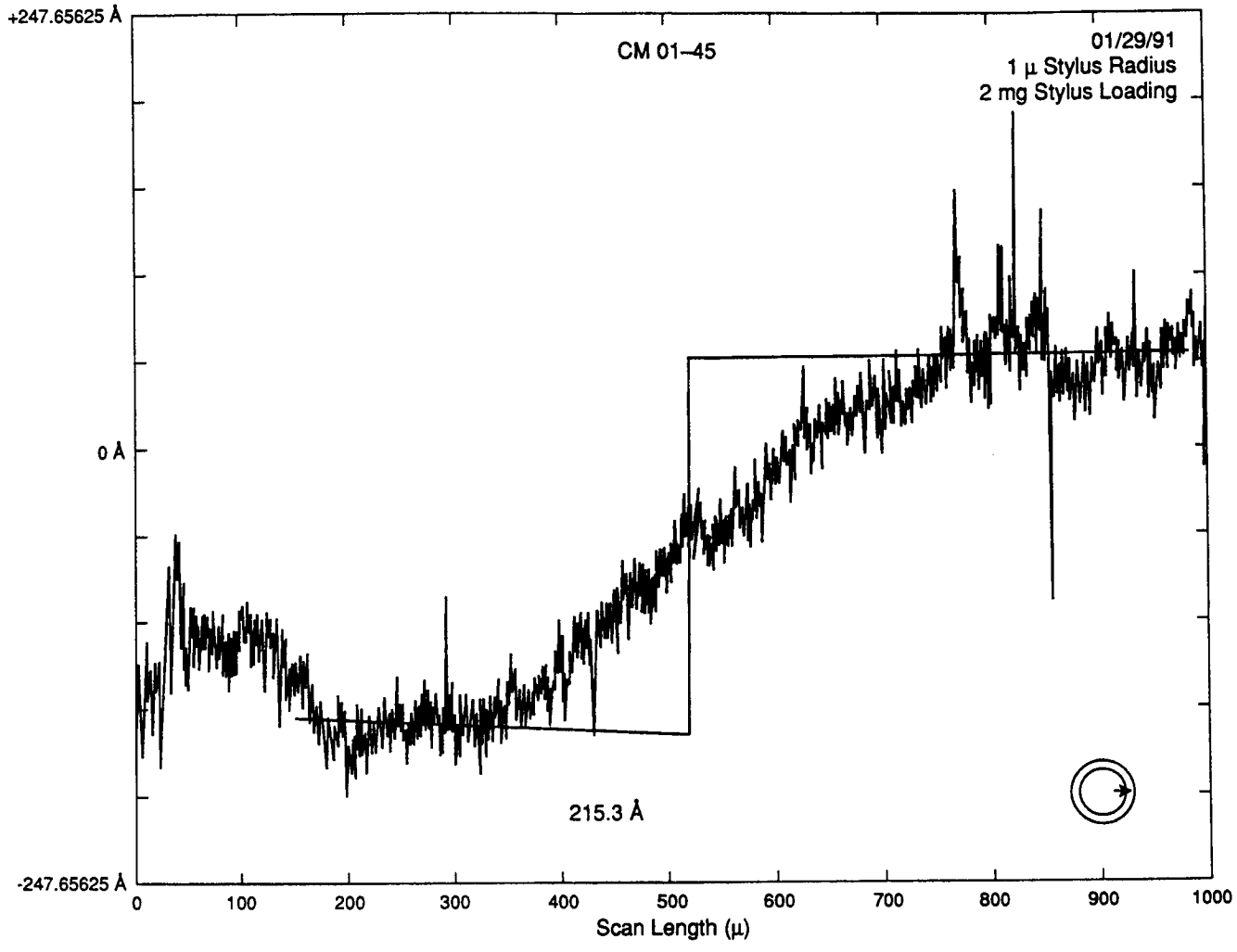

FIGURE 15 TALYSURF PROFILE FOR A0034 COLLECTOR MIRROR EXPOSED TO ATOMIC OXYGEN ON THE LEADING EDGE

N93-28284

THE INTERACTION OF ATOMIC OXYGEN WITH COPPER: AN XPS, AES, XRD, OPTICAL TRANSMISSION AND STYLUS PROFILOMETRY STUDY

Ganesh N. Raikar, John C. Gregory and Ligia C. Christl
The University of Alabama in Huntsville
Huntsville, AL 35899.
Phone: 205/895-6076, Fax: 205/895-6819

Palmer N. Peters
ES64, Space Science Laboratory
NASA, Marshall Space Flight Center
Huntsville, AL 35812.
Phone: 205/544-7728, Fax: 205/544-7754

ABSTRACT

The University of Alabama in Huntsville (UAH) experiment A-0114 was designed to study the reaction of material surfaces with LEO atmospheric oxygen. The experiment contained 128 one inch circular samples; metals, polymers, carbons and semiconductors. Half of these samples were exposed on the front of the LDEF and remaining on the rear.

Among metal samples, copper has shown some interesting new results. There were two forms of copper samples : a thin film sputter-coated on fused silica and a solid piece of OFHC copper. They were characterized by x-ray and Auger electron spectroscopies, x-ray diffraction and high resolution profilometry. Cu 2p core level spectra were used to demonstrate the presence of Cu_2O and CuO and to determine the oxidation states.

Experiment No: A-0114

1: INTRODUCTION

We know that the environment at altitudes of 200-700 km, where satellites orbit the earth, is extremely harsh due to the presence of atomic oxygen. An understanding of the nature of hyperthermal atomic oxygen with materials is essential to the design of long-lived satellites. In this regard the Long Duration Exposure Facility (LDEF), which carried samples of metals, alloys, ceramics, polymers, semiconductors, paints and a host of other materials and remained in space for nearly six years, is proving to be a source of data unrivalled in the history of space flight [1].

The copper samples, in both thin film and solid forms, were flown on the leading edge, C9 tray of LDEF with matching trailing edge samples in the C3 tray. The trailing C3 samples showed little effect of atomic oxygen. In this paper we discuss the effect of atomic oxygen seen on the C9 samples.

The surfaces of most metals and alloys in contact with the atmosphere are covered by a thin layer of oxide which protects the underlying metal. A knowledge of the composition, structure and thickness of this oxide layer is vital in understanding the relationship between the surface and the properties of various metals such as adhesion, corrosion resistance and optical performance. Its use in space is of interest because of its similarity to silver, which has superior electrical properties but catastrophically poor resistance to atomic oxygen.

Copper has been one of the elements most extensively studied in the laboratory with several surface sensitive techniques. Interpretation of oxide spectral structures is easier for copper than for other transition metals. The x-ray photoelectron core level line-shapes of Cu in copper-oxide based compounds have been widely studied in recent years. After the discovery of copper oxide based high temperature superconductors, great interest has been prompted in the understanding of the electronic structure of the Cu-O bond [2].

Copper is known to form two common oxide phases, depending on the oxidation conditions: cuprous oxide (Cu_2O) and cupric oxide (CuO) whose properties are listed in Table 1. Cuprous oxide is a semiconductor with a band gap of 2.17 eV and has essentially a full 3d ($3d^{10}$) shell while cupric oxide is an antiferromagnetic semiconductor with a band gap of 1.4 eV and has an open 3d ($3d^9$) shell. Cuprous oxide is the most stable at low oxygen pressures, particularly under vacuum conditions, and is the main phase formed at room temperature in contact with the atmosphere. Cupric oxide grows only at higher temperatures in the presence of high enough pressures, and is found to reduce to Cu_2O when heated under vacuum [3]. An unstable cupric hydroxide $Cu(OH)_2$

also exists on some surfaces due to moisture absorption. An understanding of these three compounds which are the likely surface products of the corrosion of copper metal is thus important.

ESCA (Electron Spectroscopy for Chemical Analysis) has proved to be a very powerful tool in the identification of metallic Cu [Cu(0)], Cu_2O [Cu(I)], and CuO [Cu(II)] species through the analysis of the Cu (2p) peaks and of the corresponding "shake-up satellites", as well as the x-ray excited Auger Cu $L_{2,3}M_{4,5}M_{4,5}$ [4]. In this study, we have utilized x-ray photoelectron spectroscopy (XPS), x-ray excited Auger electron spectroscopy (AES), high resolution stylus profilometry, scanning optical microdensitometry, electrical measurements and x-ray diffraction techniques.

2: EXPERIMENTAL

Thin films of copper were prepared at Space Sciences Laboratory, NASA Marshall Space Flight Center. Substrates were fused silica optical flats, obtained from Acton Research Corporation. These were coated with ca. 68 ± 1 nm copper using an RF sputtering system. The solid copper sample was cut from OFHC copper rod of one inch diameter and polished with 1 μm diamond powder. XPS was used to monitor the surface cleanliness of all these samples.

X-ray diffraction measurements were made using a Rigaku x-ray diffractometer with a thin film attachment. The angle between the thin film sample and the x-ray beam was constant at 1 degree to maximize surface sensitivity.

We used a Taylor-Hobson Talystep, Model # 223-27 instrument for profilometer measurements only on the thin film sample. Both exposed and unexposed areas could easily be scratched down to substrate interface with a fine tungsten wire. The square negative pulse-like traces gave good indications of the thickness of the exposed and unexposed regions at several locations across the sample [5]. This technique could not be used on the solid metal sample.

Transmission measurements were made using a white light source and scanning microdensitometer to verify uniformity of the exposed and unexposed areas. Additional transmission measurements were made using 4 different colored filters in a densitometer with 1 mm diameter aperture, but with the sample slightly elevated above the aperture by a shim support at the edges to avoid physical contact with the copper film; calibration standards were similarly supported and included a bare substrate.

XPS and x-ray excited AES measurements were made with a Perkin-Elmer 5400 ESCA system with an Apollo 4500 Domain series workstation. Typical operating conditions were:

System Pressure:	2-5 x 10^{-9} Torr
Anode (Mg $K\alpha_{1,2}$,1253.6 eV)Power:	300 watts (15 kVand 20 mA)
Area of Analysis:	1.2 mm^2
Pass energy:	89.5 eV (XPS survey scans)
	17.9 eV (XPS multiplex, Auger lines)
	8.95 eV (XPS core lines)
Take-off angle:	45°

Sample charging was measured by the displacement of the adventitious surface C 1s peak at 284.8±0.2 eV. The reproducibility of the peak positions obtained was within ±0.2 eV. The effect of the Mg $K\alpha_{3,4}$ satellites has been removed from the Cu 2p peaks and the Auger line-shapes.

3: RESULTS AND DISCUSSION

3.1: X-Ray Diffraction

Figure 1 shows the x-ray diffraction pattern of the unexposed region of the copper thin film. Three main peaks at $2\theta = 36.5°$ (Cu_2O), 43.5° (Cu) and 50.5° (Cu) are observed. The intense main peak at 21° is due to the fused silica substrate. The data is interpreted as characteristic of metallic Cu with a thin film of Cu_2O on its surface.

Figure 2 shows the XRD pattern of the exposed region. There are three main peaks at $2\theta = 36.5°$ (Cu_2O), 43.5° (Cu) and 50.5° (Cu) with a small peak at 39° (CuO) plus the intense silica peak as seen before. The observed distribution of phases for this region can be described as a mixture of mainly Cu_2O and metallic Cu with some CuO being present.

3.2: Stylus Profilometry

It has been shown in a previous paper [5] that the stylus profilometer can be used to measure changes in the roughness, erosion depths and material growth on a flat surface. This technique has the unique ability to measure a range of dimensional changes from 1mm to 0.1 nm. If the molar

volume of metal oxide produced is different from that of the native metal, as is usually the case, the method is capable of detecting extremely low levels of oxidation.

Figure 3 shows a representative trace taken on the unexposed region showing a film thickness of ca. 68± 1 nm. Figure 4 shows that the thickness of the exposed region was 105.3 ±1 nm, or 40% greater than the unexposed region. The average height of the step measured at the mask edge as shown in Fig.5 was ca. 34.3±0.5 nm , in agreement with the difference in total film thickness.

If all the copper in the 68 nm film were converted to one or other of the oxides, the thickness of these oxide films would be 114 nm for Cu_2O and 117 nm for CuO. This calculation assumes the theoretical maximum densities for the solids (see table 1) . Since the exposed film is only 105 nm thick, we may assume that the metal is not entirely oxidized through to the substrate. Although the profilometry data cannot distinguish between the two oxides, the XRD analysis clearly shows a mixture of Cu_2O and native metal, but cannot be used quantitatively. Again assuming theoretical densities we calculate that the exposed film consists of 92 nm of Cu_2O and 13 nm of Cu. Thus 55 nm of Cu were oxidized during the full LDEF exposure.

3.3: Optical Measurements

Visual inspection of the copper film shows that the exposed portion is much more transmissive than the unexposed. White light optical density measurements on the unexposed and exposed portions of the copper film gave transmissions of 5 and 13% respectively. The transmittance and reflectance versus thickness of a pure copper film were calculated [6] using equations for normal incidence from air onto a homogeneous copper film on fused silica; corrections for contamination were neglected. Optical constants for pure copper and its oxides were used in separate calculations, assuming a single film on a fused silica substrate.

A pure copper film with the measured optical density of the exposed portion should be less than 35 nm thick, as determined from Fig.6 while stylus measurements of the exposed area indicated 105.3 nm thickness. The same analysis was performed assuming a 100% Cu_2O film in the exposed area. Figure 7 shows that pure Cu_2O would be much more transparent than that observed for the exposed portion. This also suggests only partial conversion of the exposed copper film to copper oxide, although visually the film does not appear metallic in nature. This also supports the conclusion reached from the XRD and profilometry results on the thin film sample. More detailed analysis of the transmission and reflectance of these films has been made using a multi-layer model. The results have provided quantitative support of the profilometer and XRD data, but will be reported later.

3.4: Electrical Measurements

Limited resistivity measurements of the exposed and unexposed halves of the copper thin film were made with two-terminal contacts and a digital ohmmeter. Because contact resistances were not eliminated, only rough comparisons can be made; although the resistivity of the exposed area was higher than the unexposed area, it appeared to be too good a conductor to be cuprous oxide. Again incomplete conversion of copper to an oxide is indicated.

3.5: XPS and AES Measurements

For this study, we have made use of both photoelectron and Auger line shifts and changes in the lineshapes to determine the presence of various oxides on the thin film and solid samples of copper. The spectra were analyzed in terms of relative peak area intensities, full width at half maximum (FWHM), chemical shifts in the Cu $2p_{3/2}$ and Cu $2p_{1/2}$, Cu $L_3M_{4,5}M_{4,5}$ Auger lines and satellite structure associated with the Cu $2p_{3/2}$ peak.

Figure 8 shows the survey scans measured on the exposed and unexposed regions of the solid Cu. The atomic concentrations measured on the thin film and solid samples are tabulated in Table 2. Contaminants observed are C and Si. Silicone contamination on LDEF samples has been reported by several groups. Carbon contamination was roughly 50-60 % on all the samples which we attribute to hydrocarbon contamination.

The O 1s line (ca. 530 eV) has been extensively used in the analysis of oxide surface species. The line has a relatively narrow width and a symmetric shape. However, the presence of more than one species complicates the analysis and accurate fitting of the complex band combinations. It has been observed that the O 1s electrons in metal oxide species with a formal charge assignment of O^{2-} have a lower binding energy than in "adsorbed" oxygen which may be present in the formal modes of O_2^-, O_2^{2-} or O^- .

Normally chemical shifts of several eV are observed between the O 1s lines from a bulk oxide (O^{2-}), hydroxide (OH^-) or molecular water (H_2O). As shown in Fig.9 the O 1s spectrum taken from the exposed region of the solid sample, three main bands can be fitted. The peak A at ca. 529.5 ± 0.2 eV (FWHM= 1.1) is attributed to the main oxide O^{2-} species on the surface. The peak B at ca. 530.8 ± 0.2 eV (FWHM=1.32) arises from OH^- species while the wide intense peak C at ca. 532.5 ± 0.2 eV (FHWM=1.77) may be due to silica [7].

One major difference between the XPS spectra of Cu(I) and Cu(II) is the presence of prominent satellite structures called "shake-up" satellites on the high binding energy side of the Cu 2p lines in Cu(II) oxide. More generally, these effects have been associated with paramagnetic species. Cu(II) has a paramagnetic $3d^9$ structure while Cu(I) has a filled 3d subshell. Similar shake-up satellites occur on the 2p lines of copper halides and also in paramagnetic nickel independent of valence or stereochemistry [8]. These shake-up satellites arise due to the interaction between the Cu $2p_{3/2}$ core hole and the valence electrons. It is now well accepted that the mainpeak corresponds to a final state of $2p^5 3d^{10} \underline{L}$ (where $\underline{L}$ means a ligand hole) and the satellite to a $2p^5 3d^9$ final state. The structure seen in the Cu $2p_{3/2}$ satellite is a result of multiplet splitting in the $2p^5 3d^9$ final state [9].

Such satellites are seen only on the exposed region of the solid sample and are absent in the thin film sample. In Fig.10 we have plotted Cu 2p peaks measured from both exposed and unexposed regions of the thin film along with that taken from a pure Cu control. The FWHM of Cu $2p_{3/2}$ increases from nearly 1 eV in the control sample to 1.8 eV in the unexposed and exposed regions. The shape of Cu 2p peaks in the exposed and unexposed regions is quite similar to that from pure Cu (I) oxide. The B.E shifts for these peaks are less than 0.2 eV when compared with those from metallic Cu. Thus the species on both sides of the sample are mostly Cu_2O.

Similar comparison is made for the Cu 2p peaks in Fig.11 measured from both exposed and unexposed regions of solid copper. The shape and the FWHM of Cu $2p_{3/2}$ peak in the unexposed region are the same as on the exposed and unexposed regions of the thin film sample. We can infer from this observation that the oxide present on the unexposed region is similar in composition to Cu_2O oxide. The shake-up satellites that appear in the Cu 2p peaks measured on the exposed region are characteristic of CuO oxide. This is reinforced by a larger FWHM of the main peak (3.7 eV) , and a chemical shift of ca. 1.3 eV with respect to the metallic Cu(0) and Cu(I) species. Similar satellites have been observed by de Rooij from copper strips flown on LDEF [10].

Angle-resolved XPS (ARXPS) measurements can provide a surface composition of thin films [11]. The information depth is limited to 3λ where λ is the inelastic mean free path for electrons in the materials and typically 5 to 30Å. We have performed ARXPS measurements on all the samples. It is interesting to notice that as we increase the angle of collection of photoelectrons and probe deeper into the sample, we observe changes in the corresponding Cu 2p spectra from the exposed side of the LDEF solid copper sample as shown in Fig.12. In particular the satellite peaks, prominent at the outer surface and attributed to CuO, are observed to decrease to almost zero at maximum probing depth. As the maximum depth probed in the ARXPS [12] is about 7 nm, we roughly

estimate the thickness of CuO on the exposed region of the solid copper sample as ca. 2-3 nm, and beneath this depth the oxide resembles Cu_2O.

A detailed analysis of the Auger-line shape for those transitions involving valence electrons, in principle, should provide valance-band information and also effective Coulomb repulsion between the final two electrons in the Auger process . Now the Coulomb interaction for the Cu $L_3M_{4,5}M_{4,5}$ Auger line can be determined from the relation:

$$U_{eff} = E_{kin} - E_b(2p) - 2E_b(3d)$$

where $E_b(2p)$ is the Cu 2p binding energy and $E_b(3d)$ is the binding energy of the 3d electrons, and U_{eff} is the effective Coulomb interaction. Generally, if U_{eff} is less than twice the one-electron band width [Γ] as measured from XPS, the resulting LVV Auger spectrum is characterized as "band-like" and should have the same shape as a self-convolution of the density of electronic states within the valence band. If $U_{eff} \geq 2\Gamma$, electron correlation effects will be important and the resulting Auger transitions are termed "quasi-atomic", as they exhibit fine structure [13] as seen in the Cu Auger lines.

In Fig.13 we have plotted on a binding energy scale the Cu $L_{2,3}M_{4,5}M_{4,5}$ Auger spectra measured from the exposed regions of thin film and copper solid samples which are in turn compared with that from the Cu control. The scales are normalized to the C 1s fiducial at 284.6 eV. There are clear differences in these spectra. The Auger spectra from the LDEF samples are broader and lack the fine structure seen in the control sample. The two features marked A and B in the spectrum 3 (lab control) are "double ionization satellites" arising from the $L_2L_3M_{4,5}$ Coster-Kronig type of Auger transitions which results in a $3d^7$ final state. After this process has taken place, the created L_3 hole decays via the normal $L_3M_{4,5}M_{4,5}$ Auger process. The Auger spectral shape of spectrum 1 is different from that of spectrum 2. Also the intensity of the ionization satellites is considerably less in spectrum 1. It has been suggested that the shake-up $3d^9$ states which are responsible for the XP shake-up satellites in Cu (II) materials will enhance the intensity of the ionization satellites as seen in spectrum 2 [14]. The spectrum 2 thus identifies the presence of Cu (II) species in larger amount than in spectrum 1. The most prominent line in the Cu Auger $L_3M_{4,5}M_{4,5}$ spectrum and its energy is used for the chemical state identification. A peak shift of ca. 2.3 eV to lower kinetic energy (i.e higher binding energy) is observed between the Cu (0) and Cu (I) Auger lines, and nearly 1 eV between the Cu (0) and Cu (II) Auger lines as seen in the Fig.13. Again, we deduce that the surface copper species on the exposed portions of the solid sample and the thin film are Cu (II) and Cu (I) respectively.

4: SUMMARY

A battery of surface and thin film techniques has been applied to the analysis of the oxidized copper surfaces exposed in LDEF experiment A0114. These surfaces on row 9 received a total fluence of 8.72×10^{21} oxygen atoms per square cm.

XRD and high resolution profilometry have shown that on the thin film sample, 55 nm of copper was converted stoichiometrically to Cu_2O. Optical transmission measurements were consistent with this result. ESCA analysis has shown that the outermost layers of the cuprous oxide (ca. 2-3 nm) have been oxidized to a cupric oxide on the solid sample. This may be hydrated and in the form of $Cu(OH)_2$. It is our hypothesis that this oxidation from Cu (I) to Cu (II) occurred after the samples were returned to earth. The difference in re-oxidation between the two samples is probably due to different storage and analysis histories. The re-oxidation hypothesis has recently been substantiated by oxygen-18 isotope measurements by Saxon et al [15] on copper grounding strips. We note that our results and conclusions are entirely consistent with those of de Rooij [10], also made on the copper grounding strips.

5: REFERENCES

[1] Bland A. Stein and H. Gary Pippin, Proceedings of "First LDEF Post-Retrieval Symposium", Kissimmee, June 2-8, 1991; Ed. Arlene S. Levine, NASA CP-3134, P.617.

[2] P.A.P. Lindberg, Z.X.Shen, I. Lindau and W.E.Spicer, Surf.Sci.Rep., 11 (1991) 1.

[3] A.F. Wells, *Structural Inorganic Chemistry*, 5th Ed (Clarendon Press, Oxford, 1984) 1 ; A. Billi, E. Marinelli, L. Pedocchi and G. Rovida, Proceedings of 11th Int. Corrosion Congress, Florence, 1990, P.129.

[4] N.S. McIntyre, S. Sunder, D.W. Shoesmith and F.W. Stanchell, J. Vac. Sci. Technol. 18, (1981) 714; C. Malitesta, T. Rotunno, L. Sabbatini, and P.G. Zambonin, J. Chem. Soc. Faraday Trans. 86 (1990) 3607.

[5] Ligia C. Christl, John C. Gregory and Palmer N. Peters, Proceedings of "First LDEF Post-Retrieval Symposium", Kissimmee, June 2-8, 1991; Ed. Arlene S. Levine, NASA CP-3134, P.723.

[6] Hass, Georg, and Lawrence Hadley, "Optical Properties of Metals", in American Institute of Physics Handbook, Ed. D.E Gray et al (McGraw-Hill, N.Y, 1963), P.6.

[7] Terry L.Barr, J.Vac.Sci. Technol. A 9(3) (1991) 1793.

[8] G. van der Laan, C. Westra, C. Haas and G.A. Sawatzky, Phys. Rev. B 23, (1981) 4369.

[9] J. Ghijsen, L. H. Tjeng, J. van Elp, H. Eskes, J. Westerink, G. A. Sawatzky and M. T. Czyzyk, Phys. Rev. B 38 (1988) 11322.

[10] A. De Rooj, Proceedings of "Materials in a Space Environment", Cannes, Sept , 1991, P.119.

[11] C. S. Fadley, Prog. Solid State Chem. 2 (176) 265.

[12] I. Dalins and M. Karimi, J. Vac. Sci. Technol, A 10(4) 1992, 1.

[13] J. C. Fuggle in, "Electron Spectroscopy: Theory, Techniques and Applications", Vol.4, Eds. C. R. Brundle and A. D. Baker (Academic Press, N.Y, 1981) P.86.

[14] D.E. Ramaker, J.Electron Spectroscopy and Related Phen. 52 (1990) 341.

[15] J. M. Saxton, I. C. Lyon, E. Chatzitheodoredis, J. D. Gilmour and G. Turner, Presented at the "Second LDEF Post-Retrieval Symposium", San Diego, June 1-5, 1992; NASA CP-10067, P.78.

TABLE 1

Properties of Cu and Its Oxides

Species	Oxidation State	Color	Structure	Formula Weight	Specific Gravity	Refractive Index
Cu	0	Red	Cubic	63.5	8.92	-----
Cu_2O	+1	Red	Cubic	143	6.0	2.70
CuO	+ 2	Black	Monoclinic	79.5	6.3-6.5	2.63

TABLE 2

Surface Atomic Concentration

Photo Peak		Copper Thin Film, C9-16 Exposed	Copper Thin Film, C9-16 Unexposed	Solid Copper, C9-30 Exposed	Solid Copper, C9-30 Unexposed
Cu 2p	A.C (%)	4.3	2.7	8.9	5.6
O 1s	"	37.4	21.6	55.0	25.2
C 1s	"	44.4	65.8	18.5	62.9
Si 2p	"	13.9	9.3	16.9	4.9
Na 1s	"	0.0	0.0	0.0	0.5
Cl 2p	"	0.0	0.6	0.7	1.0

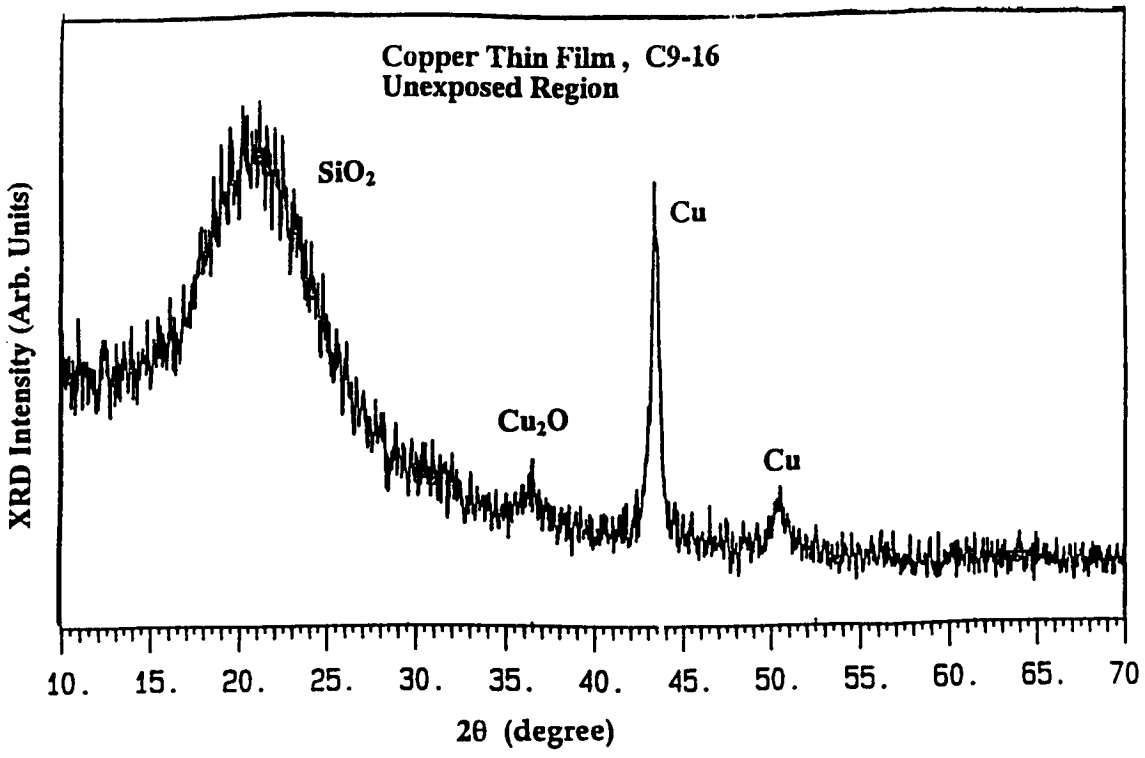

Fig. 1: XRD pattern of the unexposed region of Cu thin film.

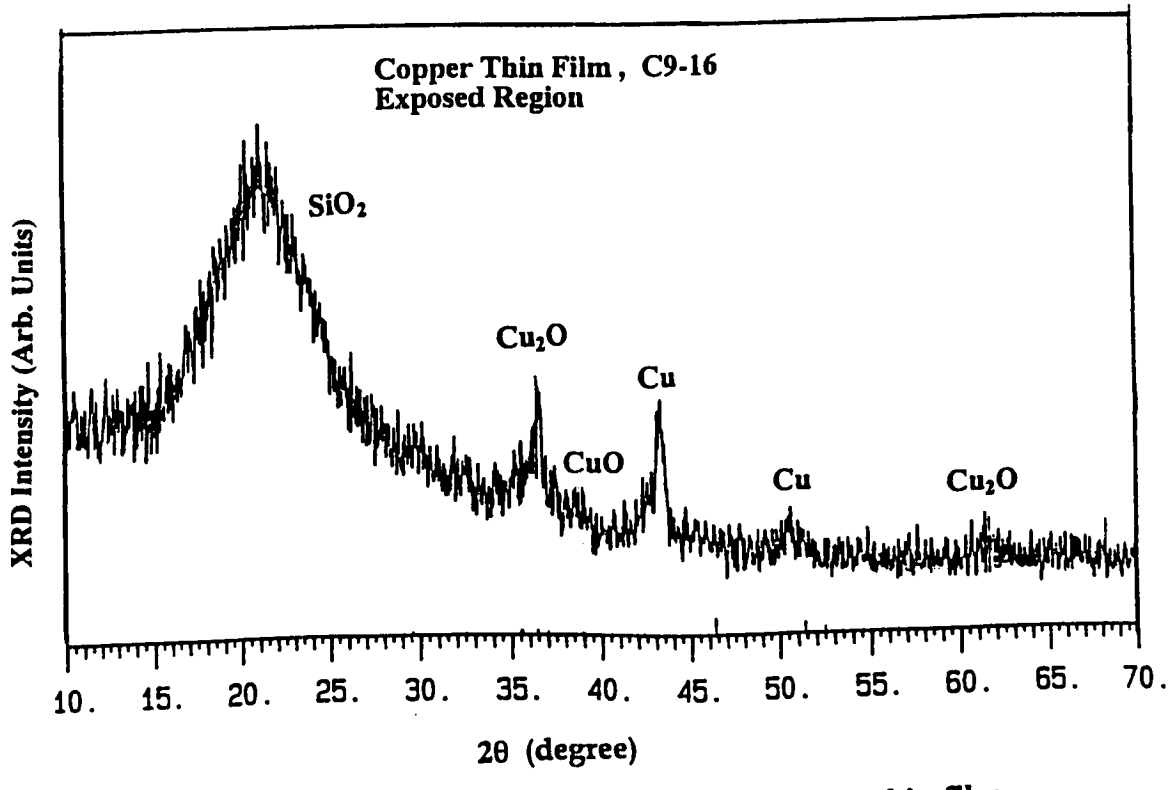

Fig. 2: XRD pattern of the exposed region of Cu thin film.

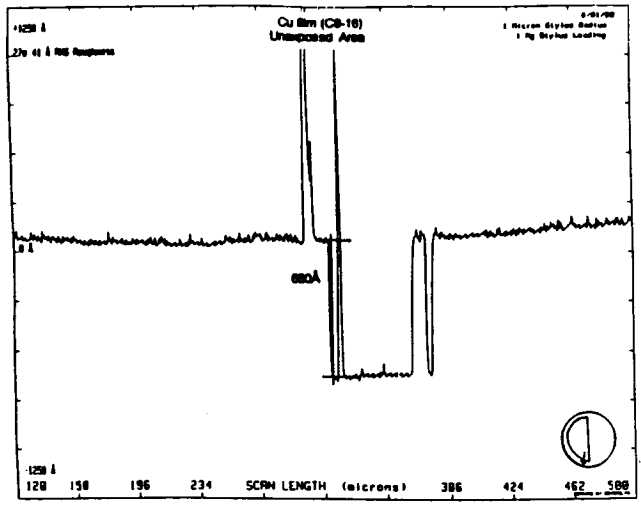

Fig. 3: Surface profile of the unexposed region of Cu thin film

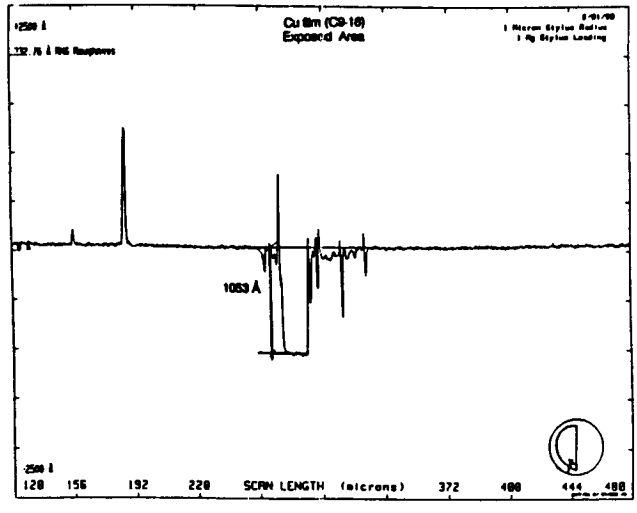

Fig. 4: Surface profile of the unexposed region of Cu thin film

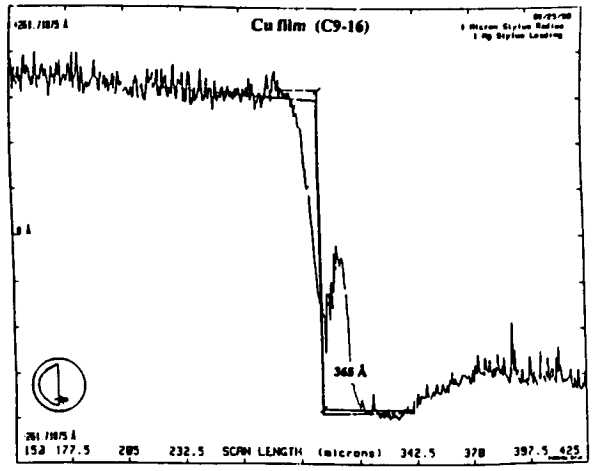

Fig. 5: Surface profile of transition from the exposed to the unexposed region of Cu thin film

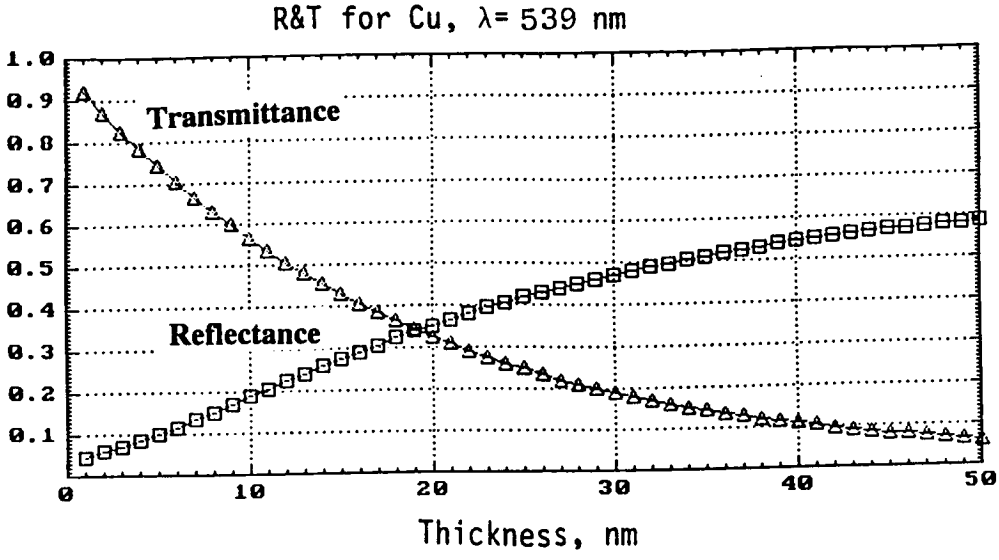

Fig. 6: Calculated Reflectance and Transmittance curves for Cu

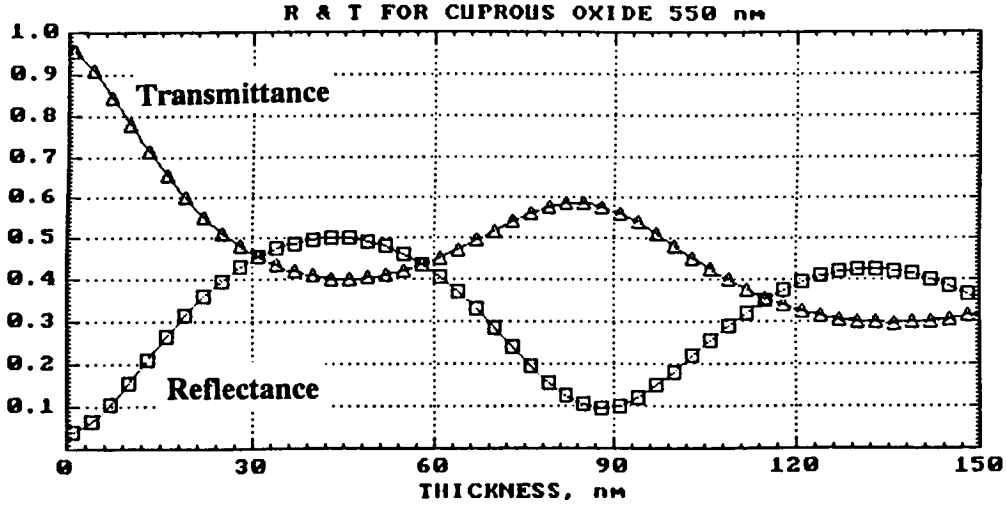

Fig. 7: Calculated Reflectance and Transmittance curves for Cu_2O

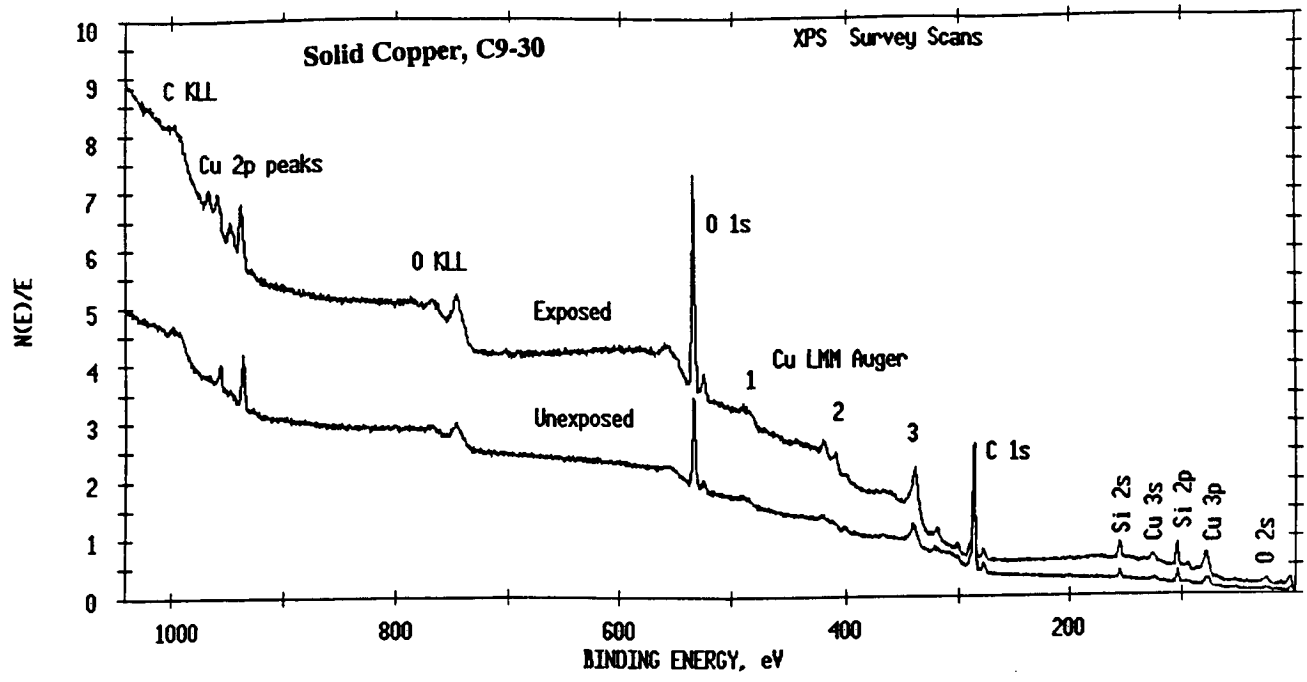

Fig. 8: XPS survey scans of the unexposed and exposed regions of Solid Cu

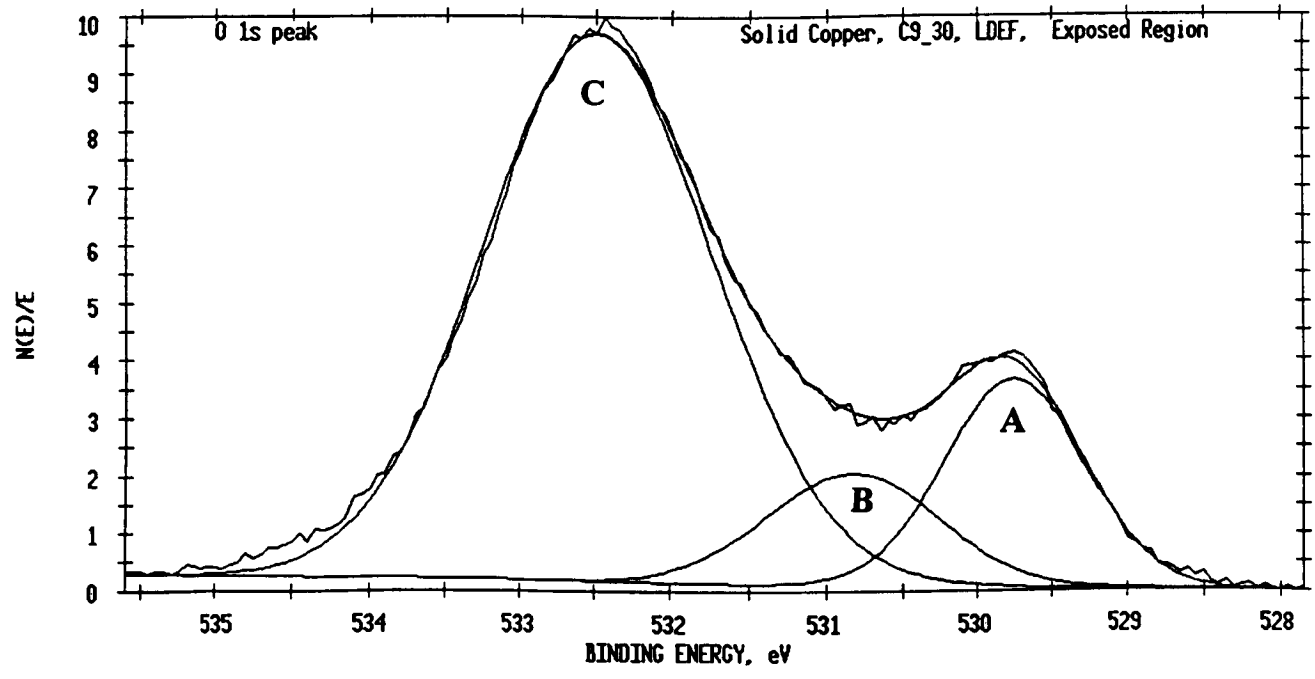

Fig. 9: Curve synthesis for the O 1s core-line from the exposed region of solid Cu

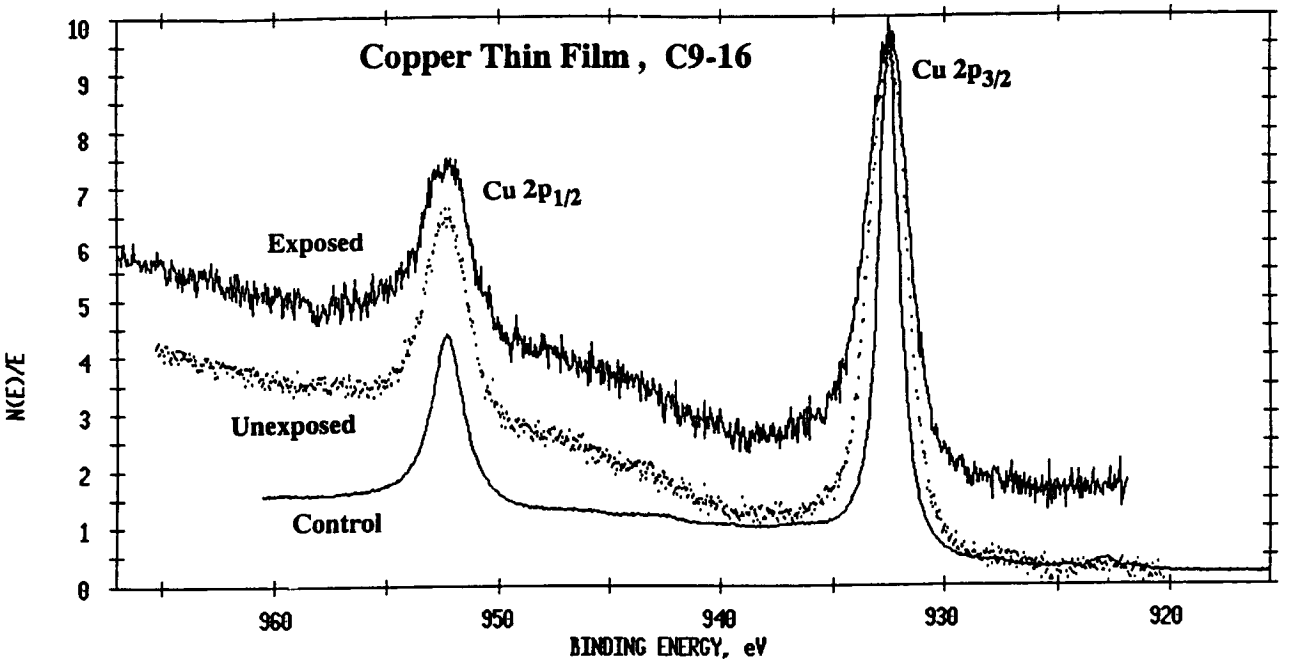

Fig.10: Cu 2p core-level peaks of the exposed and unexposed regions of Cu thin film

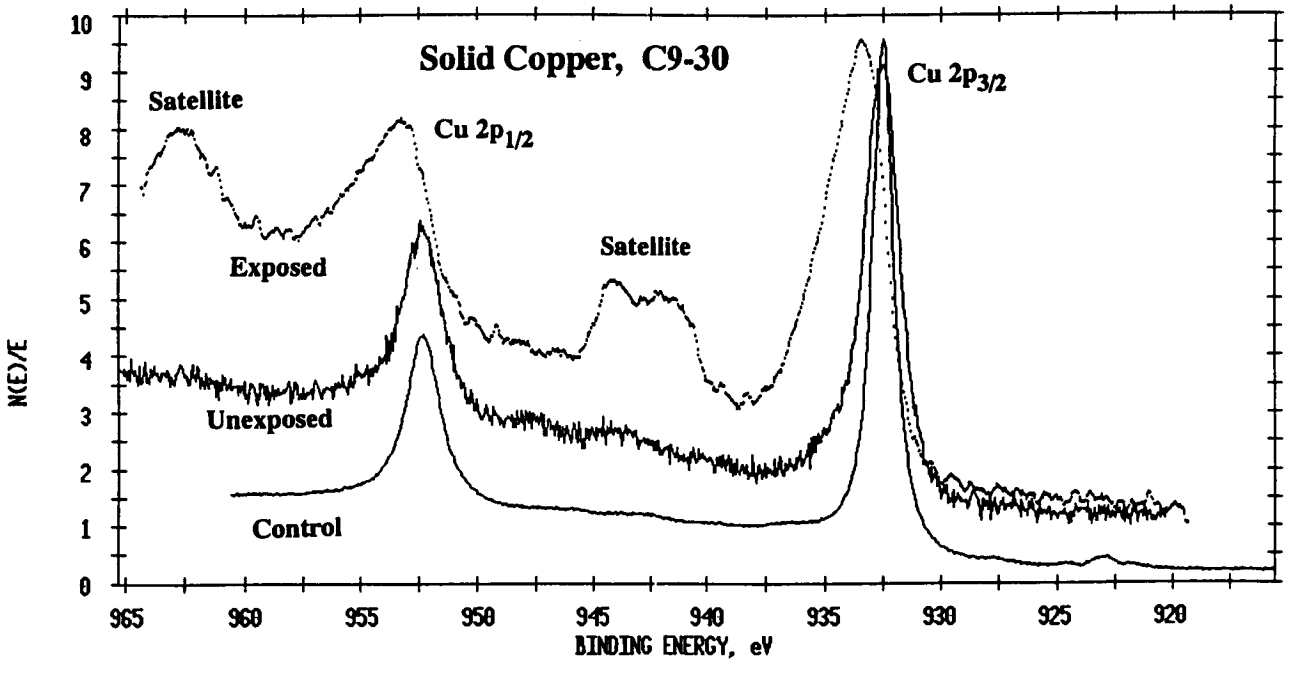

Fig. 11: Cu 2p core-level peaks of the exposed and unexposed regions of solid Cu

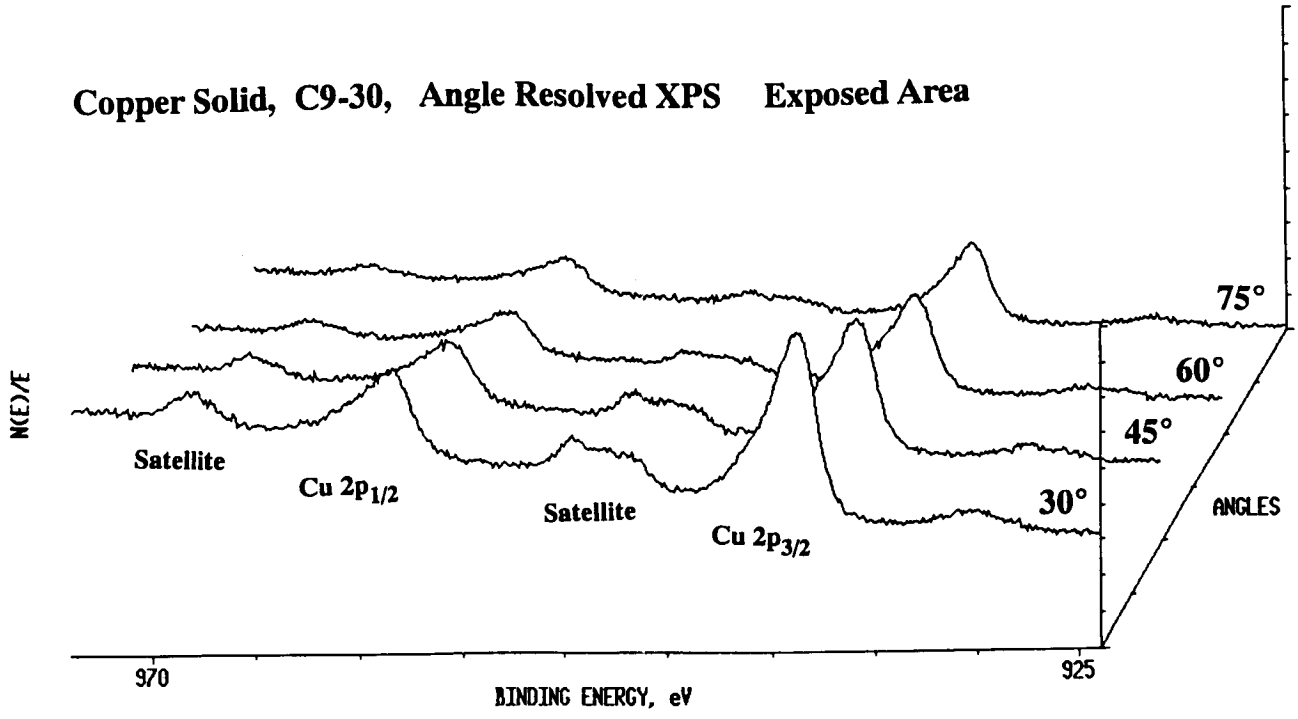

Fig. 12: Angle resolved XPS montage plot of Cu 2p core-level peaks of the exposed region of solid Cu sample. A larger take-off angle for the electrons correlates with a sampling depth deeper into the surface

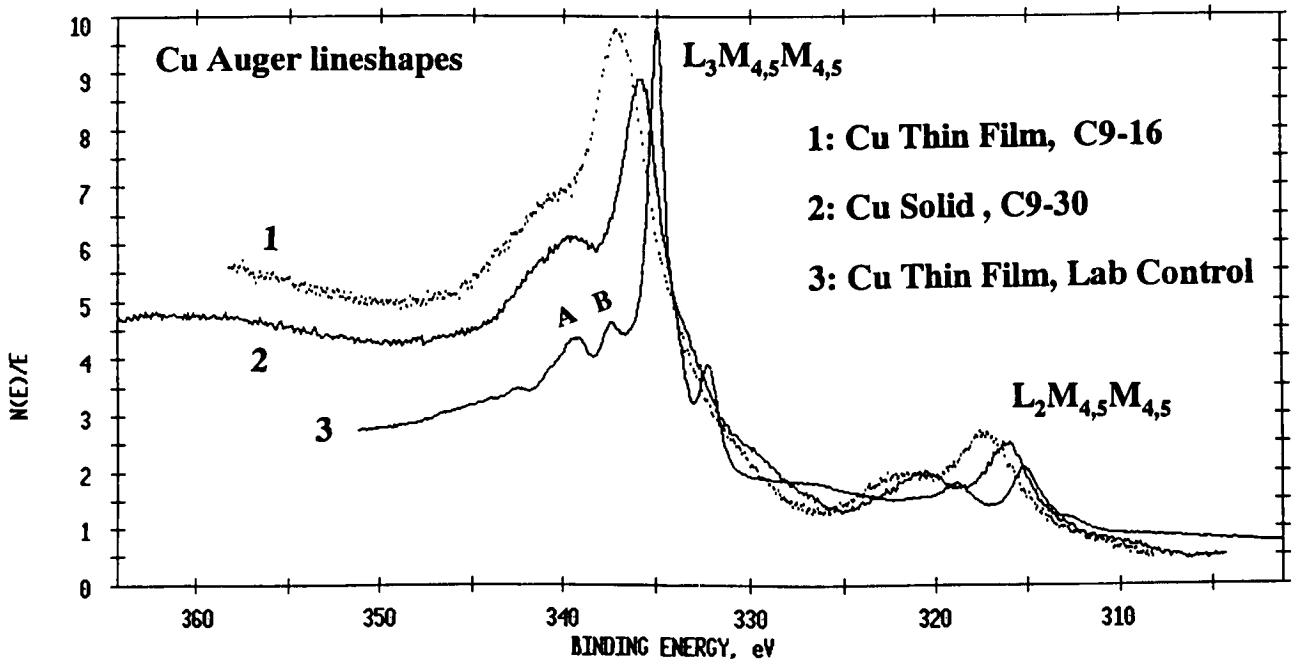

Fig. 13: Cu Auger ($L_{2,3}M_{4,5}M_{4,5}$) line-shapes of Cu thin film and solid Cu samples

N93-28285

LDEF MATERIALS DATA ANALYSIS: REPRESENTATIVE EXAMPLES

Gary Pippin and Russ Crutcher
Boeing Defense & Space Group
Seattle, WA 98124-2499
Phone:206/773-2846, Fax:206/773-4946

Part of the philosophy which guided the examination of hardware from the Long Duration Exposure Facility (LDEF) was that materials present at multiple locations should have fairly high priority for investigation. Properties of such materials were characterized as a function of exposure conditions to obtain as much data as possible for predicting performance lifetimes. This paper summarizes results from examination of several materials from interior locations of LDEF, selected measurements on silverized teflon blanket specimens, and detailed measurements on the copper grounding strap from tray D11.

Visual observations of interior locations of LDEF made during deintegration at KSC showed apparent changes in particular specimens. This inspection lead to testing of selected nylon clamps, fiberglass shims and heat shrink tubing from wire harness clamps, and visually discolored silver coated hex nuts.

Ten nylon wire support clamps were taken from a sampling of the same locations as the heat shrink tubing samples we tested, examined and compared with the condition of a virgin nylon 6/6 specimen. In general only slight changes in the properties of the space exposed nylon hardware were noted. All nylon clamps performed their function; although cracking was observed in five of the ten space exposed specimens we examined.

There was no change in the shore D hardness or the melting points of the space hardware relative to the ground control specimens. Specific heats of the space flown hardware increased by 10-20% relative to the nylon 6/6 control specimen. However, there is considerable variation in the value of specific heat of nylons so the difference may not be real.

All the space flown specimens show increased degradation products during pyrolysis gas chromatography. Infrared measurements showed peaks associated with bond rupture at amide linkages for all flight specimens, one of which also showed evidence of slight surface oxidation.

The changes observed are all indicative of some UV exposure but this is hard to quantify. These specimens likely received solar exposure for short periods of time through small gaps at the corners of the experiment trays. The slight oxidation on one individual specimen suggests that specimen was directly aligned with an opening near the leading edge. Thermal vacuum cycling also likely contributed to the crack development and embrittlement as the materials outgassed over time.

Initial inspection showed substantial discoloration on the surface of the silver coated hex nuts which held titanium clamps on the interior of the space and earth ends. Surface examination showed that this was due to a molecular contamination layer and that the silver surface was not oxidized to any significant degree. A few of the hex nuts were cross sectioned and the good condition of the hardware was confirmed.

Visual inspection of aluminum wire harness clamps, partially covered by heat shrink tubing with fiberglass shims inside, showed a distinctly different pattern along the longeron between rows 3 and 4 relative to all other locations. Around each wire harness clamp assembly on this longeron was a discolored area which appeared to be the result of outgassing from components of the wire harness clamp assembly. This pattern was not evident on any of the other longerons. Outgassing measurements from selected pieces of heat shrink tubing and shims lead to the following conclusions. Flight specimens of heat shrink tubing show total mass loss (TML) from outgassing measurements about 65-75% of the TML measured for

ground control specimens. Table 1 shows average TML and collectable volatile condensible materials (CVCM) for heat shrink tubing specimens from selected locations. These specimens were taken from a portion of the tubing directly exposed to the interior of LDEF. An additional set of measurements were made on specimens from a portion of each tubing piece facing the longeron. Each number in the table is an average of four individual measurements.

There are two populations among the space exposed specimens, leading and trailing edge locations form one group and all other locations form the second group with the lowest TML values. The CVCM values are generally lower for space exposed specimens relative to the ground specimens, and the non leading or trailing edge specimens have the lowest CVCMs. The reason for these differences is not well understood. However, the leading and trailing edges did see the most solar UV and the thermal cycling patterns varied from location to location, so indirect heating effects could have caused the differences. Another possibility is that differing amounts of intermittent direct solar UV radiation reached the clamps through gaps at the tray corners. Figures 1 and 2 show the TML and CVCM data plotted as a function of the angle from the nearest of either the leading or trailing edge.

Outgassing of a small sampling of fiberglass composite shims was measured. TML for flight specimens was 85-95% of the ground control value, with no apparent differentiation due to location.

Modeling efforts have now provided a reasonable estimate of solar fluence to each major surface of LDEF. Earlier measurements characterizing the effects of solar UV on fluorinated ethylene propylene (FEP) have been revisited. X-ray photoelectron spectroscopy (XPS) measurements were carried out on the surface of FEP films from many locations on LDEF. The carbon 1s peak heights for carbon atoms in different locations in the FEP polymer change with exposure to solar UV. This change is induced by the breaking of carbon-carbon bonds, subsequent crosslinking between polymer chains or decomposition and loss of volatile fragments, leading to a polymer of different structure than the initial FEP. While exposure to AO leads to oxidation, volatilization and recession of the UV altered material, trailing edge specimens retain the altered layer of material and allows characterization of the solar UV effects.

It is observed that increased UV exposure increases the fraction of -CF and CF_3 functional groups at the expense of the CF_2 groups along the chain. The structural changes associated with this are increased crosslinking and embrittlement of the near surface material.

Detailed measurements have been carried out on two trailing edge blankets, D01 and C05. Measurements at selected locations in protected areas, exposed areas and in the curved region of each blanket show variation in the surface properties. The UV exposure for each location in the curved region has yet to be determined.

Specimens from the leading edge show ratios essentially independent of the UV exposure. This is consistent with the removal of UV damaged material by atomic oxygen, leaving virgin FEP on the surface, particularly since the majority of the oxygen exposure occurred in the last six months of the mission, after most of the UV damage had occurred. Figures 3-4 summarize these results graphically. Figure 5 shows how the ratio varies around LDEF, with row 6 clearly a transition region from atomic oxygen dominated processes to solar UV dominated processes.

The curved transition region of each blanket between the exposed face and shielded edge provides the basis for extensive recession vs angle data. Several methods were used to determine the angle from ram of the surface as a function of distance from the shielded edge of the blanket. SEM images were obtained and the angle from ram estimated from the direction of the textured peaks. This provided angles to within about 5 degrees and allowed identification of the location on the blanket surface facing the ram direction to within 2mm. We also examined photographs of blanket edges, taken with the blankets still mounted on the flight experiments, to attempt to define the radius of curvature. A spare blanket was remounted in a tray at ESTEC in an attempt to determine the flight configuration geometry and measure the curvature of the transition region from exposed to shielded areas. To calculate recession of FEP using our AO exposure

model we assumed the radius of curvature was constant. This reproduced the experimental values to within the measurement uncertainty.

An angle bracket from the McDonnell-Douglas heat pipe experiment on tray F9 provided an exposed area of FEP mounted with a well defined orientation with respect to ram. The FEP/Ag blanket was adhesively bonded to an aluminum bracket, shown in cross section in Figure 6. The rigid aluminum established a continuous range of well defined angles from about 8°to 90° from ram. An area of the angle bracket was mounted in a potting compound, cut and polished in cross section, 100X photomicrographs were taken of the cross section all along the length of the bracket, and the thickness of the FEP layer measured directly from the photomicrograph images. The thickness of the FEP along the bracket measured in this manner agrees with results obtained using our atomic oxygen exposure model, which includes the contribution from directly impacted and scattered atomic oxygen, to within the measurement uncertainty. To determine recession rates we used a reaction efficiency of 0.34×10^{-24} cm^3/atom, independent of angle of incidence.

Figure 7 shows the thickness vs angle data. The diamond shaped individual data points are from the raised part and the convex curved portion of the bracket. The triangle shaped individual data points are from the lower part and the concave curved portion of the bracket. The decreased thickness at or near the concave region, relative to the thickness of the raised portion is attributed to enhanced atomic oxygen exposure due to indirect scattering. Figure 8 shows the thickness vs location from photomicrograph cross-sections of two specimens from the edge of the blanket on tray D11. Curved and flat refers to the way the specimens were mounted in the potting compound for cross sectioning. The two specimens gave virtually identical results.

The exposed surfaces of the copper grounding straps had a rather complex geometry. Two areas on each clamp had well defined orientations; the portion on top of the clamps holding the experiment trays and the portion along each tray lip. Each exposed clamp and tray lip were at a 15° angle from one another. Measurements of solar absorbance and thermal emittance taken on surfaces from the areas with constant, well defined exposures, are shown as functions of atomic oxygen fluence and solar exposure in figures 9 and 10, respectively. Values for ground control specimens are plotted as zero exposure. No change in emittance is observed due to either leading or trailing conditions. The absorptance values for trailing edge specimens show no change over the exposure range 7000 to 11,000 equivalent sun hours, but these values are all substantially higher than the value for the ground control. This means that net UV induced changes occurred during the first half of the mission. The changes in absorbance on the leading edge exposed copper surfaces is a strong function of atomic oxygen fluence. Preliminary examination showed the darkened surface layer to be extremely thin, but the actual thickness has not been quantified.

The copper straps were made by bonding together two strips of 3M (X-1181) adhesive backed tape. The tape is manufactured into a roll and the release paper which protected the adhesive prior to use was coated with silicone. This caused a layer of silicone to be left on the copper as the tape was removed from the roll. Figure 11 shows a cross sectional view of the D11 copper strap flight configuration. The actual strap continued underneath the FEP where it was completely shielded from the UV and AO. XPS measurements were taken at many locations along the strap.

The surface elemental composition of the strap portion shielded by the aluminum shim was essentially identical to the surface elemental composition of a ground control strap. The relative atomic oxygen flux was determined along the D11 strap by using our atomic oxygen exposure model. The curve plotted in Figure 12 shows the flux from where the strap appears from under the FEP/Ag blanket (~22mm) to past the point where it goes beneath the shim. At distances greater than ~105mm the exposed surface is the aluminum shim and bolt rather than the copper. The copper surface was directly exposed to ram oxygen around 40mm from the physical end of the copper strap. XPS shows wide variation in copper, oxygen, carbon and silicon mol fractions on the surface. Figures 13 and 14 show the copper and silicone data. Figure 15 shows a comparison of O/C XPS ratios vs. location on the strap in comparison with relative oxygen flux levels. The XPS analysis shows the mol % copper on the surface is very low for shielded regions under the FEP and shim, falls to zero for the strap portion between the tray wall and FEP, goes

through a small peak along the curved portion of the strap which passes through the ram direction, and then goes through a very large peak for the region of the strap along the edge of the clamp. This area saw enhanced atomic oxygen exposure due to scattered oxygen from the part of the clamp on the tray tip as well as direct impacts. This relatively "clean' area of the strap shows copper to be the major constituent on the surface. Examination of the silicon data shows a corresponding drop in intensity in this same area. The silicon elemental % shows two distinct patterns in the exposed portion of the strap. The area from the edge of the FEP along the tray wall and tray lip which was in view of the vent slots in the FEP blankets, showed increased mol % relative to the ground control sample and shielded part of the strap under the shim.

The exposed areas along the edge of the tray, and the tray clamp, which was directly exposed to atomic oxygen but not the potential contamination source from the blanket adhesive, showed decreased Si content relative to the ground control and covered areas of D11. Figure 15, showing a comparison of O/C surface elemental % ratio and oxygen flux as location on the strap, also supports the fact that outgassed siloxane material deposited on the lower exposed area of the clamps, increasing the % silicon and oxygen on these areas above that expected from the ground based contamination and the ambient atmosphere, respectively.

The nylon materials exhibited change consistent with some UV exposure. The heat shrink tubing and fiberglass shim flight specimens all show lower outgassing than corresponding ground control specimens. Contaminant deposits were observed on the trailing edge longeron and on the silver coated hex nuts. The heat shrink tubing space exposed specimens have two distinct populations, those from the leading and trailing edge longeron, and those from all other locations. Further differentiation would require measurements on a larger sample population.

The UV exposed FEP showed evidence of surface and near surface structural changes as measured by XPS. These changes, characteristic of bond breaking and molecular rearrangements by crosslinking between polymer chains, correspond to previous data showing embrittlement as measured by decreased elongation to failure, and lower tensile strength, with increasing UV.

Data was presented for recession due to exposure to atomic oxygen for locations with well-defined angles from ram. Related theoretical modeling work has shown that some indirect scattering by atomic oxygen is necessary to predict observed results.

The 3M X-1181 adhesive backed copper tape had a silicone coated release paper protecting the adhesive on the roll. This left a deposit of silicon on the bare copper. This deposit was enhanced in areas directly exposed to venting from the blanket interior and was reduced in areas with the greatest exposure to atomic oxygen. This implied that processes which compete with oxidation of silicones to silicates occurred and that these processes produced volatile silicon containing species which were removed. Areas with the largest fluence of oxygen had the most reduced levels of silicon, carbon, and oxygen.

The discolored, oxidized layer is extremely thin. Copper tape could be used as interconnects for solar cell arrays without the need for a protective coating. Examination of the copper straps also provided significant data on deposition of silicone based contamination.

Each of the materials discussed in this paper performed their engineering functions for the duration of the flight. Observed changes for materials on the interior were slight. UV induced changes in the FEP polymer film were considerable and did not appear to have reached equilibrium at 11000 hours. The recession data reported covers the most extensive range of angles from ram to date. This work was carried out at the direction of NASA Langley Research Center under contract NAS1-19247, as part of Boeing's responsibilities in support of the LDEF Materials Special Investigation Group.

Table 1 Outgassing Data for Heat Shrink Tubing Specimens

SPECIMEN LOCATION LONGERON BETWEEN ROWS, & BAY	TML(%)	CVCM(%)
3-4, A	0.113	0.050
3-4, B	0.130	0.069
3-4, C	0.122	0.060
8-9, B	0.137	0.051
8-9, B	0.123	0.053
5-6, B	0.100	0.049
D-8, D-E	0.103	0.050
9-10, B	0.132	0.061
9-10, F	0.113	0.047
10-11, C	0.115	0.057
Space End	0.111	0.044
2-3, E	0.136	0.061
12-1, E	0.114	0.045
Earth End	0.102	0.042
8-9, F	0.126	0.056
3-4, B	0.139	0.054
Ground Control	0.170	0.061

C-6

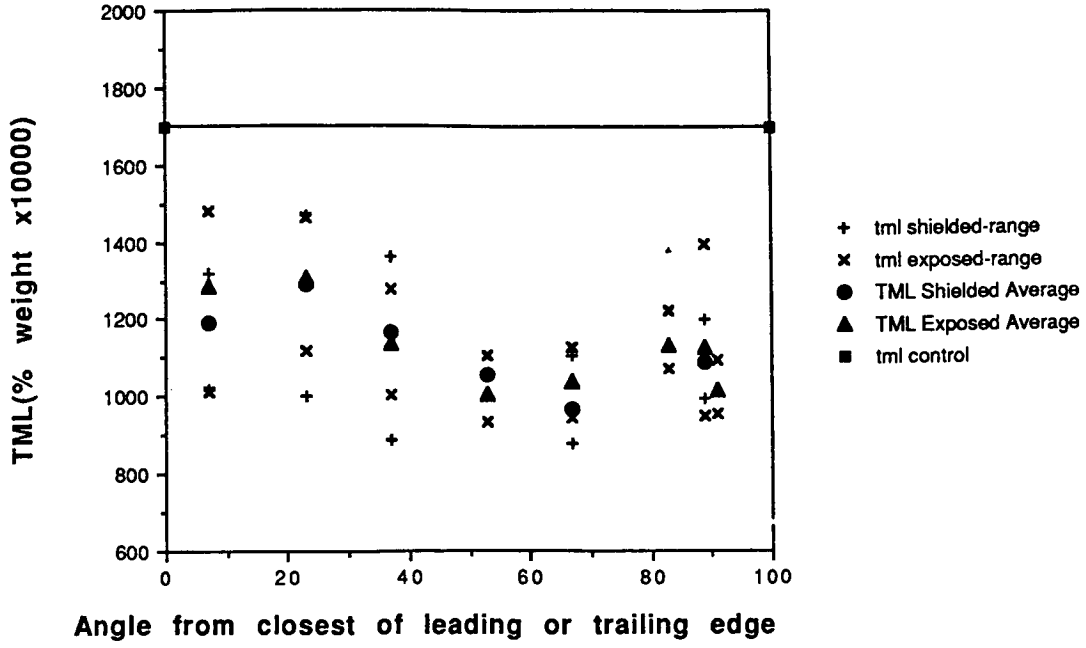

Figure 1 Total Mass Loss Outgassed from LDEF Heat Shrink Tubing Specimens

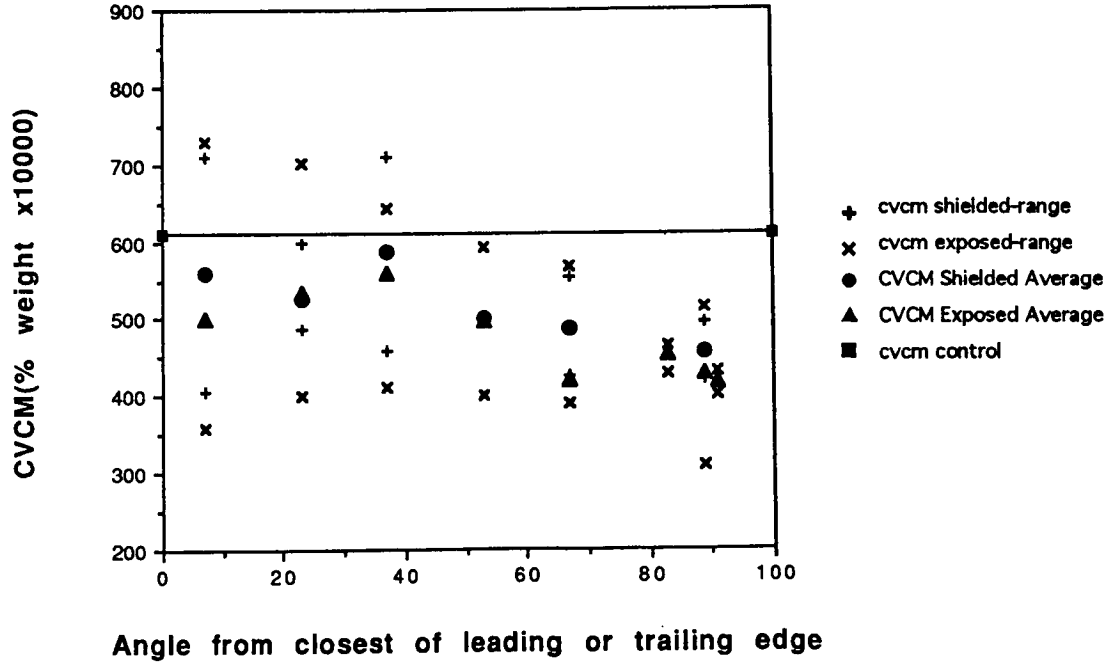

Figure 2 Collectable Volatile Condensible Materials Outgassed from LDEF Heat Shrink Tubing Specimens

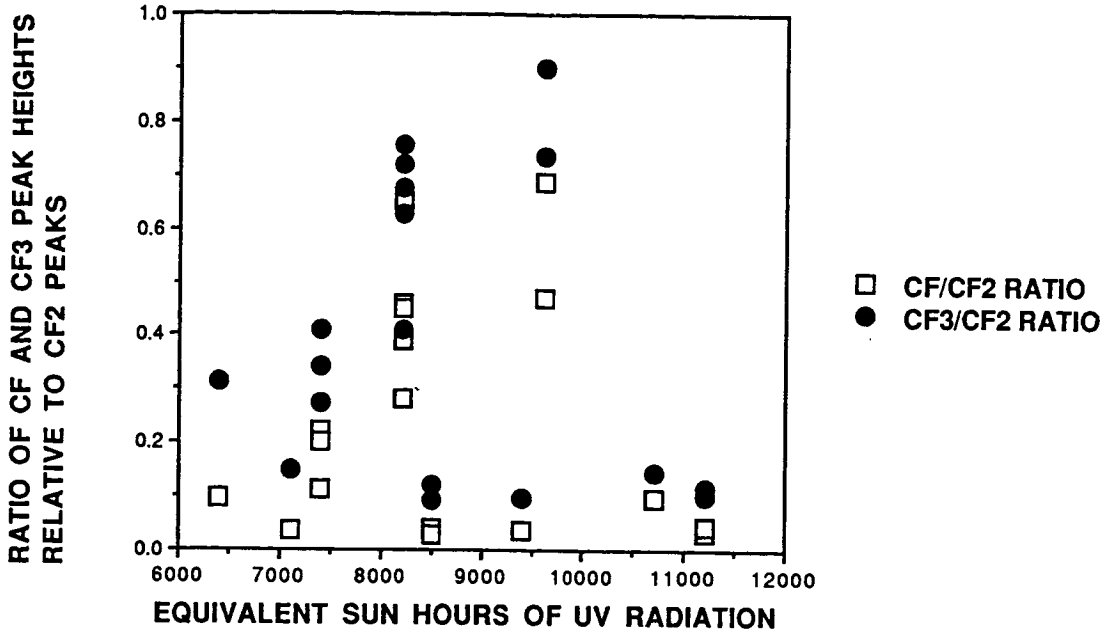

Figure 3 Structural Changes in FEP vs Solar Exposure for Silverized Teflon Blankets from LDEF

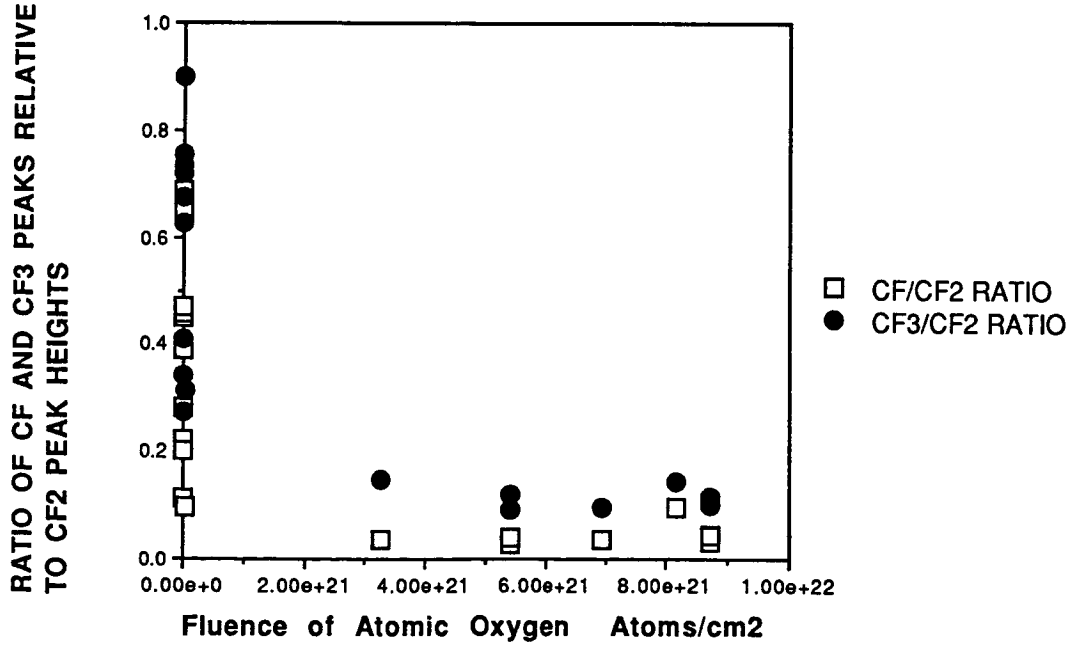

Figure 4 Structural Changes in FEP vs Atomic Oxygen Exposure for Silverized Teflon Blankets from LDEF

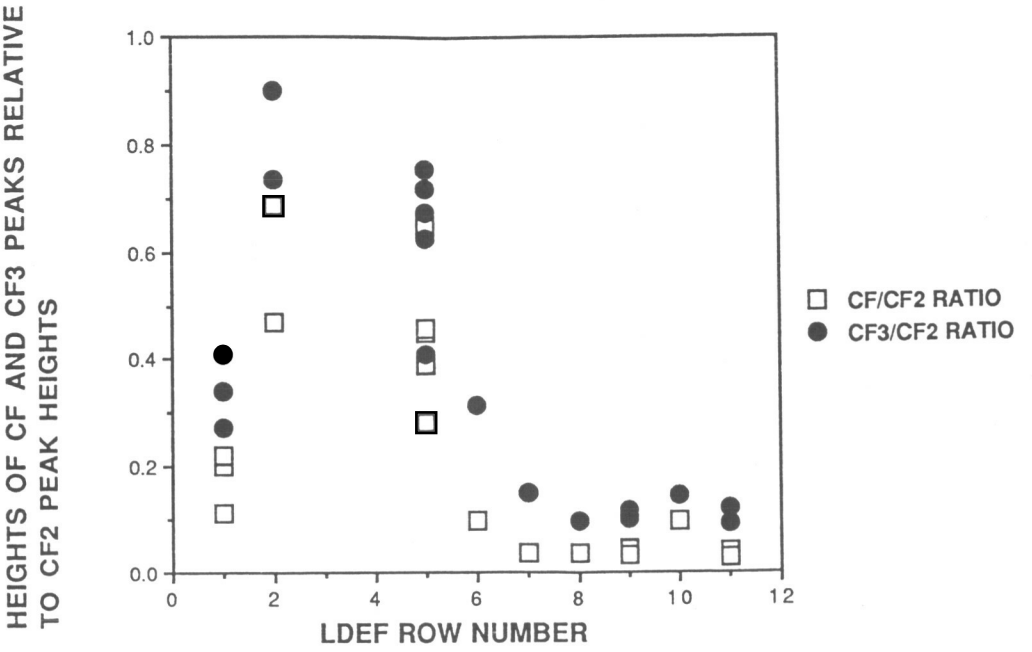

Figure 5 Evidence for Structural Changes in FEP Layer of Silverized Teflon vs Location on LDEF

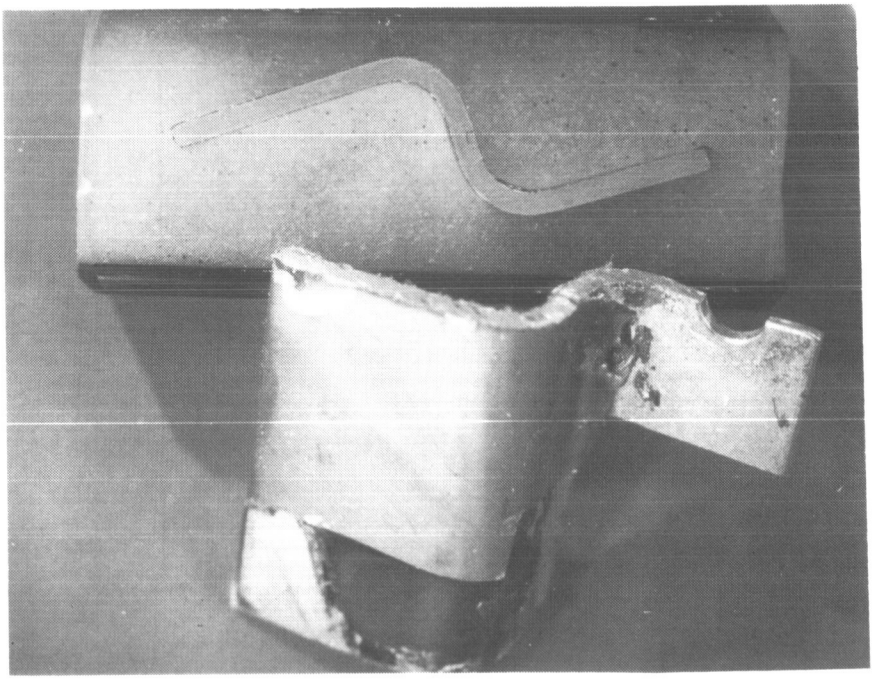

Figure 6 Photograph of Piece of Angle Bracket and Mounted Specimen for Photomicrograph Cross-Section Thickness Determination

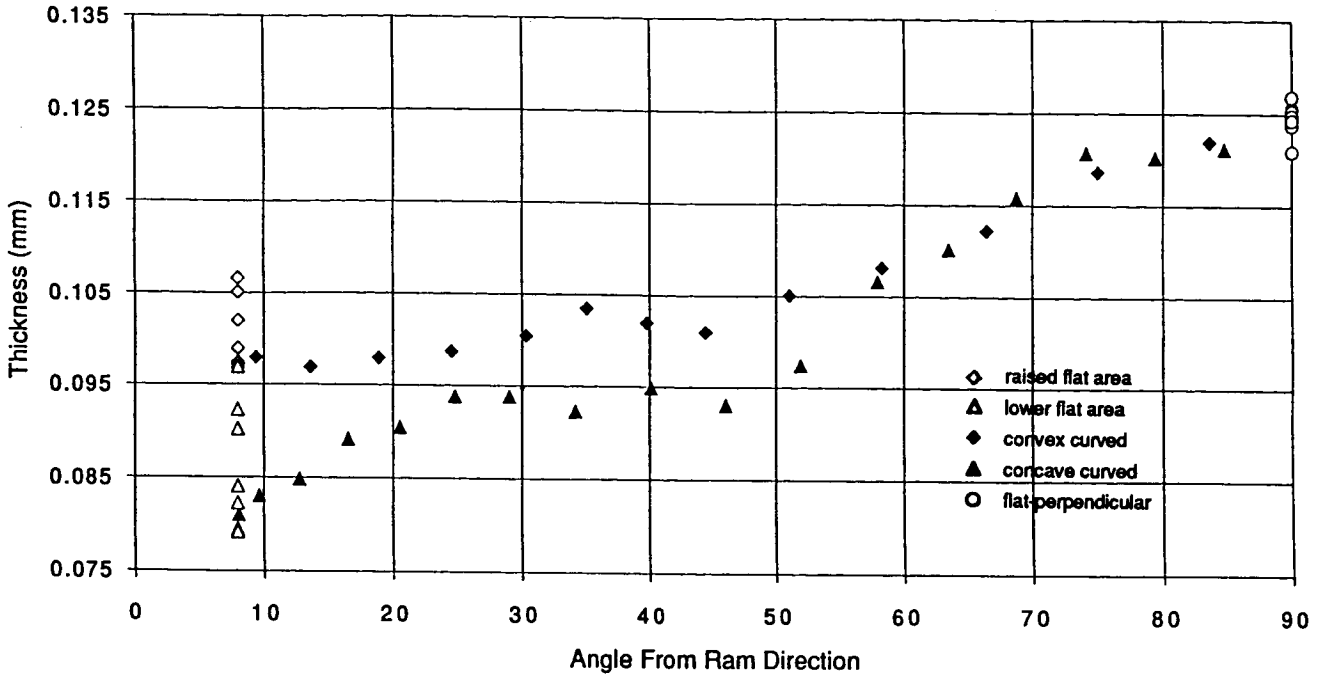

Figure 7 Erosion Rate Data for Exposed FEP from Silverized Teflon Thermal Control Blanket on Angle Bracket Mounted on LDEF Tray F9

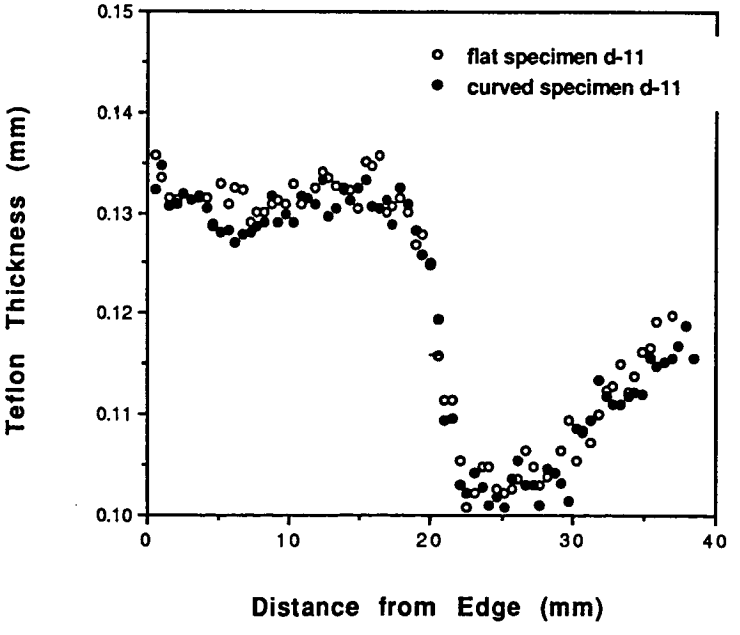

Figure 8 Atomic Oxygen Induced Erosion of FEP as a Function of Distance Along a Curved Portion(varying angle to ram) of Silverized Teflon Blanket from Tray D11

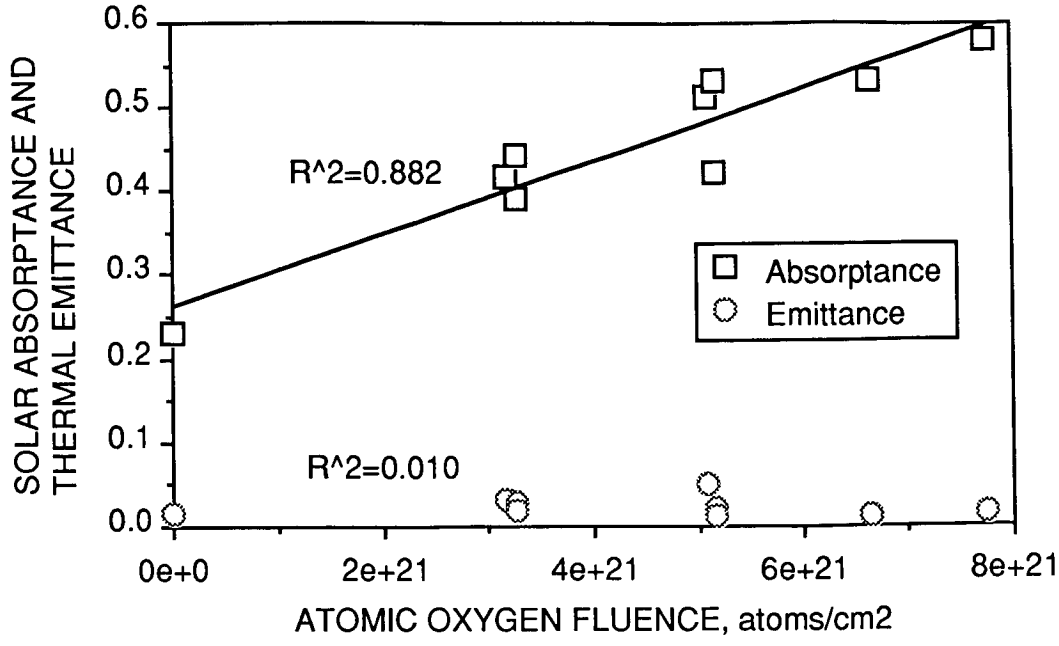

Figure 9 Optical Properties of Copper Grounding Straps from LDEF as a Function of Atomic Oxygen Exposure

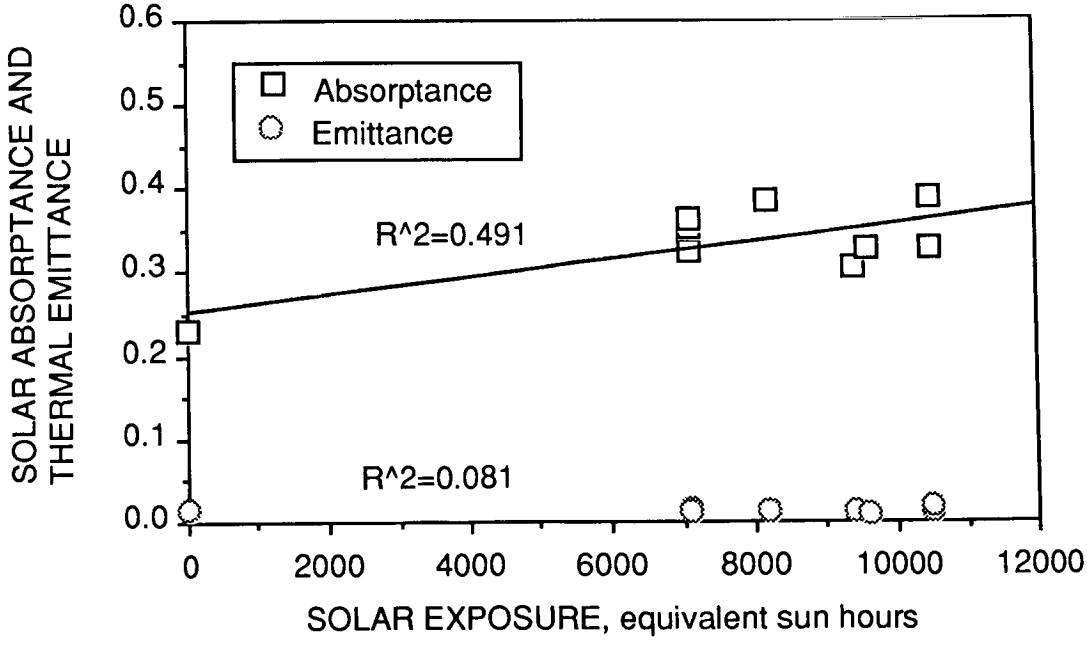

Figure 10 Optical Properties of Copper Grounding Straps from LDEF as a Function of Solar Exposure

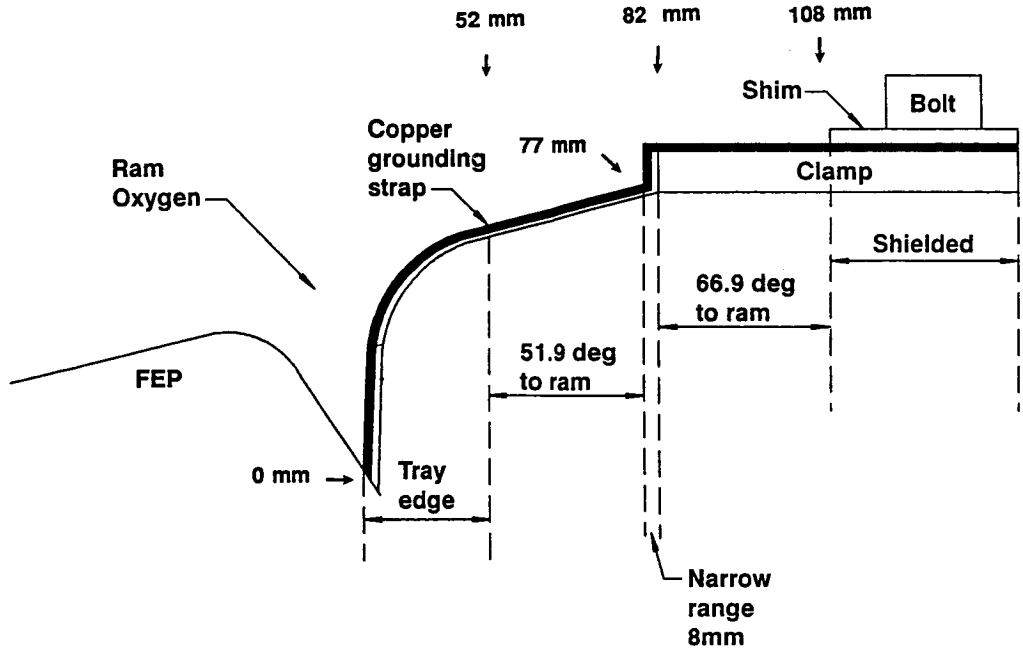

Figure 11 Cross Section View of Copper Grounding Strap, Tray D11, and Surrounding Structure

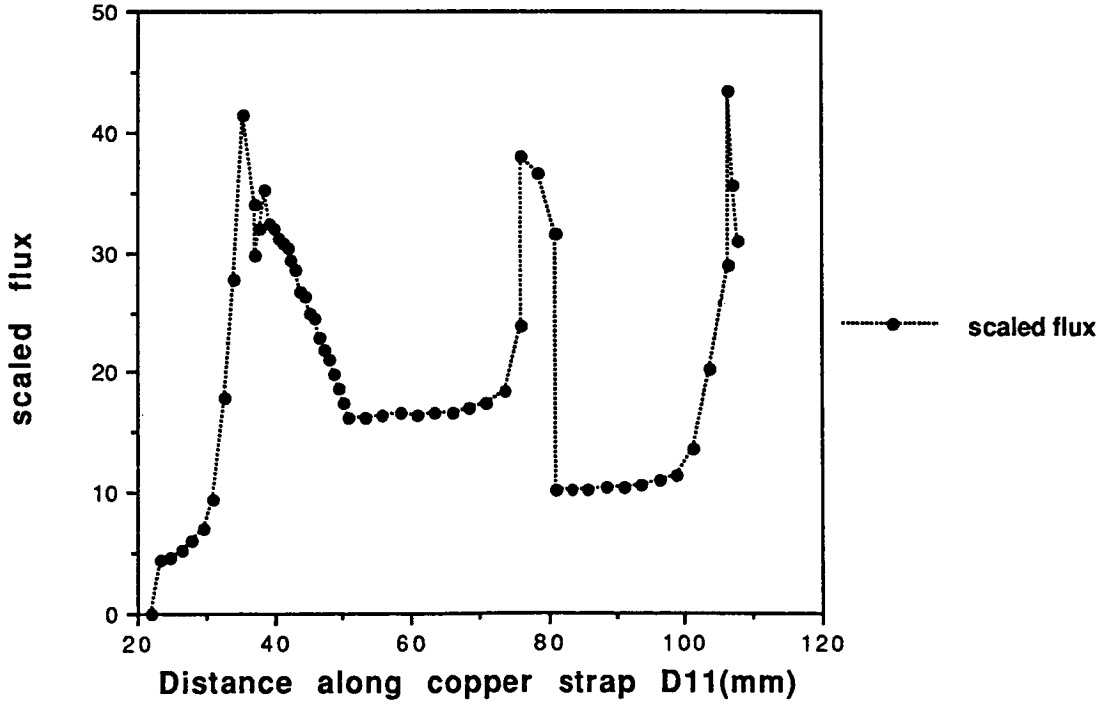

Figure 12 Relative Flux of Atomic Oxygen as a Function of Location on Copper Grounding Strap D11

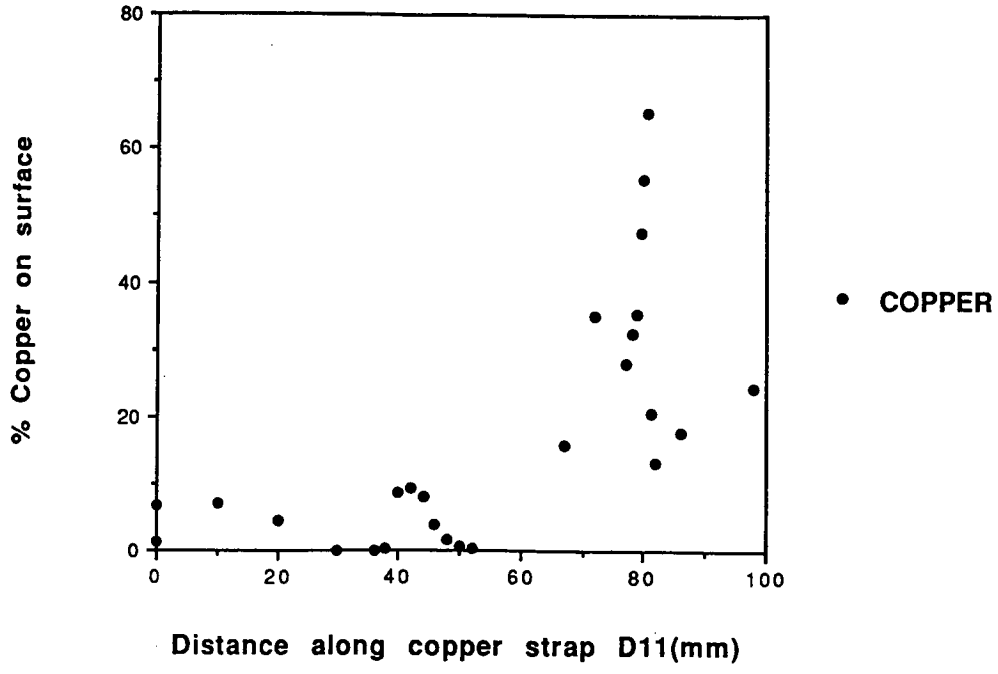

Figure 13 Copper Mol% as Measured by XPS, as a Function of Location on Surface of Copper Grounding Strap D11

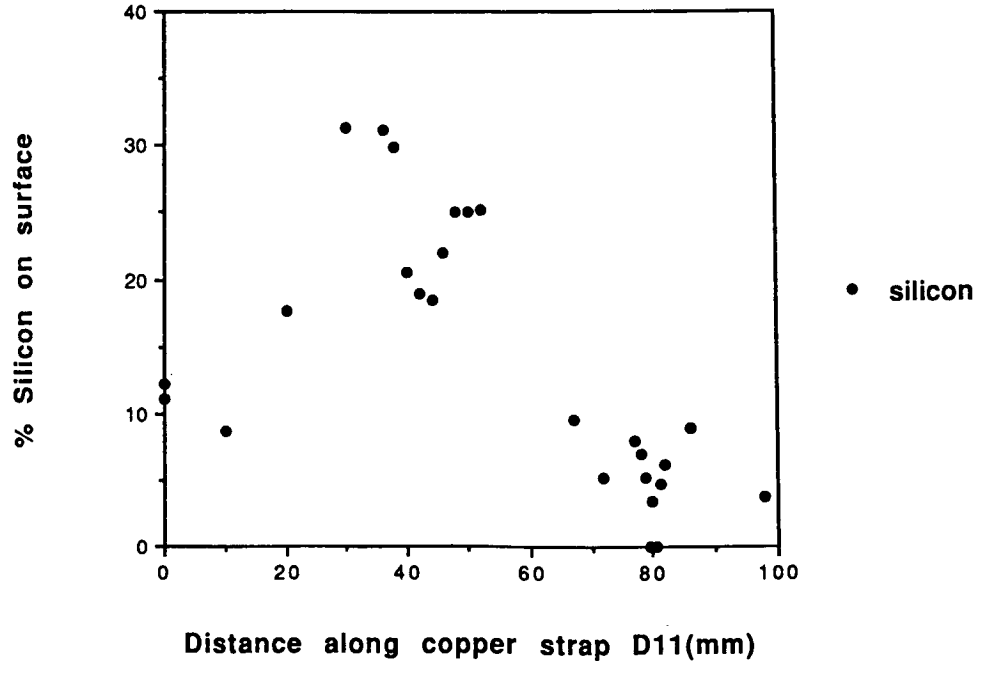

Figure 14 Silicon Mol % as Measured by XPS, as a Function of Location on Surface of Copper Grounding Strap D11

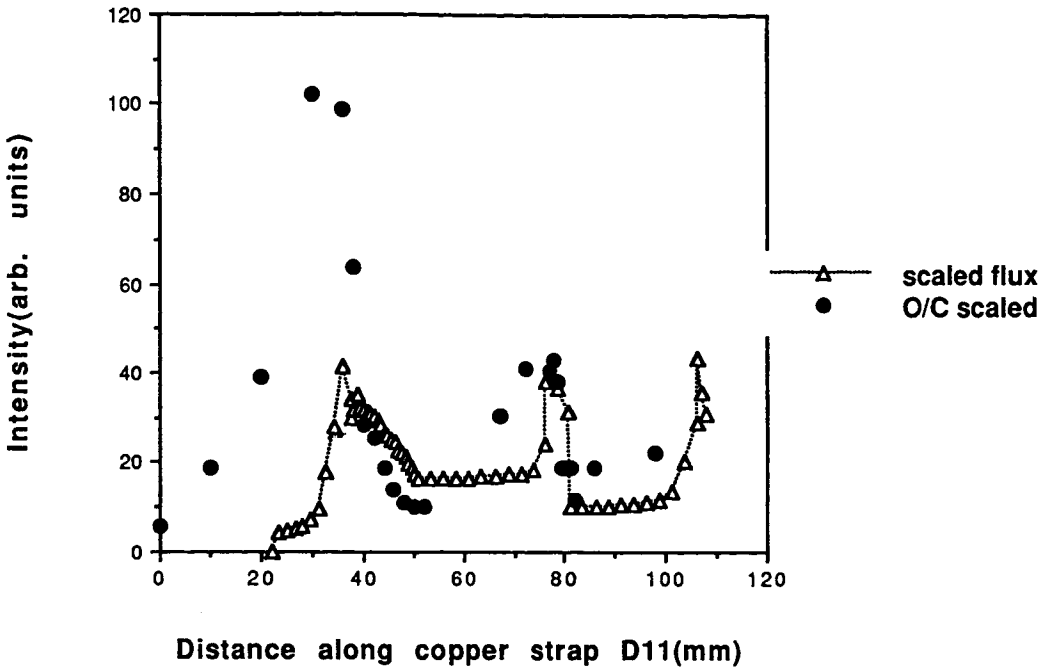

Figure 15 Comparison of Ratio of Oxygen to Carbon Mol % vs Location on Copper Strap with Atomic Oxygen Flux

data search. At the main LDEF Materials Data Base menu (fig. 3) select option 1 and the LDEF Materials Data Base Basic Data Search Criteria screen, shown in figure 6, is displayed. At this point the user may choose up to three search criteria. The first optional criteria is "1. Material Code". The material code is a five digit number that is assigned by NASA Marshall Space Flight Center to identify a specific material, part, or assembly. The material code is the primary means of linking materials in the rest of the MAPTIS. At this time the majority of the entries in the LDEF Materials Data Base have not been given material codes and are not correlated to the rest of the MAPTIS. The second optional criteria is "2. Use type". The use type defines the actual use or application of the material. Possible use types currently available are adhesive, coating/paint, composite, film, mirror/reflector, miscellaneous, structural/cover plates/clamps, and thermal control blankets. The wildcard character, %, is available for use in the use type search criteria as well as in the other search criteria screens. For example, a search on "cover%" would return all use types starting with "cover". However, a search on "%cover%" would return all use types containing "cover". The third optional criteria is "3. Designation". The designation is the manufacturers identification or name for a product. Examples of designations include Chemglaze, and T300 graphite fibers/5208 epoxy. The fourth optional criteria is "4. Composition", which is the chemical or generic name of the material. Teflon and graphite fibers/epoxy are examples of composition listings. The fifth optional criteria is "5. Designation/Composition" which searches both the designation and composition fields and returns information on the materials that meet either criteria. This search criteria is specifically designed to allow the user to find the information requested without requiring the user to know the specific designation or composition. The sixth optional criteria is "6. Specification" which allows the user to search for a specific NASA, military or commercial specification. The seventh optional search criteria is "7. Manufacturer/Supplier" which allows the user to search for a specific manufacturer. For example, by searching on "%3m% the user would get a listing of all materials manufactured by 3M Corp. that are contained in the data base. The last optional search criteria is "8. Category (metals/non-metals)". This search criteria allows the user to search on metals, non-metals or both and is frequently used in conjunction with other search criteria.

As an example of a search, suppose the user wanted to know if there were any data in the data base on a composite material made from 934 epoxy resin. A basic data search using the fifth optional criteria, designation and composition, and using "%934%" would return any entry containing 934 in the designation or composition fields. The step-by-step screens with user required inputs shaded are shown in figure 7. The output from the aforementioned search is shown in figure 8. The output shows that data from a number of composites with 934 as the resin system are contained in the data base. The user may then request more specific information on a specific 934 composite. Also included in the output is any atomic concentration data that exists in the data base as shown in figure 8. The atomic concentration data are results of X-ray photoelectron spectroscopic (XPS) analyses. The first column is the specimen location on the LDEF. The second column describes whether the specimen was coated, uncoated, covered or uncovered. The third through the ninth columns list the percentage of atomic concentration of a specific element in the first 5 nanometers of the surface. The data source or reference is noted in the last column of the table under the heading DS for data

source. In the example shown in figure 8, data from two sources, data source numbers 1032 and 1035, are listed. Currently the user is required to go to the data source option of the data base and query on the data source numbers to determine what the reference is for the atomic concentration data. In the near future the data source listed in the atomic concentration data tables will be listed at the conclusion of the query as is currently done for other data source listings. For completeness the data in the atomic concentration table are from two papers published in *LDEF Materials Workshop '91*, NASA Conference Publication 3162. Data source 1032 is reference 4 and data source 1035 is reference 5.

Specific Property Searches

Options 2, and 4 through 7 of the main LDEF Materials Data Base menu(fig. 3) all deal with properties of the material and all have the same search criteria. The search criteria screen for these options is shown in figure 9. Options 1 through 8 have been previously described in the basic data search criteria. Option "9. Location" allows the user to search by specific location on the LDEF. For example if the user was interested in the leading edge only, the user could search on the location row 9 and would input "%9%" at the location prompt. Option "10. Experiment Number" allows the user to search on up to three specific experiment numbers. Option "11. E (eV) Value" allows the user to search on materials which meet a given range of energy of atomic oxygen. Options "12. Est. Sun Hours", "13. AO Flux Values", and "14. Angle of Incidence Values" also allow the user to search on a range of numerical values. In this case the values are estimated sun hours, atomic oxygen flux, and angle of incidence of the atomic oxygen, respectively. The last option, "15. Data Sources" is discussed in the next section.

As an example, suppose the user wants to search on all of the absorptivity data on T300/934 composites that received more than 9E13 atoms/cm^{2}s of atomic oxygen. The user would select option number "7B" from the main LDEF Materials Data Base menu which specifies absorptivity data as shown in figure 10. Then the user would select options "5,13" from the LDEF Materials Data Base search criteria menu. At the designation/composition screen the user would be prompted to enter "%T300%934%". The user would then been prompted to enter the values of atomic oxygen required. In this example, the user would then enter ">" and "9E13". The data base then would return the output shown in figure 11. The atomic concentration data was discussed in the previous section. Two data sets are listed. Both are from the same location, experiment and data source. The output lists the test apparatus used to conduct the test, the pre- and post-flight measurements and , in this case, the side of the material being measured. Immediately following the data listing is a list of the data source. The data source output correlates the data with the title, and author(s) of the published paper containing the original data. Currently all data in the data base are from a published paper. However, in the future, the data base will contain unpublished data which will be correlated by primary facility and principal investigator(s).

Data Source Searches

The last type of search available from the main LDEF Materials Data Base screen

is the data sources search. Option "3. Data Sources" from the main screen allows the user to search by data source number, primary facility, author or document title. For example, if the user wanted to know all the papers from which data were extracted for the data base by a specific author, the user would follow the steps shown in figure 12. First, option "3. Data Sources" would be chosen from the main screen. Second, since the user wanted to know about data sources written by a specific author, the user would choose option "3. Author or Secondary Facility" from the LDEF Materials Data Base Data Source Search Criteria. At the prompt the user would input the author's name. Using the wildcard character in front and behind the author's name, for example "%pippin%" assures that all data sources containing the author's name will be listed. The output from this search is shown in figure 13.

CHANGES TO THE LDEF MATERIALS DATA BASE

As stated in the introduction of this paper, the LDEF Materials Data Base is a preliminary version of this data base. The data base has and will continue to change and grow as more information becomes available. During the Second LDEF Post-Retrieval Symposium, a group of industry and government advisors met. This advisory group, called the LDEF Materials Data Base Format Committee, was given the goal of critiquing the initial format and content of the data base to ensure that it would develop into a valuable tool for both the space researcher and the spacecraft designer. A listing of the committee members is shown in figure 14. The committee's input has guided the changes that the data base is currently undergoing. These changes include adding atomic oxygen fluence data and in general, adding features to aid the novice user.

ACCESS TO THE DATA BASE

As previously stated, the LDEF Materials Data Base is a part of the MAPTIS. For those parties interested in accessing the LDEF Materials Data Base and thus MAPTIS, a form, figure 15, is included in this paper. By filling out the form and returning it to the fax number listed on the bottom of the form, the requestor will be given a user identification name and password to the MAPTIS. Users are requested to send their comments and suggestions to the people listed on the LDEF Materials Data Base attention screen which is displayed each time a user accesses the data base.

ADDITIONS TO THE DATA BASE

The developers of the LDEF Materials Data Base are currently acquiring additional data to incorporate into the data base. One of the purposes of the LDEF Materials Data Base is to collect and disseminate unpublished data so that valuable LDEF data will not be lost to future designers and researchers. Researchers having data they would like to have incorporated into the LDEF Materials Data Base are asked to contact the first author of this paper.

CONCLUDING REMARKS

The Materials Special Investigation Group of LDEF has developed the LDEF Materials Data Base on MAPTIS. The LDEF Materials Data Base is an electronic data base which users can access remotely. Although preliminary in nature, the LDEF Materials Data Base is designed to eventually contain the vast quantity of materials data generated from the 5.8-year flight of the Long Duration Exposure Facility.

REFERENCES

1. Stein, Bland A.: "An Interim Overview of LDEF Materials Findings", NASA TM-107664, August 1992.

2. Levine, Arlene S.: *LDEF- 69 Months In Space: First Post-Retrieval Symposium*, NASA CP-3134, June 1991.

3. User and Operations Guide For the Marshall Space Flight Center Materials and Processes Technical Information System (MAPTIS), available from NASA- MSFC, Mail Code EH02, Huntsville, AL 35812, Jan. 1992.

4. Young, Philip R.; and Slemp, Wayne S.: "Characterization of Selected LDEF-Exposed Polymeric Films and Resins," *LDEF Materials Workshop '91*, NASA CP-3162, Part 1, Nov. 19-22, 1991.

5. Tennyson, R. C. : "Additional Results On Space Environmental Effects on Polymer Matrix Composites- Experiment AO180", *LDEF Materials Workshop '91*, NASA CP-3162, Part 2, Nov. 19-22, 1991, pp. 571-592.

CHOICE: _____ MAPTIS - MAIN MENU Page 1 of 2
PRESS RETURN FOR NEXT PAGE

1. MECHANICAL/PHYSICAL PROPERTIES
   A. Metals
   B. Nonmetals
   C. Acoustics
   D. Atomic Oxygen
   D. Atomic Oxygen
   E. Magnetic Materials
   F. High Temperature
   G. Bondline Information System
   H. Nozzles Materials

2. MATERIAL SELECTION
   A. Metals (MSFC-SPEC-522, etc)
   B. Nonmetals (NHB 8060.1, etc)
   C. Standard/Commercial Parts

3. VERIFICATION & CONTROL
   A. MUA - Mtrl Usage Agreements
   B. Foreign Alloy Cross Reference
   C. MIUL - Mtrl Id and Usage List
   D. Intercenter Agreement Cert. Letter
   D. Intercenter Agreement Cert. Letters

4. LONG DURATION EXPOSURE FACILITY DATA
   A. Overview
   B. Materials SIG Data

5. FAILURE ANALYSIS

6. (NOET) INFORMATION SYSTEM (NSI)
   A. Replacement Technology
   B. Propulsion Technology (TBD)

CHOICE: ENTER NUMBER & ALPHA (1C GETS THE ACOUSTICS DATABASE)
FOR HELP: ENTER H PRIOR TO CHOICE (H1C GETS HELP FOR ACOUSTICS DATABASE)
NOTE: ENTER DO FOR LIST OF STANDARD MENU OPTIONS

CHOICE: _____ MAPTIS - MAIN MENU Page 2 of 2
PRESS RETURN FOR PREVIOUS PAGE

7. MANAGEMENT SYSTEMS FOR PROJECTS
   A. SSF - Space Station Freedom II
   B. NLS - National Launch System

8. SPECIFICATIONS AND STANDARDS

9. ADMINISTRATIVE
   A. MSFC Form 512.5
   B. MSFC Form 424

CHOICE: ENTER NUMBER & ALPHA (1C GETS THE ACOUSTICS DATABASE)
FOR HELP: ENTER H PRIOR TO CHOICE (H1C GETS HELP FOR ACOUSTICS DATABASE)
NOTE: ENTER DO FOR LIST OF STANDARD MENU OPTIONS

Figure 1. MAPTIS main screens.

CHOICE: _____ MAPTIS - STANDARD MENU OPTIONS

OPTION	ACTION
0 /PM	Previous Menu
97/MM	Main Menu
98/CM	Change menu display from full to brief or brief to full.
99/LO	Log off the MAPTIS VAX
AM	Activate the Action Menu
BB	Display Bulletin Board
BO	Toggle between running queries online (default) & batch.
CF	Toggle report format between 132 (default) & 80.
CU	Toggle report unit of measure between standard (def) & metric
CQ	Change action mode to Canned Query.
DF	Display report format selection.
TIME	Display the Date and Time
PHONE	Activate the VAX Phone Utility
MAIL	Activate the VAX Mail Utility

OPTION	ACTION
DO	Display this list of menu options
DU	Display report unit of measure selection.
ID	Change your Query ID
PW	Allow user to change their VAX Password.
SF	Activate System Functions Menu

**NOTE: FOR NONMETALS MATERIAL SELECTION TEST REPORT DATA QUERIES ONLY

EXPERT	Turns off NOVICE Function
NOVICE	Automatic material count/screen at time scroll
MC	Material count prior to query report generation
SS	Scroll query report screen at a time
DN	Display NOVICE Functions

Figure 2. Standard menu options for MAPTIS.

CHOICE: _____ MAPTIS - LDEF MATERIALS DATABASE

1. Basic Data
2. All Data
3. Data Sources

4. Electrical Properties
   A. Surface Resistance

5. Mechanical Properties
   A. All Mechanical Properties
   B. Elastic Modulus
   C. Tensile Strength
   D. Hardness
   E. Maximum Load
   F. Shear
   G. Flexural
   I. Compression Strength
   J. Load Deflection

6. General Properties
   A. All General Properties
   B. Change in Mass
   C. Change in Thickness
   D. Optical Density
   E. Surface Roughness
   F. Glass Transition Temperature
   G. VCM

7. Optical/Thermal Properties
   A. All Optical/Thermal Properties
   B. Absorptivity
   C. Emissivity
   D. Absorptivity/ Emissivity
   E. Reflectance
   F. Transmittance
   G. Coeff. Thermal Expansion

CHOICE: ENTER UP TO 3 CHOICES DELIMIT WITH A COMMA (5C,6A,7D)
FOR HELP: ENTER H FOR GENERAL HELP OR H AND CHOICE FOR MORE SPECIFIC HELP (H7B)
NOTE: ENTER DO TO LIST STANDARD MENU OPTIONS

Figure 3. The LDEF Materials Data Base main menu screen.

MAPTIS - LDEF MATERIALS DATA BASE GENERAL HELP

VCM - this data found in the data base is defined as Volatile Condensible Materials according to the paper(s) from which the data has been taken.

When a query is run on the system, any data that is available that meets your search criteria will scroll across the screen as it is being retrieved and when the query is complete, you will receive a "Query Complete" message. If you receive a "Query Complete" message without seeing any data, this means that there is no data currently in the system that meets your given search criteria.

The convention used for naming and describing all composites in this data base is fibers first, followed by matrix material (example: GY70 graphite fibers/934 epoxy, SP288 graphite fibers/V108 epoxy, etc...)

In this data base and throughout MAPTIS, Designation refers to the manufacturer's designation or name for a given material or the commonly refered to trade name (i.e., KAPTON, GY70 graphite fibers, etc...). Composition refers to the "generic" composition of a given material (i.e., polyimide, graphite, PTFE, FEP, etc...).

PRESS RETURN TO CONTINUE:

Figure 4. The LDEF Materials Data Base general help screen.

MAPTIS - LDEF MATERIALS DATABASE HELP

BASIC DATA - is the general information about the material being returned.

This data includes:

MATERIAL CODE	- NASA assigned material identifier
DESIGNATION	- Manufacturers' product identification
COMPOSITION	- Generic material makeup
USE TEMPERATURE	- Recommended temperature range for the product
USE TYPE	- Generic use of the material *Example: Adhesive, Coating
REMARKS	- Other information relating to the material
SPECIFICATION	- Specifications pertaining to the material
MANUFACTURER/ SUPPLIER	- Company that makes and/or supplies the material
ADDRESS	- Address of manufacturer/supplier

ATOMIC CONCENTRATION data will also be provided when available.

NOTE: BASIC DATA will be slightly different for metallic materials.

Figure 5. The LDEF Materials Data Base basic data help screen.

CHOICE: _____ LDEF MATERIALS DATABASE BASIC DATA SEARCH CRITERIA

1. Material Code
2. Use Type
3. Designation
4. Composition
5. Designation / Composition
6. Specification
7. Manufacturer / Supplier
8. Category (metals / non-metals)

CHOICE: ENTER UP TO 3 SEARCH CRITERIAS DELIMIT WITH A COMMA (2,5,6)
FOR HELP: ENTER H PRIOR TO ANY CHOICE (H1 GETS HELP ON DESIGNATION)
NOTE: ENTER DO TO LIST STANDARD MENU OPTIONS

Figure 6. The LDEF Materials Data Base basic data search screen.

CHOICE: 1 MAPTIS - LDEF MATERIALS DATABASE

1. Basic Data
2. All Data
3. Data Sources

4. Electrical Properties
   A. Surface Resistance

5. Mechanical Properties
   A. All Mechanical Properties
   B. Elastic Modulus
   C. Tensile Strength
   D. Hardness
   E. Maximum Load
   F. Shear
   G. Flexural
   I. Compression Strength
   J. Load Deflection

6. General Properties
   A. All General Properties
   B. Change in Mass
   C. Change in Thickness
   D. Optical Density
   E. Surface Roughness
   F. Glass Transition Temperature
   G. VCM

7. Optical/Thermal Properties
   A. All Optical/Thermal Properties
   B. Absorptivity
   C. Emissivity
   D. Absorptivity/ Emissivity
   E. Reflectance
   F. Transmittance
   G. Coeff. Thermal Expansion

CHOICE: ENTER UP TO 3 CHOICES DELIMIT WITH A COMMA (5C,6A,7D)
FOR HELP: ENTER H FOR GENERAL HELP OR H AND CHOICE FOR MORE SPECIFIC HELP (H7B)
NOTE: ENTER DO TO LIST STANDARD MENU OPTIONS

CHOICE: 5 LDEF MATERIALS DATABASE BASIC DATA SEARCH CRITERIA

1. Material Code
2. Use Type
3. Designation
4. Composition
5. Designation / Composition
6. Specification
7. Manufacturer / Supplier
8. Category (metals / non-metals)

CHOICE: ENTER UP TO 3 SEARCH CRITERIAS DELIMIT WITH A COMMA (2,5,6)
FOR HELP: ENTER H PRIOR TO ANY CHOICE (H1 GETS HELP ON DESIGNATION)
NOTE: ENTER DO TO LIST STANDARD MENU OPTIONS

Enter up to three designations

You must supply all wildcards (%). Enter <CR> to terminate entry.

%934% KEVLAR%

MYLAR%

%ALUMINUM%

Figure 7. Example input for basic data search on 934 resin system.

```
                    PROCESSING YOUR QUERY


          IF YOU MUST EXIT QUERY BEFORE IT HAS FINISHED PROCESSING

          PRESS CTRL & C KEYS SIMULTANEOUS ONE TIME (MAY TAKE FEW SECONDS)


          CTRL-Y(s) AND MULTIPLE CTRL-Cs WILL BACK YOU UP TO SOME
          PREVIOUS MENU AND MAY POSSIBLY LOG YOU OFF THE SYSTEM IF
          TOO MANY ARE ENTERED.

*************** MAPTIS - LDEF MATERIALS DATABASE *******************************

MATERIAL CODE:

     USE TYPE:  COMPOSITE

  DESIGNATION:  HMS 934

  COMPOSITION:  GRAPHITE FIBERS/EPOXY

 USE TEMP MIN:                  USE TEMP MAX:

      REMARKS:

SPECIFICATION:

*************** MAPTIS - LDEF MATERIALS DATABASE *******************************

MATERIAL CODE:
     USE TYPE:  COMPOSITE

  DESIGNATION:  P75S/934

  COMPOSITION:  GRAPHITE FIBERS/EPOXY

 USE TEMP MIN:                  USE TEMP MAX:


*************** MAPTIS - LDEF MATERIALS DATABASE *******************************

MATERIAL CODE:

     USE TYPE:  COMPOSITE

  DESIGNATION:  ALUMINUM HONEYCOMB (4.40 AG5) WITH CFRP FACE SHEETS OF GY70
                FIBERS/934 EPOXY, AND BSL 312 BOND FILM

  COMPOSITION:  ALUMINUM 4.40 AG5, FIBER/EPOXY, AND  OND FILM

 USE TEMP MIN:                  USE TEMP MAX:

      REMARKS:

SPECIFICATION:


*************** MAPTIS - LDEF MATERIALS DATABASE *******************************

MATERIAL CODE:

     USE TYPE:  COMPOSITE

  DESIGNATION:  GY70 FIBERS/934 EPOXY, UNIDIRECTIONAL, RECTANGULAR TUBE

  COMPOSITION:  FIBERS/EPOXY

 USE TEMP MIN:                  USE TEMP MAX:

      REMARKS:


SPECIFICATION:
```

Figure 8. Screen output for basic data search on 934 resin.

```
*************** MAPTIS - LDEF MATERIALS DATABASE *********************************

MATERIAL CODE:
     USE TYPE:  COMPOSITE
  DESIGNATION:  GY70 FIBERS/934 EPOXY, UNIDIRECTIONAL
  COMPOSITION:  FIBER/EPOXY
 USE TEMP MIN:                    USE TEMP MAX:
      REMARKS:

SPECIFICATION:


     SUPPLIER:  FIBERITE
     DIVISION:
      ADDRESS:
         CITY:       STATE:      COUNTRY:

*************** MAPTIS - LDEF MATERIALS DATABASE *********************************

MATERIAL CODE:
     USE TYPE:  COMPOSITE
  DESIGNATION:
  COMPOSITION:  T300 GRAPHITE/934 EPOXY
 USE TEMP MIN:                    USE TEMP MAX:
      REMARKS:

SPECIFICATION:


ATOMIC CONCENTRATION DATA

LOCATION             MATERIAL SIDE        C    CL   CU   F    NA   O    SI   DS
-------------------- -------------------- ---- ---- ---- ---- ---- ---- ---- ---
B9                   EXPOSED SIDE,NO COAT 54.3                      33.0 7.5  1032
B9                   COVERED SIDE,NO COAT 62.8                 2.0  1.7  24.8 3.4  1032
B9                   EXPOSED SIDE,COATED  28.9                      47.6 11.8 1032
B9                   COVERED SIDE, COATED 65.1                      29.7 2.4  1032
D12, #1              EXPOSED SIDE         49.7                 0.5  34.0 13.0 1035
D12, #1              UNEXPOSED SIDE       66.1                 0.40 23.3 3.60 1035
D12, #2              EXPOSED SIDE         52.7                 1.70 32.1 11.8 1035
D12, #2              UNEXPOSED SIDE       64.5                 0.50 25.7 4.30 1035

Query complete - press return to continue:
```

Figure 8 (concluded). Screen output for basic data search on 934 resin.

CHOICE: _____ LDEF MATERIALS DATABASE ALL DATA SEARCH CRITERIA

1. Material Code
2. Use Type
3. Designation
4. Composition
5. Designation / Composition
6. Specification
7. Manufacturer / Supplier
8. Category (metals / non-metals)
9. Location
10. Experiment Number
11. E (eV) value
12. Est. Sun Hours
13. AO Flux value
14. Angle of Incidence value
15. DATA SOURCES
    A. Data Source Number
    B. Primary Facility
    C. Author or Secondary Facility
    D. Document Title

CHOICE: ENTER UP TO 3 SEARCH CRITERIAS DELIMIT WITH A COMMA (2,5,6)
FOR HELP: ENTER H PRIOR TO ANY CHOICE (H1 GETS HELP ON DESIGNATION)
NOTE: ENTER DO TO LIST STANDARD MENU OPTIONS

Figure 9. The LDEF Materials Data Base all data search screen.

CHOICE: 7B

MAPTIS - LDEF MATERIALS DATABASE

1. Basic Data
2. All Data
3. Data Sources

4. Electrical Properties
   A. Surface Resistance

5. Mechanical Properties
   A. All Mechanical Properties
   B. Elastic Modulus
   C. Tensile Strength
   D. Hardness
   E. Maximum Load
   F. Shear
   G. Flexural
   I. Compression Strength
   J. Load Deflection

6. General Properties
   A. All General Properties
   B. Change in Mass
   C. Change in Thickness
   D. Optical Density
   E. Surface Roughness
   F. Glass Transition Temperature
   G. VCM

7. Optical/Thermal Properties
   A. All Optical/Thermal Properties
   B. Absorptivity
   C. Emissivity
   D. Absorptivity/ Emissivity
   E. Reflectance
   F. Transmittance
   G. Coeff. Thermal Expansion

CHOICE: ENTER UP TO 3 CHOICES DELIMIT WITH A COMMA (5C,6A,7D)
FOR HELP: ENTER H FOR GENERAL HELP OR H AND CHOICE FOR MORE SPECIFIC HELP (H7B)
NOTE: ENTER DO TO LIST STANDARD MENU OPTIONS

CHOICE: 5, 13

LDEF MATERIALS DATABASE ALL DATA SEARCH CRITERIA

1. Material Code
2. Use Type
3. Designation
4. Composition
5. Designation / Composition
6. Specification
7. Manufacturer / Supplier
8. Category (metals / non-metals)
9. Location
10. Experiment Number
11. E (eV) value
12. Est. Sun Hours
13. AO Flux value
14. Angle of Incidence value
15. DATA SOURCES
    A. Data Source Number
    B. Primary Facility
    C. Author or Secondary Facility
    D. Document Title

CHOICE: ENTER UP TO 3 SEARCH CRITERIAS DELIMIT WITH A COMMA (2,5,6)
FOR HELP: ENTER H PRIOR TO ANY CHOICE (H1 GETS HELP ON DESIGNATION)
NOTE: ENTER DO TO LIST STANDARD MENU OPTIONS

Enter up to three designations

You must supply all wildcards (%).

%T300%934%

Enter <CR> to terminate entry.

KEVLAR%

MYLAR%

%ALUMINUM%

Do you want the value in AO Flux to be (=, NOT=, <, <=, >, >=)

>

Enter value for AO Flux

9E13 (atom/sq.cm*s)

Figure 10. Input screens for example search for absorptivity data on T300/934 exposed to atomic oxygen flux greater than 9E13 atoms/cm^{2}s.

PROCESSING YOUR QUERY

IF YOU MUST EXIT QUERY BEFORE IT HAS FINISHED PROCESSING

PRESS CTRL & C KEYS SIMULTANEOUS ONE TIME (MAY TAKE FEW SECONDS)

CTRL-Y(s) AND MULTIPLE CTRL-Cs WILL BACK YOU UP TO SOME PREVIOUS MENU AND MAY POSSIBLY LOG YOU OFF THE SYSTEM IF TOO MANY ARE ENTERED.

******* MAPTIS - LDEF MATERIALS DATABASE ********** 31-AUG-92

MATERIAL CODE:
USE TYPE: COMPOSITE
MANUF DESIGNATION:
COMPOSITION: T300 GRAPHITE/934 EPOXY
USE TEMP MIN: USE TEMP MAX:
REMARKS:
SPECIFICATION:

MANUF/SUPP:
DIVISION:
ADDRESS:
CITY: STATE:
COUNTRY:

ATOMIC CONCENTRATION DATA

LOCATION	MATERIAL SIDE	C	CL	CU	F	NA	O	SI	DS #
B9	EXPOSED SIDE,NO COAT	54.3					33.0	7.5	1032
B9	COVERED SIDE,NO COAT	62.8			2.0	1.7	24.8	3.4	1032
B9	EXPOSED SIDE,COATED	28.9					47.6	11.8	1032
B9	COVERED SIDE, COATED	65.1					29.7	2.4	1032
D12, #1	EXPOSED SIDE	49.7				0.5	34.0	13.0	1035
D12, #1	UNEXPOSED SIDE	66.1				0.40	23.3	3.60	1035
D12, #2	EXPOSED SIDE	52.7				1.70	32.1	11.8	1035
D12, #2	UNEXPOSED SIDE	64.5				0.50	25.7	4.30	1035

Figure 11. Output from example search in figure 10.

```
OPTICAL / THERMAL PROPERTY EFFECTS DATA

PROPERTY NAME: ABSORPTIVITY                        QUALIFIER: SOLAR
      PRE-FLT: 0.90        POST-FLT: 0.90            UNITS:
MATERIAL SIDE: UNEXPOSED SIDE                     LOCATION: D9
    SUBSTRATE:                                  EXPERIMENT #: M0003-8
TST WAVELNGTH:                                  SAMPLE THICK:
TST APPARATUS: PERKIN-ELMER LAMBDA 9 USED PER ASTM E424A
  SAMPLE TEMP:                                 EXPOSURE TIME: 5.77 (yrs)
 EST. SUN HRS: 11100                            A-O FLUX AOI: 82 (deg)
         FLUX:   9.16E+13 (atom/cm2*s)                    E: 5 (eV)
  A-O FLUENCE:
    COMMENT #:                                          DS #: 1015

PROPERTY NAME: ABSORPTIVITY                        QUALIFIER: SOLAR
      PRE-FLT: 0.90        POST-FLT: 0.93            UNITS:
MATERIAL SIDE: EXPOSED SIDE                       LOCATION: D9
    SUBSTRATE:                                  EXPERIMENT #: M0003-8
TST WAVELNGTH:                                  SAMPLE THICK:
TST APPARATUS: PERKIN-ELMER LAMBDA 9 USED PER ASTM E424A
  SAMPLE TEMP:                                 EXPOSURE TIME: 5.77 (yrs)
 EST. SUN HRS: 11100                            A-O FLUX AOI: 82 (deg)
         FLUX:   9.16E+13 (atom/cm2*s)                    E: 5 (eV)
  A-O FLUENCE:
    COMMENT #:                                          DS #: 1015

DATA SOURCE
   DATA SOURCE:  1015          DATE:  30-JUN-91
      FACILITY:  BOEING DEFENSE AND SPACE GROUP
 DOCUMENT TYPE:  TECHNICAL PAPER PRESENTED AT LDEF SYMPOSIUM, JUNE 1991
IDENTIFICATION:  CP-3134, PART 2
         TITLE:  RESULTS FROM ANALYSIS OF BOEING COMPOSITE SPECIMENS FLOWN ON
                 LDEF EXPERIMENT M0003
        REMARK:  PETE E. GEORGE, SYLVESTER G. HILL
Query complete - press return to continue:
```

Figure 11 (concluded). Output from example search in figure 10.

CHOICE: 3 MAPTIS - LDEF MATERIALS DATABASE

1. Basic Data
2. All Data
3. Data Sources

4. Electrical Properties
   A. Surface Resistance

5. Mechanical Properties
   A. All Mechanical Properties
   B. Elastic Modulus
   C. Tensile Strength
   D. Hardness
   E. Maximum Load
   F. Shear
   G. Flexural
   I. Compression Strength
   J. Load Deflection

6. General Properties
   A. All General Properties
   B. Change in Mass
   C. Change in Thickness
   D. Optical Density
   E. Surface Roughness
   F. Glass Transition Temperature
   G. VCM

7. Optical/Thermal Properties
   A. All Optical/Thermal Properties
   B. Absorptivity
   C. Emissivity
   D. Absorptivity/ Emissivity
   E. Reflectance
   F. Transmittance
   G. Coeff. Thermal Expansion

CHOICE: ENTER UP TO 3 CHOICES DELIMIT WITH A COMMA (5C,6A,7D)
FOR HELP: ENTER H FOR GENERAL HELP OR H AND CHOICE FOR MORE SPECIFIC HELP (H7B)
NOTE: ENTER DO TO LIST STANDARD MENU OPTIONS

CHOICE: 3 LDEF MATERIALS DATABASE DATA SOURCE SEARCH CRITERIA

1. Data Source Number
2. Primary Facility
3. Author or Secondary Facility
4. Document Title

CHOICE: ENTER UP TO 3 SEARCH CRITERIAS DELIMIT WITH A COMMA (1,2,4)
FOR HELP: ENTER H PRIOR TO ANY CHOICE (H1 GETS HELP ON DESIGNATION)
NOTE: ENTER DO TO LIST STANDARD MENU OPTIONS

Enter up to three AUTHORS or SECONDARY FACILITIES

You must supply all wildcards (%)!! Enter <CR> to terminate entry.

%pippin% %MULKEY%

%RUTLEDGE%

%UNIVERSITY%

Figure 12. Input screens for example screen on data sources by author named Pippin.

```
                    PROCESSING YOUR QUERY

          IF YOU MUST EXIT QUERY BEFORE IT HAS FINISHED PROCESSING

          PRESS CTRL & C KEYS SIMULTANEOUS ONE TIME (MAY TAKE FEW SECONDS)


          CTRL-Y(s) AND MULTIPLE CTRL-Cs WILL BACK YOU UP TO SOME
          PREVIOUS MENU AND MAY POSSIBLY LOG YOU OFF THE SYSTEM IF
          TOO MANY ARE ENTERED.

DATA SOURCE

   DATA SOURCE:  1001          DATE:  30-JUN-91
      FACILITY:  NASA, LANGLEY RESEARCH CENTER
 DOCUMENT TYPE:  TECHNICAL PAPER PRESENTED AT LDEF SYMPOSIUM, JUNE 1991
IDENTIFICATION:  CP-3134, PART 2
         TITLE:  PRELIMINARY FINDINGS OF THE LONG DURATION EXPOSURE FACILITY
                 MATERIALS SPECIAL INVESTIGATION GROUP
        REMARK:  BLAND A. STEIN; BOEING DEFENSE AND SPACE GROUP, H. GARY
                 PIPPIN

   DATA SOURCE:  1005          DATE:  30-JUN-91
      FACILITY:  BOEING AEROSPACE AND ELECTRONICS DIVISION
 DOCUMENT TYPE:  TECHNICAL PAPER PRESENTED AT LDEF SYMPOSIUM, JUNE 1991
IDENTIFICATION:  CP-3134, PART 2
         TITLE:  RESULTS OF EXAMINATION OF SILVERED TEFLON FROM THE LONG
                 DURATION EXPOSURE FACILITY
        REMARK:  KEN ROUSSLANG, RUSS CRUTCHER, GARY PIPPIN

   DATA SOURCE:  1014          DATE:  30-JUN-91
      FACILITY:  BOEING DEFENSE AND SPACE GROUP
 DOCUMENT TYPE:  TECHNICAL PAPER PRESENTED AT LDEF SYMPOSIUM, JUNE 1991
IDENTIFICATION:  CP-3134, PART 2
         TITLE:  SURVEY OF RESULTS FROM THE BOEING MODULES ON THE M0003
                 EXPERIMENT ON LDEF
        REMARK:  H. G. PIPPIN, OWEN MULKEY, JURIS VERZEMNIEKS, EMMETT MILLER,
                 SYLVESTER HILL, HARY DURSCH

   DATA SOURCE:  1037          DATE:  30-NOV-91
      FACILITY:  EUROPEAN SPACE AGENCY, ESTEC
 DOCUMENT TYPE:  TECHNICAL PAPER PRESENTED AT LDEF MATERIALS WORKSHOP, NOV 91
IDENTIFICATION:
         TITLE:  EFFECTS OF THE LDEF ENVIRONMENT ON THE SILVER/FEP THERMAL
                 BLANKETS
        REMARK:  FRANCOIS LEVADOU; BOEING DEFENSE AND SPACE GROUP, GARY
                 PIPPIN


 Query complete - press return to continue:
```

Figure 13. Output from example search in figure 12 on a specific author.

LDEF Materials Data Base Format Committee

Chairman: Joan Funk
NASA- Langley Research Center

Co-Chairman: John Davis
NASA-Marshall Space Flight Center

Kaia David
McDonnell Douglas SSC

Bruce Drolen
Hughes Aircraft, Space
& Communications Group

James Gehen
McDonnell Douglas SSC

Dave Harden
Boeing

William T. Lee
Rocketdyne

Ray LeVesque
McDonnell Douglas SSC

Steve McKinney
Space Systems/Loral

Glenn G. Ormbrek
Wright Labs/MLB

Brian Petrie
Lockheed Missiles & Space Co.

Dr. Lou Rosales
TRW

Bland Stein
NASA-Langley Research Center

John Strickland
BAMSI Inc.

Wayne Stuckey
The Aerospace Corporation

Alan Tribble
Rockwell International
Space Systems Div.

Figure 14. Members of the LDEF Materials Data Base Format Committee.

User Request Form for MAPTIS and the LDEF Materials Data Base

Employee Name:_____ ____. _____

Company/Mail Code:_____

Work Address:_____

City:_____ **State:**___ **Country:**_____

Zip Code:_____

Office Telephone Number:(___)____-_____

FAX:(___)____-_____

Signature:_____ **Date:**__/__/____

Do Not Write Below This Line

----------System Information----------

Username:_____ Uic:(_____,_____)

Check only one:

Govt Contractor _____ Industry User _____ NASA (MSFC) _____

Bamsi/BCSS Programmer ____ EHO2 Personnel _____ NASA (OTHER) _____

NPSS/PSCN ID: _____ Initial Password: _____

Creation Date: ____/____/_____ By: _____

Deletion Date: ____/____/_____ By: _____

Complete and fax to Rene Hitson/ John Davis (205) 544-5786. If you have any problems, contact Rene Hitson at (205) 544-6972 or John Davis at (205) 544-2494.

Figure 15. User request form for access to MAPTIS and the LDEF Materials Data Base.

DATA BASES FOR LDEF RESULTS

N93-28287

Gail Bohnhoff-Hlavacek
Boeing Defense & Space Group
Seattle, WA. 98124-2499
Phone: 206/773-6892, Fax: 206/773-1249

INTRODUCTION

The Long Duration Exposure Facility (LDEF) carried 57 experiments and 10,000 specimens for some 200 LDEF experiment investigators. The external surface of LDEF had a large variety of materials exposed to the space environment which were tested preflight, during flight, and postflight. Thermal blankets, optical materials, thermal control paints, aluminum, and composites are among the materials flown. The investigations have produced an abundance of analysis results. One of the responsibilities of the Boeing Support Contract, Materials and Systems Special Investigation Group, is to collate and compile that information into an organized fashion. This paper describes the databases developed at Boeing to accomplish this task.

DATABASE OBJECTIVES

The main objective of this task was to compile and organize the LDEF results into a database as part of the LDEF contract data analysis. After a trade study of various database software and an examination of the available investigators papers, a prototype database was developed. Important field names were chosen to serve as a framework upon which to build information and make it easy for a user to follow and understand the data in the database. Once the framework was established, initial data was inputted, in order to evaluate the database performance. When the framework was found to be acceptable, the bulk of the data was inputted. The Optical Materials Database was the first database developed. Because of the good response received from the LDEF community with the Optical Materials Database, additional databases were developed for Treated Aluminum Hardware, Silverized Teflon, Thermal Control Paints, and the LDEF Environments. These database subjects were chosen because of the large amount of data available for compilation, and because there was a need to disseminate the information quickly, especially to support materials research for future spacecraft applications.

DATABASE CHARACTERISTICS

The LDEF database design has several important and distinguishing characteristics. Because of the intuitive user interface, it requires no computer experience to operate, and is very easy to use. The data provided in the database is entirely traceable back to the original source of the information. The principal investigators in charge of the LDEF experiment, and other experimenters who authored papers are always acknowledged. Database users are encouraged to consult the original papers, or contact the experimenters for their first-hand accounts. A database password protection mechanism is employed which enables the user to have full access to the LDEF information in order to read all available data, print

copies, or download into other medium, but it does not give the user an opportunity to edit the results. Even though upgrading the information in the database is quite easy, all corrections and additions are done at Boeing. Exporting data can be done to a variety of formats, including ASCII, the WKS worksheet format used in the Lotus 1-2-3 software™, SYLK a spreadsheet format for Microsoft Excel™, and the dBase format used in the Ashton Tate dBase software™. This way information can be downloaded into the user's own spreadsheets, reports, or databases like M/VISION™ of PDA Engineering or the Materials and Processes Technical Information System (MAPTIS) which is the NASA-wide storage, retrieval, and display system for materials and processes information managed by the NASA Marshall Space Flight Center. The user is not limited to a single layout design, but can create whatever layout they prefer. The application software results in a flat file database, which can contain text, tables, graphs, diagrams and even picture files. (A flat file database was chosen over other types of databases because most of the information being produced by LDEF investigators came in the form of text, graphs, pictures, and small tables; rarely was the information contained in long narrow columns of tabulated data which is most appropriate for relational databases.) Further, the principal investigator's interpretation of the results is considered vital to the databasing process, and every attempt was made to capture it intact within the database. In essence the LDEF databases prepared at Boeing are a compilation of results summaries, conclusions, lessons learned, descriptions of flight hardware, and the full spectrum of environmental exposure parameters the samples were exposed to. The database was not intended for, nor was it designed to archive every data point or perform relational studies. Further, the database is only as complete as the information that is available from the investigators for input.

STATUS OF DATABASES

To date five databases have been created and respective LDEF data inputted. The first, in 1991, was funded by the Systems Special Investigative Group (SSIG) effort to compile information on the optical materials that flew on LDEF. As a follow-on to this task, we will update the Optical Materials Database in fiscal year 1993. The other four databases were started in 1992 and funded by the Materials SIG effort including: Silverized Teflon Thermal Blankets; Treated Aluminum Hardware (chromic acid anodize, alodyne, sulfuric acid, polished and untreated aluminum); Thermal Control Paints (e.g. A276, S13-GLO) and the LDEF Environment. The LDEF Environment Database compiles extensive overall data charts, graphs, diagrams, images of the LDEF environment including such parameters as the thermal environment, solar ultraviolet (UV), meteroid and debris (M/D) impacts, atomic oxygen (AO) exposure, and LDEF historical information. In addition, it will contain information on the LDEF microenvironments.

All of these databases are run on the Filemaker Pro software developed by the Claris Corporation.[1] Presently the software is available for Macintosh computers only. However, as mentioned earlier, information contained in the databases is exportable to DOS computers, by saving to a variety of formats that are readable on the receiving computer. By the third quarter of 1992, the Claris Corporation has advised us that there will be a DOS / Windows version that will allow one to use the full capability of the Filemaker Pro database structure on IBM-compatible personal computers. In addition, an upgraded Mac version will be available to the Macintosh users by that time as well. This is important for network users, since the user's network resident fileserver will have access to both types of computer, and the data will be transparent between the Mac and PC.

DATABASE DEMONSTRATION

The database design is built upon a structure of "field names". Some field name entries provide necessary background information such as: experiment name, experiment number, principal investigators (PIs), and experiment objectives as shown in Figure 1. Other field names detail the environmental parameters specific to that experiment or location (AO, UV, M/D impacts, etc.). Figure 2 shows the ensuing field name titles that indicate the hardware that flew on the experiment, and what measurements were performed on those parts. Following these field names are others that provide a results summary and the principal investigator's conclusions (Figure 3). Along with the PI's system analysis and recommendations for future designs, the database also contains a list of other published papers by this author, the references used to make up this database record, the experiment status, the hardware archive locations, and a date describing the latest database upgrade, as shown in Figure 4. The amount of information contained under each field name is not limited to a certain number of characters.

In addition to text, the database can utilize tables, graphs and picture files. These inputs add greatly to the user's understanding of the text or tables already in the database. For example, Figure 5 is an example of a picture file within the LDEF Environmental Database. It documents the atomic oxygen fluence around the LDEF structure.[2] This information could just as easily have been put into a numerical table, but the diagram gives the reader an excellent perspective of LDEF, and a better understanding of the directionality associated with the AO fluence. The second example illustrated in Figure 6 is a graph of the bidirectional reflectance distribution function (BRDF) results from a piece of silverized teflon (AgFEP).[3] This plot provides the viewer a better opportunity to evaluate the variation of diffuse reflectance scatter on samples exposed to AO at various locations on LDEF. Further it shows the slight asymmetry in the measurement due to the orientation of the sample with respect to the measuring laser beam, and the directionality of the roughened surface of these specimens. Figure 7 shows a micrometeroid debris impact in metal, which has a different appearance than that of an M/D impact in glass or in an organic coating, all of which can be seen in the database.[4] The last example (Figure 8) shows a scanning tunneling microscope 3-D analysis plot illustrating the surface projections that are on the order of a wavelength of light on a diffuse area of the AgFEP. This picture supports the author's interpretation that the opaqueness seen on the AgFEP is likely due to the interaction of visible light with the roughened surface through classical reflection-refraction processes.[5] In summary, these four examples illustrate how important it is to be able to include graphics in the various LDEF databases.

The following is a demonstration of how easy it is to utilize the database to search and query information. In this example, we will use the database to find any information concerning Experiment S0050. We place S0050 in the Experiment Number slot, and press "find" as shown in Figure 9. The database searches and finds Experiment S0050, "Effects of Long Duration Exposure on Active Optical System Components" as shown in Figure 10. Using the computer we can read through the entire entry, gathering a great deal of information on the various optical materials (Figure 11) that were exposed on this experiment.

GETTING PRELIMINARY COPIES OF THE DATABASE

To receive a free preliminary copy of the LDEF databases for review, please send a written request with an empty 3.5" floppy disk for each database you request to: Dr. Gary Pippin, Technical Lead LDEF Materials Data Analysis, Boeing Defense and Space Group, P.O. Box 3999, M/S 82-32, Seattle, WA 98124-2499. For your convenience, the table below summarizes which databases are available, and the date of their most recent upgrade at the time of this conference.

Table 1. Available LDEF Databases

LDEF Database	Latest Upgrade Date
Optical Materials	12/91
Silverized Teflon	05/92
Treated Aluminum	05/92
Thermal Control Paints	05/92
LDEF Environment	05/92

CONCLUSIONS

In conclusion, the database fulfills our main objective, namely to compile the LDEF materials exposure results into an organized database. Even more than that, the Boeing LDEF databases serve as a unique research tool. The databases are application specific, and each database is an independent self-contained unit of information. This database design allows for efficient and easy transfer of LDEF findings to the space community.

ACKNOWLEDGEMENT

The author gratefully acknowledges the LDEF Project Office at the National Aeronautics and Space Administration Langley Research Center for supporting the development of this database under contract NAS1-19247

---

[1]Claris Corporation, 5201 Patrick Henry Drive, Box 58168, Santa Clara, CA. 95052-8168, Telephone 408/727-8227.

[2]Bourrassa, R. and Gillis, J.R.: "Atomic Oxygen Exposure of LDEF Experiment Trays", *LDEF Supporting Data,* NASA Contract NAS1-19247 Report, pg. 12, March 1992.

[3]Rousslang, Ken, Crutcher, E.R. and Pippin, H.G.: "Results of Examination of Silvered Teflon from the Long Duration Exposure Facility", *LDEF 69 Months in Space: First LDEF Post-Retrieval Conference Proceedings*, NASA CP-3134, February 1992.

[4]See, T.H., Allbrooks, M.K., Atkinson, D.R., Simon, C.G., and Zolensky, M.E.: *Meteroid and Debris Impact Features Documented on the Long Duration Exposure Facility,* NASA Publication #84, JSC #24608, pg. 9, 1990.

[5]Young, P.R. and Slemp,W.: "An Analysis of LDEF-Exposed Silvered FEP Teflon Thermal Blanket Material", NASA Technical Memorandum 104096, December 1991.

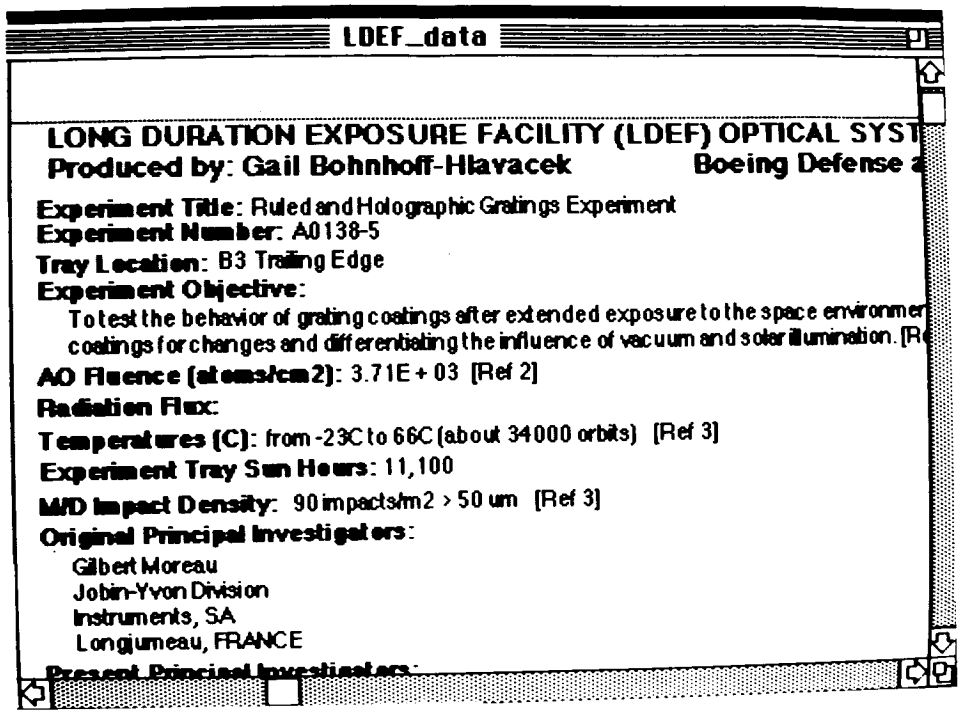

Figure 1. Database record with field names and referenced data entries.

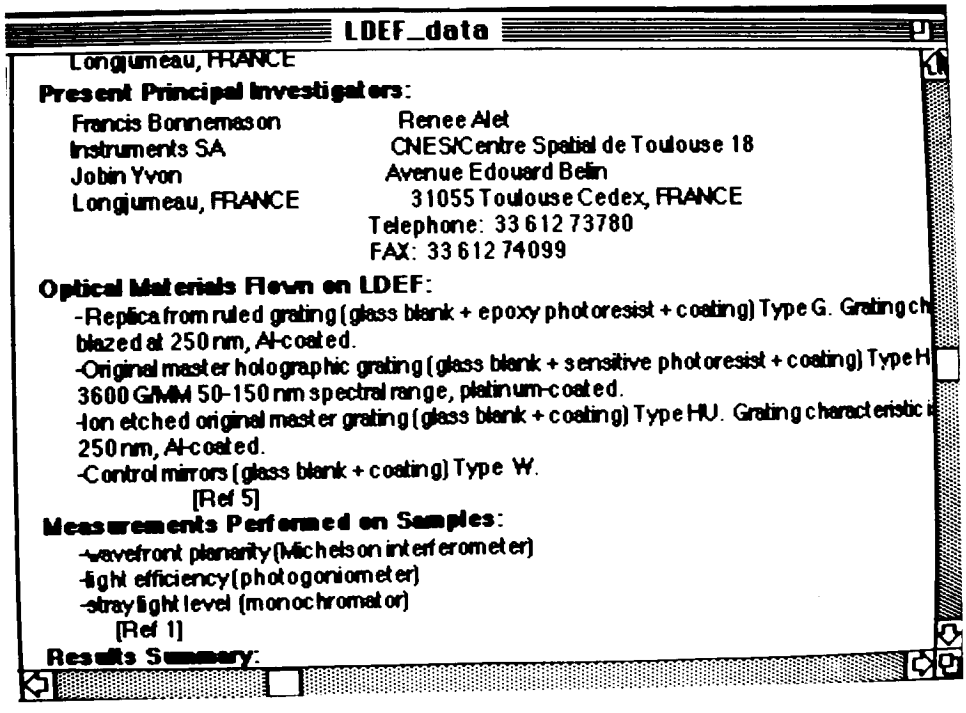

Figure 2. Continuation of database record from Figure 1.

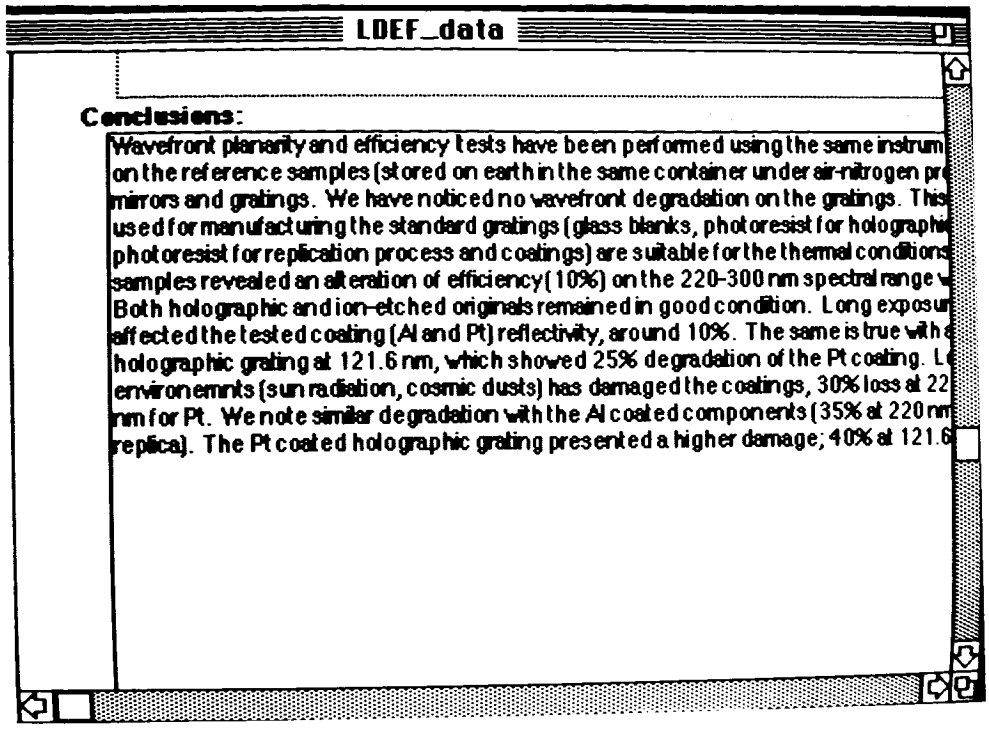

Figure 3. Continuation of database record from Figure 2.

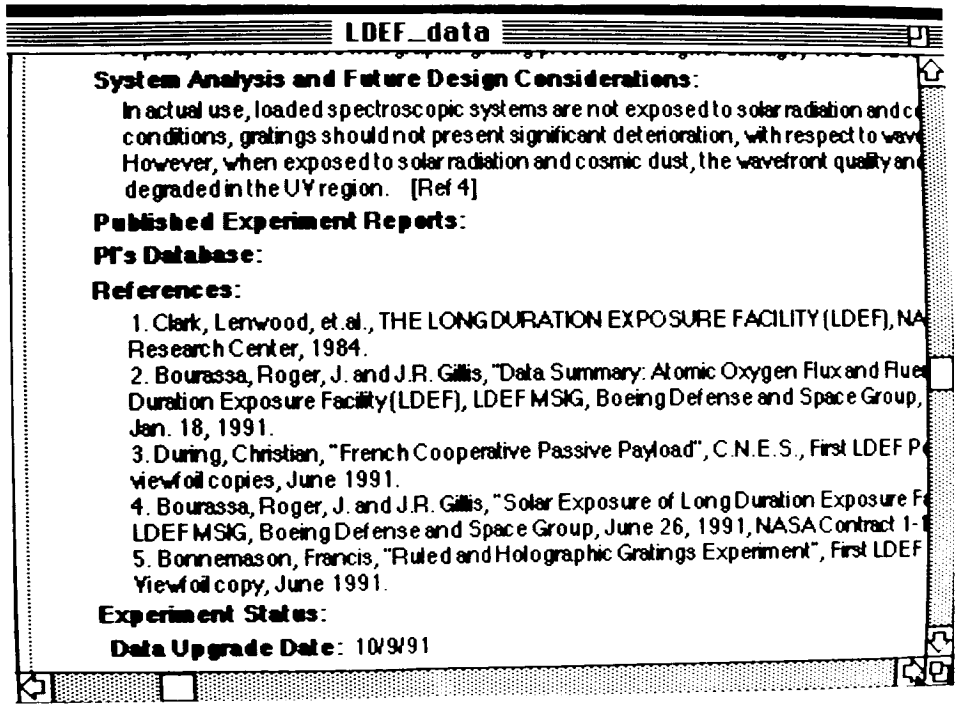

Figure 4. Continuation of database record from Figure 3.

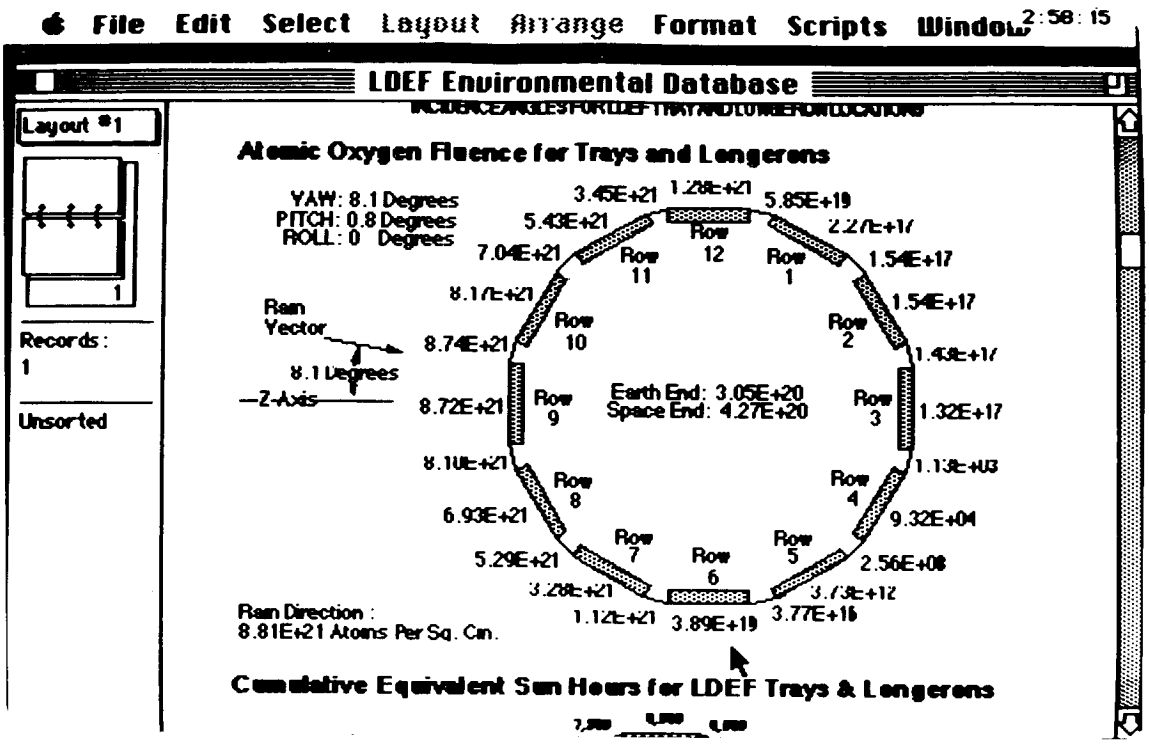

Figure 5. Example of a drawing in database.

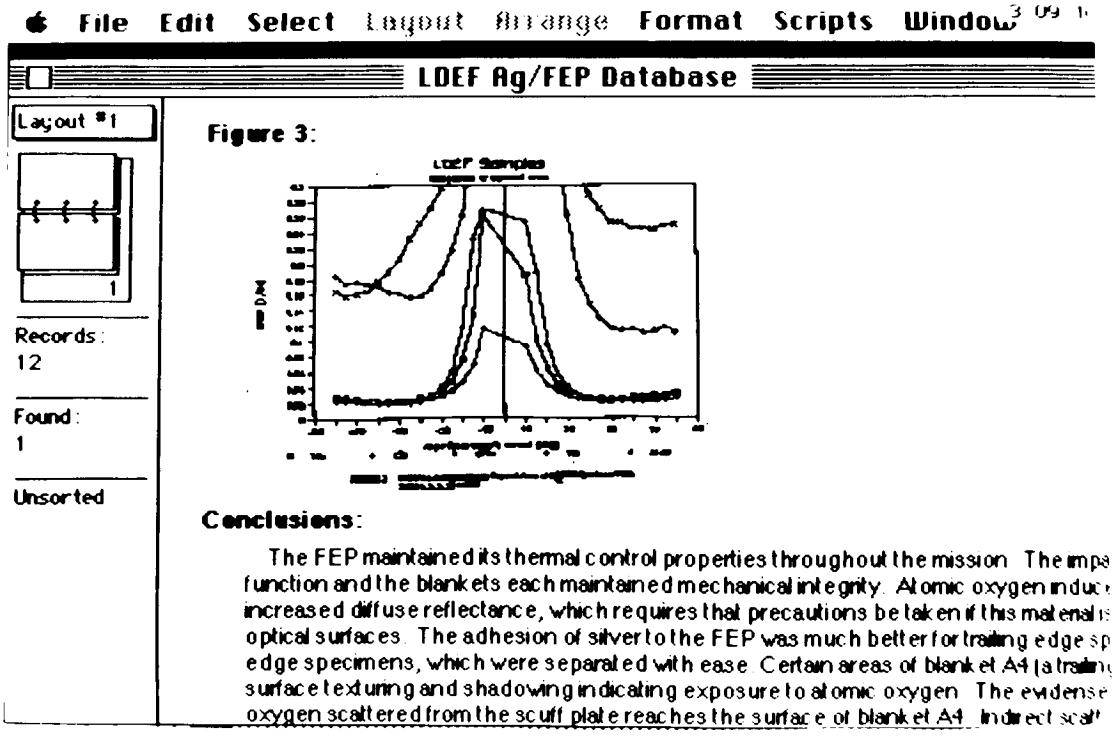

Figure 6. Example of graphical plot in database.

ORIGINAL PAGE IS
OF POOR QUALITY

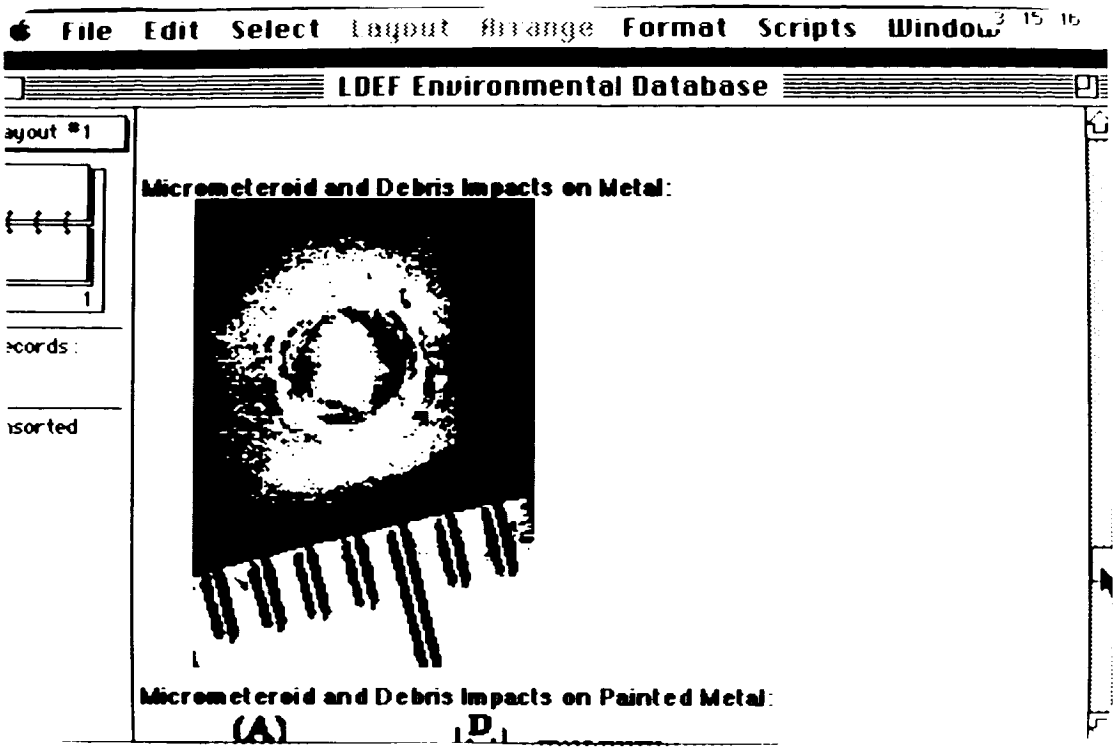

Figure 7. Example of picture file in database.

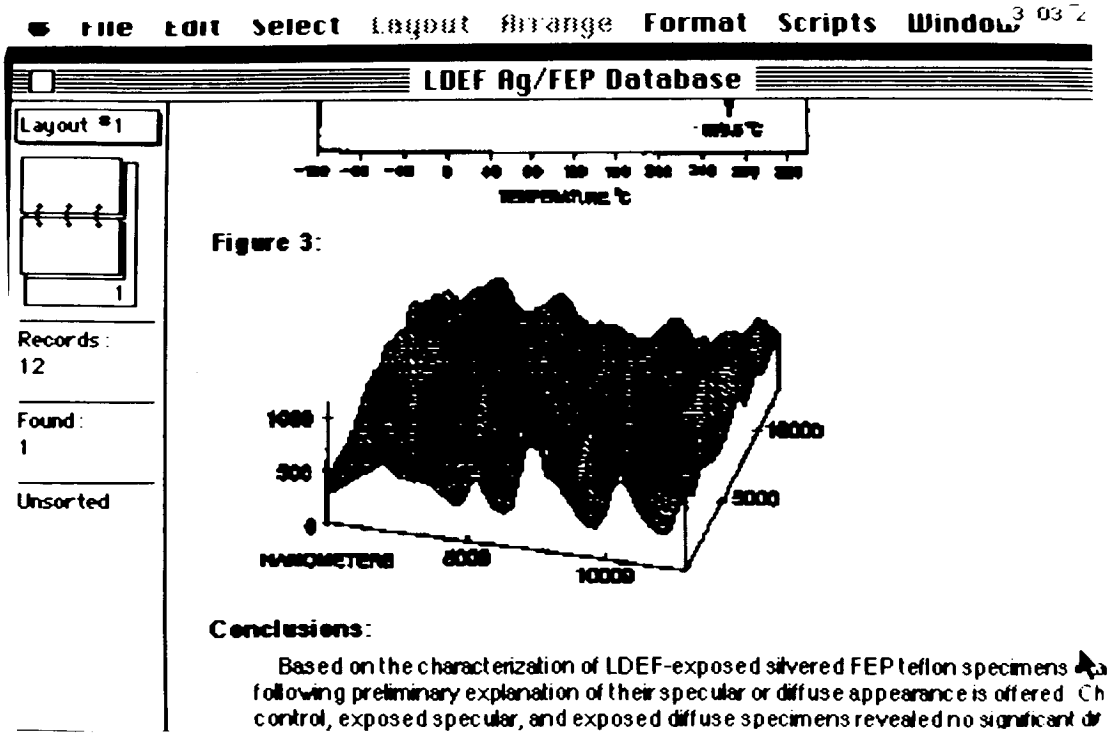

Figure 8. Example of 3-D plot in database.

ORIGINAL PAGE IS
OF POOR QUALITY

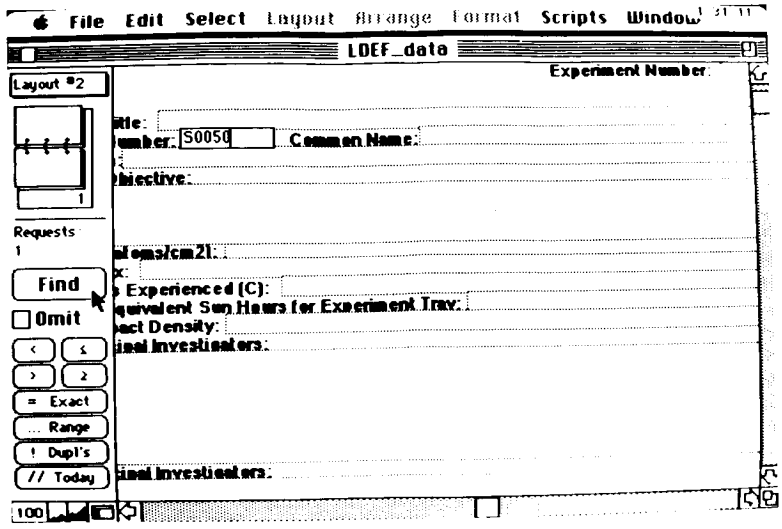

Figure 9. Search function on database.

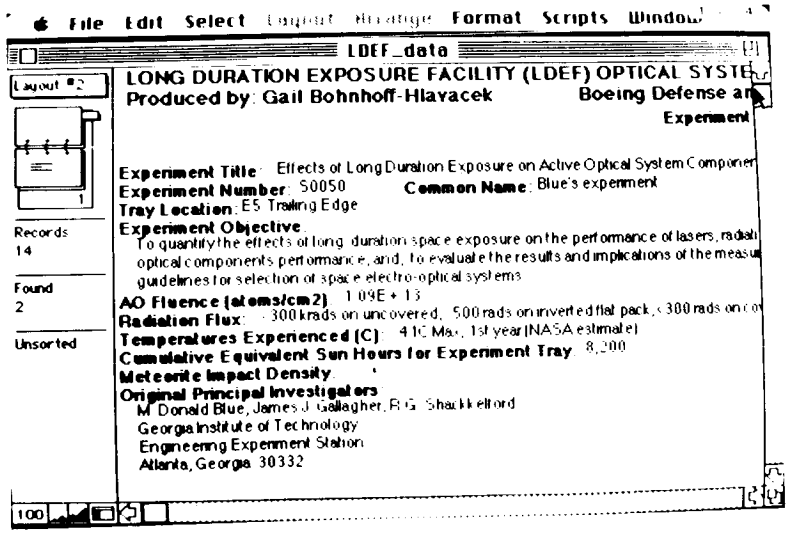

Figure 10. Database retrieves Experiment S0050.

ORIGINAL PAGE IS
OF POOR QUALITY

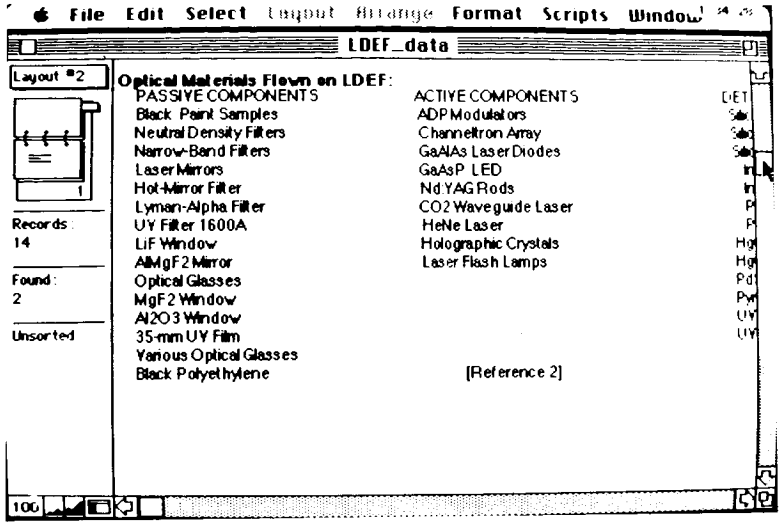

Figure 11. Scanning the "Optical Materials Flown on LDEF" field name in this database record.

ORIGINAL PAGE IS
OF POOR QUALITY

N93-28288

LONG DURATION EXPOSURE FACILITY EXPERIMENT M0003 DEINTEGRATION OBSERVATION DATA BASE

S. R. Gyetvay
J. M. Coggi
M. J. Meshishnek
The Aerospace Corporation
El Segundo, CA 90245

ABSTRACT

The four trays (2 leading edge and 2 trailing edge) of the M0003 materials experiment on LDEF contained 1274 samples from 20 subexperiments. The complete sample complement represented a broad range of materials, including thin film optical coatings, paints, polymer sheets and tapes, adhesives, and composites, for use in various spacecraft applications, including thermal control, structures, optics, and solar power. Most subexperiments contained sets of samples exposed on both the leading and trailing edge trays of LDEF. Each individual sample was examined by high resolution optical microscope during the deintegration of the subexperiments from the M0003 trays. Observations of the post-flight condition of the samples made during this examination were recorded in a computer data base. The deintegration observation data base is available to requesters on floppy disk in 4th Dimension for the Macintosh format. Over 3,000 color macrographs and photomicrographs were shot to complement the observation records and to document the condition of the individual samples and of the M0003 trays. The photographs provide a visual comparison of the response of materials in leading and trailing edge LDEF environments. The Aerospace Corporate Archives is distributing photographs of the samples and hard copies of the database records to the general public upon request. Information on obtaining copies of the data base disks and for ordering photographs and records of specific samples or materials are given in this paper.

INTRODUCTION

The Aerospace Corp. M0003 Experiment

Of the 57 experiments flown on the 86 experiment-holding trays arrayed around the LDEF, M0003 was one of the most comprehensive materials experiments. Experiment M0003 resided on four trays, two on the leading edge of LDEF and two on the trailing edge. This experiment, planned and integrated by the Aerospace Corporation Mechanics and Materials Technology Center, was designed to study the effects of the space environment on current and developmental spacecraft materials. The M0003 experiment was a collection of 20 subexperiments from the Aerospace Corporation Laboratories, Air Force and Navy Laboratories, and Department of

PRECEDING PAGE BLANK NOT FILMED

Defense (DoD) contractors, fielded under the sponsorship of the Air Force Space Systems Division and the Space Test Program. The 20 subexperiments are described in Table I; the current point of contact for each is given.

M0003 Trays And Samples

The M0003 hardware consisted of four encircling trays, two Experiment Power and Data Systems (EPDS), two Environment Exposure Control Canisters (EECCs), and several Li/SO_2 batteries to satisfy power requirements. The trays were flown in pairs, one pair consisting of a 6-inch deep tray (carrying a data system and a canister) that was connected by wiring harness to a 3-inch deep tray (carrying mostly sample coupons). One tray pair was located on the LDEF leading edge and a similar pair was located on the trailing edge. Aerospace designated the trays as "L3", "L6", "T3", and "T6", according to the tray depth and leading or trailing edge location, before NASA had assigned the trays to an exact location on the LDEF. Subsequently, these trays were named by NASA according to their row and ring location and are more commonly known as "D9", "D8", "D3", and "D4", respectively. The Aerospace tray designations were ensconced in the unique identification code assigned to each subexperimenter sample for the coordination and data base accounting of the M0003 experiment integration and deintegration and these could not easily be changed.

The design of the M0003 trays was modular, allowing samples to be thermally coupled or decoupled from the tray and therefore, the LDEF structure. Each tray had six of the experiment-carrying modules, designated by Roman Numerals I through VI. The 1274 samples were mounted on anodized black aluminum hardware plates on the modules. The materials in the M0003 experiment included a variety of thermal control paints and coatings, polymers, optics, structural materials, and solar power materials. The M0003 sample complement is diagrammed by these material types in Figures 1 through 5. For brevity, not all samples types are shown in these diagrams.

For the 69 month duration of the LDEF exposure at Low Earth orbit, the four trays of samples experienced different environments which varied according to their location on LDEF, but all trays, leading and trailing edge, experienced the same number of thermal cycles, were exposed to roughly the same number of hours of UV exposure and received the same low levels of electron and proton irradiation. Only the leading edge trays, D8 (L6) and D9 (L3), were subjected to a significant atomic oxygen dose; these trays also received a greater number of hypervelocity impacts than did the trailing edge trays (Ref. 1, 2, 3).

Most of the subexperiments in M0003 contained duplicate sets of samples exposed on the leading and the trailing edge trays. A few had duplicate sets exposed for shorter durations in the canisters as well. Some subexperiments also included a set of "flight control" samples that were mounted within the modules and that were not directly exposed to the space environment, but were subject to the thermal vacuum cycling.

Environment Exposure Control Canisters

The canisters on trays D4 (T6) and D8 (L6) were programmed to open in three stages in order to obtain different duration exposures on some materials. Two weeks after the initiate

signal, the canisters opened to expose a large (~3/4 area) of samples. The next canister stepped movement occurred approximately 23 weeks after deployment and exposed another row of samples (1/8 additional area). The next canister stepped movement was at approximately 33 weeks and exposed the last row of samples (1/8 area) by opening to the canister's fullest extension. The canister drawer closed completely at 42 weeks after initiate and remained closed during the remainder of the LDEF mission. Thus, varying exposure times of 9, 19, and 40 weeks were obtained for some samples in addition to the full mission exposure of 69 months for identical samples on the other M0003 trays. The canisters were opened in a clean room at Aerospace roughly five months after LDEF retrieval. LDEF special investigation group (SIG) personnel were present during this event and sampled the canister gases and assisted in helium leak testing of the seals. The canisters were both essentially at atmospheric pressure and some leakage of the front seals was detected.

THE M0003 EXPERIMENT DEINTEGRATION

Following retrieval of the LDEF, the Aerospace Corporation was charged by the Space Test Program, with documentation of the handling and disassembly of the M0003 experimental trays and with providing support to the subexperimenters. The support included full photographic documentation of the trays, modules, and quarter-modules from the earliest stages of retrieval through the complete deintegration of the trays; photographic documentation of the condition of the individual samples; packaging and return of the samples to the subexperimenters; and providing flight data to the subexperimenters. The deintegration tasks were documented in a relational computer data base, 4th Dimension for the Macintosh.

Inspection at Kennedy Space Center

The deintegration tasks began with inspection of the M0003 trays at Kennedy Space Center following the removal of LDEF from the payload bay of the Shuttle Columbia to the SAEF (Spacecraft Assembly and Encapsulation) II clean room facility. Observations were recorded and NASA photographic surveys were made to document the condition of the trays and samples following their reintroduction into the earth environment (air, humidity, gravity, etc.).

Tray Disassembly at The Aerospace Corporation

The four M0003 trays were air-shipped to the Aerospace Corporation and unpacked and disassembled in a class 10,000 clean room. As test samples were removed from the trays, they were individually examined by optical microscopy and photographed, preserving the orientation of the samples as mounted on the LDEF. Many of the samples experienced space-induced damage effects such as crazing, surface roughening, discoloration, erosion, contamination staining, and hypervelocity impact crater formation. Not all samples exhibited discernible changes, however. Observations of the condition of the samples were made by a single examiner who maintained a consistent criteria for the qualitative descriptions of the condition of all the M0003

samples. Each sample was examined and photographed using optical microscopy at magnifications from 3X to 1000X. A Wild-Heerbrug stereomacroscope and a Zeiss Axioplan Pol research microscope were used for the examinations. Microscopy techniques used included bright field, dark field, and Nomarski differential interference contrast. The observations of the condition of the samples were entered in real time into the computer data base. It should be noted that in-depth analysis of the effects of the space exposure on the samples was the prerogative of the subexperimenters and was not the role of the examiner or the deintegration team. The microscopy examination was performed to provide a record of the post-flight condition of all samples in the event that some subexperiments were not reclaimed by the original subexperiments.

All entries in the M0003 database were keyed on a simple database number and unique sample identification code assigned to each sample . How each is used is illustrated in the example in Figure 6. The database number for the sample in this example is #73. Encoded in the sample identification is the sample's location on the trays, the module on which it was mounted, the subexperiment number, the sample location number on the module, and the identification code number given it by the subexperimenter. In the example, L3II-7-65-10, an optical coating specimen, was fielded on L3 (D9), the leading edge 3-in. deep tray, on module II. It was part of subexperiment 7 and was sample #65 on module II on D9 . It was designated as "10" by the principal investigator of the subexperiment.

Photographic And Observation Documentation

Over 3,000 macrographs and photomicrographs were made at the Aerospace Corporation to document the effects observed on the M0003 trays and the individual samples. Overall photographs of the trays, modules, and quarter-modules, (front and back) were shot using large format print film in color and in black and white. An example of one such photograph, a view of the D9 (L3) tray before deintegration of the samples, is shown in Figure 7. As the individual samples were dismounted from the modules, the underlying layers of the module hardware were also photo-documented. In addition, photographs of side-by-side leading and trailing edge pieces of hardware were made for visual comparison of the differences in degree of contamination staining, erosion, discoloration, etc. Photomicrographs made during the optical microscopy examination were recorded on high resolution 35 mm color print film. An example of a series of photographs made of an optical sample is shown in Figure 8. This sample, identified by both database number and sample identification code is a ZnS optical thin film coating on a fused silica substrate. Photographs of this type and the accompanying observation records are available for specific samples by request to the Aerospace Corporation Corporate Archives . The observation record for this sample is shown in Figure 9. The ZnS coating buckled during the 69 months of exposure. In addition, ring-like features, discernible at 200 times magnification, were observed on the buckled surface.

OBTAINING DATA AND PHOTOGRAPHS

The M0003 Deintegration Observation Record Database is available to requesters on an 1.4 MB (HD) diskette in Macintosh 4th Dimension™ format. A user instruction text file is provided on the

disk. The text file includes the detailed examination criteria used in compiling the observation records. A copy of the Aerospace form for ordering records and photographs of samples is also included in this file. The database file contains various layouts for examining the contents of the database by location on the M0003 trays, by sample identification code, or by spacecraft application. Searches may be made by material type, damage effects, categories, or text strings. Observation records in the database file include the dimensions of the samples, the subexperimenter-supplied descriptions of their composition or configuration, the observations made at Kennedy Space Center, the observations made during the deintegration process at Aerospace Corporation, and the subexperiment contacts for additional information on the samples.

The photographic portion of the database is not included on the diskette. The Aerospace Corporate Archives maintains a copy of the entire database to coordinate requests for photographs of specific samples. Requests should be addressed to the Aerospace Corporate Archives, P. O. Box 92957, Mail Station M2/326, Los Angeles, CA 90009-2957, phone (310) 336-5319; FAX (310) 336-5912). The requester should be as specific as possible in stating the type of materials desired (e. g., color prints of full trays, black and white photographs of certain modules, color micrographs of a specific samples, data records , etc.). This service will be provided as long as resources allow.

REFERENCES

1. Bourassa, R. J. and Gillis, J. R.: *Data Summary Atomic Oxygen Flux and Fluence Calculation for Long Duration Exposure Facility (LDEF),* NAS1-18224, Task 12, Boeing Defense and Space Group, Seattle, WA, January 18, 1991.

2. Bourassa, R. J. and Gillis, J. R.: *Solar Exposure of LDEF Experiment Trays*, NASA Contractor Report 189554, Boeing Defense and Space Group, Seattle, WA, February 1992.

3. See, T. H.; Allbrooks, M. A.; Atkinson, D. R.; Simon, C. G.; and Zolensky, M.: *Meteoroid and Debris Impact Features Documented on the Long Duration Exposure Facility, A Preliminary Report*, Publication #84, JSC #24608, 1990.

TABLE I. SUMMARY OF M0003 EXPERIMENTS

Subexperiment number	Scope	Subexperiment Point of Contact	Organization/ Address
-1	Radar camouflage materials and electro-optical signature coatings	Charles Hurley	Univ. of Dayton Research Inst. 300 College Park Dayton, OH 45469-0001
-2	Laser optics	Linda De Hainaut	Phillips Lab/LIDA Kirtland AFB, NM 87117-6008
-3	Structural materials	Charles Miglionico	Phillips Lab/PL/VTSI Kirtland AFB, NM 87117-6008
-4	Solar power components	Terry Trumble	Wright Labs/POOC Wright Patterson AFB, OH 45433-6533
-5	Thermal control materials	Charles Hurley	Univ. of Dayton Research Inst. 300 College Park Dayton, OH 45469-0001
-6	Laser communication components	Randall R. Hodgson	McDonnell Douglas Astronautics Corp. Mail Code 1067267 P. O. Box 516 St. Louis, MO 63166
-7	Laser mirror coatings	Terry M. Donovan	3481 Murdoch Dr. Palo Alto, CA 94306
-8	Composite materials, electronic piece parts, fiber optics	Gary Pippin	Boeing Aerospace Co. MaterialsTechnology Dept., MS 2E-01 P. O. Box 3999 Seattle, WA 98124
-9	Thermal control materials, antenna materials, composite materials, and cold welding	Brian C. Petrie	Lockheed Missiles & Space Co. Dept. 62-92, Bldg. 564 P. O. Box J04 Sunnyvale, CA 94086
-10	Advanced composite materials	Gary L. Steckel	The Aerospace Corp. P. O. Box 92957, M2/242 Los Angeles, CA 90009
-11, -12	Contamination monitoring, Radiation measurements	Eugene N. Borson, F. B. Sinsheimer	The Aerospace Corp. M2/270
-13	Laser hardened materials	Randall R. Hodgson	McDonnell Douglas Astronautics Corp. Mail Code 1067267 P. O. Box 516 St. Louis, MO 63166
-14	Quartz crystal microbalance	Donald A. Wallace	QCM Research 2825 Laguna Canyon Road P. O. Box 277 Laguna Beach, CA 92652
-15	Thermal control materials	Oscar Esquivel	The Aerospace Corp. M2/241
-16	Advanced polymer composites	Gary L. Steckel	The Aerospace Corp. M2/242
-17	Radiation dosimetry	Sam S. Imamoto, J. Bernard Blake	The Aerospace Corp. M2/260
-18	Thermal control paints	Christopher H. Jaggers	The Aerospace Corp. M2/271
-19	Electronic Piece Parts	Seymour Feuerstein	The Aerospace Corp. M2/244
-20	Tray Hardware	Michael J. Meshishnek	The Aerospace Corp. M2/271

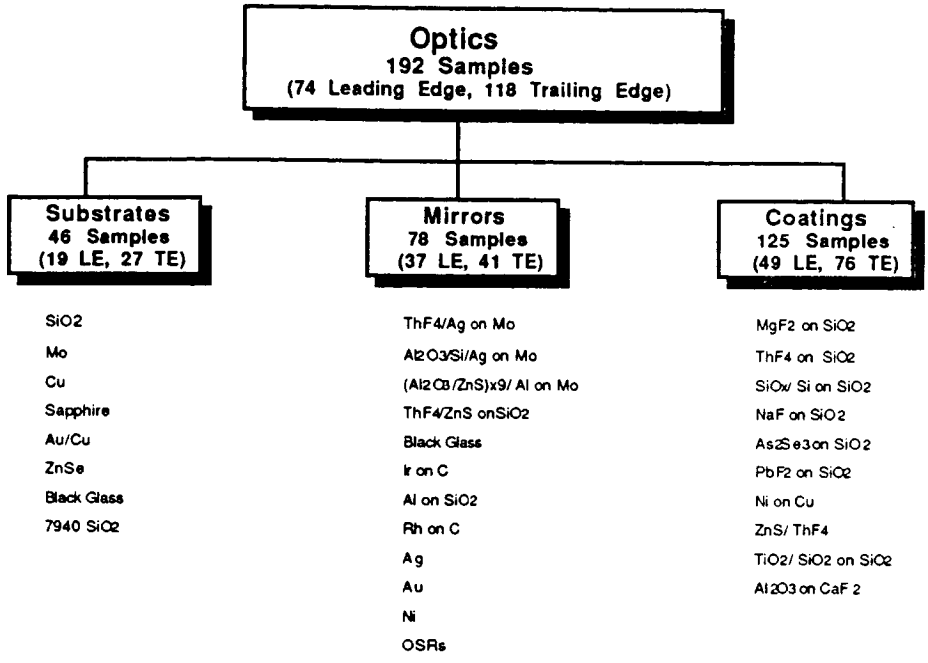

Figure 1. Diagram of Optics samples in database.

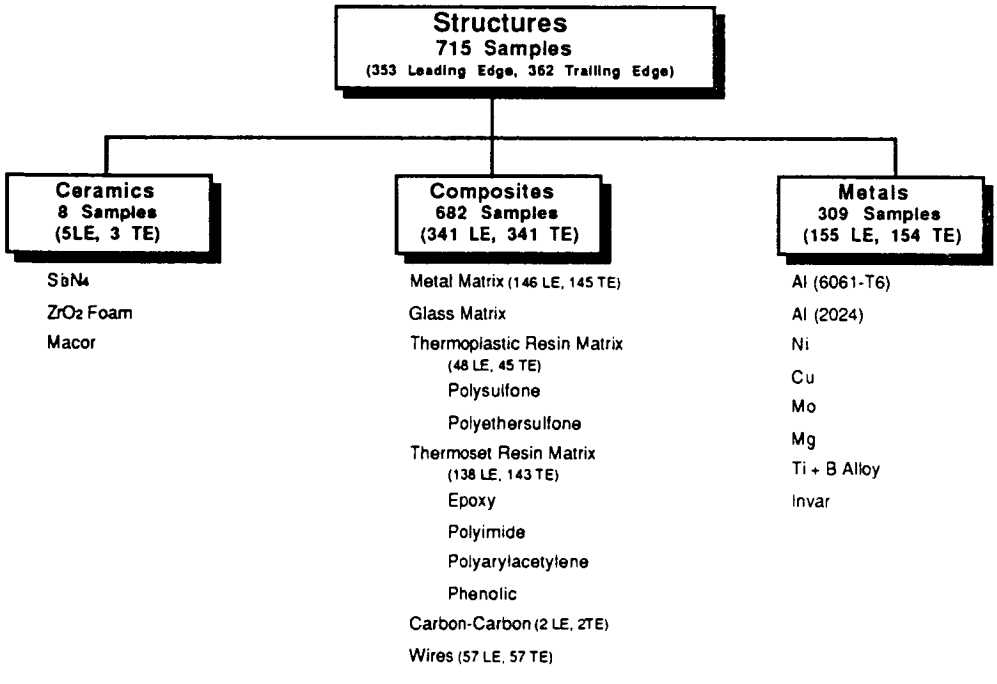

Figure 2. Diagram of Structure samples in database.

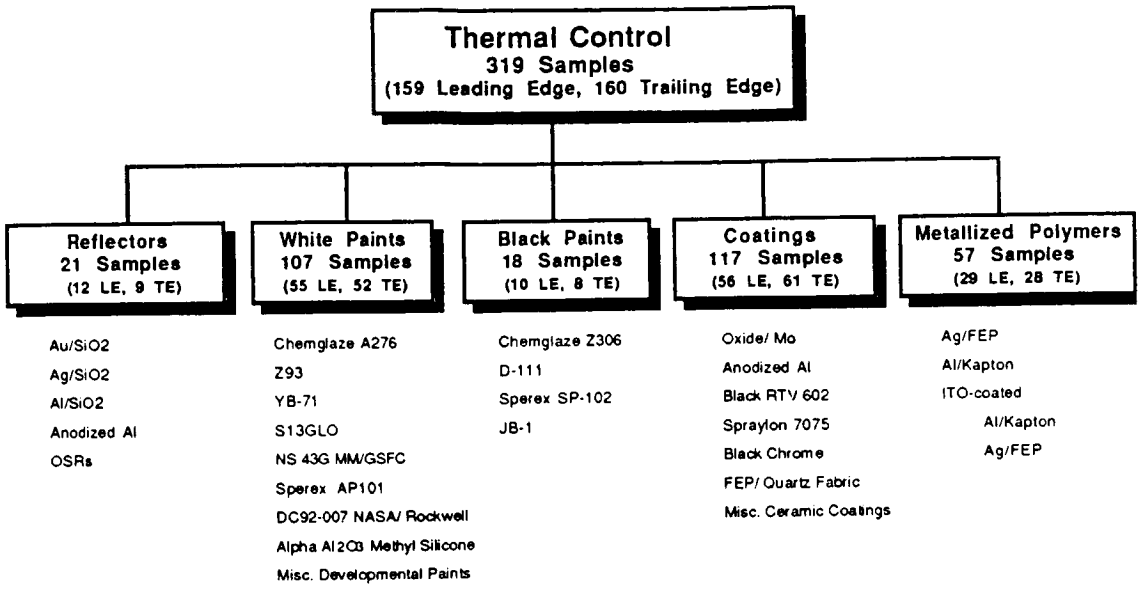

Figure 3. Diagram of Thermal Control samples in database.

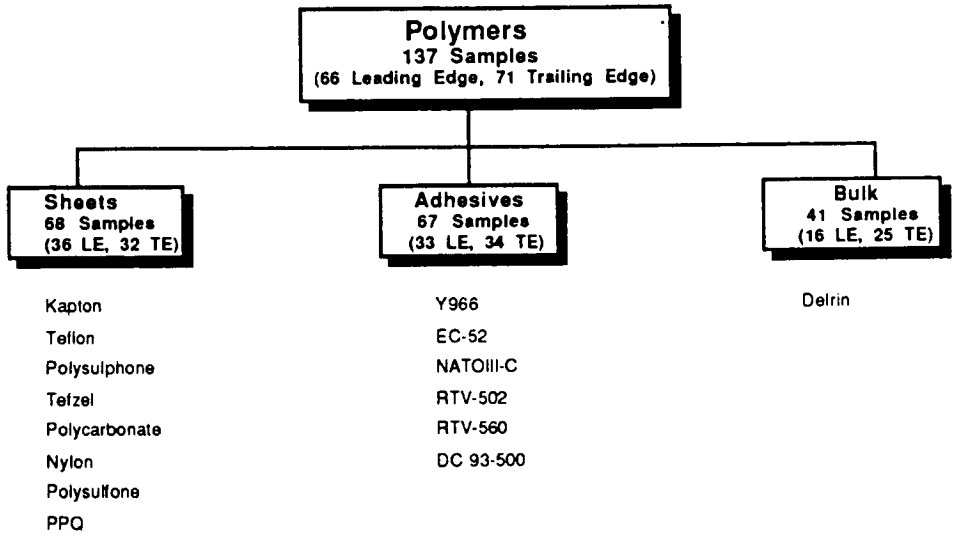

Figure 4. Diagram of Polymer samples in database.

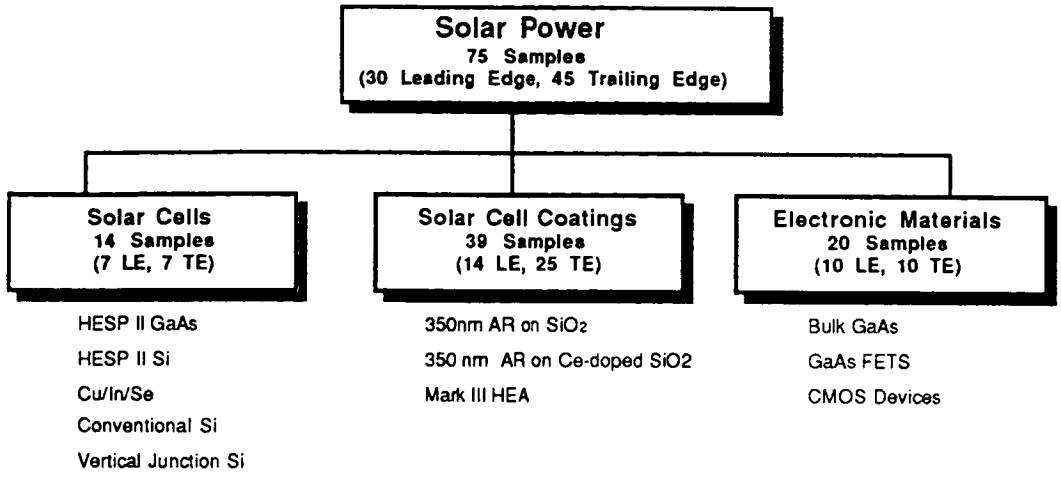

Figure 5. Diagram of Solar Power samples in database.

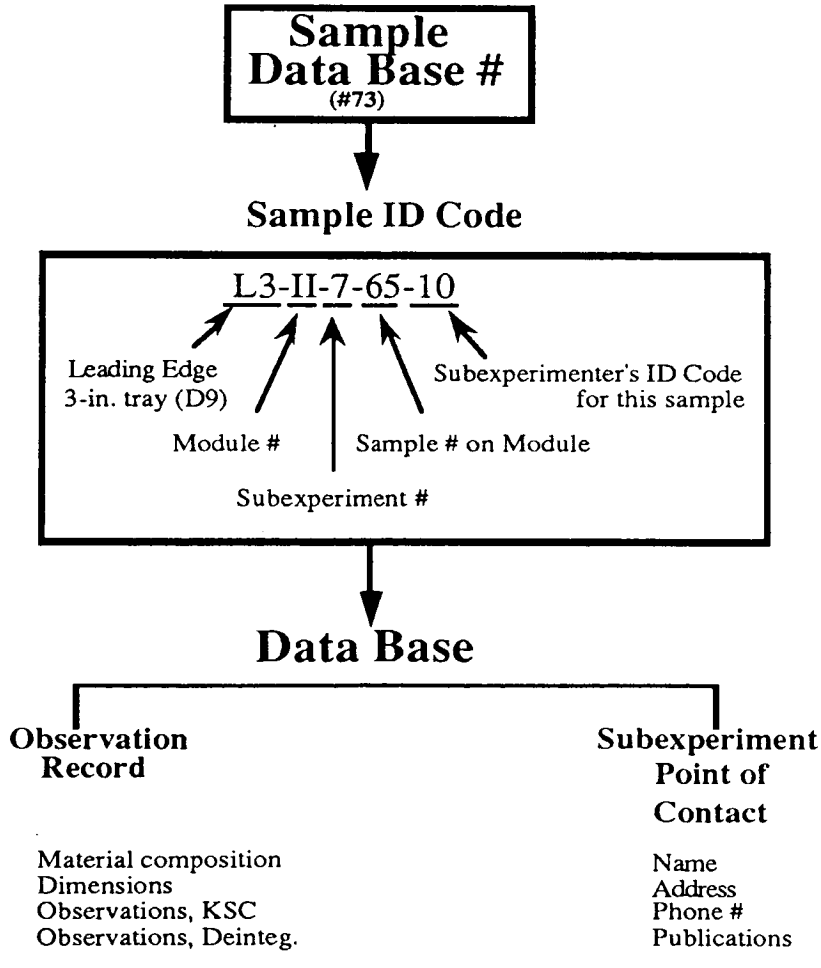

Figure 6. Diagram of M0003 database.

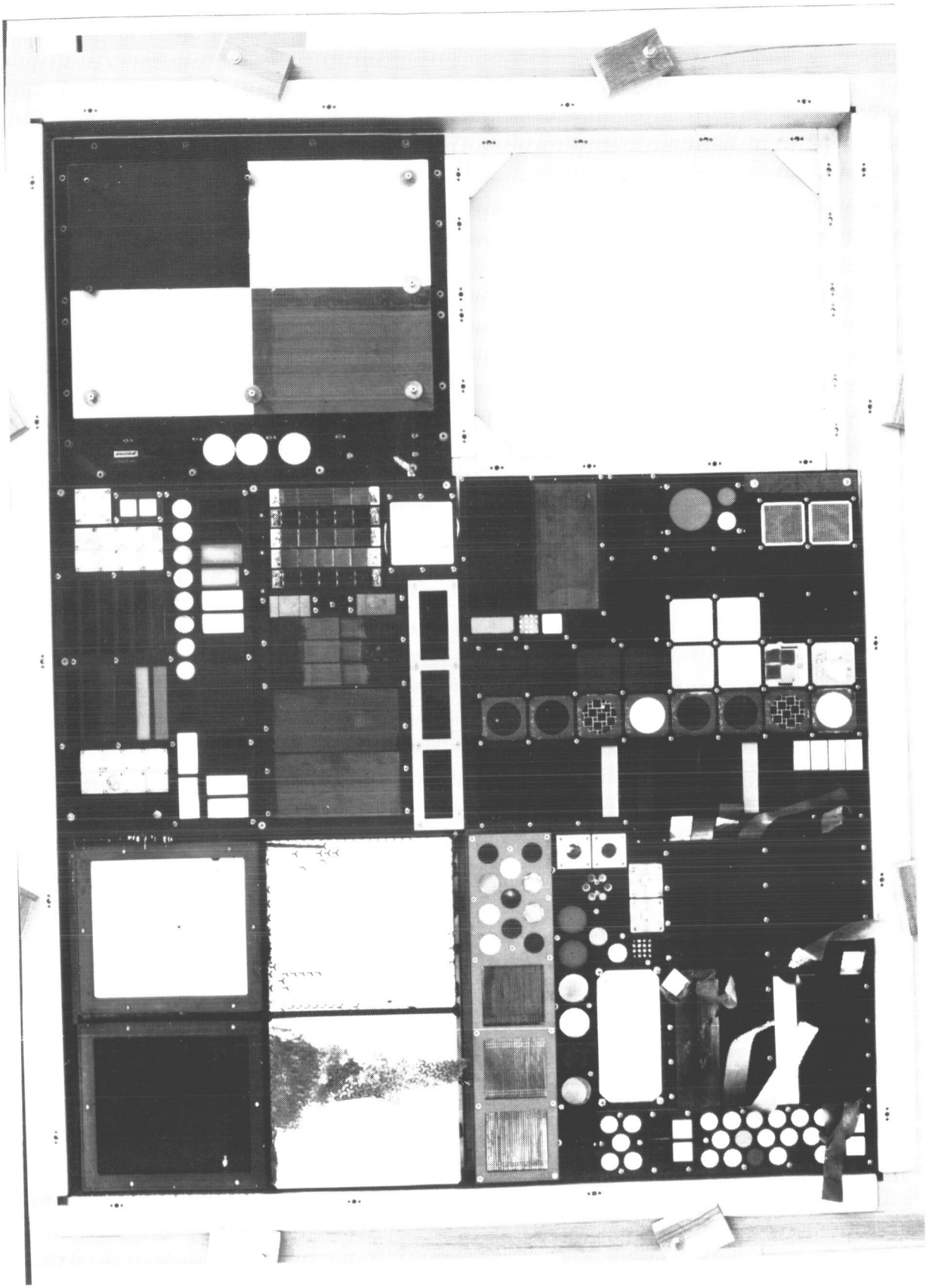

Figure 7. View of the D9 (L3) tray before deintegration of the samples.

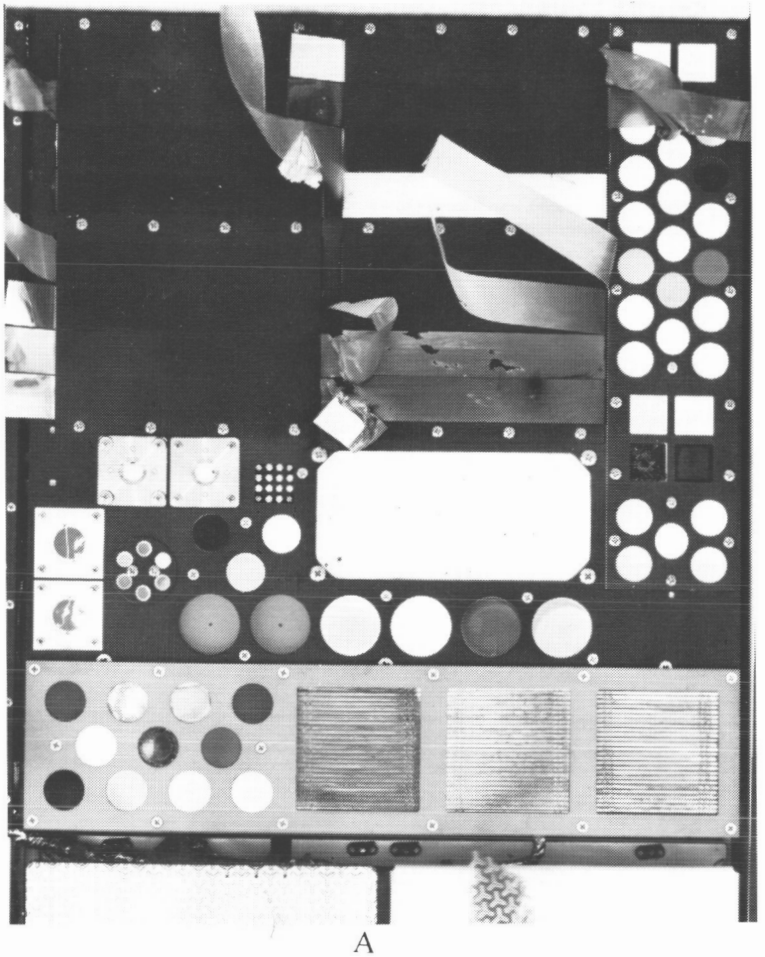

A

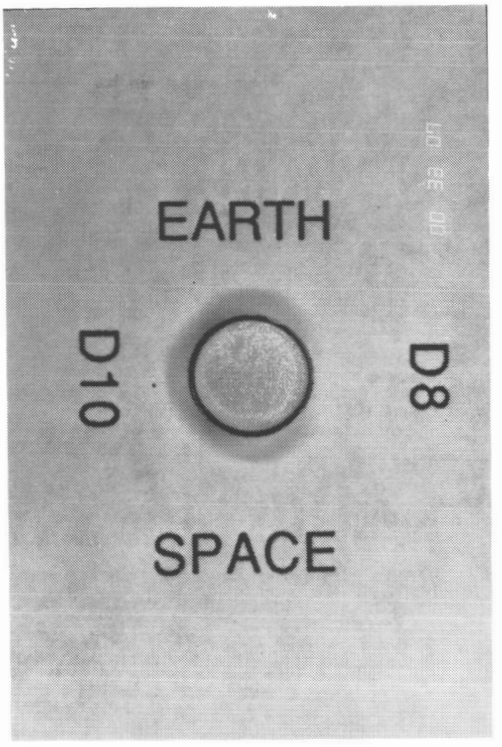

B

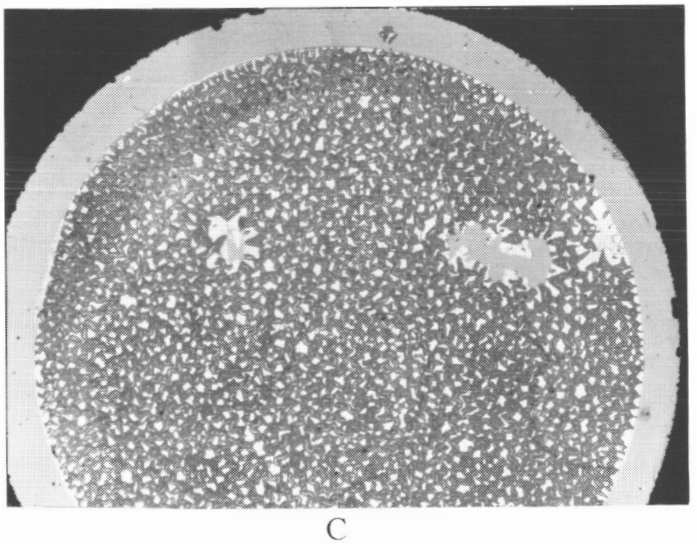

C

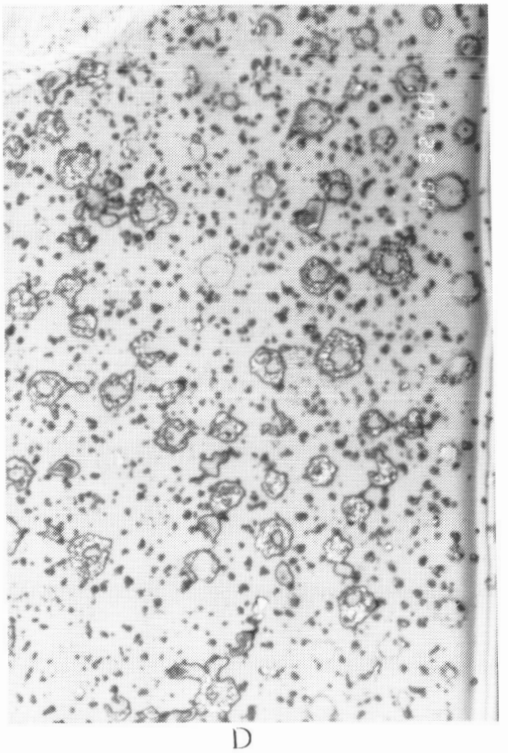

D

Figure 8. Macrographs and micrographs of sample Database #73.
View A. Module macrograph - Module II on Tray D9 .
View B. Sample macrograph of DB#73 (L3II-7-65-10, ZnS coating on fused silica, .375 in. dia.).
View C. Low magnification micrograph of buckled coating on surface of DB#73.
View D. High magnification micrograph of annular features on buckled coating on DB#73.

LDEF M0003 Sample Observation

Sample ID: L3II-7-65-10

Database #: 73

Tray: D9 **Module:** II **Experiment #:** 7

Description: Coating, ZnS on SiO2 (SiO2 substrate, ZnS coating)

Width: 0.375
Length: -
Thickness: 0.100

Category: Coating, glass
Subcategory: Coated substrate
Application: Optics

Exposure: 69 months

Post-flight Condition: Buckled (+), delaminated

Observations at KSC Before Deintegration:

SURFACE CRAKED, FLAKING

Observations at The Aerospace Corporation:

Date: Tuesday, May 15, 1990

The exposed coating appears uniformly buckled; some areas have buckled so severely that the coating has flaked. In the flaked areas, the residual surface (the substrate) is smooth. Another phase appears to have nucleated on the top of the buckled surface. This phase is manifested, in various stages of formation, as crescent-, ring- or circular-shaped features on the surface.

Point of Contact:
Terry Donovan

3481 Murdoch Dr.

Stanford CA 94306
(000) 000-0000 FAX: (___) 000-0000

Publications:

1. T. M. Donovan, J. M. Bennett, and S. Gyetvay, "Space Environmental Effects on Coated Optics," Proceedings of the First Post-Retrieval Symposium, Kissimmee, FL, Jun 2-8, 1991, NASA Conference Publication 3134, Part 3

Mechanics and Materials Technology Center
THE AEROSPACE CORPORATION

Figure 9. Example of hard copy database observation record (DB#73).

ORIGINAL PAGE
COLOR PHOTOGRAPH

COLOR PHOTOGRAPHS

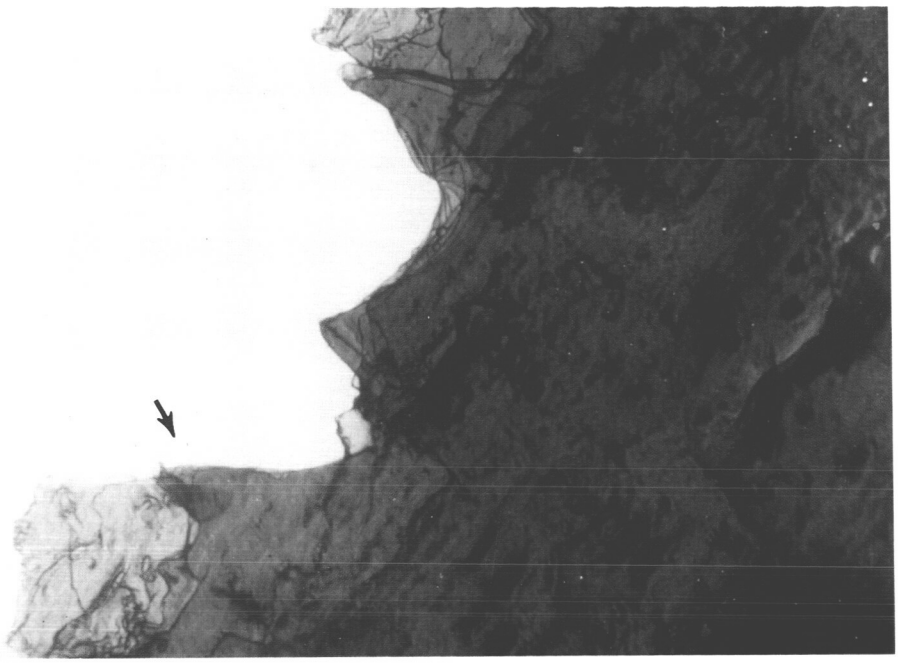

Figure 3. Layered contaminant films from Tray C12.
(Color version of black and white photograph shown on page 1028.)

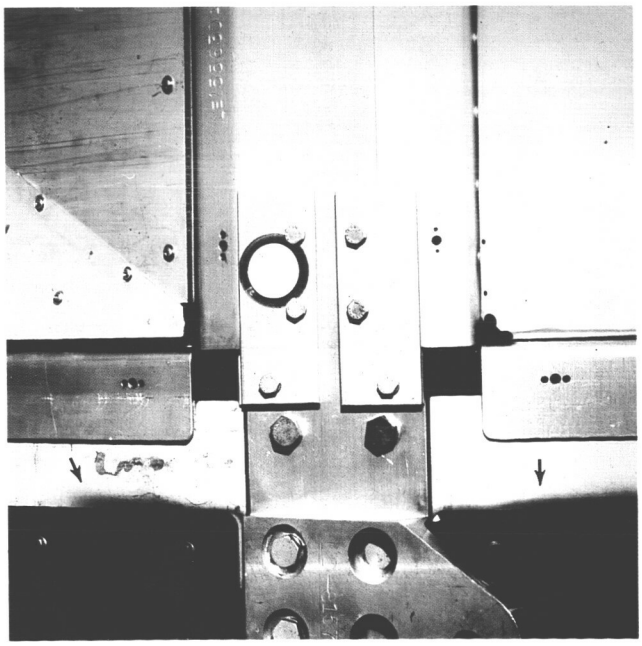

Figure 5. Outgassed material on LDEF structure near vents from interior.
(Color version of black and white photograph shown on page 1029.)

ORIGINAL PAGE
COLOR PHOTOGRAPH

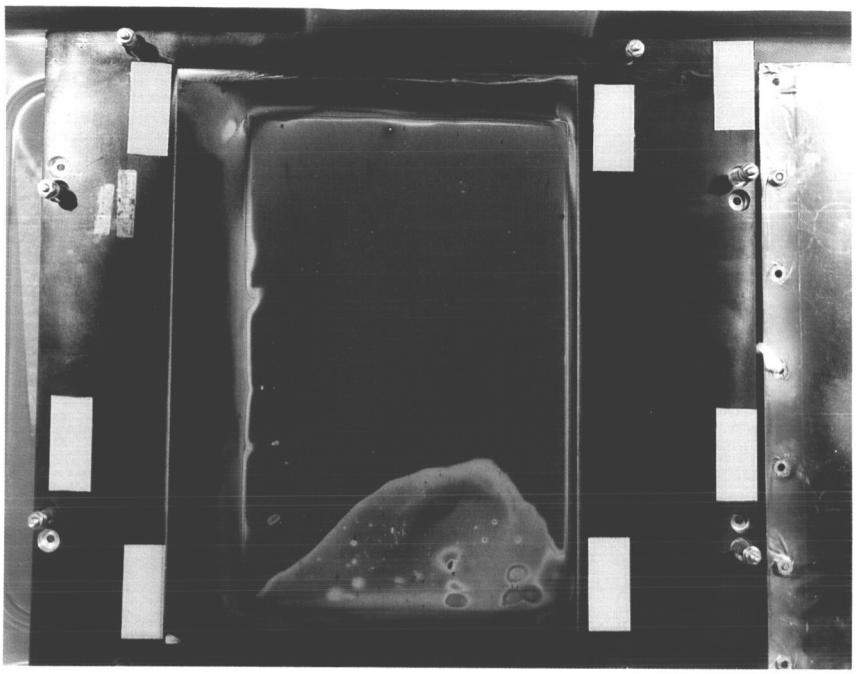

Figure 1. Photograph of black chromium plated solar absorber panel, experiment AO076, tray F9.
(Color version of black and white photograph shown on page 1106.)

AUTHOR INDEX

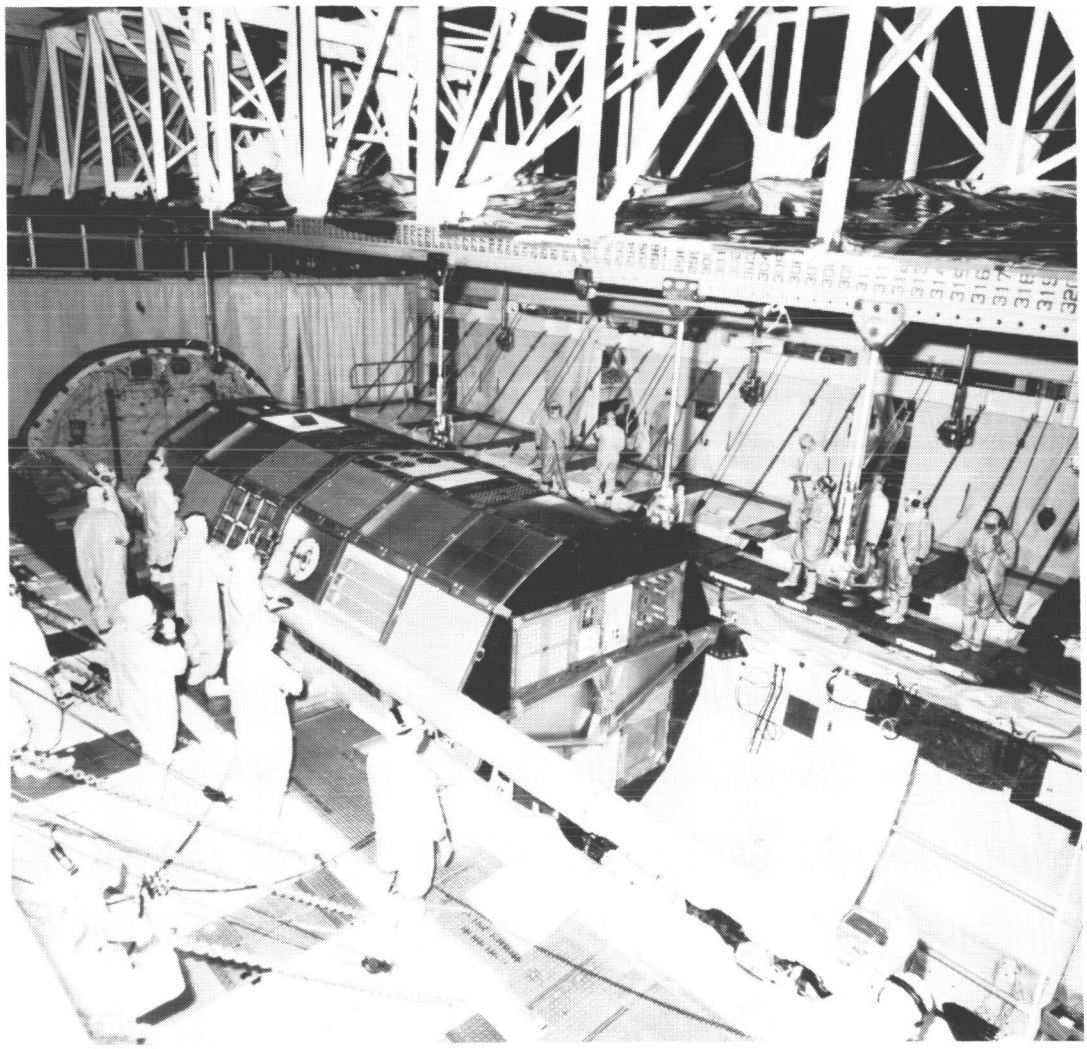

ORIGINAL PAGE
BLACK AND WHITE PHOTOGRAPH

L-90-11206

Author Index

Index Guide

Part 1, pages 1–274; Part 2, pages 275–738

Part 3, pages 739–1254; Part 4, pages 1255–1570

Adams, J.H., Jr. 247, 1551

Agüero, R.C. 665

Ahearn , J.S. 1285

Albrecht, A. 231

Allbrooks, M.K. 595

Alston, J.A. 1493

Amari, S. 513

Armstrong, T.W. 137, 163, 187, 195, 207, 221

Arthur, R.J. 79

Atkinson, D.R. 277, 595, 619, 1399

Auer, B.M. 1137

Bada, J. 453

Banks, B.A. 431, 1137

Beahm , L.P. 247

Beaujean , R. 239

Becker, L. 453

Benton, E.R., 171, 181

Benton, E.V. 163, 171, 181, 187

Bergman, L.A. 1439

Bernhard, R.P. 541, 551

Berry, J.N. 1425

Best, S. 479

Blake, J.B. 147

Blakkolb, B.K. 1035, 1343

Blue, M.D., 1333

Boberg, P.R. 247

Bobias, S.G. 87

Bohnhoff-Hlavacek, G. 1223

Bonnemason, F. 1401

Borg, J. 347

Borson, E.N. 1033

Bosch, J. 261

Bourassa, R.J. 13

Bourrieau, J. 157

Bowen, H.S. 1035

Bradley, J. 577

Brennan, P.J. 1455

Brinker, D.J. 1291, 1375

Brodzinski, R.L. 79

Brownlee, D.E. 577, 677

Bühler, F. 705

Bunch, T.E. 347, 453

Burns, F. 107

Cagle, J.A. 1511

Callen, W.R. 1403

Carabétian, Ch. 1355

Chaloupka, T. 479

Champetier, R.J. 1399

Chang, A.C. 827

Chapman, S.P. 1425

Chatzitheodoridis, E. 791

Coggi, J.M. 357, 1075, 1235

Christl, L.C. 1169

Colborn, B.L. 137, 163, 187, 195, 207, 221

Cooke, W.J. 667, 693

Coombs, C.R. 277, 595, 619

Crawford, G. 479

Cromer, T.F. 1015

Cromwell, B.K. 1001

Crutcher, E.R. 1023, 1187

PRECEDING PAGE BLANK NOT FILMED

Csige, I. 171, 181, 187
Dardano, C.B. 277
Davis, J.M. 1201
de Groh, K.K. 1137
DeHainaut, L.L. 1361
Delaboudinère, J.P. 1355
Derrickson, J.H. 171
Deshpande, S.P. 417
De Vries, C. 431
DeWalt , S.A. 1413
Dezfouly-Arjomandy, B. 231
Divine, N. 665
Domingo, C. 261
Drolshagen, G. 325
Durin, C. 541, 1315
Dursch, H.W. 923, 1041, 1257
Edelman, Joel 1257
Edwards, J.L. 1137
Enge, W. 239
Erlichman, J. 453
Eugster, O. 705
Farrow, A. 849
Felbeck, D.K. 889
Finckenor, M.M. 1125
Fishman, G.J. 111, 125
Fleming, R.H. 453
Foote, J. 513
Ford, D.I. 811
Frank, A.L. 163, 171
Frigo, L.A. 171, 187
Funk, J.G. 1201
Gaylord, T.K. 1403
Gebauer, L. 1137
Geiss, J. 705
George, G.A. 867
George, P.E. 923
Gillis, J.R. 13
Gilmour, J.D. 791
Golden, J.L. 1099
Grammer, H.L. 1015
Green, S.F. 417
Gregory, J.C. 3, 231, 1111, 1169
Griffis, D.P. 677
Grigsby, D.K. 1479
Gursky, H. 1535
Gyetvay, S.R. 357, 1235
Harmon, B.A. 111, 125, 231
Hartmayer, R. 1439
Harvey, G.A. 797
Havey, K. 1389
Hemminger, C.S. 963
Hennessy, C.J. 595
Henke, R.P. 171
Herzog, G. 231
Hickey, J.R. 1291, 1375
Hill, D.J.T. 867
Hill, S.G. 923
Hochedez, J.F. 1355
Hörz, F. 277, 551, 577
Hunter, J.L. 677
Hurley, D.L. 97
Imamoto, S.S. 147
Jaggers, C.H. 1075
Jansen, F. 261
Jenkins, P. 1375
Johnson, R.E. 811
Johnston, A.R. 1439
Jonathal, D. 239
Joswiak, D. 577
Kamenetzy, R.R. 1125, 1151
Kassel, Jr., P.C. 667, 693
Keegan, R. 261

Kemp, W.T. 1399
Kenemuth, J.R. 1361
Keough, B. 1041
Kessler, D.J. 585
Kinard, W.H. 277
Kinser , D.L. 529
Klein, J. 231
Kosic, T.J. 1035
Laird, C.E. 111, 125
Lange, G. 513
Lauriente, M. 51
Le, T.D. 977
Lee, M. 957
Letton, A. 849
Lind, D.L. 705
Lind, M.D. 725
Linton, R.C. 1151
Lyon, I.C. 791
Mack, K.S. 313
Mackay, N. 417
Macklin, J. 453
Mallon, J.J. 963
Mandeville, J.-C. 303, 347
Manuelpillai, G. 493
Masarik, J. 87
Mason, J.B. 1257
Matthews, R. 877
McCreight, C. 1455
McDonnell, J.A.M. 417
McKibben, R.B. 1535
McIntosh, R. 1455
Mell, R.J. 1061, 1111
Merrow, J.E. 431
Meshishnek, M.J. 357, 1075, 1235
Middleton, R. 231
Miglionico, C.J. 905
Miller, E.R. 1061, 1111
Mirtich, M.J. 431
Misra, V. 677
Monarski, T.W. 1425
Moss, C.E. 87
Motley, W.R. III 667
Mulholland, J.D. 667, 693
Murr, L.E. 905
Mustico, A. 1389
Newman, P.J. 417
Newman, S.C. 1511
Nielsen, K.F. 725
Norwood, J.K. 1125
Oda, K. 171
O'Donnell, J.H. 867
Oliver, J.P. 667, 693
Olmez, I. 107
O'Sullivan, D. 261
Padden, R.J. 1425
Parnell, T.A. 69, 111, 125, 171, 187
Paschen, K.W. 357
Pender, C.W. 1001
Perry, A.T. 1511
Peters, P.N. 3, 1111, 1169
Pippin, H.G. 13, 1023, 1041, 1187
Pomery, P.J. 867
Radhakrishnan, G. 1269
Radicati di Brozolo, F. 347, 453
Raikar, G.N. 1169
Rasoul, F.A. 867
Reedy, R.C. 87
Reeves, J.H. 79
Ricks, D.A. 677
Rooney, W. 957
Rose, M.F. 479
Roybal, R.E. 905

Rutledge, S.K. 431
Ryan, L.E. 1035, 1343
Sagalyn, P. 107
Sampair, T.R. 27, 51
Sanchez, A.D. 1425
Sapp, C.A. 339
Saxton, J.M. 791
Scheiman, D.A. 1291
Schurig, H.J. 1343
See, T.H. 277, 313, 339, 551
Seegmiller, D.W. 1361
Shepherd, S.D. 1001
Simon, C.G. 277, 677, 693
Simpson, J.A. 1535
Sinsheimer, F.B. 1033
Singer, S.F. 667
Slemp, W.S. 827, 1015, 1093
Smith, A.R. 97
Soundararajan, S. 181
Steckel, G.L. 977
Stein, B.A. 741
Stein, C. 905
Stella, P.M. 1303
Stephens, B. 479
Strganac, T. 849
Strickland, J.W. 1201
Stuckey, W.K. 1269
Swan, P. 513
Taylor, E.W. 1413, 1425
Taylor, W.W.L. 1343
Tennyson, R.C. 493, 877
Thompson, A. 261
Tidler, C.E. 1361
Turner, G. 791
Tuzzolino, A.J. 1535
Tylka, A.J. 247
Uht, J.C. 963
Vallimont, J. 1389
Van Lierde, P. 791
Venables, J.D. 1285
Voss, H.D. 1535
Vyhnal, R.F. 941
Wagner, J.D. 595, 619
Walker, R.M. 513
Wallace, D. 1269
Warren, J.L. 313
Watts, A.J. 277, 595, 619
Watts, J.W., Jr. 137, 171, 187
Weinberg, J.L. 667
Wenzel, K.-P. 261
Whitaker, A.F. 1125
Whitehouse, P.L. 3
Whiteside, J. 957
Wiedlocher, D.E. 529
Wightman, J.P. 1015
Wilkes, D.R. 1061, 1111, 1521
Wilson, B.K. 1499
Wong, W.C. 1343
Wood, B.E. 1001
Wortman, J.J. 667, 677
Yaung, J.Y. 1343
Young, P.R. 827, 1015, 1093
Zinner, E. 513
Zolensky, M.E. 277, 313, 339, 541
Zook, H.A. 277, 313, 339, 575
Zwiener, J.M. 1061, 1111

REPORT DOCUMENTATION PAGE

Form Approved
OMB No. 0704-0188

Public reporting burden for this collection of information is estimated to average 1 hour per response, including the time for reviewing instructions, searching existing data sources, gathering and maintaining the data needed, and completing and reviewing the collection of information. Send comments regarding this burden estimate or any other aspect of this collection of information, including suggestions for reducing this burden, to Washington Headquarters Services, Directorate for Information Operations and Reports, 1215 Jefferson Davis Highway, Suite 1204, Arlington, VA 22202-4302, and to the Office of Management and Budget, Paperwork Reduction Project (0704-0188), Washington, DC 20503.

1. AGENCY USE ONLY *(Leave blank)*	2. REPORT DATE	3. REPORT TYPE AND DATES COVERED
	April 1993	Conference Publication

4. TITLE AND SUBTITLE
69 Months In Space—Second LDEF Post-Retrieval Symposium

5. FUNDING NUMBERS
506-48-91-11

6. AUTHOR(S)
Arlene S. Levine, Editor

7. PERFORMING ORGANIZATION NAME(S) AND ADDRESS(ES)
NASA Langley Research Center
Hampton, VA 23681-0001

8. PERFORMING ORGANIZATION REPORT NUMBER
L-17196

9. SPONSORING/MONITORING AGENCY NAME(S) AND ADDRESS(ES)
National Aeronautics and Space Administration
Washington, DC 20546-0001

10. SPONSORING/MONITORING AGENCY REPORT NUMBER
NASA CP-3194, Part 3

11. SUPPLEMENTARY NOTES

12a. DISTRIBUTION/AVAILABILITY STATEMENT
Unclassified–Unlimited

Subject Category 99

12b. DISTRIBUTION CODE

13. ABSTRACT *(Maximum 200 words)*
This document is a compilation of papers presented at the Second Long Duration Exposure Facility (LDEF) Post-Retrieval Symposium. The papers represent the data analysis of the 57 experiments flown on the LDEF. The experiments include materials, coatings, thermal systems, power and propulsion, science (cosmic ray, interstellar gas, heavy ions, micrometeoroid, etc.), electronics, optics, and life science.

14. SUBJECT TERMS
Space experiment

15. NUMBER OF PAGES
528

16. PRICE CODE
A23

17. SECURITY CLASSIFICATION OF REPORT	18. SECURITY CLASSIFICATION OF THIS PAGE	19. SECURITY CLASSIFICATION OF ABSTRACT	20. LIMITATION OF ABSTRACT
Unclassified	Unclassified	Unclassified	

NSN 7540-01-280-5500

Standard Form 298(Rev. 2-89)
Prescribed by ANSI Std. Z39-18
298-102

NASA-Langley, 1993